Group 4 Indenyl Complexes for Ethylene Polymerisation

by

Thomas A. Q. Arnold



This thesis is submitted in partial fulfilment of the requirement for the degree of Doctor of Philosophy at the University of Oxford

Balliol College, Oxford

February 2015

The work described in this thesis was carried out in the Chemistry Research Laboratory, Mansfield Road, Oxford between October 2011 and February 2015 under the supervision of Professor Dermot O'Hare. All the work is my own unless stated to the contrary, and has not been previously submitted for any degree at this or any other university.

Thomas Allan Quartermaine Arnold
Balliol College
February 2015

Abstract

Group 4 Indenyl Complexes for Ethylene Polymerisation

Thomas A. Q. Arnold **D.Phil. Thesis**

Balliol College **Hilary Term 2015**

The aim of this project has been to develop the field of group 4 indenyl metallocene complexes based upon highly methylated ligands. Previous studies have shown that these compounds can be extremely active ethylene polymerisation catalysts, and, as such, are of both significant academic and commercial interest

Chapter One introduces metallocene chemistry, discussing developments within the field and the effects of permethylation on indenyl rings. A synopsis of the rise of the *ansa*-bridge is provided, in addition to highlights from recent zirconocene chemistry. A feature on olefin polymerisation is included, spanning heterogeneous catalysts, homogeneous metallocenes and post metallocenes, as well immobilised complexes and their supports.

Chapter Two charts updates to syntheses of bridged and unbridged permethylindenyl ligands. The developments have allowed for their use as viable industrial procedures.

Chapter Three is an account of the group 4 organometallic chemistry of the indenyl ligands from Chapter Two. Four bridged metallocenes, including *rac*-SBI*$ZrCl_2$ and *meso*-EBI*$Zr(CH_2Ph)_2$, are reported. In addition, six unbridged analogues comprising *rac*/*meso*-$Ind^{\#}_2MCl_2$ (M = Zr, Hf) and *rac*/*meso*-$Ind^{\#}_2(CH_2Ph)_2$ are described as well as a half-metallocene. The complexes are characterised by single crystal X-ray diffraction and variable temperature NMR spectroscopy. DFT calculations have been performed, with representations of their optimised geometries and frontier MOs given.

Chapter Four describes a reliable, reproducible procedure for immobilising group 4 complexes on the surface of solid supports; in total 19 catalysts are prepared. In addition to SSMAO, two new inorganic supports (LDHMAO and Solid MAO) are utilised. The latter has never previously been described in the academic literature. These catalysts have been characterised by IR, UV/visible and solid-state NMR spectroscopy in addition to SEM imaging. Zr K-edge EXAFS experiments were conducted and exceptionally clear data are reported.

Chapter Five investigates the aforementioned complexes as both solution- and slurry-phase ethylene polymerisation catalysts. Numerous parameters are tested including temperature and time dependence and all of the catalysts produce high molecular weight polymer in the range 150-300,000 daltons. The activity of *rac*-SBI*$ZrCl_2$ in solution exceeds 22,500 $kg_{PE}/mol_{Zr}/h/bar$, and 7,500 $kg_{PE}/mol_{Zr}/h/bar$ immobilised on Solid MAO. *meso*-EBI*$Zr(CH_2Ph)_2$ displays double the activity of its dichloride analogue. 1-hexene co-polymerisation is carried out as part of a high throughput screening study and activities in excess of 30,000 $kg_{PE}/mol_{Zr}/h/bar$ are reported. Scale-up polymerisation runs are also disclosed. The resultant polymer has been characterised by GPC, as well as X-ray diffraction, SEM, ^{13}C NMR and IR spectroscopy.

Chapter Six provides the experimental details and characterising data for the previous chapters. An **Appendix** consists of crystal structure data while the **Electronic Appendix** contains the CIFs, DFT output files and the raw polymerisation data.

Acknowledgements

Firstly I would like to thank Dermot for accepting me into his group back in 2010 and for agreeing to have me continue. With the extra three years in Balliol under his tutelage, it has been a long (and happy) road. Secondly, I am hugely indebted to SCG Chemicals for their financial support which has not only kept me in bread and wine, and the Magdalen Arms propped up, but has also taken me to Japan, Thailand and Cambodia.

A number of people have played a large part in the chemistry reported in this thesis, but first and foremost amongst these is JC – I couldn't have wanted a better partner-in-crime in the battle against the permethylated ligands. Not only have I received the odd result, but copious advice (and ignored a lot of it) and plenty of encouragement along the way. It has been a great three years in S4 and I have learnt and laughed a lot. Mark is also to blame for kindling the organometallic fire within and teaching me what little I know. He doubles as a great housemate and a reliable leader in adventures to the Uni Club, the PT and beyond.

Dr. Amber Thompson helped Mark to teach me the basics of crystallography and for that I am very grateful. I am similarly grateful to the ever-present Dr. Nick Rees for his help with all things NMR and for running all of my solid-state samples. Colin Sparrow is also thanked for the early morning mass spectrometry results – an excellent way to start a day! Dr. Peter Wells and Dr. Emma Gibson at Harwell have done invaluable work guiding JC and I though the murky waters of EXAFS and for generating some excellent results so I thank them hugely for that. Zoë was kind enough to share her wisdom on DFT and this has proven very useful. Thanks also to Golf for running SEM samples for me under duress and to Chunping for powder XRDs. SCG Chemicals have provided me with all-important GPC data as well as endless discussion on the synthetic procedures used here in Oxford. A number of people (Chris, Coops, Yue, Duncan, Zoë and JC) have dedicated a significant number of hours to proof-reading this work – it is a thankless task and one for which I am very lucky. However, it is their contributions to making the lab a great place to work that will forever have my gratitude.

Coops for some great conversations after one too many; Charles for his ridiculous quizzing knowledge; Joyce for her insatiable appetite (and making me look restrained!); Saul for introducing me to the Gin-Rum; Henry for organising some cracking socials and endless lunch amusement; Dave for the short-suit and some great partying; Golf for making me look hard-working; Chris for football, squash, plenty of cinema and Uni Club amusement as well as for actually being a good Part II. The post-docs have been invaluable in making the group run efficiently and have provided their share of amusement along the way. Many others have chipped in, from fun Part IIs to brilliant visiting professors and everything in between. It has been such fun taking on the journey with Sam and Hannah – I never would have made it through without them: stalwarts on a social and at tea-time and fantastic fun on a night out – what a three (and a bit) years.

I have had some excellent housemates (Aileen, Alice, Tom and Mark) during my D.Phil. and I am impressed that Hannah and I stuck it out for the whole hog! Thanks also to my Balliol cohort (Emily, Mike, Larry, Steve, Catherine, Andy and Euan), who made the undergraduate slog such fun, and to Alex Wykeham, amongst others, for providing plenty of distraction. I have hugely enjoyed lining my pockets with titbits from demonstrating, teaching

and interviewing, and Phil Wiseman, Fraser Armstrong, Dermot, Rachel Quarrell and William Barford have all played their parts. Wine has, quite literally, sustained me for the last few years and William Kelley, Henry Little and Ren Lim have played key roles in that ludicrous adventure.

Finally a huge debt is due to my parents, and to Alice, who have helped and encouraged me throughout and have always been loving and supportive; all without having a clue as to what I might be doing – thank you so much.

Introduction **1**
1.1 Organometallic chemistry 1
1.1.1 Cyclopentadienyl chemistry 1
1.1.2 Methylated cyclopentadienyl chemistry 1
1.1.3 Indenyl chemistry 5
1.1.4 Methylated indenyl chemistry 6
1.1.5 *ansa*-bridged organometallic chemistry 10
1.1.5.1 One-atom bridges 10
1.1.5.2 Two-atom bridges 12
1.1.5.3 Longer, and multiple, bridges 12
1.1.5.4 The *ansa*-effect 13
1.6.1 Recent zirconocene chemistry 16
1.1 Olefin polymerisation 20
1.2.1 The polyolefin market 20
1.2.2 Heterogeneous olefin polymerisation 20
1.2.3 Homogeneous olefin polymerisation 20
1.2.4 Mechanism of polymerisation 25
1.2.5 Supported single-site olefin polymerisation 28
1.2.6 Industrial processes 31
1.3 Aims 31
1.4 References 32
Ligand Development **41**
2.1 Introduction 41
2.2 An updated synthesis 42
2.2.1 Rationale for the update 42
2.2.2 Synthesis of tigloyl chloride (**2.2**) 43
2.2.3 Synthesis of 2,3,4,5,6,7-hexamethylindanone (**2.4**). 44
2.2.4 Synthesis of 1,2,3,4,5,6,7-heptamethylindan-1-ol (**2.5**). 47
2.2.5 Synthesis of lithium 1,2,3,4,5,6,7-heptamethylindenide (**2.7**). 52
2.2.6 Synthesis of 1-methylene-2,3,4,5,6,7-hexamethylindene (**2.8**) 53
2.2.7 Synthesis of ethylenebis[1-(2,3,4,5,6,7-hexamethylindenide)] dilithium (**2.9**). 55
2.3 A route to EBI*H_2 (**2.13**) from **2.4** 56
2.3.1 Synthesis of 2,3,4,5,6,7-hexamethylindan-1-ol (**2.10**) 57
2.3.2 Synthesis of 2,3,4,5,6,7-hexamethylindene (**2.11**) 57
2.3.3 Synthesis of lithium 2,3,4,5,6,7-hexamethylindenide (**2.12**) 60

2.3.4 Synthesis of ethylenebis[1-(2,3,4,5,6,7-hexamethylindene)] (**2.13**).....61
2.4 An improved route in preparation for industrial scale-up.....63
2.4.1 Synthesis of 2,3,4,5,6,7-hexamethylindanone (**2.4**) 63
2.4.2 Synthesis of 2,3,4,5,6,7-hexamethylindene (**2.11**) 65
2.4.3 Synthesis of ethylenebis[1-(2,3,4,5,6,7-hexamethylindene)] (**2.13**).....66
2.4.4 Synthesis of ethylenebis[1-(2,3,4,5,6,7-hexamethylindenide)] dilithium (**2.9**) 67
2.5 Ligand variations 69
2.5.1 Synthesis of dimethylsilylbis[1-(2,3,4,5,6,7-hexamethylindene)] (**2.14**).....69
2.5.2 Synthesis of dimethylsilyl[1-(2,3,4,5,6,7-hexamethylindene)]chloride (**2.16**).....71
2.5.3 Synthesis of dimethylsiliconbis[1-(2,3,4,5,6,7-hexamethylindenide] dilithium (**2.15**) 72
2.5.4 Synthesis of lithium *n*-butyldimethylsilicon(1-(2,3,4,5,6,7-hexamethylindenide) (**2.17**) 72
2.6 Conclusions.....73
2.7 References.....74
Synthesis of Group 4 Indenyl Complexes 76
3.1 Introduction.....76
3.2 Definitions of structural parameters.....76
3.3 Metallation improvements 78
3.3.1 Protonolysis 78
3.3.2 Salt metathesis 79
3.4 Synthesis of silyl-bridged group 4 complexes 80
3.4.1 Synthesis of dimethylsilylbis[1-(2,3,4,5,6,7-hexamethylindenyl)]zirconium dichloride, SBI*$ZrCl_2$ (**3.1**).....80
3.4.2 Synthesis of dimethylsilylbis[1(2,3,4,5,6,7-hexamethylindenyl)]zirconium dibenzyl, SBI*$Zr(CH_2Ph)_2$ (**3.2**) 86
3.5 Synthesis of ethylene bridged group 4 complexes.....88
3.5.1 Synthesis of ethylenebis[1-(2,3,4,5,6,7-hexamethylindenyl)] zirconium dibenzyl, EBI*$Zr(CH_2Ph)_2$ (**3.3**) 88
3.5.2 Synthesis of ethylenebis[1-(2,3,4,5,6,7-hexamethylindenyl)] zirconium neopentyl chloride, EBI*$Zr(CH_2{}^tBu)Cl$ (**3.4**).....100
3.6 Synthesis of unbridged group 4 complexes 107
3.6.1 Synthesis of bis(2,3,4,5,6,7-hexamethylindenyl)zirconium dichloride, $Ind^{\#}_2ZrCl_2$ (**3.5**) 107
3.6.2 Synthesis of bis(2,3,4,5,6,7-hexamethylindenyl)hafnium dichloride, $Ind^{\#}_2HfCl_2$ (**3.6**).....113

3.6.3 Synthesis of bis(2,3,4,5,6,7-hexamethylindenyl)zirconium dibenzyl, $Ind^{\#}_2ZrBz_2$ (**3.7**) 121
3.7 Synthesis of {*n*-butyldimethylsilyl[1-(2,3,4,5,6,7-hexamethylindenyl)]} zirconium trichloride (**3.8**) 127
3.8 Further reactivity 132
3.8.1 Synthesis of hydride species 132
3.8.2 Synthesis of cationic species 132
3.8.3 Reactivity with alkyl aluminium species 132
3.9 Conclusion 133
3.10 References 133
Supported Catalysts and Solid-State Characterisation 136
4.1 Introduction 136
4.2 Immobilising the complexes 139
4.3 Characterisation of the supported catalysts 144
4.3.1 Scanning electron microscopy 144
4.3.2 UV/visible spectroscopy 146
4.3.3 IR spectroscopy 148
4.3.4 Solid-state NMR spectroscopy 149
4.4 EXAFS studies 151
4.5 SANS experiment 158
4.6 Conclusion 158
4.7 References 159
Ethylene Polymerisation Studies 161
5.1 Introduction 161
5.2 Solution-phase polymerisation 161
5.3 Slurry-phase polymerisation 169
5.3.1 EBI* complexes 169
5.3.2 SBI* complexes 176
5.3.3 $Ind^{\#}$ complexes 182
5.3.4 $Ind^{\#}SiMe_2{}^{n}BuZrCl_3$ 184
5.3.5 Summary 186
5.4 High-throughput screening 188
5.5 Large-scale polymerisation runs 192
5.6 Polymer characterisation 192
5.7 Conclusion 197
5.8 References 197
Experimental Details 200

6.1 General Procedures 200
6.2 Physical measurements 200
6.2.1 Single crystal X-ray diffraction 200
6.2.2 Density functional theory calculations 201
6.2.3 Solution phase NMR spectroscopy 202
6.2.4 Solid-state NMR spectroscopy 202
6.2.5 Infrared spectroscopy 202
6.2.6 Ultraviolet/visible spectroscopy 202
6.2.7 Mass spectrometry 203
6.2.8 Scanning electron microscopy 203
6.2.9 Powder X-ray diffraction 203
6.2.10 Gel permeation chromatography 203
6.2.11 Elemental analysis 203
6.2.12 EXAFS measurements 203
6.3 Starting Materials 204
6.3.1 Commercially supplied reagents 204
6.3.2 Literature preparations 204
6.4 Experimental details for Chapter Two 205
6.4.1 Synthesis of tigloyl chloride (**2.2**) 205
6.4.2 Synthesis of hexamethylindanone (**2.4**) 205
6.4.3 Synthesis of Ind*OH (**2.5**) 206
6.4.4 Synthesis of Ind*H (**2.6**) 206
6.4.5 Synthesis of Ind*Li (**2.7**) 207
6.4.6 Synthesis of hexamethylindenyl fulvene (**2.8**) 207
6.4.7 Synthesis of EBI*Li_2 (**2.9**) 208
6.4.8 Synthesis of Ind$^{\#}$OH (**2.10**) 208
6.4.9 Synthesis of Ind$^{\#}$H (**2.11**) 209
6.4.10 Synthesis of Ind$^{\#}$Li (**2.12**) 210
6.4.11 Synthesis of EBI*H_2 (**2.13**) 210
6.4.12 Synthesis of hexamethylindanone (**2.4**) *via* a one-pot method 211
6.4.13 Synthesis of Ind$^{\#}$H (**2.11**) *via* a one-pot method 211
6.4.14 Synthesis of EBI*H_2 *via* a one-pot method 212
6.4.15 Synthesis of EBI*Li_2 (**2.9**) from EBI*H_2 212
6.4.16 Synthesis of SBI*H_2 (**2.14**) 213
6.4.17 Synthesis of HIndSiMe_2Cl (**2.16**) 213
6.4.18 Synthesis of SBI*Li_2 (**2.15**) 214

6.4.19 Synthesis of LiInd$^{\#}$SiMe$_2$^{n}Bu (**2.17**) 214
6.4.20 Synthesis of HInd$^{\#}$SiMe$_2$^{n}Bu (**2.18**) 215
6.5 Experimental details for Chapter Three 215
6.5.1 Synthesis of EBI*ZrCl$_2$ 215
6.5.2 Synthesis of SBI*Zr(NMe$_2$)$_2$ 216
6.5.3 Synthesis of SBI*ZrCl$_2$ (**3.1**) 216
6.5.4 Synthesis of SBI*ZrBz$_2$ (**3.2**) 217
6.5.5 Synthesis of EBI*ZrBz$_2$ (**3.3**) 217
6.5.6 Synthesis of EBI*ZrNpCl (**3.4**) 218
6.5.7 Synthesis of Ind$^{\#}_2$ZrCl$_2$ (**3.5**) 219
6.5.7 Synthesis of Ind$^{\#}_2$HfCl$_2$ (**3.6**) 221
6.5.8 Synthesis of Ind$^{\#}_2$ZrBz$_2$ (**3.7**) 222
6.5.9 Synthesis of Ind$^{\#}$SiMe$_2$^{n}BuZrCl$_3$ (**3.8**) 223
6.6 Experimental details for Chapter Four 224
6.6.1 Synthesis of supported catalysts 224
6.6.2 UV/visible spectroscopy data 225
6.6.3 Solid-state NMR spectroscopy data 225
6.6.4 EXAFS fit data 226
6.7 Experimental details for Chapter Five 226
6.7.1 Laboratory polymerisation runs 226
6.7.2 Polymer characterisation 227
6.8 References 227

List of Abbreviations

°C	degrees Celsius
Å	ängstrøm, 10^{-10} m
AF	amorphous fraction
AMO-LDH	high surface area LDH synthesised using AMOST
AMOST	aqueous miscible organic solvent treatment
Ar^F	pentafluorophenyl, C_6F_5
b	broad
BET	Brunauer-Emmett-Teller
btmsa	bis(trimethylsilyl)acetylene
^{i}Bu	*iso*-butyl, CH_2CHMe_2
^{n}Bu	*n*-butyl, $CH_2CH_2CH_2CH_3$
^{t}Bu	*tert*-butyl, CMe_3
Bz	benzyl, CH_2Ph
cent	centroid
c.	*circa*
CEF	crystallisation elution fractionation
CGC	constrained geometry catalyst
COD	cyclooctadiene, C_8H_{12}
COSY	correlation spectroscopy
Cp	cyclopentadienyl, C_5H_5
Cp*	pentamethylcyclopentadienyl, C_5Me_5
Cp′	methylcyclopentadienyl, C_5H_4Me
CSD	crystal structure database
CV	cyclic voltammmetry
δ	chemical shift
$\Delta_{M\text{-}C}$	ring slip
d	doublet
DBU	diazabicyclo[5.4.0]undec-7-ene
DCM	dichloromethane, CH_2Cl_2
DEAC	diethylaluminium chloride, $AlEt_2Cl$
DFT	density functional theory
DIPP	2,6-diisopropylphenyl, 2,6-^{i}Pr-C_6H_3

DMAD	dimethylacetylenedicarboxylate
DMF	N,N-dimethylformamide
DMSO	dimethylsulphoxide, Me_2SO
η	hapticity
E_0	standard reduction potential
EBI	ethylenebis(indenyl), $IndCH_2CH_2Ind$
EBI*	ethylenebis(hexamethylindenyl), $Ind^{\#}CH_2CH_2Ind^{\#}$
EBTHI	ethylenebis(tetrahydroindenyl), $(C_9H_{10})CH_2CH_2(C_9H_{10})$
EI	electron ionisation (formerly known as electron impact)
EPR	electron paramagnetic resonance
ESD	estimated standard deviation
Et	ethyl, CH_2CH_3
EXAFS	extended X-ray absorption fine structure
FA	fold angle
FADE	fumaric acid dimethylester
FLP	frustrated Lewis pair
Flu	fluorenyl, $C_{13}H_9$
Flu*	nonamethylfluorenyl, $C_{13}Me_9$
FT	Fourier transform
GPC	gel permeation chromatography
h	hour
HA	hinge angle
HDPE	high density polyethylene
HOMO	highest occupied molecular orbital
HRMS	high-resolution mass spectrometry
Ind	indenyl, C_9H_7
Ind*	heptamethylindenyl, C_9Me_7
$Ind^{\#}$	hexamethylindenyl, C_9Me_6H
IR	infrared
K	kelvin
KIE	kinetic isotope effect
λ_{max}	wavelength of maximum absorption
LDH	layered double hydroxide

LDHMAO	LDH supported MAO ($MgAlSO_4$ unless specified otherwise)
LDPE	low density polyethylene
LMCT	ligand-to-metal charge transfer
Ln	lanthanide
LUMO	lowest unoccupied molecular orbital
μ	bridging
m	multiplet
M	mol dm^{-1} ; metal
M_n	number-average molecular weight
M_w	weight-average molecular weight
MADE	maleic acid dimethyl ester
MAO	methylaluminoxane
Me	methyl, CH_3
MO	molecular orbital
MS	mass spectrometry
MWD	molecular weight distribution
NBS	N-bromosuccinimide
NMR	nuclear magnetic resonance
Np	neopentyl, CH_2CMe_3
NOE	nuclear Overhauser effect
p.a.	*per annum*
PDI	polydispersity index
PE	polyethylene
PES	photoelectron spectroscopy
Ph	phenyl, C_6H_5
pip	piperazine, $C_4H_8N_2$
Pn*	hexamethylpentalene, C_8Me_6
PP	polypropylene
ppm	parts per million
^{i}Pr	*iso*-propyl, $CHMe_2$
q	quartet
RA	rotation angle
ROESY	rotating-frame nuclear Overhauser effect spectroscopy

s	singlet
SANS	small-angle neutron scattering
SBI	dimethylsilylbis(indenyl), Ind_2SiMe_2
SBI*	dimethylsilylbis(hexamethylindenyl), $Ind^{\#}_2SiMe_2$
SEM	scanning electron microscopy
SSMAO	silica supported MAO
SQUID	superconduction quantum interference device
T	temperature
t	triplet; time
TA	torsion angle
TA′	adapted torsion angle
TEA	triethylaluminium, $AlEt_3$
THF	tetrahydrofuran, C_4H_8O
TIBA	triisobutylaluminium, $Al^{i}Bu_3$
TM	transition metal
TMA	trimethylaluminium, $AlMe_3$
TMEDA	tetramethylethylenediamine, $Me_2NCH_2CH_2NMe_2$
TMS	tetramethylsilane, $SiMe_4$
ULDPE	ultra-low density polyethylene
UV	ultraviolet
VLDPE	very-low density polyethylene

Key to Compound Identification

Chapter Two

2.1	tiglic acid (*trans*-2-methylbutenoic acid)
2.2	tigloyl chloride (*trans*-2-methylbutenoyl chloride)
2.3	1,2,3,4-tetramethylbenzene
2.4	1,2,3,4,5,6-hexamethylindanone
2.5	1,2,3,4,5,6,7-heptamethylindan-1-ol
2.6	Ind*H
2.7	Ind*Li
2.8	1-methylene-2,3,4,5,6,7-hexamethylindene
2.9	EBI*Li_2
2.10	2,3,4,5,6,7-hexamethylindan-1-ol
2.11	$Ind^{\#}H$
2.12	$Ind^{\#}Li$
2.13	EBI*H_2
2.14	SBI*H_2
2.15	SBI*Li_2
2.16	$HInd^{\#}SiMe_2Cl$
2.17	$LiInd^{\#}SiMe_2{}^{n}Bu$
2.18	$HInd^{\#}SiMe_2{}^{n}Bu$

Chapter Three

***rac*-3.1**	*rac*-SBI*$ZrCl_2$
***rac*-3.2**	*rac*-SBI*$ZrBz_2$
***meso*-3.3**	*meso*-EBI*$ZrBz_2$
***meso*-3.4**	*meso*-EBI*ZrNpCl
***rac*/*meso*-3.5**	*rac*/*meso*-$Ind^{\#}_2ZrCl_2$
***rac*/*meso*-3.6**	*rac*/*meso*-$Ind^{\#}_2HfCl_2$
***rac*/*meso*-3.7**	*rac*/*meso*-$Ind^{\#}_2ZrBz_2$
3.8	$Ind^{\#}SiMe_2{}^{n}BuZrCl_3$

Ind* = C_9Me_7; $Ind^{\#}$ = C_9Me_6H; EBI* = $Ind^{\#}CH_2CH_2Ind^{\#}$; SBI* = $Ind^{\#}_2SiMe_2$; Bz = CH_2Ph; Np = $CH_2{}^{t}Bu$.

Chapter One
Introduction

1.1 Organometallic chemistry

1.1.1 Cyclopentadienyl chemistry

For over 60 years, the field of organometallic chemistry has been dominated by the use of the cyclopentadienyl ligand (Cp). Its first appearance, the complex ferrocene (Cp_2Fe; Figure 1.1a) in 1951 heralded a new dawn from which organometallics has never looked back.[1] Cp was quickly incorporated into new complexes spanning the periodic table,[2–7] and formed the backbone for much key research into its uses including olefin polymerisation,[8] organic synthesis,[9] and nitrogen activation.[10] Its excellent properties as a ligand are primarily derived from its ability to coordinate to metals through an anionic η^5 bonding motif where the delocalised electron density in the carbocyclic π-orbitals is able to interact with empty metal d- and f-orbitals forming a strong σ- or π-bond.[4] This interaction can often be enhanced by the strong electrostatic attraction between the anionic ligand and a positively charged metal centre. The combination of these factors leads to its typical use as a non-labile ancillary ligand. The use of the Cp ligand with group 4 metals followed swiftly, with Cp_2TiCl_2 and Cp_2ZrCl_2 (Figure 1.1b) reported by Wilkinson in 1954,[11] and Cp_2HfCl_2 by Lynch just three years later.[12] Cp ligands were quickly modified and Cp'_2Fe ($Cp' = C_5H_4Me$) was published eight years after its non-methylated equivalent.[13]

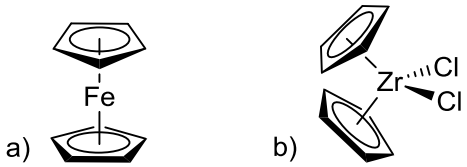


Figure 1.1: a) Cp_2Fe, ferrocene;[1] b) Cp_2ZrCl_2, zirconocene dichloride.[11]

1.1.2 Methylated cyclopentadienyl chemistry

The advent of pentamethylcyclopentadiene (Cp*H; C_5Me_5H) and its organometallic derivatives has greatly enhanced the field, and metal complexes containing Cp* are near ubiquitous today.[14] This permethylated variant confers greater stability on its complexes, both kinetically and thermodynamically compared to its non-methylated analogue.[15–17] Broadly speaking, permethylation can impart steric and electronic effects. Due to the differing electronegativities of C and H, the methyl groups accrue electron density and act as inductive electron donors through the sigma framework of the carbocycle, funnelling electron density

into the aromatic Cp ring. This is in turn passed into the metal-carbon (M-C) bond, strengthening it. This increased donor ability of the ligand can also be measured indirectly by looking at the decrease in infrared (IR) stretching frequency of carbonyl ligands upon permethylation of the cyclopentadienyl moiety as seen in the compounds $Cp^{R}M(CO)_2$ (M = Co, Rh, Ni; Cp^{R} = Cp or Cp*).[18,19] Both papers report a drop in CO stretching frequency of between 20 and 40 cm^{-1} and attribute it to the increased electron density on the metal centre backbonding into the carbonyl π^* and weakening the C≡O bonding interaction, as a result of the increased electron density from the Cp*. Mise *et al.* also comment on the change in ^{13}C NMR spectroscopic shift for the carbonyl resonance, shifting 12.1 ppm downfield for Cp* from 226.2 to 238.3 ppm. As the metal-ligand backdonation increased, the M-L bond distance decreased, increasing the deshielding on the carbon and increasing its relative chemical shift.[20,21]

This effect can also be measured directly using ultraviolet (UV)/visible spectroscopy where the lowest unoccupied molecular orbital (LUMO), consisting mainly of metal d-orbital character, is raised in energy as the number of methyl substituents in Cp^{R} increases for the compound $Cp^{R}TiCl_3$.[22] It is shown that on each successive methylation of the Cp ligand, the LUMO is raised by approximately 0.1 eV deduced by the changing energy of the charge transfer band in the UV spectrum, consistent with increased electron density on the metal centre where the LUMO is based. This effect is also seen when comparing decamethylmetallocenes across the first row of the periodic table which see the Racah parameter, B, and the ligand field splitting parameter, Δ_0, both measured by UV/visible spectroscopy, increased relative to the unmethylated analogues.[15] This increased thermodynamic stability can be measured using other techniques including cyclic voltammetry (CV), used to measure the changing reduction potential (E_0) of the metal. Analysis of a series of increasingly methylated zirconocene dichlorides elucidates a remarkably smooth trend of increased reduction potential with electron density on the metal.[23] The addition of a methyl group to each of the Cp groups reduces the E_0 value by approximately 50 mV across the range Cp_2ZrCl_2 to $Cp^*_2ZrCl_2$, decreasing to a relative E_0 of −244 mV. This remarkably detailed study improves upon a previous array of results which were, at times, contradictory,[24–26] and confirms that $Cp^*_2ZrCl_2$ has a more negative E_0 than $Cp^{Me4}_2ZrCl_2$. Furthermore it proves, perhaps unsurprisingly, that this effect can be attributed to methyl groups in the same manner in a mixed ring system, displaying a reduction in potential of 129 mV from Cp_2ZrCl_2 to $CpCp^*ZrCl_2$. It continues, analysing the effects of both

more bulky alkyl and silyl substituents but also the effect of *ansa*-bridges and indenyl ligands (see section 1.1.5). In addition, the paper addresses the questions of carbonyl stretching frequencies and ^{13}C NMR shifts (*vide supra*) in the series $Cp_2Zr(CO)_2$ to $Cp^*_2Zr(CO)_2$ and $CpCp^*Zr(CO)_2$. The carbonyl resonance in the ^{13}C NMR shifts downfield 8.1 ppm from $Cp_2Zr(CO)_2$ to $Cp^*_2Zr(CO)_2$ in good agreement with the results from Mise. The IR values are similarly correlated, with the CO stretching frequency dropping on average 33 and 12 cm^{-1} from $Cp_2Zr(CO)_2$ to $Cp^*_2Zr(CO)_2$ and $CpCp^*Zr(CO)_2$ respectively.

The trend in reduction potential seen above for zirconocenes is replicated across the first row transition metals with Cp^*_2M (M = Cr, Co, Ni) more easily oxidised than the unmethylated congeners and with the decamethylated Cp^*_2M (M = Mg, V) not reported.[15] However, the author does highlight another advantage of permethylated ligands with the synthesis of the formally 18-electron $[Cp^*_2Ni][PF_6]_2$, with a central Ni^{4+} ion stabilised by the strong electron donation from the Cp* ligands. No such equivalent has been synthesised using Cp, although 20-electron Cp_2Ni is well documented. As well as the capability to stabilise high oxidation states, permethylated ligands have been isolated with low valent non-metals such as those in group 14. A rare example of a silicon (II) organometallic complex, Jutzi's Cp^*_2Si, is this time stabilised by the Cp* ligand's steric bulk rather than its formidable electron donation ability.[28,29] The isolation of this complex proved to be a major breakthrough in low valent non-metal chemistry. Cp* was also used to stabilise a rare zinc (I) organometallic, $(Cp^*Zn)_2$, and the first example of Zn(I)-Zn(I) bonding.[29] Unlike mercury, which has extensive +1 oxidation state chemistry, zinc primarily adopts the +2 state. Once again it is the kinetic stability imparted by the sterically imposing ligand that protects the complex, rendering it stable in solution and in the solid state, although the compound is exceedingly reactive towards both air and moisture. Unusually, the complex exhibits eclipsed Cp* rings although their large separation, including the Zn-Zn bond of 2.305(3) Å, would preclude much interaction.

Cp*'s steric bulk also played a major part in the isolation of some of the first metal-metal multiple bonds.[17] It was found that when CpLi was reacted with $Mo(CO)_6$, $[CpMo(CO)_3]_2$ could be isolated as a stable 18-electron complex with a single Mo-Mo bond, as was also shown for rhenium. However, when Cp*Li was used, an unusual stoichiometry was identified. Further analysis led to the conclusion that $[Cp^*Mo(CO)_2]_2$ contained the unusual Mo≡Mo triple bond, satisfying the 18-electron criterion with the loss of one carbonyl per

metal.[30] A similar scenario is seen with a double Co=Co bond in $[Cp^*Co(CO)]_2$ which is also stabilised by the additional bulk of the ten methyl groups and has no direct Cp congener.[31]

The most obvious difference is its steric bulk which shields the metal centre and provides kinetic stability. It also is able to offer kinetic stability by another means: the absence of α-hydrogens. This removes an intramolecular decomposition pathway, clearly illustrated by the different species formed by the related titanocenes, Cp_2Ti[32,33] and Cp^*_2Ti (Figure 1.2).[34]

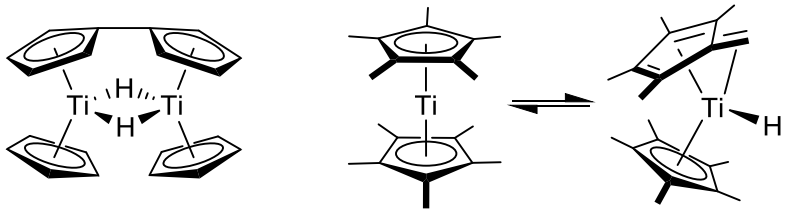


Figure 1.2: dimeric and monomeric structures of "$TiCp_2$" and "$TiCp^*_2$" respectively.[32–34]

In both cases the neutral monomer would be a 14-electron compound and, hence, electron deficient. To relieve this pressure, titanocene deviates from the pattern seen for the rest of the first row metallocenes (Cp_2M) and the titanium abstracts a hydride from the Cp ligand, forming a fulvalene moiety and two hydrides, leaving the titanium as a 16-electron species. In contrast, decamethyltitanocene exists in equilibrium with a monomeric fulvene hydride species (also 16-electron).

The principles of inductive donation from the methyl groups on the ring naturally extend to other conjugated ring systems with cyclopentadienyl type rings, such as pentalenes (Pn; C_8H_6), arenes,[35] and their combinations: systems such as indenyl (Ind; C_9H_7 and fluorenyl (Flu; $C_{13}H_8$). Many of these species, and in particular their permethylated analogues have been extensively investigated by O'Hare and co-workers. The permethylpentalene (Pn*) ligand, first synthesised by Ashley *et al.* in 2007,[36] has been used extensively to bring about interesting chemistry all over the periodic table: group 14,[37] lanthanides,[38] actinides,[39–41] and the first row of the d-block.[42] Perhaps most pertinently of all, Pn* has been used to elucidate numerous structures of the group 4 metals,[37] some of which have been proven active catalysts for the polymerisation of ethylene,[43] or initiators for the polymerisation of lactide.[44] The challenge of permethylating fluorene, a Cp with two ring fused benzene groups, was overcome in 2006, and the new ligand was used to coordinate metals using both the arene and the Cp fragment.[45–47] η^6,η^6-Flu*H$[Cr(CO)_3]_2$ was shown to be both more stable than its non-methylated analogue and more soluble, facilitating further chemistry, while [η^6,η^6-

Flu*H(FeCp)$_2$][PF$_6$]$_2$ was additionally catalytically active towards the dechlorination of aromatic species such as polychlorinated biphenyls (PCBs) (Figure 1.3).[46]

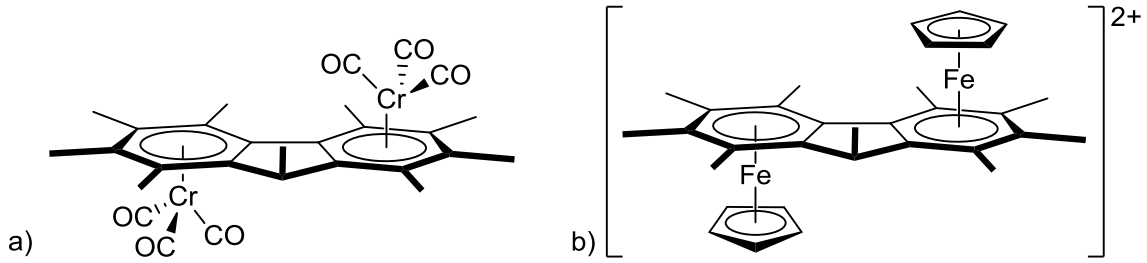
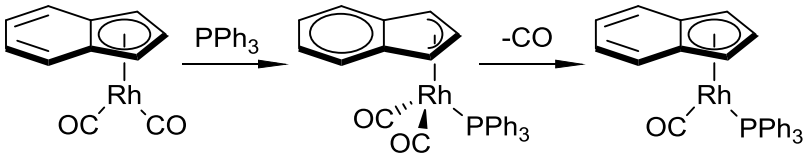


Figure 1.3: a) η^6,η^6-Flu*H[Cr(CO)$_3$]$_2$; b) [η^6,η^6-Flu*H(FeCp)$_2$][PF$_6$]$_2$. [PF$_6$]$^-$ anions omitted for clarity).[45–47]

While Flu* can be considered an extended subset of permethylindenyl (Ind*; C$_9$Me$_7$), its chemistry is dominated by η^6 interactions with the incorporated arenes and not with the Cp fragment which had, until recently, only been successfully used for one η^5 species, (Flu*ZrCl$_3$)$_2$, and one η^1, Flu*InCl$_2$(THF), both of which are dimeric. Bazinet *et al.* were able to use Flu* (and Flu″, its octamethyl congener) to generate mixed ligand systems with both zirconium and hafnium.[48] In addition they were able to reduce the dichlorides to dicarbonyls – the first time that this had been achieved with a fluorenyl system.

1.1.3 Indenyl chemistry

As illustrated above, methylation is far from the only means of derivitising Cp; the benzannulated version, indenyl, has also been the subject of much investigation. Indene was first isolated from coal tar in 1890,[49] but its use as an organometallic ligand is significantly less developed than that of Cp as illustrated by 517 hits in the Cambridge Structural Database (CSD) as opposed to over 10,000 for Cp. It shows a variety of binding modes which characterise its chemistry and differentiate it from Cp.[50] Most notable amongst these is the so-called "indenyl effect" where the ligand is able to ring slip from η^5 coordination to η^3, allowing the metal to gain electrons in its valence shell without having to change oxidation state. This ability is clearly highlighted in the reaction of Basolo's famous IndRh(CO)$_2$ complex with PPh$_3$ (Scheme 1.1), which is seen to undergo S$_N$2 (associative) 10^8 times faster than the corresponding Cp complex.[51]



Scheme 1.1: ligand substitution in an indenyl rhodium complex illustrating the η^5-η^3 ring slippage, demonstrated by Basolo.[51]

The indenyl effect is facilitated by the aromaticity of the benzene ring which is maintained whether the group coordinates in an η^5 or an η^3 manner, whereas the Cp has to lose the stabilising aromaticity introducing a larger energetic barrier to reaction. This allows the rhodium centre to maintain 18 valence electrons throughout the addition and subsequent elimination. However, this feature also leads to the increased lability of the indenyl ring, reducing a complex's overall stability compared to its Cp counterpart. This relative instability was observed with the first indenyl group 4 complexes reported.[52] Both Ind_2TiCl_2 and Ind_2ZrCl_2 were synthesised using a salt metathesis method from IndNa and anhydrous MCl_4 (M = Ti, Zr) but the complexes were found to decompose rapidly on extraction into organic solvents, and instead were washed with dilute aqueous HCl to remove the salt impurities. Indenyl complexes of the group 4 metals continue to feature prominently in the field of olefin polymerisation and more details will be discussed in Section 1.2.3.

1.1.4 Methylated indenyl chemistry

The chemistry of Ind* is dominated by metals bound η^5 to the ligand. However η^6 arene interactions are observed in four complexes: η^6-Ind*HCr(CO)$_3$ – both *endo*- and *exo*-isomers, and (Cr(CO)$_3$)Ind*RhCOD (COD = cyclooctadiene).[50] In each of these cases, it is a chromium(0) species that is coordinated to the carbocycle η^6; the rhodium, where applicable, attaches *via* an η^5 binding mode (Figure 1.4).

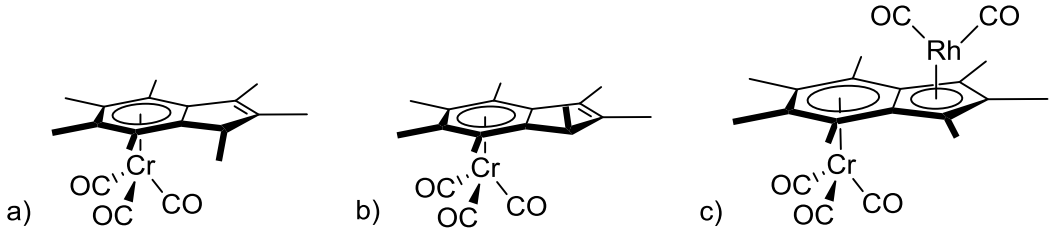


Figure 1.4: a) *endo*-η^6-Ind*Cr(CO)$_3$; b) *exo*-η^6-Ind*Cr(CO)$_3$; c) (Cr(CO)$_3$)Ind*Rh(CO)$_2$.[50]

The *endo*- and *exo*-isomers of η^6-Ind*HCr(CO)$_3$ were not found to form in a 50:50 ratio but 85:15, with the exo-methyl preferred, presumably on the grounds of a steric repulsion. Both isomers were found to deprotonate on reaction with butyllithium and further reaction with (Rh(μ-Cl)COD)$_2$ was facile even at low temperature leading to *anti*-(Cr(CO)$_3$)Ind*RhCOD with the metal moieties found on opposite faces of the ligand. Conversion to (Cr(CO)$_3$)Ind*Rh(CO)$_2$ simply required the addition of carbon monoxide and proceeded in quantitative yield. The paper also details the synthesis of Ind*RhCOD and Ind*Rh(CO)$_2$. Mantovani *et al.* continued their work, showing that (Cr(CO)$_3$)Ind*Rh(CO)$_2$

was an effective catalyst precursor in the cyclotrimerisation of deactivated acetylene derivatives to substituted to benzenes.[53] The active catalyst for this transformation, $(Cr(CO)_3)Ind^*Rh(DMAD)_2$ (DMAD = dimethylacetylenedicarboxylate; $MeO_2CC{\equiv}CCO_2Me$), is achieved by a direct ligand substitution of the starting precatalyst, a reaction that has a temperature dependent induction period. After all the monomer is consumed, a reaction intermediate, $(Cr(CO)_3)Ind^*Rh(CO)(FADE)$ (FADE = fumaric acid dimethyl ester) was isolated and structurally characterised along with its separately synthesised geometric isomer $(Cr(CO)_3)Ind^*Rh(CO)(MADE)$ (MADE = maleic acid dimethyl ester). The use of Ind* was found to effect the complete conversion of the starting material with no observed drop in rate whereas the non-methylated analogue only attained a conversion of 80%.

In contrast to the η^6 compounds outlined above, Ind* was first described in 1981 by Miyamoto *et al.* in the ferrocene analogue, Ind^*_2Fe, postulated to bind η^5, which was characterised solely by elemental analysis.[54] A synthesis of Ind*H and its subsequent lithiation were also published. The following year, they published numerous heptamethylindenyl lanthanide complexes where the steric bulk and electronic character of the ligand were seen to encourage strong covalent bonding with the largely ionic rare earth metals.[55] Up until that point, synthesis of early lanthanide complexes of the form Cp_2LnCl or $CpLnCl_2$ had proven challenging as a result of their large ionic radii, and the weakness of their ligand field interaction due to the core-like nature of the 4f subshell. The successful synthesis of compounds involving lanthanum, neodymium and erbium was well received and Ind^*LnCl_2 and Ind^*_3Ln (Ln = La, Nd, Er) were reported along with Ind^*_2LaCl.

In 1986, the Ind* ligand was used in the synthesis of actinide containing organometallics for the first time and, although no different stoichiometries were observed from the use of the unsubstituted analogue, five new Ind*Th containing species were characterised.[56] Four years later the room temperature crystal structure of Ind^*_2Fe was reported, which was found to be ordered at room temperature, unlike its non-permethylated congener.[57] The authors looked to quantify a variety of parameters to fully describe the bonding seen in indenyl ligands, choosing to focus on the slip parameter ($\Delta_{M\text{-}C}$), the hinge angle (HA), and the fold angle (FA). Depictions of the parameters are given in Figure 1.5. Unsurprisingly, it was reported that the values for all three parameters were significantly lower for Ind_2Fe and Ind^*_2Fe than for Ind_2Co or Ind_2Ni where the ligand distorts away from classic η^5 bonding so the 18-

electron rule is not violated. The parameters of Ind_2Fe and Ind^*_2Fe were comparable with each other and also with $[Ind_2Co]^+$.

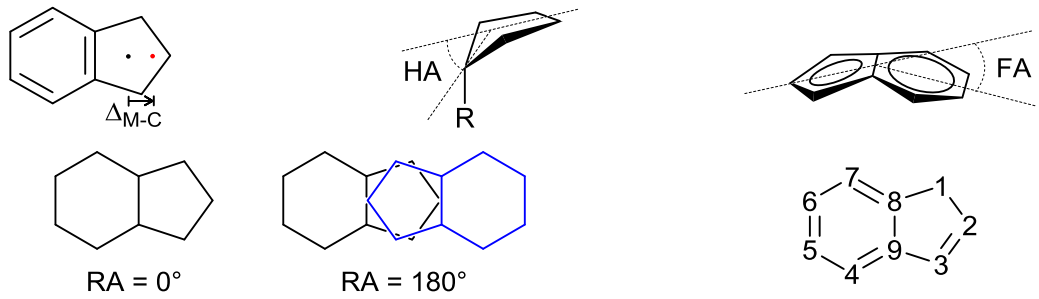


Figure 1.5: depictions of important bonding parameters for indenyl rings and the indenyl numbering scheme.

Marder and co-workers developed the subject area with publications studying indenyl rhodium complexes including Ind^*RhL_2 (L_2 = $(CO)_2$, $(C_2H_4)_2$, COD) by photoelectron spectroscopy (PES) combined with DFT studies by Green.[58,59] It was concluded that indenyl ligands proved to be more effective electron donors to d^8 ML_2 fragments than their Cp counterparts as evidenced by the ionisation energies of the metal based nonbonding orbitals. Furthermore they concluded that permethylated ligands increase this ability to donate electrons, as expected, and suggested that this would enhance rhodium's oxidative addition chemistry. Interestingly, the authors note that the π-backbonding to other coordinated ligands is less efficient despite the higher electron density on rhodium. This is attributed to the lowered energy of the indenyl π_4 orbital relative to the e_1 for Cp and is consistent with increased rates of S_N1 at the rhodium centre. O'Hare's first foray into Ind* chemistry came with an update to the ligand synthesis as well as a full electronic characterisation (PES, DFT, EPR, CV, and SQUID) of both the previously described Ind^*_2Fe, and Ind^*_2Co and their respective monocations achieved using a chemical oxidation.[60] A subsequent paper extended the study to include the complexes of chromium as well as reporting the crystal structures of $[Ind^*_2M][PF_6]$ (M = Cr, Co) and Ind^*_2Cr.[61] These were the first structurally characterised indenyl chromocenes, and subsequent work by Meredith *et al.* has established a relationship between substitution on the ring, and the conformation and spin-state of the chromocene.[62,63] This original work was built upon with the reporting of the first group 4 metal species involving Ind*: Ind^*MCl_3 (M = Ti, Zr, Hf), $Ind^*_2MCl_2$ (M = Zr, Hf) and $Ind^*_2HfMe_2$.[64] Both the metallocene dichlorides were found to be air stable in the solid-state while the half-sandwich trichlorides were both air and moisture sensitive. Analysis of the values for Δ_{M-C}, HA, and FA found the bonding to be essentially η^5 although strong bond alternation was

observed in the benzene ring. In 1995, Kakkar *et al.* synthesised and structurally characterised an Ind* rhodium(III) chloride dimer, $[Ind^*RhCl(\mu\text{-}Cl)]_2$, as well as the first Ind* complex with a coordinated phosphine, $Ind^*RhCl_2(PMe_2Ph)$.[65] The following year, Ind* was used in the synthesis of *closo*- and *pseudocloso*- carbametallaboranes based on Kakkar's rhodium starting material, $[Ind^*RhCl(\mu\text{-}Cl)]_2$.[66] In this case, as in many previously described, the vastly increased solubility of the Ind* starting material make this an ideal entry point to indenyl carbarhodaborane chemistry.

The first report of η^1 Ind* binding was described in 1997 in the compound Ind^*SnMe_3, although the hapticity was seen to change by NMR spectroscopy on elevating the temperature.[67,68] η^5 complexes involving both Ind* and rhenium including $Ind^*Re(CO)_3$, $[Ind^*Re(CO)NO][BF_4]$, and $Ind^*Re(CO)_2P(OEt)_3$ were also characterised (Figure 1.6). Molybdenum was also added to the heptamethylindenyl roster in the same year with crystal structures of $Ind^*Mo(CO)_2(\eta\text{-}C_3H_5)$ and $Ind^*MoCO(\eta^2\text{-}MeC{\equiv}CMe)_2$ alongside numerous other neutral and cationic species.[69]

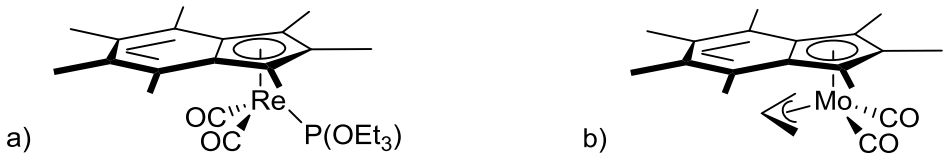


Figure 1.6: a) $Ind^*Re(CO)_2P(OEt)_3$; b) $Ind^*Mo(CO)_2(\eta\text{-}C_3H_5)$.[67,69]

A 2002 review of bonding and structural preferences of indenyl compounds introduces a valid additional parameter for bent metallocenes where the rotation angle (RA) no longer holds due to the tilt of the indenyl rings, α (Figures 1.5 and 1.9).[70] This parameter is the torsion angle (TA) measured for $C2\text{-}Cp_{cent}\text{-}Cp'_{cent}\text{-}C2'$ (Figure 1.5). Calhorda *et al.* also perform geometry optimisation calculations on numerous indenyl metallocenes from the literature. Of particular note is the calculation that shows that certain ligand orientations of $Ind^*_2ZrCl_2$ can be up to 21.5 kcal/mol less favourable in energy than others,[64] compared to a maximum energy gap of just 2.4 kcal/mol for unsubstituted indenyls. One of the more recent papers focusing on permethylindenyl complexes describes the synthesis of Ind^*_2YCl and related compounds including the THF adduct and the methyl congeners.[71] This paper highlights the ability of Ind^*_2 to trap the transient hydride intermediate (Ind^*_2YH), unstable even with the bulky Cp*.

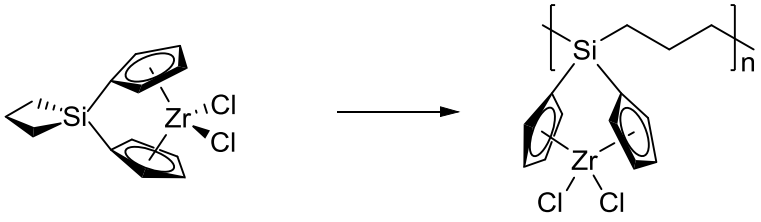
A recent work by the O'Hare group is the preparation of the first low spin indenyl manganocene, Ind^*_2Mn, which undergoes a spin crossover on warming to room temperature with significant population of a high spin state.[72]

1.1.5 *ansa*-bridged organometallic chemistry

Replacing the term metallocenophane (for all except group 8 metals), *ansa*, from the latin meaning "bent handle, attached at both ends" was first suggested for use in a chemical context in 1942 and was used to indicate the bridge between Cp fragments by Brintzinger in the late 1970s.[73,74] The introduction of an *ansa*-bridge changes the symmetry of a ligand and therefore endows a Cp-type moiety with enantiotopic faces. When both cyclopentadienes are considered, this gives rise to both enantiomers and diastereomers, and in the case of many bridged metallocene complexes, two distinguishable isomers: *rac*- and *meso*-. The *meso*-form comprises just one enantiopure isomer, while the *rac*- consists of a racemic mixture of two enantiomers. It is, of course, possible to introduce more complexity than this, typically through the use of an asymmetric bridge.[75] A bridge is not a requirement for chiral metallocenes – two non-symmetric ligands are sufficient.

1.1.5.1 One-atom bridges

Silyl bridges have proven exceptionally popular due to their ease of manufacture. Facile reaction of an alkali metal cyclopentadienide (e.g. NaCp) with dichlorodimethylsilane ($SiMe_2Cl_2$) quickly affords a bridged species (Me_2SiCp_2),[76] and the technique is easily transferrable to other ring systems such as benzindene derivatives.[77] Moreover, sequential addition of different carbocycles can lead to mixed ring systems (e.g. $Me_2Si(Cp^*)Cp$),[78,79] while there is a large variety of silicon based bridges available (e.g. $(CH_2)_3SiInd_2$).[80,81] In one silicon based system by Manners and co-workers, a silacyclobutane backbone is used to form $(CH_2)_3SiCp_2ZrCl_2$ which then undergoes ring-opening polymerisation to yield a polymer with pendant zirconocenes (Scheme 1.2).[82]



Scheme 1.2: ring-opening polymerisation of Manners' silacyclobutane *ansa*-zirconocene, $(CH_2)_3SiCp_2ZrCl_2$.[82]

In 1997, O'Hare and co-workers synthesised a new indenyl ligand in both bridged and unbridged forms.[83] 2,3,4,5,6,7-hexamethylindene ($Ind^{\#}H$) was synthesised in a route adapted from the preparative methodology employed for Ind*,[60] simply avoiding the extra methylation. The advantage of the new ligand was that it could both be used as a ligand in its own right and as a precursor to a series of bridged ligand frameworks. In the paper, a dimethylsilicon bridge was employed and complexes were synthesised using iron based metal fragments. SBI*Fe (SBI* = dimethylsiliconbis(hexamethylindenyl); $Me_2Si(C_9Me_6)_2$), the first *ansa*-indenyl ferrocene, and $Ind^{\#}_2Fe$ were both reported as mixtures of isomers. Most of the ligand sets previously discussed (*vide supra*) have had C_{2v} symmetry at least, but *rac*- and *meso*-isomers are observed for $Ind^{\#}_2Fe$.

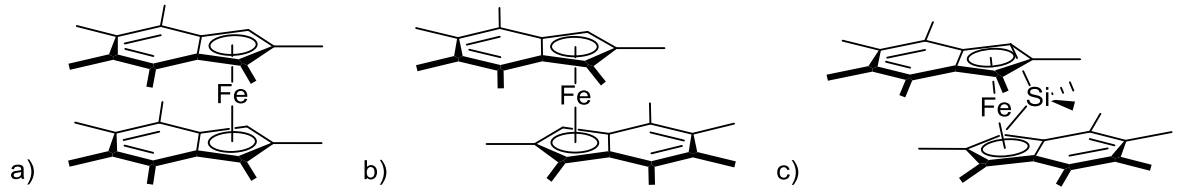


Figure 1.7: a) *meso*-$Ind^{\#}_2Fe$; b) *rac*-$Ind^{\#}_2Fe$; c) *rac*-SBI*Fe.[83]

Silicon need not be the only bridging atom; a single, sp^3-hybridised carbon is one of the smallest bridging units. A methylene bridge was first introduced by Katz *et al.* in 1970, in the compound $CH_2Cp_2TiCl_2$.[84] The ligand backbone was assembled by reacting two equivalents of sodium cyclopentadienide with dichloromethane (DCM), akin to the preparation of silyl bridges.[85] However, this synthetic route is typically low-yielding for *geminal* haloalkanes.[86] It is preferable to prepare methylene bridges, particularly those with additional substitutions, from Cp and an appropriate fulvene,[87] which can even be intermolecular.[88] If both ring systems are intended to be identical, then a carbonyl group can be used to couple their alkali metal salts: formaldehyde leading to a methylene bridge with acetone yielding the dimethyl substituted congener.[89] Other group 14 elements can be used as bridging groups although there are many fewer examples in the literature; tin bridges have been used to synthesise *ansa*-zirconocenes analogous to their silyl counterparts. When activated with methylaluminoxane (MAO), both complexes displayed the same ethylene polymerisation activity and the stannylene-bridged variety yielded a polymer with a higher molecular weight, suggesting fewer chain terminations.[90] A tin bridge has also been used to support bis(*ansa*-zirconocenes) with two active polymerisation centres (Figure 1.8). Both Sn and Ge have been utilised as bridging atoms for permethyl metallocene complexes: both elements being used for lanthanide complexes and dimethylgermylenes for group 4 metals.[91,92]

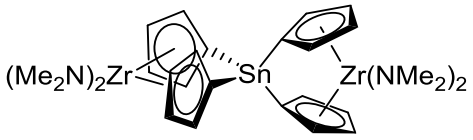


Figure 1.8: tin-bridged bis(*ansa*-zirconocene), $Sn(Cp_2Zr(NMe_2)_2)_2$.[90]

1.1.5.2 Two-atom bridges

Ethylene bridges can be easily synthesised from dibromoethane and two appropriate cyclopentadienide-type alkali metals salts, although intermolecular cyclisations can prevent the substitution of the second ring.[93,94] Another widely adopted method for inserting a two carbon bridge is to use the reductive coupling of fulvenes. There are two sides to this approach: directly using the required metal which can include the alkaline earths,[95,96] lanthanides,[97] and group 4 elements.[98] Alternatively, reduction using a alkali metal napthalenide solution affords the appropriate salt ready for metalation.[99] One of the numerous advantages to this system is the wide variety of easily accessible fulvenes, in particular those where the *exo*-double bond is contained within an annulated ring.[100–102] Ring based bridges can also alter the reactivity of an olefin polymerisation catalyst, typically increasing the rigidity and concomitant selectivity towards propene.[103,104] Mixed ring systems can be generated using a system pioneered by Rieger *et al.*[105] using an epoxide building block. sp^2-hybridised carbons may also be incorporated and have been seen in systems by Brintzinger and co-workers, amongst others.[106] Mixed C-Si and Si-Si bridges have also been reported (e.g. $(Me_2Si(Flu)CH_2Flu)ZrCl_2$),[107,108] as have those involving elements other than those from group 14 (e.g. $(CpBCl_2PMe_2Cp)ZrCl_2$).[109]

1.1.5.3 Longer, and multiple, bridges

Bridges comprising more than two atoms tend to offer less structural rigidity to the resulting complexes and, hence, less selectivity, and have in general been disfavoured. However, both sp^3-[110] and sp^2-hybridised[111,112] examples exist, as do those containing heteroatoms such as Si-O-Si.[113] Even longer bridges, up to five atoms, have been reported for *ansa*-zirconocenes.[114]

In certain cases, more than one bridge has been employed and while two bridges at most have ever been incorporated into group 4 metallocenes,[115,116] up to five have been incorporated for ferrocenophanes.[117] These bridges are considerably more strained and can be susceptible to degradation by MAO, although their rigidity can be used to promote the stereospecific formation of C_2 metallocenes or those primed for syndiotactic polypropylene

(PP) catalysis. Contrasting with the double silylenes above, double ethylene bridges barely increase the bridge strain.[118]

1.1.5.4 The *ansa*-effect

Typically, bridges are attached to the Cp group, usually in the 1-position for indenes, with more elaborate methods required to introduce them elsewhere. Halterman was able to include a bridge at the 7-position on the arene ring, first coupling two benzyl groups before building on the Cp rings to form indenes.[119] Complexes with both Ti and Zr were achieved. *ansa*-titanocenes have also been prepared with a bridge at the 2-position by a titanium(III) mediated reductive coupling step,[120] as well as a disulfone methodology.[121]

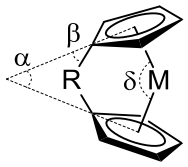
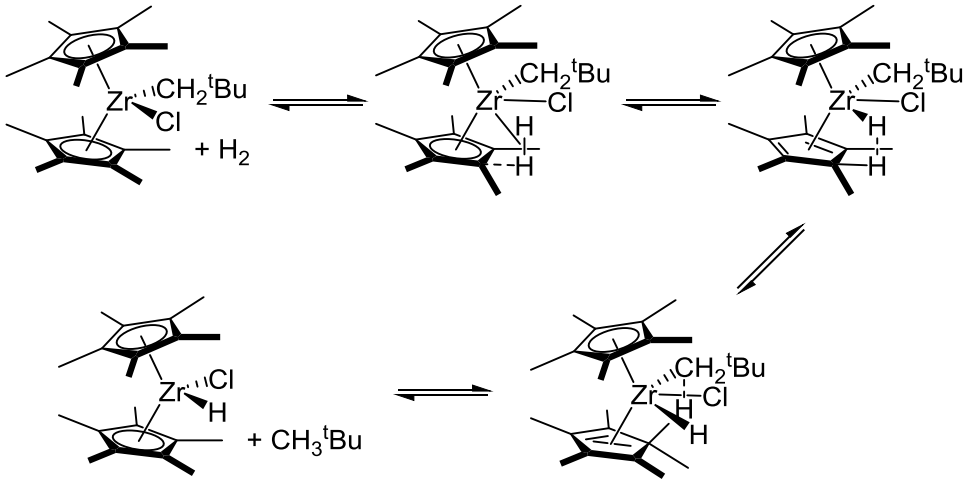


Figure 1.9: a selection of geometric parameters to describe *ansa*-metallocenes, and the numbering system used for indenyl rings.

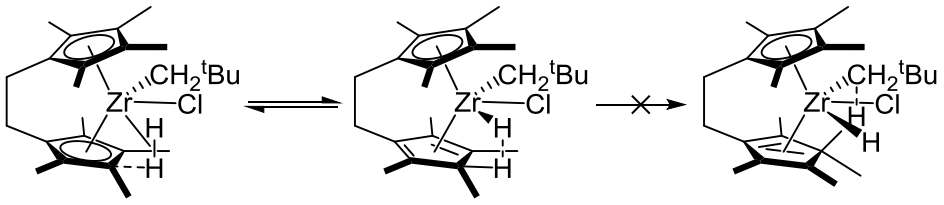
The effect of the introduction of the *ansa*-bridge to a metallocene can be measured in two ways: through structural differences, as measured by numerous geometric parameters, and through the changes in reactivity seen. A large number of parameters have been established to fully describe the bonding in *ansa*-metallocenes, including those outlined previously (HA, FA and $\Delta_{M\text{-}C}$).[122] Others of particular interest include α, the dihedral angle between the planes of the rings, and the related δ, the angle subtended by the Cp centroids at the metal centre (Figure 1.9). β, the angle between the first bridging atom and the plane of the ring can be thought of as a measure of the strain imparted by the bridge. In addition to $\Delta_{M\text{-}C}$, the ring slip can be measured by the angle between the normal of the ring planes, φ, and δ. A parameter, D, measures the "protrusion" of the metal from the line connecting the centroids, with the suggestion that the greater that distance, the more reactive the centre.[122,123]

In the early 1970s, it was noted that the reactivity of ferrocenophanes differed substantially from their unbridged analogues, displaying increased Lewis basicity but resistance to Friedel-Crafts acylation and deprotonation by butyllithium.[93,124] Brintzinger extended this work to zirconocenes,[125] titanocenes,[126] and chromocenes,[127] citing numerous examples of differing reactivities. Titanocenes generally displayed decreased reactivity, but increased stability relative to their unbridged analogues. Electrochemical reduction of the

titanium(IV) complex $[(CH_2)_2Cp_2]TiCl_2$ was found to occur −0.3 V below that of titanocene.[126,128] Bridged $[(CH_2)_2Cp_2]CrCO$ is isolable whereas chromocene carbonyl is not; DFT calculations have attributed this to the relative destabilisation of the ligand prior to complexation.[129,130] A significant difference between the reactivity of permethylated zirconocenes was noted in the decomposition pathways for alkyl hydrides.[125] $Cp^*_2ZrNpCl$ (Np = $CH_2{}^tBu$) reacts easily with dihydrogen whereas the ethylene bridged species does not. It was proposed that this was due to the restricted rotation of the Cp ring, inhibiting the hydrogen transfer suggested as the first step (Schemes 1.3 and 1.4).



Scheme 1.3: proposed mechanism by Brintzinger and co-workers for the hydrogenolysis of $Cp^*_2ZrNpCl$.[125]

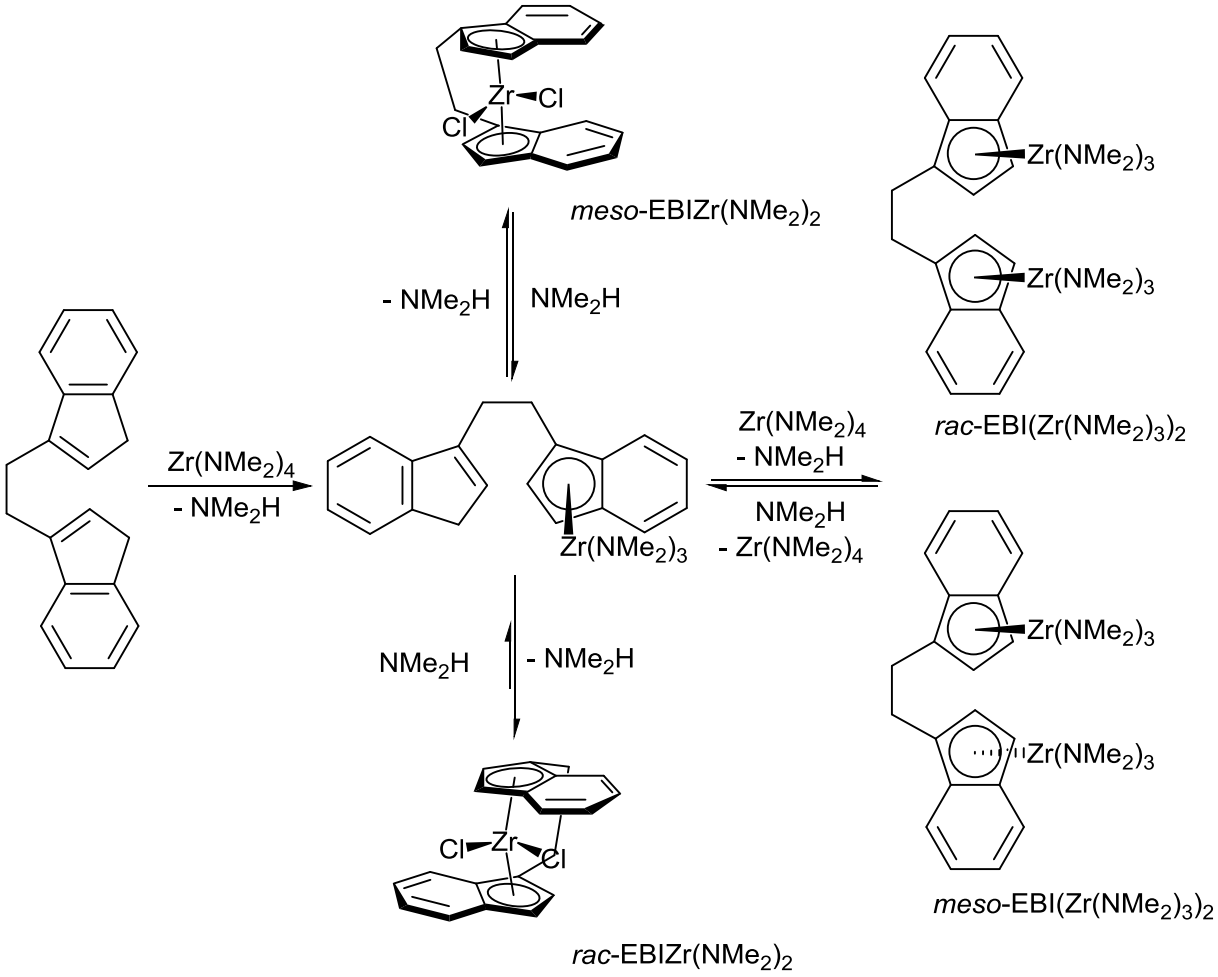


Scheme 1.4: restricted rotation inhibiting hydrogenolysis of $[(CH_2)_2Cp^*]_2ZrNpCl$.[125]

Parkin's work on permethylated zirconocenes illustrates an opposite trend, one of activation. Whereas $Cp^*_2ZrH_2$ does not react, $Me_2SiCp^*_2ZrH_2$ activates a benzene C-H bond forming $Me_2SiCp^*_2ZrPhH$.[131] Similar behaviour was noted with *ansa*-tantalocenes[132] and molybdocenes,[133,134] while permethylated *ansa*-lanthanocenes were seen to be more active towards sterically demanding oligomerisation reactions.[135]

As previously indicated, the introduction of a bridge brings the concomitant challenge of separating out the desired isomers. While the *rac*- and *meso*-isomers are chemically different and are often separable by fractional crystallisation, numerous other methodologies also exist for preferentially selecting one isomer over another. Appropriate bridge chirality can help,

and *spiro*-germylenes or silylenes have been shown to select for C_2-symmetric rings on transmetallation, suppressing the formation of unwanted *meso*-isomers.[136,137] Eisch *et al.* reported that the reductive coupling of 6-arylfulvenes with group 4 dihalides gives high stereoselectivity for the *rac*-isomer, due to the steric bulk of the arene groups.[98] The downside to these methodologies is that the choice of bridge is limited. However, Diamond *et al.* reported an alternative approach which involves alteration of the ancillary ligands, allowing the selective formation of the *rac*-isomer regardless of the bridge introduced.[138–140] By switching from salt metathesis to amine elimination, the reaction proceeds to the thermodynamic product due to a series of microreversible steps. Even if the undesired *meso*-product is formed, the zirconium amide moiety can disconnect and reconnect in the more favourable *rac*-orientation (Scheme 1.5).



Scheme 1.5: The proposed pathway for the synthesis of *rac*-EBIZr$(NMe_2)_2$ by Diamond *et al.*[140]

Jordan and co-workers were able to extend this idea to a silyl-bridged indenyl zirconocene,[141] before the use of chelating diamide ligands was introduced giving better control of the stereochemistry.[142]

In 2009, O'Hare and co-workers synthesised the permethylated ethylenebis(hexamethylindenide) alkali metals, EBI*M_2 (M = Li, Na, K), in a seven-step procedure by the alkali metal-mediated reductive coupling of fulvenes.[99] This new ligand was used to synthesise and structurally characterise one neutral and two cationic strained *ansa*-cobaltocenes. These were further investigated by CV and SQUID magnetometry, with EBI*Co a Curie-Weiss paramagnet. A cerium analogue, EBI*CeI(THF), was also synthesised – the first example of an *ansa*-indenyl cerocene – and more recently, iron and tin equivalents.[143,144] Zirconium and hafnium analogues have also been reported and showed excellent polymerisation results - they are discussed in detail in section 1.2.3.

1.6.1 Recent zirconocene chemistry

Some 60 years after Wilkinson began his quest for sandwich complexes across the periodic table and discovered Cp_2TiCl_2, the field of group 4 metallocenes remains remarkably current.[145] While some of the emphasis has shifted away from olefin polymerisation, the number of new avenues under investigation continues to grow. Chirik's report of a zirconocene with a side-on bound dinitrogen in 2003,[146] stoked the fire in a field which had already taken hold of titanium chemistry many years before (Figure 1.10).[147] It was further reported that at room temperature, in the presence of H_2, the activated N_2 will react forming N-H bonds.[10] Gentle heating to 45 °C causes the N-N bond to cleave, and finally, heating at 85 °C in an atmosphere of H_2 will result in its complete fixation to ammonia. More recently, near identical complexes have been prepared using photochemically induced reductive elimination.[148] Similar complexes had been reported in titanium chemistry achieving end-on N_2 binding with highly substituted Cp derivatives, $(Cp^R_2Ti)N_2$ (Cp^R = 1,2,3,4-Me-Cp and Cp*).[149,150]

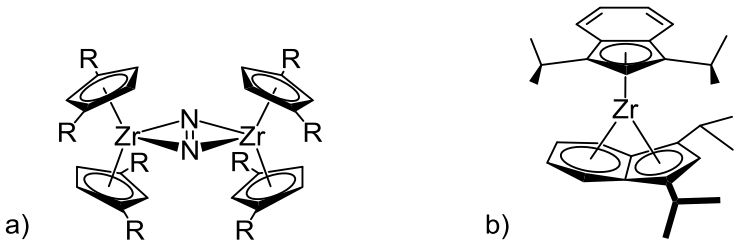
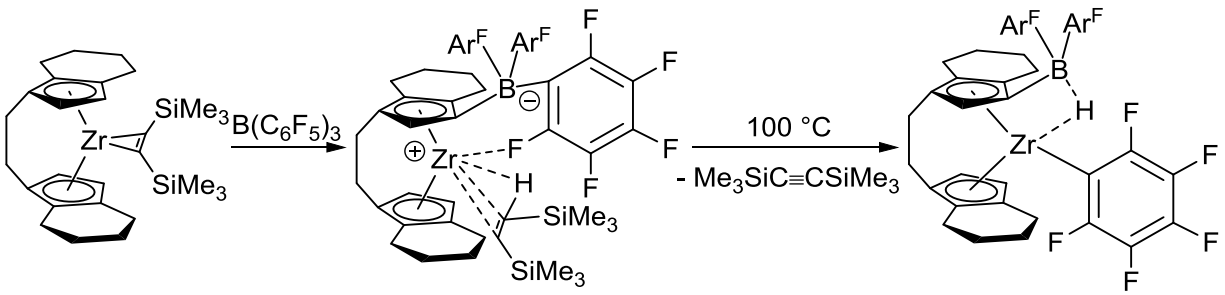


Figure 1.10: a) Chirik's side-on bound N_2 zirconocene complex (R = $SiMe_3$); b) η^9,η^5-bis(indenyl)zirconium.[146,151]

The Chirik group has also pursued a number of attempts to isolate a *bona fide* "zirconocene", a Cp_2Zr fragment with no coordinated ligands. Permethylated variants of titanocene have been isolated (*vide supra*) but both the Zr and Hf congeners have proven elusive. Rosenthal and co-workers have been able to stabilise zirconium(II) species using a labile alkyne; this has provided them an excellent starting point for investigations into metallacycles (*vide infra*).[152,153] Bradley *et al*. were able to use indenyl ligands to stabilise "zirconocene" fragments including the three coordinate η^5,η^6-$Ind^R_2Zr(THF)$ (Ind^R = 1,3-$SiMe_3$-Ind).[154] Numerous incidences of η^5,η^9-bonding were observed for the indenyl fragments including Ind^R_2Zr (Ind^R = 1,3-$^iPr_2$-Ind, 1,3-$(SiMe_2{}^tBu)_2$-Ind) but it is a stretch to consider these genuinely analogous to zirconocene.[151] It was noted that while the hapticity was alternating between the rings in these complexes, there was an opportunity to bind dinitrogen. This was realised in the form of reversible end-on N_2 binding in $[Ind^RCp^*Zr]2(\mu$-$N_2)$ (Ind^R = 1-Me-3-^{i}Pr-Ind) where the zirconium is coordinated η^5 to both Cp rings, η^1 to the N_2, and η^2 to a localised π-bond in the arene portion of the indenyl ring.[155] Further N_2 activation was noticed in bis(indenyl) complexes of the same ligand where the diatomic first coordinates end-on as an *ate*-complex, with the arene stabilising the sodium and then, on addition of H_2, side-on to both zirconium centres.[156] Similar alkali metal complexes were noted have unusual N_2 binding, and it was discovered that the hapticity changes, for certain systems, on redox activity.[157] *ansa*-systems have also been used in the reduction of dinitrogen, and it was reported that CO induced N_2 cleavage was attained using a hafnocene system, $[(Me_2SiCp^*)_2Hf]_2(\mu$-η^2-$N_2)$.[158] In addition, carboxylation of N_2 to hydrazine has been achieved using an *ansa*-zirconocene.[159]

N_2 activation is just one current use of zirconocenes. The Arndt and Rosenthal group, who begin swathes of their chemistry with $Cp_2M(btmsa)$ (M = Ti, Zr; btmsa = η^2-$Me_3SiC{\equiv}CSiMe_3$) variants, have used *ansa*-zirconocenes such as EBTHIZr(btmsa) (EBTHI = ethylenebis(tetrahydroindenyl) to study interactions with perfluoroarylboron species (Scheme 1.6).[160]



Scheme 1.6: deactivation of EBTHIZr(btmsa) with $B(C_6F_5)_3$.[160]

Initially, a zwitterionic species is reported with the C-H bond at the 3-position activated, before loss of the btmsa on heating to 100 °C and restoration of a neutral zirconium centre by the transfer of a perfluoroaryl ring. It is noted that if the zirconocene is first treated with ethylene, a zirconacyclopentane is formed, which, when activated with the Lewis acid, is active for the polymerisation of ethylene. However, in this case, neither species generated on prior treatment with $B(C_6F_5)_3$ leads to ethylene polymerisation.

$Cp^*_2Zr(\eta^2\text{-}RC{\equiv}CR)$ (R = piperazine [pip], NEt_2) exists in equilibrium with a "tuck-in" complex, activating one of the C-H bonds on the Cp*, clearly demonstrating how reactive these species can be (Figure 1.11).[161] Numerous other examples of unusual metallacycles have been reported including a tetra-piperazine-substituted zirconacyclopentadiene (Figure 1.15) and a zirconacyclopentatriene, also known as a zirconacyclocumulene.[162] These exotic species can be synthesised using two equivalents of a terminal alkyne or a 1,3-dialkyne. Zirconaheterocycles can also be formed in a rare incidence of nitrile coupling, giving a ring-strained zirconadiazacyclopentadiene (Figure 1.11).[163]

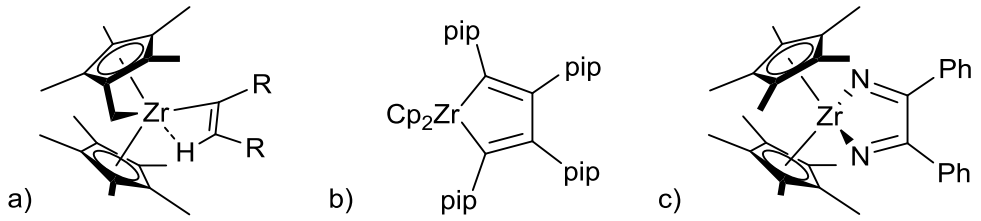


Figure 1.11: a) Rosenthal's "tuck-in" complex (R = pip, 4-Me-pip, NEt_2); b) zirconacyclopentadiene; c)nitrile coupled zirconadiazacyclopentadiene.[161,163]

Since frustrated Lewis pairs (FLPs) were reported by Stephan in 2006, they have received significant attention.[164] Initial investigations were based firmly in the p-block but recently a number of group 4 based FLPs have been reported.[165] Recent research in the Wass group has seen the development of a zirconocene-phosphine FLP system.[166] As with most FLPs, the aim is to activate small molecules and these cationic systems, stabilised in their resting state by the lone pair donation from the phosphine to the electronically and coordinatively unsaturated zirconium; these have proven to be active with both CO_2 and H_2 (Figure 1.12).[167]

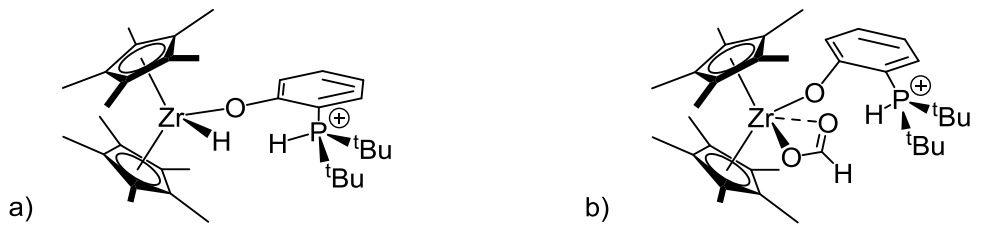


Figure 1.12: Wass' cationic zirconocene FLP systems a) having split H_2, b) and subsequently CO_2. $[B(C_6F_5)_4]^-$ counterions are not shown.[166,167]

In 2012, Erker and co-workers described the activation of dihydrogen using another unsaturated zirconocene system, not unlike those employed by Rosenthal (*vide supra*).[168] A bis-substituted alkyne with a bulky, inert $SiMe_3$ group at one end and a Lewis acidic perfluoroaryl borane at the other was used to stabilise the zirconium centre. On addition of hydrogen gas, the formally zirconium(II) centre is able to reduce dihydrogen, yielding a zwitterionic dihydride species (Figure 1.13). On the replacement of the alkyne substituents with Ph and PPh_2, the system becomes active towards CO_2 (Figure 1.13) and numerous other derivatives including azides and isonitriles, combining typical cationic zirconocene activity with the more modern FLP aspect.[169] The creation of the new reactive synthon came about by 1,1-carbozirconation which had been developed within their group.[170,171] Considered analogous to 1,1-carboboration, it is unusual to see such reactivity from a system, $[Cp_2ZrMe]^+$, that is so well known for the 1,2-insertion carried out during olefin polymerisation. It was found to depend significantly upon the ability of the $SiMe_3$ group to migrate and on the Lewis basicity of the phosphine substituent.

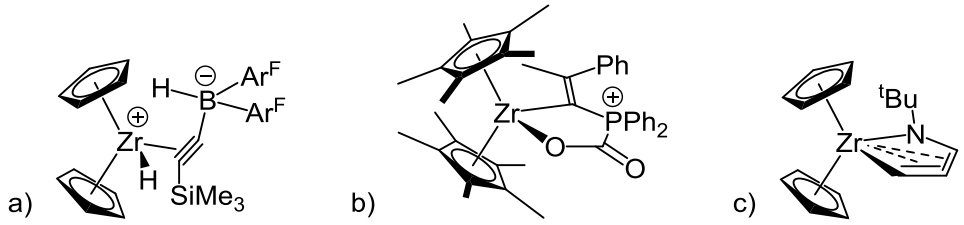


Figure 1.13: a) heterolytically cleaved H_2 and b) activated CO_2 by two of Erker's zirconocene FLP systems ($[B(C_6F_5)_4]^-$ counterions are not shown).[170,171] c) One resonance form of a zirconacycloallenoid.[172]

Erker recently published a number of strained, multiply bonded ring systems such as the zirconacycloallenoids (Figure 1.13).[172,173] Although not true analogues of the unisolable cycloallenoids, they have proven interesting species for further chemistry, and they too have been shown to bind both H_2 and CO_2.[174,175]

A recent publication by Tilley and co-workers has shown early/late transition metal heterobimetallics with both zirconocenes and hafnocenes. The M-Ir bond (M = Zr, Hf) has been able to incorporate sulphur, azides and other substrates. However, the metal-metal bond was prone to oxidative cleavage and protonation.[176]

1.1 Olefin polymerisation

1.2.1 The polyolefin market

The polymer market is dominated by polyolefins, which account for more than 70% of the total production.[177] Annual production of polyethylene (PE) is approximately 80 million tonnes,[178] representing the highest volume production of any single polymer type, ahead of polypropylene (PP) at 40 million tonnes. With PE costing in the region of £1,000/tonne, it is simple to understand why the industry is so important globally, and why research therein remains of the utmost importance. The reason for the continued dominance of polyolefins, and PE more specifically, is its comparatively low cost and its wide-ranging applications in our everyday lives, as well as our ever expanding understanding of its synthesis and make-up. Indeed, its chemical stability has become a problem, as large quantities of polyolefins end up in landfill.

1.2.2 Heterogeneous olefin polymerisation

In the first half of the twentieth century, the only PE known was low density polyethylene (LDPE) produced under high pressures and temperatures by radical polymerisation. The revolutionary discovery of Ziegler,[179,180] for which he went on to receive the Nobel prize in 1963, paved the way to "high molecular-weight polyethylenes", and changed the industry forever. Natta, who named the catalysts "Ziegler catalysts" and was a co-recipient of the Nobel prize, turned his attention to PP and published the seminal work on the stereoselective polymerisation of propene, which in turn led to its commercialisation.[181,182] Both of these catalysts typically involved trivalent metal chlorides (e.g. $TiCl_3$) and tri-alkyl aluminium species (e.g. $AlMe_3$), and were heterogeneous in two senses: they were insoluble in the reaction solvent, and in the low uniformity of their catalytic sites. This leads to broad molecular weight distributions, poor and uneven co-monomer incorporation and restricts their use to low cost, bulk resins. Despite this, it is expected that they will retain the largest proportion of polyethylene production for the foreseeable future.[177] Today the vast majority of polymer plants are based around these catalysts in either gas-phase or slurry-phase processes, as the required expertise has been honed for more than 50 years.[183]

1.2.3 Homogeneous olefin polymerisation

Just a couple of years after Ziegler's breakthrough discovery, Natta and Breslow reported the use of titanocene dichloride, along with aluminium activators, for the polymerisation of

ethylene.[184,185] It was noted that, on addition of diethylaluminium chloride (DEAC) or triethylaluminium (TEA), the orange solution of Cp_2TiCl_2 turned blue and ethane was evolved. The compound was isolated and was found to be a paramagnetic Ti(III) complexed with DEAC; it was reported to be a poor ethylene polymerisation catalyst but that a freshly prepared solution was very active. They also commented, presciently, that the polymerisation proceeded a lot faster with the addition of a small quantity of oxygen to the ethylene feed. These discoveries proved revolutionary, not due to their activity but as they were precise and characterisable models of Ziegler-Natta catalysis that could be further studied.[186,187] These well-defined metallocenes came to be known as single-site catalysts. Unfortunately, it was found that they lacked the requisite stability for commercialisation.

The interest in single-site catalysts was revitalised due to the discovery that the adventitious addition of water to alkylaluminium activators dramatically increases the activities recorded.[188–191] This led Kaminsky to the use of methylaluminoxane (MAO) which has now become almost ubiquitous for complex activation,[192] and revived the interest in metallocenes as olefin polymerisation catalysts. The key advantage of single-site catalysts is their tuneability, allowing for alteration of activity, molecular weight, co-monomer incorporation and numerous other structural parameters.[193–195]

Metals such as yttrium and scandium (*vide infra*) have also been used as olefin polymerisation catalysts;[196,197] an *ansa*-bridged yttrocene yielded iso-specific poly(1-butene). Naturally, it was found that it was the C_2 symmetric *rac*-isomer that yielded the isotactic polymer, while the *meso*-isomer had to be removed by a tedious separation.

While metallocenes remain at the forefront of the field, numerous other single-site systems have been developed. Of particular note are the following:[198–200] bis(imino)pyridines,[201–206] α-diimines,[207,208] constrained geometry catalysts (CGCs)[8,197,209] and phosphinamides.[210]

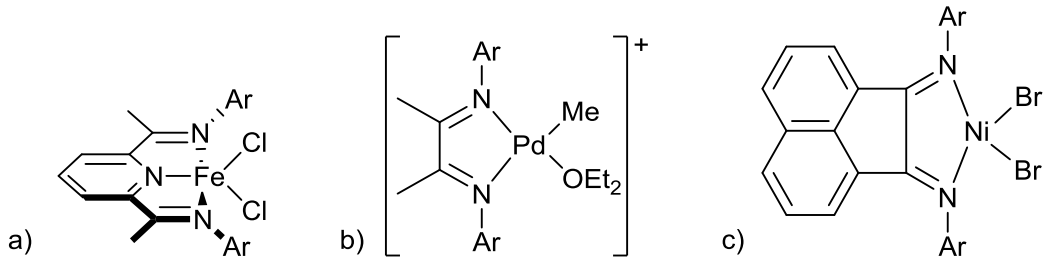


Figure 1.14: a) Britovsek *et al.*'s bis(imino)pyridine iron;[201] Brookhart's cationic α-diimino palladium (b) and neutral nickel (c) olefin polymerisation catalysts.[207] $[B(3,5\text{-}CF_3\text{-}C_6H_3)_4]^-$ counterions are not shown. Ar = 2,6-diisopropylphenyl (DIPP).

The bis(imino)pyridines developed by Gibson and co-workers were among the first catalysts in the literature based on iron that exhibited commercially viable olefin polymerisation activities.[201,206] At the time of their publication in 1998, the majority of polymerisation initiators focused on the early transition metals (TMs), known not to be tolerant of heteroatom containing functional groups. While this is advantageous for the late TMs, most complexes were found to undergo oligomerisation due to their propensity towards β-hydride elimination. A structural characterisation carried out on the compound pictured in Figure 1.14a found that the iron sits above the plane of the pyridyl group, and that the ligands are coordinated in a *pseudo*-square pyramidal geometry around the metal centre with the "top" chlorine sitting at the apex with a noticeable longer bond than its counterpart. An activity of 5,430 $kg_{PE}/mol_M/h/bar$ was reported for the complex shown, with a methyl-substituted analogue recording 11,020 $kg_{PE}/mol_M/h/bar$; this was comparable to some of the highest values seen at the time. Earlier examples of late transition metal catalysts exist, and Brookhart's 1995 report of initiators based on palladium and nickel was among the first.[207] The complexes, with a rigid α-diimino backbone (Figure 1.14), also exhibited activities comparable to those reported for metallocenes, with a nickel-based initiator recording activities of 11,000 $kg_{PE}/mol_M/h/bar$. The palladium catalyst pictured in Figure 1.14b is generated *in situ* by the addition of $[H(OEt_2)_2][B(3,5\text{-}CF_3\text{-}C_6H_3)_4]$ to the dimethyl complex, liberating methane. The mechanism of action was also investigated and they were the first catalysts where an olefin alkyl complex was demonstrated to be the resting state. Further investigation led to the publication of successful ethylene co-polymerisation with functionalised vinyl co-monomers such as methylacrylate (MA), and a suggested mechanism was published.[211] Due to the formation of a resting state chelate complex that requires insertion of ethylene for further chain growth, the rate of both ethylene and MA turnovers depends on the ethylene pressure. The slow chain-transfer processes of these catalysts was exploited in the "living" polymerisation of block co-polymers of different α-olefins.[212]

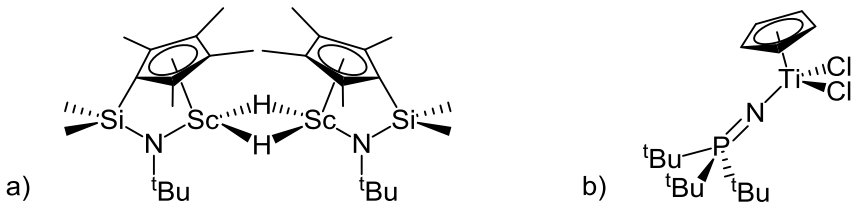


Figure 1.15: a) Shapiro *et al.*'s constrained geometry (CG) scandium complex; b) Stephan's titanium phosphinamide developed with NOVA Chem. Corp. (right).[197,210]

Another class of catalysts was developed in the early 1990s which tended to incorporate early TMs but contained only one Cp ring as well as a pendant amide ligand. The first published example of this came from Bercaw's group and comprised a scandium hydride dimer (Figure 1.15), each scandium bearing a Cp* ligand and an amide, with a bridging dimethylsilyl group.[197] While the complex was only able to produce PP with a low molecular weight, it provided an alternative to metallocenes, and proved a rare example of a single-component α-olefin polymerisation catalyst. Monitoring by ^{1}H NMR spectroscopy on addition of propene confirmed that all the sites were active, leading to oligomers with a low molecular weight distribution. Only a few months later, Okuda published iron and titanium compounds bearing the same Cp-amido motif, although no polymerisation data were reported.[209] Industrial interest in these CG catalysts quickly grew and the following year, both Dow and Exxon had filed a number of patents.[213–216] There was interest in tuning the catalysts, but attempts to try and exert chain end control proved unsuccessful and they were found to be relatively intolerant to other functional groups.[8] In contrast to the metallocenes, the many advantages of CGCs derive from the open nature of the metal centre which allows incorporation of a variety of olefins. These include longer chain α-olefins such as 1-hexene and 1-octene, cyclic alkenes such as norbornene, and even styrene. In addition, CGCs tend to exhibit greater thermal stability than metallocenes, are less susceptible to degradation by MAO, and often generate high molecular weight polymers.[8] These robust properties and their high activities mean that they were among the first homogeneous Ziegler-Natta systems to be employed commercially.[217]

Approximately a decade after the first CGC systems were reported, Stephan *et al.* introduced a new, related class of ethylene polymerisation catalysts: the phosphinamides (Figure 1.15).[210] Drawing inspiration from a bulky ligand, tritox, (OC^tBu_3), described as being a steric analogue of Cp,[218] and the electronic properties of the phosphoraneiminato substituent,[219] they were able to create a system that sits neatly between the CGCs and metallocenes. It was noted that the cone angle subtended by the phosphinamide ligand pictured above (Figure 1.15) is greater than that for Cp at a similar metal; 87° and 83° respectively. The Cp_{cent}-Ti-N angle is greater for phosphoriminato complexes than for Ti CGCs (107.6°),[220] suggesting that the metal centre is less exposed.[210] This may affect the polymerisation activities which were reported as being up to 2000 $kg_{PE}/mol_{Ti}/h/bar$, with molecular weight in several instances nearing 1,000,000 daltons.

The activities reported above for non-metallocene single-site catalysts compare very favourably with those for metallocenes. It is important to note when comparing activities, how much of an effect the alteration of a relatively minor component can have.[221] Lee *et al.* report that almost no activity was seen on decreasing the solvent volume of a polymerisation run from 500 ml to 50 ml, despite maintaining the same amount of catalyst and MAO. The authors record ethylene polymerisation activities for Ind_2ZrCl_2 of 14,000 $kg_{PE}/mol_{Zr}/h/bar$ and note the effect the ligand's substitution pattern can have (Table 1.2).

Table 1.2: effect of substitution pattern and ethylene bridge on activity and molecular weight of PE for indenyl zirconocenes.[221]

Substitution Pattern	Activity ($kg_{PE}/mol_{Zr}/h/bar$)		Molecular Weight, M_w (daltons)	
$Ind^R_2ZrCl_2$	No bridge	C_2H_4 bridge	No bridge	C_2H_4 bridge
R = H_7	14,000	10,000	250,000	145,000
R = 5,6-Me_2	25,200	22,200	278,000	125,000
R = 4,7-Me_2	13,800	13,000	352,000	205,000

Double methyl substitution at the 5- and 6-positions on both indenyl ligands increases the activity dramatically to 25,200 $kg_{PE}/mol_{Zr}/h/bar$, while the same substitution at the 4- and 7-positions has little effect (13,800 $kg_{PE}/mol_{Zr}/h/bar$). The molecular weight of the resulting PE is seen to increase on substitution, with a marked effect at the 4- and 7-positions. The introduction of an ethylene *ansa*-bridge at the 1-position, and exclusive use of the *rac*-isomer, decreases the activity relative to the unbridged analogues but follows the same pattern with regards to substitution. A similar effect is noted with the molecular weight. Permethylation of the ethylenebis(indenyl) (EBI) ligand used above increases the ethylene polymerisation activity further.[222] Ransom *et al.* reported activities of 61,800 and 38,300 $kg_{PE}/mol_{Zr}/h/bar$ for *rac*- and *meso*-EBI*$ZrCl_2$, some of the highest in the literature. The activities for the hafnium congeners were 1,250 and 3,350 $kg_{PE}/mol_{Hf}/h/bar$ respectively. The molecular weights for the zirconium catalysed PE were similar to those reported by Lee *et al.* at 215,000 and 203,000 daltons respectively, and they were found not to polymerise propene. Studies into the effects of differing ring substitutions and their quantification have been summarised in an excellent review by Möhring *et al.*[223]

The homogeneous olefin polymerisation catalysts thus far described have almost exclusively been mononuclear in nature, containing only one metal centre. However, a significant amount of research has gone into the design and testing of multinuclear catalysts.[224] These can incorporate two (or more) identical metal centres or can comprise

different procatalysts which can operate cooperatively and need not even be based on the same metal. Each individual centre can be selected from any of the classes of single-site catalyst described above, and no doubt many more.

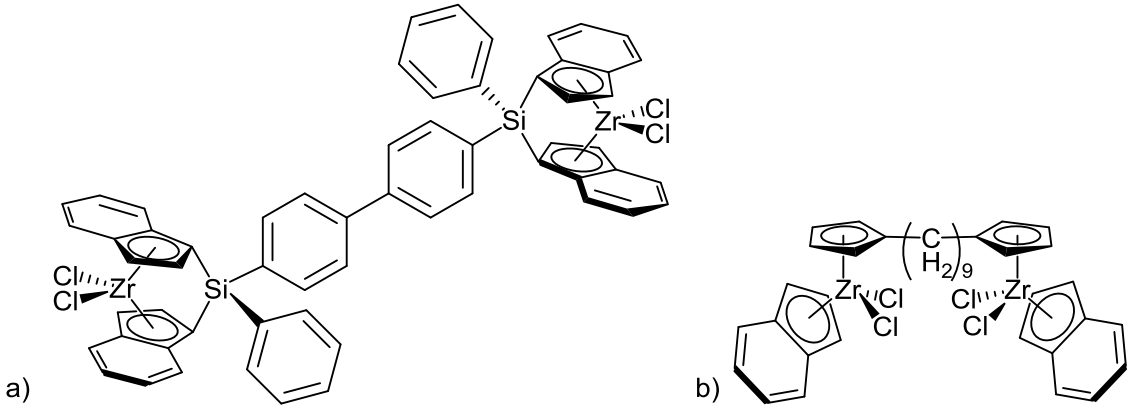


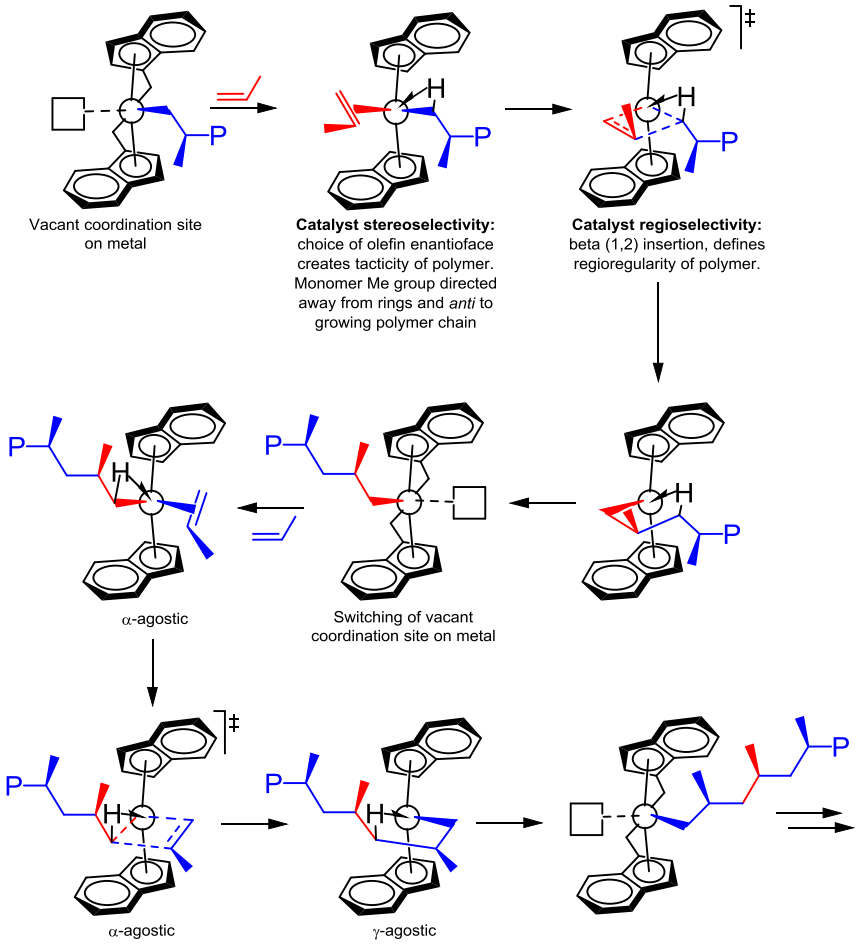
Figure 1.16: binuclear indenyl zirconocenes with a rigid bridge (a)[80,225] and a flexible bridge (b).[226]

The incorporation of a biphenylene bridge between two *ansa*-silyl zirconocene centres by Noh *et al*. was noted to increase the rate of ethylene polymerisation at each metal centre from 3,500 $kg_{PE}/mol_{Zr}/h/bar$ for the monomeric $Ph_2SiInd_2ZrCl_2$ to 11,400 $kg_{PE}/mol_{Zr}/h/bar$ for the binuclear analogue (Figure 1.16).[80,225] Although the molecular weight was seen to drop from one-centre to two (74,000 and 47,200 daltons respectively), activities of more than 70,000 $kg_{PE}/mol_{Zr}/h/bar$ were reported for the complex shown under the right conditions. Lee and co-workers observed that varying the number of methylene groups between flexibly linked zirconocenes affected the balance of steric and electronic effects.[226–228] If the bridge is too short, steric crowding around the metal centres inhibits activity and the binuclear catalyst is seen to be less active than its mononuclear counterpart. However, once the bridge is lengthened beyond a certain point, these steric effects are far outweighed by the electronic benefits of the inductive push from the longer alkyl chain. Ethylene polymerisation activity was seen to increase with increasing chain length (n = 3<5<7<9) with a top activity of 5,550 $kg_{PE}/mol_{Zr}/h/bar$ reported in the case of the complex shown.

1.2.4 Mechanism of polymerisation

Given the levels of research into Ziegler-Natta catalysts, there has been much interest in the mechanism of polymerisation and a few alternatives have been proposed. In 1964, Cossee elucidated a proposed mechanism for the growing polymer chain for Ziegler-Natta catalysts.[229] It required that a transition metal had one vacant coordination site and no (or at least very few) electrons in the t_{2g} orbital, consistent with the d^0 group 4 metallocenes. The

vacant site is quickly occupied by the alkene which coordinates to the metal η^2. For heterogeneous catalysts, the overlap between the metal d_{yz} and the alkene π^* lowers the energy of the lowest unoccupied molecular orbital (LUMO), decreasing the energy required to break the bond between the metal and the growing polymer chain. The 1,2 insertion that follows *via* a metallacyclobutane transition state simply requires an electronic rearrangement and not a steric one. This helps to explain why the propagation step has such a low activation energy. Due to the lifetime of the active species, it was supposed that the highest occupied molecular orbital (HOMO)-LUMO gap must be large enough to prevent the M-R bond breaking in the absence of a coordinating olefin. Arlman, working with Cossee, developed the argument further to explain the stereospecific polymerisation of propene in a heterogeneous system.[230] Based on the assumption that the correct electronic interaction requires alignment of the olefin with the growing polymer chain, there is only one sterically feasible orientation of the propene (of the four theoretical positions); the others are blocked by chloride ligands around the metal centre in α-$TiCl_3$. For the specific requirement of isotactic polypropylene, the mechanism only requires a series of identical propagation steps. This has come to be known as the Cossee-Arlman mechanism. In Scheme 1.7, the coordination geometry of the incoming propene is controlled by the bulky asymmetric indenyl ligands in a manner similar to that observed in the heterogeneous case above. When the polymer chain site switches after 1,2 insertion of the alkene, the opposite site favours the opposite coordination from the next monomer due to the C_2 symmetry of the complex, generating isotactic PP.



Scheme 1.7: representation of the stereo- and regio-selectivity imposed by a C_2-symmetric *ansa*-indenyl ligand on a growing polypropylene chain – the Brookhart-Green mechanism based on the Cossee-Arlman mechanism.[229–231] Adapted from Paul Ransom: metal centres represented by circles, vacant coordination sites by squares and positive charges not shown.[232] The bridging atoms have been omitted for the most part for clarity.

In 1978, Green and Rooney suggested an alternative mechanism to that put forward by Cossee and Arlman.[233] At the time, there was no evidence to suggest that the 1964 mechanism was correct or otherwise. Inspiration was taken from metathesis chemistry, and an α-hydride transfer to the metal was proposed, requiring an oxidative addition step and generating an M=R double bond and a metal hydride. Coordination of the alkene then led to a metathesis-type step, again involving a metallacyclobutane, followed by reductive elimination. It was suggested that this mechanism was unsuitable for d^0 metals as they were unable to facilitate oxidative addition due to the lack of electrons in a suitable MO. A comprehensive rebuttle of this mechanism was provided by Grubbs and co-workers who showed that there was no kinetic isotope effect (KIE) and that there was an even distribution of isomers on using deuterated olefins.[234,235] Both of these might have been expected if an α-hydride transfer step were involved. However, Brookhart and Green proffered another

alternative that can be thought of as intermediary between the two previous mechanistic suggestions, and one which would not incur any significant KIE.[231] An α-agostic interaction between the hydrogen on the α-carbon of the growing chain and the metal centre mediates the breaking of the M-C bond and facilitates the close approach of the olefin and the polymer chain, and, hence, C-C bond formation. This suggestion has been backed up by experimental evidence,[236,237] and more recently, DFT calculations.[238]

1.2.5 Supported single-site olefin polymerisation

While the activity of homogeneous olefin polymerisation catalysts has greatly improved since inception, they are still rarely used for industrial processes, being retained typically for co-polymerisation procedures including Dowlex (Dow) and Sclairtech (Nova Chem. Corp.) or those producing low molecular weight polymer.[177] This is partially due to the prerequisite that the polymer is soluble within the diluent, meaning that high temperatures are often employed putting significant demands on the catalyst in terms of thermal stability and typically causing them to yield lower crystallinity polymer. Another problem of solution phase polymerisation, particularly on an industrial scale, is reactor fouling, caused by the large exotherm generated by the exergonic propagation step causing the polymer to stick to the sides of the reaction vessel. One increasingly popular way of controlling this problem while retaining the advantageous characteristics of single-site catalysts (narrow molecular weight distribution, high activity and uniform incorporation of co-monomer) is to immobilise the organometallic species on an insoluble support. This is seen as the future of the polyolefin industry and, as such, is the subject of considerable research and investment.[177]

A key aspect to controlling the resultant polymer during supported single-site olefin polymerisation is the manipulation of particle growth. Uniform particle growth, as well as widespread fragmentation of the particle, is essential to efficient control over the localised temperatures as well as resulting polymer morphology.[239] It is important that the particle has an appropriate mechanical strength: too low and it falls apart rapidly, but low enough that it disintegrates during the polymerisation process, allowing an even distribution of active sites throughout the growing polymer particle. Typically the morphology of the support particle is replicated in the final polymer with approximately ten-fold growth in each dimension. The ability to fragment during polymerisation is important as it allows access of the monomer to all the catalytic sites, maximising the potential activity. This is not always possible and in diffusion-limited cases, a layered "onion" like morphology can be seen.[240] This challenge

can, of course, be overcome and a typical procedure is a prepolymerisation. For PE, which can pack very tightly around a growing particle, and hence lead to diffusion-limitation,[241] prepolymerisation with propene can lift this barrier,[242] allowing for even growth. A similar effect is noted for an *ansa*-silylindenyl zirconocene system carrying out ethene/1-hexene co-polymerisation on a SiO_2/MAO support where the build-up of polymer prevents the larger monomer reaching the active sites and homopolymerisation is allowed to occur.[243] A similar system provided an example where the particle did not break apart uniformly but instead underwent a layer-by-layer disintegration, leading to a lag time prior to maximum activity.[244] The advantage over solution-phase polymerisation becomes clearer if each particle is thought of as an individual reactor, able to regulate its own temperature.[241] These "microreactors" have been observed and analysed by high resolution digital photography by Fink and co-workers in a specially designed cell yielding accurate kinetic data on the progress of a polymerisation run.[245]

Given the physical properties required and their widespread availability, inorganic supports are the mainstay immobilisation surface, with silicas proving by far the most popular. Many other supports have also been used including alumina and clays such as monmorillonite and hydrotalcite.[177] A typical silica support will have a uniform particle size in the range 10-100 μm and a spherical morphology. As they are most commonly unmodified, they are normally subjected to some form of thermal dihydroxylation to remove superfluous silanol groups. This calcination process is most typically run at between 150 and 800 °C, with different temperatures removing different proportions of silanol groups (Figure 1.17) and adsorbed H_2O.

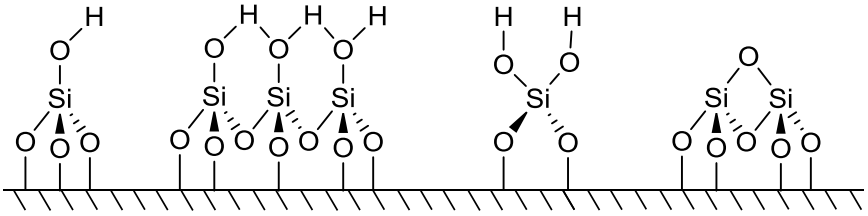


Fig 1.17: (left to right) representations of isolated, vicinal and geminal silanols and a silyl ether (siloxane) on a silica surface.[177]

The effect of different temperatures of calcination is to remove varying degrees of silanol groups by conversion to silyl ethers and the effects on polymerisation activities have been extensively studied.[246–248] Perhaps surprisingly, the results show that high calcination temperatures lead to lower catalyst loadings but higher activities when contacted with MAO.

It was noted by Collins *et al*. that the supporting of $EBIZrCl_2$ directly onto uncalcined silica lead to appreciable quantities of the *protio*-ligand in the grafting solution whereas this was not found to be the case for $EBTHIZrCl_2$.[249] They also reported that higher calcination temperatures led to increased activity, but, despite this, the values still fell short of the solution-phase by a factor of 10^1-10^2.

Kaminsky *et al.* reported that while precontacting the silica surface with MAO afforded PP resins akin to those of the homogeneous system, $EBIZrCl_2$, treatment of the SiO_2, calcined at 100 °C, followed by exposure to MAO led to greatly increased stereoregularity and increased molecular weights.[250] Dos Santos and co-workers published that precontacting with MAO enabled the achievement of higher catalyst loadings, but that those observed for the bulky dimethylsilyl-bridged bis(indenyl)zirconium dichloride ($SBIZrCl_2$) were lower than that of its ethylene bridged counterpart.[251,252] In addition to pre- and postcontacting the support with MAO, it is also possible to treat the organometallic precatalyst with MAO in advance, which may carry several advantages: reduction in volume of solvent used, a more effective activation of the metal centre, and purification and solubilisation of a barely soluble precatalyst.[253,254]

There are reports in the patent literature of how the heat treatment of MAOs at an elevated temperature for a prolonged period (up to 80 °C for seven hours) can lead to an increase in the reported polymerisation activity of up to 25%.[255,256] This is believed to be caused by a more stable form of MAO, resulting in improved performance. These insoluble MAOs have even been used to support metallocenes in slurry-phase polymerisations.[257–260] A particulate "solid MAO" can be formed by the controlled hydrolysis of $AlMe_3$ in hexane with the use of a surfactant.[261] The insolubility of the aluminoxanes in aliphatic hydrocarbon solvents can be used to precipitate out MAO from a toluene solution, rendering a solid support.[262–264]

Naturally, considerable effort has been expended better to understand the active species on an inorganic support, as they can often be ill defined. Silsesquioxanes can provide a realistic structural model of a silica surface and have been studied in great detail.[265] Typically, silsesquioxanes show comparatively poor activity relative to their silica-immobilised counterparts as they are highly mobile in solution, tending to aggregate. A study by Basset and co-workers using half metallocenes has attempted to probe the nature of supported single-site catalysts using surface organometallic chemistry.[266] Their results included an extended X-ray absorption fine structure (EXAFS) analysis of an alumina

zirconocene, allowing the short-range order to be determined in an otherwise amorphous system. Two earlier papers by O'Hare and co-workers report studies of EXAFS experiments on *ansa*-metallocenes supported on silica.[267,268] The chiral zirconocene, EBIZrCl_2, was analysed, confirming the presence of the indenyl rings as well as an additional methyl bond at the zirconium centre.

1.2.6 Industrial processes

As previously mentioned, the majority of PE is currently produced under heterogeneous conditions, within slurry- or gas-phase reactors, and the production of high density polyethylene (HDPE) is carried out almost exclusively by this method.

Slurry-phase reactors are typically continuously stirred vessels with an aliphatic hydrocarbon diluent (most usually hexane), and with operating temperatures and pressures within the range 70-90 °C and 2-24 bar. As polymerisation is an exothermic process, reactors are normally cooled to maintain optimum conditions and to stop agglomeration of polymer particles which can lead to reactor fouling. Due to their higher polymer capacity by volume, batch polymerisation times are typically between 30 minutes and two hours, and the polymer is typically removed from solution by centrifugation. The largest slurry plants are capable of producing 350,000 tonnes of PE *p.a.*[177]

Gas-phase reactors comprise immobilised catalyst through which is flowed a gas mixture, comprising an inert carrier gas (e.g. N_2), the monomer(s) to be polymerised and a chain transfer agent (e.g. H_2). The polymer is discharged from lower in the reactor while the gas is recycled through the top. Batch processing times are typically longer than for a slurry reactor and they can be operated at higher temperatures and pressures. Gas-phase reactors make up the majority of new production plants and can have a maximum capacity of 660,000 tonnes *p.a.*[177]

1.3 Aims

This thesis aims to build upon the recent synthesis of the permethylated *ansa*-indenyl EBI* and its metallocene chemistry with group 4 metals (zirconium and hafnium).[222] A redesign of the ligand synthesis procedure is desirable if these complexes are to be successful industrial catalysts. Moreover, an appropriate route opens numerous other potential ligands in order to tune the properties of the system. A major focus of this work will be to characterise a number of permethylindenyl organometallics based on group 4, and to understand their structure and bonding both in solution and in the solid-state. An eventual aim is to have a

number of well-defined and characterised supported catalysts for the polymerisation of ethylene, with the hope of better understanding the structure-function relationship of immobilised metallocenes. The solid catalysts will be characterised by a number of lab based techniques as well as EXAFS. Polymerisation studies will examine the activity of the catalysts under a variety of conditions while the polymer samples will be analysed externally.

1.4 References

(1) Kealy, T. J.; Pauson, P. L. *Nature* **1951**, *168*, 1039.
(2) Fischer, E. O.; Jira, R. *Z. Naturforsch. B* **1953**, *8b*, 1.
(3) Wilkinson, G.; Pauson, P. L.; Cotton, F. A. *J. Am. Chem. Soc.* **1954**, *76*, 1970.
(4) Reynolds, L.; Wilkinson, G. *J. Inorg. Nucl. Chem.* **1956**, *2*, 246.
(5) Wilkinson, G.; Cotton, F. A.; Birmingham, J. M. *J. Inorg. Nucl. Chem.* **1956**, *2*, 95.
(6) Harder, S. *Coord. Chem. Rev.* **1998**, *176*, 17.
(7) Arndt, S.; Okuda, J. *Chem. Rev.* **2002**, *102*, 1953.
(8) McKnight, A. L.; Waymouth, R. M. *Chem. Rev.* **1998**, *98*, 2587.
(9) Li, C. L.; Liu, R. S. *Chem. Rev.* **2000**, *100*, 3127.
(10) Pool, J. A.; Lobkovsky, E.; Chirik, P. J. *Nature* **2004**, *427*, 527.
(11) Wilkinson, G.; Birmingham, J. M. *J. Am. Chem. Soc.* **1954**, *76*, 4281.
(12) Lynch Jr., M. A.; Brantley, J. C. Cyclopentadienyl derivatives of transition metals. GB785760, November 06, 1957.
(13) Reynolds, L. T.; Wilkinson, G. *J. Inorg. Nucl. Chem.* **1959**, *9*, 86.
(14) De Vries, L. *J. Org. Chem* **1960**, *25*, 1838.
(15) Robbins, J. L.; Edelstein, N.; Spencer, B.; Smart, J. C. *J. Am. Chem. Soc.* **1982**, *104*, 1882.
(16) Jutzi, P.; Reumann, G. *J. Chem. Soc. Dalton Trans.* **2000**, 2237.
(17) King, R. B. *Coord. Chem. Rev.* **1976**, *20*, 155.
(18) Rerek, M. E.; Basolo, F. *Organometallics* **1983**, *2*, 372.
(19) Mise, T.; Yamazaki, H. *J. Organomet. Chem.* **1979**, *164*, 391.
(20) Bodner, G. M.; Todd, L. J. *Inorg. Chem.* **1974**, *13*, 1335.
(21) Braterman, P. S.; Milne, D. W.; Randall, E. W.; Rosenberg, E. *J. Chem. Soc. Dalton Trans.* **1973**, 1027.
(22) Mach, K.; Varga, V.; Antropiusová, H.; Poláček, J. *J. Organomet. Chem.* **1987**, *333*, 205.
(23) Zachmanoglou, C. E.; Docrat, A.; Bridgewater, B. M.; Parkin, G.; Brandow, C. G.; Bercaw, J. E.; Jardine, C. N.; Lyall, M.; Green, J. C.; Keister, J. B. *J. Am. Chem. Soc.* **2002**, *124*, 9525.
(24) Lappert, M. F.; Pickett, C. J.; Riley, P. I.; Yarrow, P. I. W. *J. Chem. Soc. Dalton Trans.* **1981**, 805.
(25) Antiñolo, A.; Bristow, G. S.; Campbell, G. K.; Duff, A. W.; Hitchcock, P. B.; Kamarudin, R. A.; Lappert, M. F.; Norton, R. J.; Sarjudeen, N.; Winterborn, D. J. W.; Atwood, J. L.; Hunter, W. E.; Zhang, H. *Polyhedron* **1989**, *8*, 1601.
(26) Langmaier, J.; Samec, Z.; Varga, V.; Horáček, M.; Choukroun, R.; Mach, K. *J. Organomet. Chem.* **1999**, *584*, 323.
(27) Jutzi, P. The Versatility of the Pentamethylcyclopentadienyl Ligand in Main-Group Chemistry. *Comments on Inorganic Chemistry*, 1987, *6*, 123–144.
(28) Jutzi, P. *Pure Appl. Chem.* **2003**, *75*, 483.

(29) Resa, I.; Carmona, E.; Gutierrez-Puebla, E.; Monge, A. *Science* **2004**, *305*, 1136.
(30) King, R. B.; Bisnette, M. B. *J. Organomet. Chem.* **1967**, *8*, 287.
(31) Bailey, W. I.; Collins, D. M.; Cotton, F. A.; Baldwin, J. C.; Kaska, W. C. *J. Organomet. Chem.* **1979**, *165*, 373.
(32) Brintzinger, H.; Bercaw, J. E. *J. Am. Chem. Soc.* **1970**, *92*, 6182.
(33) Troyanov, S. I.; Antropiusová, H.; Mach, K. *J. Organomet. Chem.* **1992**, *427*, 49.
(34) Bercaw, J. E.; Marvich, R. H.; Bell, L. G.; Brintzinger, H. H. *J. Am. Chem. Soc.* **1972**, *94*, 1219.
(35) Bailey, M. F.; Dahl, L. F. *Inorg. Chem.* **1965**, *4*, 1298.
(36) Ashley, A. E.; Cowley, A. R.; O'Hare, D. *Eur. J. Org. Chem.* **2007**, *2007*, 2239.
(37) Cooper, R. T.; Chadwick, F. M.; Ashley, A. E.; O'Hare, D. *Organometallics* **2013**, *32*, 2228.
(38) Ashley, A.; Balazs, G.; Cowley, A.; Green, J.; Booth, C. H.; O'Hare, D. *Chem. Commun.* **2007**, *1*, 1515.
(39) Chadwick, F. M.; Ashley, A.; Wildgoose, G.; Goicoechea, J. M.; Randall, S.; O'Hare, D. *Dalton Trans.* **2010**, *39*, 6789.
(40) Chadwick, F. M. *D.Phil. Thesis*, University of Oxford, **2013**.
(41) Chadwick, F. M.; O'Hare, D. M. *Organometallics* **2014**, *33*, 3768.
(42) Ashley, A. E.; Cooper, R. T.; Wildgoose, G. G.; Green, J. C.; O'Hare, D. *J. Am. Chem. Soc.* **2008**, *130*, 15662.
(43) Chadwick, F. M.; Cooper, R. T.; Ashley, A. E.; Buffet, J.-C.; O'Hare, D. M. *Organometallics* **2014**, *33*, 3775.
(44) Turner, Z. R.; Buffet, J.-C.; O'Hare, D. *Organometallics* **2014**, *33*, 3891.
(45) Moss, J.; Thomas, J.; Ashley, A.; Cowley, A. R.; O'Hare, D. *Organometallics* **2006**, *25*, 4279.
(46) Fletcher, A. E. D.; Moss, J.; Cowley, A. R.; O'Hare, D. *Chem. Commun.* **2007**, *1242*, 2971.
(47) Moss, J. *D.Phil. Thesis*, University of Oxford, **2007**.
(48) Bazinet, P.; Tilley, T. D. *Organometallics* **2008**, *27*, 1267.
(49) Kraemer, G.; Spilker, A. *Ber. Dtsch. Chem. Ges.* **1890**, *23*, 3276.
(50) Bonifaci, C.; Ceccon, A.; Gambaro, A.; Ganis, P.; Mantovani, L.; Santi, S.; Venzo, A. *J. Organomet. Chem.* **1994**, *475*, 267.
(51) Rerek, M. E.; Ji, L.; Basolo, F. *J. Chem. Soc. Chem. Commun.* **1983**, 1208.
(52) Samuel, E.; Setton, R. *J. Organomet. Chem.* **1965**, *4*, 156.
(53) Mantovani, L.; Ceccon, A.; Gambaro, A.; Santi, S.; Ganis, P.; Venzo, A. *Organometallics* **1997**, *16*, 2682.
(54) Miyamoto, T. K.; Tsutsui, M.; Chen, L.-B. *Chem. Lett.* **1981**, 729.
(55) Tsutsui, M.; Chen, L. B.; Bergbreiter, D. E.; Miyamoto, T. K. *J. Am. Chem. Soc.* **1982**, *104*, 855.
(56) Beeckman, W.; Goffart, J.; Rebizant, J.; Spirlet, M. R. *J. Organomet. Chem.* **1986**, *307*, 23.
(57) Westcott, S. A.; Kakkar, A. K.; Stringer, G.; Taylor, N. J.; Marder, T. B. *J. Organomet. Chem.* **1990**, *394*, 777.
(58) Frankcom, T. M.; Green, J. C.; Nagy, A.; Kakkar, A. K.; Marder, T. B. *Organometallics* **1993**, *12*, 3688.
(59) Kakkar, A. K.; Jones, S. F.; Taylor, N. J.; Collins, S.; Marder, T. B. *J. Chem. Soc. Chem. Commun.* **1989**, 1454.
(60) O'Hare, D.; Green, J. C.; Marder, T.; Collins, S.; Stringer, G.; Kakkar, A. K.; Kaltsoyannis, N.; Kuhn, A.; Lewis, R. *Organometallics* **1992**, *11*, 48.

(61) O'Hare, D.; Murphy, V. J.; Kaltsoyannis, N. *J. Chem. Soc. Dalton Trans.* **1993**, 383.
(62) Meredith, M. B.; Crisp, J. A.; Brady, E. D.; Hanusa, T. P.; Yee, G. T.; Pink, M.; Brennessel, W. W.; Young, V. G. *Organometallics* **2008**, *27*, 5464.
(63) Brady, E. D.; Overby, J. S.; Meredith, M. B.; Mussman, A. B.; Cohn, M. A.; Hanusa, T. P.; Yee, G. T.; Pink, M. *J. Am. Chem. Soc.* **2002**, *124*, 9556.
(64) O'Hare, D.; Murphy, V.; Diamond, G. M.; Arnold, P.; Mountford, P. *Organometallics* **1994**, *13*, 4689.
(65) Kakkar, A. K.; Stringer, G.; Taylor, N. J.; Marder, T. B. *Can. J. Chem.* **1995**, *73*, 981.
(66) Grädler, U.; Weller, A. S.; Welch, A. J.; Reed, D. *J. Chem. Soc. Dalton Trans.* **1996**, 335.
(67) Herrmann, W. A.; Geisberger, M. R.; Kühn, F. E.; Artus, G. R. J.; Herdtweck, E. *Z.Anorg. Allg. Chem.* **1997**, *623*, 1229.
(68) Stradiotto, M.; McGlinchey, M. J. *Coord. Chem. Rev.* **2001**, *221*, 311.
(69) Green, M.; McGrath, T. D.; Thomas, R. L.; Walker, A. P. *J. Organomet. Chem.* **1997**, *532*, 61.
(70) Calhorda, M. J.; Félix, V.; Veiros, L. F. *Coord. Chem. Rev.* **2002**, *230*, 49.
(71) Gavenonis, J.; Don Tilley, T. *J. Organomet. Chem.* **2004**, *689*, 870.
(72) Arnold, T. A. Q.; Ransom, P. Unpublished results.
(73) Lüttringhaus, A.; Gralheer, H. *Justus Liebig's Ann. der Chemie* **1942**, *550*, 67.
(74) Smith, J. A.; von Seyerl, J.; Huttner, G.; Brintzinger, H. H. *J. Organomet. Chem.* **1979**, *173*, 175.
(75) Tang, G.; Jin, G.-X.; Weng, L. *J. Organomet. Chem.* **2004**, *689*, 678.
(76) Bajgur, C. S.; Tikkanen, W.; Petersen, J. L. *Inorg. Chem.* **1985**, *24*, 2539.
(77) Schneider, N.; Huttenloch, M. E.; Stehling, U.; Kirsten, R.; Schaper, F.; Brintzinger, H. H. *Organometallics* **1997**, *16*, 3413.
(78) Stern, D.; Sabat, M.; Marks, T. J. *J. Am. Chem. Soc.* **1990**, *112*, 9558.
(79) Alt, H. G.; Jung, M. *J. Organomet. Chem.* **1998**, *562*, 229.
(80) Ban, H. T.; Uozumi, T.; Soga, K. *J. Polym. Sci. Part A Polym. Chem.* **1998**, *36*, 2269.
(81) Luttikhedde, H. J. G.; Leino, R. P.; Näsman, J. H.; Ahlgrén, M.; Pakkanen, T. *J. Organomet. Chem.* **1995**, *486*, 193.
(82) Peckham, T. J.; Nguyen, P.; Bourke, S. C.; Wang, Q.; Harrison, D. G.; Zoricak, P.; Russell, C.; Liable-Sands, L. M.; Rheingold, A. L.; Lough, A. J.; Manners, I. *Organometallics* **2001**, *20*, 3035.
(83) Alias, F. M.; Barlow, S.; Tudor, J. S.; O'Hare, D.; Perry, R. T.; Nelson, J. M.; Manners, I. *J. Organomet. Chem.* **1997**, *528*, 47.
(84) J. Katz, T.; Acton, N. *Tetrahedron Lett.* **1970**, *11*, 2497.
(85) Katz, T. J.; Acton, N.; Martin, G. *J. Am. Chem. Soc.* **1973**, *95*, 2934.
(86) Reddy, K. P.; Petersen, J. L. *Organometallics* **1989**, *8*, 2107.
(87) Green, M. L. H.; Ishihara, N. *J. Chem. Soc. Dalton Trans.* **1994**, *1*, 657.
(88) Erker, G.; Psiorz, C.; Fröhlich, R.; Grehl, M.; Krüger, C.; Noe, R.; Nolte, M. *Tetrahedron* **1995**, *51*, 4347.
(89) Resconi, L.; Balboni, D.; Baruzzi, G.; Fiori, C.; Guidotti, S.; Mercandelli, P.; Sironi, A. *Organometallics* **2000**, *19*, 420.
(90) Herrmann, W. A.; Morawietz, M. J. A.; Herrmann, H.-F.; Küber, F. *J. Organomet. Chem.* **1996**, *509*, 115.
(91) Suzuki, N.; Masubuchi, Y.; Yamaguchi, Y.; Kase, T.; Miyamoto, T. K.; Horiuchi, A.; Mise, T. *Macromolecules* **2000**, *33*, 754.
(92) Schumann, H.; Esser, L.; Loebel, J.; Dietrich, A.; Van der Helm, D.; Ji, X. *Organometallics* **1991**, *10*, 2585.

(93) Lentzner, H. L.; Watts, W. E. *Tetrahedron* **1971**, *27*, 4343.
(94) Grossman, R. B.; Doyle, R. A.; Buchwald, S. L. *Organometallics* **1991**, *10*, 1501.
(95) Gutmann, S.; Burger, P.; Hund, H.-U.; Hofmann, J.; Brintzinger, H.-H. *J. Organomet. Chem.* **1989**, *369*, 343.
(96) Sinnema, P.; Höhn, B.; Hubbard, R. L.; Shapiro, P. J.; Twamley, B.; Blumenfeld, A.; Vij, A. *Organometallics* **2002**, *21*, 182.
(97) Recknagel, A.; Edelmann, F. T. *Angew. Chem. Int. Ed.* **1991**, *30*, 693.
(98) Eisch, J. J.; Shi, X.; Owuor, F. A. *Organometallics* **1998**, *17*, 5219.
(99) Ransom, P.; Ashley, A.; Thompson, A.; O'Hare, D. *J. Organomet. Chem.* **2009**, *694*, 1059.
(100) Burger, P.; Hund, H.-U.; Evertz, K.; Brintzinger, H.-H. *J. Organomet. Chem.* **1989**, *378*, 153.
(101) Könemann, M.; Erker, G.; Fröhlich, R.; Kotila, S. *Organometallics* **1997**, *16*, 2900.
(102) Fedushkin, I. L.; Dechert, S.; Schumann, H. *Angew. Chem. Int. Ed.* **2001**, *40*, 561.
(103) Chen, Z.; Halterman, R. L. *Organometallics* **1994**, *13*, 3932.
(104) Erker, G.; Wilker, S.; Krueger, C.; Nolte, M. *Organometallics* **1993**, *12*, 2140.
(105) Dietrich, U.; Hackmann, M.; Rieger, B.; Klinga, M.; Leskelä, M. *J. Am. Chem. Soc.* **1999**, *121*, 4348.
(106) Burger, P.; Brintzinger, H. H. *J. Organomet. Chem.* **1991**, *407*, 207.
(107) Schertl, P.; Alt, H. G. *J. Organomet. Chem.* **1997**, *545-546*, 553.
(108) Finckh, W.; Tang, B. Z.; Lough, A.; Manners, I. *Organometallics* **1992**, *11*, 2904.
(109) Ostoja Starzewski KA; Kelly, W.; Stumpf, A.; Freitag, D. *Angew. Chem. Int. Ed.* **1999**, *38*, 2439.
(110) Schnutenhaus, H.; Brintzinger, H. H. *Angew. Chem. Int. Ed.* **1979**, *18*, 777.
(111) Knüppel, S.; Erker, G.; Fröhlich, R. *Angew. Chem. Int. Ed.* **1999**, *38*, 1923.
(112) Bai, S.; Wei, X.; Guo, J.; Liu, D.-S.; Zhou, Z.-Y. *Angew. Chem. Int. Ed.* **1999**, *38*, 1926.
(113) Lofthus, O. W.; Slebodnick, C.; Deck, P. A. *Organometallics* **1999**, *18*, 3702.
(114) Qian, C.; Guo, J.; Ye, C.; Sun, J.; Zheng, P. *J. Chem. Soc. Dalton Trans.* **1993**, 3441.
(115) Mengele, W.; Diebold, J.; Troll, C.; Roell, W.; Brintzinger, H. H. *Organometallics* **1993**, *12*, 1931.
(116) Herzog, T. A.; Zubris, D. L.; Bercaw, J. E. *J. Am. Chem. Soc.* **1996**, *118*, 11988.
(117) Mueller-Westerhoff, U. T. *Angew. Chem. Int. Ed.* **1986**, *25*, 702.
(118) Dorer, B.; Prosenc, M.; Rief, U.; Brintzinger, H. H. *Organometallics* **1994**, *13*, 3868.
(119) Halterman, R. L.; Combs, D.; Khan, M. A. *Organometallics* **1998**, *17*, 3900.
(120) Palandoken, H.; Wyatt, J. K.; Hitchcock, S. R.; Olmstead, M. M.; Nantz, M. H. *J. Organomet. Chem.* **1999**, *579*, 338.
(121) Nantz, M. H.; Hitchcock, S. R.; Sutton, S. C.; Smith, M. D. *Organometallics* **1993**, *12*, 5012.
(122) Shapiro, P. J. *Coord. Chem. Rev.* **2002**, *231*, 67.
(123) Shaltout, R. M.; Corey, J. Y.; Rath, N. P. *J. Organomet. Chem.* **1995**, *503*, 205.
(124) Lentzner, H. L.; Watts, W. E. *J. Chem. Soc. D Chem. Commun.* **1970**, 26.
(125) Wochner, F.; Brintzinger, H. H. *J. Organomet. Chem.* **1986**, *309*, 65.
(126) Smith, J. A.; Brintzinger, H. H. *J. Organomet. Chem.* **1981**, *218*, 159.
(127) Schwemlein, H.; Zsolnai, L.; Huttner, G.; Brintzinger, H. H. *J. Organomet. Chem.* **1983**, *256*, 285.
(128) Schwemlein, H.; Tritschler, W.; Kiesele, H.; Brintzinger, H. H. *J. Organomet. Chem.* **1985**, *293*, 353.

(129) Schaper, F.; Rentzsch, M.; Prosenc, M.; Rief, U.; Schmidt, K.; Brintzinger, H. *J. Organomet. Chem.* **1997**, *534*, 67.
(130) Green, J. C.; Jardine, C. N. *J. Chem. Soc. Dalton Trans.* **1999**, 3767.
(131) Lee, H.; Desrosiers, P. J.; Guzei, I.; Rheingold, A. L.; Parkin, G. *J. Am. Chem. Soc.* **1998**, *120*, 3255.
(132) Shin, J. H.; Parkin, G. *Chem. Commun.* **1999**, 887.
(133) Churchill, D.; Shin, J. H.; Hascall, T.; Hahn, J. M.; Bridgewater, B. M.; Parkin, G. *Organometallics* **1999**, *18*, 2403.
(134) Churchill, D. G.; Bridgewater, B. M.; Parkin, G. *J. Am. Chem. Soc.* **2000**, *122*, 178.
(135) Jeske, G.; Schock, L. E.; Swepston, P. N.; Schumann, H.; Marks, T. J. *J. Am. Chem. Soc.* **1985**, *107*, 8103.
(136) Mansel, S.; Rief, U.; Prosenc, M.-H.; Kirsten, R.; Brintzinger, H.-H. *J. Organomet. Chem.* **1996**, *512*, 225.
(137) Chen, Y. X.; Rausch, M. D.; Chien, J. C. W. *Organometallics* **1994**, *13*, 748.
(138) Diamond, G. M.; Rodewald, S.; Jordan, R. F. *Organometallics* **1995**, *14*, 5.
(139) Diamond, G. M.; Jordan, R. F.; Petersen, J. L. *Organometallics* **1996**, *15*, 4030.
(140) Diamond, G. M.; Jordan, R. F.; Petersen, J. L. *J. Am. Chem. Soc.* **1996**, *118*, 8024.
(141) Christopher, J. N.; Diamond, G. M.; Jordan, R. F.; Petersen, J. L. *Organometallics* **1996**, *15*, 4038.
(142) Zhang, X.; Zhu, Q.; Guzei, I. A.; Jordan, R. F. *J. Am. Chem. Soc.* **2000**, *122*, 8093.
(143) Ransom, P.; Arnold, T. A. Q.; Thompson, A. L.; Buffet, J.-C.; O'Hare, D. *Dalton Trans.* **2012**, *41*, 11267.
(144) Ransom, P.; Arnold, T. A. Q.; Thompson, A. L.; Buffet, J.-C.; O'Hare, D. *J. Organomet. Chem.* **2014**, *774*, 48.
(145) Chirik, P. J. *Organometallics* **2010**, *29*, 1500.
(146) Pool, J. A.; Lobkovsky, E.; Chirik, P. J. *J. Am. Chem. Soc.* **2003**, *125*, 2241.
(147) Vol'pin, M. E.; Shur, V. B. *Nature* **1966**, *209*, 1236.
(148) Margulieux, G. W.; Semproni, S. P.; Chirik, P. J. *Angew. Chem. Int. Ed.* **2014**, *53*, 9189.
(149) De Wolf, J. M.; Blaauw, R.; Meetsma, A.; Teuben, J. H.; Gyepes, R.; Varga, V.; Mach, K.; Veldman, N.; Spek, A. L. *Organometallics* **1996**, *15*, 4977.
(150) Bercaw, J. E. *J. Am. Chem. Soc.* **1974**, *96*, 5087.
(151) Bradley, C. A.; Keresztes, I.; Lobkovsky, E.; Young, V. G.; Chirik, P. J. *J. Am. Chem. Soc.* **2004**, *126*, 16937.
(152) Rosenthal, U.; Burlakov, V. V.; Arndt, P.; Baumann, W.; Spannenberg, A. *Organometallics* **2003**, *22*, 884.
(153) Rosenthal, U.; Burlakov, V.; Arndt, P.; Baumann, W.; Spannenberg, A.; Shur, V. *Eur. J. Inorg. Chem.* **2004**, *2004*, 4739.
(154) Bradley, C. A.; Lobkovsky, E.; Chirik, P. J. *J. Am. Chem. Soc.* **2003**, *125*, 8110.
(155) Pun, D.; Lobkovsky, E.; Chirik, P. J. *J. Am. Chem. Soc.* **2008**, *130*, 6047.
(156) Pun, D.; Bradley, C. A.; Lobkovsky, E.; Keresztes, I.; Chirik, P. J. *J. Am. Chem. Soc.* **2008**, *130*, 14046.
(157) Semproni, S. P.; Knobloch, D. J.; Milsmann, C.; Chirik, P. J. *Angew. Chem. Int. Ed.* **2013**, *52*, 5372.
(158) Knobloch, D. J.; Lobkovsky, E.; Chirik, P. J. *J. Am. Chem. Soc.* **2010**, *132*, 10553.
(159) Knobloch, D. J.; Toomey, H. E.; Chirik, P. J. *J. Am. Chem. Soc.* **2008**, *130*, 4248.
(160) Burlakov, V. V; Shur, V. B.; Pellny, P.; Arndt, P.; Baumann, W.; Spannenberg, A.; Rosenthal, U. *Chem. Commun.* **2000**, 241.

(161) Àrias, Ò.; Petrov, A. R.; Bannenberg, T.; Altenburger, K.; Arndt, P.; Jones, P. G.; Rosenthal, U.; Tamm, M. *Organometallics* **2014**, *33*, 1774.
(162) Rosenthal, U.; Burlakov, V. V.; Arndt, P.; Baumann, W.; Spannenberg, A. *Organometallics* **2005**, *24*, 456.
(163) Becker, L.; Arndt, P.; Jiao, H.; Spannenberg, A.; Rosenthal, U. *Angew. Chem. Int. Ed.* **2013**, *52*, 11396.
(164) Welch, G. C.; San Juan, R. R.; Masuda, J. D.; Stephan, D. W. *Science* **2006**, *314*, 1124.
(165) Frömel, S.; Kehr, G.; Fröhlich, R.; Daniliuc, C. G.; Erker, G. *Dalton Trans.* **2013**, *42*, 14531.
(166) Chapman, A. M.; Haddow, M. F.; Wass, D. F. *J. Am. Chem. Soc.* **2011**, *133*, 8826.
(167) Chapman, A. M.; Haddow, M. F.; Wass, D. F. *J. Am. Chem. Soc.* **2011**, *133*, 18463.
(168) Podiyanachari, S. K.; Fröhlich, R.; Daniliuc, C. G.; Petersen, J. L.; Mück-Lichtenfeld, C.; Kehr, G.; Erker, G. *Angew. Chem. Int. Ed.* **2012**, *51*, 8830.
(169) Xu, X.; Kehr, G.; Daniliuc, C. G.; Erker, G. *J. Am. Chem. Soc.* **2013**, *135*, 6465.
(170) Xu, X.; Kehr, G.; Daniliuc, C. G.; Erker, G. *Angew. Chemie* **2013**, *125*, 13874.
(171) Xu, X.; Kehr, G.; Daniliuc, C. G.; Erker, G. *J. Am. Chem. Soc.* **2014**, *136*, 12431.
(172) Podiyanachari, S. K.; Fröhlich, R.; Daniliuc, C. G.; Petersen, J. L.; Kehr, G.; Erker, G.; Suzuki, N.; Yuasa, S.; Hagimori, K.; Inoue, S.; Asada, T.; Takemoto, T.; Masuyama, Y. *Dalton Trans.* **2012**, *41*, 10811.
(173) Bender, G.; Kehr, G.; Fröhlich, R.; Petersen, J. L.; Erker, G. *Chem. Sci.* **2012**, *3*, 3534.
(174) Bender, G.; Kehr, G.; Daniliuc, C. G.; Dao, Q. M.; Ehrlich, S.; Grimme, S.; Erker, G. *Chem. Commun.* **2012**, *48*, 11085.
(175) Podiyanachari, S. K.; Bender, G.; Daniliuc, C. G.; Kehr, G.; Erker, G. *Organometallics* **2014**, *33*, 3481.
(176) Curley, J. J.; Bergman, R. G.; Tilley, T. D. *Dalton Trans.* **2012**, *41*, 192.
(177) Severn, J. R.; Chadwick, J. C.; Duchateau, R.; Friederichs, N. *Chem. Rev.* **2005**, *105*, 4073.
(178) Piringer, O. G.; Baner, A. L. *Plastic Packaging: Interactions with Food and Pharmaceuticals*; 2nd Ed.; Wiley, **2008**.
(179) Ziegler, K.; Holzkamp, E.; Breil, H.; Martin, H. *Angew. Chemie* **1955**, *67*, 541.
(180) Ziegler, K.; Gellert, H. G.; Zosel, K.; Lehmkuhl, W.; Pfohl, W. *Angew. Chemie* **1955**, *67*, 424.
(181) Natta, G. *J. Polym. Sci.* **1955**, *16*, 143.
(182) Natta, G.; Pino, P.; Corradini, P.; Danusso, F.; Mantica, E.; Mazzanti, G.; Moraglio, G. *J. Am. Chem. Soc.* **1955**, *77*, 1708.
(183) Knuuttila, H.; Lehtinen, A.; Nummila-Pakarinen, A. *Long Term Properties of Polyolefins*; Albertsson, A.-C., Ed.; Advances in Polymer Science; Springer Berlin Heidelberg: Berlin, Heidelberg, **2004**; Vol. 169, pp. 13–27.
(184) Breslow, D. S.; Newburg, N. R. *J. Am. Chem. Soc.* **1957**, *79*, 5072.
(185) Natta, G.; Pino, P.; Mazzanti, G.; Giannini, U. *J. Am. Chem. Soc.* **1957**, *79*, 2975.
(186) Cozewith, C.; Strate, G. Ver. *Macromolecules* **1971**, *4*, 482.
(187) Doi, Y.; Ueki, S.; Keii, T. *Macromolecules* **1979**, *12*, 814.
(188) Reichert, K. H.; Meyer, K. R. *Makromol. Chemie* **1973**, *169*, 163.
(189) Long, W. P.; Breslow, D. S. *Liebigs Ann. Chem.* **1975**, *1975*, 463.
(190) Andresen, A.; Cordes, H.-G.; Herwig, J.; Kaminsky, W.; Merck, A.; Mottweiler, R.; Pein, J.; Sinn, H.; Vollmer, H.-J. *Angew. Chemie* **1976**, *88*, 689.
(191) Kaminsky, W.; Sinn, H. *Liebigs Ann. Chem.* **1975**, *1975*, 424.

(192) Sinn, H.; Kaminsky, W.; Vollmer, H.-J.; Woldt, R. *Angew. Chem. Int. Ed.* **1980**, *19*, 390.
(193) Resconi, L.; Cavallo, L.; Fait, A.; Piemontesi, F. *Chem. Rev.* **2000**, *100*, 1253.
(194) Brintzinger, H. H.; Fischer, D.; Miilhaupt, R.; Rieger, B.; Waymouth, R. M. *Makromol. Chemie* **1995**, 1143.
(195) Busico, V.; Cipullo, R. *Prog. Polym. Sci.* **2001**, *26*, 443.
(196) Coughlin, E. B.; Bercaw, J. E. *J. Am. Chem. Soc.* **1992**, *114*, 7606.
(197) Shapiro, P. J.; Bunel, E.; Schaefer, W. P.; Bercaw, J. E. *Organometallics* **1990**, *9*, 867.
(198) Gibson, V. C.; Spitzmesser, S. K. *Chem. Rev.* **2003**, *103*, 283.
(199) Hlatky, G. G. *Coord. Chem. Rev.* **1999**, *181*, 243.
(200) Hlatky, G. G. *Chem. Rev.* **2000**, *100*, 1347.
(201) Britovsek, G. J. P.; Gibson, V. C.; McTavish, S. J.; Solan, G. A.; White, A. J. P.; Williams, D. J.; Kimberley, B. S.; Maddox, P. J. *Chem. Commun.* **1998**, 849.
(202) Britovsek, G. J. P.; Bruce, M.; Gibson, V. C.; Kimberley, B. S.; Maddox, P. J.; Mastroianni, S.; McTavish, S. J.; Redshaw, C.; Solan, G. A.; Strömberg, S.; White, A. J. P.; Williams, D. J. *J. Am. Chem. Soc.* **1999**, *121*, 8728.
(203) Britovsek, G. J. P.; Cohen, S. A.; Gibson, V. C.; Van Meurs, M. *J. Am. Chem. Soc.* **2004**, *126*, 10701.
(204) Karpiniec, S. S.; McGuinness, D. S.; Britovsek, G. J. P.; Wierenga, T. S.; Patel, J. *Chem. Commun.* **2011**, *47*, 6945.
(205) Britovsek, G. J. P.; Cohen, S. A.; Gibson, V. C.; Maddox, P. J.; van Meurs, M. *Angew. Chem. Int. Ed.* **2002**, *41*, 489.
(206) Small, B. L.; Brookhart, M.; Bennett, A. M. A. *J. Am. Chem. Soc.* **1998**, *120*, 4049.
(207) Johnson, L. K.; Killian, C. M.; Brookhart, M. *J. Am. Chem. Soc.* **1995**, *117*, 6414.
(208) Mecking, S. *Angew. Chem. Int. Ed.* **2001**, *40*, 534.
(209) Okuda, J. *Chem. Ber.* **1990**, *123*, 1649.
(210) Stephan, D. W.; Stewart, J. C.; Guérin, F.; Courtenay, S.; Kickham, J.; Hollink, E.; Beddie, C.; Hoskin, A.; Graham, T.; Wei, P.; Spence, R. E. v. H.; Xu, W.; Koch, L.; Gao, X.; Harrison, D. G. *Organometallics* **2003**, *22*, 1937.
(211) Johnson, L. K.; Mecking, S.; Brookhart, M. *J. Am. Chem. Soc.* **1996**, *118*, 267.
(212) Killian, C. M.; Tempel, D. J.; Johnson, L. K.; Brookhart, M. *J. Am. Chem. Soc.* **1996**, *118*, 11664.
(213) Stevens, J. C.; Timmers, F. J.; Wilson, D. R.; Schmidt, G. F.; Nickias, P. N.; Rosen, R. K.; Knight, G. W.; Lai, S. Y. Constrained geometry addition polymerization catalysts, processes for their preparation, precursors therefor, methods of use, and novel polymers formed therewith. EP0416815 A2, March 13, **1991**.
(214) Stevens, J. C.; Neithamer, D. R. Metal complex compounds, process for preparation and method of use. EP0418044 A2, **1991**.
(215) Canich, J. A. M.; Licciardi, G. F. Mono-Cp heteroatom containing group IVB transition metal complexes with MAO: supported catalyst for olefin polymerization. US5057475, **1991**.
(216) Canich, J. A. M. Process for producing crystalline poly-.alpha.-olefins with a monocyclopentadienyl transition metal catalyst system. US5026798, **1991**.
(217) Stevens, J. C. *Stud. Surf. Sci. Catal.* **1996**, *101*, 11.
(218) Lubben, T. V; Wolczanski, P. T.; Van Duyne, G. D. *Organometallics* **1984**, *3*, 977.
(219) Dehnicke, K.; Krieger, M.; Massa, W. *Coord. Chem. Rev.* **1999**, *182*, 19.
(220) Stevens, J. C. *Stud. Surf. Sci. Catal.* **1994**, *89*, 277.
(221) Lee, I. M.; Gauthier, W. J.; Ball, J. M.; Iyengar, B.; Collins, S. *Organometallics* **1992**, *11*, 2115.

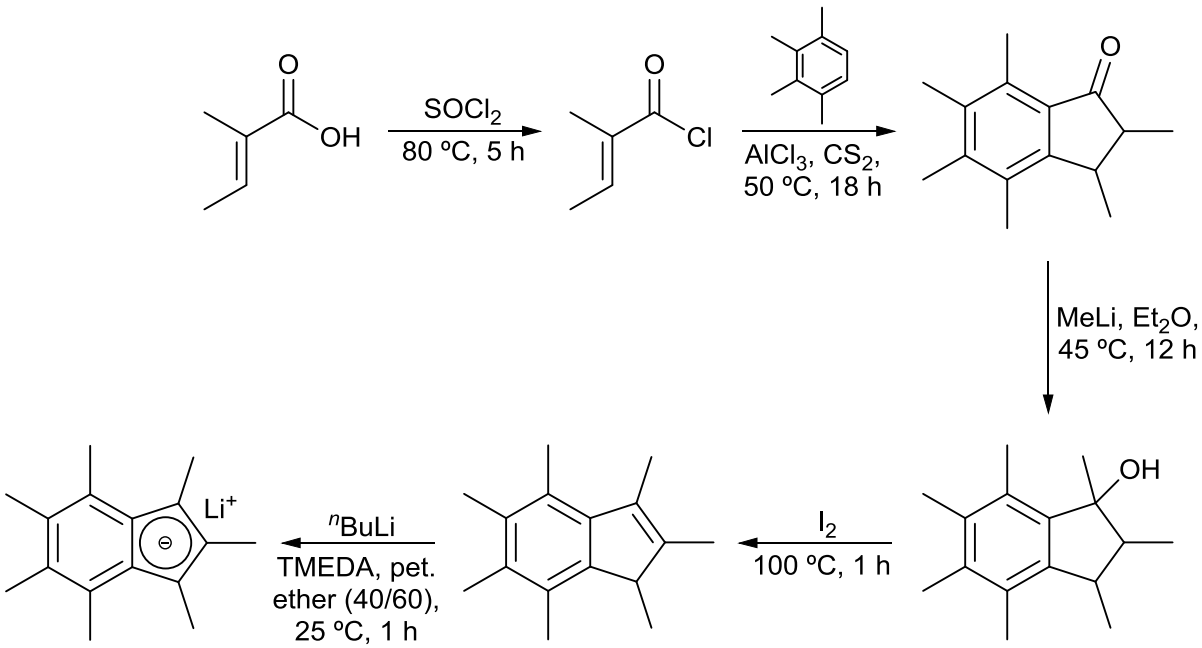
(222) Ransom, P.; Ashley, A. E.; Brown, N. D.; Thompson, A. L.; O'Hare, D. *Organometallics* **2011**, *30*, 800.
(223) Möhring, P. C.; Coville, N. J. *Coord. Chem. Rev.* **2006**, *250*, 18.
(224) Delferro, M.; Marks, T. J. *Chem. Rev.* **2011**, *111*, 2450.
(225) Soga, K.; Ban, H. T.; Uozumi, T. *J. Mol. Catal. A Chem.* **1998**, *128*, 273.
(226) Noh, S. K.; Kim, J.; Jung, J.; Ra, C. S.; Lee, D.; Lee, H. B.; Lee, S. W.; Huh, W. S. *J. Organomet. Chem.* **1999**, *580*, 90.
(227) Lee, H.-W.; Park, Y.-H. *Catal. Today* **2002**, *74*, 309.
(228) Lee, H.; Ahn, S.; Park, Y. *J. Mol. Catal. A Chem.* **2003**, *194*, 19.
(229) Cossee, P. *J. Catal.* **1964**, *3*, 80.
(230) Arlman, E.; Cossee, P. *J. Catal.* **1964**, *3*, 99.
(231) Brookhart, M.; Green, M. L. H. *J. Organomet. Chem.* **1983**, *250*, 395.
(232) Ransom, P. *D.Phil. Thesis*, University of Oxford, **2009**.
(233) Ivin, K. J.; Rooney, J. J.; Stewart, C. D.; Green, M. L. H.; Mahtab, R. *J. Chem. Soc. Chem. Commun.* **1978**, 604.
(234) Soto, J.; Steigerwald, M. L.; Grubbs, R. H. *J. Am. Chem. Soc.* **1982**, *104*, 4479.
(235) Clawson, L.; Soto, J.; Buchwald, S. L.; Steigerwald, M. L.; Grubbs, R. H. *J. Am. Chem. Soc.* **1985**, *107*, 3377.
(236) Krauledat, H.; Brintzinger, H.-H. *Angew. Chem. Int. Ed.* **1990**, *29*, 1412.
(237) Piers, W. E.; Bercaw, J. E. *J. Am. Chem. Soc.* **1990**, *112*, 9406.
(238) Xu, Z.; Vanka, K.; Ziegler, T. *Organometallics* **2004**, *23*, 104.
(239) McKenna, T. F.; Soares, J. B. P. *Chem. Eng. Sci.* **2001**, *56*, 3931.
(240) Galli, P.; Haylock, J. C. *Prog. Polym. Sci.* **1991**, *16*, 443.
(241) Böhm, L. L. *Angew. Chem. Int. Ed.* **2003**, *42*, 5010.
(242) Zakharov, V. A.; Bukatov, G. D.; Barabanov, A. A. *Macromol. Symp.* **2004**, *213*, 19.
(243) Przybyla, C.; Tesche, B.; Fink, G. *Macromol. Rapid Commun.* **1999**, *20*, 328.
(244) Bonini, F.; Fraaije, V.; Fink, G. *J. Polym. Sci. Part A Polym. Chem.* **1995**, *33*, 2393.
(245) Knoke, S.; Ferrari, D.; Tesche, B.; Fink, G. *Angew. Chem. Int. Ed.* **2003**, *42*, 5090.
(246) Dos Santos, J. H. Z.; Dorneles, S.; Stedile, F. C.; Dupont, J.; de Camargo Forte, M. M.; Baumvol, I. J. R. *Macromol. Chem. Phys.* **1997**, *198*, 3529.
(247) Dos Santos, J. H. Z.; Larentis, A.; da Rosa, M. B.; Krug, C.; Baumvol, I. J. R.; Dupont, J.; Stedile, F. C.; de Camargo Forte, M. *Macromol. Chem. Phys.* **1999**, *200*, 751.
(248) Dos Santos, J. H. Z.; Krug, C.; Da Rosa, M. B.; Stedile, F. C.; Dupont, J.; De Camargo Forte, M. *J. Mol. Catal. A Chem.* **1999**, *139*, 199.
(249) Collins, S.; Kelly, W. M.; Holden, D. A. *Macromolecules* **1992**, *25*, 1780.
(250) Kaminsky, W.; Renner, F. *Macromol. Rapid Commun.* **1993**, *14*, 239.
(251) Guimarães, R.; Stedile, F. C.; dos Santos, J. H. . *J. Mol. Catal. A Chem.* **2003**, *206*, 353.
(252) Galland, G. B.; Seferin, M.; Guimarães, R.; Rohrmann, J. A.; Stedile, F. C.; dos Santos, J. H. Z. *J. Mol. Catal. A Chem.* **2002**, *189*, 233.
(253) Burckhart, T. J.; Murata, M.; Brandley, W. B. Method for making and using a supported metallocene catalyst system. US5240894, **1993**.
(254) Burckhart, T. J.; Brandley, W. B. Method for preparing metallocene catalyst systems. US5635437, **1997**.
(255) Krzystowczyk, N. L.; Diefenbach, S. P.; Burt, E. A. Use of heat treated alumoxanes in preparing supported catalysts. US5739368, **1998**.
(256) Krzystowczyk, N. L.; Diefenbach, S. P.; Burt, E. A. Heat treated alumoxanes. US6034024, **2000**.

(257) Geerts, R. L.; Kufeld, S. E.; Hill, T. G. Preparation of organoaluminoxy product and its use as polymerization cocatalyst. US5354721, August 31, **1994**.
(258) Geerts, R. L. Organoaluminoxy product and use as cocatalysts with metallocenes in ethylene polymerization., October 11, **1994**.
(259) Geerts, R. L.; Hill, T. G.; Kufeld, S. E. Organo-aluminoxy product and use. US5411925, **1995**.
(260) Geerts, R. L. Organoaluminoxy product, preparation, and use. US5436212, 1995.
(261) Lu, B.; Wang, J.; Hong, X.; Jing, Z. Preparation of supported metallocene/aluminoxane solid catalyst. US5728640, **1998**.
(262) Kioka, M.; Kashiwa, N. Finely divided aluminoxane, process for producing same and its use. US4952540, **1990**.
(263) Kioka, M.; Kashiwa, N. Catalyst for olefin polymerization and processes for its production. US4923833, **1990**.
(264) Kioka, M.; Kashiwa, N.; Tsutsui, T.; Toyota, A. Catalyst for polymerizing an olefin and process for polymerizing an olefin. US5122491, **1992**.
(265) Duchateau, R. *Chem. Rev.* **2002**, *102*, 3525.
(266) Jezequel, M.; Dufaud, V.; Ruiz-Garcia, M. J.; Carrillo-Hermosilla, F.; Neugebauer, U.; Niccolai, G. P.; Lefebvre, F.; Bayard, F.; Corker, J.; Fiddy, S.; Evans, J.; Broyer, J.-P.; Malinge, J.; Basset, J.-M. *J. Am. Chem. Soc.* **2001**, *123*, 3520.
(267) O'Brien, S.; Tudor, J.; Maschmeyer, T. *Chem. Commun.* **1997**, 1905.
(268) O'Brien, S.; Tudor, J.; Barlow, S.; Drewitt, M. J.; Heyes, S. J.; O'Hare, D. *Chem. Commun.* **1997**, 641.

Chapter Two
Ligand Development

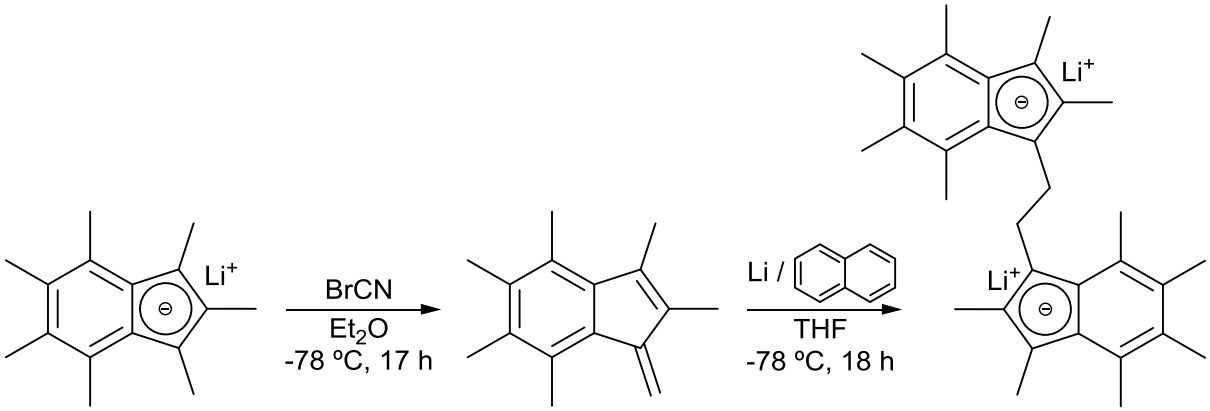
2.1 Introduction

As discussed briefly in Chapter One, the first synthesis of a permethylated indenyl synthon was reported by Miyamoto *et al.* in 1981 in response to the varied applications and advantages found for Cp*.[1] The ligand was synthesised from trans-2-methylbutenoic acid (tiglic acid, **2.1**) which was chlorinated (**2.2**), and reacted with 1,2,3,4-tetramethylbenzene (**2.3**) by means of a Friedel-Crafts acylation, affording a yellow oil: 2,3,4,5,6,7-hexamethylindanone (**2.4**). Methylation using methyllithium, iodine and sodium dithionite ($Na_2S_2O_4$) yielded the indene, Ind*H (**2.6**), in high yield. The resulting ligand was used to create the permethylindenyl congener of ferrocene, Ind^*_2Fe.[1] A further publication extended the chemistry of this new ligand to the lanthanides, and compounds with varying indenyl stoichiometries were reported for lanthanum, erbium and neodymium.[2] Despite the obvious significance of this breakthrough, the synthetic route was outlined with only meagre details including the complete omission of analytical data or reaction conditions. A flurry of activity at the beginning of the 1990s revived the interest in permethylindenyl chemistry,[3–5] and its synthesis was republished by O'Hare *et al.* replete with characterising data and practical information (Scheme 2.1).[6]



Scheme 2.1: O'Hare *et al.*'s 1992 synthesis of Ind*Li.[6]

No other synthetic routes to the ligand have been published although the original procedure was developed in a further paper by O'Hare and co-workers in 2009,[7] with the synthesis of the *ansa*-bridged analogue, EBI*Li_2 (**2.9**). The method consists of the creation of an *exo*-double bond in a fulvene-like species *via* the addition/elimination of an electrophilic bromine species, and an alkali-metal mediated reductive coupling (Scheme 2.2).



Scheme 2.2: Ransom *et al.*'s 2009 synthesis of EBI*Li_2.[7]

2.2 An updated synthesis

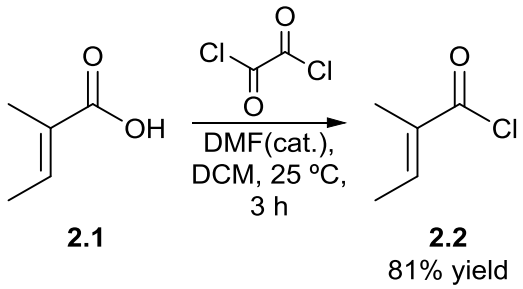
2.2.1 Rationale for the update

A number of factors came together in the requirement to update the synthetic route described in the two papers by O'Hare and co-workers.[6,7] First and foremost was the sponsorship of the project by an industrial company, SCG Chemicals, with an interest in the polyolefin industry. The aim of the project was to develop active ethylene polymerisation catalysts based on *ansa*-permethylindenyl complexes of the group 4 metals, as covered by O'Hare *et al.*'s patent.[8] For the project to be feasible, the ligand synthesis involved had to be reproducible on a large scale in preparation for its potential industrial manufacture. This involved the removal of all steps requiring "hazardous" chemicals; those which are forbidden for use on an industrial scale, or those which necessitate the introduction of significant additional safety precautions. Moreover, it was envisaged that a new synthesis might be higher yielding and less time consuming than its predecessor which takes 72 straight hours to complete.

Another significant contributing factor was the vastly inflated cost of one of the key starting materials, **2.3**. 1,2,3,4-tetramethylbenzene had seen a four-fold increase in price from key laboratory suppliers in a six year period from £3.50/g (2006) to £12.04/g (2012).[9] Attempts were made to circumvent this increase in cost by the synthesis of **2.3** from

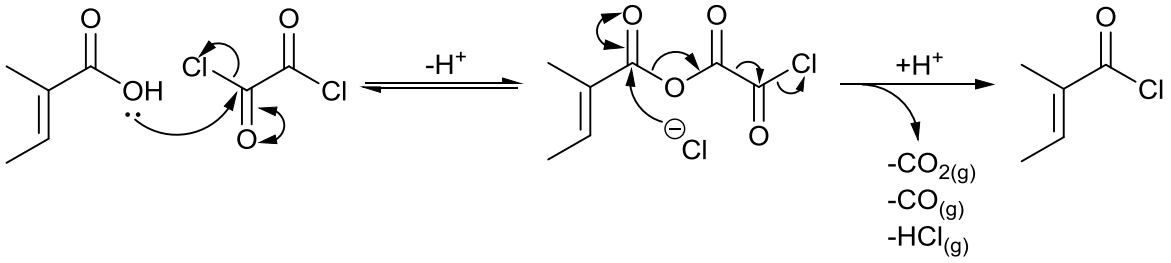
alternative starting materials.[10] A large quantity of 5,6-dinitro-1,2,3,4-tetramethylbenzene was available but the reduction of this *via* the 5,6-diamino-1,2,3,4-tetramethylbenzene was considered dangerous due to the toxicity of the intermediate *ortho*-diaminobenzene and the potentially violent decomposition of the starting material. 5,6-dibromo-1,2,3,4-tetramethylbenzene and 5-bromo-1,2,3,4-tetramethylbenzene were successfully reduced using a Grignard reagent and catalytic iron dichloride but this was not seen as a viable alternative due to their lack of commercial availability. More promising, however, were 1,2,4-trimethylbenzene (£0.35/g) and 1,2,3-trimethylbenzene (£1.49/g),[9] with the latter favoured due to its propensity to react at the 4- and 6-positions because of its electron-donating methyl groups. Unfortunately, iodination, prior to methylation with methyllithium, led to a mixture of isomers which proved inseparable.[10] No viable synthesis of **2.3** was devised, and it was necessary to purchase the reagent at the inflated price.

2.2.2 Synthesis of tigloyl chloride (2.2).



Scheme 2.3: synthesis of tigloyl chloride (**2.2**).

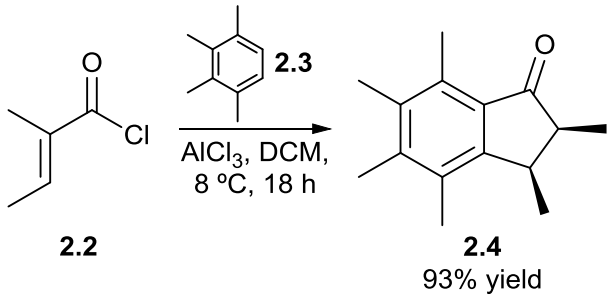
The original 1981 synthesis used thionyl chloride as the chlorinating agent, which has the advantage of being used neat, acting as both reagent and solvent. However it has a very high toxicity and it was desired to replace this with a more benign alternative. Oxalyl chloride was chosen as the replacement due to the irreversible nature with which it reacts with **2.1**. Its reaction with even weak oxygen nucleophiles causes its degradation into CO_2, CO and HCl as well as chlorinating the reagent. As the gases are bubbled off from solution, the reaction is irreversible (Scheme 2.4), as well as the considerable entropic gain through their evolution. Another advantage over thionyl chloride is that oxalyl chloride effects the chlorination at room temperature.



Scheme 2.4: irreversible chlorination mechanism by oxalyl chloride.

Dichloromethane (DCM) was chosen as the solvent due to its volatility.[11] Only 0.9 equivalents of oxalyl chloride were added to the reaction mixture for ease of separation as both **2.2** and oxalyl chloride are volatile and can be challenging to isolate from one another. Upon mixing the reagents together, the solution began to bubble slowly, and on addition of a catalytic amount of dry N,N-dimethylformamide (DMF), the effervescence increased dramatically. When no more gas was evolved, *circa* three hours, the product was distilled off to obtain a clear, colourless, moisture-sensitive liquid in 81% yield.

2.2.3 Synthesis of 2,3,4,5,6,7-hexamethylindanone (2.4).

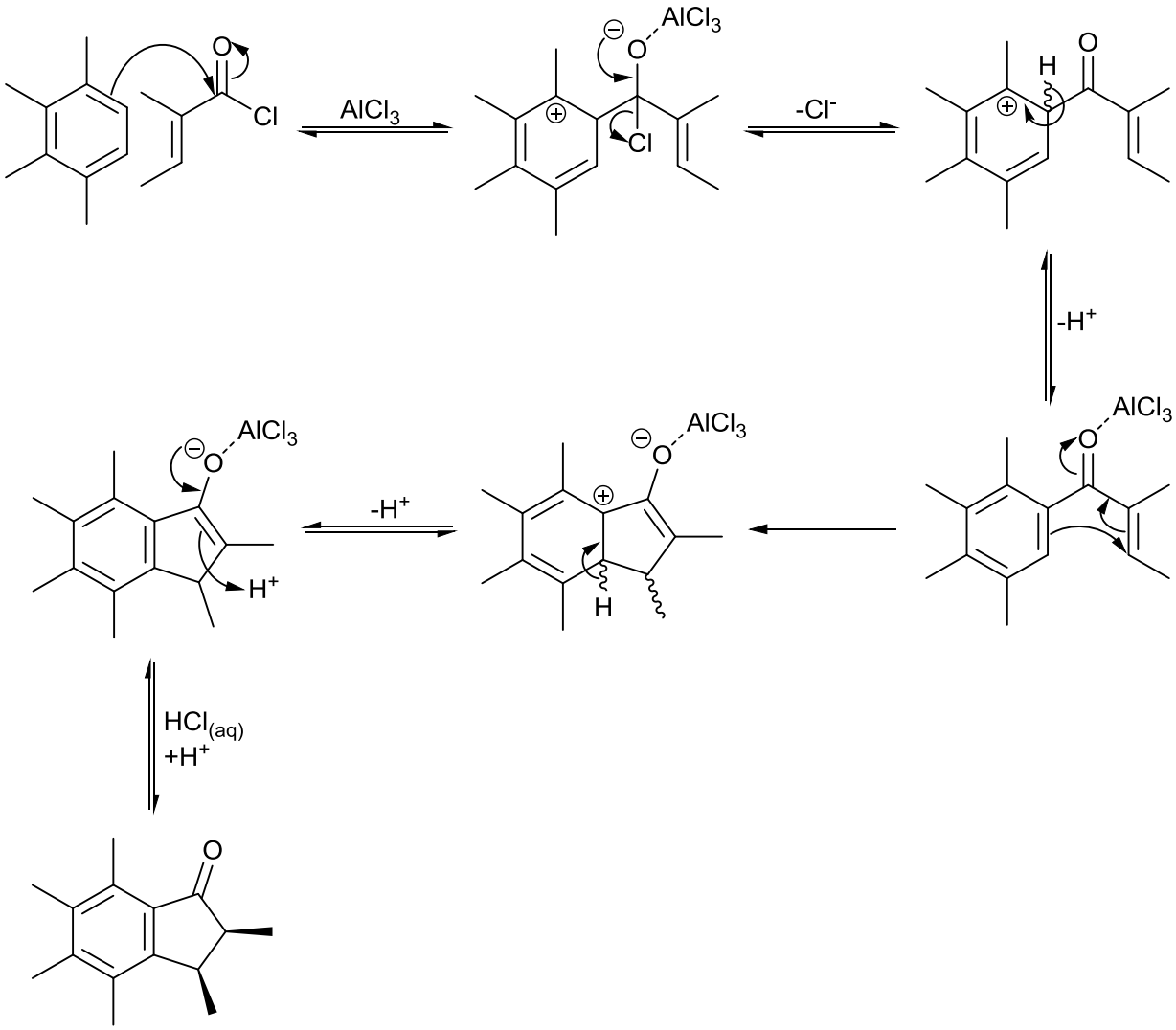


Scheme 2.5: synthesis of 2,3,4,5,6,7-hexamethylindanone (**2.4**).

The synthesis of **2.4** was only modified slightly; a change of solvent away from carbon disulfide was desired by our industrial collaborators to reduce toxicity and DCM enabled the reaction to proceed at 8 °C, as opposed to the elevated 50 °C.

The five-membered ring-system is closed by a Nazarov cyclisation which is concomitant with the Friedel-Crafts acylation as it is also catalysed by a Lewis acid (Scheme 2.6).[12] Once the Friedel-Crafts reaction is complete, it is not worked-up but allowed to undergo a Nazarov cyclisation. The Lewis acidic $AlCl_3$ interacts with the ketone exacerbating the partial positive charge on the *ipso*-carbon and facilitating a conrotatory pericyclic reaction fusing the rings. Aromaticity is restored by the removal of a proton and an acidic work-up causes a keto-enol tautomerisation to restore the ketone. The reactivity of the substrate is enhanced by substitution at the positions α to the ketone, promoting the *s-trans* enone conformers, and

hence cyclisation.[13] The reactivity can be diminished, however, by electron-donating substituents at the α-positions as these can stabilise the oxyallyl cation and not the pentadienyl one. As in this case, substrates with this substitution pattern require stoichiometric quantities of a strong Lewis acid, and they can cyclise to give the *cis*-isomer.[14] This is also encouraged by the reversible acidic work-up where the double bond will be protonated from the less hindered face.



Scheme 2.6: Lewis acid catalysed mechanism of the Nazarov cyclisation with relative stereochemistry shown.

Anhydrous aluminium trichloride was stirred in DCM under a flow of N_2 for 15 minutes before cooling to 8 °C. Tigloyl chloride was combined with 1,2,3,4-tetramethylbenzene and was added dropwise by syringe to the pale yellow $AlCl_3$ suspension effecting a rapid change in colour to dark orange. It was stirred at room temperature for 12 hours, turning dark red-brown, before quenching with a mixture of conc. hydrochloric acid and ice 1:1 (v/v), causing it to decolourise to pale pink. A standard organic work-up afforded **2.4** as a white crystalline

solid in 93% yield. This was a marked improvement on the reported 85% yield of a yellow oil previously documented. Single crystals suitable for analysis by X-ray diffraction were grown by trituration of the product with hexane at 5 °C overnight (Figure 2.1). The crystals grew as colourless blocks.

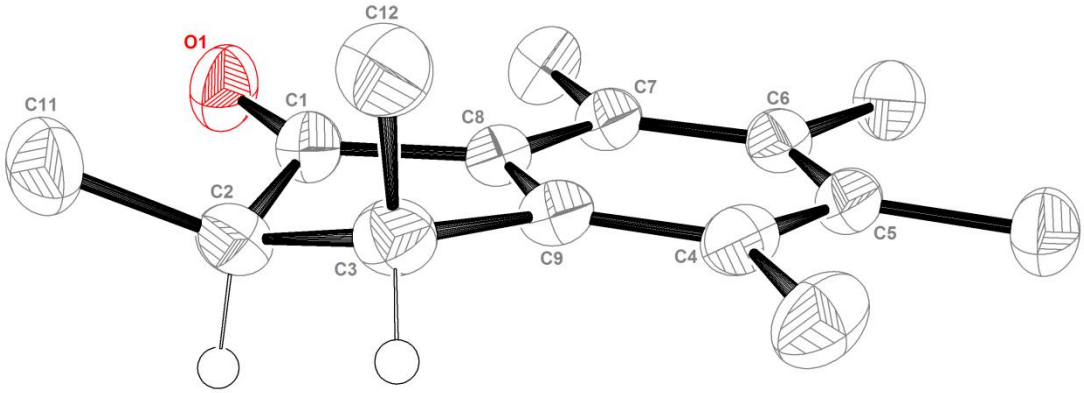


Figure 2.1: solid-state molecular structure of (*2R,3S*)-**2.4**. Methyl protons omitted for clarity. Thermal ellipsoids drawn at 50% probability.

Table 2.1: selected bond lengths for **2.4**. ESDs in parentheses.

Bond Lengths (Å)			
C(1)-C(2)	1.528(3)	C(4)-C(5)	1.409(3)
C(2)-C(3)	1.545(3)	C(5)-C(6)	1.412(3)
C(3)-C(9)	1.525(3)	C(6)-C(7)	1.404(3)
C(8)-C(9)	1.396(2)	C(7)-C(8)	1.405(2)
C(1)-C(8)	1.483(3)	C(1)-O(1)	1.218(3)
C(4)-C(9)	1.390(3)		

2.4 was found to crystallise in the orthorhombic spacegroup *Pca2₁*, with one molecule in the asymmetric unit and two molecules of each enantiomer in the unit cell. The bond lengths and angles observed for **2.4** are unremarkable. The C=O double bond (1.218(3) Å) is almost identical for that reported for the equivalent diketone precursor to permethylpentalene, $WeissMe_4$, (1.219(2) Å).[15] Naturally the average C-C bond distances exclusively observed for the five-membered ring are significantly longer than those in the six-membered ring: 1.520 and 1.403 Å respectively. This is hardly surprising as the six membered ring is aromatic, containing three unsaturations. There is very little bond alternation within the benzene ring – good evidence for full delocalisation of the π-electrons. A substantial hinge angle (HA),

which quantifies envelope conformations, is measured for C(2) (22.72°) which explains why the methyl group, C(12), seems significantly further removed from the ring plane than C(11).

^{1}H NMR spectroscopic analysis of the bulk sample confirms only one diastereoisomer is present with both C(11) and C(12) on the same face (Figure 2.2). This species comprises two enantiomers (*2R,3S* and *2S,3R*) which are indistinguishable by NMR spectroscopy.

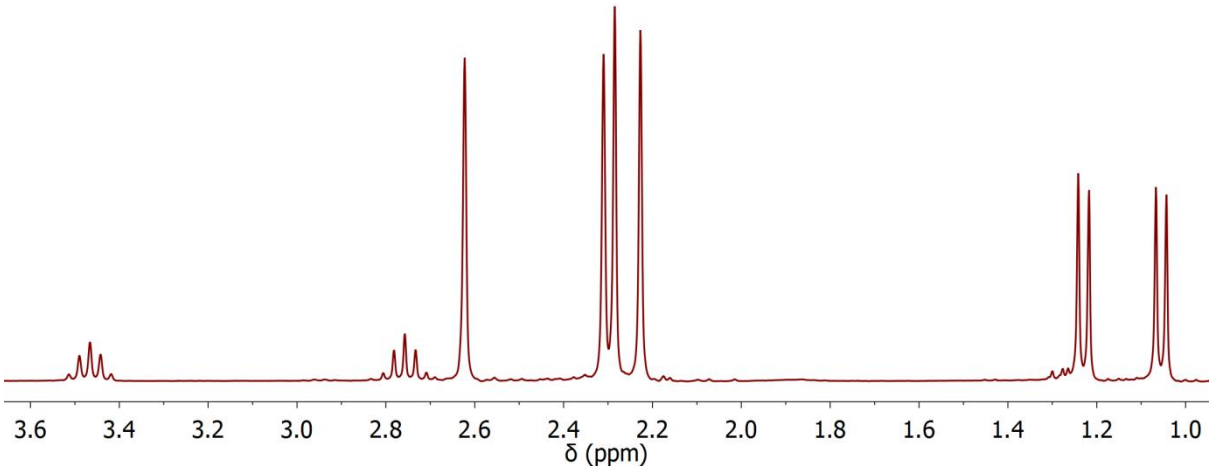
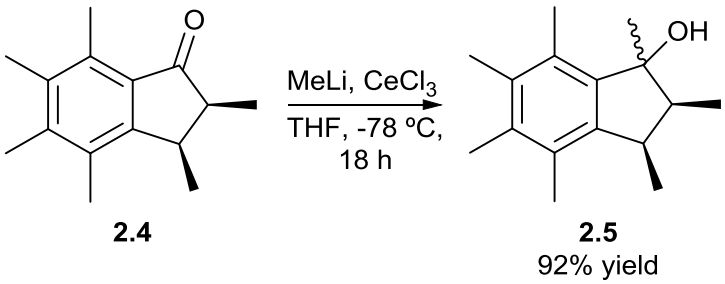


Figure 2.2: ^{1}H NMR (400 MHz) spectrum of **2.4** in chloroform-d_1.

The ^{1}H NMR spectrum is quite simple with two methyl doublets at low frequency split by the aliphatic ring protons which occur at 2.75 and 3.47 ppm as multiplets. Four singlets, each with intensity three occupy the region from 2.2-2.7 ppm and correspond to the methyl groups on the aromatic ring.

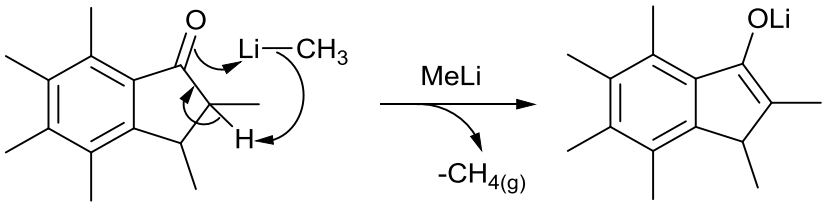
2.2.4 Synthesis of 1,2,3,4,5,6,7-heptamethylindan-1-ol (2.5).



Scheme 2.7: synthesis of 1,2,3,4,5,6,7-heptamethylindan-1-ol (**2.5**) with relative stereochemistry shown.

Whereas methyllithium was used as the reducing agent in the syntheses from both 1981 and 1992,[1,6] it was found, in this instance, to be too basic to carry out this transformation, resulting in ligand degradation as observed by ^{1}H NMR spectroscopy. This is no doubt due to the enolisation reaction which competes with the nucleophilic attack at the carbonyl carbon (Scheme 2.8).[16] Once the deprotonation is complete, the gaseous by-product, methane, is

given off making the reaction irreversible. In its enolate form, the C=O bond is immune to further nucleophilic attack, greatly reducing the yield.



Scheme 2.8: the competitive enolisation reaction, which is rendered irreversible by the evolution of methane.

Earlier reports on this synthesis suggested that using methyllithium in a non-polar solvent decreased its basicity relative to its nucleophilicity but attempts at this did not improve the yield. It was therefore decided to use a Grignard reagent in place of the alkali metal reagent as a marginally "softer" methylating agent and a better nucleophile. This had shown promise in earlier studies. The appropriate methylation was effected by MeMgBr, as determined by ^{1}H NMR spectroscopy, but it was a significant challenge to separate the desired product from a brown oil, found by ^{1}H NMR spectroscopy to contain a multitude of methyl resonances. Given this unwanted intricacy, it was decided to pursue a different route.

Similar problems had been encountered with a number of bicyclic compounds,[17,18] including permethylpentalene,[15] with a proposed carbonyl methylation leading to product degradation.[19] In all cases, it was found that an even "softer" methyl transfer agent was required for successful conversion of the hindered ketone to the *ipso*-methylated alcohol. Quast *et al.* were able to use copper based reagents, while Beckmann and co-workers drew on earlier reports in the literature of an alternative procedure based on cerium.[17,18] In 1984, Imamoto *et al.* published a report on the "nucleophilic addition to easily enolisable ketones" in which they advocate the use of a cerium reagent.[20] A follow-up study five years later demonstrated the method's applicability to a wide range of substrates, particularly those with unsaturations in the ring systems.[21] Reaction of cerium trichloride with the desired alkyllithium in a donor solvent (e.g. THF) generates the non-basic "$CeCl_2R$", which is able to attack the nucleophilic *ipso*-carbon, enacting the alkylation in high yield.[22] It is key to the reaction that the cerium trichloride is completely dehydrated and that the bound water of the heptahydrate is removed at the correct temperature to prevent hydrolysis of the $CeCl_3$ and deactivation of the reagent.

A solution of **2.4** in THF was slowly added to the "$CeCl_2Me$" mixture at −35 °C and, after an hour, the reaction allowed to warm up to room temperature and stir under N_2 for eleven hours. The mixture was quenched with a saturated solution of NH_4Cl and a standard

organic work-up afforded the product as an oily mixture of isomers in 92% yield. Crystals of **2.5** suitable for X-ray diffraction were obtained by recrystallisation from pentane at −18 °C (Figure 2.3).

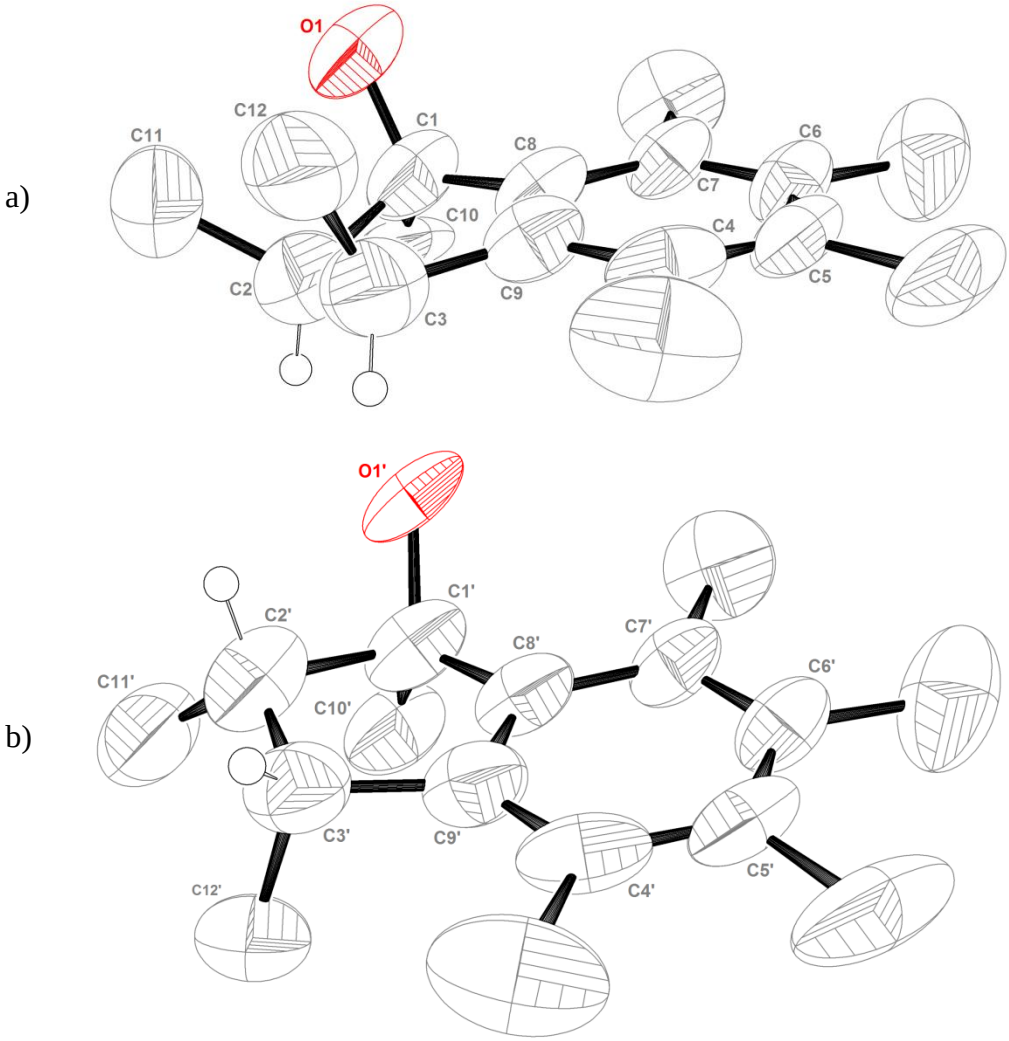


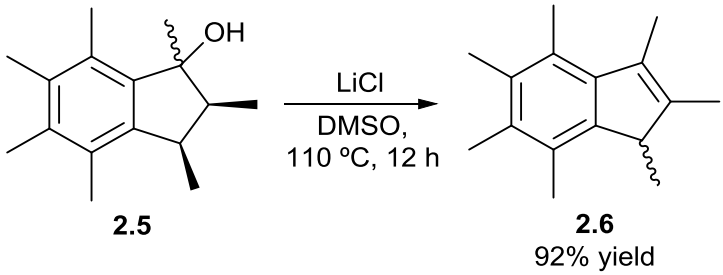
Figure 2.3: solid-state molecular structures of (*1R,2R,3S*)-**2.5** (a) and (*1R,2S,3R*)-**2.5** (b). Methyl protons omitted for clarity. Thermal ellipsoids drawn at 50% probability.

2.5 was found to crystallise in the tetragonal spacegroup $I4_1/a$, with 16 molecules in the unit cell and one molecule in the asymmetric unit. This molecule was, however, found to be disordered with partial occupancy of two different diastereomers on the same site. When this was modelled, 65% were found to be the *1R,2R,3S* (Figure 2.3a) and the remaining 35% the *1R,2S,3R* (Figure 2.3b). The molecules within the unit cell comprise eight enantiomeric pairs (of both diastereomers). No evidence was seen of the isomers where the methyls at the 2- and 3-positions were *anti* to one another. This is hardly surprising given that its precursor, **2.4**, was diastereomerically pure *syn* as well. Given the level of disorder, it is inappropriate to

comment in any significant way on the bond lengths observed but the features seen were similar to those reported for **2.4**. Synthesis of 1,2,3,4,5,6,7-heptamethylindene (2.6).

Table 2.2: selected bond lengths for **2.5**. ESDs in parentheses.

Bond Lengths (Å)			
(*1R,2R,3S*)-**2.5**		(*1R,2S,3R*)-**2.5**	
C(1)-C(2)	1.793(6)	C(1)′-C(2)′	1.787(6)
C(2)-C(3)	1.465(6)	C(2)′-C(3)′	1.475(6)
C(3)-C(9)	1.540(5)	C(3)′-C(9)′	1.538(6)
C(8)-C(9)	1.379(5)	C(8)′-C(9)′	1.379(5)
C(1)-C(8)	1.490(4)	C(1)′-C(8)′	1.490(4)
C(4)-C(9)	1.419(8)	C(4)′-C(9)′	1.419(8)
C(4)-C(5)	1.379(10)	C(4)′-C(5)′	1.379(10)
C(5)-C(6)	1.371(9)	C(5)′-C(6)′	1.371(9)
C(6)-C(7)	1.377(9)	C(6)′-C(7)′	1.377(9)
C(7)-C(8)	1.411(7)	C(7)′-C(8)′	1.411(7)
C(1)-O(1)	1.351(7)	C(1)′-O(1)′	1.439(8)

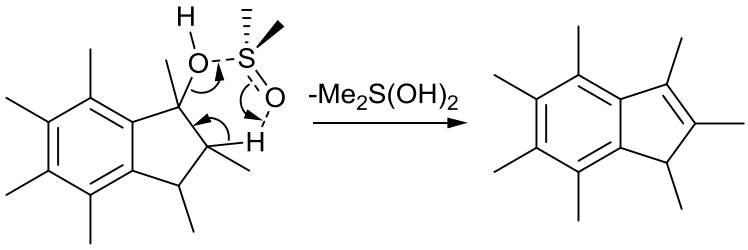


Scheme 2.9: synthesis of 1,2,3,4,5,6,7-heptamethylindene (**2.6**) with relative stereochemistry shown.

Initial attempts to replicate the procedure reported by O'Hare *et al.* were unsuccessful with the use of iodine as the dehydration agent, despite heating to elevated temperatures in excess of 100 °C. Alternative methods were sought and it was thought suitable to try reaction with tosic acid [4-Me-PhSO$_2$(OH)] which can be used in catalytic amounts.[19] Initially, the reaction was attempted in DCM with a stoichiometric quantity of tosic acid and anhydrous magnesium sulfate to absorb the water (10 g/ml). A series of aliquots, analysed by ^{1}H NMR spectroscopy, suggest that the reaction does begin but that it never reaches completion, and a colour change from off-white to dark yellow and then red was noted. Gentle heating was applied which was not successful in driving the reaction to completion. A change of the

reaction solvent to toluene and use of Dean-Stark apparatus at 130 °C did not appear to change the extent of reaction either, and other synthetic routes were tried. Concentrated sulfuric acid was partially successful, but seemed to degrade some of the ligand in addition to dehydrating the majority, leading to unsatisfactory yields.[16]

The reduction of a hindered and electronically deactivated cyclopentanol is effected by LiCl in dimethylsulfoxide (DMSO).[15] Two reports by Traynelis *et al.* in the 1960s describe the efficacy of DMSO as a dehydrating agent for secondary and tertiary alcohols, proposing a cyclic six-membered transition state (Scheme 2.10).[23,24]



Scheme 2.10: the proposed six-membered transition state for the dehydration of **2.5** to **2.6** using DMSO.

Further work by Ashley *et al.* ascertained that the dehydration was catalysed by the addition of anhydrous lithium chloride, and confirmed its wide-ranging applicability including better yields than the acidic dehydration reported in the preparation of Cp*H from the corresponding alcohol.

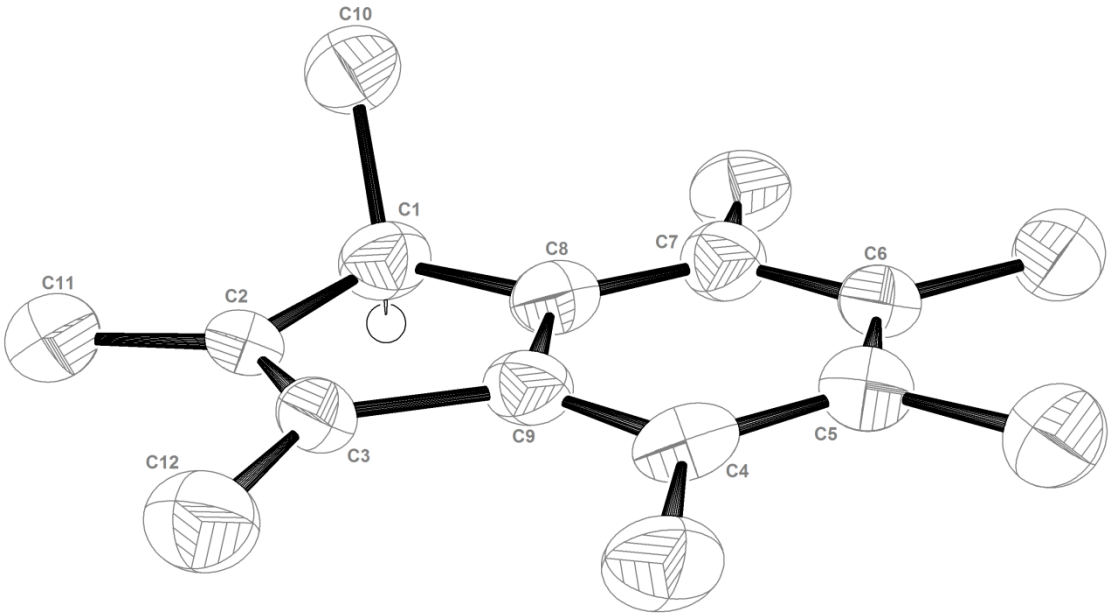


Figure 2.4: solid-state molecular structure of (*1R*)-**2.6**. Methyl protons omitted for clarity. Thermal ellipsoids drawn at 50% probability.

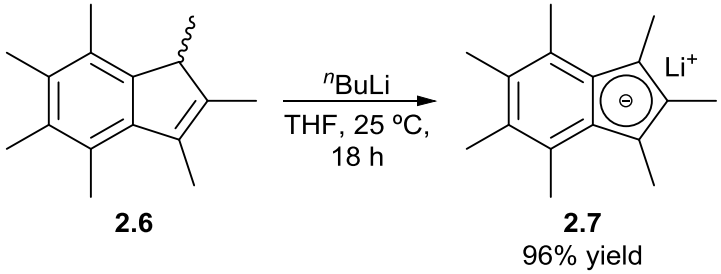
Anhydrous LiCl was added to a reflux condenser containing **2.5** and dry DMSO which was heated at 110 °C for 12 hours. On cooling, the product was extracted with pentane and worked-up giving **2.6** as a light brown oil in 92% yield. Trituration with pentane afforded an off-white crystalline solid, from which crystals, suitable for X-ray diffraction were obtained (Figure 2.4).

Table 2.3: selected bond lengths for **2.6**. ESDs in parentheses.

Bond Lengths (Å)			
C(1)-C(2)	1.515(7)	C(4)-C(9)	1.392(6)
C(2)-C(3)	1.324(6)	C(4)-C(5)	1.390(7)
C(3)-C(9)	1.504(6)	C(5)-C(6)	1.418(6)
C(8)-C(9)	1.414(6)	C(6)-C(7)	1.412(6)
C(1)-C(8)	1.487(6)	C(7)-C(8)	1.391(6)

2.6 was found to crystallise in the monoclinic spacegroup $P2_1/a$, with one molecule in the asymmetric unit and four in the unit cell, comprising two pairs of enantiomers. While all the bond lengths and angles were much as expected, the first point of note is the localised double bond in the five membered ring, determined by the C=C bond distance of 1.324(6) Å, which is considerably shorter than any other carbon-carbon bonds in the structure; either the bond average ring C-C single bond (1.502 Å) or the average bond in the benzene ring (1.403 Å). Moreover, it matches well with other values reported for methyl-substituted cyclopentadienes.[25,26] As with both **2.4** and **2.5**, there is no appreciable alternation in the bonds of the benzene ring. Moreover C(3)-C(9) is not shortened now that it is comprised in the conjugated π-system, suggesting that the two areas of electron density are quite separate. As the five-membered ring now contains four rigid sp^2 centres there is very little puckering with an HA at C(2) of only 2.28°.

2.2.5 Synthesis of lithium 1,2,3,4,5,6,7-heptamethylindenide (2.7).



Scheme 2.11: synthesis of lithium 1,2,3,4,5,6,7-heptamethylindenide (**2.7**).

The synthesis of **2.7** proved facile using the reported methodology although the solvent was changed to THF from petroleum ether (b.p. 40/60), which resulted in a very modest improvement in the yield. *n*-butyllithium in hexane was added dropwise at room temperature to a stirred solution of **2.6** in THF and allowed to stir overnight under an atmosphere of N_2. On reduction *in vacuo*, the beige solid was washed with toluene and pentane (being insoluble in all but the most coordinating of solvents), affording a white powder in 96% yield. Analysis by ^{1}H NMR spectroscopy, revealed that **2.7** is symmetric (C_{2v}) in solution as only four resonances corresponding to the ligand were observed (Figure 2.5).

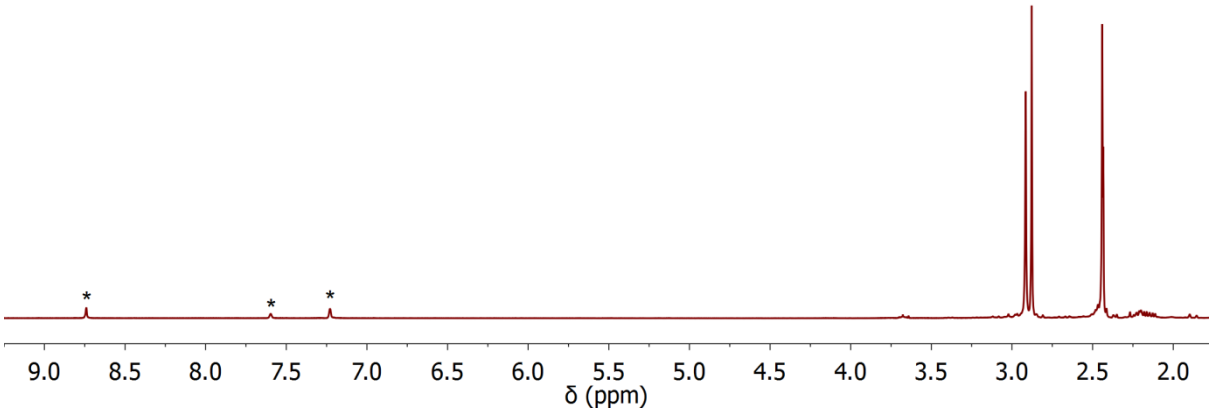
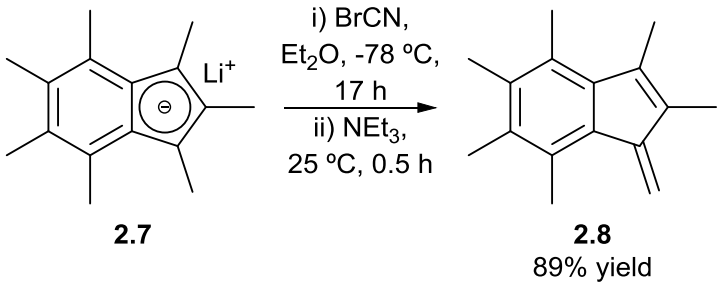


Figure 2.5: ^{1}H NMR of **2.7** in pyridine-d_5. Asterisks mark residual *protio*-solvent resonances.

Two of these resonances were almost coincident in pyridine-d_5 (2.43 and 2.44 ppm) and the whole spectrum was found to agree well with that reported for complexes of Ind*, showing the characteristic 2:2:2:1 intensity ratio for the methyl groups.[27]

2.2.6 Synthesis of 1-methylene-2,3,4,5,6,7-hexamethylindene (2.8)

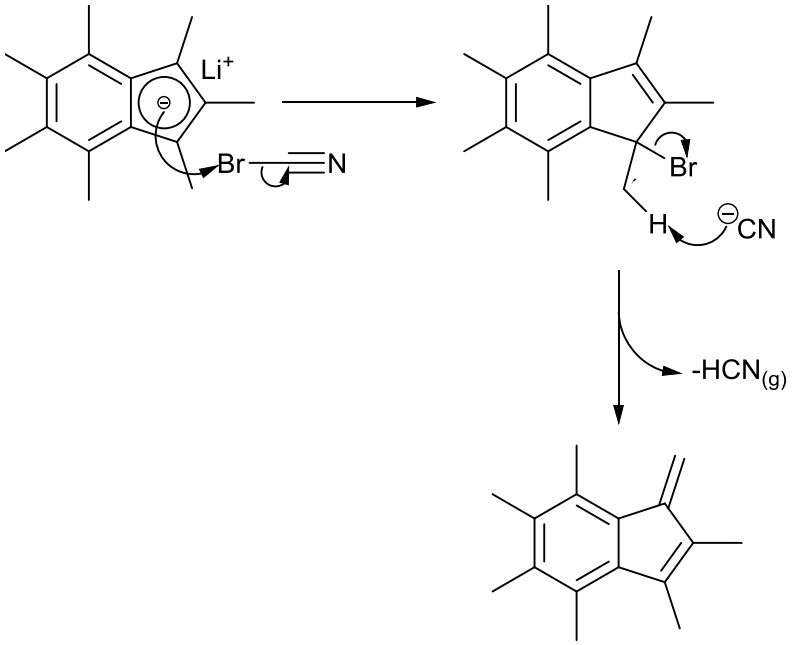


Scheme 2.12: synthesis of 1-methylene-2,3,4,5,6,7-hexamethylindene (**2.8**).

Given the large quantities of hydrogen cyanide liberated by the reported procedure for this step, it was imperative for an industrial scale-up that an alternative was found. It was decided to follow the halogenation/elimination methodology and 1,8-diazabicyclo[5.4.0]undec-7-ene (DBU) was selected as the reagent to carry out the

elimination due to its ability to sequester halide ions as well as acting as a non-nucleophilic base, known to promote elimination *via* E2. A variety of halogenation agents were tried including Br_2, I_2 and N-bromosuccinimide (NBS) and these were able, at least partially, to effect the formation of 1-bromo-1,2,3,4,5,6,7-heptamethylindene as adjudged by ^{1}H NMR spectroscopy. However, their combination with DBU typically led to inseparable mixtures of products of which the desired fulvene, **2.8**, was only a small fraction.

It was decided to revert to the reported synthesis, with a more recent update comprising the addition of trimethylamine to ensure completion,[28] and to return to the challenge of avoiding cyanogen bromide at a later date. It was noted that the reaction did not proceed if the less volatile THF was used in place of Et_2O, a change typically made by toll manufacturers.[29] Although some **2.8** was observed, significant quantities of **2.6** were also seen.

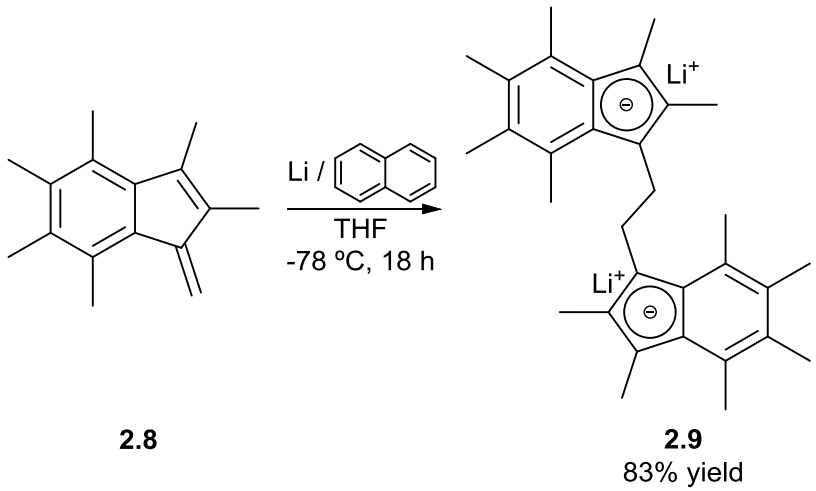


Scheme 2.13: suggested mechanism for the addition elimination reaction of BrCN. Alternative bases such as NEt_3 or DBU may replace the CN^- in the second step.

A slurry of **2.7** in Et_2O was cooled to −78 °C and the lachrymator, BrCN, was added quickly under a flush of N_2, effecting an immediate but subtle change in colour from a white suspension to a pale yellow. On warming to room temperature and stirring for a further 12 hours, the mixture had turned a dark red-brown. Addition of excess triethylamine by syringe caused an instantaneous change in colour to tan, and monitoring by ^{1}H NMR spectroscopy showed the reaction to be complete. The solvent was removed under reduced pressure and the residue extracted with hexane giving a dark yellow solution. On drying, **2.8** was collected as

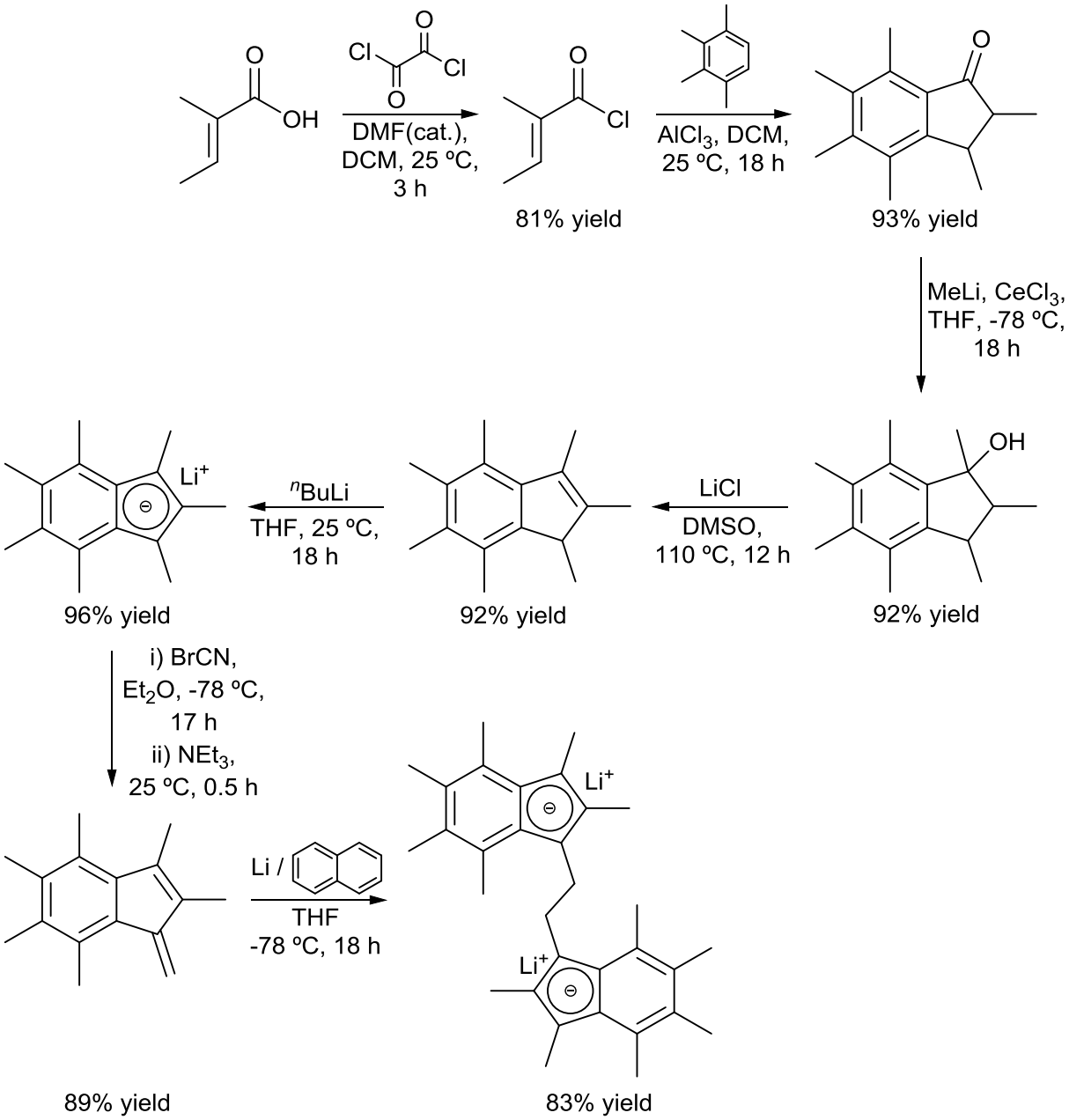
a bright yellow solid in 89% yield; a significant improvement on the previously reported 71%.

2.2.7 Synthesis of ethylenebis[1-(2,3,4,5,6,7-hexamethylindenide)] dilithium (2.9).



Scheme 2.14: synthesis of ethylenebis[1-(2,3,4,5,6,7-hexamethylindenide] dilithium (**2.9**).

The alkali-metal/naphthalenide-mediated reductive coupling of fulvenes reported by O'Hare and co-workers was employed for the synthesis of **2.9**, although a higher yield is reported here (83% as opposed to 76%).[7] The product was obtained as a THF adduct: EBI*Li_2·0.29THF. The completed procedure goes in overall 45% yield (or 56% from **2.3**) with well characterised intermediates (Scheme 2.15). It was noted that this final step is very effective when it works although empiricism suggested that this was only approximately half of the time. These failed reactions, despite no apparent changes to the experimental conditions, crystallised our thoughts to devise an improved procedure, without the need for hazardous chemicals such as BrCN which seemed unavoidable. Inspiration was taken from Alias *et al.* who reported the synthesis of hexamethylindene and subsequent attachment of a bridging moiety.[30]

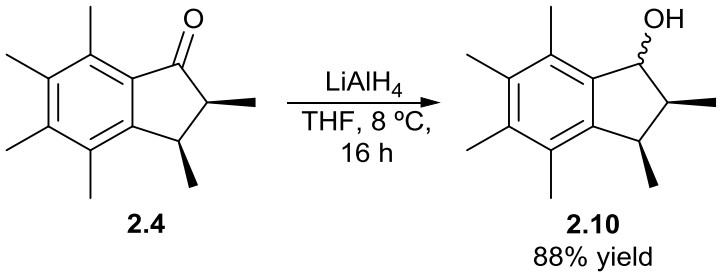


Scheme 2.15: revised synthesis of EBI*Li_2 *via* Ind*H.

2.3 A route to EBI*H_2 (2.13) from 2.4

While section 2.2 was successful in terms of the characterisation of intermediates and improved yields, a number of hazardous chemicals, including BrCN, were still required to bring about the synthesis of **2.9**. Section 2.3, details a new approach without the need for such hazardous and unreliable reagents, starting from **2.4**.

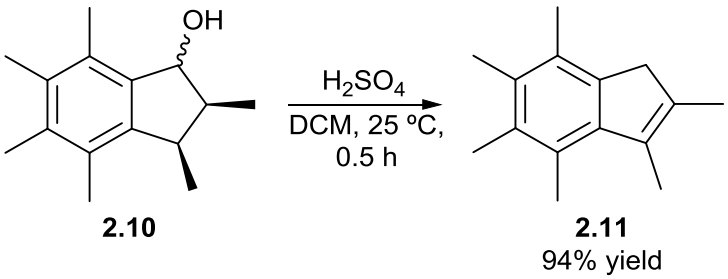
2.3.1 Synthesis of 2,3,4,5,6,7-hexamethylindan-1-ol (2.10)



Scheme 2.16: synthesis of 2,3,4,5,6,7-hexamethylindan-1-ol (**2.10**).

Attempts were made to replace the reported $LiAlH_4$ with the less reactive and more industrially suitable $NaBH_4$ but this did not react at all with the substrate, even upon heating. Solid $LiAlH_4$ was stirred in THF, cooled to 8 °C and to this a THF solution of **2.4** was added dropwise, causing an exotherm. The reaction was quenched after 16 hours and worked-up using dilute HCl, added to aid the separation of the layers. **2.10** was afforded as a pale yellow oil in 88% yield. Attempts to obtain crystals suitable for X-ray diffraction failed, despite the use of a spectrum of common laboratory solvents for the recrystallistion. The compound was observed, however, as an off-white solid following trituration with pentane.

2.3.2 Synthesis of 2,3,4,5,6,7-hexamethylindene (2.11)



Scheme 2.17: synthesis of 2,3,4,5,6,7-hexamethylindene (**2.11**).

Alias *et al*. reported the use of phosphoric acid for the synthesis of an alternative isomer of hexamethylindene with the two Cp methyl groups vinylic and allylic, in addition to a vinylic proton. **2.10** was dissolved in DCM at room temperature and conc. H_2SO_4 was added dropwise to the mixture causing it to turn first orange, then bright red. After 30 minutes, the mixture had turned an opaque dark red and was quenched by the slow addition of water. The product was dried from the organic layer and obtained as an off-white crystalline solid in 94% yield, improving the previously reported yield (81%).[30] The crystal **2.11** (Figure 2.6) grown by George Harris.[10] The procedure, using the temperature controlled reactor, is illustrated in Figure 2.7.

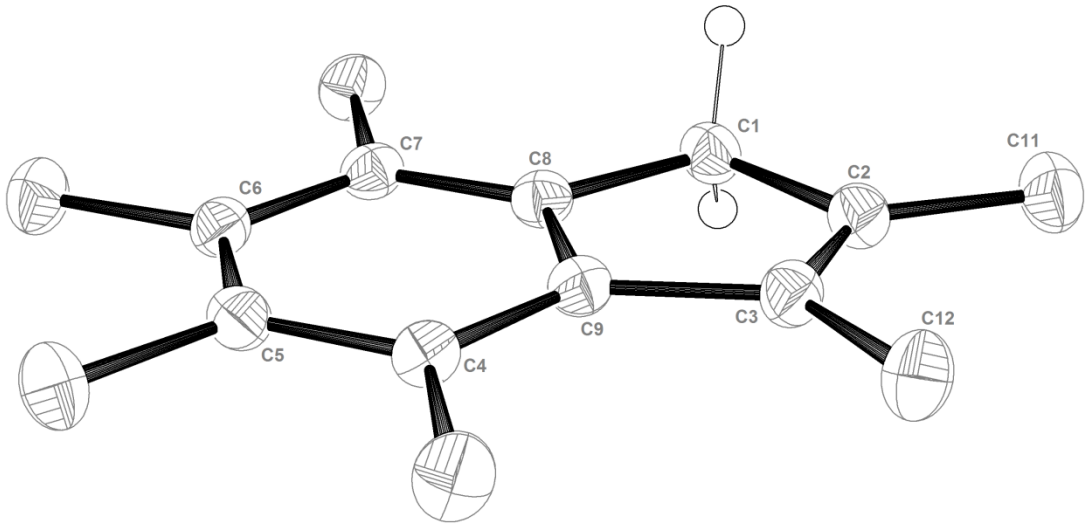


Figure 2.6: solid-state molecular structure of **2.11**. Methyl protons omitted for clarity. Thermal ellipsoids drawn at 50% probability. Crystal was grown by George Harris.

Table 2.4: selected bond lengths for **2.11**. ESDs in parentheses.

Bond Lengths (Å)			
C(1)-C(2)	1.504(2)	C(4)-C(9)	1.400(2)
C(2)-C(3)	1.352(2)	C(4)-C(5)	1.411(2)
C(3)-C(9)	1.492(2)	C(5)-C(6)	1.407(2)
C(8)-C(9)	1.405(2)	C(6)-C(7)	1.408(2)
C(1)-C(8)	1.498(2)	C(7)-C(8)	1.388(2)

2.11 crystallises in the monoclinic spacegroup $P2_1/c$, with one molecule in the asymmetric unit and four in the unit cell. As with **2.6** there is a localised double bond between C(2) and C(3) (1.352(2) Å) which is in good agreement with the value reported for **2.6** (1.324(6) Å).[10] The ring system is planar without any carbons atoms deviating significantly. The bond lengths in the benzene ring are not seen to alternate and C(3)-C(9) is not appreciably shortened from a single bond, suggesting that there is little conjugation of the π-electrons between the two delocalised systems.

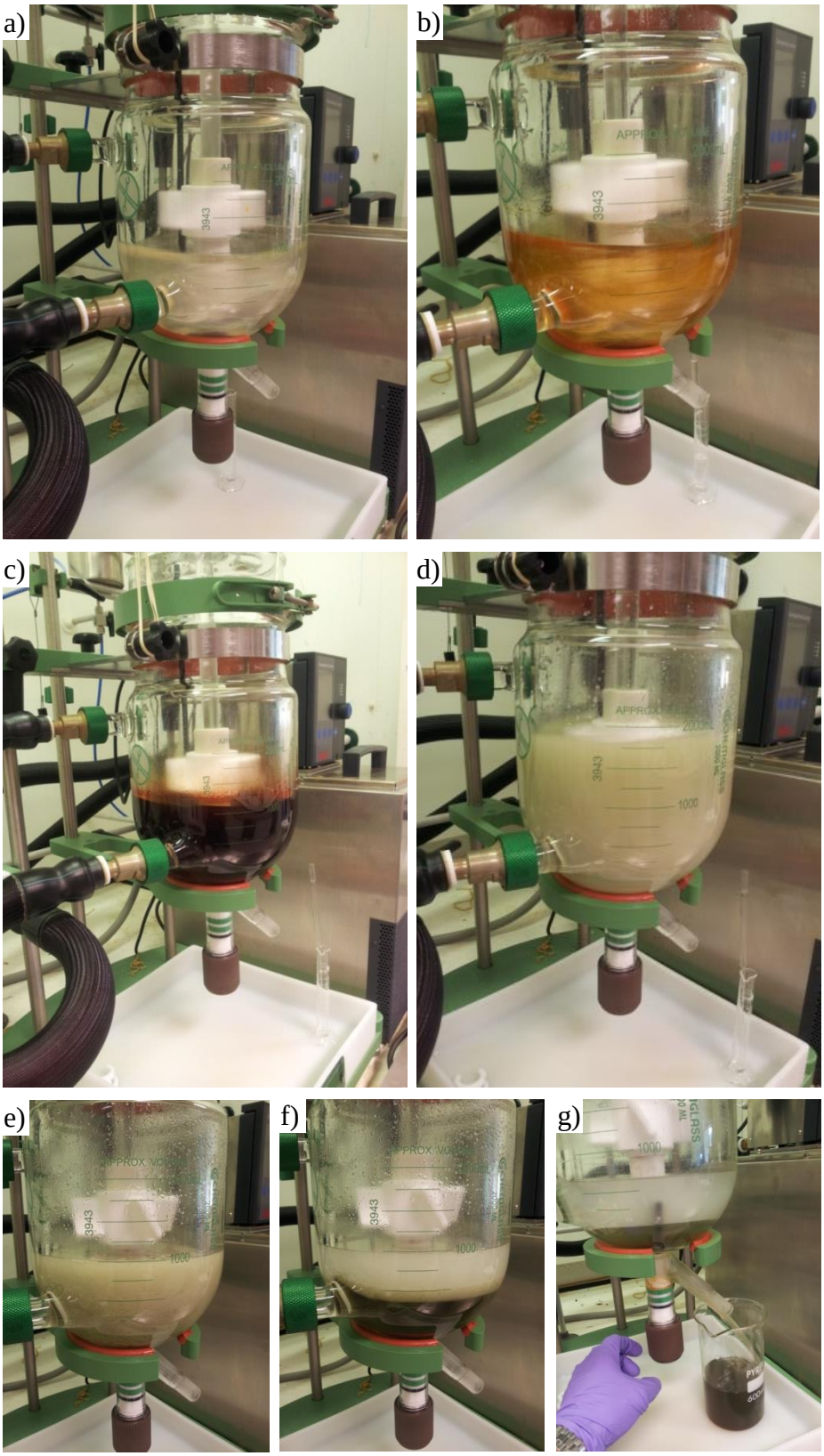


Figure 2.7: synthesis of **2.11** using the reactor. a) dissolution of **2.10** in DCM; b) dropwise addition of conc. H_2SO_4; c) stirring for 30 minutes; d) quenching with water; e) cessation of stirring; f) mixture allowed to settle for 10 seconds; g) mixture allowed to settle for 20 seconds and product decanted.

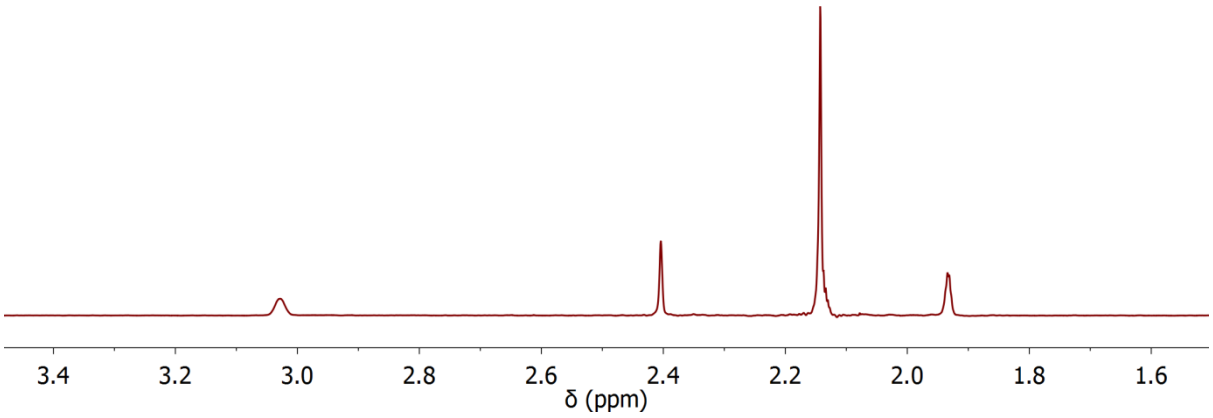
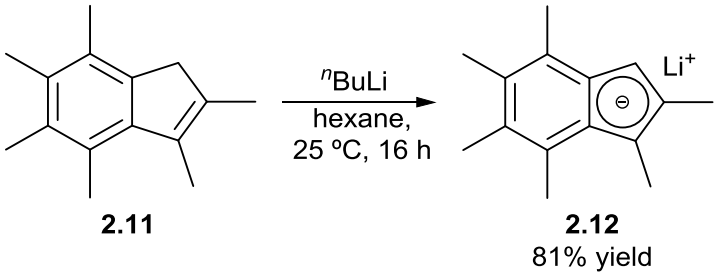


Figure 2.8: ^{1}H NMR spectrum of **2.11** in chloroform-d_1.

Naturally the ^{1}H NMR spectrum (Figure 2.8) of **2.11** differs significantly from that reported for the other regioisomer. All the seven resonances are singlets of intensity 2:3:3:3:3:3:3 although four of the methyl signals are coincident in chloroform-d_1 (2.24 ppm) with the allylic protons occurring at 3.13 ppm.

2.3.3 Synthesis of lithium 2,3,4,5,6,7-hexamethylindenide (2.12)



Scheme 2.18: synthesis of lithium 2,3,4,5,6,7-hexamethylindenide (**2.12**).

Previously **2.12** was synthesised using *n*-butyllithium and tetramethylethylenediamine (TMEDA) by Alias *et al.* It was decided to avoid TMEDA, and the reaction was found to proceed as described and the off-white product was precipitated from the reaction in 81% yield. Somewhat to our surprise given the nature of Ind*Li (**2.7**), **2.12** was found to be soluble in all common laboratory solvents including short-chain aliphatic hydrocarbons.

2.12 does not contain a C_2 axis (unlike **2.7**, *vide supra*) and therefore the ^{1}H NMR spectrum in pyridine-d_5 (Figure 2.9) comprises six methyl resonances (2.42-2.91 ppm), each with intensity three, and a singlet, corresponding to the Cp proton with an intensity of one (6.30 ppm).

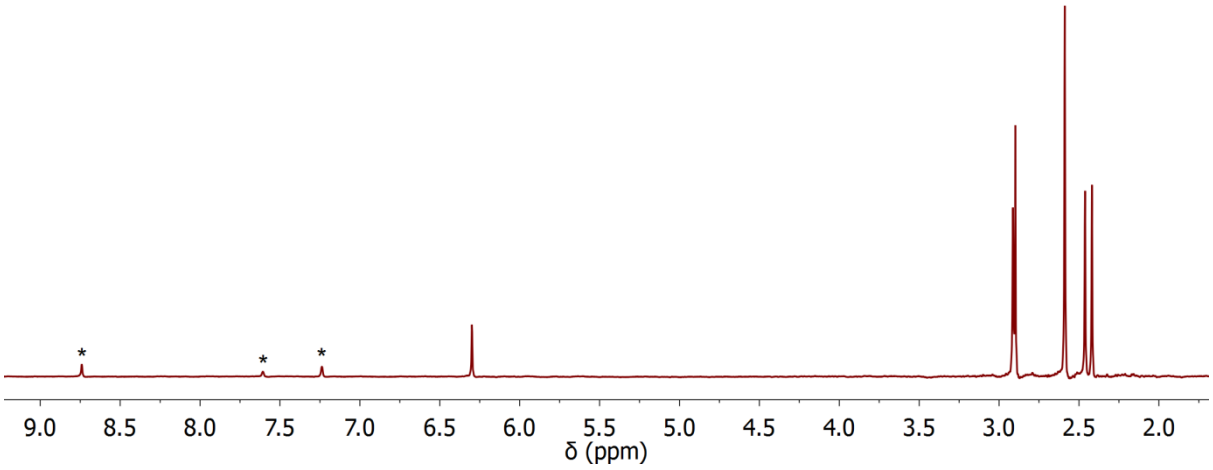
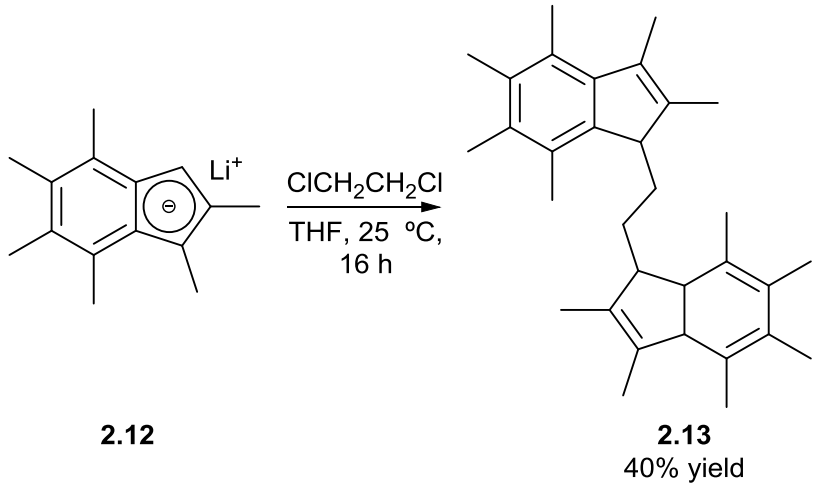


Figure 2.9: ^{1}H NMR spectrum of **2.12** in pyridine-d_5. Asterisks mark residual *protio*-solvent resonances.

2.3.4 Synthesis of ethylenebis[1-(2,3,4,5,6,7-hexamethylindene)] (2.13)



2.12 **2.13**
40% yield

Scheme 2.19: synthesis of ethylenebis[1-(2,3,4,5,6,7-hexamethylindene)] (**2.13**).

$SiCl_4$ was used for the synthesis of the bridged permethylindene in the 1997 paper and it was decided to mimic the procedure for the synthesis of EBI*H_2, **2.13** using 1,2-dichloroethane ($ClCH_2CH_2Cl$). A THF solution of $ClCH_2CH_2Cl$ was added, in a dropwise fashion, to a stirred orange solution of **2.12** in THF at room temperature. Care was taken to ensure that the dropwise addition of the ethylene dichloride was slow and that the solution of **2.12** was dilute (approximately 0.05 M), since this yielded the best results. The colour of the solution changed to a clear yellow and the reaction was left to stir for 15 hours, before drying *in vacuo*. Work-up afforded **2.13** as an off-white solid in 40% yield. This was the first bulk isolation of **2.13**, which had previously only been observed as a decomposition product.

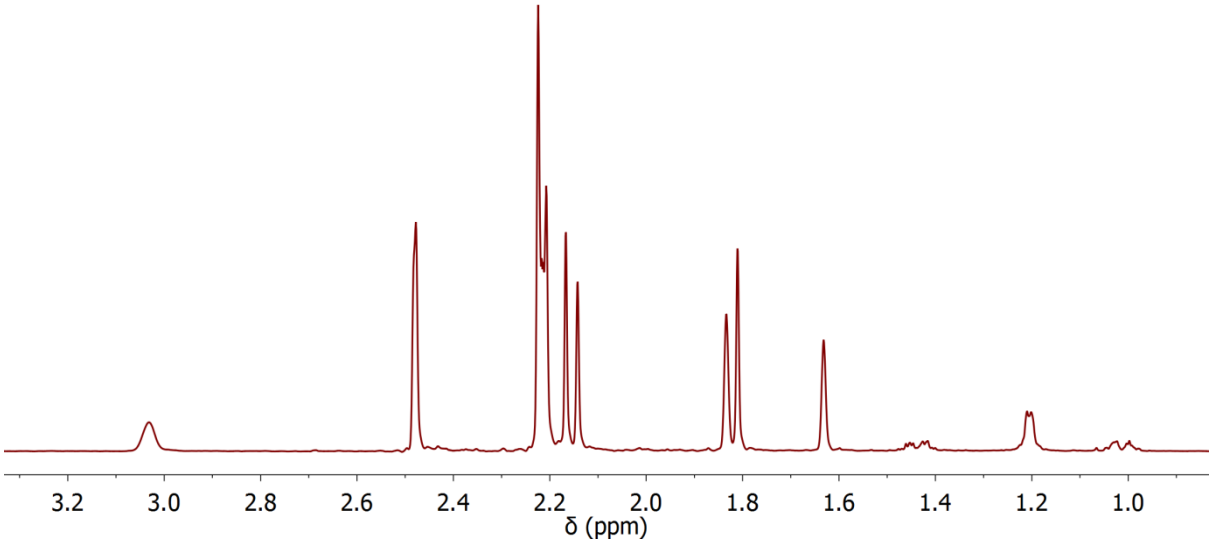
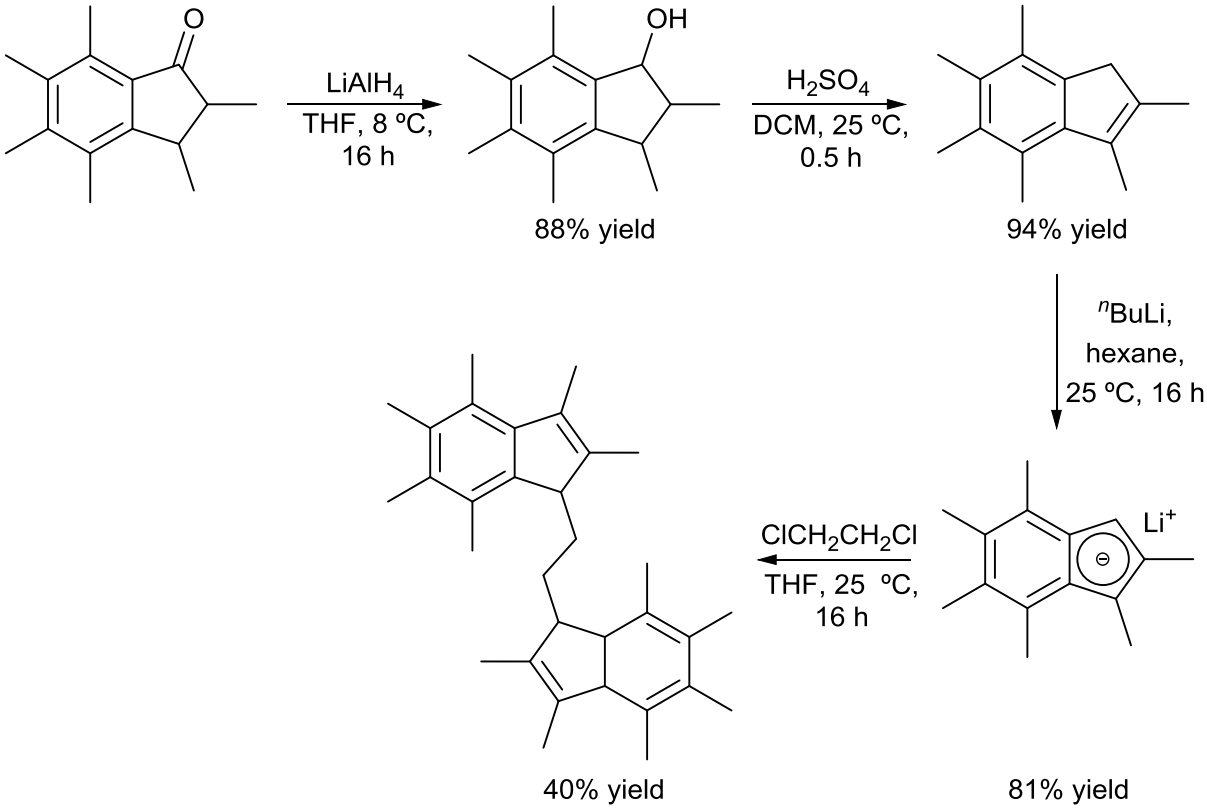


Figure 2.10: ^{1}H NMR spectrum of **2.13** in chloroform-d_1.

Figure 2.10 illustrates the ^{1}H NMR spectrum obtained for a 1:1 mixture of the *rac*- and *meso*- isomers of **2.13** in chloroform-d_1. The signals relating to the ethylene bridge can be found in the region from 1-1.5 ppm with a complex multiplicity. The rest of the spectrum, which occurs entirely between 1.6 and 3.1 ppm, comprises 12 singlets corresponding to each of the methyl groups, each isomer comprising two identical ring systems, and one broader singlet for the ring allylic protons which occur at nearly the same chemical shift. The spectrum is complicated slightly by the coincidence of a number of the methyl resonances which appear in the ratio 1:1:1:1:1:5:2. The isomers were not separated by fractional crystallisation.

Scheme 2.20 illustrates the whole synthetic procedure for **2.13** which represents an overall yield of 27% from the **2.4**. While this represents a decrease in yield from the synthetic route outlined in section 2.2, the reliability of the individual steps and the absence of toxic and hazardous chemicals favoured the new route.

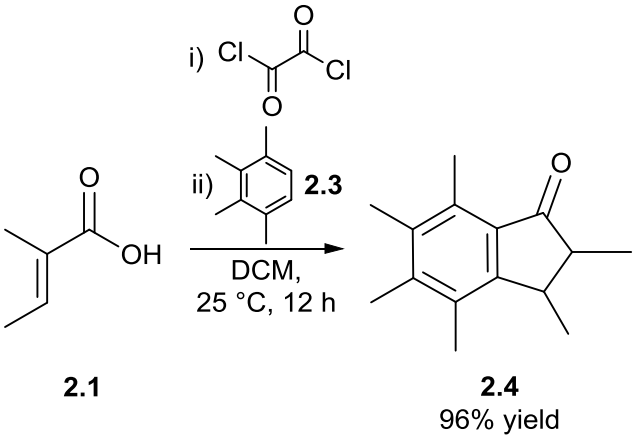


Scheme 2.20: revised synthesis of EBI*Li_2 *via* Ind$^{\#}$H.

2.4 An improved route in preparation for industrial scale-up

Section 2.3 and Scheme 2.20 describe the preparation of **2.13** from **2.4**. It was envisaged the a number of time-saving improvements could be made in order to ready the synthesis for use on an industrial scale.

2.4.1 Synthesis of 2,3,4,5,6,7-hexamethylindanone (2.4)



Scheme 2.21: synthesis of 2,3,4,5,6,7-hexamethylindanone (**2.4**) in a one-pot procedure from **2.1**.

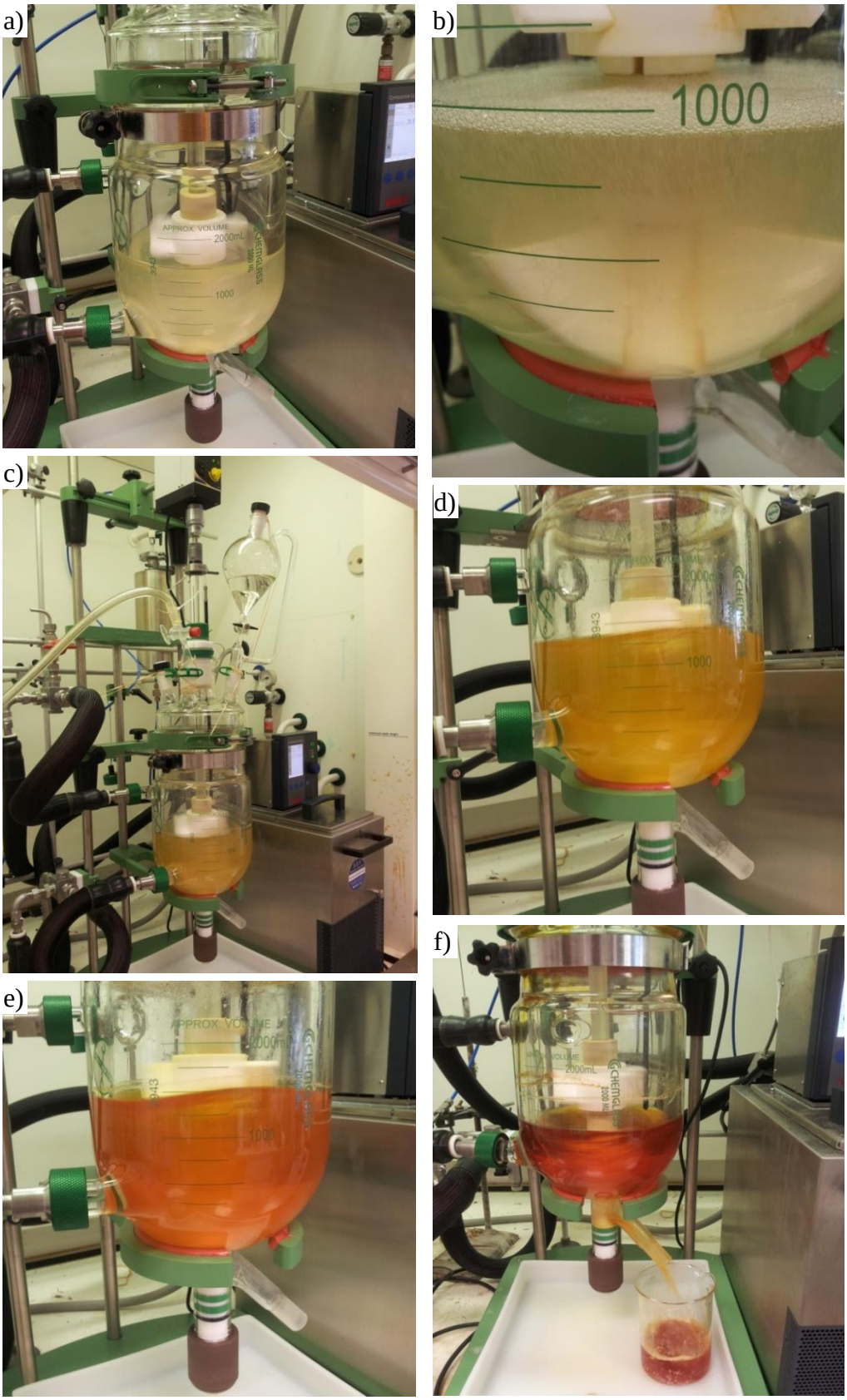


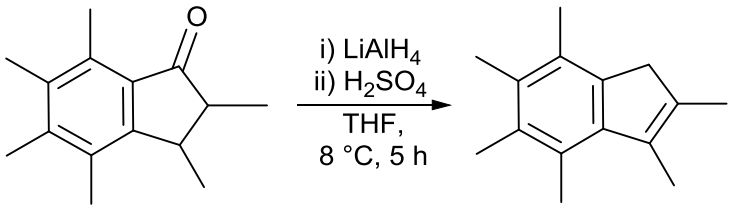
Figure 2.11: one-pot synthesis of **2.4** using the reactor. a) on immediate mixing of **2.1** and oxalyl chloride in DCM; b) effervescence on addition of four drops of DMF; c) use of an equilibrated addition funnel for addition of **2.3**; d) colour of solution after complete addition of **2.3**; e) colour of solution after stirring for one hour; f) final colour of solution.

Regular aliquots, taken during the chlorination of **2.1** and analysed by ^{1}H NMR spectroscopy, revealed that the reaction proceeds very quickly initially, being 50% complete within approximately an hour, and that the effervescence (of CO, CO_2 and HCl) ceases after approximately another hour. The complete procedure is illustrated in Figure 2.11.

As adjudged by ^{1}H NMR spectroscopy, the reaction never seems to reach completion, and is even observed to degrade to the starting material, **2.1**, if left for more than 12 hours. In addition, it was felt that any additional **2.1** left in the reaction mixture might help as an acid catalyst in the Friedel-Crafts acylation and that the reactions could therefore be combined. Both steps were already performed in the same solvent which eased the problem.

Equimolar reaction of **2.1** with oxalyl chloride in DCM with a drop of DMF as a catalyst was carried out. After five hours, the reaction was cooled to 8 °C, and finely powdered $AlCl_3$ was added to the mixture and the temperature was allowed to equilibrate. A DCM solution of **2.3** was slowly added to the mixture effecting a similar colour change to that seen previously, and after seven hours, the reaction was worked up as before (Section 2.2.2). **2.4** was obtained in a hugely improved yield of 96%.

2.4.2 Synthesis of 2,3,4,5,6,7-hexamethylindene (2.11)



2.4 **2.11**
98% yield

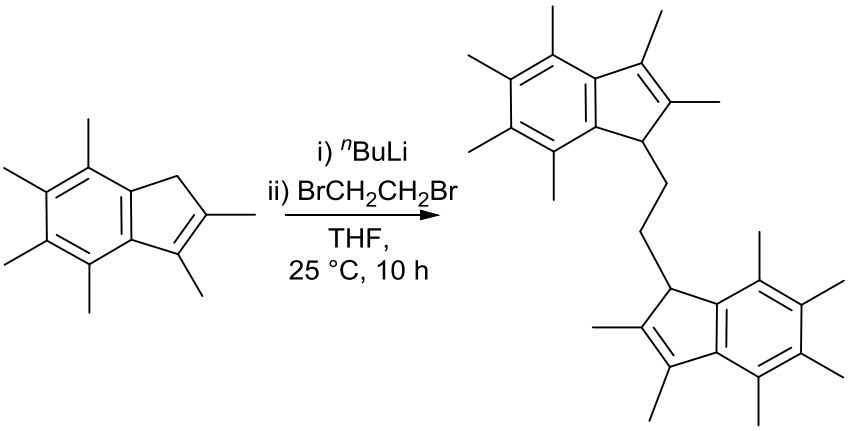
Scheme 2.22: synthesis of 2,3,4,5,6,7-hexamethylindene (**2.11**) in a one-pot procedure from **2.4**.

The reaction to generate **2.11** involved two steps and a change of solvent, meaning that it is more time-consuming and wasteful to carry out on an industrial scale. Two developments significantly changed our approach to this transformation: the use of a THF solution of $LiAlH_4$ (as opposed to a slurry) was found to have a far greater efficacy for the reduction of **2.4**, and the ability of conc. H_2SO_4 to effect the dehydration in THF. The new hydride source was able to complete the reduction of a large batch of **2.4** (*c*. 50 g) in only two hours. Tests revealed that the volume of conc. H_2SO_4 required to dehydrate **2.10** was significantly higher in miscible THF than in the biphasic mixture with DCM and that five equivalents was sufficient. It was also desirable to quench the remaining $LiAlH_4$ with a stoichiometric

quantity of H_2O to reduce the diluting effect of the excess and solvent volumes were kept to a minimum where possible.

$LiAlH_4$ (1.0 M in THF) was cooled to 8 °C and a THF solution of **2.4** was added and the mixure stirred at room temperature for four hours before careful quenching with a stoichiometric amount (calculated as 0.5 eq. $LiAlH_4$) of H_2O. Addition of conc. H_2SO_4, slowly at first and then more quickly, caused the pale reaction mixture to turn dark grey over the course of 30 minutes. The reaction was quenched with excess water and the product extracted with DCM, affording **2.11** as a brown oil in 98% yield.

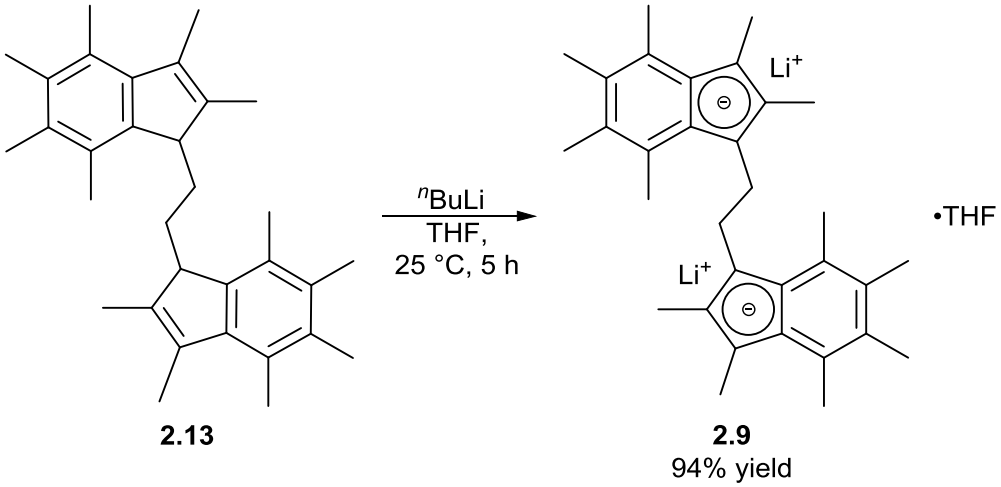
2.4.3 Synthesis of ethylenebis[1-(2,3,4,5,6,7-hexamethylindene)] (2.13)



Scheme 2.23: synthesis of ethylenebis[1-(2,3,4,5,6,7-hexamethylindene)] (**2.13**) in a one-pot procedure from **2.11**.

Combination of the final two steps from the previous procedure (Sections 2.3.3 and 2.3.4) and the introduction of 1,2-dibromoethane have led to an improvement in the overall yield of almost 40%. The absence of the lithium indenide isolation step greatly improves the efficiency of the process, which can now be completed in just ten hours, with the potential for further curtailment. **2.11** is dissolved in THF and a stoichiometric amount of ^{n}BuLi was added dropwise as before (Section 2.3.3). After six hours, $BrCH_2CH_2Br$ is slowly added and stirring is continued for a further two hours, by which time the reaction was deemed to be complete by ^{1}H NMR spectroscopy. **2.13** was obtained in 45% isolated yield as a white powder.

2.4.4 Synthesis of ethylenebis[1-(2,3,4,5,6,7-hexamethylindenide)] dilithium (2.9)

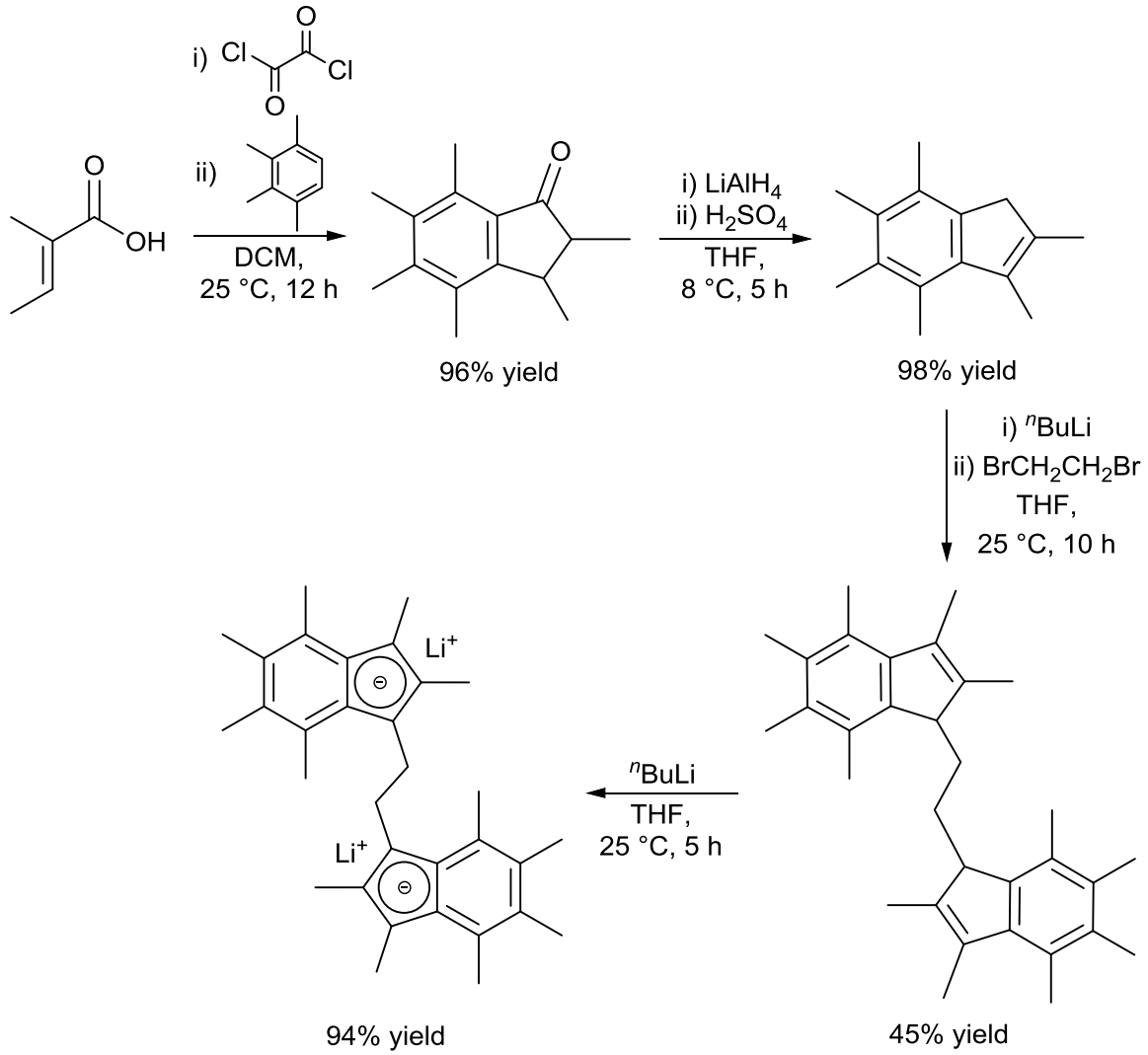


Scheme 2.24: synthesis of ethylenebis[1-(2,3,4,5,6,7-hexamethylindenide)] dilithium (**2.9**).

Remarkably, crystalline **2.13**, is completely insoluble in all common solvents rendering it untransformable. Even in its micro-crystalline or powdered form, it is only very weakly soluble, with DCM or chloroform being most amenable.

A slurry of **2.13** in THF was treated with *n*-butyllithium, causing a slight exotherm and all of the substrate to dissolve, forming a pale green solution. After approximately one hour, a precipitate is seen to form, comprising pure **2.9** in a 94% yield with one bound THF (*vide supra*).

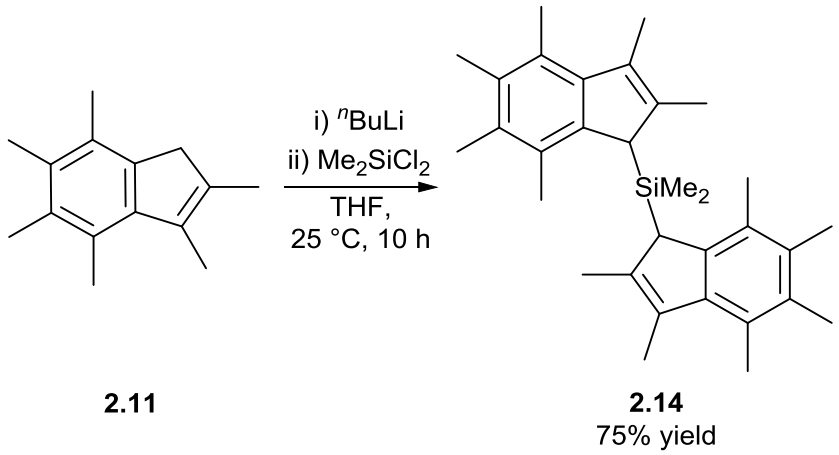
A comparison of this shortened and updated route with its direct predecessor makes for enjoyable reading as all the stages have been improved quite dramatically (Scheme 2.25). A total overall yield to **2.9** of 40% is only slightly lower than the mercurial route *via* Ind*H, and its reliability, ease, speed and scaleability make its use preferable. With the appropriate starting materials in place, the new procedure means that **2.9** could be prepared on a 12 g scale in 36 hours of real lab time, whereas the previously reported route would take at least a week. This procedure was submitted for patent protection in November 2014.[31] In addition to the aforementioned benefits, the ability to vary the bridge represents a great advantage in chemistry as sensitive to subtle steric and electronic changes as that of ethylene polymerisation catalysis.



Scheme 2.25: synthesis of EBI*Li_2 *via* $Ind^{\#}H$ modified to a four step procedure proceeding in an overall 40% yield.

2.5 Ligand variations

2.5.1 Synthesis of dimethylsilylbis[1-(2,3,4,5,6,7-hexamethylindene)] (2.14)



Scheme 2.26: synthesis of dimethylsilylbis(1-(2,3,4,5,6,7-hexamethylindene) (**2.14**).

Given the success had by Alias *et al.* with **2.14**, SBI*H_2, with its facile metalation,[30] it was decided to pursue it as a ligand for group 4 metals. Given the ready availability of dimethyldichlorosilane, this was chosen as a suitable reagent with which to form the bridge.

As in Section 2.4.3, **2.11** was reacted with ^{n}BuLi in THF for six hours at room temperature before the slow addition of the Me_2SiCl_2. Again care was taken to ensure that the dichloride was added slowly and that the solution was dilute to ensure good results. A white solid was obtained on extraction of the solid with toluene and subsequent removal of solvent *in vacuo*. **2.14** was obtained in 75% yield and was found to comprise an 1:1 mixture of *rac*- and *meso*-isomers (as determined by ^{1}H NMR spectroscopy). As with **2.12** these were not routinely separated as they form a single isomer on lithiation. A suitable single crystal of ***rac*-2.14** for X-ray diffraction was obtained by Dr. Jean-Charles Buffet *via* recrystallisation from hexane at 5 °C.

***rac*-2.14** crystallises in the triclinic spacegroup $P\bar{1}$, with one molecule in the asymmetric unit and two in the unit cell. The two molecules in the unit cell are enantiomers of one another and Figure 2.12 shows the *S,S*-isomer. While crystallographically distinct, the two ring systems are chemically identical, both displaying localised double bonds in the five membered ring with bond lengths 1.347(6) and 1.341(6) Å. This compares well with that reported for the parent indene, **2.11**: 1.352(2) Å, as do the rest of the structural parameters. No bond length alternation is observed within the benzene ring and the average ring bond length is intermediate between the localised double bond and the C-C single bonds.

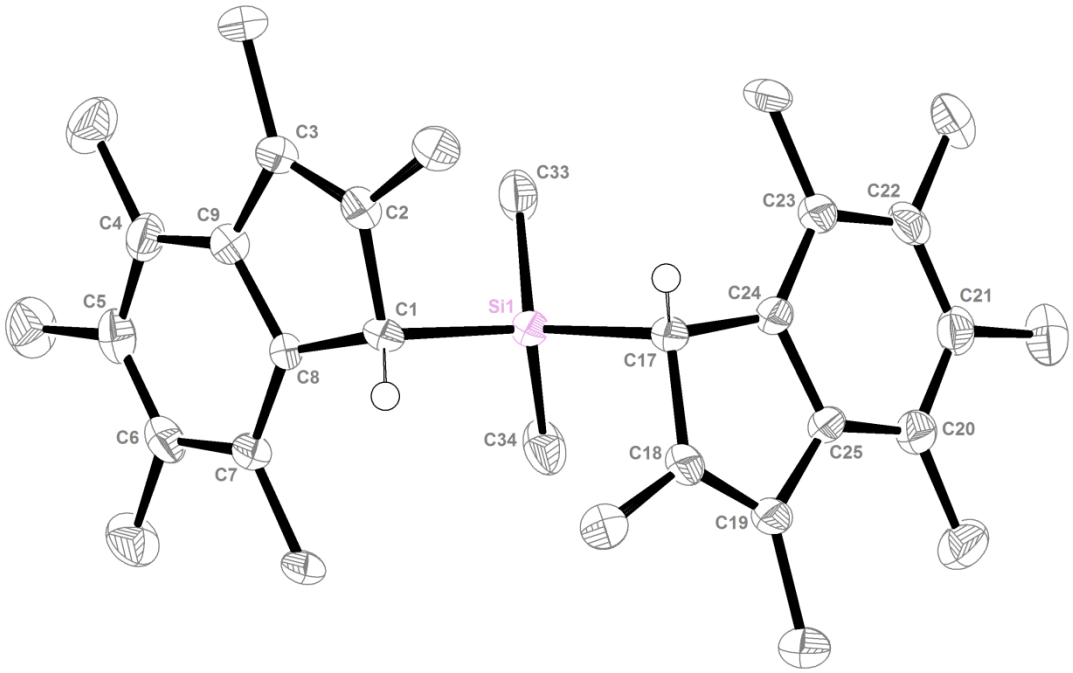


Figure 2.12: solid-state molecular structure of (*S*,*S*)-***rac*-2.14**. Methyl protons omitted for clarity. Thermal ellipsoids drawn at 50% probability.

Table 2.5: selected bond lengths and angles for ***rac*-2.14**. ESDs in parentheses.

Bond Lengths (Å)			
C(1)-C(2)	1.502(5)	C(17)-C(18)	1.500(6)
C(2)-C(3)	1.347(6)	C(18)-C(19)	1.341(6)
C(3)-C(9)	1.477(6)	C(19)-C(25)	1.492(6)
C(8)-C(9)	1.410(5)	C(24)-C(25)	1.410(6)
C(1)-C(8)	1.510(6)	C(17)-C(24)	1.498(5)
C(4)-C(9)	1.406(6)	C(20)-C(25)	1.404(6)
C(4)-C(5)	1.407(6)	C(20)-C(21)	1.406(7)
C(5)-C(6)	1.416(6)	C(21)-C(22)	1.391(7)
C(6)-C(7)	1.399(6)	C(22)-C(23)	1.413(6)
C(7)-C(8)	1.395(6)	C(23)-C(24)	1.400(6)
C(1)-Si(1)	1.937(4)	C(17)-Si(1)	1.941(4)
Si(1)-C(33)	1.876(5)	Si(1)-C(34)	1.864(5)
Bond Angles (°)			
C(1)-Si(1)-C(17)	110.69(18)	C(33)-Si(1)-C(34)	106.3(2)

C(1), C(17) and Si(1) are tetrahedral. Due to the bulk of the substituted indenyl rings, the C(1)-Si(1)-C(17) bond angle (110.69(18)°) is greater than that between the two methyls,

C(33)-Si(1)-C(34) (106.3(2)°), but this effect is only marginal. The Si-Ind bond lengths (1.937(4) and 1.941(4) Å) agree well with those of SBIZr(O-2,6-$Me_2C_6H_3$)Cl (1.876 Å), although they are slightly lengthened to account for the increased bulk of the permethylated ligand.[32]

As is clearly illustrated in the solid-state structure of ***rac*-2.14** (Figure 2.12), the two silicon methyl groups, C(33) and C(34), are in equivalent environments and this is replicated in the solution-phase (Figure 2.13). ^{1}H NMR spectroscopy in chloroform-d_1 shows only one methyl resonance with intensity six at −0.59 ppm. This is also noted for the ring systems which are not duplicated, as in **2.13** (*vide supra*), but appear in the same environment with six ring methyl resonances (2.16-2.52 ppm), each intensity six, and one proton resonance of intensity two (3.71 ppm).

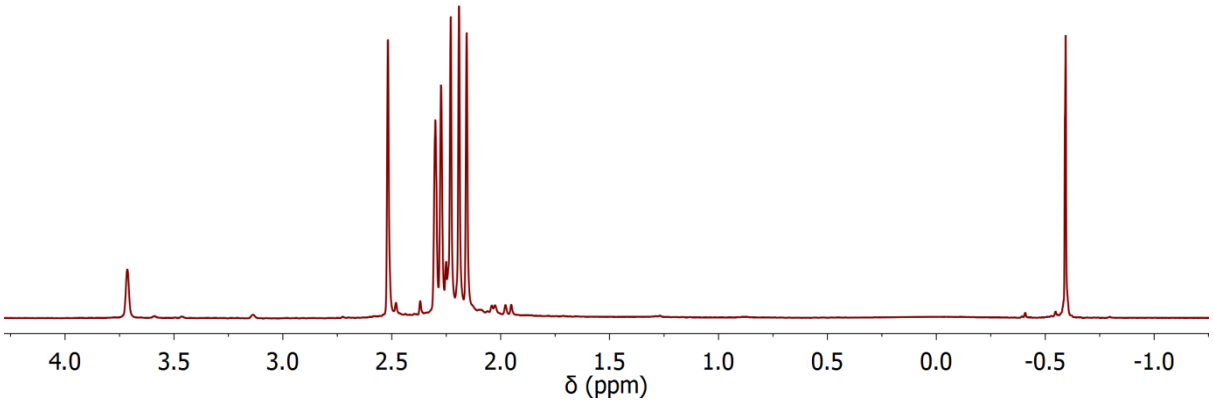
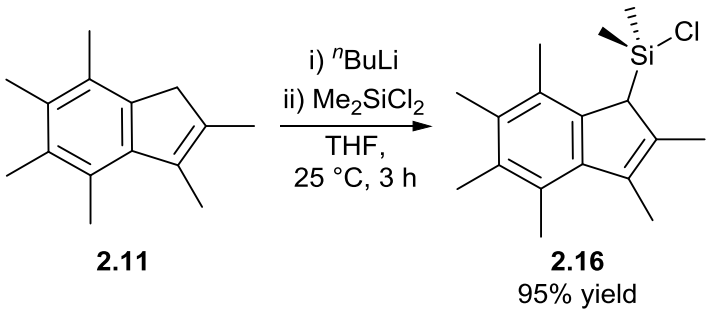


Figure 2.13: ^{1}H NMR spectrum of ***rac*-2.14** in chloroform-d_1.

2.5.2 Synthesis of dimethylsilyl[1-(2,3,4,5,6,7-hexamethylindene)]chloride (2.16)

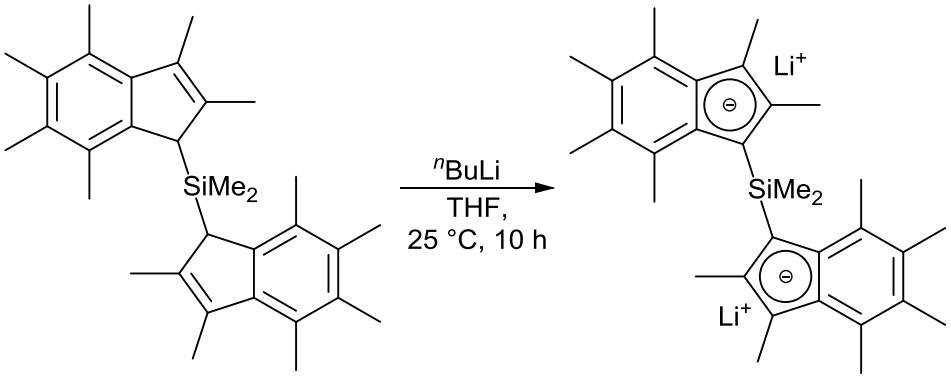


Scheme 2.27: synthesis of dimethylsilyl(1-(2,3,4,5,6,7-hexamethylindene))chloride (**2.16**).

In an attempt to improve the yield of **2.14**, it was decided to add the indenyl rings sequentially, and the intermediate **2.16** was synthesized. While the reaction of **2.16** with a further equivalent of **2.12** does work, it has no augmentative effect upon the final yield of **2.14** and a deleterious effect on the reaction time. With the exception of changing the reaction

time and stoichiometry, increasing the equivalents of the silane to five, the reaction conditions were unchanged from Section 2.5.1. It was, however, noted that **2.16** offered a pathway to mixed-ring systems.

2.5.3 Synthesis of dimethylsiliconbis[1-(2,3,4,5,6,7-hexamethylindenide] dilithium (2.15)

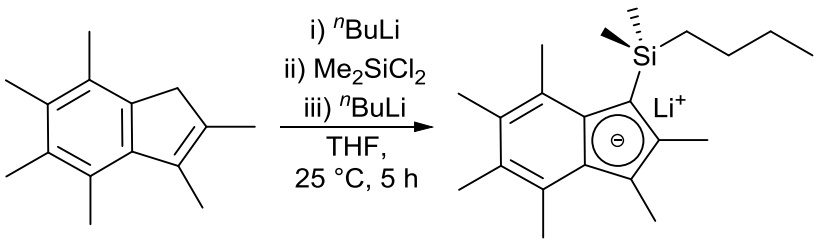


2.14 **2.15** 68% yield

Scheme 2.28: synthesis of dimethylsiliconbis(1-(2,3,4,5,6,7-hexamethylindenide) dilithium (**2.15**)

This lithiation proceeded much as described by Alias *et al*. with the omission of TMEDA. Although some changes were noted in the solubility regime, as described for EBI*Li_2 (*vide supra*), some ligand degradation was also observed with unbridged indenyl fragements noted in the ^{1}H NMR spectrum, accounting for the surprisingly low isolated yield for this facile transformation.

2.5.4 Synthesis of lithium *n*-butyldimethylsilicon(1-(2,3,4,5,6,7-hexamethylindenide) (2.17)



2.11 **2.17** 83% yield

Scheme 2.29: synthesis of lithium *n*-butyldimethylsilicon(1-(2,3,4,5,6,7-hexamethylindenide) (**2.17**).

In an attempt to decrease the reaction time required to synthesise **2.15** (and concomitantly **2.14**), and remove an extra work-up step, it was attempted to carry out the whole procedure

from **2.11**. However, **2.12** (formed *in situ*) had incompletely reacted with the dimethylchlorosilane forming **2.16** (*vide infra*). On addition of two equivalents of *n*-butyllithium, not only was the ring deprotonated but the chloride was replaced by a butyl chain, giving **2.17**. Further investigation led to the isolation of the *protio*-congener, HInd$^{\#}$SiMe$_2$^{n}Bu, **2.18**. While not quite an anticipated result, it was hoped that **2.17** might prove a suitable ligand for group 4 metals, and a potential backbone to a highly active ethylene polymerisation catalyst.

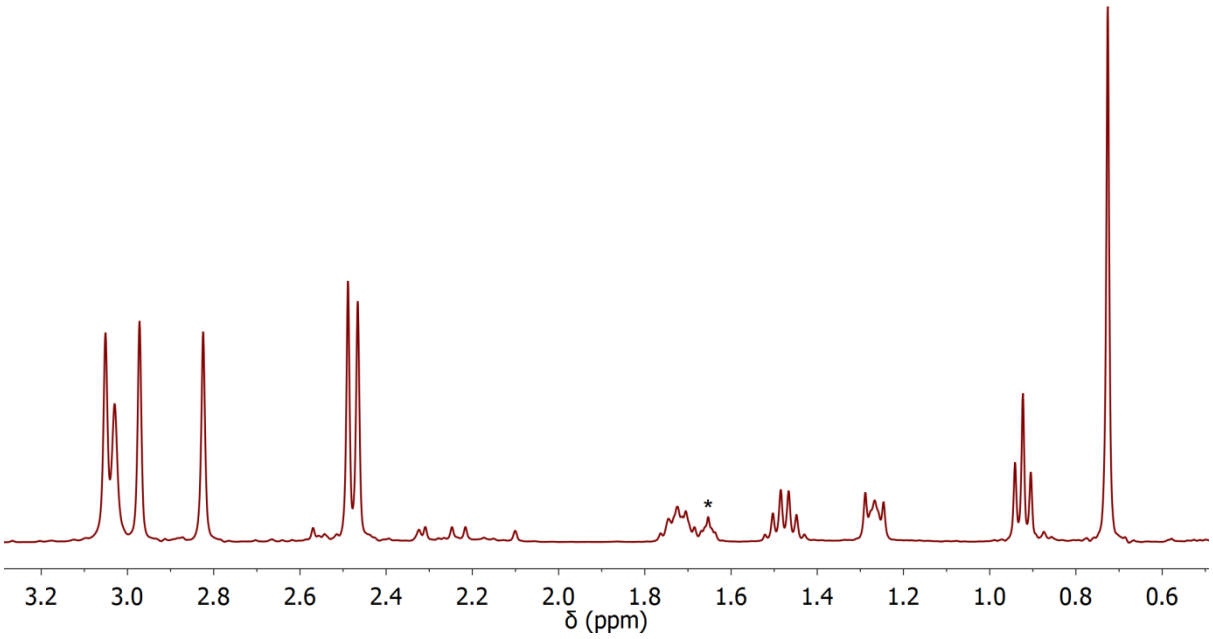


Figure 2.14: ^{1}H NMR spectrum of **2.17** in pyridine-d_5. The asterisk denotes residual THF.

The ^{1}H NMR spectrum of **2.17** in pyridine-d_5 (Figure 2.14) revealed intricate multiplicities as might be expected from a butyl chain. The "methyl region" of approximately 2.4-3.1 ppm reveals the six distinct ring methyl groups. A singlet at 0.73 ppm, with intensity six, is attributed to the silicon methyl groups. A distinct triplet at 0.92 ppm corresponds to the butyl terminal CH_3, while the three multiplets at 1.27, 1.47 and 1.72 ppm are attributed to the methylene groups α, γ and β to the silicon respectively, verified by 2-D NMR spectroscopic experiments.

2.6 Conclusions

Chapter Two describes the successful update of three permethylindenyl ligand syntheses in addition to four complexes not previously described and five compounds not previously isolated or characterised. In the vast majority of cases, not only were potentially hazardous or undesirable chemicals removed, but the yields were significantly improved and the number of

stages required greatly diminished. The reliability of the new synthetic routes means any resultant complexes are viable for industry. The procedures described have been submitted for patent approval, and are currently in industrial scale-up with a variety of toll manufacturers.

2.7 References

(1) Miyamoto, T. K.; Tsutsui, M.; Chen, L.-B. *Chem. Lett.* **1981**, 729.
(2) Tsutsui, M.; Chen, L. B.; Bergbreiter, D. E.; Miyamoto, T. K. *J. Am. Chem. Soc.* **1982**, *104*, 855.
(3) Westcott, S. A.; Kakkar, A. K.; Stringer, G.; Taylor, N. J.; Marder, T. B. *J. Organomet. Chem.* **1990**, *394*, 777.
(4) Kakkar, A. K.; Jones, S. F.; Taylor, N. J.; Collins, S.; Marder, T. B. *J. Chem. Soc. Chem. Commun.* **1989**, 1454.
(5) Kakkar, A. K.; Taylor, N. J.; Marder, T. B.; Shen, J. K.; Hallinan, N.; Basolo, F. *Inorg. Chim. Acta* **1992**, *198-200*, 219.
(6) O'Hare, D.; Green, J. C.; Marder, T.; Collins, S.; Stringer, G.; Kakkar, A. K.; Kaltsoyannis, N.; Kuhn, A.; Lewis, R. *Organometallics* **1992**, *11*, 48.
(7) Ransom, P.; Ashley, A.; Thompson, A.; O'Hare, D. *J. Organomet. Chem.* **2009**, *694*, 1059.
(8) Ransom, P.; Ashley, A. E.; O'Hare, D. Catalysts. WO2011/051705 A1, **2011**.
(9) Alfa Aesar, Cat No. L19756.
(10) Harris, G. R. *Part II Thesis*, University of Oxford, **2012**.
(11) Snider, B. B.; Che, Q. *Org. Lett.* **2004**, *6*, 2877.
(12) Nazarov, I. N.; Zaretskaya, I. I. *Izv. Akad. Nauk. SSSR, Ser. Khim* **1941**, 211.
(13) Marino, J. P.; Linderman, R. J. *J. Org. Chem.* **1981**, *46*, 3696.
(14) Frontier, A. J.; Collison, C. *Tetrahedron* **2005**, *61*, 7577.
(15) Ashley, A. E.; Cowley, A. R.; O'Hare, D. *Eur. J. Org. Chem.* **2007**, *2007*, 2239.
(16) Murphy, V. J. *D.Phil. Thesis*, University of Oxford, **1993**.
(17) Quast, H.; Carlsen, J.; Herkert, T.; Janiak, R.; Röschert, H.; Peters, E.-M.; Peters, K.; von Schnering, H. G. *Liebigs Ann. Chem.* **1992**, *1992*, 495.
(18) Beckmann, E.; Bahr, N.; Cullmann, O.; Yang, F.; Kegel, M.; Vögtle, M.; Exner, K.; Keller, M.; Knothe, L.; Prinzbach, H. *Eur. J. Org. Chem.* **2003**, *2003*, 4248.
(19) Ashley, A. E. *D.Phil. Thesis*, University of Oxford, **2006**.
(20) Imamoto, T.; Sugiura, Y.; Takiyama, N. *Tet. Lett.* **1984**, *25*, 4233.
(21) Imamoto, T.; Takiyama, N.; Nakamura, K.; Hatajima, T.; Kamiya, Y. *J. Am. Chem. Soc.* **1989**, *111*, 4392.
(22) Dimitrov, V.; Kostova, K.; Genov, M. *Tetrahedron Lett.* **1996**, *37*, 6787.
(23) Traynelis, V. J.; Hergenrother, W. L.; Livingston, J. R.; Valicenti, J. A. *J. Org. Chem.* **1962**, *27*, 2377.
(24) Traynelis, V. J.; Hergenrother, W. L.; Hanson, H. T.; Valicenti, J. A. *J. Org. Chem.* **1964**, *29*, 123.
(25) Enders, M.; Ludwig, G.; Pritzkow, H. *Organometallics* **2001**, *20*, 827.
(26) Jakob, A.; Ecorchard, P.; Rüffer, T.; Linseis, M.; Winter, R. F.; Lang, H. *J. Organomet. Chem.* **2009**, *694*, 3542.
(27) O'Hare, D.; Murphy, V.; Diamond, G. M.; Arnold, P.; Mountford, P. *Organometallics* **1994**, *13*, 4689.
(28) Ransom, P. *D.Phil. Thesis*, University of Oxford, **2009**.

(29) Mayalarp, S. Private Communication.
(30) Alias, F. M.; Barlow, S.; Tudor, J. S.; O'Hare, D.; Perry, R. T.; Nelson, J. M.; Manners, I. *J. Organomet. Chem.* **1997**, *528*, 47.
(31) Buffet, J.-C.; Arnold, T. A. Q.; Mayalarp, S.; O'Hare, D. Optimised indenyl ligand synthesis. Application No: 1410202, **2014**.
(32) Buffet, J.-C.; Arnold, T. A. Q. Unpublished results.

Chapter Three

Synthesis of Group 4 Indenyl Complexes

3.1 Introduction

As described in Chapter One, group 4 metallocenes have a long history stretching back to 1954.[1] As highlighted in section 1.1.6, zirconocenes have recently been investigated for many reasons including N_2 binding,[2] as FLPs capable of activating small molecules such as CO_2 and H_2,[3–5] and their ability to form isolable high-hapticity indenyl complexes.[6] Nevertheless, the primary reason for the continued investigation into the d^0 metallocenes of group 4 has remained their activity in olefin polymerisation, providing the basis for a unique, mutually beneficial collaboration with industry. This chapter seeks to build upon the publication by O'Hare and co-workers of a variety of methylated indenyl group 4 complexes to build a library of polymerisation catalysts.[7,8] The aim is to report new complexes, both based on previously synthesised ligands and those developed in Chapter Two, and to characterise those compounds fully so as to understand their interaction in the solid- and solution-states.

3.2 Definitions of structural parameters

The indenyl rings in this work will be labelled according to the following rules (Figure 3.1). A subsequent, distinct indenyl ring will continue the same pattern starting from C(17).

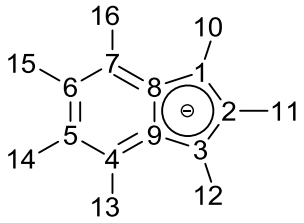


Figure 3.1: labelling scheme for the first indenyl ring.

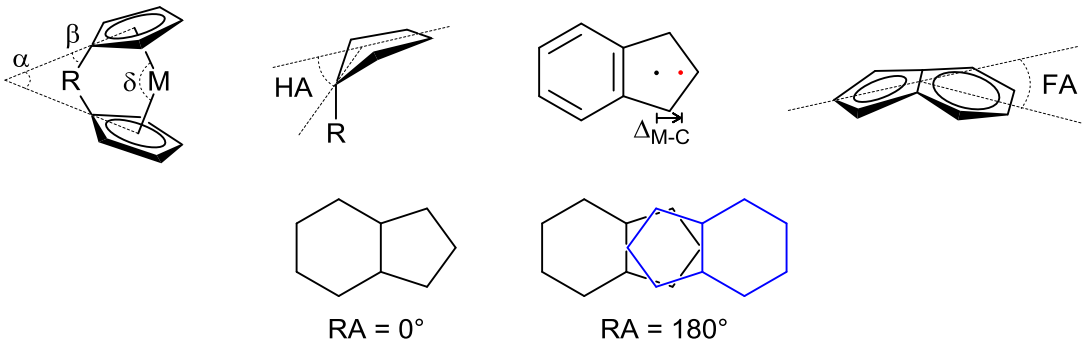


Figure 3.2: a variety of structural parameters used throughout this chapter.

While some of the more common structural parameters have been briefly outlined in sections 1.1.4 and 1.1.5, they are described here in more detail (Figure 3.2).

Perhaps the most discussed parameter for group 4 metallocenes is α, a measure of the tilt between the two cyclopentadienyl rings. This parameter is measured as the dihedral angle between two planes, each calculated as the least squares mean of the five atoms comprising the Cp ring. For a perfectly tetrahedral metal centre, a value of 70.53° is expected. Angles smaller than this indicate a lesser degree of ring tilt, such as in zirconocene or titanocene dichloride (53.46 and 51.58° respectively), and *vice versa*.[9] A closely related angle is that of δ, which is the angle subtended at the metal centre by the normal of the two ring planes. Consequently, it is expected to be the supplementary angle to α; 109.47° for a perfect tetrahedral structure. In practice, it is measured in this work as the angle subtended at the metal centre by the two metal centroids. Any deviation between this angle (sometimes referred to elsewhere as β) and δ can indicate a degree of ring slippage; this is not expected to be significant in the d^0 metallocenes.[10] For Cp_2MCl_2 (M = Zr, Ti), δ is calculated as 129.03 and 130.72° respectively displaying little deviation from the expected values.

β, as used in this text and elsewhere,[11] measures the angle between the first bridging atom and the plane of the Cp ring, and is used as another indicator of the strain placed on the ring by the *ansa*-bridge. While some examples display values of 30° or more, it is typically much lower than this for multi-atomic bridges. In this work, it is measured as the angle subtended at C(1) by the nearest bridging atom, Si(1) or C(10), and the Cp_{cent}. With small values for β (<7°), its significance can largely be ignored, as the direction of the bend can be away from the metal centre.

The hinge angle (HA) can be used to describe two effects, depending on where the hinge is defined. Seen more for late transition metal indenyl chemistry, it can quantify folding in the Cp ring to accommodate a change in hapticity from η^5 to η^3 – this typically takes place at the 2-position, across the C(1)-C(3) line.[12] In this thesis, and in other works pertaining to the chemistry of *ansa*-metallocenes, it quantifies the Cp ring folding induced by the strain of the bridge and is normally seen at C(1). It is calculated as the dihedral angle between the mean planes calculated from C(1), C(2), C(8) and C(2), C(3), C(8), C(9). A related parameter is the fold angle (FA), which defines the dihedral angle between the planes of the benzene and cyclopentadiene rings, along the C(8)-C(9) ring annulation. This parameter can indicate interaction with the delocalised π-system of the arene, used to stabilise electronically

deficient complexes, with values as high as 37.62° observed for the η^9 bis(indenyl) zirconocene reported by Bradley *et al.*[6]

$\Delta_{M\text{-}C}$, also called the ring-slip parameter, is a measure of how far the metal distorts from η^5 bonding towards η^3 and is a good quantifier of the "indenyl effect". It is measured in angstroms and is calculated using Equation 3.1 where C(#) = M-C(#).

$$\Delta_{M-C} = \left\{\frac{C(8) + C(9)}{2}\right\} - \left\{\frac{C(1) + C(2) + C(3)}{3}\right\}$$

Equation 3.1: definition of $\Delta_{M\text{-}C}$.

The rotation angle (RA), and the torsion angle (TA and TA′) all measure the twist of the two indenyl rings relative to one another with 0° being eclipsed, 180° being staggered and anything in between gauche. However, all three parameters are calculated in different ways. RA is the most prevalent, and is calculated as the dihedral angle between two planes, each containing M(1). While a very apt measure for co-planar metallocenes, its use is ill-judged for the bent-metallocenes of the early TMs as it comprises a significant component of α and the two are impossible to disentangle. A much better measure is TA, which measures the torsion angle: C(2)-Cp_{cent}-Cp_{cent}-C(18), first introduced by Calhorda *et al.*[12] This has been adapted in this work to TA′ [C(11)-C(2)-C(18)-C(27)] for ease of measurement and clarity, given the abundance of methyl groups, but it retains the elegance and advantages of its predecessor and negates the effect of α.

3.3 Metallation improvements

3.3.1 Protonolysis

One of the biggest advantages of the new synthetic route to bridged permethylindenyl derivatives (section 2.4), is the large scale synthesis of the pro-ligand bearing comparatively acidic protons. Given the low yields reported for the transformation of EBI*Li_2 to EBI*$ZrCl_2$ *via* salt metathesis,[8] it was anticipated that protonolysis of EBI*H_2 could effect a similar transformation.[13] There is significant precedent for the use of such moieties in the literature; Diamond *et al*. reported the use of zirconium amides for the transformation of the related $EBIH_2$ to EBIZr$(NMe_2)_2$.[14] Moreover, the advantage of these reagents, as discussed in section 1.1.5.4, is that they selectively form the *rac*-isomer as the thermodynamic product, reducing the need for wasteful isolation procedures. Alternative methods also exist for preferentially synthesising the *rac*-isomer, but typically require sterically bulky bridges.[15–17]

A test reaction containing one equivalent of EBI*H_2, **2.13**, with one equivalent of $Zr(NMe_2)_4$ was carried out in an NMR tube in benzene-d_6. No reaction was observed by ^{1}H NMR spectroscopy over the course of 48 hours at 25 °C, and the mixture was heated first to 60 °C and then 80 °C for a period of 72 hours. No reaction was seen to occur even when the tube was placed under a partial static vacuum to encourage the removal of the amine byproduct. The reaction was scaled up in a small ampoule to allow for stirring of the reagents, but this also yielded no reaction. It was conceived that the reaction might not have taken place, due to the decreased acidity of the indenyl ring proton, compared to the unmethylated analogue.[13] In the series CpH, IndH, Ind$^{2\text{-Me}}$H, Ind$^{3\text{-Me}}$H and Cp^{Me4}H, the pK_a (in DMSO) increases (18.0, 20.1, 21.8, 22.5 and 26.1 respectively).[18–20] It is, therefore, a small extrapolation to see that the pK_a of permethylindene would be higher still (given the inductive electron donation from all the methyl groups) and to suspect that the proton was far less acidic than had been considered. Given that approximate pK_a of NMe_2H is 35 or higher, this should prove no barrier to reaction. An NMR scale test reaction in chloroform-d_1 was performed with SBI*H_2, **2.14**, with the product, SBI*$Zr(NMe_2)_2$, clearly observed by ^{1}H NMR spectroscopy but attempts to scale this reaction up failed as no reaction took place.

The more basic zirconium benzyl (pK_a toluene = 43)[21] was also employed but no reaction was observed at room temperature, even with sonication. On heating, the $ZrBz_4$ was seen to decompose before any reaction was noted with either **2.13** or **2.14**.

Further studies were carried out using $Y(N(SiMe_3)_2)_3$ and $Ca(N(SiMe_3)_2)_2$·2THF with Ind*H, **2.6**. The calcium amide was seen to react by ^{1}H NMR spectroscopy affording Ind*$Ca(N(SiMe_3)_2)$·xTHF, but with a conversion of approximately 40% after 144 hours at 110 °C, it was not pursued further.

3.3.2 Salt metathesis

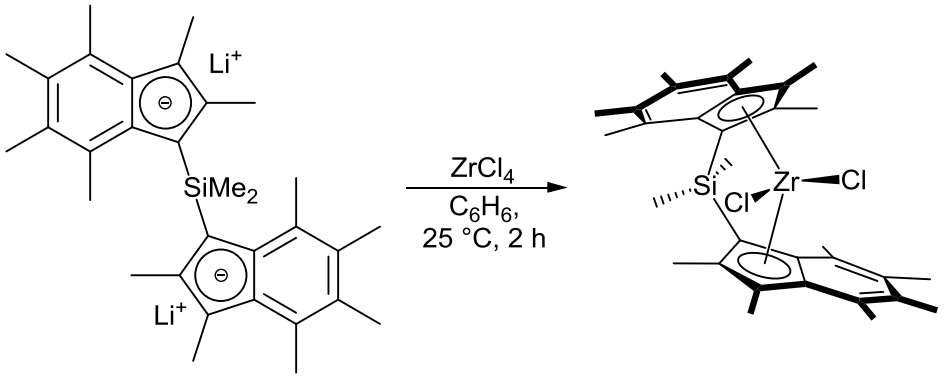
Following the recent publication of the EBI*$(SnMe_3)_2$ complexes, it was hoped that these would enable an increase in the synthetic yield for the formation of EBI*$ZrCl_2$.[22,23] However, attempts to use tin complexes for this purpose were unsuccessful as they were unreactive towards zirconium tetrachloride under any conditions employed. Given the failure to update the transmetallation procedures for these ligands, a salt metathesis methodology is employed throughout the remainder of this chapter.

Work on resynthesising EBI*$ZrCl_2$ by the published route had encountered problems and acceptable yields were hard to achieve. Despite the prudent cooling of the reagents to −78 °C

before mixing, no change in colour was observed until warming to room temperature, suggesting that the reaction was inhibited, and actively negating the slow reagent addition. A room temperature repeat with the slow addition of the $ZrCl_4$·2THF yielded similar results. Since the EBI*Li_2 is synthesised with bound THF, attempts were made to perform the transformation using $ZrCl_4$. The reaction was tested on an NMR scale first and benzene-d_6 was selected as the solvent. An instantaneous colour change to bright orange was noted on addition of the benzene and the ^{1}H NMR spectrum showed the formation of both *rac*- and *meso*-EBI*$ZrCl_2$. Since this simple reaction showed more promise than the alternative in toluene, it was scaled-up in benzene.

3.4 Synthesis of silyl-bridged group 4 complexes

3.4.1 Synthesis of dimethylsilylbis[1-(2,3,4,5,6,7-hexamethylindenyl)]zirconium dichloride, SBI*$ZrCl_2$ (3.1)



2.15 **3.1**
34% yield

Scheme 3.1: synthesis of dimethylsilylbis[1(2,3,4,5,6,7-hexamethylindenyl)]zirconium dichloride, SBI*$ZrCl_2$ (**3.1**)

Following on from the synthesis of EBI*$ZrCl_2$ in 2011, and its promising ethylene polymerisation activity (61,800 $kg_{PE}/mol_{Zr}/h/bar$), it was hoped that silyl-bridged analogues would have equally impressive properties.[8]

The same approach was applied to the synthesis of *rac*-SBI*$ZrCl_2$, **3.1**. Benzene was added to a Schlenk tube charged with **2.15** and $ZrCl_4$ and on stirring the mixture was seen to turn orange over the course of five minutes. The mixture was stirred for a further two hours before hot filtration afforded a dark orange solution and a red/brown residue. The solution was allowed to stand overnight at 5 °C, precipitating a small quantity of a bright orange powder identified by ^{1}H NMR spectroscopy as ***rac*-3.1**. The remaining decanted solution was

dried *in vacuo*, extracted into hexane and left to stand at −35 °C for two days affording bright orange crystals. These were collected and combined with the orange powder, affording ***rac*-3.1** in a 34% yield. No evidence of ***meso*-3.1** was seen in any reaction aliquots analysed by ^{1}H NMR spectroscopy – a marked change from the previous syntheses of EBI*$ZrCl_2$ and SBI*Fe where even isomeric mixtures were obtained.[8,24]

The crystals, grown from hexane by Dr. Jean-Charles Buffet,[25] were suitable for analysis by single crystal X-ray diffraction and two views of the solid state molecular structure are given in Figure 3.3. Selected bond lengths and angles are given in Table 3.1. ***rac*-3.1** crystallises in the monoclinic spacegroup $P2_1/n$, with one molecule in the asymmetric unit and four molecules in the unit cell – two of each enantiomer. The first point of note is that the value of TA′ (and to a lesser extent RA), 145.15° (and 116.89°), are larger than 90° showing that the two indenyl rings are pointed in opposite directions as is expected for a *rac*-isomer. This value of TA′ agrees well with that reported for *rac*-SBI$ZrCl_2$, 145.20°.[26] This suggests that the constraints of the dimethylsilicon bridge outweighs any steric effects from the permethylation. It also suggests that the one atom bridge seen here is less flexible than the ethylene bridge of EBI*$ZrCl_2$ which has a TA′ calculated as 152.68°, with the indenyl rings more staggered.[8]

The tilt angle (58.50°), α, is slightly lower than that reported for either SBI$ZrCl_2$ (61.80°) or $^{2,4,6\text{-}Me_3}$SBI$ZrCl_2$ (59.18°) suggesting that the increased methylation and bulk of the indenyls causes the rings to sit more parallel to one another so as to avoid any steric clashing.[27] The value of α is also in good agreement with that of *rac*-EBI*$ZrCl_2$ (57.15°), although slightly larger suggesting that the silyl bridge imparts slightly more strain than its ethylene counterpart. However, all of these values for α are much larger than that reported for $Ind^{*}_{2}ZrCl_2$ (41.02°), suggesting that both the ethylene and the silyl bridge confer significant constraints on the bulky indenyl ligands.[7] This is borne out by the large βs for ***rac*-3.1** of 18.49° and 18.89°, slightly exceeding those reported for $^{2,4,6\text{-}Me_3}$SBI$ZrCl_2$ (17.05°) or SBI$ZrCl_2$ (16.45°). However the values for both HA and FA are small and unremarkable.

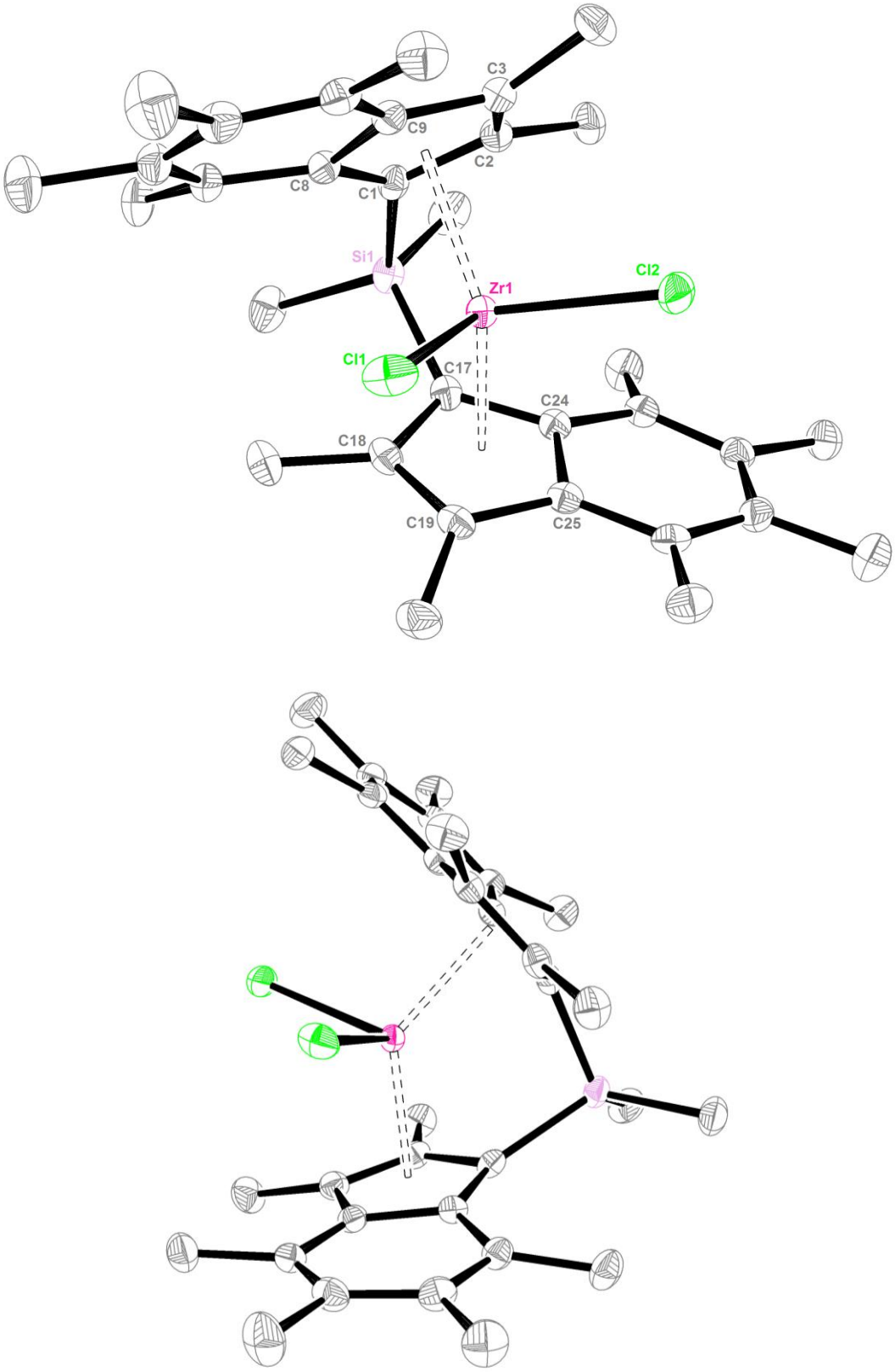


Figure 3.3: two views of molecular structure of ***rac*-3.1**. Methyl protons omitted for clarity. Thermal ellipsoids drawn at 50% probability. Crystals were grown by Dr. Jean-Charles Buffet.

Table 3.1: selected bond lengths (Å), angles (°), and geometric parameters (Å/°) for ***rac*-3.1**. Estimated standard deviations (ESDs) given in parentheses.

Bond Lengths (Å)			
Zr(1)-Cp_{cent}	2.257	Zr(1)-Cp_{cent}	2.244
Zr(1)-C(1)	2.4741(17)	Zr(1)-C(17)	2.4624(17)
Zr(1)-C(2)	2.4698(17)	Zr(1)-C(18)	2.4802(17)
Zr(1)-C(3)	2.5989(18)	Zr(1)-C(19)	2.5957(18)
Zr(1)-C(8)	2.6441(17)	Zr(1)-C(24)	2.6347(18)
Zr(1)-C(9)	2.6417(17)	Zr(1)-C(25)	2.6007(17)
Zr(1)-Cl(1)	2.4191(5)	Zr(1)-Cl(2)	2.4257(5)
C(1)-Si(1)	1.8975(19)	C(17)-Si(1)	1.8987(19)
Si(1)-C(33)	1.874(2)	Si(1)-C(34)	1.871(2)
Avg. Cp C-C	1.439	Avg. Cp C-C	1.439
Avg. Cp C-Me	1.506	Avg. Cp C-Me	1.506
Avg. C_6 C-C	1.418	Avg. C_6 C-C	1.419
Avg. C_6 C-Me	1.511	Avg. C_6 C-Me	1.509
Δ_{M-C}	0.105	Δ_{M-C}	0.129
Bond Angles (°)			
C(1)-Si(1)-C(17)	96.20(7)	C(33)-Si(1)-C(34)	98.72(10)
Cl(1)-Zr(1)-Cl(2)	97.806(19)		
α	58.50	δ	130.35
β	18.49	β	18.89
TA′	145.15	RA	116.89
HA	5.01	HA	4.13
FA	9.80	FA	5.81

The average Zr-Cp_{cent} distance (2.251 Å) fits well with other values reported in the literature for *ansa*-bridged species including EBI*$ZrCl_2$ (2.240 Å), SBI$ZrCl_2$ (2.241 Å) and $^{2,4,6\text{-Me}_3}$SBI$ZrCl_2$ (2.231 Å). It is also in good agreement with unbridged examples such as $Ind^*_2ZrCl_2$ (2.257 Å) and Ind_2ZrCl_2 (2.231 Å).[7,28]

It is also noted that there is a slight bond alternation in the benzene ring, with C(4)-C(5) and C(6)-C(7) shortened (avg. 1.381 Å) relative to the other C-C bonds within the indenyl ring, suggesting slight double bond localisation, not seen in the pro-ligand, **2.14**.

Table 3.2: comparison of selected bond lengths (Å), angles (°) and geometric parameters (°) between the crystal structure of ***rac*-3.1** and DFT geometry optimisations using two basis sets: B3LYP and BP86.

Bond/Angle	Crystal	B3LYP	BP86
Avg. Zr-Cp_{cent} (Å)	2.251	2.308	2.288
Avg. Zr-Cl (Å)	2.423	2.442	2.428
C(1)-Si(1)-C(17) (°)	96.20	96.31	95.85
α (°)	58.50	61.28	59.95
TA′ (°)	145.15	148.44	146.30

Density functional theory (DFT) calculations, comprising a geometry optimisation and a molecular orbital (MO) analysis, have been performed in two basis sets (B3LYP[29–31] and BP86[32,33]). A comparison of the reported values from the X-ray structure of ***rac*-3.1** and the calculated parameters is contained within Table 3.2. All three sets of values are in good agreement although both calculations indicate a preference for a slightly increased rotation and larger tilt angles. The changes observed, however, are marginal. Illustrations of the DFT (B3LYP) computed highest occupied molecular orbital (HOMO) and the lowest unoccupied molecular (LUMO) are given in Figure 3.4.

The HOMO primarily consists of ligand p-orbitals, particularly those involved in the partially localised double bonds within the benzene ring which can be clearly seen in Figure 3.4. In contrast, the LUMO is primarily based on the d^0 metal centre with 20.0% of the electron density on the Zr d_{yz} and 28.2% on the $d_{x^2-y^2}$.

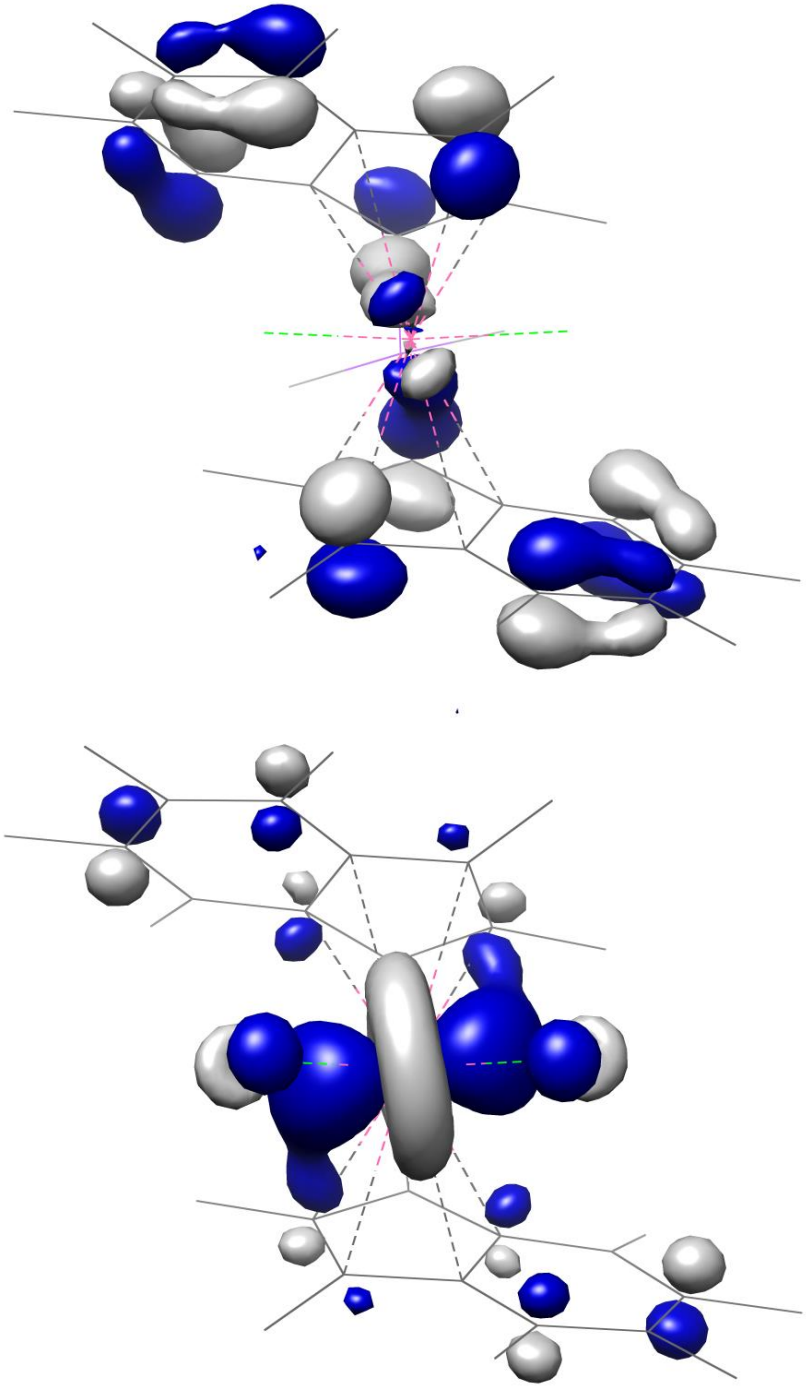


Figure 3.4: illustration of the DFT computed HOMO (top) and LUMO (bottom) of ***rac*-3.1** at the B3LYP level.

The ^{1}H NMR spectrum of ***rac*-3.1** in chloroform-d_1 shows six singlets between 1.25 and 2.5 ppm. One of these has double the intensity of the others (2.45 ppm) corresponding to two coincident methyl resonances on each ring; the rest each correspond to two methyl groups. The *rac*-form has one resonance for the two silyl methyl groups, C(33) and C(34), which are in the same environment in solution and low frequency (1.34 ppm) due to the shielding silicon. This echoes the solid state structure (Figure 3.3) where the complex is C_2 symmetric.

As is also typical of the *rac*-isomer of *ansa*-indenyls, one of the ring methyl resonances is 0.3 ppm upfield from the rest (1.88 ppm).[8]

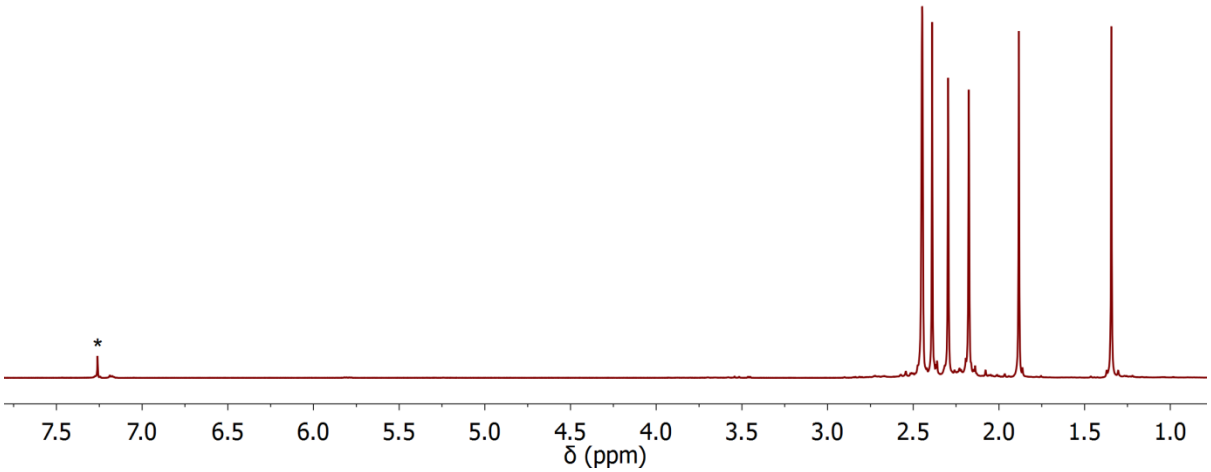
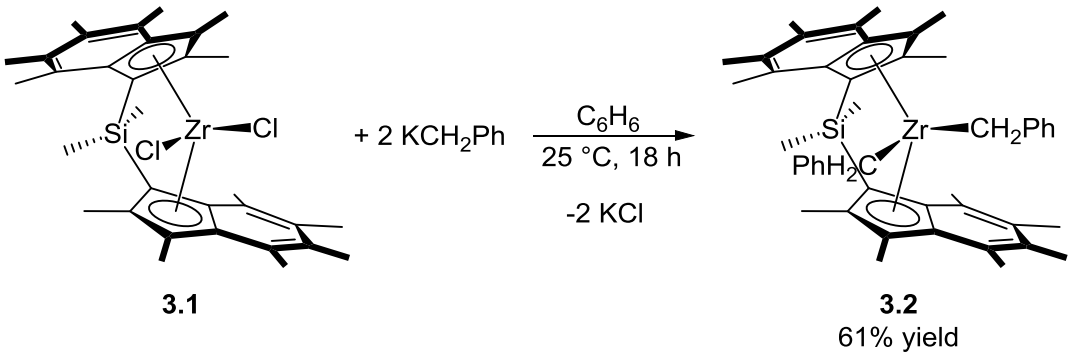


Figure 3.5: ^{1}H NMR (400 MHz) spectrum of ***rac*-3.1** in chloroform-d_1. Asterisk marks the residual *protio*-solvent resonance.

3.4.2 Synthesis of dimethylsilylbis[1(2,3,4,5,6,7-hexamethylindenyl)]zirconium dibenzyl, SBI*Zr(CH_2Ph)$_2$ (3.2)



3.1 **3.2** 61% yield

Scheme 3.2: synthesis of dimethylsilylbis[1(2,3,4,5,6,7-hexamethylindenyl)]zirconium dibenzyl, SBI*Zr(CH_2Ph)$_2$ (**3.2**)

Following on from the successful synthesis of ***rac*-3.1,** it was hoped to use the dichloride as an entry into the synthesis of SBI* alkyl complexes. During activation of dichlorides with MAO, methylation is seen to occur, before methyl abstraction.[34,35] For this reason, the synthesis of alkyl complexes of group 4 is desirable. It was decided to focus our efforts on three particular target alkyl groups: benzyl (CH_2Ph, Bz), neopentyl ($CH_2{}^tBu$, Np) and neosilyl (CH_2SiMe_3). Initial ^{1}H NMR spectroscopic studies in benzene-d_6 suggested that the reaction of ***rac*-3.1** with potassium benzyl proceeded quickly on sonication at room temperature and in good yield. In contrast, no reaction at all was observed with lithium neopentyl, even upon

extensive heating, while unexpected resonances were seen for the reaction with $NaCH_2SiMe_3$ (*vide infra*).

Benzene was added to a Schlenk tube containing ***rac*-3.1** and 2.2 equivalents of KBz and stirred overnight turning from a dark orange to a red/brown. Monitoring by ^{1}H NMR spectroscopy suggested that the reaction had not gone to completion and the tube was sonicated for a further 30 minutes before drying *in vacuo*. Extraction of the dark-brown solid with hexane afforded a yellow solution which was dried to afford ***rac*-3.2** as a yellow powder in 61% yield. Numerous attempts were made to generate crystals suitable for an X-ray structure analysis. However, crystallisation from a variety of solvents afforded thin, yellow plates which were found to be too weakly diffracting for successful data collection even when employing synchrotron radiation.

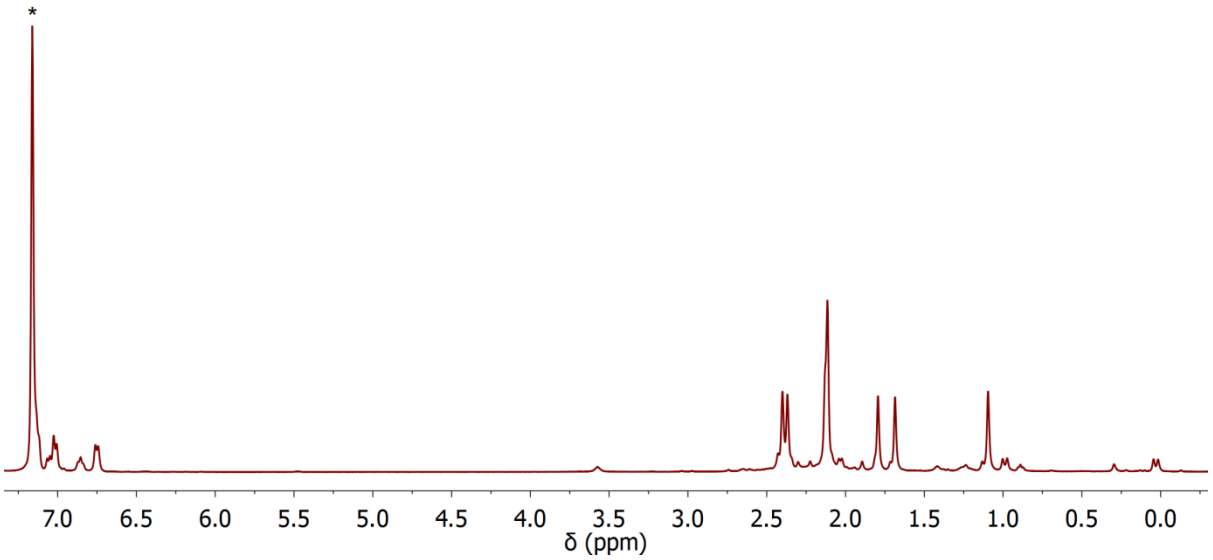


Figure 3.6: ^{1}H NMR (400 MHz) spectrum of ***rac*-3.2** in benzene-d_6. Asterisk marks the residual *protio*-solvent resonance which is coincident with a multiplet in the aromatic region.

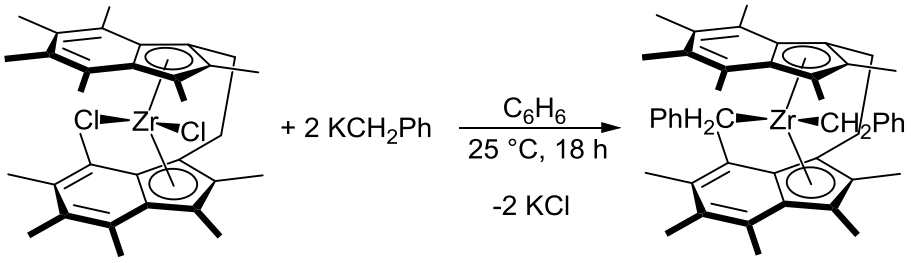
The ^{1}H NMR spectrum recorded for ***rac*-3.2** in benzene-d_6 (Figure 3.6) was found to contain resonances in three broadly distinct regions. The "methyl region" (1.10-2.40 ppm) was found to be similar to that reported for ***rac*-3.1**. Seven methyl singlets are observed with two being almost coincident (2.11 and 2.13 ppm). The signal corresponding to the silicon methyl is separated from the rest by 0.59 ppm at 1.10 ppm. Beyond this are two doublet resonances (0.03 and 0.99 ppm), each corresponding to the diastereotopic benzylic protons with intensity two. These values and multiplicities along with the very slight roofing effects also observed, are typical of the zirconocene benzyl groups.[36–39] Significantly deshielded, a doublet (6.75 ppm) and two triplets (6.86 and 7.05 ppm) are also observed corresponding to

the protons on the phenyl ring. In addition, significant quantities of toluene and unidentified resonances in the "methyl region" were seen in the ^{1}H NMR spectrum when allowed to stand at room temperature, no doubt indicative of a decomposition product in solution. This may explain the comparatively poor yield.

Reaction of ***rac*-3.1** with $NaCH_2SiMe_3$ led to the observation of three resonances in the ratio 2:2:6 which did not fit with the expected mono- or bis(neosilyl) complex in addition to a large peak at 0.00 ppm, identified as $SiMe_4$, and with an intensity of approximately 12. The presence of TMS suggested that *rac*-SBI*Zr$(CH_2SiMe_3)_2$ had not formed and suitable crystals of the metallocene fragment were grown. X-ray analysis showed that a metallasilacyclobutane, SBI*Zr(η^2-$CH_2Si(CH_3)_2CH_2$), had formed. It is suggested that this came about after γ-hydride abstraction by the other neosilyl group, forming neosilane, and closing of the cyclobutane.[25]

3.5 Synthesis of ethylene bridged group 4 complexes

3.5.1 Synthesis of ethylenebis[1-(2,3,4,5,6,7-hexamethylindenyl)] zirconium dibenzyl, EBI*Zr$(CH_2Ph)_2$ (3.3)



3.3
64% yield

Scheme 3.3: synthesis of ethylenebis[1-(2,3,4,5,6,7-hexamethylindenyl)] zirconium dibenzyl, EBI*Zr$(CH_2Ph)_2$ (**3.3**)

As in section 3.3.2, three alkyl groups were targeted: benzyl, neopentyl and neosilyl. Test reactions showed that sonication was required to solubilise the KBz, and that heating caused decomposition of the reagent. In contrast to section 3.3.2, no toluene was observed in the NMR spectrum if the complex was left in solution.

Similar reaction conditions were employed to those used in the synthesis of ***rac*-3.2**; benzene was added directly to the solid reagents, *meso*-EBI*ZrCl_2 and KBz, and stirred for 42 hours. After work-up, ***meso*-3.3** was obtained as a yellow microcrystalline solid in 64% yield. Crystals suitable for X-ray diffraction were obtained from hexane at −35 °C.

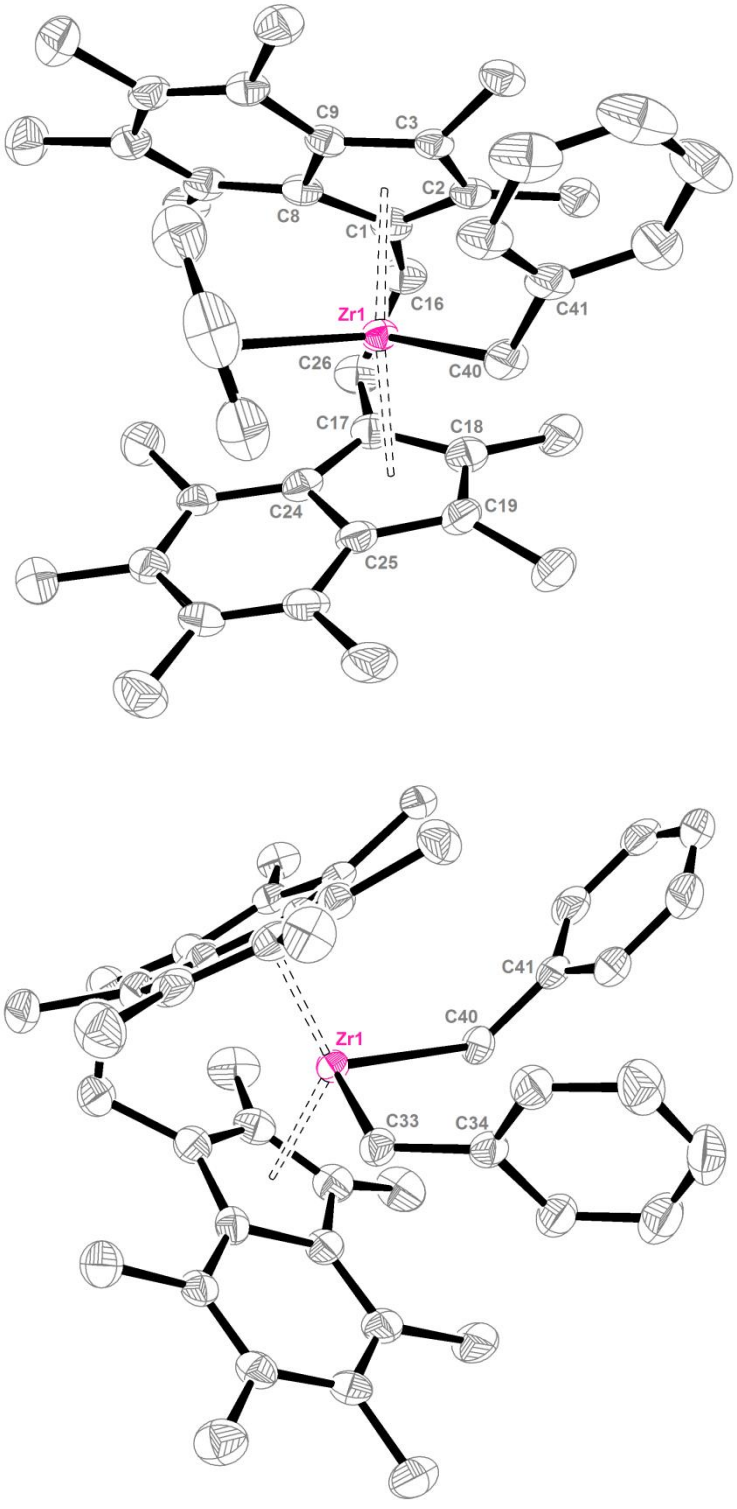


Figure 3.7: two views of the solid-state molecular structure of ***meso*-3.3**. Hydrogens omitted for clarity. Thermal ellipsoids drawn at 50% probability.

Table 3.3: selected bond lengths (Å), angles (°), and geometric parameters (Å/°) for ***meso*-3.3**. ESDs given in parentheses.

Bond Lengths (Å)			
Zr(1)-Cp_{cent}	2.290	Zr(1)-Cp_{cent}	2.307
Zr(1)-C(1)	2.514(4)	Zr(1)-C(17)	2.474(4)
Zr(1)-C(2)	2.544(4)	Zr(1)-C(18)	2.570(4)
Zr(1)-C(3)	2.614(3)	Zr(1)-C(19)	2.680(4)
Zr(1)-C(8)	2.627(3)	Zr(1)-C(24)	2.612(4)
Zr(1)-C(9)	2.665(3)	Zr(1)-C(25)	2.698(4)
Zr(1)-C(33)	2.335(4)	Zr(1)-C(40)	2.322(3)
C(33)-C(34)	1.492(5)	C(40)-C(41)	1.478(5)
Avg. Cp C-C	1.431	Avg. Cp C-C	1.430
Avg. Cp C-Me	1.501	Avg. Cp C-Me	1.512
Avg. C_6 C-C	1.418	Avg. C_6 C-C	1.418
Avg. C_6 C-Me	1.517	Avg. C_6 C-Me	1.512
Δ_{M-C}	0.088	Δ_{M-C}	0.080
Bond Angles (°)			
Zr(1)-C(33)-C(34)	119.5(2)	Zr(1)-C(40)-C(41)	128.8(3)
C(33)-Zr(1)-C(40)	103.25(14)	Ph-Ph planes	89.39
α	61.85	δ	127.27
β	2.74	β	6.85
TA′	17.42	RA	46.68
HA	3.51	HA	4.86
FA	5.53	FA	5.30

***meso*-3.3** was found to crystallise in the monoclinic spacegroup $P2_1/n$, with one molecule in the asymmetric unit and four in the unit cell (Figure 3.7 and Table 3.3). Unsurprisingly, ***meso*-3.3** contrasts sharply in structure from ***rac*-3.1** with the rings aligned in the same direction, indicating the *meso*-form. This is borne out in the value for TA′ of 17.42° which is in stark contrast to the 145.15° reported for ***rac*-3.1**. The value for TA′ for ***meso*-3.3** agrees well with that measured for *meso*-EBI*$ZrCl_2$ (18.97°), suggesting either that the benzyl groups have a small effect on the molecular geometry or that the bridge exercises considerable constraint. Another feature in common with *meso*-EBI*$ZrCl_2$, is the way that the

methyls on the five membered rings splay back, away from the centroid and the plane of the ring by approximately 10° (8.09-9.74°) with a particularly large effect in close proximity to the benzyl groups (14.12°). These values match well with *meso*-EBI*$ZrCl_2$ where the range is 4.77-10.37°.

The value for α (61.85°) significantly exceeds that reported for *meso*-EBI*$ZrCl_2$ (56.87°), hypothesised to be because of the increased steric bulk of the benzyl groups compared to the chloride. This fits well with bending of C(11) away from the plane of the Cp ring (*vide supra*). The tilt angle is larger even than that reported for ***rac*-3.1** (58.50°) and fits much better with that seen for the unmethylated analogue, SBI$ZrCl_2$ (61.80°).[26] The values of β (2.74 and 6.85°) are negligible compared with those for ***rac*-3.1** (18.49 and 18.89°), and this difference is attributed to there being two atoms in the bridge. The "splaying" of the methyl groups is thought to contribute to the small values of β. The values for HA and FA for ***meso*-3.3** are unremarkable.

The average Zr-Cp_{cent} distance (2.299 Å) for ***meso*-3.3** is marginally longer than *meso*-EBI*$ZrCl_2$ (2.248 Å) and ***rac*-3.1** (2.250 Å), expected to be caused by the better σ-donation ability of the benzyl groups, relative to the chlorides, with the consequent increase in electron density on the metal centre, leading to a weaker electrostatic interaction with the ligand. In addition to the electronic effects, it is also suspected that the metal-centroid distance is somewhat expanded due to the steric crowding at the metal centre due to the clash of the permethylated ligand and the benzyl rings. Other reported indenyl benzyl compounds, such as EBTHI$ZrBz_2$ [EBTHI = ethylenebis(1-tetrahydroindenyl)] and $Ind^R_2ZrBz_2$ (Ind^R = 4,7-F_2-Ind) exhibit slightly shorter Zr-Cp_{cent} distances (2.226 and 2.254 Å respectively) indicating that the steric effects dominate the electronic ones in ***meso*-3.3**.[36,38]

The zirconium benzyl distances (2.335(4) and 2.322(3) Å) are in good agreement with those in the literature,[37,39,40] and match most closely with the only other *ansa*-indenyl benzyl compound reported: EBTHI$ZrBz_2$ (2.314 Å).[38] Similarly, the twist of the two phenyl rings relative to one another (89.35°) in ***meso*-3.3** falls within the typical range (approximately 70-90°).[37,38] The Zr-C-C bond angles subtended at the benzyl carbons (119.5(2) and 128.8(3)°) also fall within the literature range for analogous zirconocenes.[37,39] It is perhaps interesting to note that the significantly different angles reported for the different benzyl groups is also a feature of these structures and can sometimes be indicative of different benzyl binding modes.[39,41] According to the investigation by Parkin *et al.* into a variety of benzyl compounds found in the CSD and $Zr(CH_2Ph)_4$ itself,[42] these angles are far greater than the 97° proposed

for anything other than an η^1 benzyl bonding motif. Moreover, a δ_{ipso}, calculated as the difference between the M-C_{ipso} distance (Zr1-C34/41) and the M-CH_2 distance (Zr1-C33/40), should not be greater than 0.5 Å. In ***meso*-3.3**, these distances are reported as 0.998 and 1.126 Å respectively, confirming both benzyl moieties as indubitably η^1.

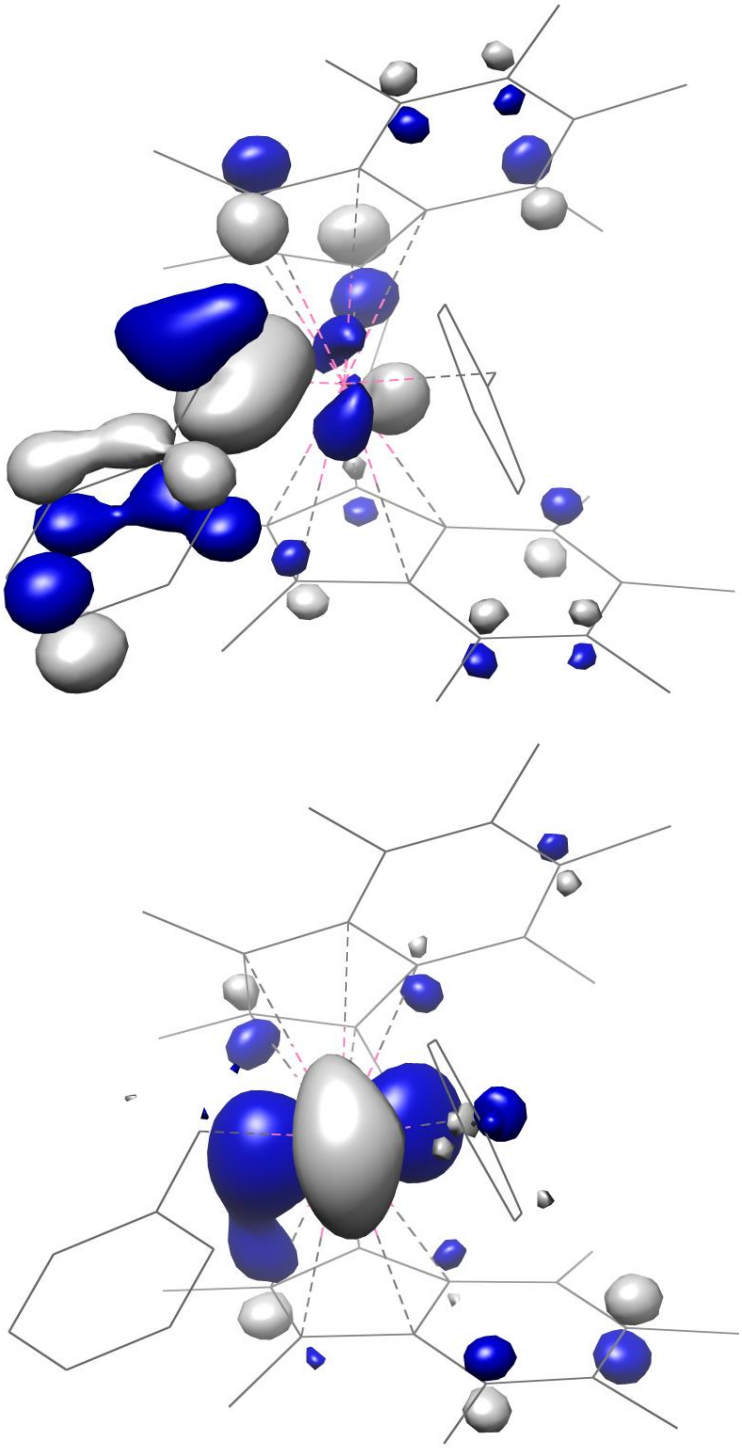


Figure 3.8: illustration of the DFT computed HOMO (top) and LUMO (bottom) of ***meso*-3.3** at the BP86 level.

The DFT studies (Figure 3.8) at both the BP86 and the B3LYP levels corroborate the crystal data, fitting the geometry optimisation well (Table 3.4). Analysis of the HOMO shows a bonding interaction between Zr(1) and C(40) with 17.6% of the electron density shared between the Zr(1) d_{yz} and the C(33) p_z. Additionally there is significant electron density on the phenyl ring of the same benzyl group, primarily in the p_z orbitals.

Table 3.4: comparison of selected bond lengths (Å), angles (°) and geometric parameters (°) between the crystal structure of ***meso*-3.3** and DFT geometry optimisations using two basis sets: B3LYP and BP86.

Bond/Angle	Crystal	B3LYP	BP86
Avg. Zr-Cp_{cent} (Å)	2.299	2.363	2.337
Avg. Zr-C(33)/(40) (Å)	2.328	2.341	2.344
Zr(1)-C(33)-C(34) (°)	119.49	124.10	119.21
Zr(1)-C(40)-C(41) (°)	128.85	129.05	131.30
α (°)	61.85	62.92	63.17
TA′ (°)	17.42	12.91	15.08

The ^{1}H NMR spectrum of ***meso*-3.1** (Figure 3.9) contains the same diagnostic ligand resonances as *meso*-EBI*$ZrCl_2$, with six singlets falling between 1.85 and 2.7 ppm, each of intensity six and two of which are coincident (2.04 ppm). The bridge protons are observed as two quartets, each of intensity two, in the range 3-4 ppm. Further upfield of the methyl resonances are two singlets at 1.83 and −0.70 ppm which were attributed to the benzyl protons, each having an integration of two. The chemical shift of the protons was found to be more significantly separated from one another than was previously anticipated; separations of up to 1 ppm are commonplace for zirconium benzyl compounds.[36,39] These separations only arise at room temperature for *ansa*-species as the free rotation of the indenyls in complexes such as $Ind^R_2ZrBz_2$ (Ind^R = 4,7-F_2-Ind, 4,7-Me_2-Ind, 4,7-$(OMe)_2$-Ind) lead to the observation of just one benzylic environment.[38] The separation reported for ***meso*-3.3** is unusually large and this was investigated further (*vide infra*). It was perhaps surprising to identify the benzylic protons as singlets as it was anticipated that they would occupy diastereotopic environments and show more complex multiplicities within the spectrum, as this was seen for the only previously characterised *ansa*-indenyl zirconium benzyl species, *rac*-EBTHIZrBz_2.[38]

The solid state molecular structure of ***meso*-3.3** indicates that, as *meso*-forms no longer have the same C_2 rotational symmetry, the two pairs of benzyl protons sit in different environments (Figure 3.7). One pair of benzyl protons lies directly between the two arenes (Figure 3.13) and might be affected by the ring currents.[43] To ascertain this, a rotating-frame

nuclear Overhauser effect spectroscopy (ROESY) experiment was conducted on ***meso*-3.3** (Figure 3.12).

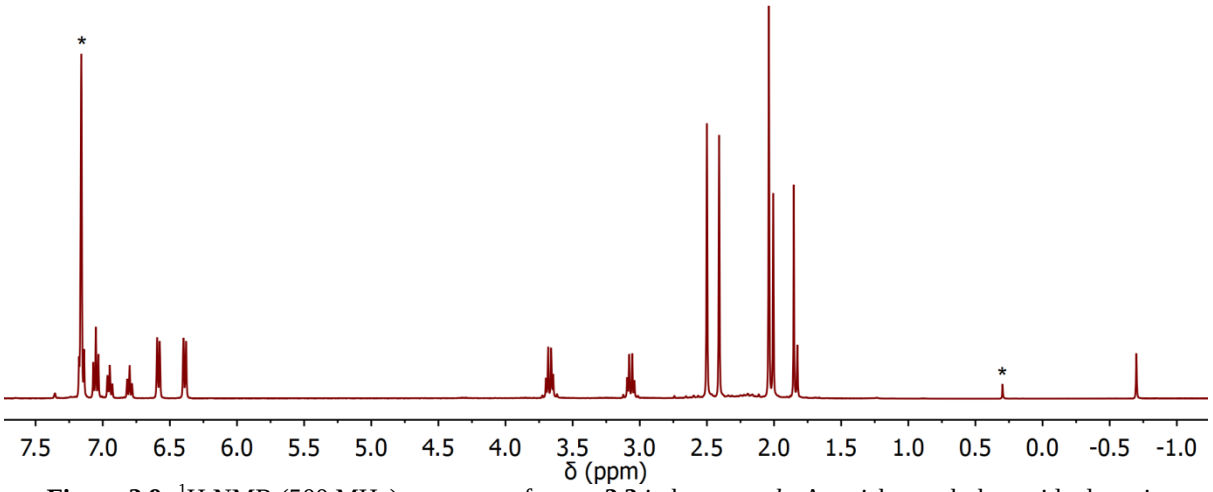


Figure 3.9: ^{1}H NMR (500 MHz) spectrum of ***meso*-3.3** in benzene-d_6. Asterisks mark the residual protio-solvent resonance and trace silicon grease.

Analysis of the aromatic region revealed six resonances (one of which is partially obscured by the residual *protio*-solvent): two doublets at lower frequency (6.39 and 6.59 ppm) and four triplets at higher frequency (6.80, 6.95, 7.05 and 7.15 ppm). Given their respective intensities: 2:2 for the doublets, and 1:1:2:2 for the triplets (totalling ten), it was proposed that the system comprised two distinct benzyl groups, with each phenyl ring able to freely rotate. This hypothesis was confirmed by two-dimensional homonuclear proton correlation spectroscopy (^{1}H-^{1}H COSY) in Figure 3.10.

If we label the resonances shown in Figure 3.10 from **1** to **6** (from low field to high) then we see that resonances **1**, **3** and **5** all couple (as seen from the cross-peaks) to one another, as do signals **2**, **4** and **6**. This allows us to identify two separate phenyl groups in different environments and to assign them. As the only doublets, **5** and **6** are assigned as the *ortho*-protons; with half the intensity of the other signals **3** and **4** were attributed to the *para*-protons. **1** and **2** are ascribed as *meta*-resonances – a good fit with their triplets and intensities of two each. This free rotation about the benzyl bond also explains the singlet nature of the benzylic protons which are rendered equivalent.

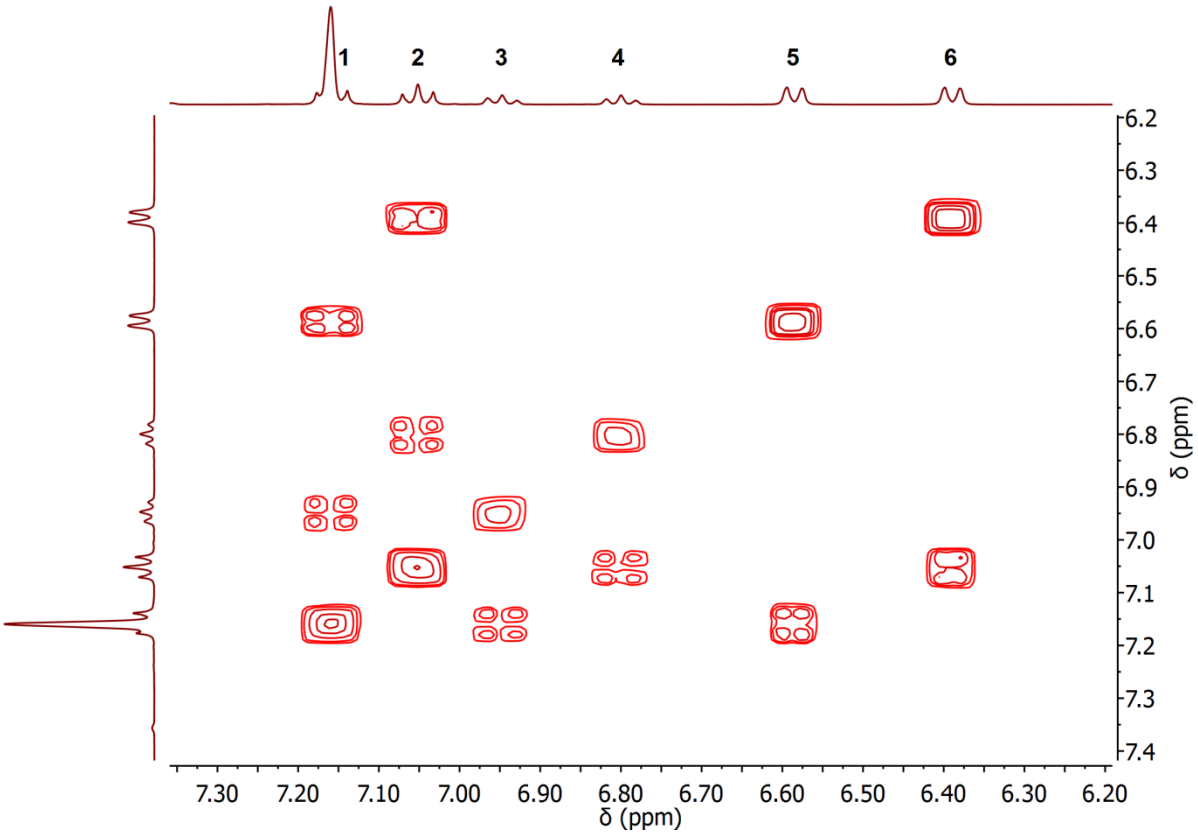


Figure 3.10: homonuclear ^{1}H correlation NMR spectrum of ***meso*-3.3** in benzene-d_6.

It was anticipated that further complexity could be identified on cooling the system, in the hopes of slowing the rotation around the benzyl bond below the NMR timescale (Figure 3.11). The sample was dissolved in tetrahydrofuran-d_8 since the residual *protio*-solvent resonances are not coincident with any of the signals in the spectrum, and it allows cooling to beyond −80 °C (Figure 3.11).

On cooling ***meso*-3.3** in THF-d_8, the rotation of the phenyl rings was not seen to slow on the NMR timescale, as evidenced by the singlets corresponding to the benzylic protons seen at 193 K. Similarly, six resonances for the phenyl rings are seen to remain, maintaining their respective multiplicities although their relative chemical shifts change. One pair of *ortho*-protons, **5**, move 0.48 ppm over 100 K, from 6.27 ppm at 293 K to 5.79 ppm at 193 K. Large movements such as this even cause the signals interchange positions. At 253 K, **5** and **6** are coincident, appearing as one doublet with an integration of four. Similarly, resonances **1** and **2** form a coincident triplet at 223 K and overlap to a greater or lesser extent for 20 K either side. Naturally it is not only the aromatic multiplets that shift on changing the temperature but all the resonances. For instance, the signals corresponding to the benzylic CH_2 move from 1.59 and −1.01 ppm at 298 K to 1.48 and −1.40 ppm at 193 K.

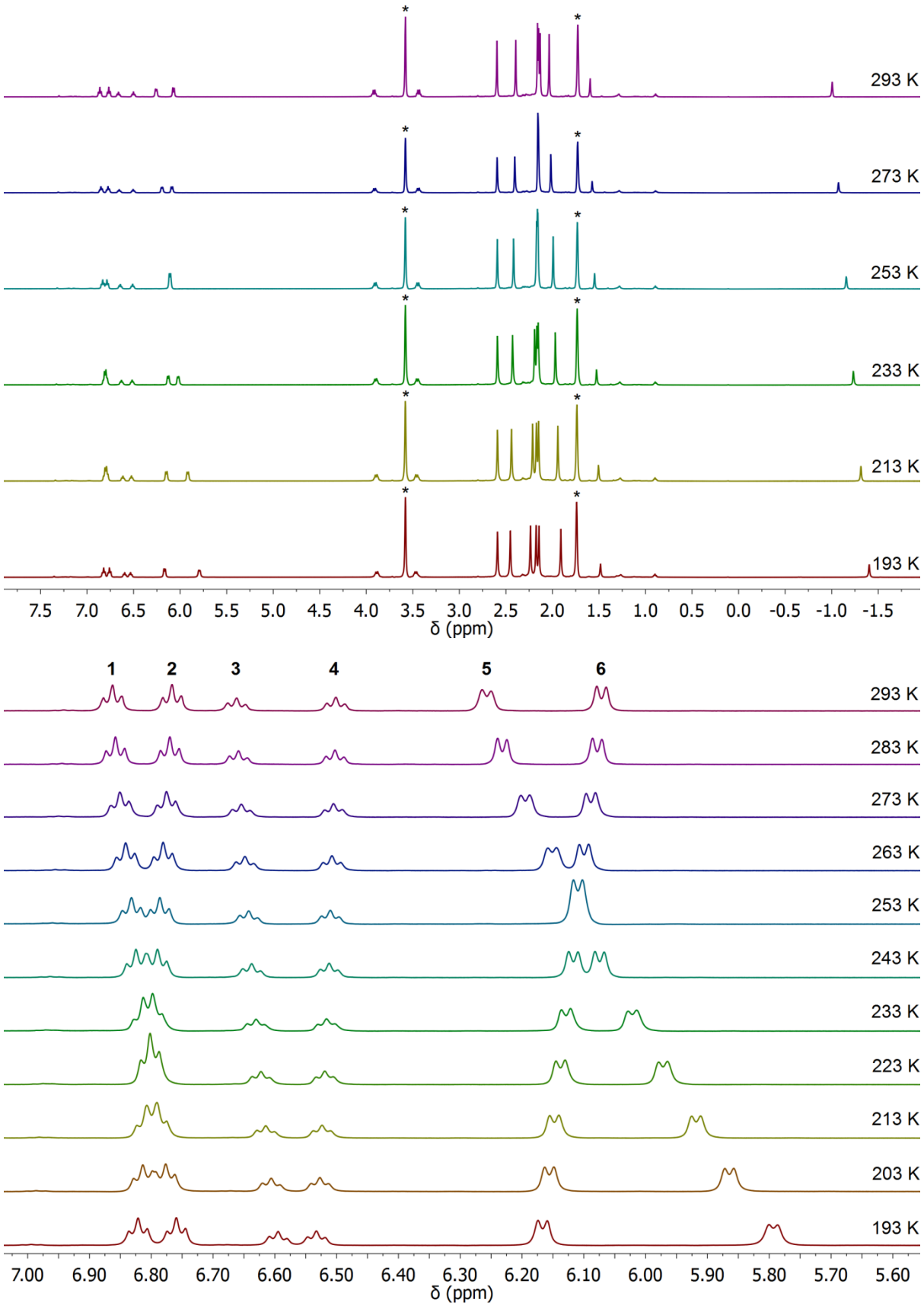


Figure 3.11: two variable temperature ^{1}H NMR (500 MHz) spectra of ***meso*-3.3** in THF-d_8; the full spectral width (top) and the aromatic region (bottom) are shown.

As mentioned above, it was noted that the two benzyl resonances were significantly separated from one another, and in particular that the resonance at −1.01 ppm (298 K, THF-d_8) is significantly shielded compared to other examples in the literature. It could easily be reasoned that the close proximity of the benzyl protons to the zirconium centre could lead them being shifted upfield due to the presence of the electropositive metal and that small changes in environment could lead to slight differences in chemical shift. However, as it is a tetravalent d^0 zirconium, it might be expected to be electron deficient (and hence a more electronegative species). Couple this with the surprisingly large difference in chemical shift, and the model falls apart.

Analysis of the ROESY experiment (Figure 3.12), allows better understanding of the molecular structure of ***meso*-3.3** in the solution-state. Cross-peaks in the spectrum highlight a through-space proximity of two protons (<4 Å). Focusing on the cross-peaks of the benzylic resonance at −1.01 ppm (bottom spectrum in Figure 3.12), six signals are seen, of which two appear to be of greater intensity than the others. This greater intensity can be caused either by greater proximity or by overlapping signals. Two of these fall in the aromatic region demonstrating interactions with the *ortho*-proton doublets of the phenyl ring, **5** and **6**. It is clear that the cross-peak with **6** is stronger than that with **5**, allowing us to infer that the signals at 6.07 (**6**) and −1.01 ppm are on the same benzyl group. This represents a much smaller separation than that between the two benzyl groups: 2.551 Å as opposed to 4.149 Å in the solid state orientation (Figure 3.13). A focus on the region from 1.5 to 2.75 ppm shows four signals again, one of which is more intense. This signal of greater intensity occurs at a chemical shift where three of the methyl groups are almost coincident (2.13-2.16 ppm) and a more precise examination of the cross-peak suggested it correlated with the resonances at both 2.13 and 2.15 ppm. Reference to the crystal structure suggested that these and two other cross peaks (2.39 and 2.60 ppm) might be methyls on the aryl ring confirming that the proton is in close proximity (<4 Å) to the aryl rings. The distances from the benzyl protons to the arene ring centroids in the solid-state structure are 2.318 and 2.543 Å and should certainly be susceptible to ring current effects. The final interaction seen is with the other benzyl protons, deemed in the solid-state to be only 3.793 Å (Figure 3.13).

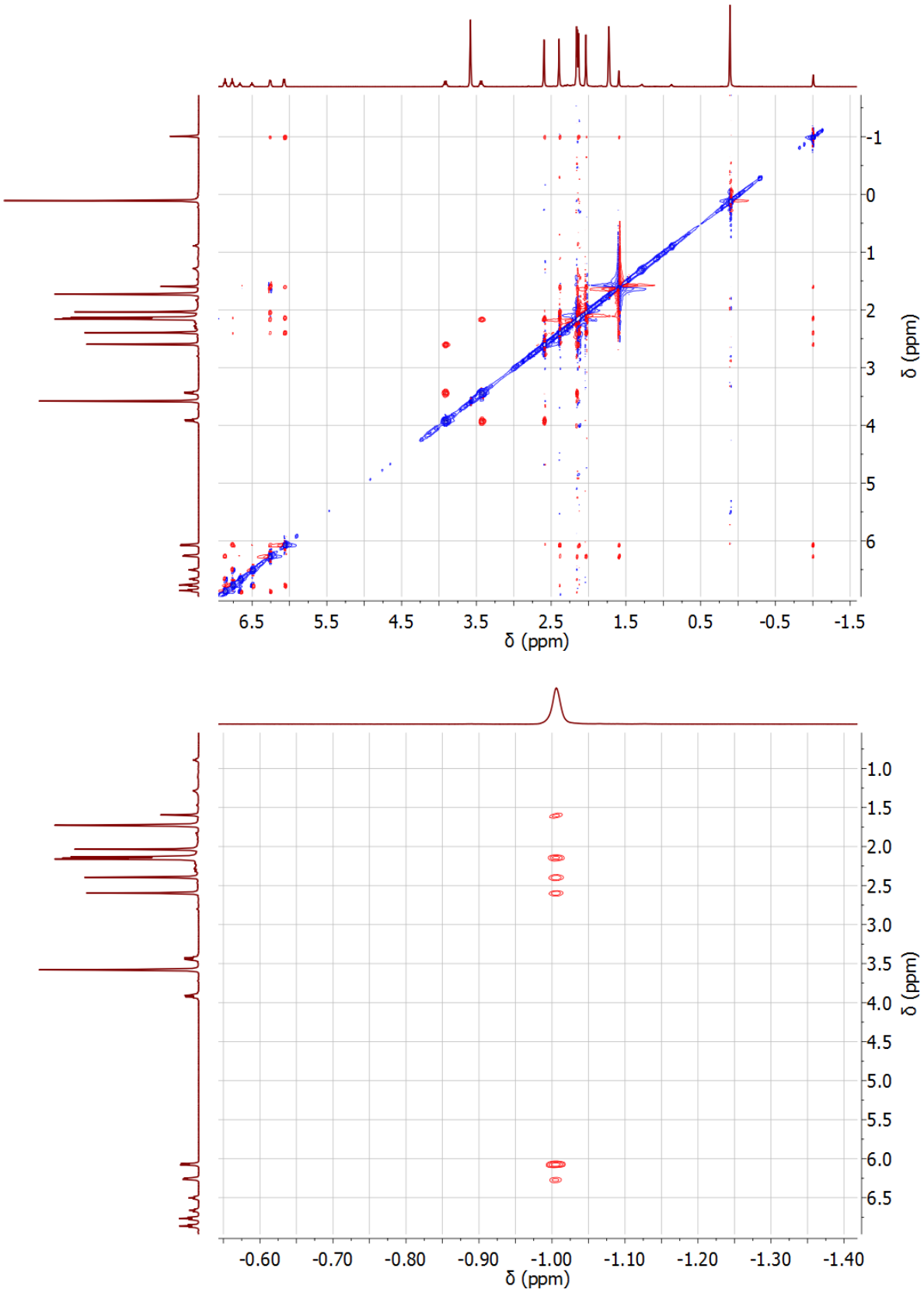


Figure 3.12: two rotating-frame nuclear Overhauser effect spectra of ***meso*-3.3** in THF-d_8; the full spectral width is shown (top) and a focus on the resonance corresponding to the benzylic protons at −1.01 ppm (bottom).

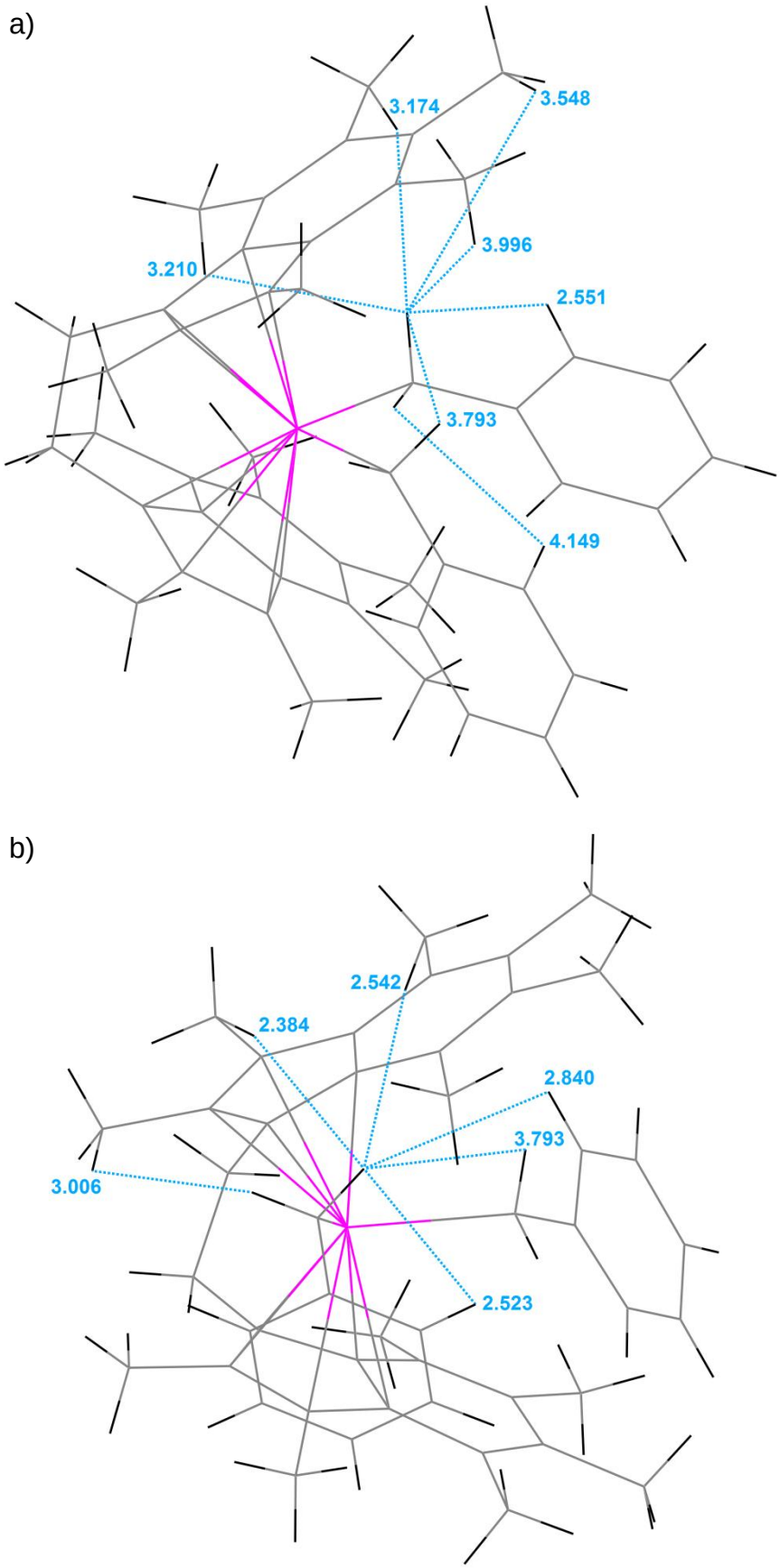


Figure 3.13: two views of the solid-state molecular structure of ***meso*-3.3** illustrating the interactions causing cross peaks in the ROESY for the a) upfield and b) downfield benzylic protons. Distances given in Å.

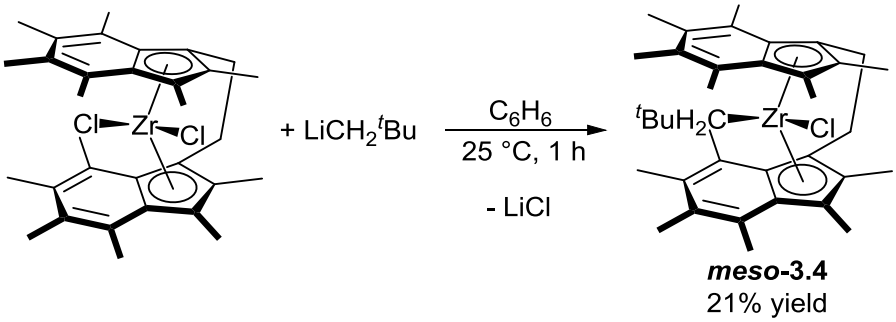
A similar analysis can be performed on the benzyl resonance at 1.59 ppm which shows cross peaks with the two Cp methyls, C(11) and C(12), at 2.16 and 2.03 ppm respectively. Additional cross peaks are seen with C(13), one of the arene methyl resonances, at 2.39 ppm, and with the *ortho*-protons, **5** and **6**, where **5** is more intense. Similar separations are also shown in Figure 3.13.

Using the ROESY spectrum (Figure 3.12), it is easy to fully assign the methyl resonances using the through-space interactions, with even the bridge protons being assignable. Those closer to the arene show strong cross-peaks with C(16) at 2.60 ppm (1.994 Å) while the others are much closer (1.955 Å) to C(11) at 2.16 ppm. All the data from a variety of NMR experiments complement perfectly to help elucidate the solution-phase structure of ***meso*-3.3**, and to explain the unusual chemical shift observed for the benzylic protons.

***meso*-3.3** was further characterised by high resolution mass spectrometry, finding not only the molecular ion peak (expected: 726.3198, found: 726.2760) but also numerous degradation fragments at m/z = 635, 544 and 91 corresponding to $[EBI*ZrBz]^+$, $[EBI*Zr]^+$ and $[Bz]^+$ respectively.

In addition, attempts were made to synthesise a mono-benzyl species, *meso*-EBI*ZrBzCl, but when one equivalent of KBz was added and the reaction mixture sonicated, it appeared by ^{1}H NMR spectroscopy that the reaction was unsuccessful. Resonances attributed to ***meso*-3.3** and the starting material, *meso*-EBI*$ZrCl_2$ were observed but no new species.

3.5.2 Synthesis of ethylenebis[1-(2,3,4,5,6,7-hexamethylindenyl)] zirconium neopentyl chloride, EBI*Zr($CH_2{}^t$Bu)Cl (3.4)



Scheme 3.4: synthesis of ethylenebis[1-(2,3,4,5,6,7-hexamethylindenyl)] zirconium neopentyl chloride, EBI*Zr($CH_2{}^t$Bu)Cl (**3.4**)

After the successful synthesis of ***meso*-3.3**, it was decided to attempted to synthesise the neopentyl analogue by a similar means. Addition of one equivalent of lithium neopentyl to *meso*-EBI*$ZrCl_2$ showed no reaction, except for the formation of neopentane, while two

equivalents generated *meso*-EBI*ZrNpCl, ***meso*-3.4**. The addition of more LiNp provoked no further reaction, but caused the mono-neopentyl complex to decompose. The use of the less basic NpMgCl didn't change the reactivity and the bis(neopentyl) complex was not synthesised. In both cases, ***meso*-3.4** was found to decompose in solution at room temperature over the course of 48 hours.

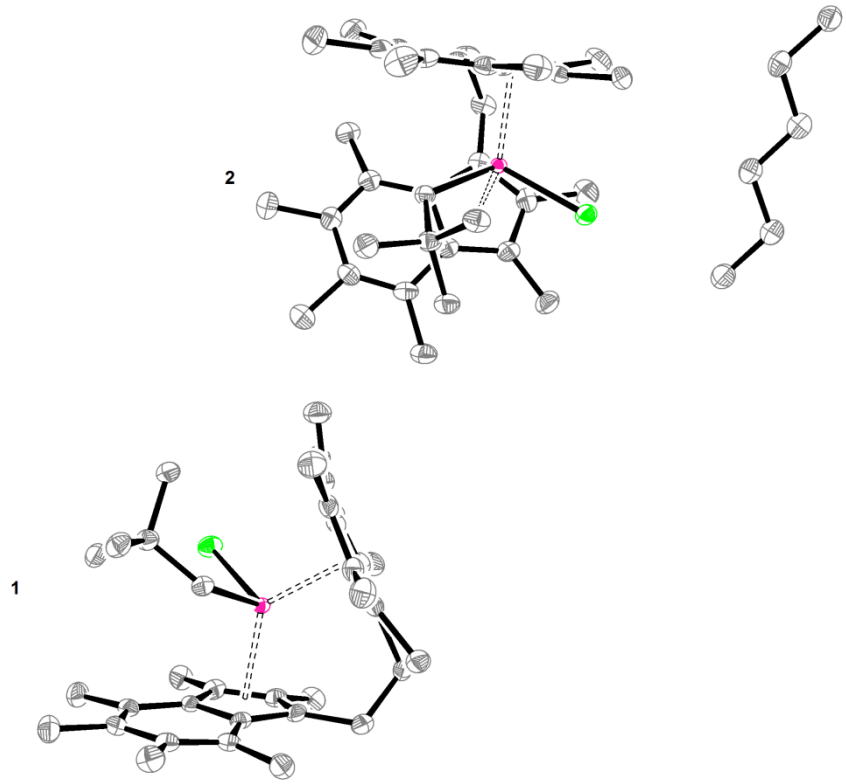


Figure 3.14: solid-state molecular structure of ***meso*-3.4** depicting the two independent molecules, co-crystallised with hexane, within the asymmetric unit. Hydrogens omitted for clarity. Thermal ellipsoids drawn at 50% probability.

It was decided to repeat the reaction with lithium neopentyl on a larger scale in the hopes of isolating ***meso*-3.4**. Attempts were made to add the reagent at both −78 °C and −20 °C, but in each case, no reaction was observed. A repeat of the procedure at room temperature with two equivalents of LiNp and one of *meso*-EBI*$ZrCl_2$ was allowed to stir for one hour in benzene before drying *in vacuo* and extraction in hexane. The resultant, dark-yellow solution was quickly dried and a small portion was dissolved in hexane at left to stand in the glovebox freezer at −35 °C. A microcrystalline solid was seen to form after four days which was removed from solution, and placed in a perfluoropolyether oil, also at −35 °C. The crystals were deemed too small for X-ray analysis on laboratory diffractometers, and the sample was taken to the synchrotron, Diamond Light Source. Data collection was carried out on a

specialist small molecule crystallography beamline, I19, and was seen to co-crystallise with hexane and two molecules of ***meso*-3.4** in the asymmetric unit, labelled **1** and **2** in Figure 3.14.

***meso*-3.4** crystallises in the triclinic spacegroup $P\bar{1}$, with four molecules in the unit cell as well as two molecules of hexane. All of the molecules were seen to be the same isomer, mirroring the simple pattern observed by ^{1}H NMR spectroscopy. Both molecules in the asymmetric unit show the chloride below the cyclopentadienyl ring and the neopentyl group positioned below the arene. This could be predicted from the NMR spectroscopic data as the shift of the methylene protons on the neopentyl group is drastically shielded (−2.23 ppm). This is attributed to similar ring current effects seen in ***meso*-3.3**.

The average zirconium-centroid distance (2.286 Å) reported for ***meso*-3.4** (isomer **1**) agrees well with that of both *meso*-EBI*$ZrCl_2$ (2.248 Å) and ***meso*-3.3** (2.299 Å), being intermediary which could be anticipated on either steric or electronic grounds. Only one previous zirconocene neopentyl chloride structure has previously been reported in the literature, with Bercaw and coworkers' report of Cp*CpZrNpCl in 2007.[44] This crystallises with both enantiomers in the unit cell and the average Zp-Cp_{cent} distance is 2.234 Å, with the bonds to the permethylated ligands slightly longer in each case. In addition to the neopentyl chloride complex above, Klamo *et al.* reported a bis(neopentyl) congener which joins two other structurally characterised bis(neopentyl) zirconocene in the literature. All of these mirror the reported metal-centroid distances (2.241-2.301 Å) although the mixed cyclopentadienyl system reports a shorter distance for the Cp*.[45,46]

The Zr(1)-C(33) distance in ***meso*-3.4** (2.293(3) Å) agrees well with that for the other structurally characterised zirconocene neopentyl chloride (2.3258(12) and 2.3287(12) Å for the two isomers) as well as with other zirconium neopentyl bonds in the literature (2.256-2.352 Å).[44–46] It also matches very closely to the Zr(1)-C(33)/C(40) bond distances reported for ***meso*-3.3** (2.325(4) and 2.322(3) Å). Meanwhile the zirconium chloride distance (2.4365(8) Å) matches well with the averages reported for ***rac*-3.1**, *meso*-EBI*$ZrCl_2$, and both isomers of Cp*CpZrNpCl (2.4224, 2.443 and 2.4473 Å).

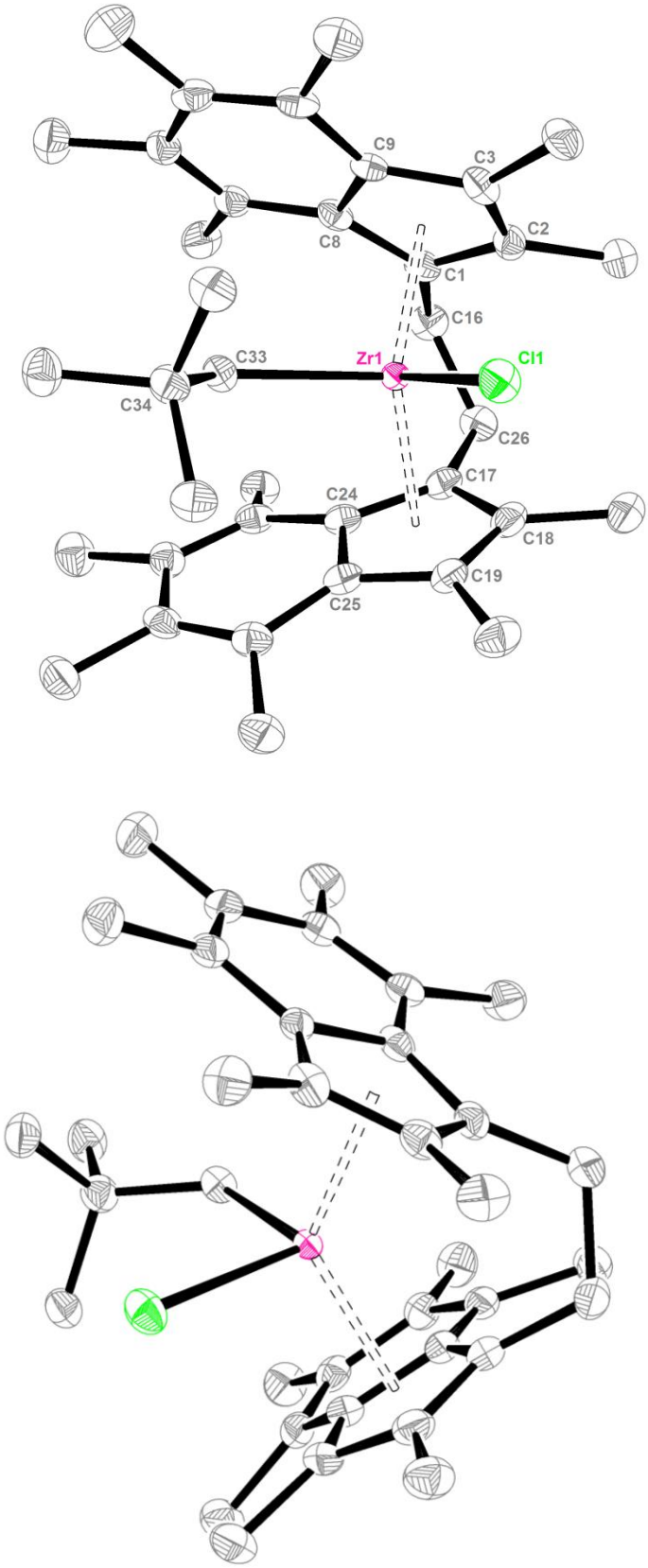


Figure 3.15: two views of the solid-state molecular structure of ***meso*-3.4** (isomer **1** shown). Hydrogens omitted for clarity. Thermal ellipsoids drawn at 50% probability.

Table 3.5: selected bond lengths (Å), angles (°), and geometric parameters (Å/°) for ***meso*-3.4** (isomer **1**). ESDs given in parentheses.

Bond Lengths (Å)			
Zr(1)-Cp_{cent}	2.285	Zr(1)-Cp_{cent}	2.287
Zr(1)-C(1)	2.482(3)	Zr(1)-C(17)	2.503(3)
Zr(1)-C(2)	2.552(3)	Zr(1)-C(18)	2.518(3)
Zr(1)-C(3)	2.626(3)	Zr(1)-C(19)	2.596(3)
Zr(1)-C(8)	2.662(3)	Zr(1)-C(24)	2.631(3)
Zr(1)-C(9)	2.619(3)	Zr(1)-C(25)	2.697(3)
Zr(1)-C(33)	2.293(3)	Zr(1)-Cl(1)	2.4365(8)
C(33)-C(34)	1.549(4)		
Avg. Cp C-C	1.431	Avg. Cp C-C	1.430
Avg. Cp C-Me	1.507	Avg. Cp C-Me	1.504
Avg. C_6 C-C	1.416	Avg. C_6 C-C	1.416
Avg. C_6 C-Me	1.510	Avg. C_6 C-Me	1.515
Δ_{M-C}	0.253	Δ_{M-C}	0.125
Bond Angles (°)			
C(33)-Zr(1)-Cl(1)	101.47(8)	Zr(1)-C(33)-C(34)	128.3(2)
α	60.49	δ	128.28
β	4.36	β	2.10
TA′	20.11	RA	46.80
HA	5.49	HA	2.44
FA	2.89	FA	3.29

The tilt angle (60.49°) is intermediary between *meso*-EBI*$ZrCl_2$ (56.87°) and ***meso*-3.3** (61.85°) which is very much as expected with just one bulky alkyl ligand at the metal centre forcing the rings apart. The value observed for ***meso*-3.4** is much closer to that of ***meso*-3.3** due to the comparable bulk of the $CH_2{}^tBu$ and the CH_2Ph moieties. The angle subtended at C(33) fits well with those reported for ***meso*-3.3**: 128.3(2), 119.5(2) and 128.8(3)° respectively. The value for TA′ (20.11°) shows the rings in ***meso*-3.4** to be close to eclipsed as in *meso*-EBI*$ZrCl_2$ (18.97°) and ***meso*-3.3** (17.42°).

One parameter which has not yet been discussed due to the insignificant values reported for the compounds so far is Δ_{M-C}. In one of the rings of ***meso*-3.4**, this value is recorded as 0.253 Å, suggesting that the mapping of the metal centre onto the ring is positioned significantly towards C(2). In bis(allyl) nickel complexes with fused rings, determined to bind η^3, the values reported are approximately 0.26 Å, suggesting that one of the rings in ***meso*-3.4** might also interact in this manner.[47] If we consider the valence electrons seen by the zirconium centre in ***meso*-3.4**, ten are expected from the two cyclopentadienyl rings, four from the neutral metal centre and one each from the chloride and the neopentyl group, totalling 16. It would be most unusual for a ring slip to occur at an electron deficient metal centre such as Zr(IV) and this effect is therefore attributed to the crystal packing. It should also be considered that as the nickel is held closer to the cyclopentadienyl ring (r_{Ni} = 0.55 Å, r_{Zr} = 0.59 Å),[48] the effect is more pronounced. No similar effect is noted for the other ring and the ^{1}H NMR spectroscopy determines that the complex has only one equivalent ring environment in solution.

DFT studies were undertaken for ***meso*-3.4** and a comparison of the pertinent bond angles is given below (Table 3.6).

Table 3.6: comparison of selected bond lengths (Å), angles (°) and geometric parameters (°) between the crystal structure of ***meso*-3.3** and DFT geometry optimisations using two basis sets: B3LYP and BP86.

Bond/Angle	Crystal	B3LYP	BP86
Avg. Zr-Cp_{cent} (Å)	2.286	2.349	2.329
Zr(1)-C(33) (Å)	2.293(3)	2.318	2.319
Zr(1)-Cl(1) (Å)	2.4365(8)	2.454	2.448
Δ_{M-C} (Å)	0.253/0.125	0.164/0.134	0.158/0.137
Zr(1)-C(33)-C(34) (°)	128.3(2)	127.41	127.42
α (°)	60.49	62.81	62.23
TA′ (°)	20.11	16.82	17.15

The DFT geometry optimisations in ***meso*-3.4** do not change the molecular parameters significantly although both basis sets do lengthen all contacts with the zirconium very slightly as well as increasing the value of α by approximately 2°, suggesting that the crystal structure is slightly overcrowded at the metal centre, and that there might be steric clashing with the large neopentyl. Both models also correct the observed value for Δ_{M-C}, reducing it by approximately 0.1 Å in each case.

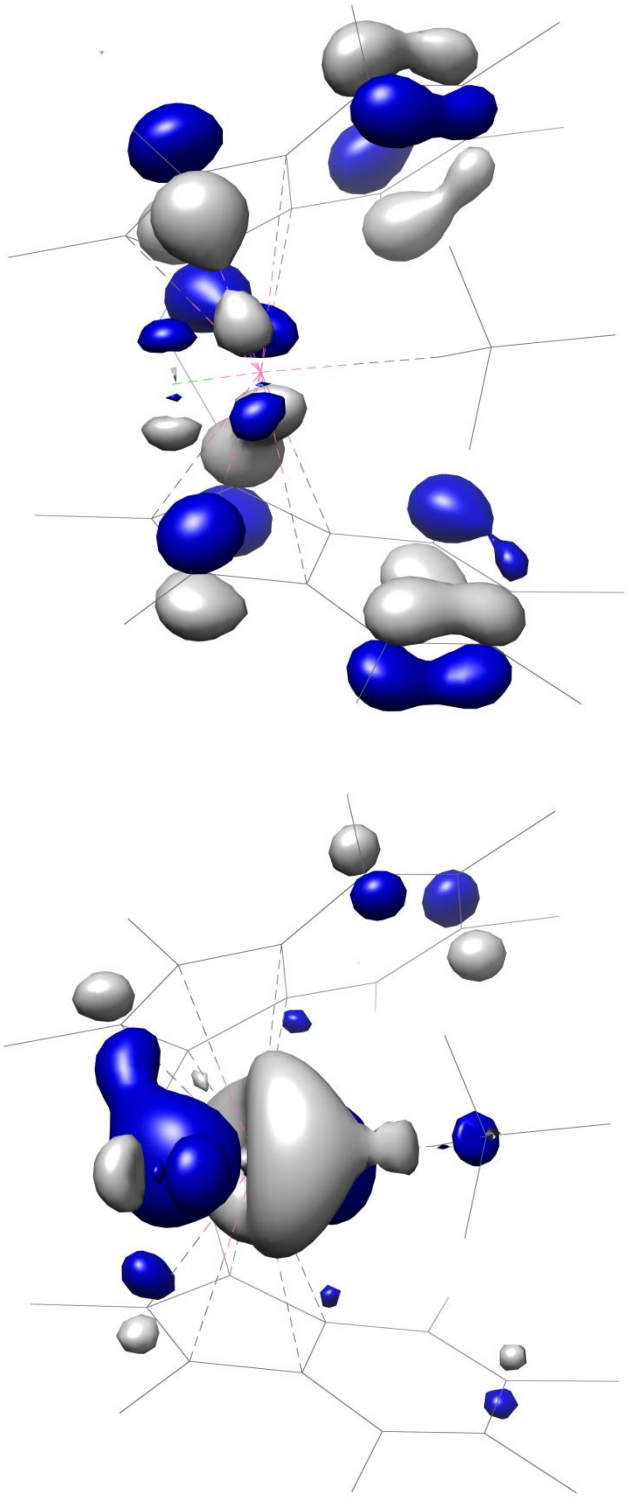


Figure 3.16: illustration of the DFT computed HOMO (top) and LUMO (bottom) of ***meso*-3.4** at the B3LYP level.

The calculated HOMO is predominantly based on the indenyl ligand, being more comparable to ***rac*-3.1**, than with it based on the ancillary ligands, as in ***meso*-3.3** (Figure

3.16). The LUMO is significantly based on the metal, as in all the reported d^0 zirconocenes, with 43.7% of the electron density based on the Zr d_{xy} orbital.

The ^{1}H NMR spectrum of ***meso*-3.4** in benzene-d_6 has an extremely shielded methylene group (−2.23 ppm) and a resonance with intensity nine (0.74 ppm) corresponding to the *tert*-butyl group of the neopentyl. Six methyl singlets fall in the range 1.91-2.53 ppm and the bridge multiplets are seen at 3.17 and 3.63 ppm. Co-crystallised hexane is also observed in the spectrum.

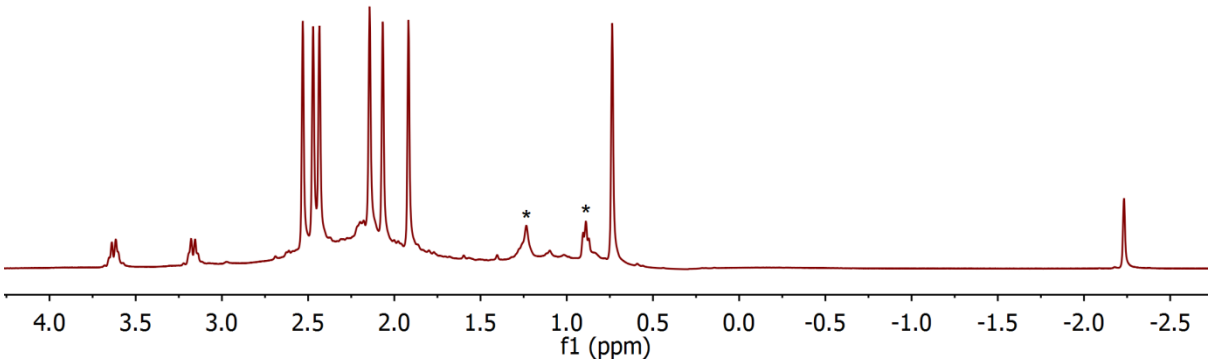
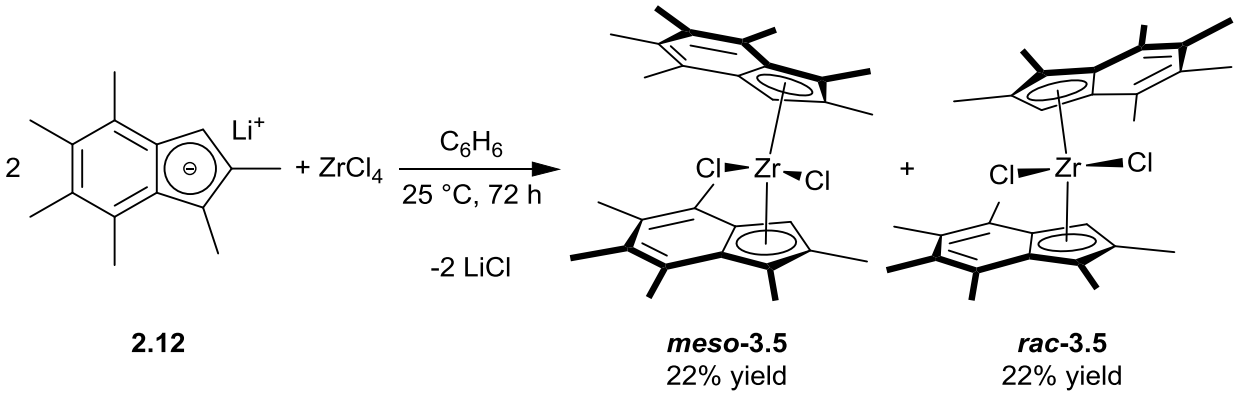


Figure 3.17: ^{1}H NMR spectrum of ***meso*-3.4** in benzene-d_6. Resonances relating to the co-crystallised hexane are marked with asterisks.

3.6 Synthesis of unbridged group 4 complexes

3.6.1 Synthesis of bis(2,3,4,5,6,7-hexamethylindenyl)zirconium dichloride, $Ind^{\#}_2ZrCl_2$ (3.5)



Scheme 3.5: synthesis of bis(2,3,4,5,6,7-hexamethylindenyl)zirconium dichloride, $Ind^{\#}_2ZrCl_2$ (**3.5**)

Given the success of the new synthetic route described in Chapter Two, and the previous ease of synthesis of the $Ind^{\#}_2Fe$, it was decided to use the hexamethylindenyl ligand for the synthesis group 4 metal complexes.[24] $Ind^{\#}_2ZrCl_2$, **3.5,** was first prepared as a mixture of isomers by John Coward in very low yield (<10%),[49] and crystals of both isomers were obtained. The crystal structure views and data are included here primarily for comparison to

***rac*-3.6** and ***meso*-3.6** (*vide infra*) as well as the other compounds described within this chapter. Two equivalents of Ind$^{\#}$Li were combined with $ZrCl_4$ in a Schlenk tube in the glovebox and the mixture was stirred in benzene. After 72 hours stirring, the reaction was deemed complete by ^{1}H NMR spectroscopy. The benzene solution was removed by hot filtration and reduced *in vacuo* affording a clean, even mixture of ***rac*-3.5** and ***meso*-3.5** in 44% isolated yield. Attempts to separate the mixture by fractional crystallisation in aliphatic hydrocarbon solvents failed, and after three successive recrystallisations from hexane, no change was observed in the isomeric ratio. However, a microcrystalline solid was obtained on each occasion, and the crystals were found suitable for X-ray analysis on beamline I19 at Diamond Light Source. Solid-state molecular structures are depicted in Figures 3.18 and 3.19.

Similar attempts at fractional crystallisation were attempted using aromatic solvents including benzene and toluene but no separation was observed. Attempts at separation by column chromatography also proved unsuccessful. **3.5** was tested for air- and moisture-stability, as had been reported for $Ind^*_2ZrCl_2$, and a filtered acetone solution of **3.5** was left to stand at −35 °C for three days. On decantation of the supernatant, crystals of two habits were seen to form: one forming dark orange blocks with a side length of up to 3 mm and the other very fine pale orange crystals with maximum length no more than 0.1 mm.

These crystals were separated by eye under a microscope and were seen to contain different isomers by ^{1}H NMR spectroscopy, confirming their separability. Analysis of the ^{1}H NMR spectra showed that it was the light orange microcrystalline solid that contained the resonance separated upfield from the rest of the methyls, usually found to correspond to *rac*. A unit cell analysis confirmed the dark orange solid to be ***meso*-3.5**, with the light-orange being ***rac*-3.5**. It was found that the procedure for fractional crystallisation in acetone could be optimised to yield only ***meso*-3.5** as a solid although it proved to be quite unreliable.

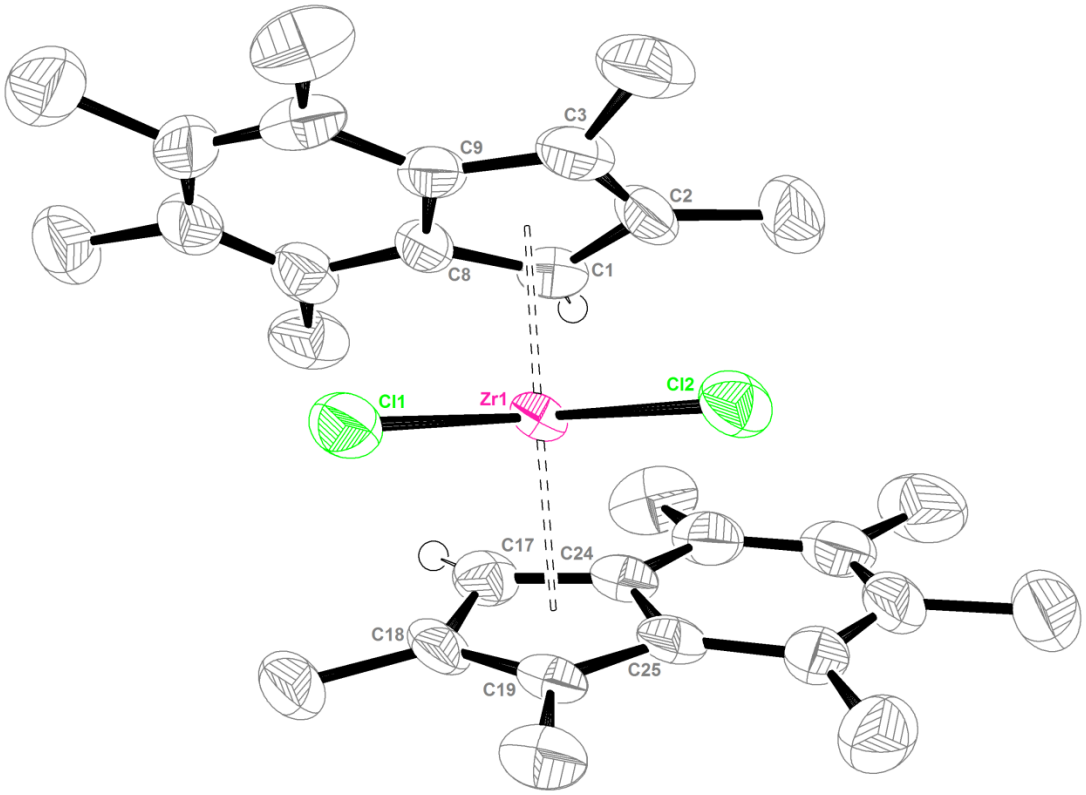


Figure 3.18: the solid-state molecular structure of ***rac*-3.5**. Methyl protons omitted for clarity. Thermal ellipsoids drawn at 50% probability. Crystals were grown by John Coward.[49]

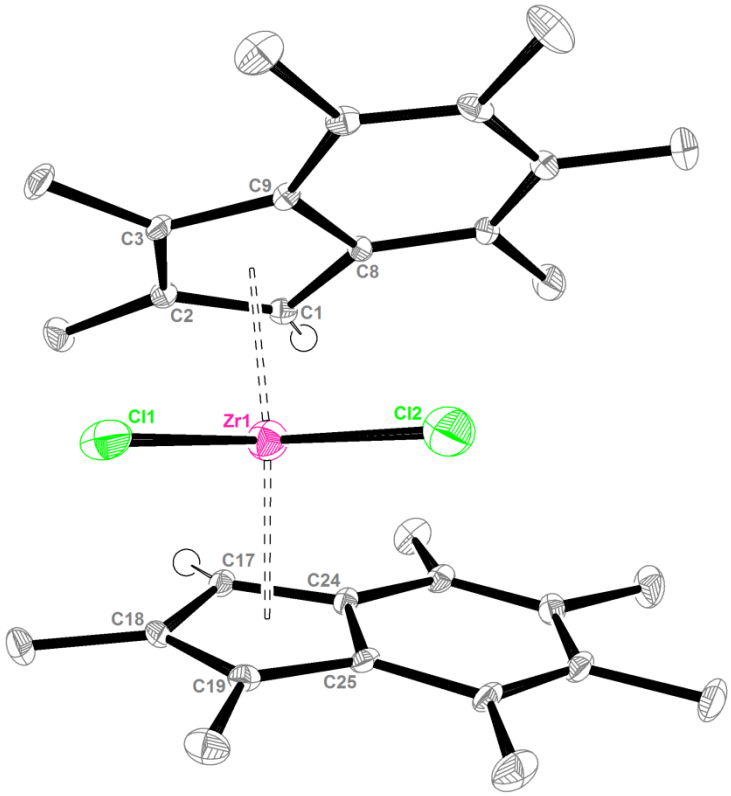


Figure 3.19: the solid-state molecular structure of ***meso*-3.5**. Methyl protons omitted for clarity. Thermal ellipsoids drawn at 50% probability. Crystals were grown by John Coward.[49]

Table 3.7: selected bond lengths (Å), angles (°), and geometric parameters (Å/°) for ***rac*-3.5**. ESDs given in parentheses.

Bond Lengths (Å)			
Zr(1)-Cp_{cent}	2.224	Zr(1)-Cp_{cent}	2.229
Zr(1)-C(1)	2.428(5)	Zr(1)-C(17)	2.447(5)
Zr(1)-C(2)	2.503(5)	Zr(1)-C(18)	2.530(4)
Zr(1)-C(3)	2.569(5)	Zr(1)-C(19)	2.530(4)
Zr(1)-C(8)	2.542(5)	Zr(1)-C(24)	2.557(5)
Zr(1)-C(9)	2.602(4)	Zr(1)-C(25)	2.598(5)
Zr(1)-Cl(1)	2.4136(14)	Zr(1)-Cl(2)	2.4279(14)
Avg. Cp C-C	1.415	Avg. Cp C-C	1.414
Avg. Cp C-Me	1.489	Avg. Cp C-Me	1.505
Avg. C_6 C-C	1.401	Avg. C_6 C-C	1.407
Avg. C_6 C-Me	1.507	Avg. C_6 C-Me	1.501
Δ_{M-C}	0.072	Δ_{M-C}	0.075
Bond Angles (°)			
Cl(1)-Zr(1)-Cl(2)	95.47(5)		
α	51.71	δ	133.59
TA′	174.77	RA	44.78
FA	5.81	FA	2.26

***rac*-3.5** was found to crystallise in the monoclinic spacegroup $P2_1/c$, with one molecule in the asymmetric unit and four in the unit cell, comprising both enantiomers. ***meso*-3.5** was also found to crystallise in a monoclinic crystal system but in a different spacegroup: $P2_1/n$. Once again only one molecule was seen in the asymmetric unit while four were observed in the unit cell. The bond lengths and angles for both forms of **3.5** are reported in Tables 3.7 and 3.8 and will be discussed with their hafnium analogues in section 3.6.2.

Table 3.8: selected bond lengths (Å), angles (°), and geometric parameters (Å/°) for ***meso*-3.5**. ESDs given in parentheses.

Bond Lengths (Å)			
Zr(1)-Cp_{cent}	2.251	Zr(1)-Cp_{cent}	2.249
Zr(1)-C(1)	2.452(2)	Zr(1)-C(17)	2.474(2)
Zr(1)-C(2)	2.518(2)	Zr(1)-C(18)	2.532(2)
Zr(1)-C(3)	2.607(2)	Zr(1)-C(19)	2.569(3)
Zr(1)-C(8)	2.573(2)	Zr(1)-C(24)	2.567(2)
Zr(1)-C(9)	2.637(2)	Zr(1)-C(25)	2.633(2)
Zr(1)-Cl(1)	2.4499(8)	Zr(1)-Cl(2)	2.4051(10)
Avg. Cp C-C	1.430	Avg. Cp C-C	1.428
Avg. Cp C-Me	1.503	Avg. Cp C-Me	1.508
Avg. C_6 C-C	1.415	Avg. C_6 C-C	1.416
Avg. C_6 C-Me	1.509	Avg. C_6 C-Me	1.513
Δ_{M-C}	0.079	Δ_{M-C}	0.075
Bond Angles (°)			
Cl(1)-Zr(1)-Cl(2)	95.35(4)		
α	53.40	δ	134.03
TA′	37.19	RA	55.96
FA	1.12	FA	3.45

The ^{1}H NMR spectrum of ***rac*-3.5** in chloroform-d_1 (Figure 3.20) comprises only singlets with a ratio of intensities of 1:3:3:3:3:3:3, corresponding to a cyclopentadienyl proton (6.26 ppm) and six methyl groups, with one at lower frequency (1.60 ppm). The spectrum is very similar to that reported for **2.12**.

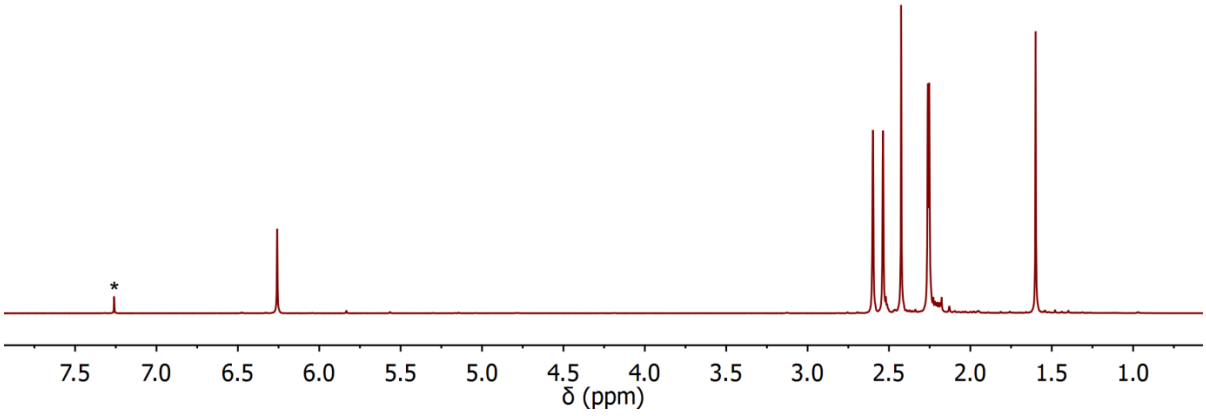


Figure 3.20: ^{1}H NMR spectrum of ***rac*-3.5** in chloroform-d_1. Asterisk marks the residual *protio*-solvent resonance.

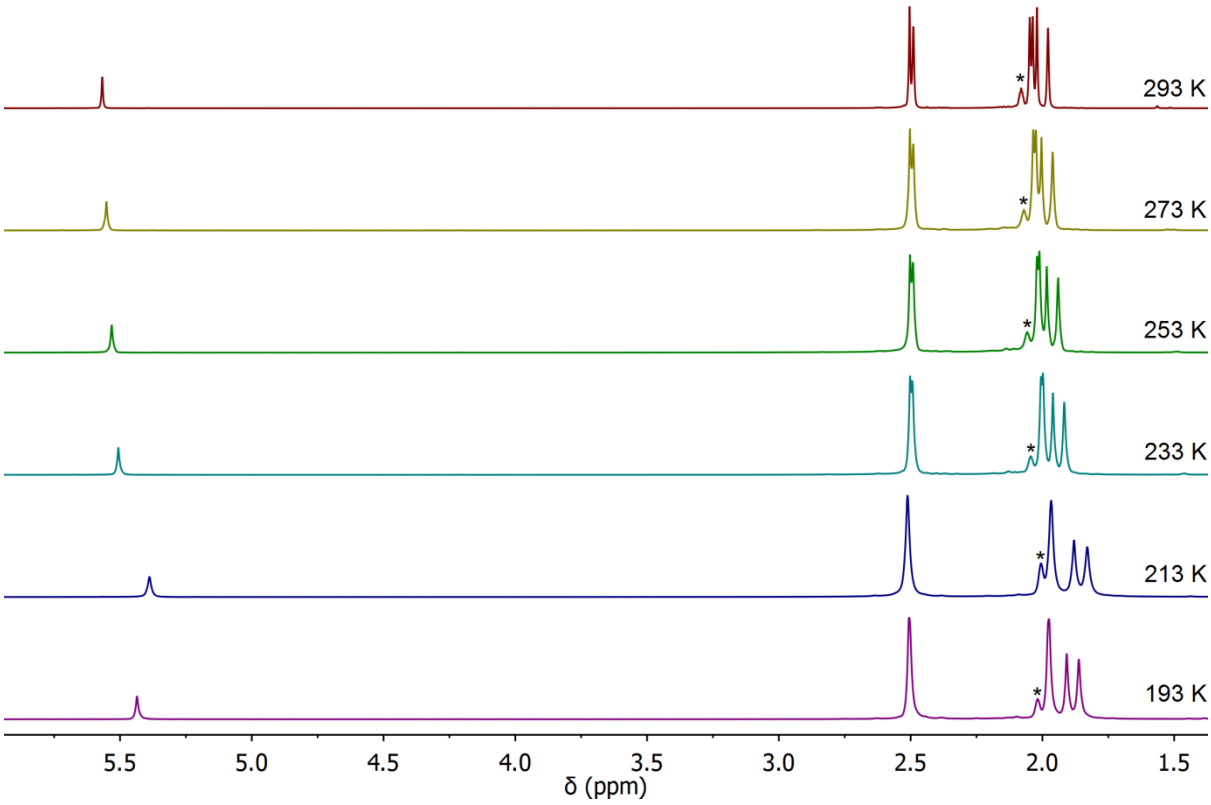


Figure 3.21: variable temperature ^{1}H NMR spectrum of ***meso*-3.5** in toluene-d_8. Asterisks mark the residual *protio*-solvent resonance.

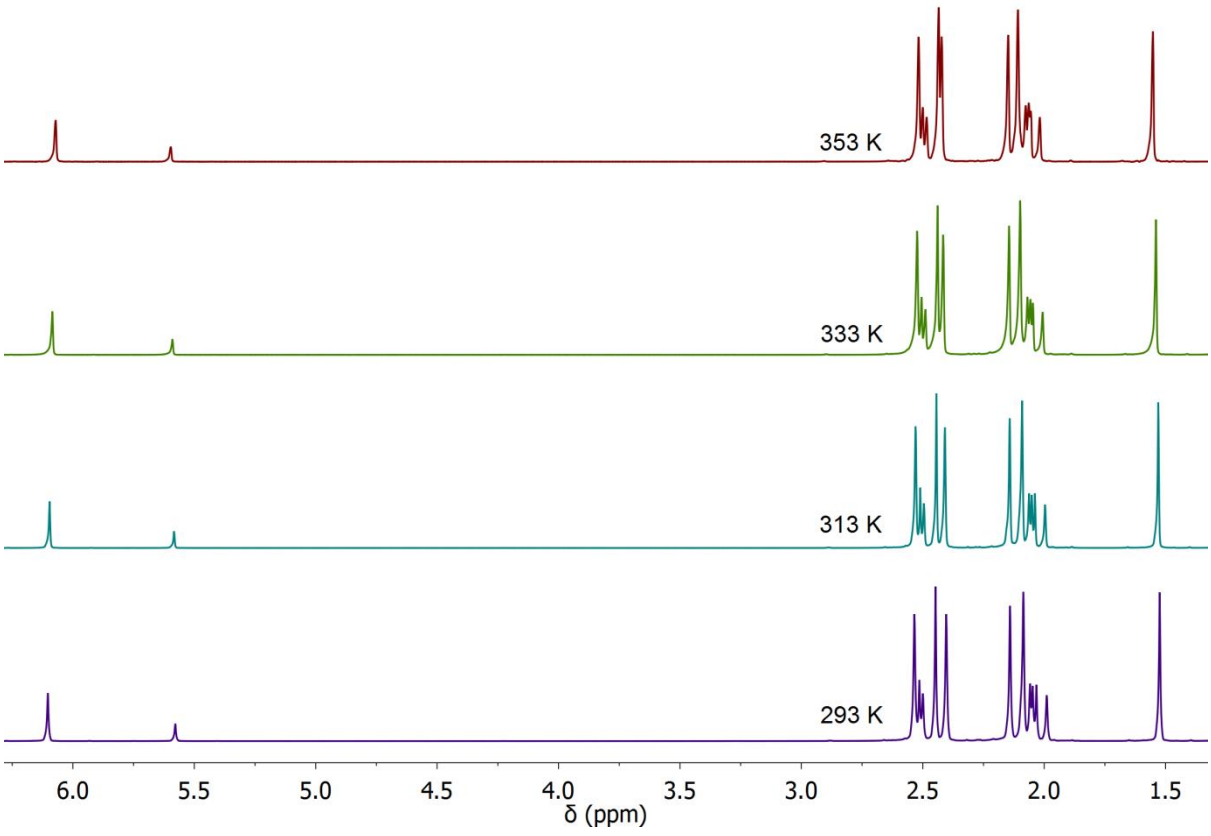
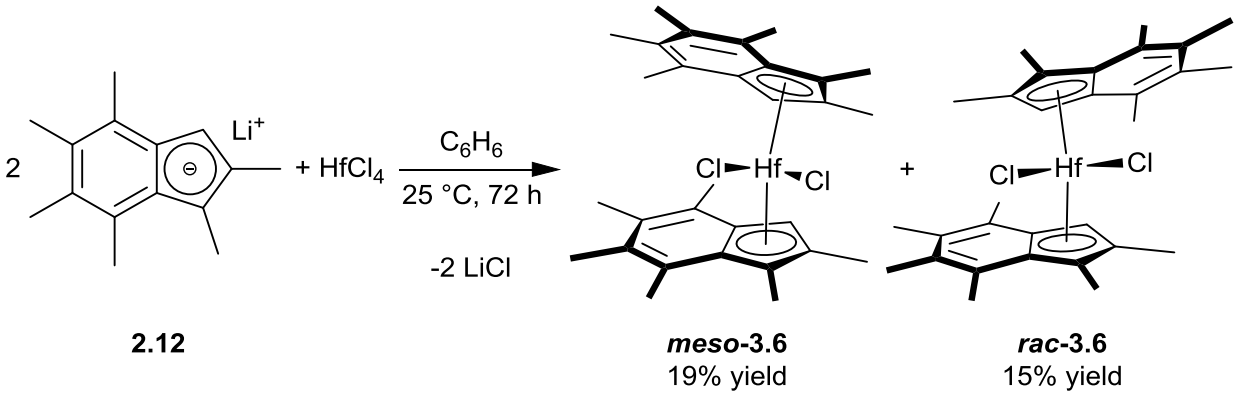


Figure 3.22: variable temperature ^{1}H NMR spectrum of both isomers of **3.5** (*rac*:*meso* 3:1) in toluene-d_8.

The ^{1}H NMR spectrum of ***meso*-3.5** in chloroform-d_1 contains the diagnostic resonances of ***rac*-3.5**, although all the methyls are grouped more closely spaced (2.13-2.52 ppm) and the cyclopentadienyl proton is shifted less far downfield (5.83 ppm). A variable temperature NMR study was carried out on ***meso*-3.5** in toluene-d_8 to investigate whether the rotation of the indenyl ligands is hindered at low temperature (Figure 3.21) – this is discussed in further detail in section 3.6.3.

A further variable temperature experiment was carried out for **3.5** (*rac*:*meso* 3:1) to ascertain whether there was any interconversion between the isomers at elevated temperatures (Figure 3.22). A sample comprising a mixture of isomers of **3.5** (*rac*:*meso* 3:1) was heated to 353 K and maintained at that temperature for one hour. No change in the isomeric ratio was noted either on heating or on re-cooling.

3.6.2 Synthesis of bis(2,3,4,5,6,7-hexamethylindenyl)hafnium dichloride, $Ind^{\#}_2HfCl_2$ (3.6)



Scheme 3.6: synthesis of bis(2,3,4,5,6,7-hexamethylindenyl)hafnium dichloride, $Ind^{\#}_2HfCl_2$ (**3.6**).

An analogous preparation to that used for **3.5** was attempted for the titanium and hafnium analogues using $TiCl_4$·2THF and $HfCl_4$. No tractable products were identified for the titanium species while the hafnium reaction proceeded as for the zirconium, reaching completion after 72 hours. A clean mixture of isomers (*rac*:*meso* 45:55) of $Ind^{\#}_2HfCl_2$ was obtained, again in moderate yield (34%). Single crystals suitable for an X-ray diffraction study were grown from hexane at −35 °C and were picked by eye for analysis of both isomers.

Solid state structures for of **3.6** are shown in Figures 3.20 and 3.21. Both pairs of isomers, ***rac*-3.5/3.6** and ***meso*-3.5/3.6** can be considered isomorphous with one another, with the *rac*-forms crystallising in $P2_1/c$ and the *meso*-isomers in $P2_1/n$. Although the volume range of the unit cells, each containing four molecules, is small across the four complexes (2594.3(4)-2633.74(4) Å^3), the cell parameters vary dramatically. The *a*, *b*, *c*, and β lattice parameters are approximately 17 Å, 9 Å, 18 Å and 115° for ***rac*-3.5/3.6**, and 13 Å, 15 Å, 14 Å and 99°

for ***meso*-3.5/3.6**. The ethylene-bridged permethylindenyl zirconium and hafnium congeners are also isostructural excepting *meso*-EBI*$ZrCl_2$ which was co-crystallised with toluene.[8]

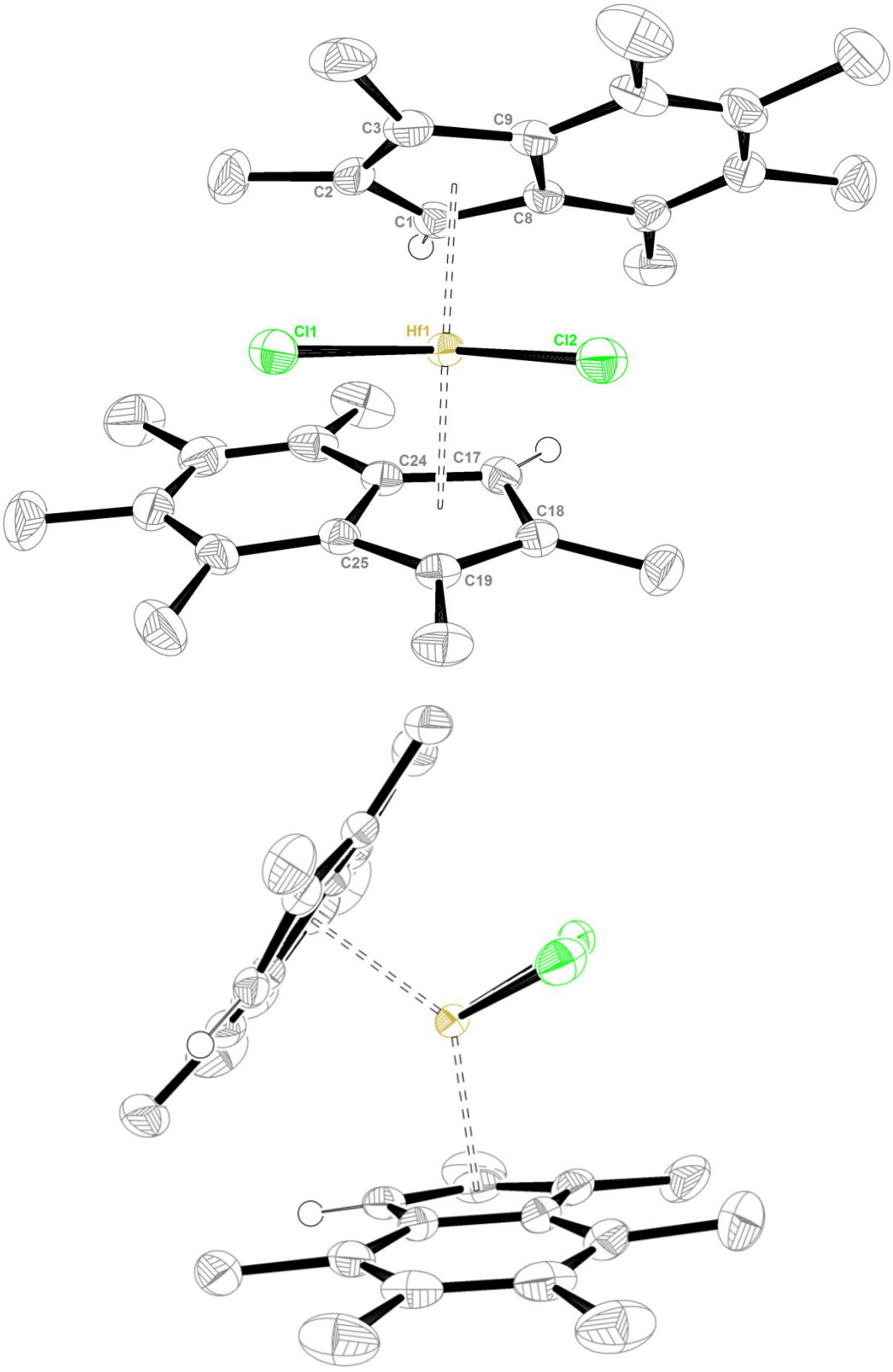


Figure 3.24: two views of the solid-state molecular structure of ***rac*-3.6**. Methyl protons omitted for clarity. Thermal ellipsoids drawn at 50% probability.

Table 3.9: selected bond lengths (Å), angles (°), and geometric parameters (Å/°) for ***rac*-3.6**. ESDs given in parentheses.

Bond Lengths (Å)			
Hf(1)-Cp_{cent}	2.216	Hf(1)-Cp_{cent}	2.217
Hf(1)-C(1)	2.4440(17)	Hf(1)-C(17)	2.4304(18)
Hf(1)-C(2)	2.5235(18)	Hf(1)-C(18)	2.4895(18)
Hf(1)-C(3)	2.5279(18)	Hf(1)-C(19)	2.5555(19)
Hf(1)-C(8)	2.5429(17)	Hf(1)-C(24)	2.5341(17)
Hf(1)-C(9)	2.5918(17)	Hf(1)-C(25)	2.6181(19)
Hf(1)-Cl(1)	2.4027(4)	Hf(1)-Cl(2)	2.4156(4)
Avg. Cp C-C	1.427	Avg. Cp C-C	1.424
Avg. Cp C-Me	1.501	Avg. Cp C-Me	1.505
Avg. C_6 C-C	1.414	Avg. C_6 C-C	1.412
Avg. C_6 C-Me	1.513	Avg. C_6 C-Me	1.511
Δ_{M-C}	0.069	Δ_{M-C}	0.084
Bond Angles (°)			
Cl(1)-Hf(1)-Cl(2)	94.803(17)		
α	51.58	δ	133.85
TA′	175.29	RA	44.19
FA	2.92	FA	5.75

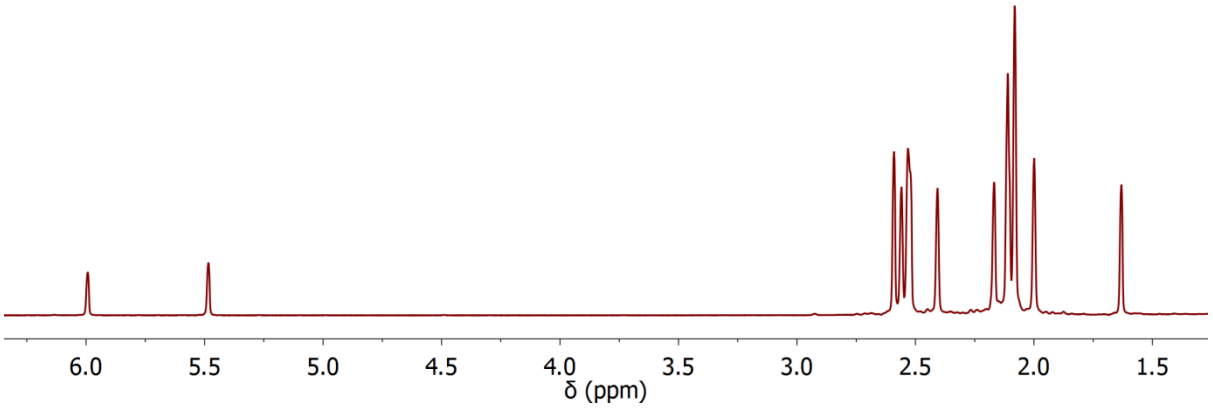


Figure 3.23: ^{1}H NMR spectrum of both isomers of **3.6** in benzene-d_6.

^{1}H NMR spectroscopy shows that the two isomers form in a nearly even mixture consisting of 55% ***meso*-3.6**. As with **3.5** they were found to have the same solubility in aliphatic and aromatic hydrocarbon solvents. Furthermore, they were found to be sensitive to moisture, immediately degrading on addition of benchtop acetone, inhibiting their separation.

Ethereal solvents were also employed to effect the isolation of one isomer in preference to the other but yielded no success.

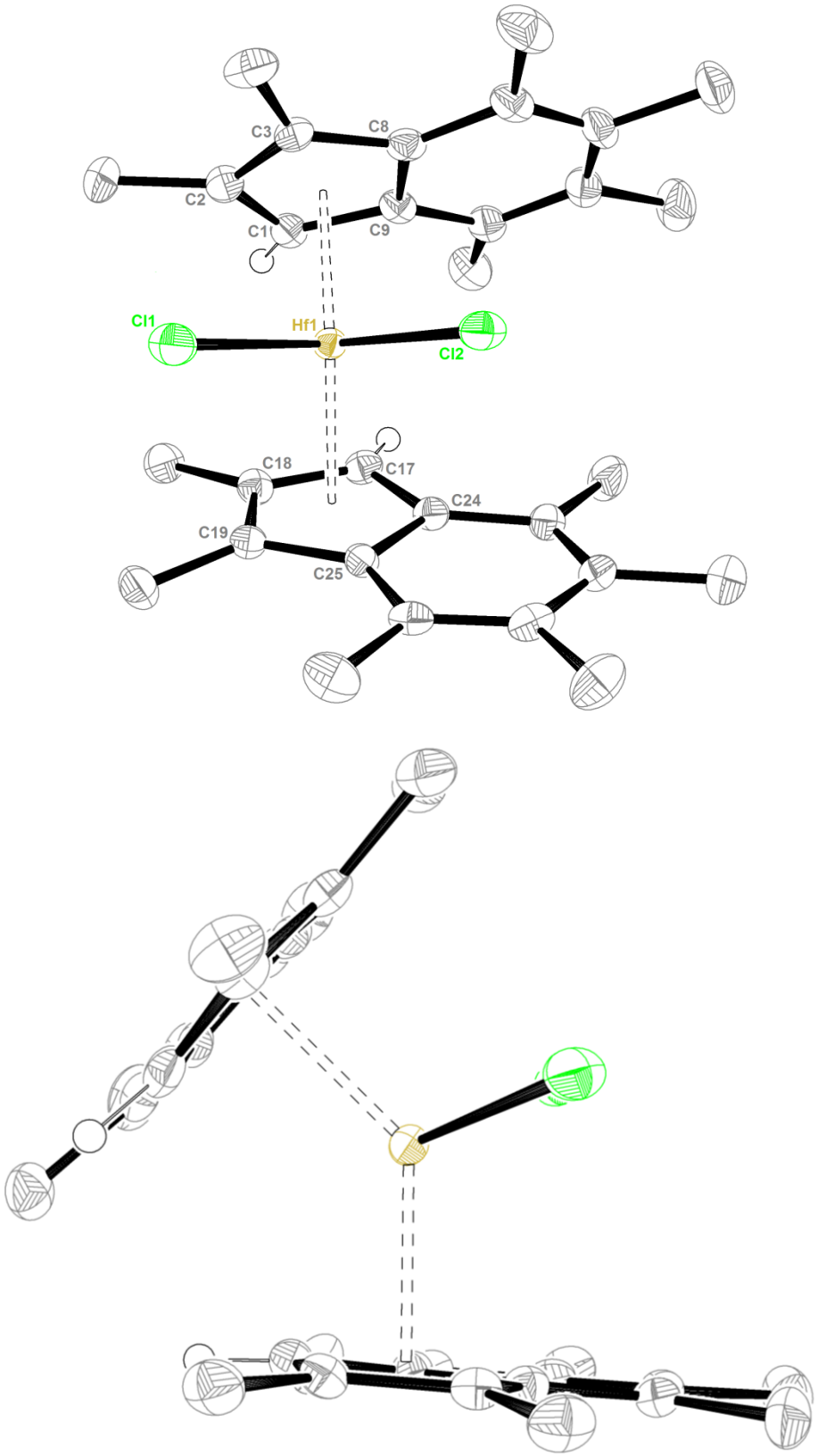


Figure 3.25: two views of the solid-state molecular structure of ***meso*-3.6**. Methyl protons omitted for clarity. Thermal ellipsoids drawn at 50% probability.

Table 3.10: selected bond lengths (Å), angles (°), and geometric parameters (Å/°) for ***meso*-3.6**. ESDs given in parentheses.

Bond Lengths (Å)			
Hf(1)-Cp_{cent}	2.225	Hf(1)-Cp_{cent}	2.229
Hf(1)-C(1)	2.462(3)	Hf(1)-C(17)	2.431(3)
Hf(1)-C(2)	2.509(3)	Hf(1)-C(18)	2.500(3)
Hf(1)-C(3)	2.540(3)	Hf(1)-C(19)	2.587(3)
Hf(1)-C(8)	2.546(3)	Hf(1)-C(24)	2.550(3)
Hf(1)-C(9)	2.616(3)	Hf(1)-C(25)	2.621(3)
Hf(1)-Cl(1)	2.4244(7)	Hf(1)-Cl(2)	2.3923(6)
Avg. Cp C-C	1.429	Avg. Cp C-C	1.429
Avg. Cp C-Me	1.503	Avg. Cp C-Me	1.498
Avg. C_6 C-C	1.416	Avg. C_6 C-C	1.413
Avg. C_6 C-Me	1.509	Avg. C_6 C-Me	1.510
Δ_{M-C}	0.078	Δ_{M-C}	0.229
Bond Angles (°)			
Cl(1)-Hf(1)-Cl(2)	94.31(3)		
α	53.50	δ	133.63
TA′	37.82	RA	57.25
FA	3.64	FA	1.40

Naturally the rotation of the indenyl rings, both RA and TA′, differ substantially between the *rac*- and *meso*-forms. The values (for ***rac*-3.5**, ***meso*-3.5**, ***rac*-3.6**, and ***meso*-3.6**) are 135.32°, 55.85°, 135.81°, and 57.25° for RA and 175.82°, 37.16°, 175.29° and 37.82° for TA′. This suggests that although the molecules are isostructural, they are not completely identical. These parameters compare moderately with those reported for *rac*-EBI*$ZrCl_2$ and *meso*-EBI*$ZrCl_2$ at 152.88° and 18.97° although there is clearly some constraining effect caused by the bridge.

In contrast, $Ind^*_2ZrCl_2$, immune to isomeric forms due to its symmetric rings, appears to be intermediate in structure with an RA of 91.27°,[50] while Ind_2ZrCl_2 registers 55.87°.[28] The values of α reported here (51.71°, 53.40°, 51.58° and 53.50°), however, compare more favourably with the unbridged analogues, $Ind^*_2ZrCl_2$ and Ind_2ZrCl_2, falling within the range 41.02° to 59.31° respectively. This might be expected on increasing the permethylation in order to create more space for the bulkier ligands. It is interesting to note that the orientation

of the rings in all four bis(hexamethylindenyl) dichloride structures leave the two cyclopentadienyl protons in alignment where one might expect to find the bridge. It is postulated that this is because it allows the rings to tilt away from the parallel to create more space for the methyl groups but the larger values of α seen for the ethylene bridged species (57.15°, 56.87°, 56.97° and 56.94°) suggests that the constraining geometry of the ethylene bridge exacerbates that effect.

The average M-Cp_{cent} distances observed for the $Ind^{\#}_2MCl_2$ (***rac*-3.5**, ***meso*-3.5**, ***rac*-3.6**, and ***meso*-3.6**) are 2.228 Å, 2.250 Å, 2.217 Å and 2.227 Å compare very favourably with those for the EBI* series (2.240 Å, 2.248 Å, 2.222 Å and 2.226 Å). In all cases the Zr-Cp_{cent} distances are longer than the hafnium equivalent, rationalised as being caused by the lanthanide contraction. This equates well with the ionic radii reported by Shannon which are nearly identical with the hafnium equivalent shorter by just 0.01 Å.[48] The *meso*-forms show longer bond lengths than the *rac*- as the steric repulsion between the eclipsed indenyl ligands might be expected to lengthen this bond. In addition the Zr-Cp_{cent} distances agree well with those reported for the Ind_2ZrCl_2 and its permethylated analogue, 2.231 Å and 2.257 Å. The M-Cl distances were also found to be in good agreement, with those for hafnium marginally shorter.

Table 3.11: comparison of selected bond lengths (Å), angles (°) and geometric parameters (°) between the crystal structures of ***rac*-3.6** and ***meso*-3.6**, and DFT geometry optimisations using two basis sets: B3LYP and BP86.

***rac*-3.6**	**Crystal**	**B3LYP**	**BP86**
Avg. Hf-Cp_{cent} (Å)	2.217	2.283	2.262
Avg. Hf-Cl (Å)	2.4092	2.427	2.414
Cl(1)-Hf(1)-Cl(2) (°)	94.803(17)	95.56	96.18
α (°)	51.58	52.47	53.20
TA′ (°)	175.29	170.16	179.64
***meso*-3.6**	**Crystal**	**B3LYP**	**BP86**
Avg. Hf-Cp_{cent} (Å)	2.227	2.282	2.262
Avg. Hf-Cl (Å)	2.4084	2.432	2.415
Cl(1)-Hf(1)-Cl(2) (°)	94.31(3)	94.66	95.94
α (°)	53.50	52.19	53.99
TA′ (°)	37.82	62.54	48.18

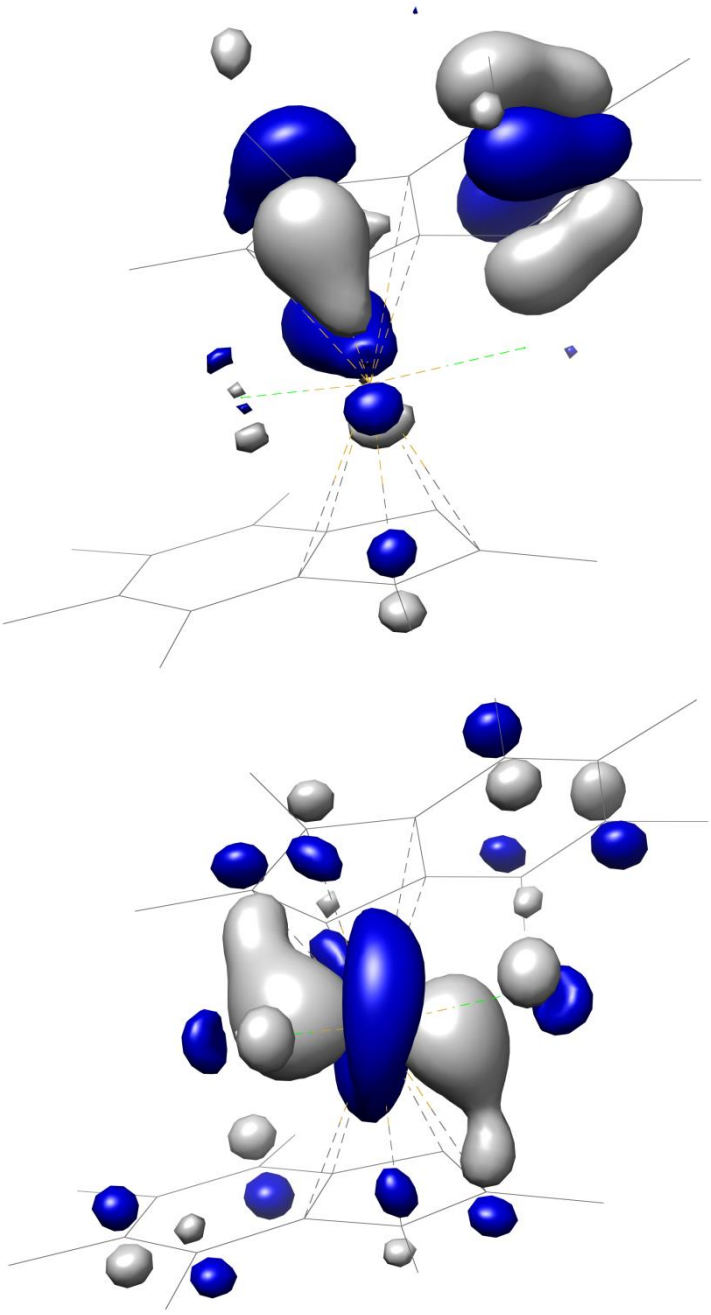


Figure 3.26: illustration of the DFT computed HOMO (top) and LUMO (bottom) of ***rac*-3.6** at the B3LYP level.

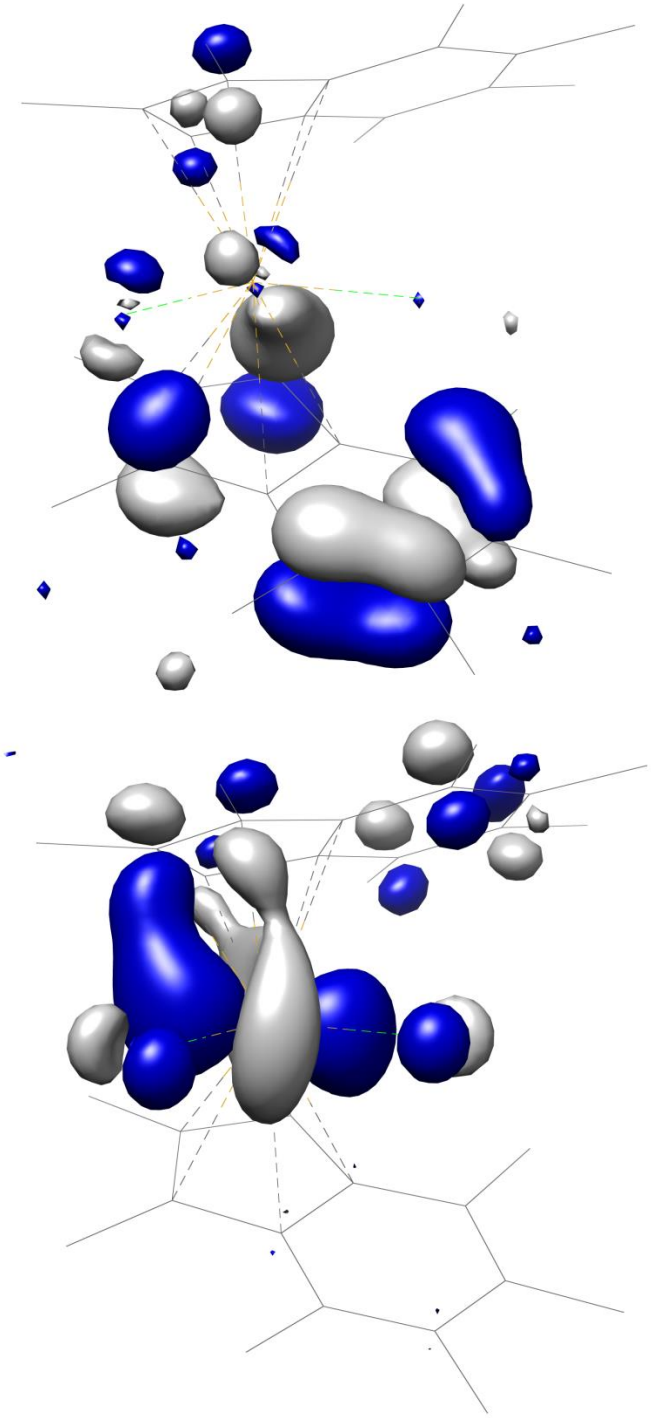


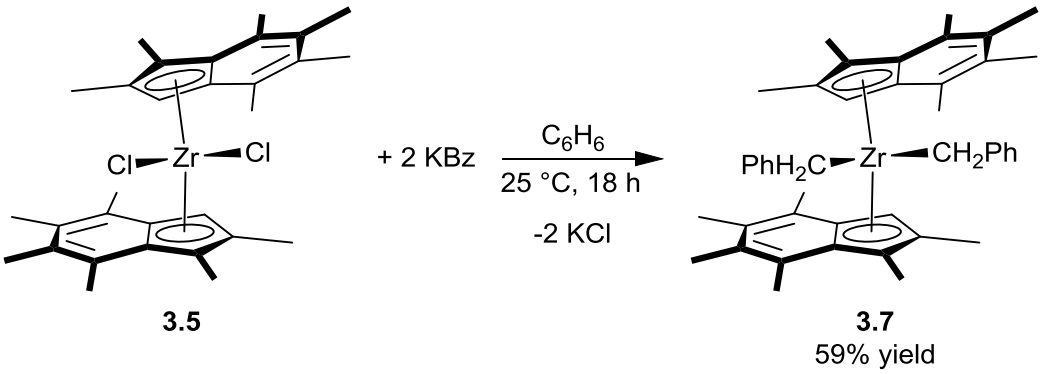
Figure 3.27: illustration of the DFT computed HOMO (top) and LUMO (bottom) of ***rac*-3.6** at the BP86 level.

DFT calculations were performed on both isomers of **3.6** and they were compared to the solid-state molecular structures. These calculations have already been reported for both isomers of **3.5**.[49] Most of the geometric parameters were found to be in excellent agreement, although the values for TA′ were seen to change quite significantly, particularly for ***meso*-3.6**. Under the calculations of both basis sets, TA′ was seen to increase, suggesting that the

structure becomes more gauche. This effect was most pronounced at the B3LYP level where an increase of approximately 25° was observed to 62.54°. The calculations were also used to confirm the occupancies of the HOMO and LUMO. While the latter are metal-based (***meso*-3.6**: 39.2% Hf d_{xy}, and ***rac*-3.6**: 20.7% Hf d_{xy} and 18.9% Hf $_{dx^2-y^2}$; BP86), as for all the zirconium species reported in this chapter, the former are based on the indenyl ligands. While electron density is spread over all the ligands in orbitals just below, the HOMO for both isomers localises the density on one of the indenyl ligands, particularly in the C p_z orbitals comprising the benzene double bonds (32.1% in ***rac*-3.6** and 30.3% in ***meso*-3.6**; BP86).

It was expected that the *rac*-isomer would have increased relative thermodynamic stabilities to the *meso*-isomer,[51,52] and the energy differences were calculated. The separations confirmed this but the values obtained were very small: 2 kJmol^{-1} and 2.5 kJmol^{-1} for **3.5** and **3.6** respectively. These are too small to be considered significant.

3.6.3 Synthesis of bis(2,3,4,5,6,7-hexamethylindenyl)zirconium dibenzyl, $Ind^{\#}_2ZrBz_2$ (3.7)



3.5 **3.7** 59% yield

Scheme 3.7: synthesis of bis(2,3,4,5,6,7-hexamethylindenyl)zirconium dibenzyl, $Ind^{\#}_2ZrBz_2$ (**3.7**)

Given the ease of the synthesis of ***meso*-3.3**, it was decided to attempt to synthesise the benzyl analogue of **3.5** using two equivalents of potassium benzyl. A quick test reaction in an NMR tube showed that the reaction proceeded smoothly on sonication. ^{1}H NMR spectroscopy revealed the cyclopentadienyl proton resonances reducing in intensity and new resonances growing into the spectrum. After sonication for two hours, the reaction appeared to have reached completion. Small singlets were noted in similar region that did not correspond either to **3.5** or **3.7**, and it was hypothesised that these might correspond to a mono-substituted, benzyl-chloride product. The reaction was repeated with only one equivalent of KBz but this simply led to the incomplete conversion of **3.5** to **3.7**.

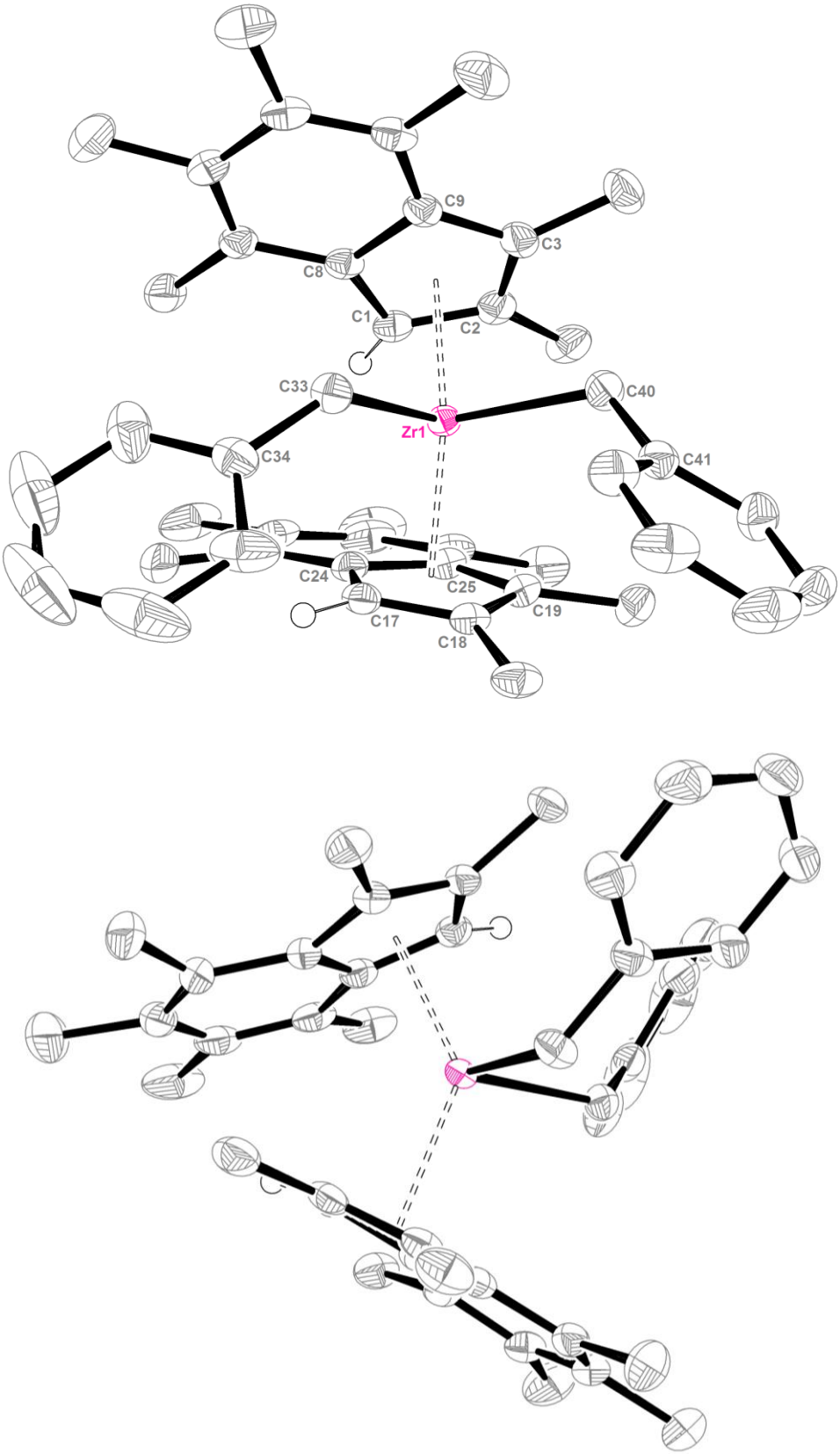


Figure 3.28: two views of the solid-state molecular structure of ***rac*-3.7**. Methyl and methylene protons omitted for clarity. Thermal ellipsoids drawn at 50% probability.

Table 3.12: selected bond lengths (Å), angles (°), and geometric parameters (Å/°) for ***rac*-3.7**. ESDs given in parentheses.

Bond Lengths (Å)			
Zr(1)-Cp_{cent}	2.306	Zr(1)-Cp_{cent}	2.263
Zr(1)-C(1)	2.4430(14)	Zr(1)-C(17)	2.4967(15)
Zr(1)-C(2)	2.5426(14)	Zr(1)-C(18)	2.5540(14)
Zr(1)-C(3)	2.6846(15)	Zr(1)-C(19)	2.5738(15)
Zr(1)-C(8)	2.6185(14)	Zr(1)-C(24)	2.5697(15)
Zr(1)-C(9)	2.7275(14)	Zr(1)-C(25)	2.6370(15)
Zr(1)-C(33)	2.3007(15)	Zr(1)-C(40)	2.3383(16)
C(33)-C(34)	1.476(2)	C(40)-C(41)	1.486(2)
Avg. Cp C-C	1.426	Avg. Cp C-C	1.425
Avg. Cp C-Me	1.503	Avg. Cp C-Me	1.505
Avg. C_6 C-C	1.414	Avg. C_6 C-C	1.415
Avg. C_6 C-Me	1.512	Avg. C_6 C-Me	1.510
Δ_{M-C}	0.116	Δ_{M-C}	0.062
Bond Angles (°)			
Zr(1)-C(33)-C(34)	131.33(11)	Zr(1)-C(40)-C(41)	127.55(11)
C(33)-Zr(1)-C(40)	94.53(6)	Ph-Ph planes	43.17
α	52.29	δ	132.74
TA′	95.90	RA	65.01
FA	6.15	FA	8.02

The reaction was repeated in a Schlenk tube and allowed to stir in benzene for 18 hours with periodic sonication, after which point the solvent was removed under vacuum. The product was extracted in hexane, and allowed to stand at −35 °C for four days, affording a ***rac*-3.7** as a bright yellow powder in 59% yield. The remaining solution still contained a mixture of isomers and despite further attempts at crystallisation, pure ***meso*-3.7** was never isolated. Crystals of ***rac*-3.7** suitable for X-ray analysis were grown from toluene in the glovebox at −35 °C (Figure 3.28). ***rac*-3.7** was found to crystallise as yellow blocks in the monoclinic spacegroup $P2_1/n$. Four molecules were found in the unit cell with only one in the asymmetric unit. However, the unit cell shape and volume (3507.48(4) $Å^3$) were notably different from the dichloride analogue.

The synthesis of ***meso*-3.7** from **3.5** was also carried out although attempts at crystallisation proved unsuccessful from either toluene or hexane, and pure ***meso*-3.7** was never isolated. It was, however analysed by ^{1}H NMR spectroscopy and found to give a spectrum with diastereotopic benzylic protons, none of which were significantly deshielded by ring current effects.

When comparing ***rac*-3.7** to ***rac*-3.5**, the striking feature is the dramatic decrease in TA′ for the benzyl complex, 95.93°, with respect to its dichloride counterpart, 175.82°. The primary cause of this must be down to the increased bulk of the ancillary ligands; by twisting one of the indenyl rings by approximately 90°, a whole face (out of the plane of the paper in Figure 3.26) of the complex has been opened up to accommodate the two benzyl groups. Similar effects are noted for $Ind^{R}_{2}ZrBz_{2}$ (Ind^{R} = 4,7-F_2-Ind) which has a TA of 110.48.[38] Both benzyl groups are seen to tilt in the same direction, presumably so as to avoid close interactions with the methyl substituents on the indenyl ring. This tilt is effected by the angles subtended at C33 and C40: 131.20(12)° and 127.57(12)° respectively. The angles between the planes of the phenyl rings (43.17°) is the lowest recorded for any zirconocene dibenzyl, attributed to space afforded by the gauche indenyl rings. As discussed for ***meso*-3.3** (*vide supra*), an η^1 benzyl bonding motif is seen for ***rac*-3.7**. Moreover, the values for δ_{ipso}, are 1.156 Å and 1.114 Å which exceeds the suggested limit allowing us to unequivocally assign the bonding as η^1 for both benzyl moieties and the formal valence electron count to 16.[42] The values for the direct zirconium-carbon bonds, Zr1-C33/40, are 2.3021(16) Å and 2.3385(16) Å. Unsurprisingly, these are shorter than the Zr-Cl distances reported for ***rac*-3.5** (2.4286(14) Å and 2.4135(14) Å) but fit well with those reported for similar species.[42] The value for α is 52.32° which is notably smaller than the values reported for the dichloride analogues. This is likely caused by the change to an intermediary TA′ of 95.93°, allowing the indenyl rings to flatten to reduce their interactions with one another, while still creating space for the benzyl groups. The Zr-Cp_{cent} distances of 2.263 Å and 2.305 Å are longer than those of ***rac*-3.5** (2.225 Å and 2.231 Å), indicating a slightly weaker indenyl-zirconium interaction to counterbalance the increased σ-donation from the benzyl groups with respect to the chlorides. A comparison of the significant bonding parameters for complexes **3.5**, **3.6** and **3.7** is given in Table 3.13.

Table 3.13: selected bond lengths (Å) and geometric parameters (°) for complexes containing Ind[#].

Complex	*rac*-3.5	*meso*-3.5	*rac*-3.6	*meso*-3.6	*rac*-3.7
Avg. M-Cp_{cent} (Å)	2.228	2.250	2.217	2.227	2.284
Avg. M-C_{Cp} (Å)	2.532	2.557	2.5986	2.536	2.5258
Avg. M-Cl* (Å)	2.4211	2.4277	2.4092	2.4084	2.3203*
TA′ (°)	175.82	37.16	175.29	37.82	95.93
α (°)	41.84	53.28	51.58	53.50	52.32

* indicates the M-C_{benzyl} distance where applicable.

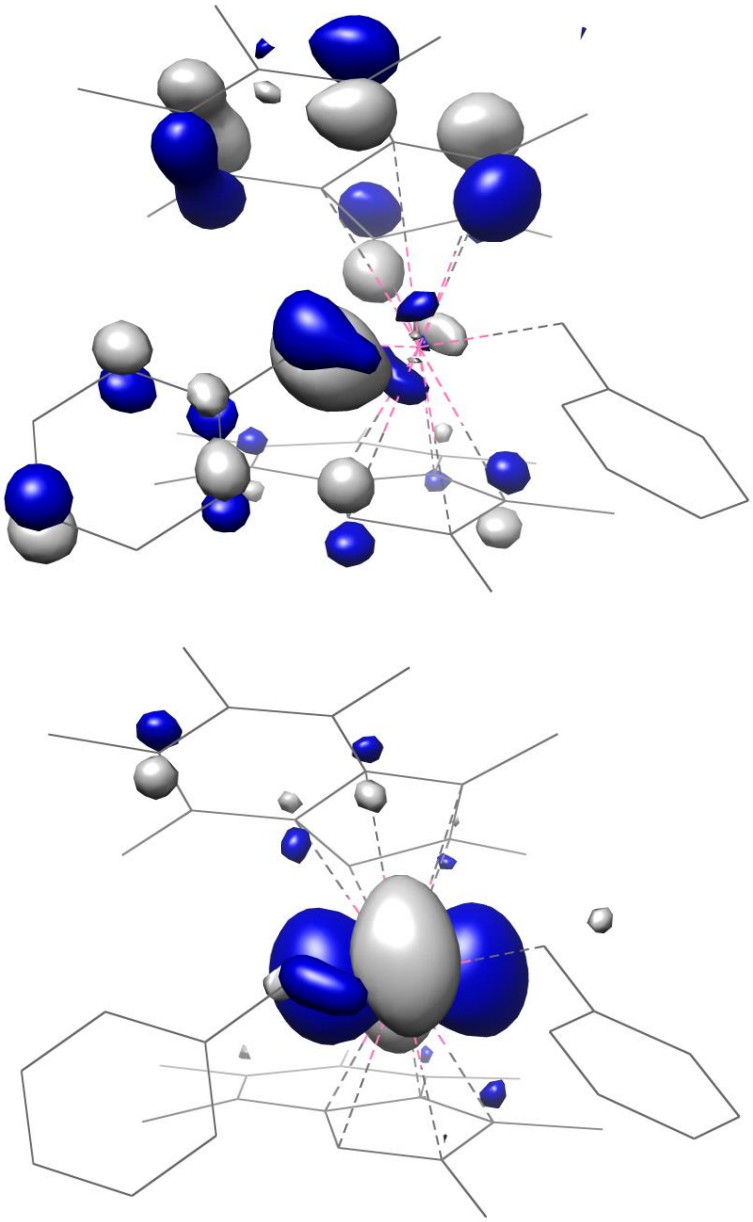


Figure 3.29: illustration of the DFT computed HOMO (top) and LUMO (bottom) of ***rac*-3.7** at the BP86 level.

Table 3.14: comparison of selected bond lengths (Å), angles (°) and geometric parameters (°) between the crystal structure of ***rac*-3.7** and DFT geometry optimisations using two basis sets: B3LYP and BP86.

Bond/Angle	Crystal	B3LYP	BP86
Avg. Zr-Cp_{cent} (Å)	2.285	2.344	2.317
Avg. Zr-C(33)/(40) (Å)	2.320	2.341	2.340
Zr(1)-C(33)-C(34) (°)	131.33	131.06	130.15
Zr(1)-C(40)-C(41) (°)	127.56	137.44	135.62
α (°)	52.32	51.74	52.12
TA′ (°)	95.93	93.06	97.11

The frontier MOs for ***rac*-3.7** are very similar to those reported for other $Ind^{\#}$ containing species with the HOMO predominantly concentrated on one indenyl ligand and the LUMO on the metal centre (Zr d_{xy} 56.7 %). Similarly the geometry optimisation agrees well with the reported parameters from the crystal structure, maintaining the low angle (*c.* 40°) between the planes of the phenyl rings and the gauche orientation of the indenyl ligands.

***rac*-3.7** was studied using ^{1}H NMR spectroscopy in toluene-d_8 and the resonances corresponding to the $Ind^{\#}$ fragment are similar to those reported for **3.5** and **3.6**, with six methyl resonances (1.78-2.38 ppm) and a singlet (4.83 ppm) corresponding to the cyclopentadienyl proton. This proton is slightly shielded compared to ***rac*-3.5**, thought to be due to the gauche orientation placing the protons within reach of the arene ring currents. Unlike ***meso*-3.3**, the benzylic protons were found to be diastereotopic, showing as a pair of roofed doublets at 0.94 and 1.10 ppm. The two benzyl groups are more similar to one another in the solid-state as well with the angles subtended at C(33) and C(40) separated by less than 4°, as opposed to more than 9° for ***meso*-3.3**.

It was anticipated that, on cooling ***rac*-3.7** (Figure 3.0)**,** the indenyl ring rotation might be hindered by the bulky benzyl groups, allowing two different environments to be identified on the NMR timescale. On cooling to 178 K, the limit of toluene-d_8, the benzylic and Cp protons were seen to broaden into the baseline. However, it was not possible to cool the sample further in order to determine the energy barrier to rotation at the coalescence point or the chemical shifts of the separate environments. The methyl and aromatic resonances were also seen to broaden and shift, although the effect is less dramatic.

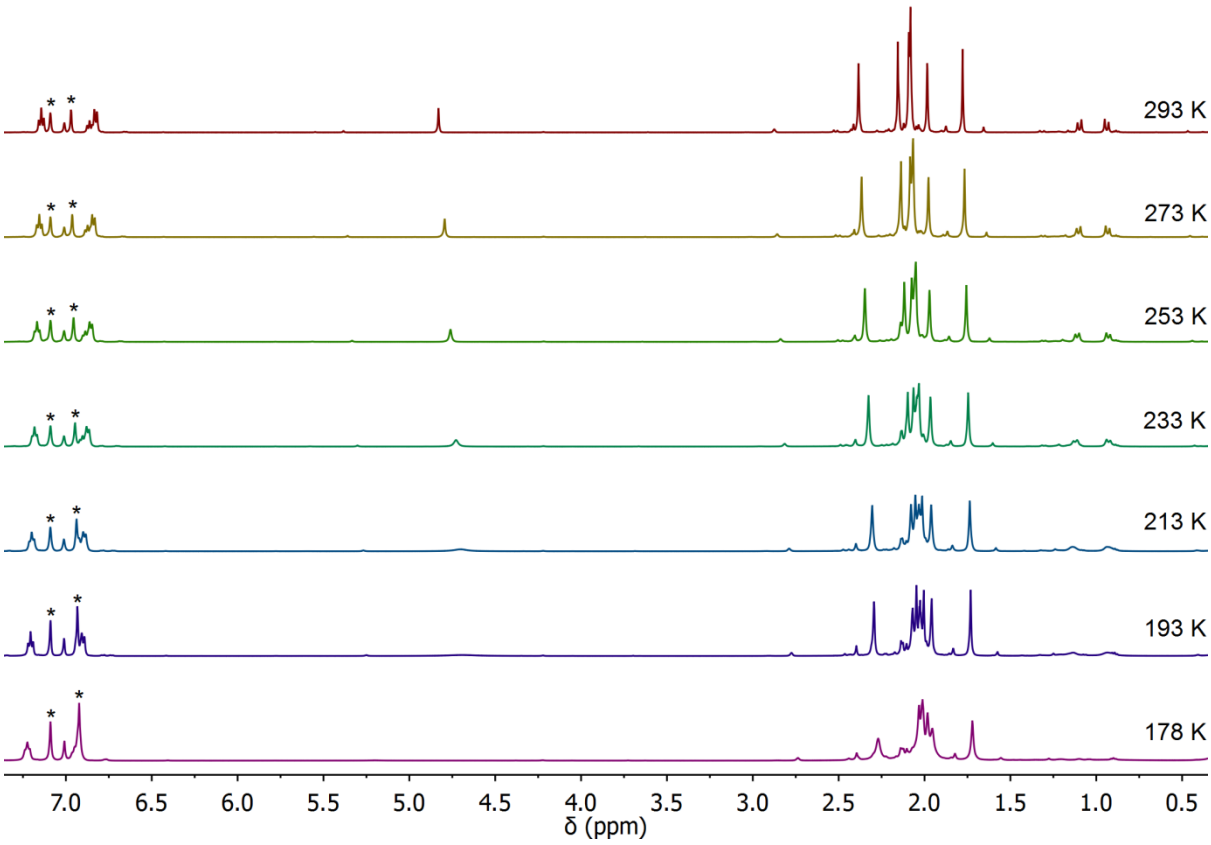
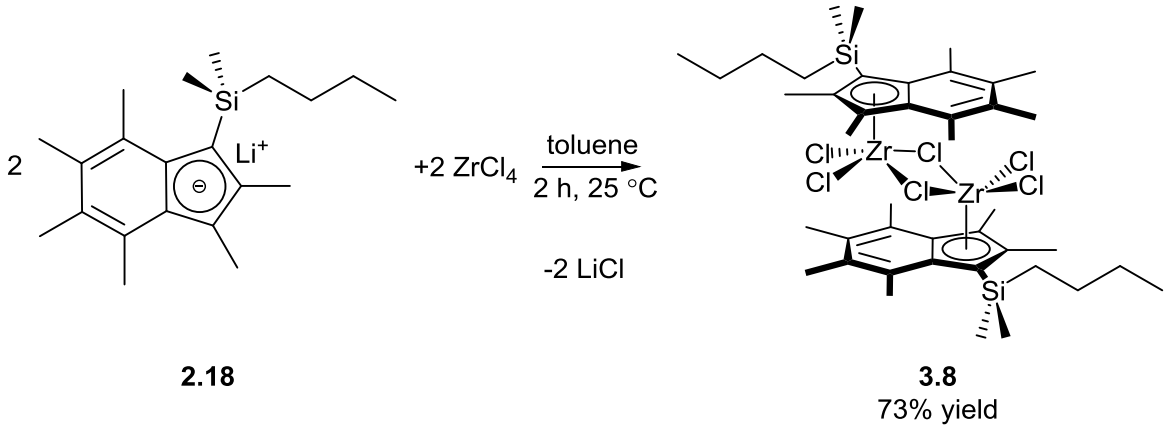


Figure 3.30: variable temperature ^{1}H NMR spectrum of ***rac*-3.7** in toluene-d_8.

3.7 Synthesis of {*n*-butyldimethylsilyl[1-(2,3,4,5,6,7-hexamethylindenyl)]} zirconium trichloride (3.8)



2.18 **3.8** 73% yield

Scheme 3.8: synthesis of {*n*-butyldimethylsilyl[1-(2,3,4,5,6,7-hexamethylindenyl)]} zirconium trichloride (**3.8**)

Stoichiometric reaction of **2.18** with $ZrCl_4$ was both facile and high yielding, and after stirring in toluene for just two hours, the red solution was filtered off and left to stand at −35 °C for three days. Decantation of the solution afforded **3.8** as a red crystalline solid in 73%

yield. The crystals were found to be suitable for analysis by X-ray diffraction and **3.8** was found to exist as a dimer, $[(Ind^{\#}SiMe_2{}^{n}Bu)Zr(\mu\text{-}Cl)Cl_2]_2$, in the solid-state.

3.8 crystallises in the triclinic spacegroup $P\bar{1}$, with half a dimer in the asymmetric unit and one dimer in the unit cell (Figure 3.31). The Zr(1)-Cp_{cent} distance (2.190 Å) is shorter than those reported for the metallocenes in this chapter – this is thought to be due to the absence of another strongly donating indenyl ligand which reduces the electron deficiency on the zirconium centre. There are no other structurally characterised indenyl zirconium trichlorides in the literature without a pendant donor atom, but the cyclopentadienyl congener exists as a polymer with Zr-Cp_{cent} distances of 2.199 Å, in excellent agreement with **3.8**.[53]

Table 3.15: selected bond lengths (Å), angles (°), and geometric parameters (Å/°) for **3.8**. ESDs given in parentheses.

Bond Lengths (Å)			
Zr(1)-Cp_{cent}	2.190	Zr(1)-C(3)	2.5626(17)
Zr(1)-C(1)	2.4298(16)	Zr(1)-C(8)	2.5203(16)
Zr(1)-C(2)	2.4655(17)	Zr(1)-C(9)	2.5678(16)
Zr(1)-Cl(1)	2.4038(5)	Zr(1)-Cl(2)	2.3983(5)
Zr(1)-Cl(3)	2.5833(4)	Zr(1)-Cl(3)′	2.5837(4)
Si(1)-C(1)	1.9114(17)	Si(1)-C(35)	1.8826(19)
Si(1)-C(33)	1.885(2)	Si(1)-C(34)	1.876(2)
Avg. Cp C-C	1.442	Avg. C_6 C-C	1.418
Avg. Cp C-Me	1.508	Avg. C_6 C-Me	1.513
$\Delta_{M\text{-}C}$	0.058		
Bond Angles (°)			
Cl(1)-Zr(1)-Cl(2)	91.215(18)	Cl(1)-Zr(1)-Cl(3)′	82.675(15)
Cl(2)-Zr(1)-Cl(3)	82.787(15)	Cl(3)-Zr(1)-Cl(3)′	74.711(14)
C(1)-Si(1)-C(35)	115.24(8)	C(33)-Si(1)-C(34)	104.37(10)
FA	3.71		

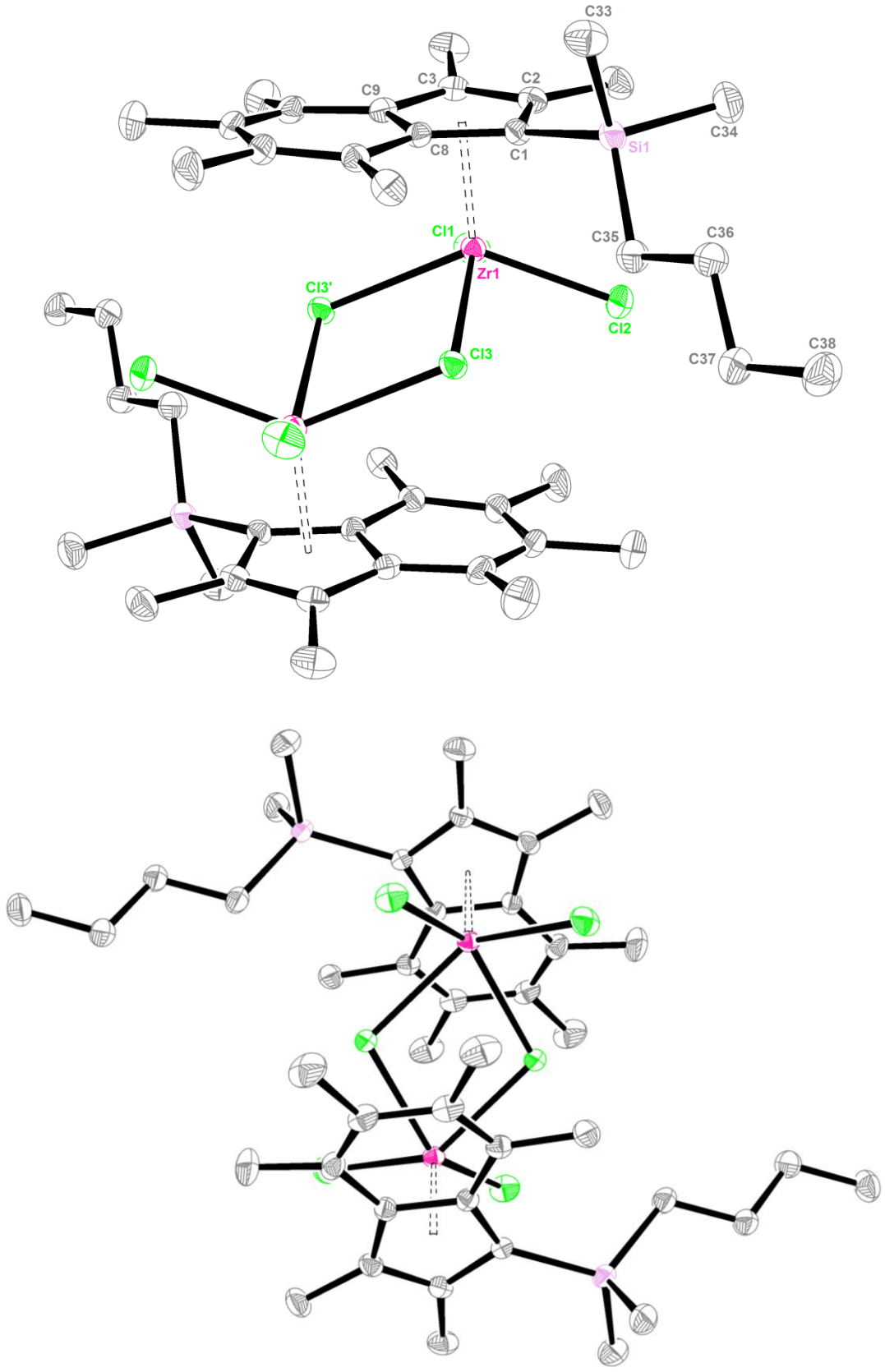


Figure 3.31: two views of the dimeric solid-state molecular structure of **3.8**. Hydrogens omitted for clarity. Thermal ellipsoids drawn at 50% probability.

As might be expected, the bond lengths for the terminal chlorides (2.4038(5) and 2.3983(5) Å) are significantly shorter than those of the bridging chlorides (2.5833(4) and 2.5837(4) Å). These agree well with the Zr-Cl distances reported for "$CpZrCl_3$" of 2.419(3) Å for the terminal chlorides and 2.518(3)-2.728(3) Å for the bridging ligands. Given the increased proximity of the terminal chlorides, Cl(1) and Cl(2), to the zirconium, the angle Cl(1)-Zr(1)-Cl(2) (91.215(18)°) is larger than that between the bridging halides (74.711(14)°). The other two Cl-Zr-Cl angles are intermediate.

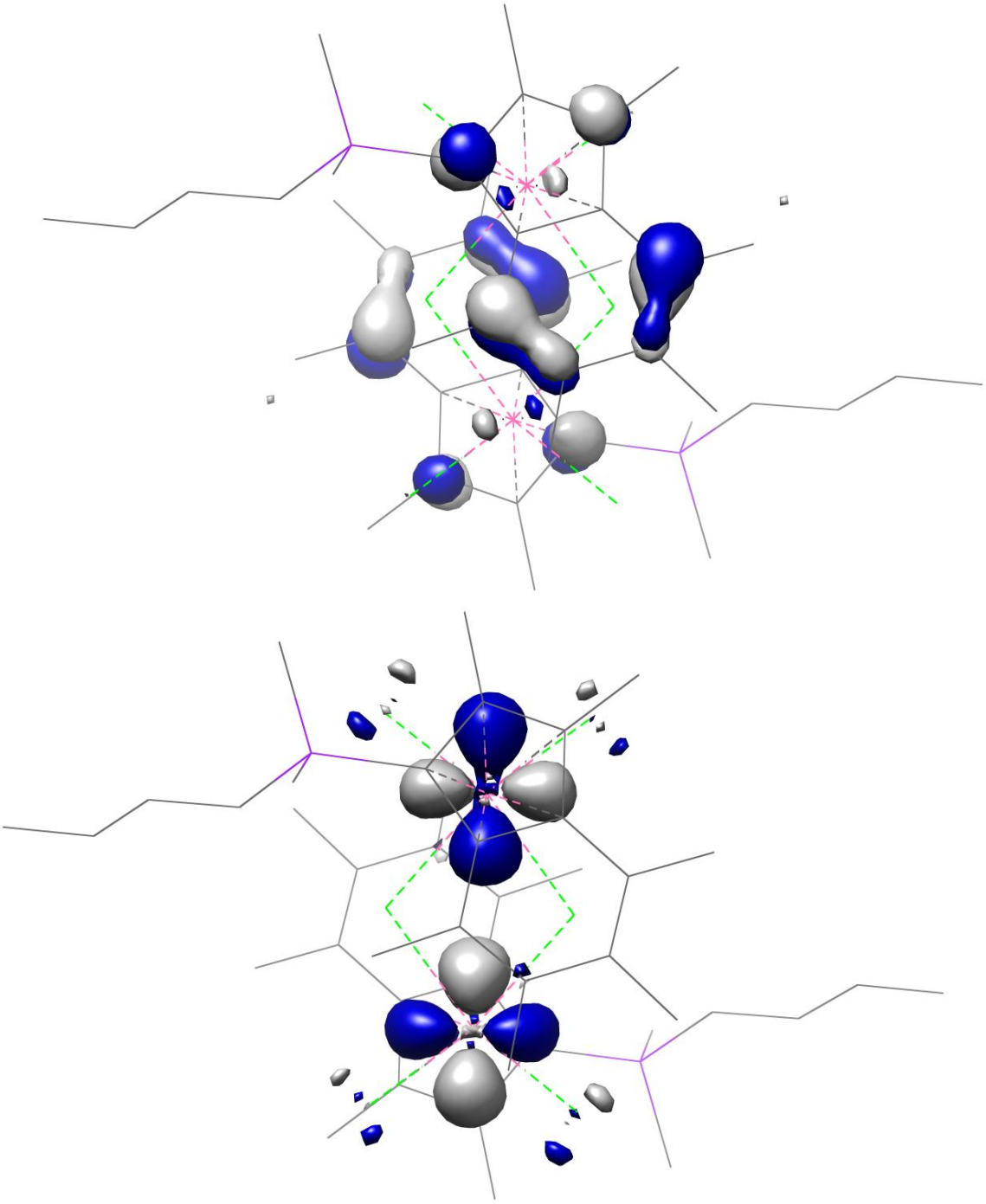


Figure 3.30: Illustration of the DFT computed HOMO (top) and LUMO (bottom) of **3.8** at the BP86 level.

Table 3.16: comparison of selected bond lengths (Å), angles (°) and geometric parameters (°) between the crystal structure of **3.8** and DFT geometry optimisations using two basis sets: B3LYP and BP86.

Bond/Angle	Crystal	B3LYP	BP86
Zr-Cp_{cent} (Å)	2.190	2.234	2.215
Avg. Zr-$Cl_{terminal}$ (Å)	2.4011	2.420	2.418
Avg. Zr-$Cl_{bridging}$ (Å)	2.5835	2.656	2.643
Cl(1)-Zr(1)-Cl(2) (°)	91.215(18)	90.74	91.59

DFT calculations were performed on **3.8**, highlighting the localised double bonds in the benzene rings in the HOMO. The LUMO is based on the zirconium d_{xy} orbital with 54.6% of the electron density. Geometry optimisations in both B3LYP and BP86 agree well with the data obtained from the crystallographic analysis (Table 3.16).

3.8 was analysed by ^{1}H NMR spectroscopy giving a spectrum very similar to that of **2.18** (Figure 3.33). In benzene-d_6, the six methyl singlets appear in the range 1.96-2.57 ppm with the silyl methyl singlets distinct from one another at 0.55 and 0.65 ppm. Multiplets relating to the butyl tether appear at 0.86, 1.00, 1.26 and 1.29 ppm for the δ, α, γ and β positions respectively. These assignments have been confirmed by ^{1}H COSY.

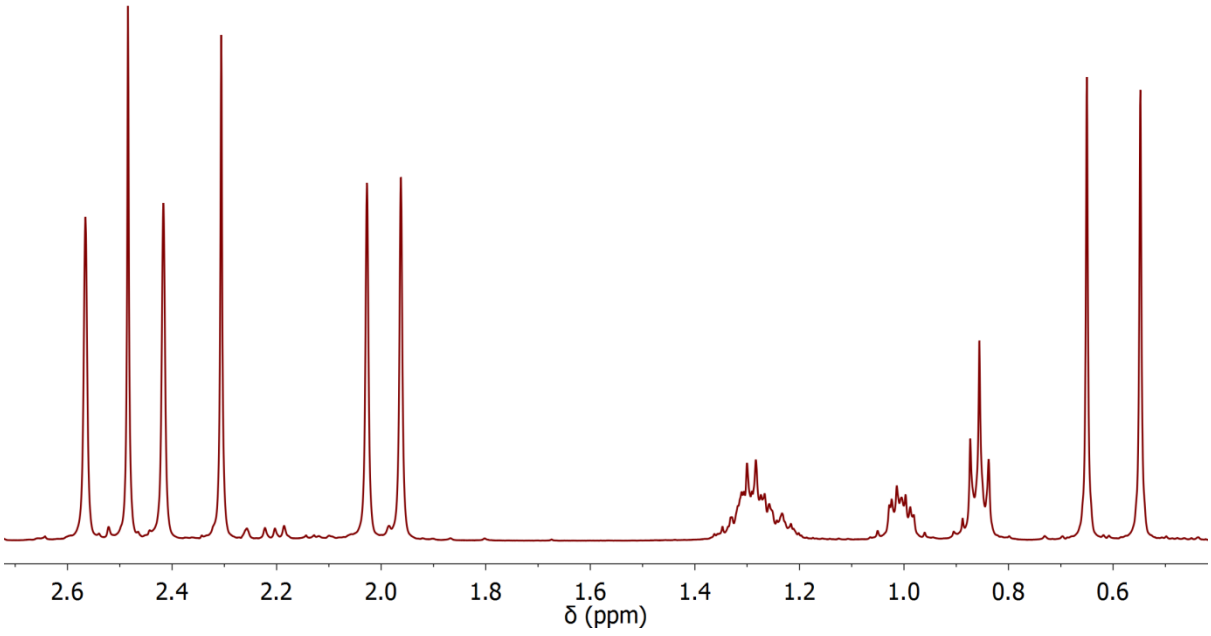


Figure 3.33: ^{1}H NMR spectrum of **3.8** in benzene-d_6.

3.8 Further reactivity

3.8.1 Synthesis of hydride species

Given the successful synthesis of group 4 alkyl complexes throughout this chapter, it was hoped to extend the library of compounds to include isolable hydride species. It is expected that they may be easily activated to give ethylene polymerisation catalysts. While only a handful of zirconocene hydride species exist,[54] and even fewer are crystallographically characterised,[6] it was anticipated that the steric bulk of the permethylated systems described might provide a suitable environment to stabilise a Zr-H bond.

***rac*-3.7** was treated with $PhSiH_3$ in order to effect the transformation from benzyl complex to hydride and was found to be unreactive at all temperatures up to 80 °C.[55,56] Similarly, treatment of ***rac*-3.7** with H_2 at 1 bar did not provoke any reaction, even upon heating.[55] Speculative attempts to synthesis a hydride species using KH were also attempted with *meso*-EBI*$ZrCl_2$ and **3.5** but no reaction was observed.

3.8.2 Synthesis of cationic species

Given the importance of transient cationic species as the active catalysts in olefin polymerisation, attempts were made to isolate and characterise a complex bearing a positive charge.[34,57] *meso*-EBI*$ZrCl_2$, ***rac*-3.1** and **3.5** were reacted with $NaB(3,5\text{-}(CF_3)_2\text{-}C_6H_3)_4$, with the intent that the formation of NaCl would drive chloride abstraction forming a cationic zirconium species, able to catalyse ethylene polymerisation without further activation. No reaction was observed with **3.5** but the orange solutions of *meso*-EBI*$ZrCl_2$ and ***rac*-3.1** turned dark brown on gentle heating, and a significant quantity of solid was seen to form. Analysis by ^{1}H NMR spectroscopy in benzene-d_6 showed no resonances relating to the starting materials in the spectrum, and it was suspected that the resultant product might be insoluble in non-coordinating solvents. The solid was filtered and dissolved in THF-d_8 but no resonances corresponding to a cationic species were observed and those attributed to the starting materials remained. Similar reactivity was seen between ***rac*-3.7** and $HB(3,5\text{-}(CF_3)_2\text{-}C_6H_3)_4$, but no products were isolated.

3.8.3 Reactivity with alkyl aluminium species

Somewhat surprisingly, given their use as activators throughout Chapter Five and their importance within the literature,[58] no reactivity was observed between *meso*-EBI*$ZrCl_2$, ***rac*-3.1**, **3.5** and **3.7**, and $AlMe_3$, Al^iBu_3 or MAO. Addition of a stoichiometric quantity of the

aluminium alkyl reagent in benzene-d_6 had no effect as adjudged by ^{1}H NMR spectroscopy, nor on the colour of the solution. This persisted on extended heating (48 hours at 80 °C), after which time the signal relating to the aluminium species has disappeared. The addition of MAO to the zirconocene species above, often precipitated a colour change, specifically turning ***rac*-3.1** pink and **3.5** dark green. However, no changes were noted in the ^{1}H NMR spectrum, even on addition of excess MAO (up to four equivalents).

3.9 Conclusion

This chapter reports the synthesis of eight group 4 complexes. All eight of these have been fully characterised while seven new crystal structures are reported. In addition, two complexes, described in part elsewhere,[49] have been further analysed and their chemistry developed. ***meso*-3.3** represents the first true *ansa*-indenyl zirconium benzyl reported and was characterised by a variety of NMR techniques including variable temperature and ROESY spectroscopy, allowing us better to understand the interactions in the solution-state. ***meso*-3.4** is only the second zirconocene neopentyl chloride to be structurally characterised and the first containing either an indenyl ligand or a bridge. ***rac*-3.1**, **3.5** and **3.6** are the first group 4 complexes with their respective ligands, and build upon their previously reported iron chemistry. **3.8** represents the only structurally characterised indenyl zirconium trichloride without a pendant donor ligand and a contrast with the metallocenes reported in this chapter. All of the new complexes have been analysed by DFT studies in order to develop our understanding of the bonding of these complexes, including looking at their relative stabilities, optimised geometries and the localisation of their frontier MOs.

3.10 References

(1) Wilkinson, G.; Birmingham, J. M. *J. Am. Chem. Soc.* **1954**, *76*, 4281.
(2) Pool, J. A.; Lobkovsky, E.; Chirik, P. J. *Nature* **2004**, *427*, 527.
(3) Chapman, A. M.; Haddow, M. F.; Wass, D. F. *J. Am. Chem. Soc.* **2011**, *133*, 18463.
(4) Xu, X.; Kehr, G.; Daniliuc, C. G.; Erker, G. *Angew. Chemie* **2013**, *125*, 13874.
(5) Xu, X.; Kehr, G.; Daniliuc, C. G.; Erker, G. *J. Am. Chem. Soc.* **2014**, *136*, 12431.
(6) Bradley, C. A.; Keresztes, I.; Lobkovsky, E.; Young, V. G.; Chirik, P. J. *J. Am. Chem. Soc.* **2004**, *126*, 16937.
(7) O'Hare, D.; Murphy, V.; Diamond, G. M.; Arnold, P.; Mountford, P. *Organometallics* **1994**, *13*, 4689.
(8) Ransom, P.; Ashley, A. E.; Brown, N. D.; Thompson, A. L.; O'Hare, D. *Organometallics* **2011**, *30*, 800.
(9) Prout, K.; Cameron, T. S.; Forder, R. A.; Critchley, S. R.; Denton, B.; Rees, G. V. *Acta Crystallogr. Sect. B* **1974**, *30*, 2290.
(10) Shapiro, P. J. *Coord. Chem. Rev.* **2002**, *231*, 67.

(11) Ransom, P.; Ashley, A.; Thompson, A.; O'Hare, D. *J. Organomet. Chem.* **2009**, *694*, 1059.
(12) Calhorda, M. J.; Félix, V.; Veiros, L. F. *Coord. Chem. Rev.* **2002**, *230*, 49.
(13) Chandra, G.; Lappert, M. F. *J. Chem. Soc. A* **1968**, 1940.
(14) Diamond, G. M.; Jordan, R. F.; Petersen, J. L. *J. Am. Chem. Soc.* **1996**, *118*, 8024.
(15) Eisch, J. J.; Shi, X.; Owuor, F. A. *Organometallics* **1998**, *17*, 5219.
(16) Mansel, S.; Rief, U.; Prosenc, M.-H.; Kirsten, R.; Brintzinger, H.-H. *J. Organomet. Chem.* **1996**, *512*, 225.
(17) Chen, Y. X.; Rausch, M. D.; Chien, J. C. W. *Organometallics* **1994**, *13*, 748.
(18) Bordwell, F. G.; Drucker, G. E.; Fried, H. E. *J. Org.Chem.* **1981**, 632.
(19) Bordwell, F. G.; Drucker, G. E. *J. Org. Chem.* **1980**, *45*, 3325.
(20) Bordwell, F. G.; Bausch, M. J. *J. Am. Chem. Soc.* **1983**, *105*, 6188.
(21) Bordwell, F. G.; Algrim, D.; Vanier, N. R. *J. Org. Chem.* **1977**, *42*, 1817.
(22) Ransom, P.; Arnold, T. A. Q.; Thompson, A. L.; Buffet, J.-C.; O'Hare, D. *J. Organomet. Chem.* **2014**, *774*, 48.
(23) Cooper, R. T.; Chadwick, F. M.; Ashley, A. E.; O'Hare, D. *Organometallics* **2013**, *32*, 2228.
(24) Alias, F. M.; Barlow, S.; Tudor, J. S.; O'Hare, D.; Perry, R. T.; Nelson, J. M.; Manners, I. *J. Organomet. Chem.* **1997**, *528*, 47.
(25) Buffet, J.-C.; Arnold, T. A. Q. Unpublished results.
(26) Herrmann, W. A.; Rohrmann, J.; Herdtweck, E.; Spaleck, W.; Winter, A. *Angew. Chem. Int. Ed.* **1989**, *28*, 1511.
(27) Churakov, A. V; Howard, J. A. K.; Voskoboynikov, A. Z. *J. Organomet. Chem.* **2005**, *690*, 1067.
(28) Repo, T.; Klinga, M.; Mutikainen, I.; Su, Y.; Leskelä, M.; Polamo, M.; Homsi, M. N.; Kuske, F. K. H.; Haugg, M.; Trabesinger-Rüf, N.; Weinhold, E. G. *Acta Chem. Scand.* **1996**, *50*, 1116.
(29) Becke, A. D. *J. Chem. Phys.* **1986**, *84*, 4524.
(30) Becke, A. D. *J. Chem. Phys.* **1993**, *98*, 5648.
(31) Lee, C.; Yang, W.; Parr, R. G. *Phys. Rev. B* **1988**, *37*, 785.
(32) Becke, A. D. *Phys. Rev. A* **1988**, *38*, 3098.
(33) Perdew, J. *Phys. Rev. B* **1986**, *33*, 8822.
(34) Bochmann, M. *J. Chem. Soc. Dalton Trans.* **1996**, 255.
(35) Mäkelä-Vaarne, N. I.; Nicholson, D. G.; Ramstad, A. L. *J. Mol. Catal. A Chem.* **2003**, *200*, 323.
(36) Jordan, R. F.; LaPointe, R. E.; Baenziger, N.; Hinch, G. D. *Organometallics* **1990**, *9*, 1539.
(37) Irwin, L. J.; Zeits, P. D.; Reibenspies, J. H.; Miller, S. A. *Organometallics* **2007**, *26*, 1129.
(38) Piccolrovazzi, N.; Pino, P.; Consiglio, G.; Sironi, A.; Moret, M. *Organometallics* **1990**, *9*, 3098.
(39) Veghini, D.; Day, M. W.; Bercaw, J. E. *Inorg. Chim. Acta* **1998**, *280*, 226.
(40) Liu, F.-C.; Liu, J.; Meyers, E. A.; Shore, S. G. *Inorg. Chem.* **1999**, *38*, 2169.
(41) Chadwick, F. M. *D.Phil. Thesis*, University of Oxford, **2013**.
(42) Rong, Y.; Al-Harbi, A.; Parkin, G. *Organometallics* **2012**, *31*, 8208.
(43) Sauriol, F.; Sonnenberg, J. F.; Chadder, S. J.; Dunlop-Brière, A. F.; Baird, M. C.; Budzelaar, P. H. M. *J. Am. Chem. Soc.* **2010**, *132*, 13357.
(44) Klamo, S. B.; Wendt, O. F.; Henling, L. M.; Day, M. W.; Bercaw, J. E. *Organometallics* **2007**, *26*, 3018.

(45) Jeffery, J.; Lappert, M. F.; Luong-Thi, N. T.; Webb, M.; Atwood, J. L.; Hunter, W. E. *J. Chem. Soc. Dalton Trans.* **1981**, 1593.
(46) Dreier, T.; Bergander, K.; Wegelius, E.; Fröhlich, R.; Erker, G. *Organometallics* **2001**, *20*, 5067.
(47) Ashley, A. E.; Cooper, R. T.; Wildgoose, G. G.; Green, J. C.; O'Hare, D. *J. Am. Chem. Soc.* **2008**, *130*, 15662.
(48) Shannon, R. D. *Acta Crystallogr. Sect. A* **1976**, *32*, 751.
(49) Coward, J. J. *Part II Thesis*, University of Oxford, **2013**.
(50) Arnold, P. L.; Turner, Z. R.; Germeroth, A. I.; Casely, I. J.; Bellabarba, R.; Tooze, R. P. *Dalton Trans.* **2010**, *39*, 6808.
(51) Diamond, G. M.; Rodewald, S.; Jordan, R. F. *Organometallics* **1995**, *14*, 5.
(52) Damrau, H. H.; Geyer, A.; Prosenc, M.; Weeber, A.; Schaper, F.; Brintzinger, H. *J. Organomet. Chem.* **1998**, *553*, 331.
(53) Engelhardt, L. M.; Papasergio, R. I.; Raston, C. L.; White, A. H. *Organometallics* **1984**, *3*, 18.
(54) Grossman, R. B.; Doyle, R. A.; Buchwald, S. L. *Organometallics* **1991**, *10*, 1501.
(55) Arndt, S.; Okuda, J. *Chem. Rev.* **2002**, *102*, 1953.
(56) Wu, F.; Jordan, R. F. *Organometallics* **2005**, *24*, 2688.
(57) Jordan, R. F.; LaPointe, R. E.; Baenziger, N.; Hinch, G. D. *Organometallics* **1990**, *9*, 1539.
(58) Chen, E. Y.; Marks, T. J. *Chem. Rev.* **2000**, *100*, 1391.

Chapter Four

Supported Catalysts and Solid-State Characterisation

4.1 Introduction

In order to preserve the single-site characteristics of metallocenes while avoiding the pitfalls of reactor fouling, it is desirable to immobilise solution-phase catalysts on solid supports. This is an area of much investigation but the majority of work is reported solely in the patent literature, if at all. Despite this, the field has been the subject of a few excellent reviews.[1,2] Another major advantage of these supported catalysts is their ability to make use of existing plants and their designs without further engineering requirements and, as such, they are considered a "drop-in" technology. The success of these immobilised catalysts should not be underestimated and they are now routinely used to synthesise many of the plastics that we rely on today.

The most commonly employed support material is silica, and, when used with an MAO activator and a metallocene complex, it forms part of the "holy trinity" of supported single-site catalysis.[3] While silica is found in numerous phases, it is most commonly the amorphous form that is used in polymerisations.[2] Silica is usually supplied in its fully hydroxylated form and requires thermal treatment before use. Depending on the temperature utilised, the silica is modified in a number of different ways. Calcination, the process of heating to remove water and dehydrate a support, at below 100 °C only removes physisorbed water molecules. Temperatures above 180 °C are typically required to remove hydrogen bonded water and as the temperature rises further still, silanol (Si-OH) surface groups can condense with one another to form silyl ethers (see Figure 1.17 and the surrounding text for a more detailed explanation). Dos Santos and co-workers have investigated the effects of differing calcination temperatures on the polymerisation performance of grafted zircononcenes and concluded that more zealous heat treatments led to lower metal loadings but higher activities and molecular weights.[4] In addition, extensive work has been carried out investigating the effect that different silicas have on the resultant ethylene polymerisation activity, with the conclusion that microporous materials with pore diameters of less than 50 Å were less potent. This is attributed to the formation of bimetallic species within the pores which are catalytically inactive.[5]

Other inorganic materials such as zeolites and clays have also been used to support metallocene catalysts. Clays are typically ion exchanged, often with ammonium salts before

precontacting with alkylaluminium reagents.[6] They have also been employed by Suga and co-workers as supports for zirconocenes,[7] and were reported as active supports for Ziegler catalysts as long ago as 1973.[8,9] O'Hare and co-workers have extensively studied layered double hydroxides (LDHs) throughout the 21st century.[10–12] Recently, applications have been found for catalysis,[13,14] immunology[15] and medical science,[16,17] optics[18] and in inorganic/organic nanocomposites.[19–22]

LDHs are a class of hydrotalcite-like clays containing positively charged layers with intercalated anions between them. The charge imbalance stems from the substitution of the dicationic metal ions (in the otherwise brucite-like structure) with trivalent ones while the anions provide a charge balance. Water is also typically found in the interlayer space. They have a general formula as shown in Equation 4.1.

$$[M^{z+}_{1-x}M^{3+}_{x}(OH)_2]^{q+}(X^{n-})_{q/n} \cdot yH_2O$$

Equation 4.1: formula for a layered double hydroxide (LDH).

It is most typical for the base metal to be divalent (i.e. z = 2) and common examples include Mg^{2+} and Ca^{2+}. The trivalent metal ion is typically Al^{3+}. The intercalated anions show more variety, and while they can include large anionic organic salts, they are more typically inorganics such as SO_4^{2-}, CO_3^{2-} or Cl^-. Recently O'Hare and co-workers have published a new generation of LDHs using an aqueous miscible solvent treatment (AMOST) method.[23] The AMO-LDHs made in this way exhibit surface areas two orders of magnitude in excess of those previously reported (*c*. 400 m^2/g).[24–26] The solvent treatment results in the displacement of interlayer H_2O with the washing solvent – this is typically acetone.

Another class of materials used as inorganic supports for metallocenes has been solid methyaluminoxanes, although no reports are available in the academic literature. A fine summary is provided in Severn's excellent review,[2] but their principal synthetic method seems to be the precipitation of MAO from solution in an insoluble form. This has been achieved in a number of ways such as the addition of water, epoxides, peroxides and carbonates to toluene solutions containing MAO.[27,28] Spherical particles of insoluble MAO were generated by adding sorbitan monoleate, an emulsifier, and water to a hexane solution of $AlMe_3$. After the immobilisation of zirconocene dichloride, the system yielded excellent activities and no evidence was found of reactor fouling.[29] Another method is to use aliphatic hydrocarbons, in which MAO is insoluble, to cause precipitation from toluene and subsequent use as a support.[30–32]

Two common procedures exist for immobilising a metallocene on a solid support. It is possible to react a metallocene with the residual silanol groups on the silica surface (depending on the calcination temperature) and the resultant catalyst is then activated with MAO or an alkylaluminium reagent. The alternative method is to precontact the support with MAO, before subsequent reaction with the complex. Kaminsky *et al*. found that the system, precontacted with MAO led to polypropylene (PP) similar in molecular weight and tacticity to that formed by the homogeneous system.[33] In contrast, when the silica was reacted with the complex directly, the resultant PP was more isotactic. If the support is activated, it has been proposed that the active species is bound by an electrostatic interaction with the surface, rather than by a covalent bond as in the case of the silanol. Another advantage of precontacting the surface is that it reduces the decomposition experienced by reaction with the silanol groups. Collins *et al*. reported appreciable quantities of the hydrolysed ligand in the supernatant.[34]

A third methodology exists for immobilising catalysts, which is to pre-activate the complex by treatment with MAO. This is particularly useful when the complex is particularly insoluble as it reduces the volume of solvent required and the by-products created.[35,36]

Given their ubiquity, it is perhaps surprising to note the relative lack of research into the active species formed on the surface of the support. One of the earliest reports on zirconocenes, by O'Hare and co-workers, used extended X-ray absorption fine structure (EXAFS) to investigate the species on the surface of an MAO activated mesoporous silica, MCM-41.[37] This built on work by Maschmeyer *et al*., who had previously studied a titanocene epoxidation catalyst using the same technique.[38] It was concluded that there was no chloride in close proximity to the zirconium centre and, unsurprisingly, that the two Cp rings remained attached. Jezequel, Basset *et al*. developed the field with a report comprising EXAFS analysis, IR and ^{13}C NMR spectroscopy data and studying Cp_2ZrMe_2 and Cp_3ZrMe precatalysts, reacted with silica and alumina supports.[39] The EXAFS fit was moderate although well corroborated by the other techniques. It was concluded that without the presence of an activator, or acidic sites (such as those provided by alumina), the species were not catalytically active towards the polymerisation of ethylene. Even on activation, a large disparity was noted between the activities of the homogeneous and heterogeneous systems. A paper from Borealis Polymers investigated a homogenous hafnocene dichloride catalyst and its immobilised form on silica supported MAO (SSMAO).[40,41] EXAFS was again employed as well as UV/visible spectroscopy. This study demonstrated the formation of a cationic

hafnocene species as well as non-bonding interactions with oxygen and silicon. It was noted that not all of the hafnocene reacted with the support surface but that this proportion increased on pre-treating the metallocene with MAO. A more recent paper by dos Santos sought to understand the relationship between the active species and the resultant polymer for a variety of silica supports.[5] It has been postulated that a reduction in the Zr-O distance between the metallocene and the support, results in polyethylene with a higher molecular weight.

The aims of this chapter are to develop a process for the repeatable immobilisation of zirconocenes on a variety of inorganic supports. These supports will consist of, or be activated by, MAO and will comprise SSMAO, LDHMAO and Solid MAO. Attempts will also be made to characterise the supported catalysts using a range of laboratory techniques and zirconium K-edge EXAFS.

4.2 Immobilising the complexes

As introduced above, it was decided to attempt the use of three different catalyst supports: silica, LDH and Solid MAO. Silica was chosen because of its ubiquity within the literature. Most reports of immobilised ethylene polymerisation catalysis are based on SiO_2 due to its ready availability in well-defined morphologies and particle sizes. In addition to this, excellent activities have been disclosed for silica supported catalysts making them an obvious choice.[5,42] The ability to easily tune LDH particle size to within a narrow distribution, dictate their morphology and control their cationic make-up makes them ideal candidates as catalytic supports. While there are no reports of their use in the open literature, their similarity to alumina made them a conducive choice for preliminary testing.[2] The well characterised AMO-LDH MgAl-SO_4 was the primary choice of LDH throughout this chapter and can be assumed to be the material in question unless specified otherwise.

Solid MAO, supplied by Tosoh Finechem, was suggested as a catalytic support by SCG Chemicals. Given its strong similarities to MAO, used worldwide for the activation of metallocene catalysts and to great effect,[43,44] it was certainly considered a highly promising material. Little is known about its structure or exact make up, although its aluminium content was disclosed as being 39.7%. Once again, there was precedence for its use within the patent literature (*vide supra*), although there are no confirmed reports as to the activities observed.

On consideration of the options, it was deemed preferable to activate the surface with MAO prior to supporting the complex. It was decided to use 0.5 equivalents of the aluminium

activator to activate the support, leading to a potential maximum of just over 15 wt% aluminium in the resulting SSMAO. The equivalent figure for LDHMAO-SO_4 is 13.5% although the exact Al weight percentage depends on which LDH is employed and is complicated by the presence of Al sites in the cationic layers. Both support materials were calcined before use: SiO_2 at 600 °C for two hours under a flow of N_2 and LDH at 150 °C for six hours under high vacuum (2×10^{-2} mbar). O'Hare and co-workers have studied the effects of different calcination temperatures on the ethylene polymerisation activity using AMO-LDH based catalysts and found the aforementioned conditions to be optimal.[45]

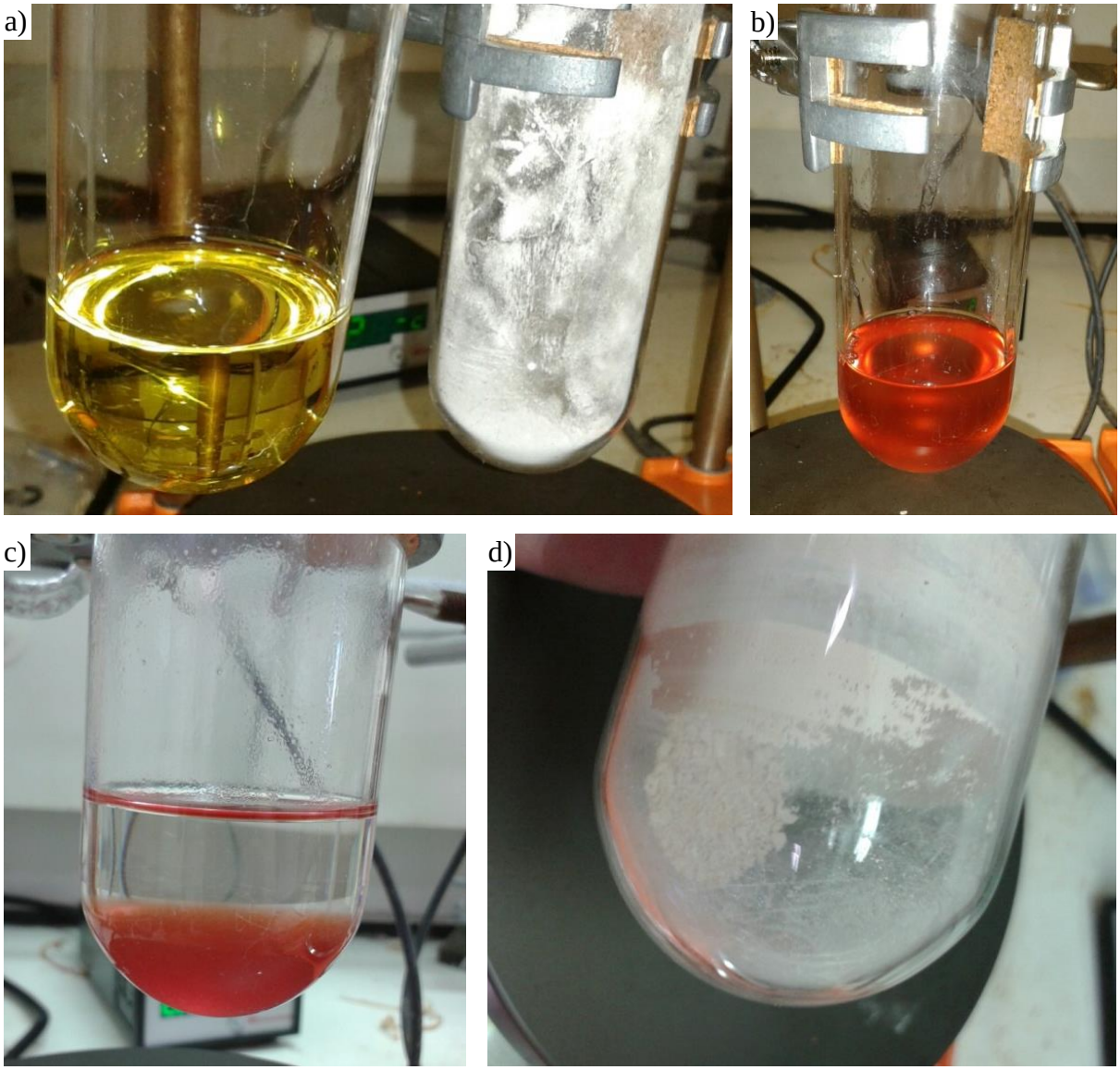


Figure 4.1: the process of supporting a catalyst. a) toluene solution of **3.8** and Solid MAO; b) on mixing the solution and the solid; c) allowing the solid to settle; d) after filtration and drying under vacuum.

In both cases, two equivalents of the calcined support and one of the activating MAO were weighed out into a Schlenk tube in the glovebox and heated at 80 °C in toluene for two

hours with constant swirling. A stirrer bar was not used to prevent aggregation of the supports. After this time, when no more evolution of gas (CH_4) was observed, the toluene was decanted and the support dried. Further heating with a heat-gun was required to remove residual toluene.

It was initially decided to immobilise the catalysts in a 1:200 ratio with the support. This give a total composition of 2:1:0.005 for support:MAO:complex. A typical support procedure is outlined below and illustrated for **3.8**, $Ind^{\#}SiMe_2{}^{n}BuZrCl_3$, in Figure 4.1. The complex and support were loaded separately into Schlenk tubes in the glovebox and the organometallic species was dissolved in toluene. The resulting solution was added to the support, typically causing an immediate colour change. The mixture was heated at 60 °C in an oil bath and swirled regularly to ensure complete immobilisation of the metallocene; stirring was again avoided to prevent aggregation. After two hours, the reaction was removed from the oil bath and allowed to settle, before decantation of the colourless supernatant and thorough drying *in vacuo*. It was of vital importance that the toluene solution contained no colour otherwise complications involving reactor fouling, caused by the simultaneous solution-phase polymerisation, were likely to occur. All the solids were afforded as pale coloured powders in good yield (>80%). The colours obtained on immobilisation bore no resemblance to the starting material and are listed in Table 4.1.

Table 4.1: colour chart of the immobilised catalysts.

Complex	Solid MAO	SSMAO	LDHMAO
rac-EBI*$ZrCl_2$	dark purple	golden brown	-
meso-EBI*$ZrCl_2$	pale beige	-	-
***rac*-3.1**	beige	beige	pale beige
***meso*-3.3**	golden brown	-	-
***meso*-3.4**	beige	-	-
***meso*-3.5**	pale brown	gold	-
***rac*-3.5**	pink	gold	-
3.6	gold	-	-
***rac*-3.7**	bright pink	-	-
3.8	gold	-	-

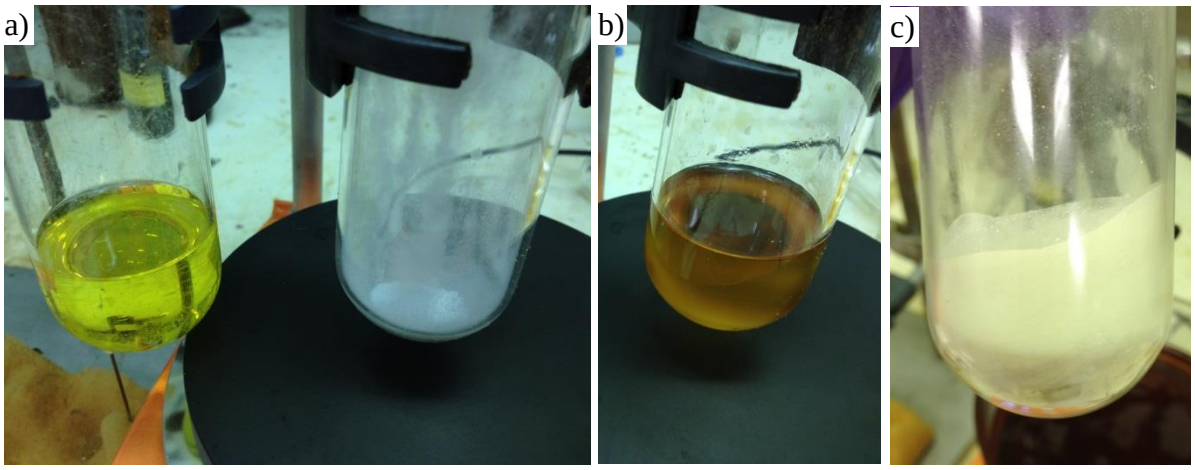


Figure 4.2: immobilisation of ***rac*-3.1** on Solid MAO. a) before mixing the toluene solution of ***rac*-3.1** (left) and the Solid MAO (right); b) immediately after mixing; c) after filtration and drying under vacuum.

The immobilisation procedure of ***rac*-3.1** on Solid MAO is shown in Figure 4.2, affording a beige solid from the orange complex. A more drastic change in colour is seen for ***rac*-3.7** where the bright yellow complex affords a bright pink heterogeneous catalyst (Figure 4.3). This catalyst was prepared with a 300:1 loading.

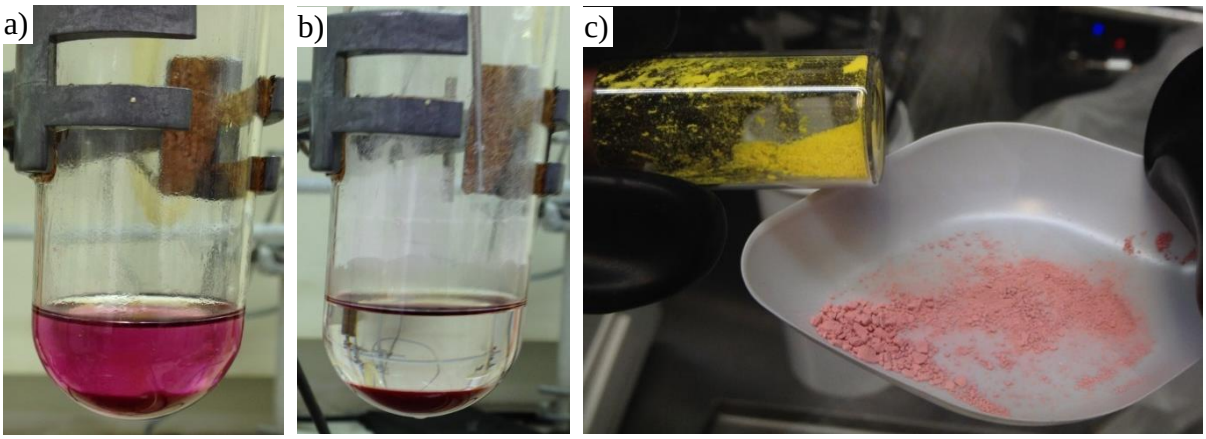


Figure 4.3: immobilisation procedure of ***rac*-3.7** on Solid MAO. a) immediately on mixing; b) on allowing the solid to settle; c) the final catalyst (pink, right) and the starting complex (yellow, left), ***rac*-3.7** for contrast.

In total, 15 different catalysts were synthesised from ten complexes and three supports. Numerous repeats were also recorded at different catalyst loadings (either 200:1 or 300:1).

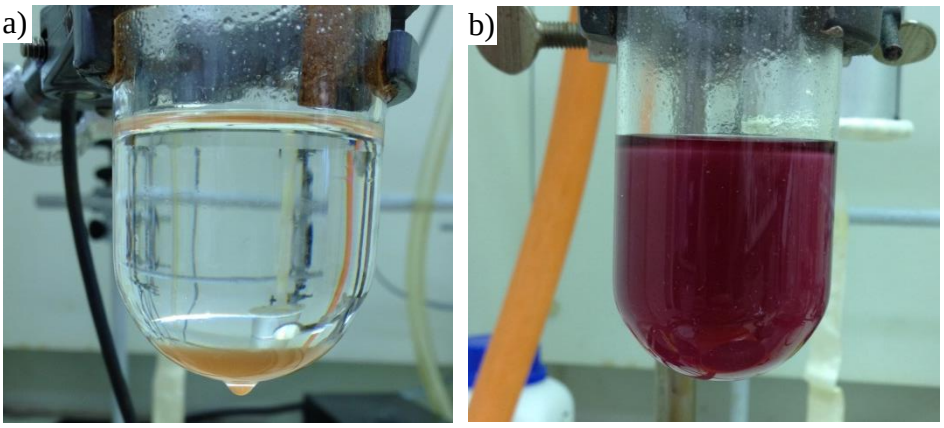


Figure 4.4: a) ***rac*-3.1** on LDHMAO; b) *rac*-EBI*$ZrCl_2$ on Solid MAO.

Table 4.1 indicates that the colours formed by complexes on complexation (with the exception of ***rac*-3.1**) are not consistent across a single support, complex or even family. Figure 4.4 highlights the contrasting colours of the final supported catalysts: the pale beige colour observed on supporting ***rac*-3.1** on LDHMAO and the bright purple of *rac*-EBI*$ZrCl_2$ on Solid MAO.

The majority of the catalysts synthesised were based on zirconocenes but the hafnium containing **3.6** was also supported (Figure 4.5) yielding a rich gold coloured catalyst. The supported catalyst containing **3.6** was not used for ethylene polymerisation due to it comprising a mixture of isomers. It was expected to show a poor activity, following the reports of other hafnocenes in the literature and yield polymer with a bimodal molecular weight distribution.[46]

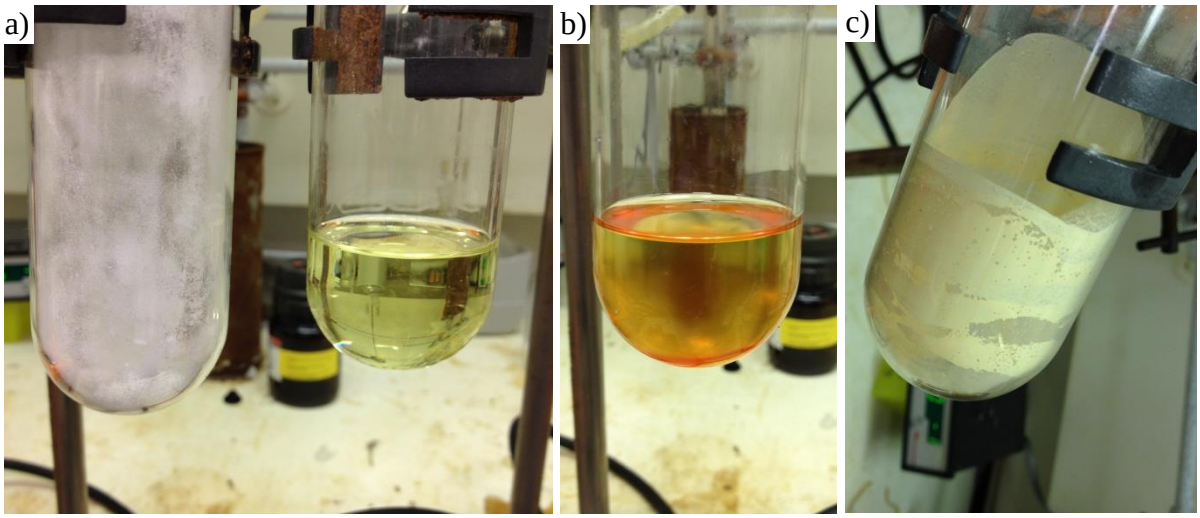


Figure 4.5: the immobilisation of **3.6** (both isomers) on Solid MAO. a) before mixing the toluene solution of **3.6** and the Solid MAO; b) immediately after mixing; c) after filtration and drying under vacuum.

4.3 Characterisation of the supported catalysts

4.3.1 Scanning electron microscopy

Scanning electron microscopy (SEM) imaging allows an assessment of the particle size and morphology of the inorganic supports. This technique was carried out in order to determine if the physical charateristics of the material have changed following treatment with MAO and the complex.

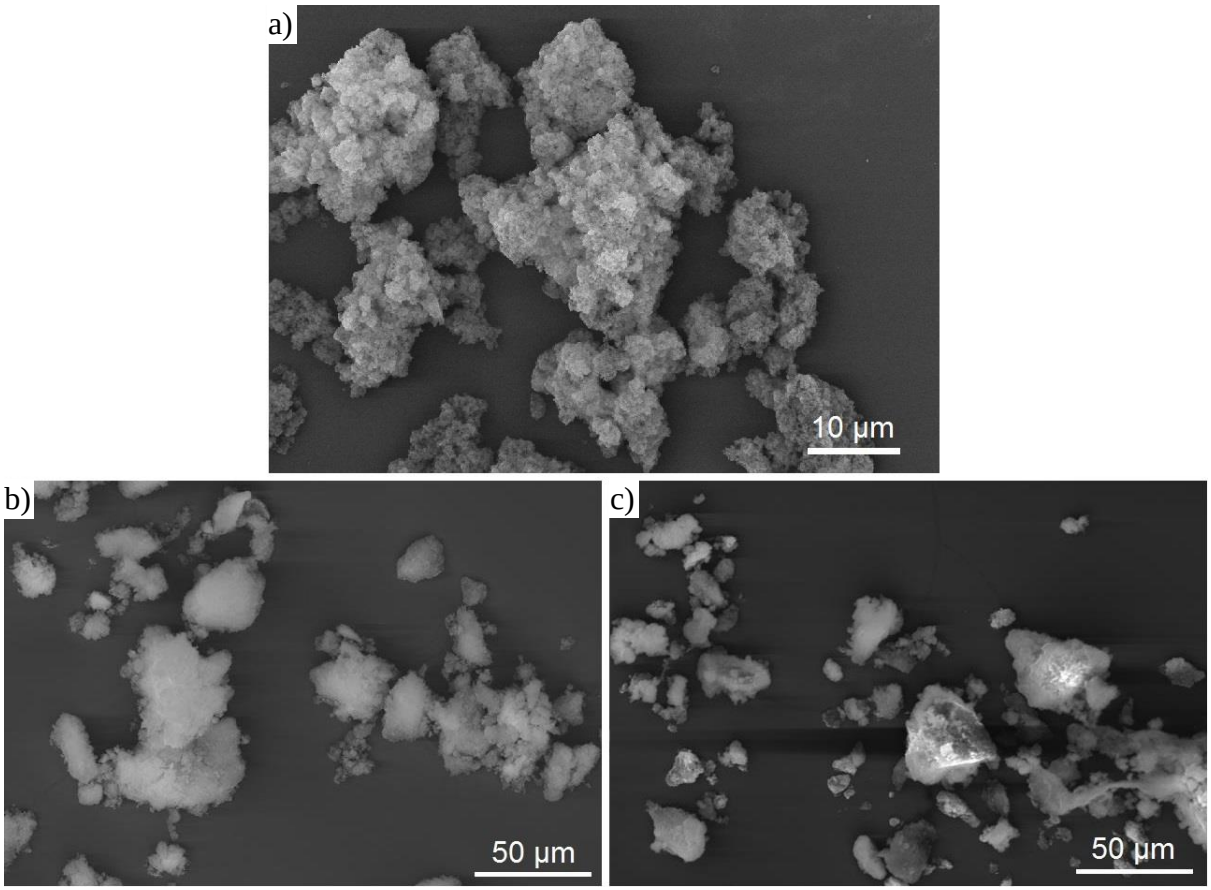


Figure 4.6: scanning electron microscopy images at 500 and 5000× magnification. a) AMO-MgAl-SO_4 LDH; b) AMO-MgAl-SO_4 LDHMAO; c) AMO-MgAl-SO_4 LDHMAO-SBI*$ZrCl_2$.

Figure 4.6 clearly reveals two points; small particle size of AMO-LDHs and the consistency of their morphology under the immobilisation process. Image a) illustrates the small diameters of the individual particles, which are poorly resolved even under 5000× magnification, and a high suface area was anticipated. This has been confirmed by BET (Brunauer-Emmett-Teller) studies in previous works.[26] It is also noteworthy that there is a significant degree of aggregation of the smaller particles. Images b) and c) display the fine detail which appears unaffected by the reaction with MAO or the complex (***rac*-3.1**) as well as the aggregation noted above.

Figure 4.7 illustrates a dramatically different particle morphology from LDH. The silica, supplied by Grace, is much more uniform in shape and size with no aggregation. The particles are not spherical but granular with an average size of approximately 10 μm. They do not change in either shape or dimension on reaction with MAO, nor on the immobilisation of ***rac*-3.1**. It can be seen that no further aggregation has occurred, justifying the omission of stirrer bars during the supporting procedure.

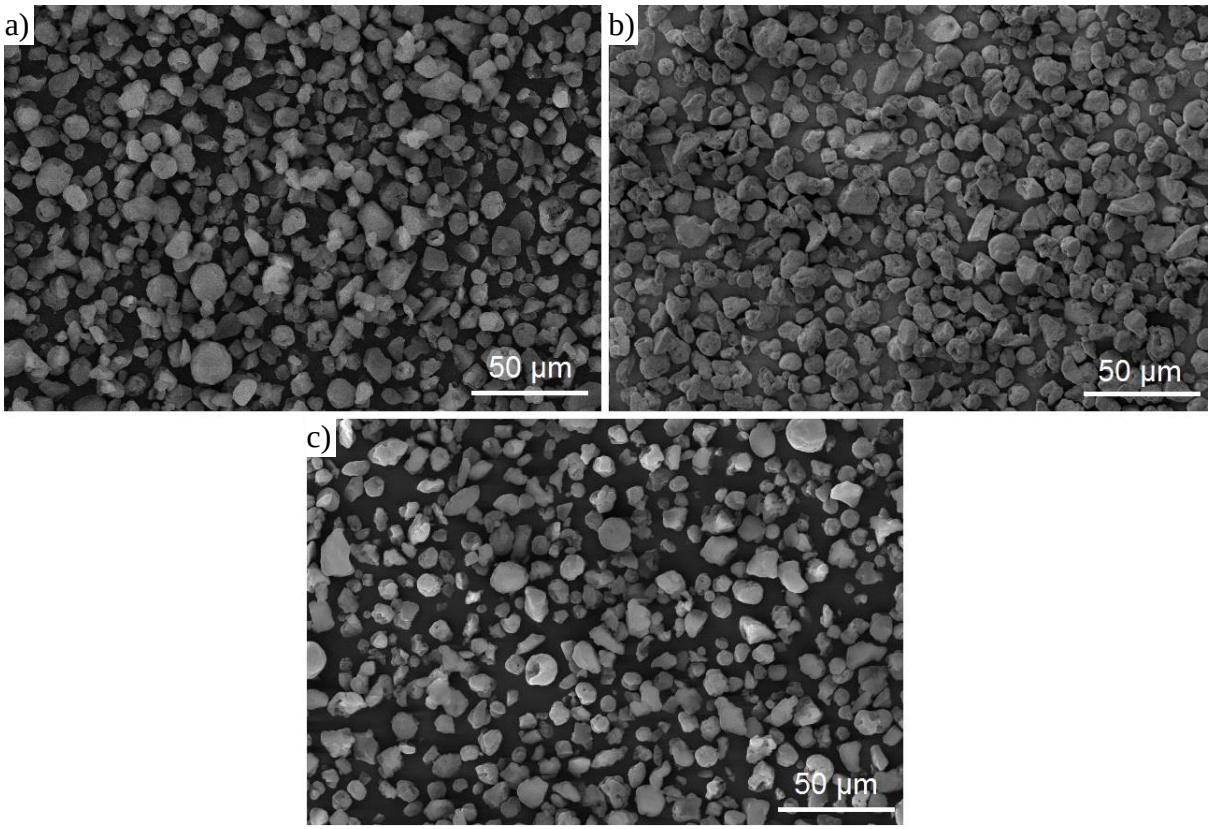


Figure 4.7: scanning electron microscopy images at 500× magnification. a) amorphous SiO_2 (Grace); b) SSMAO; c) SSMAO-SBI*$ZrCl_2$.

Solid MAO is supplied by Tosoh Finechem as a slurry in toluene, appearing as a thick gel. It is obtained in its "dry" form by the removal of the solvent *in vacuo* and it requires extensive heat treatment. Once dried, it appears as a near-spherical particulate (Figure 4.8) with a small size distribution and a mean diameter of approximately 2 μm. No effect on the size, morphology or aggregation characteristics are seen on the immobilisation of ***rac*-3.1**.

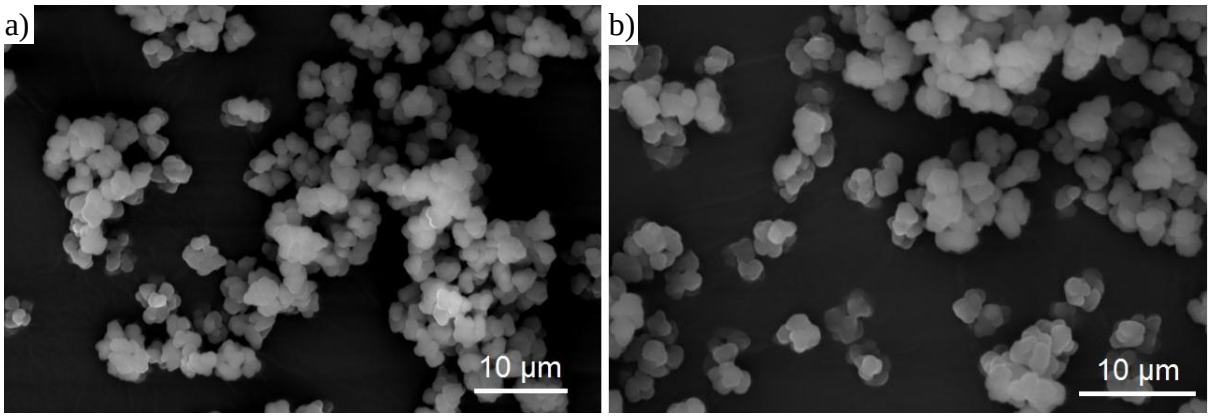


Figure 4.8: scanning electron microscopy images at 2000 and 2500× magnification. a) Solid MAO (Tosoh Finechem); b) Solid MAO-SBI*$ZrCl_2$.

4.3.2 UV/visible spectroscopy

UV/visible spectroscopy represents a key analytical technique in the analysis of metallocenes and their immobilisation on solid supports, and can give information about their structure and bonding. The electronic transition associated with d^0 metallocenes is that of ligand-to-metal charge transfer (LMCT) since the metal has no available electrons to undergo d-d transitions. This typically involves the transition of an electron from the Cp ligand HOMO to the Zr based LUMO (see DFT studies in Chapter Three).

The energy of this band changes with a variety of structural features. The introduction of an *ansa*-bridge causes bathochromic (increasing wavelength) shifts of up to 59 nm from Ind_2ZrCl_2 to $SBIZrCl_2$,.[40] This is, in part, attributed to the geometry adopted by the compound caused by the constraints of the bridge with an eclipsed orientation causing better overlap between the indenyl π-system and the empty Zr d-orbitals due to an alignment of their nodal planes. This stabilises the HOMO with respect to other alignments, increasing the energy of the LMCT band. This explains the observation of the relative colours of *rac*- and *meso*-isomers: the hypsochromic (decreasing wavelength) shift for ***meso*-3.5** (dark orange) absorbing the blue end of the spectrum better than for ***rac*-3.5** (pale orange). Figure 4.9 illustrates the diffuse-reflectance UV/visible spectra of Solid MAO, ***rac*-3.7** and Solid MAO-$Ind^{\#}_2ZrBz_2$ in the range 200-800 nm.

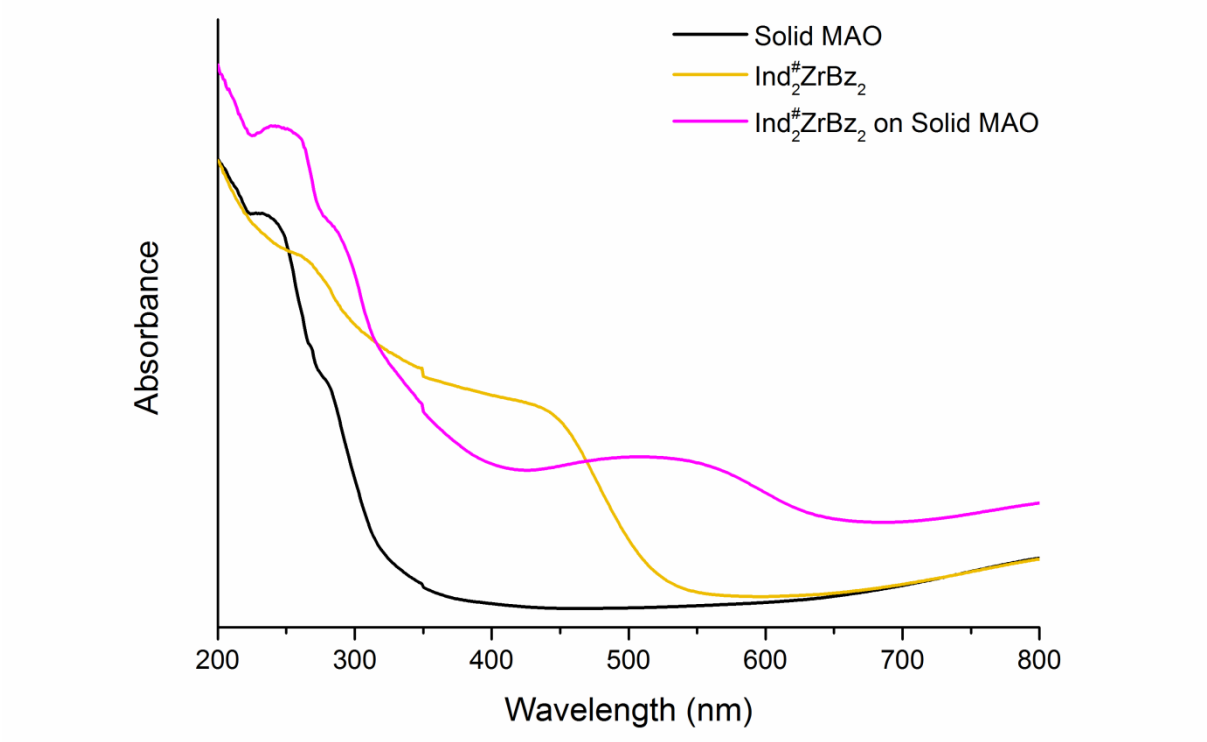


Figure 4.9: diffuse-reflectance UV/visible spectra of Solid MAO, $Ind^{\#}_{2}ZrBz_2$, and Solid MAO-$Ind^{\#}_{2}ZrBz_2$.

As is to be expected for a colourless solid, no transitions are seen in the visible region (390-700 nm) for Solid MAO although an intense band is observed in the UV at 235 nm. ***rac*-3.7** is comparatively less intense in the UV but a distinct transition at 430 nm corresponds to the LMCT band. This is an absorption in the violet region of the spectrum giving rise to a bright yellow complex. The immobilised metallocene shows an absorbance that is significantly bathochromically shifted in the visible region to 505 nm. Research by the Soga group has shown that the interaction of zirconocenes with MAO can have two distinct effects on the metal environment and, hence, on the LMCT band.[47,48] The initial methylation step, postulated to occur at low concentrations of MAO (*c*. Al:Zr 20:1) causes a hypsochromic shift due to the increased electron donation of the methyl groups, raising the energy of the Zr-based LUMO. However, on addition of a large excess of MAO, a shift in the opposite direction occurs (to higher wavelengths) caused by the formation of a cationic zirconium species, lowering the LUMO and decreasing the band energy. It is this latter shift that is observed for ***rac*-3.7** on Solid MAO, suggesting that a cationic species is formed. In addition to the LMCT band in the visible region, the characteristic absorptions of Solid MAO in the UV are also present. This provides good evidence that the complex is bound to the surface.

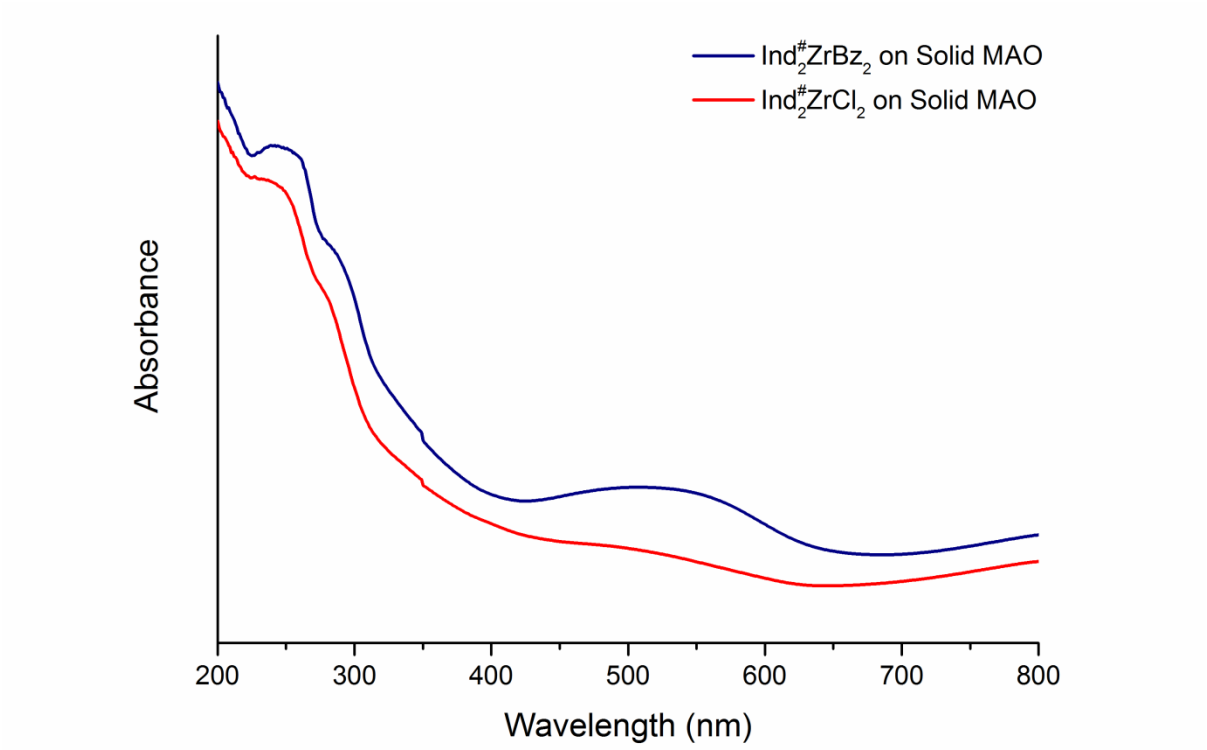


Figure 4.10: diffuse-reflectance UV/visible spectra of $Ind^{\#}_{2}ZrCl_2$ and $Ind^{\#}_{2}ZrBz_2$ supported on Solid MAO.

A shift to shorter wavelengths is observed (Figure 4.10) on substitution of the benzyl groups of ***rac*-3.7** (505 nm) for the chlorides of ***meso*-3.5** (465 nm). It is suspected that this is caused by the more challenging formation of the cationic active species on the surface of the support. The difference in intensity of the LMCT band is also evident – borne out in the lighter colour of the catalyst.

4.3.3 IR spectroscopy

Basset and co-workers determined information on surface bound zirconocenes and half-sandwich complexes using infrared (IR) spectroscopy.[39] Figure 4.11 gives the IR spectra of Solid MAO and Solid MAO-EBI*ZrNpCl. The IR spectra of the three supports documented in this chapter, show strong absorptions that coincide with those expected for a bound metallocene. The only indication of the presence of the metallocene in Figure 4.11 is the weak signal at 1673 cm^{-1} corresponding to C-C aromatic bending modes. This represents a shift of 20 cm^{-1} from 1653 cm^{-1} in the unsupported complex.

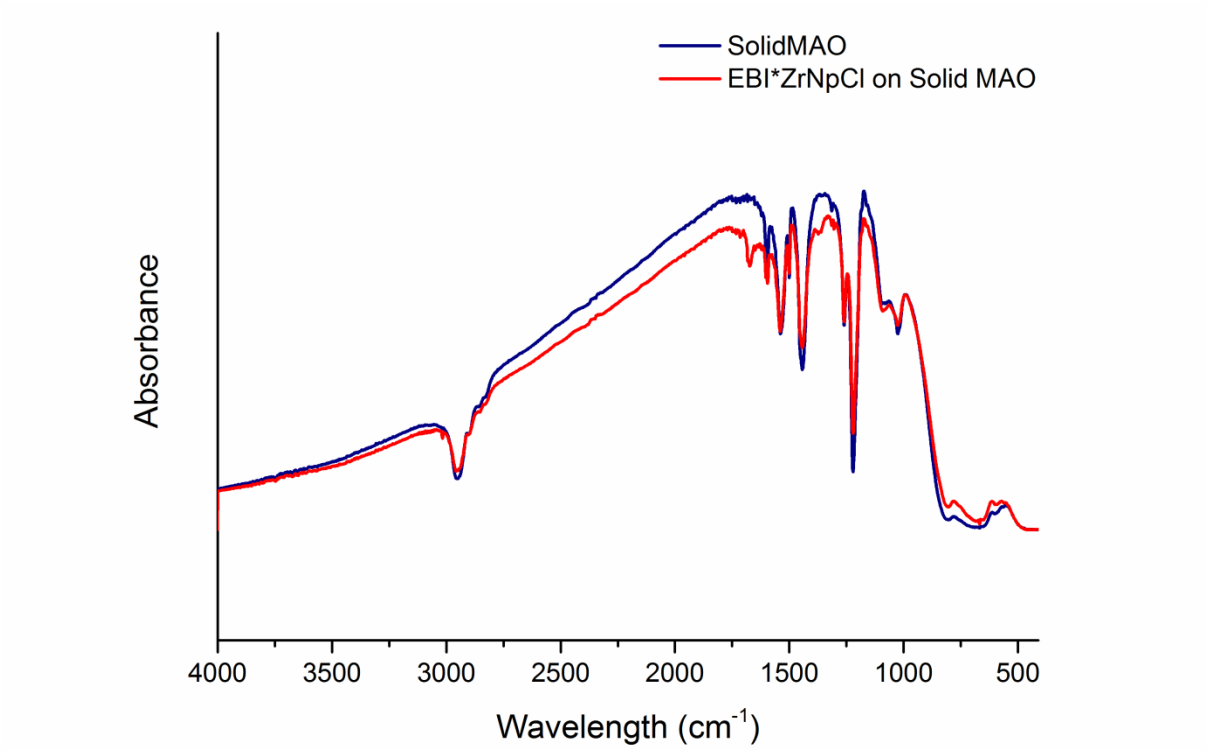


Figure 4.11: FTIR spectra of Solid MAO and Solid MAO-EBI*ZrNpCl.

4.3.4 Solid-state NMR spectroscopy

Solid-state NMR spectroscopy was performed on a number of samples in an attempt to understand the number of silicon (where applicable) and aluminium chemical environments, as well as to characterise the carbon ligand framework on the surface.

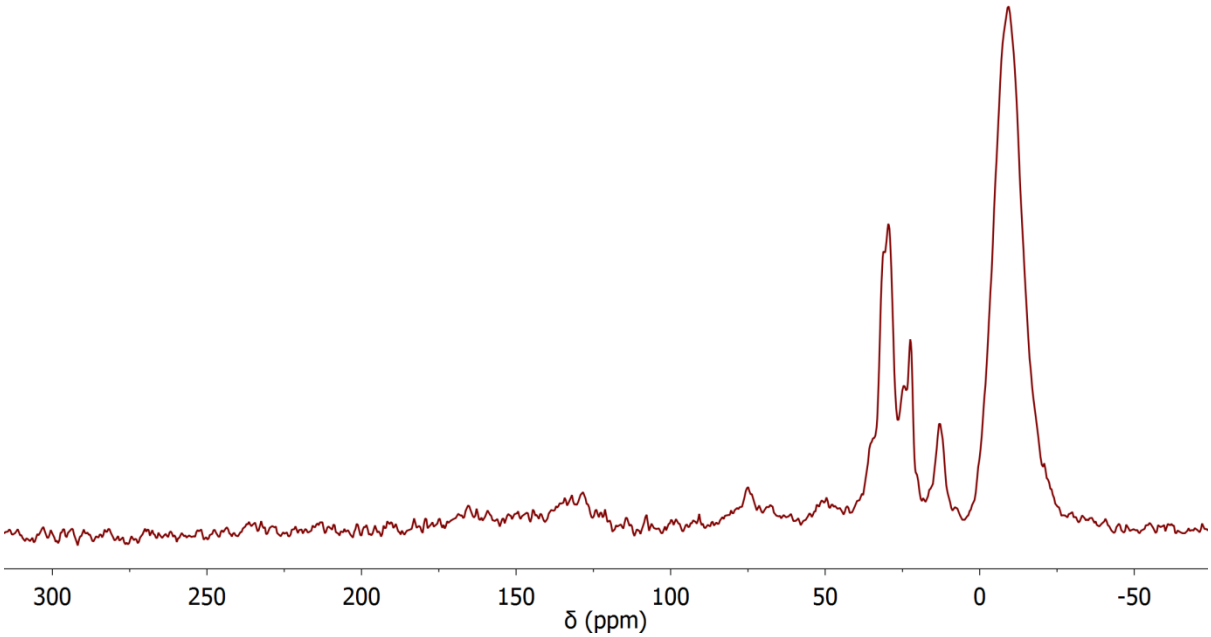


Figure 4.12: ^{13}C CPMAS (10 kHz) NMR spectrum of LDHMAO-SBI*$ZrCl_2$.

Figure 4.12 clearly shows the carbon environments in LDHMAO-SBI*$ZrCl_2$. The dominant resonance at −9 ppm corresponds to the highly shielded methyl environment of MAO. Signals between 22 and 34 ppm correspond to the methyl resonances around the rings of ***rac*-3.1** while a slightly weaker resonance is also seen at 13 ppm which corresponds to the low frequency silicon methyl resonances. All of the signals are shifted from both the solution and solid-state ^{13}C NMR spectra of pure ***rac*-3.1**. In addition, smaller resonances are noted at approximately 75 and 130 ppm which are tentatively assigned to the quaternary cyclopentadienyl and arene carbons respectively. It is noteworthy how clearly the carbon resonances of the ligand show in this spectrum considering that they make up approximately 0.6 wt% of the sample. It has been postulated that the crystalline structure of the LDH support enhances the visibility of the carbon resonances as they are all in identical environments. This is in stark contrast with the same complex supported on Solid MAO or SSMAO where the loading can reach 3 wt% and the carbon signals were not identified.

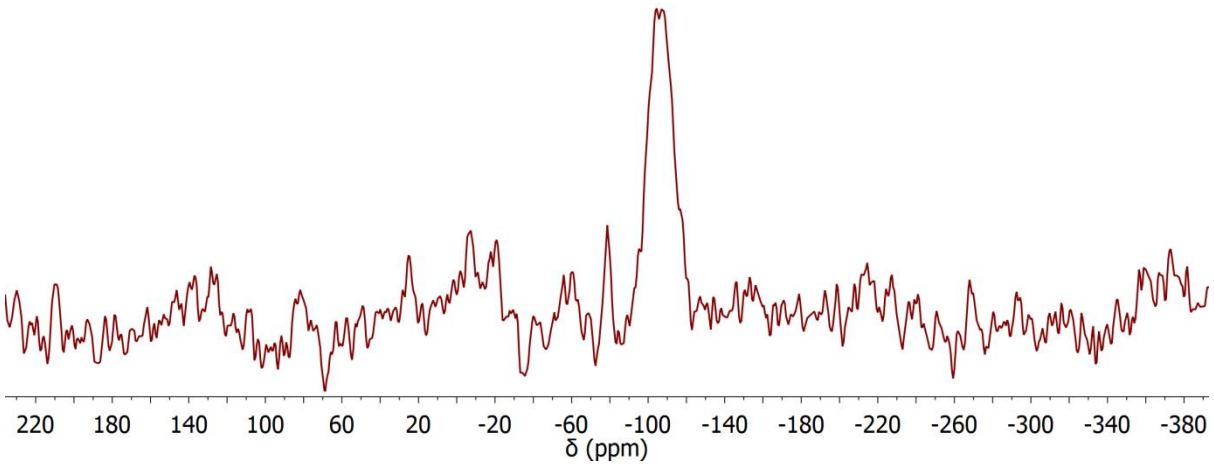


Figure 4.13: ^{29}Si CPMAS (10 kHz) NMR spectrum of SSMAO-*rac*-EBI*$ZrCl_2$.

^{29}Si NMR spectroscopy was employed where appropriate although only very weak signals were seen if the silicon was at a low loading (i.e. in the ligand). Figure 4.13 clearly shows the single silicon environment found for the SiO_2 within SSMAO which occurs at −105 ppm. Previous research in the group has demonstrated that the silicon environment remains unchanged on addition of either MAO or a complex.

^{27}Al NMR spectroscopy was also used to characterised the heterogeneous catalysts, although the signals were found to be more diagnostic than worthy of assignment. Between two and four different aluminium environments were identified within Solid MAO, as well as in SSMAO and LDHMAO, although no further information was obtained.

4.4 EXAFS studies

EXAFS experiments were run on a range of different samples across three sets of "beamtime" on beamline B18 at Diamond Light Source.[49] The intention was to obtain data that confirmed the presence of a zirconium species in a single environment on the support surface. It was envisaged that the ligand system would be clearly identifiable and possibly that a trend comparing a physical characteristic would correlate with activity.

It was decided to avoid permethylated samples due to the extra complexity they may add to an EXAFS spectrum and their involved synthesis. Samples were prepared supported on SSMAO and Solid MAO but these were found to be challenging to form into pellets suitable for analysis and they degraded in the beam. However, more success was had with LDHMAO as a support and five samples were run and analysed, each containing an LDH (Table 4.2).

Table 4.2: samples run and analysed by EXAFS at Diamond Light Source.

Sample Number	Sample contents
#1	LDHMAO-SO_4-EBIZrMe_2
#2	LDHMAO-SO_4-EBIZrCl_2 + Al^{i}Bu$_3$
#3	LDHMAO-Cl-EBIZrCl_2
#4	LDHMAO-SO_4-EBIZrCl_2
#5	LDHMAO-borate-EBIZrCl_2

Samples #3, #4 and #5 all comprise *rac*-EBIZrCl_2 supported on an LDHMAO. The difference between them lies in the anion intercalated between the layers: chloride, sulphate and borate respectively. The anions were observed to have a profound effect on the polymerisation activity of the catalysts and it was hoped that EXAFS would enable us to correlate this with a physical parameter. #1 was run to ascertain if a chloride persisted on the surface which could otherwise be demonstrated by IR spectroscopy but not if the support dominates the spectrum. #2 was selected to see if the alkylaluminium reagent was able to extract a chloride or methyl, affording a cationic species.

Samples with a high loading of zirconium (100:3) were prepared as 13 mm pellets with an approximate thickness of 4 mm and mass of 200 mg. They were pressed in the glovebox and mounted, up to three at a time, in an airtight gas cell with Kapton windows as shown in Figure 4.14.

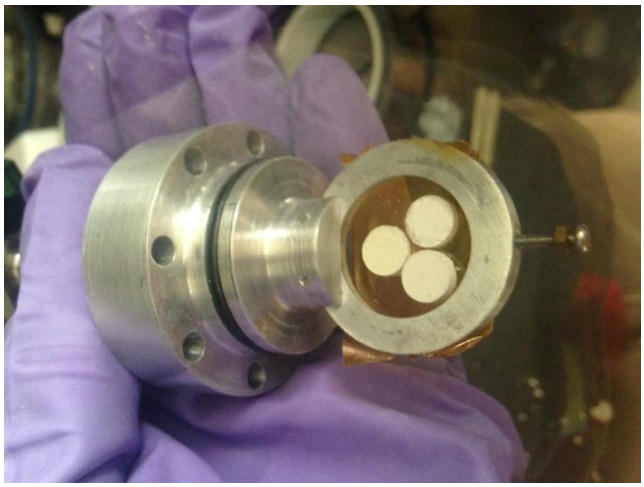


Figure 4.14: three pellets in the sample holder within the glovebox, ready for mounting into an airtight gas cell for EXAFS measurements.

The samples were mounted on a moveable stage within the experimental hutch and collected in transmission mode, measuring the difference between two ion chambers either side of the sample, I_0 and I_T (Figure 4.15).

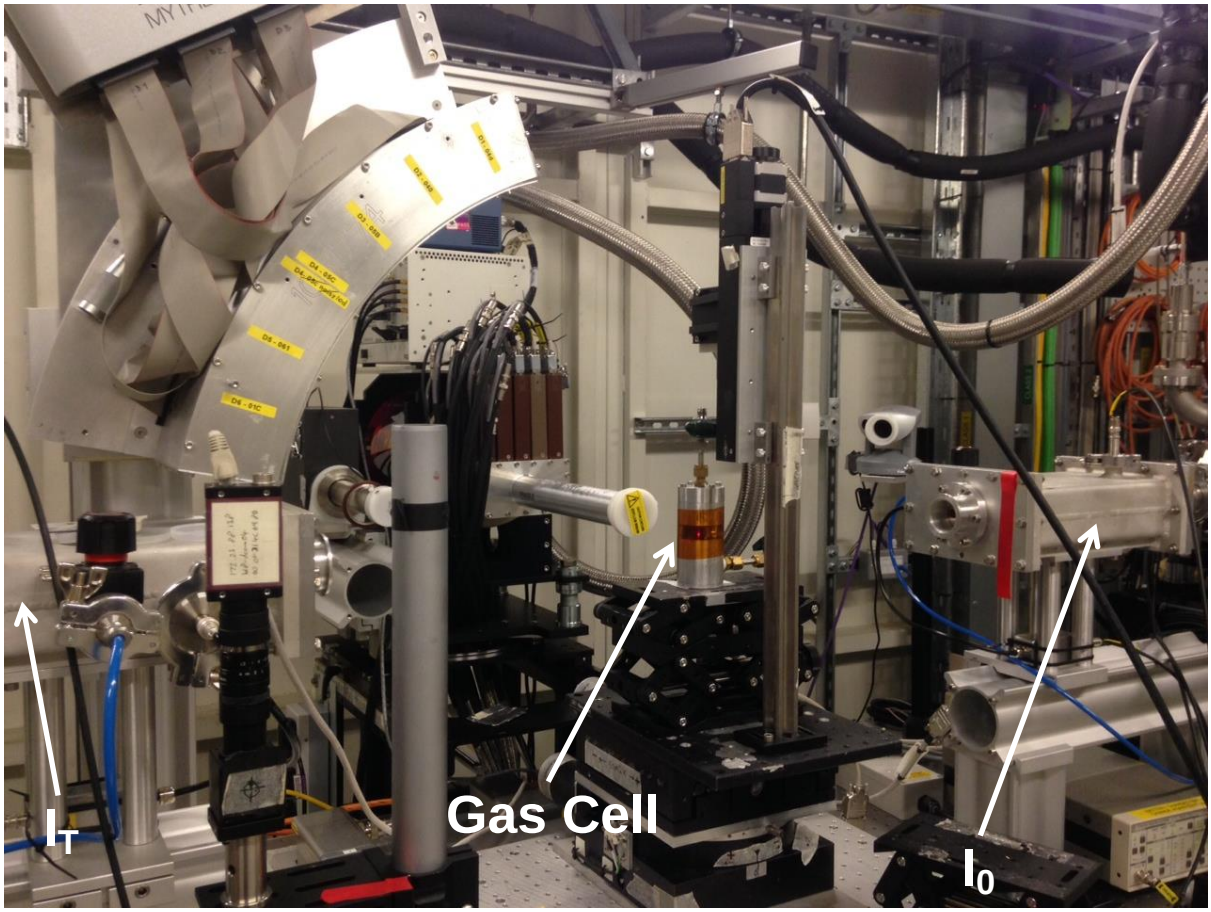


Figure 4.15: the setup with the gas cell on a moveable stage inside the experimental hutch on beamline B18 at Diamond Light Source. The ion chambers, I_0 (upstream) and I_T (downstream) are marked.

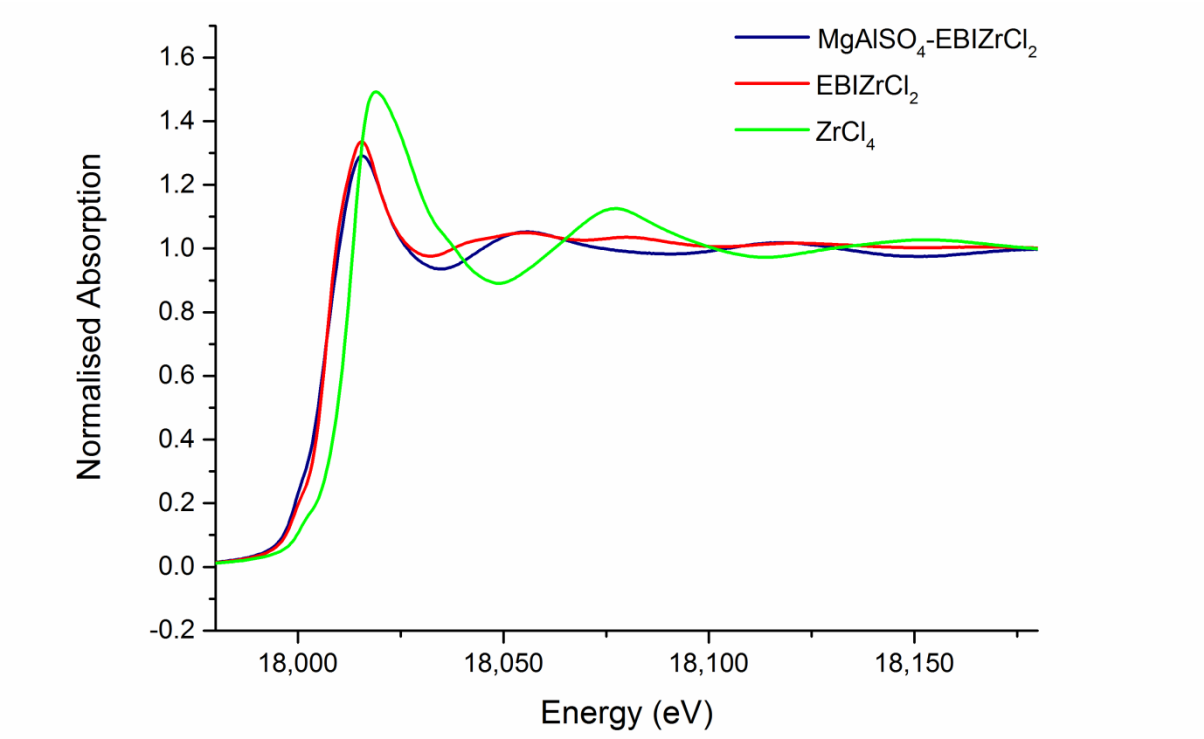


Figure 4.16: normalised XANES data for three samples: $EBIZrCl_2$ supported on LDHMAO (#4) and two standards: pure $EBIZrCl_2$ and $ZrCl_4$.

The three XANES spectra highlight a significant shift in the energy of the Zr K-edge, corresponding to approximately 5 eV, between the $ZrCl_4$ spectrum and the other two. This is attributed to the increase in electron density at the metal centre. While the formal oxidation state remains unchanged, the core electrons are held less tightly and are therefore ionised more easily. This change is caused by the covalent donation of electrons by the indenyl rings, in contrast with the highly electronegative chloride ligands.

In order to analyse EXAFS data, a model is created which can then be fitted to the data. Thanks are due to Peter Wells (UK Catalysis Hub) and Emma Gibson (UCL), both based at the Research Complex at Harwell for the generation of these models and their help collecting the EXAFS data. Figure 4.17 shows the different paths employed in the model. Zr-C corresponds to the interaction between the metal centre and the carbons in the Cp rings, while Zr-C-C takes account of multiple scattering paths. These are the strongest components on account of their multiplicities: 10 and 20 respectively. One possibility suggested was that an oxygen (from the MAO) might bind to the zirconium centre and this was found to fit well with the model. A small contribution is also made by a local aluminium atom.

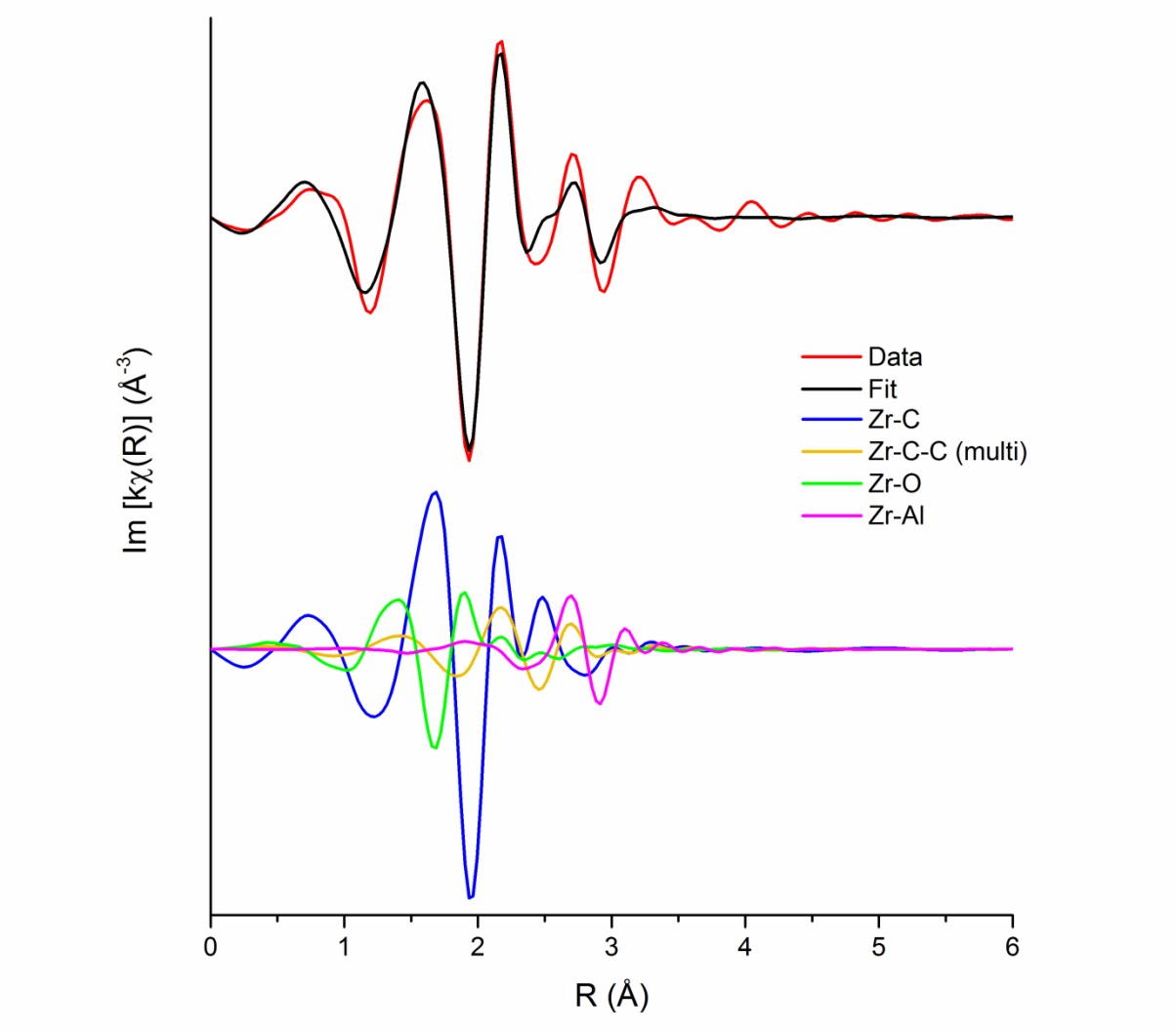


Figure 4.17: a comparison of the imaginary data for #3, the summation of the fit data and the individual components. 10-fold contribution from the Cp rings (navy), 20-fold carbon-carbon multiple scattering paths (gold), oxygen contribution (green) and aluminium contribution (magenta).

Table 4.3: EXAFS fitting parameters for #3.

Absolute Scatterers	N	Distance (Å)	Disorder, σ^2 (Å^2)
Zr-C (Cp ring)	10	2.51(2)	0.006(1)
Zr-C-C (multiple scattering)	20	3.21(4)	0.004(fixed)
Zr-O	1	2.26(4)	0.004 (fixed)
Zr-Al	1	3.34(5)	0.004 (fixed)

Fitting parameters: S_0^2 = 0.8 as deduced by ZrO_2 standard; Fit range 3<k<11.5, 1.1<R<4; number of independent points = 15; R-factor = 0.049.

On optimising the paths considered for the model, their fit with the imaginary part of the $k^2\chi(R)$ data is analysed through an iterative procedure. While Figure 4.17 shows the final fit and the experimental data for the imaginary component of $k^2\chi(R)$, Figure 4.18 gives the

magnitude of the Fourier transform of the data and the fit. Table 4.3 gives the bond lengths obtained and the other fitting parameters required. The match of the fit to the data is very good, with an R-factor of 4.9%.[39,41]

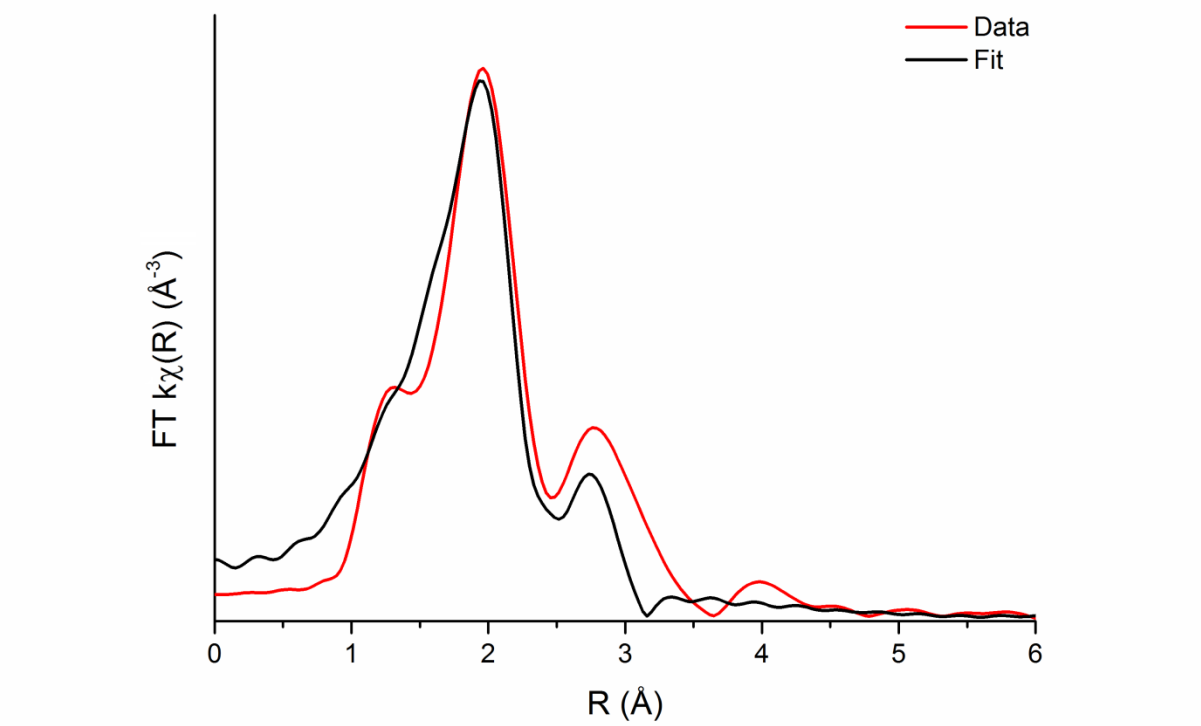


Figure 4.18: a comparison of the fit and the Fourier transform of the magnitude component of the $k^2\chi(R)$ EXAFS data for #3.

Figure 4.19 provides two illustrations of proposed models for the structure of EBIZrCl_2 supported on the surface of the LDHMAO. The interlayer chloride ions (shown in green) are between the edge-sharing metal (magnesium and aluminium) hydroxide octahedra. It is suggested that the MAO covers the surface as an amorphous layer and that there are two possible interactions with the zirconium. The first of these comprises a covalent bond between the zirconium centre and an oxygen of MAO. The suggested atomic separation from the EXAFS model is 2.26(4) Å which is longer than a typical Zr-O bond within a metallocene which fall in the range 1.94-2.01 Å.[50] Perhaps it is more likely that rather than a formal covalent bond, a closely associated ion pair is seen. This ionic model, coupled with the large separation of the Zr from the surface, would allow polymerisation to proceed *via* the Cossee mechanism (outlined in Chapter One). In addition, the Zr-C distance fits very well with that seen in similar species (2.5-2.6 Å). Figures 4.20 and 4.21 illustrate the fits and data for samples #1 to #5 – showing the EXAFS and R magnitude respectively. Their R-factors are all

excellent, varying between 3.5 and 5.2%, while the EXAFS data are of a very high quality showing low levels of noise. The fit data are shown in section 6.6.4.

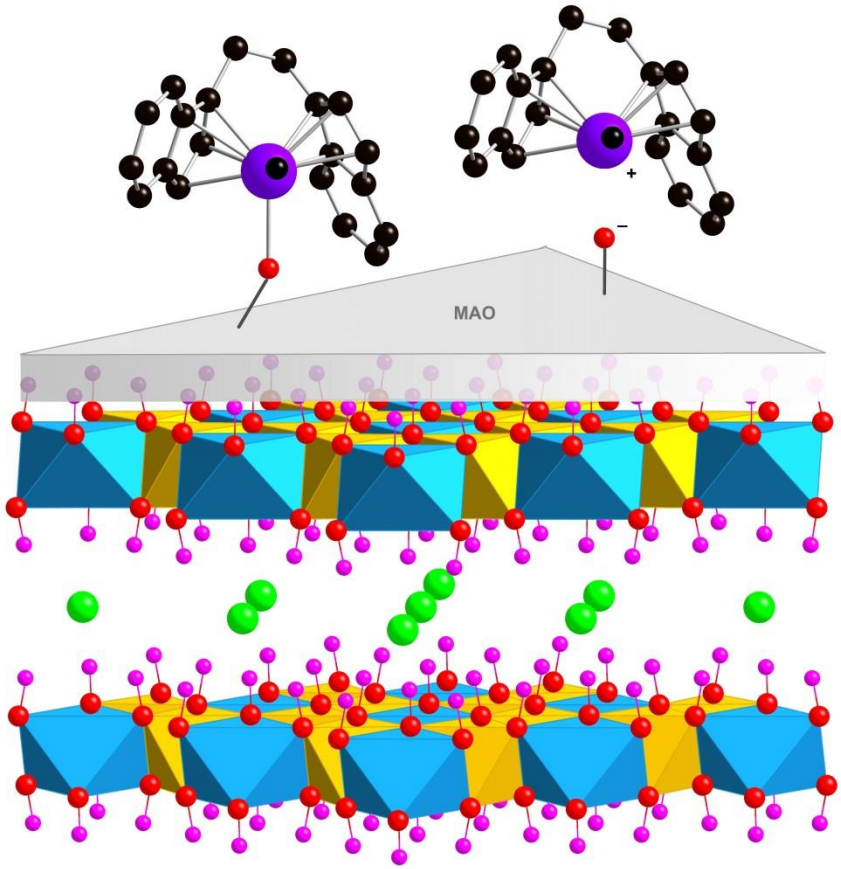


Figure 4.19: two proposed models for the structure of on the surface of LDHMAO-EBIZrCl_2 (#3); one suggestion bears a covalent linkage and the other an electrostatic attraction. Chloride, green; oxygen, red; zirconium, pink; carbon, black.

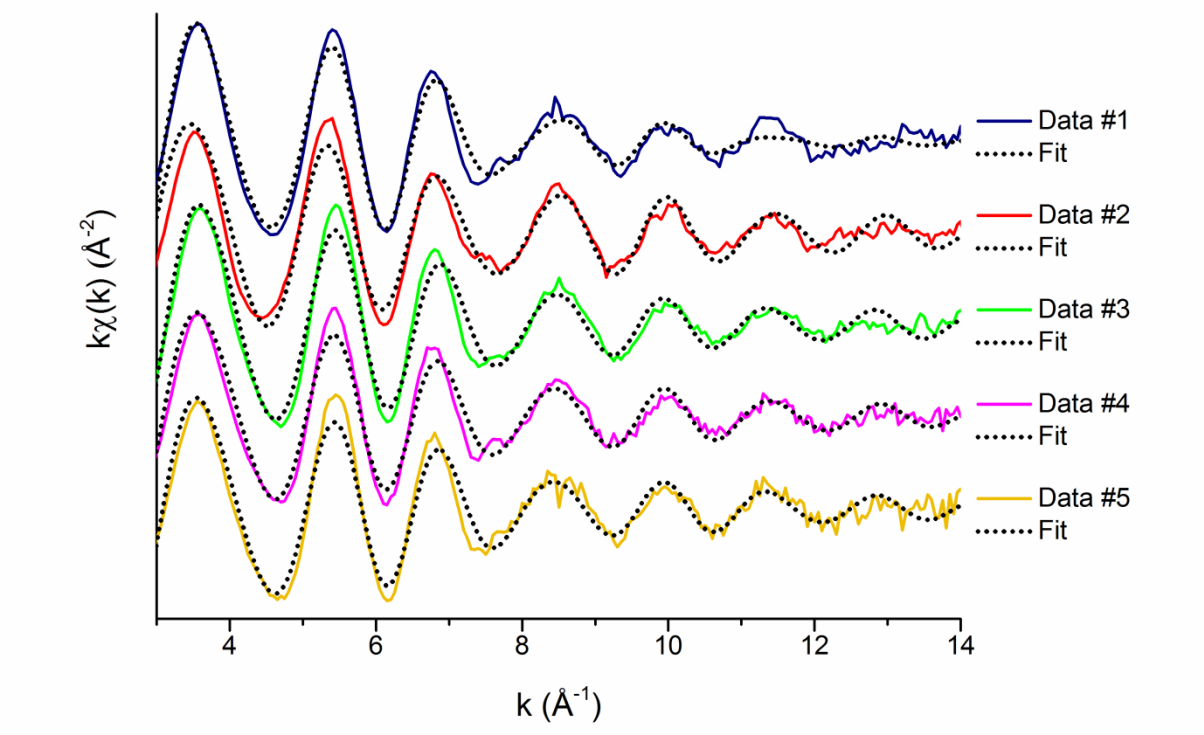


Figure 4.20: a comparison of the fit and EXAFS data for five of the supported samples analysed by EXAFS. #1 $MgAlSO_4$-MAO-EBIZrMe_2. #2 $MgAlSO_4$-MAO-EBIZrMe_2 + TIBA. #3 MgAlCl-MAO-EBIZrCl_2. #4 $MgAlSO_4$-MAO-EBIZrCl_2. #5 MgAlBorate-MAO-EBIZrCl_2.

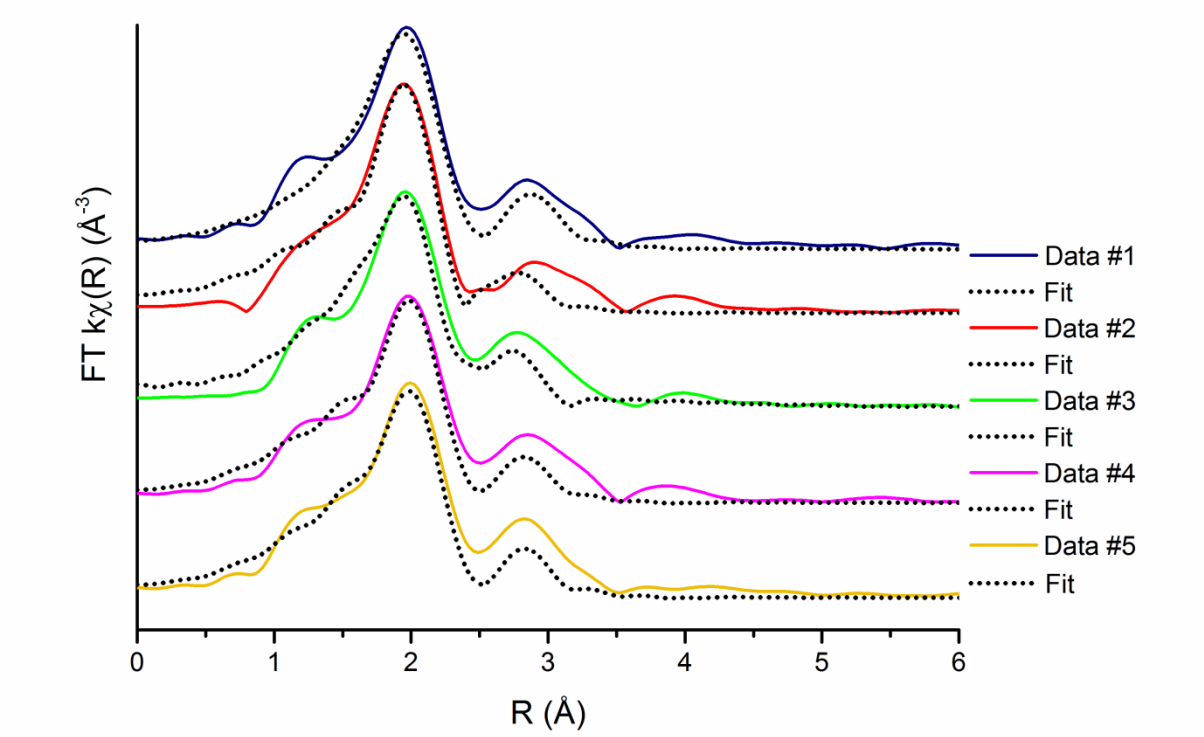


Figure 4.21: a comparison of the fit and the Fourier transform of the magnitude component of the $k^2\chi(R)$ EXAFS data for five of the supported samples analysed by EXAFS. #1 $MgAlSO_4$-MAO-EBIZrMe_2. #2 $MgAlSO_4$-MAO-EBIZrMe_2 + TIBA. #3 MgAlCl-MAO-EBIZrCl_2. #4 $MgAlSO_4$-MAO-EBIZrCl_2. #5 MgAlBorate-MAO-EBIZrCl_2.

4.5 SANS experiment

In 2013, a proposal to run a small-angle neutron scattering (SANS) experiment at ISIS Neutron Facility was accepted to provide complementary data to the EXAFS experiments conducted above. SANS, like EXAFS, allows for the determination of local order within an amorphous or disordered medium. However, it is sensitive to light elements, which is not true of small-angle X-ray scattering (SAXS), and thus can be particularly powerful in the measurement of hydrogen distances.

For this reason, it has been used to good effect in biology and biochemistry, allowing the determination of peptide folds in solution.[51] In chemistry, its use to ascertain the structure of hydrogen bound to the surface of heterogeneous catalysts has been reported and it is capable of measuring hydrogen distances at room temperature.[52]

Since hydrogen (^{1}H) and deuterium (^{2}H or D) have such different scattering lengths and cross-sections, it was decided to run difference experiments to understand the local structure. Discussion with the facility scientists encouraged the running of four samples: SSMAO, SSMAO with a *protio*-complex, SSMAO with a *deuterio*-complex and SSMAO with a mixed complex. Given the synthetic challenges posed by the deuteration of EBI*$ZrCl_2$ or even EBI$ZrCl_2$, zirconocene dichloride was chosen as an analogue. A quick analysis of the results obtained suggested that the strong signal shown by the MAO itself, obscured the differences observed. A synthetic route to deuterated MAO ($AlOCD_3$) has been devised but requires the generation of alkyl mercury compounds, which are notoriously toxic, and this avenue has not been pursued. It is still thought, however, that SANS can provide information useful for the complete determination of the surface-bound structure of immobilised metallocene catalysts, when combined with other experimental techniques such as those described in this chapter.

4.6 Conclusion

19 new catalysts have been synthesised and described, immobilised across three supports. In each case the supports have been characterised by a number of techniques including IR, UV/visible and solid-state NMR spectroscopy as well as SEM. These confirm that the morphology and particle size of the supports remain unchanged following the immobilisation procedure, as well as observing the differences shown by the heterogeneous catalysts. In every case, all of the complex was seen to be affixed to the surface, with none left in solution. This represents one of the earliest reports of the use of LDHs as the basis of a support material,[49] and five LDH samples have been analysed by EXAFS. The results published here

show EXAFS data of a very high quality and excellent fits to the data. It is also, the only report in the academic literature documenting a solid methylaluminoxane as a complete support for a single-site catalyst.

4.7 References

(1) Hlatky, G. G. *Chem. Rev.* **2000**, *100*, 1347.
(2) Severn, J. R.; Chadwick, J. C.; Duchateau, R.; Friederichs, N. *Chem. Rev.* **2005**, *105*, 4073.
(3) Severn, J. R.; Chadwick, J. C. *Taylor-Made Polymers. Via Immobilisation of Alpha-Olefin Polymerization Catalysts*; Wiley-VCH, **2008**.
(4) Dos Santos, J. H. Z.; Krug, C.; Da Rosa, M. B.; Stedile, F. C.; Dupont, J.; De Camargo Forte, M. *J. Mol. Catal. A Chem.* **1999**, *139*, 199.
(5) Silveira, F.; Alves, M. do C. M.; Stedile, F. C.; Pergher, S. B.; dos Santos, J. H. Z. *J. Mol. Catal. A Chem.* **2010**, *315*, 213.
(6) Yano, A.; Sato, M. Olefin polymerization catalyst and olefin polymerization process. US5830820, **1998**.
(7) Suzuki, T.; Suga, Y. *Polym. Prepr.* **1997**, *38*, 207.
(8) Frielingsdorf, H.; Müller-Tamm, H.; Schweier, G.; Reuter, L. Inorganic Carriers for Ziegler Catalysts. DE2163852, **1973**.
(9) Xu, Z. P.; Zhang, J.; Adebajo, M. O.; Zhang, H.; Zhou, C. *Appl. Clay Sci.* **2011**, *53*, 139.
(10) Khan, A. I.; Lei, L.; Norquist, A. L.; O'Hare, D. *Chem. Commun.* **2001**, 2342.
(11) Du, Y.; Hu, G.; O'Hare, D. *J. Mater. Chem.* **2009**, *19*, 1160.
(12) Bull, R. M. R.; Markland, C.; Williams, G. R.; O'Hare, D. *J. Mater. Chem.* **2011**, *21*, 1822.
(13) Zou, X.; Goswami, A.; Asefa, T. *J. Am. Chem. Soc.* **2013**, *135*, 17242.
(14) Zhao, Y.; Li, B.; Wang, Q.; Gao, W.; Wang, C. J.; Wei, M.; Evans, D. G.; Duan, X.; O'Hare, D. *Chem. Sci.* **2014**, *5*, 951.
(15) Williams, G. R.; Fierens, K.; Preston, S. G.; Lunn, D.; Rysnik, O.; De Prijck, S.; Kool, M.; Buckley, H. C.; Lambrecht, B. N.; O'Hare, D.; Austyn, J. M. *J. Exp. Med.* **2014**, *211*, 1019.
(16) Gao, X.; Lei, L.; O'Hare, D.; Xie, J.; Gao, P.; Chang, T. *J. Solid State Chem.* **2013**, *203*, 174.
(17) Choy, J.-H.; Park, J.; Kwak, S.-Y.; Jeong, Y.-J. *Angew. Chem. Int. Ed.* **2000**, *39*, 4041.
(18) Liu, Z.; Ma, R.; Osada, M.; Iyi, N.; Ebina, Y.; Takada, K.; Sasaki, T. *J. Am. Chem. Soc.* **2006**, *128*, 4872.
(19) Wang, Q.; Undrell, J. P.; Gao, Y.; Cai, G.; Buffet, J.-C.; Wilkie, C. A.; O'Hare, D. *Macromolecules* **2013**, *46*, 6145.
(20) Gao, Y.; Wu, J.; Wang, Q.; Wilkie, C. A.; O'Hare, D. *J. Mater. Chem. A* **2014**, *2*, 10996.
(21) Wang, Q.; Zhang, X.; Zhu, J.; Guo, Z.; O'Hare, D. *Chem. Commun.* **2012**, *48*, 7450.
(22) Wang, Q.; Wu, J.; Gao, Y.; Zhang, Z.; Wang, J.; Zhang, X.; Yan, X.; Umar, A.; Guo, Z.; O'Hare, D. *RSC Adv.* **2013**, *3*, 26017.
(23) Wang, Q.; O'Hare, D. *Chem. Commun.* **2013**, *49*, 6301.
(24) Wang, Q.; O'Hare, D. *Chem. Rev.* **2012**, *112*, 4124.
(25) Yang, M.; McDermott, O.; Buffet, J.-C.; O'Hare, D. *RSC Adv.* **2014**, *4*, 51676.

(26) Chen, C.; Yang, M.; Wang, Q.; Buffet, J.-C.; O'Hare, D. *J. Mater. Chem. A* **2014**, *2*, 15102.
(27) Geerts, R. L.; Hill, T. G.; Kufeld, S. E. Organo-aluminoxy product and use. US5411925, **1995**.
(28) Geerts, R. L.; Pettijohn, T. M.; Palackal, S. J.; Infield, R. M. Metallocene catalyst systems for polymerization of olefin. US5496781, November 22, **1995**.
(29) Lu, B.; Wang, J.; Hong, X.; Jing, Z. Preparation of supported metallocene/aluminoxane solid catalyst. US5728640, **1998**.
(30) Kioka, M.; Kashiwa, N. Finely divided aluminoxane, process for producing same and its use. US4952540, **1990**.
(31) Kioka, M.; Kashiwa, N. Catalyst for olefin polymerization and processes for its production. US4923833, **1990**.
(32) Kioka, M.; Kashiwa, N.; Tsutsui, T.; Toyota, A. Catalyst for polymerizing an olefin and process for polymerizing an olefin. US5122491, **1992**.
(33) Kaminsky, W.; Renner, F. *Macromol. Rapid Commun.* **1993**, *14*, 239.
(34) Collins, S.; Kelly, W. M.; Holden, D. A. *Macromolecules* **1992**, *25*, 1780.
(35) Burckhart, T. J.; Murata, M.; Brandley, W. B. Method for making and using a supported metallocene catalyst system. US5240894, **1993**.
(36) Burckhart, T. J.; Brandley, W. B. Method for preparing metallocene catalyst systems. US5635437, **1997**.
(37) O'Brien, S.; Tudor, J.; Maschmeyer, T.; O'Hare, D. *Chem. Commun.* **1997**, 1905.
(38) Maschmeyer, T.; Rey, F.; Sankar, G.; Thomas, J. M. *Nature* **1995**, *378*, 159.
(39) Jezequel, M.; Dufaud, V.; Ruiz-Garcia, M. J.; Carrillo-Hermosilla, F.; Neugebauer, U.; Niccolai, G. P.; Lefebvre, F.; Bayard, F.; Corker, J.; Fiddy, S.; Evans, J.; Broyer, J.-P.; Malinge, J.; Basset, J.-M. *J. Am. Chem. Soc.* **2001**, *123*, 3520.
(40) Mäkelä-Vaarne, N. *Ph.D. Thesis*, **2003**.
(41) Mäkelä-Vaarne, N. I.; Nicholson, D. G.; Ramstad, A. L. *J. Mol. Catal. A Chem.* **2003**, *200*, 323.
(42) Guimarães, R.; Stedile, F. C.; dos Santos, J. H. *J. Mol. Catal. A Chem.* **2003**, *206*, 353.
(43) Kaminsky, W.; Sinn, H. *Liebigs Ann. Chem.* **1975**, *1975*, 424.
(44) Kaminsky, W. *J. Chem. Soc. Dalton Trans.* **1998**, 1413.
(45) Buffet, J.-C.; Turner, Z. R.; Cooper, R. T.; O'Hare, D. *Polym. Chem.* **2015**, 10.1039/c4py01742k.
(46) Ransom, P.; Ashley, A. E.; Brown, N. D.; Thompson, A. L.; O'Hare, D. *Organometallics* **2011**, *30*, 800.
(47) Haag, M. C.; Krug, C.; Dupont, J.; De Galland, G. B.; Dos Santos, J. H. Z.; Uozumi, T.; Sano, T.; Soga, K. *J. Mol. Catal. A Chem.* **2001**, *169*, 275.
(48) Van Beek, J. A. M.; Pieters, P. J. J.; van Tol, M. F. H. In *Proceedings of "Metallocenes";* **1995**.
(49) Buffet, J.-C.; Wanna, N.; Arnold, T. A. Q.; Gibson, E. K.; Wells, P. P.; Wang, Q.; Tantirungrotechai, J.; O'Hare, D. *Chem. Mater.* **2015**, 10.1021/cm503433q.
(50) Buffet, J.-C.; Harris, G. R.; Coward, J. J.; Arnold, T. A. Q.; Turner, Z. R.; O'Hare, D. *Macromolecules* **2015**, Submitted.
(51) Busch, S.; Bruce, C. D.; Redfield, C.; Lorenz, C. D.; McLain, S. E. *Angew. Chem. Int. Ed.* **2013**, *52*, 13091.
(52) Parker, S. F.; Bowron, D. T.; Imberti, S.; Soper, A. K.; Refson, K.; Lox, E. S.; Lopez, M.; Albers, P. *Chem. Commun.* **2010**, *46*, 2959.

Chapter Five
Ethylene Polymerisation Studies

5.1 Introduction

As discussed in Chapter One, the polymerisation of ethylene is industrially significant with annual production in excess of 75 million tonnes.[1] It has also been a topic of huge academic importance and the focus of a number of reviews.[2–5] Interest in the field was sparked by the discovery of heterogeneous catalysts combining metals from both group 4 and group 13 by Ziegler in 1955.[6] In the 60 years since that initial research, the area has undergone a number of revolutions, revitalising the topic and opening up many new avenues of interest. The introduction of well-defined single-site metallocene catalysts by Breslow and Natta paved the way to a better understanding of the mechanism.[7,8] Kaminsky's serendipitous discovery that the addition of water greatly increased the efficacy of the aluminium cocatalysts (and the activity of the system) revived an area of interest that had not developed hugely thitherto.[9,10] Constrained geometry catalysts (CGCs) became the subject of intense industrial interest following their publication in 1990, both due to their excellent thermal stability and their co-monomer incorporation.[11–13] More recently, interest in late transition metal catalysts has taken hold, following key discoveries in 1998,[14,15] and this still remains a major topic of investigation.[16,17] However, the size of the industry supports research into a variety of themes and, to that end, both heterogeneous Ziegler catalysts and metallocenes retain their relevance today.[18–20]

While heterogeneous Ziegler catalysts are still employed for the bulk syntheses of low cost resins, tailored applications of immobilised catalysts are dominating new research.[5,21,22] Chapter Four has extensively described the immobilisation of group 4 metallocene complexes on to three solid supports (layered double hydroxides (LDHs), silica and Solid MAO), and their subsequent characterisation. This chapter aims to understand the polymerisation activity and the properties of the resultant polymer of the complexes described in this work so far under a variety of conditions.

5.2 Solution-phase polymerisation

Solution-phase polymerisation has not been adopted by industry as widely as might have been anticipated given the impact of the discoveries by Kaminsky and Sinn,[9] and the activities reported.[23] The scale-up of high-density polyethylene (HDPE) is beset with

problems, chief amongst which is that of reactor fouling. Typically, this is caused by the heat given out by the exothermic α-olefin polymerisation process, creating a localised "hot-spot" which can melt the resultant polymer causing it to stick to the reactor. As this process is repeated, reactor stirring can very quickly be inhibited or stopped entirely. This is a particular problem for solution-phase polymerisation as the activities reported are higher, and hence the exotherm greater, than in that for gas- or slurry-phase polymerisations. This limits the commercial use of solution-phase polymerisation processes to polymers which are soluble in the diluent or have melting points below the operating temperatures of the process. In practice, this means they are used for lower crystallinity polymers such as ULDPE and VLDPE (ultra- and very-low density polyethylene). However, solution polymerisation remains the gold-standard in the laboratory and within the academic literature, where reactor fouling is less problematic and where high activities are sought above all. With the aim of comparing some of the complexes prepared in Chapter Three to other reports, including that of EBI*$ZrCl_2$,[24] some solution-phase ethylene polymerisations are described here.

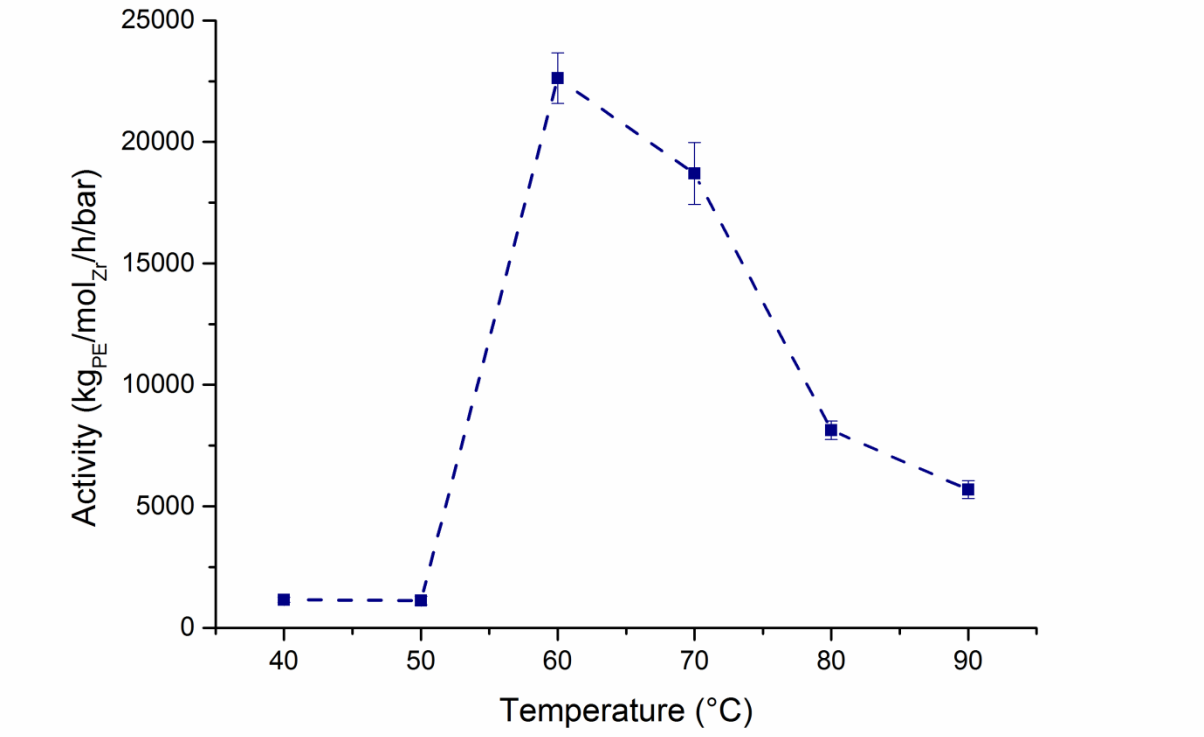


Figure 5.1: a graph showing the ethylene polymerisation activity dependence of ***rac*-3.1** on temperature. MAO (2000:1); 2 bar ethylene; 0.2 mg catalyst loading; 50 ml hexane; timed until cessation of stirring.

As described in section 6.7.1, solution phase polymerisations were all carried out under ethylene at a pressure of two bar, in 150 ml ampoules containing 50 ml hexane and 0.2 mg of

the chosen complex. All polymerisation runs were carried out in duplicate and were run for 30 minutes, or until the stirring of the vessel ceased entirely.

rac-SBI*$ZrCl_2$, ***rac*-3.1**, was used to catalyse the polymerisation of ethylene at a range of temperatures from 40-90 °C using methylaluminoxane (MAO) as the co-catalyst and scavenger (Figure 5.1). The Al:Zr ratio (MAO:***rac*-3.1**) employed was 2000:1, a typical choice for comparison with the literature, where ratios from 200-10,000 are routinely used.[23–25] The most striking feature of the temperature profile for ***rac*-3.1** in solution is the activity achieved at 60 °C (22,622 $kg_{PE}/mol_{Zr}/h/bar$) which compares well with some of the highest reported values in the literature. *rac*-EBI*$ZrCl_2$ has an activity reported as 61,800 $kg_{PE}/mol_{Zr}/h/bar$ (70 °C),[24] while *rac*-SBI$ZrCl_2$, *rac*-$^{2,4,7\text{-}Me_3}$SBI$ZrCl_2$ and Cp_2ZrCl_2 show 14,760, 44,760 and 24,360 $kg_{PE}/mol_{Zr}/h/bar$ respectively (all 30 °C).[23,26] However, the former reaction was carried out at 10 bar in a 5 l reactor and the latter three at 2.5 bar in a 1 l vessel (c.f. 2 bar/50 ml, *vide supra*). Furthermore, the solvents used in each case are different: hexane (***rac*-3.1**), isobutene (*rac*-EBI*$ZrCl_2$) and toluene (*rac*-SBI$ZrCl_2$, *rac*-$^{2,4,7\text{-}Me_3}$SBI$ZrCl_2$ and Cp_2ZrCl_2). A combination of these factors means that results are rarely comparable with those from the literature but empiricism suggests that larger volumes and larger pressures lead to higher activities. Conversely, higher loadings typically reduce the performance. A study performed within the research group on *rac*-EBI*$ZrCl_2$ showed the activity at 60 °C in 50 ml hexane at 1 bar to be 1,975 $kg_{PE}/mol_{Zr}/h/bar$;[27] more than an order of magnitude slower than the value reported for ***rac*-3.1**.

Another interesting feature of Figure 5.1 is the sharp increase in activity seen between 50 (1,123 $kg_{PE}/mol_{Zr}/h/bar$) and 60 °C (22,622 $kg_{PE}/mol_{Zr}/h/bar$). We can, perhaps, infer from this that some form of activation barrier is overcome between these temperatures, allowing the polymerisation to proceed more rapidly. Similar features were reported by Eskelinen *et al*. who attributed a sharp rise in activity between 70 and 80 °C to an increase in the solubility of the PE chain (in *n*-heptane), allowing for better monomer diffusion to the catalytic centre.[28] A marked decline in activity is also noted between 70 (18,703 $kg_{PE}/mol_{Zr}/h/bar$) and 80 °C (8,130 $kg_{PE}/mol_{Zr}/h/bar$), suggesting that the catalyst is potentially less stable at elevated temperatures – a well-documented disadvantage to metallocene catalysts.[5]

The weight average molecular weight, M_w, of the resultant polymer was seen to peak at 70 °C (261,337 daltons), up from 213,927 daltons at the activity peak (60 °C). A drop-off is also noted at 80 °C to *c*. 200,000 daltons. The molecular weight distribution (MWD),

measured by the polydispersity index (PDI), was also recorded and was found to increase with increasing temperature from 2.32 (60 °C) to 2.99 (80 °C).

A study was undertaken with ***rac*-3.1** to test the effect that the Al:Zr ratio has on activity (Figure 5.2) and the value for M_w and M_n, the number average molecular weight, were measured in each case. The polymerisation runs were carried out at 70 °C for ease of comparison since most of the catalysts tested are at or near their optima at this temperature. A very strong dependence of the activity on the Al:Zr ratio was noted. The activity at 2000:1 (18,703 $kg_{PE}/mol_{Zr}/h/bar$) is more than four times greater than that at 200:1 (3,996 $kg_{PE}/mol_{Zr}/h/bar$).

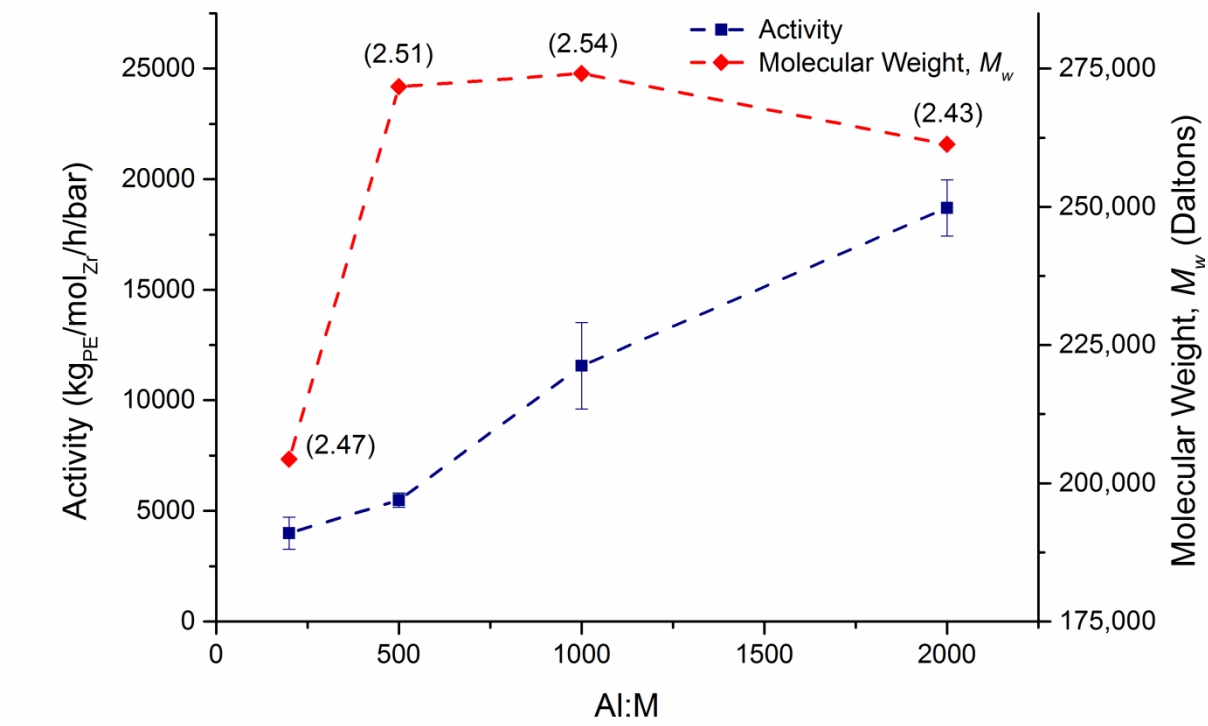


Figure 5.2: a graph showing the dependence of activity and molecular weight, M_w, for ***rac*-3.1** on the Al:Zr co-catalyst (MAO) ratio. PDIs are given in parentheses. 70 °C; 2 bar ethylene; 0.2 mg catalyst loading; 50 ml hexane; timed until cessation of stirring.

The behaviour of M_w is quite unusual, however. At an Al:Zr ratio of 200, it is recorded as 204,374 daltons rising quickly to 271,713 daltons at a ratio of 500 and plateauing on further increases. This contrasts with reports in the literature that suggest that M_w will decrease on addition of more MAO,[29] or at the very least remain constant for the same catalyst.[30]

Attempts were also made, not only to vary the Al:Zr ratio, but to vary the source of aluminium. Polymerisation attempts with 2000 equivalents of Al^iBu_3 (TIBA) and $AlMe_3$ (TMA) failed to produce any PE whatsoever, and the catalysts were deemed inactive.

Following the excellent activities reported for ***rac*-3.1**, it was hoped that the unbridged analogue, $Ind^{\#}_2ZrCl_2$, **3.5**, might also yield high activity data. Figure 5.3 shows a comparison between the solution-phase ethylene polymerisation activities of ***rac*-3.5** and ***meso*-3.5** across a range of temperatures. Unfortunately, the first point of note is that the activities fall far short of those reported for ***rac*-3.1** with peaks at 433 $kg_{PE}/mol_{Zr}/h/bar$ (50 °C) and 335 $kg_{PE}/mol_{Zr}/h/bar$ (70 °C) for ***rac*-3.5** and ***meso*-3.5** respectively. These values also compare unfavourably with a variety of other indenyl complexes reported in the literature such as Ind_2ZrCl_2 (3,866 $kg_{PE}/mol_{Zr}/h/bar$ at 34 °C and 14,000 $kg_{PE}/mol_{Zr}/h/bar$ at 25 °C).[31,32] The most likely cause of the difference is the change in Al:Zr ratios employed (*c.* 500:1 and 2000:1 respectively) as both were conducted in 500 ml toluene using MAO as a co-catalyst. Another possible explanation for the high values reported is the pre-saturation of the diluent with ethylene. Figure 5.3 shows two contrasting trends in activity with varying temperature: ***meso*-3.5** displaying a clear optimum at 70 °C while ***rac*-3.5** shows a gradual decline in activity with increasing temperature. Their activities are comparable in the range 70-90 °C but the typically faster *rac*-isomer outperforms the *meso*- significantly below 70 °C (50 °C: 433 and 181 $kg_{PE}/mol_{Zr}/h/bar$ respectively).

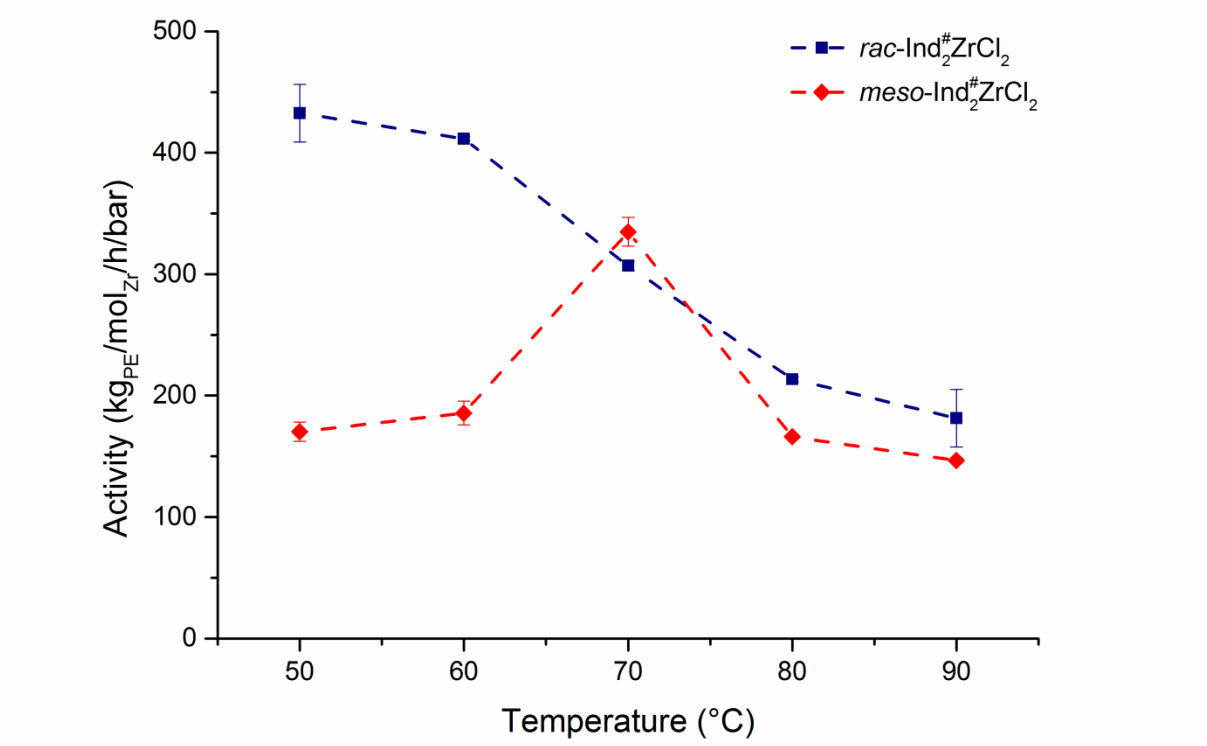


Figure 5.3: a graph showing the ethylene polymerisation activity dependence of ***rac*-** and ***meso*-3.5** on temperature. MAO (2000:1); 2 bar ethylene; 0.2 mg catalyst loading; 50 ml hexane; 30 minutes.

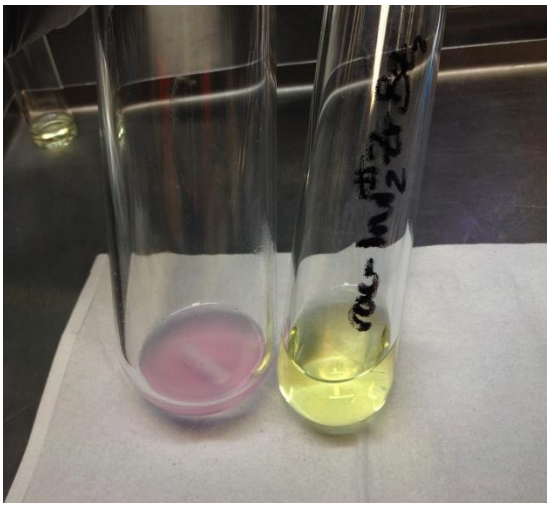


Figure 5.4: stock solution of ***rac*-3.7** immediately before (right; yellow) and after (left; pink) its addition to MAO, prior to polymerisation.

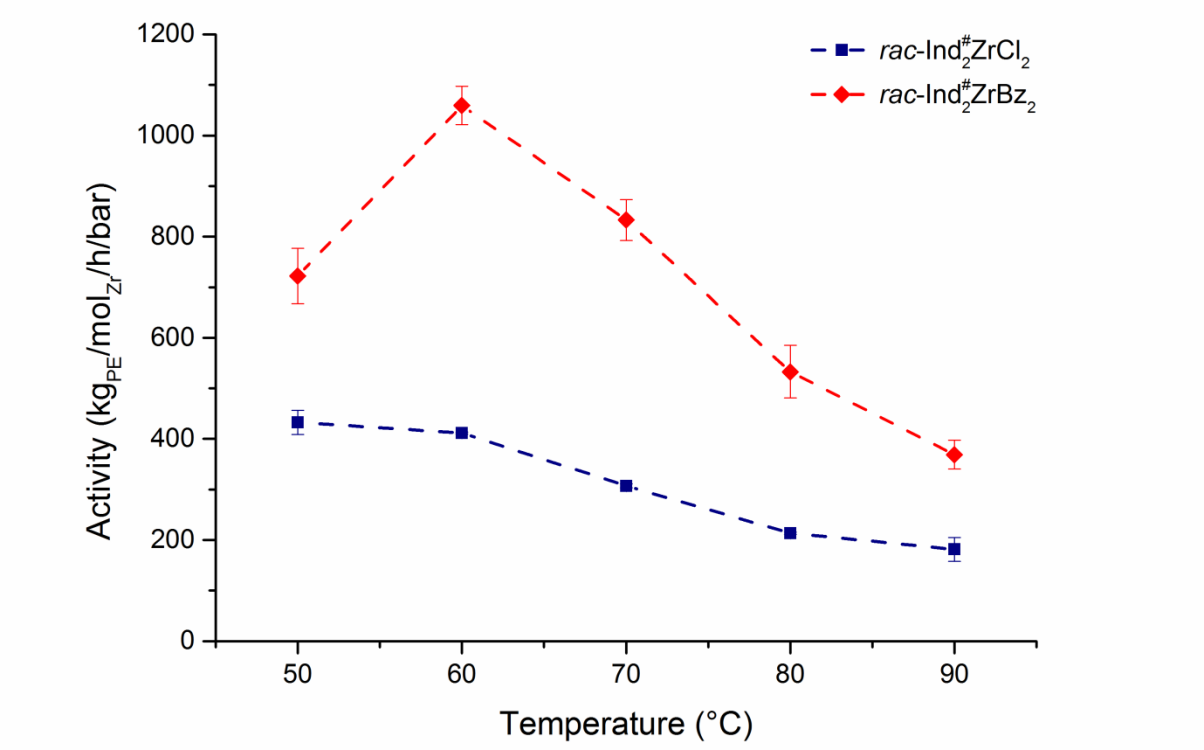


Figure 5.5: a graph showing the ethylene polymerisation activity dependence of ***rac*-3.5** and ***rac*-3.7** on temperature. MAO (2000:1); 2 bar ethylene; 0.2 mg catalyst loading; 50 ml hexane; 30 minutes.

Figure 5.4 shows the change in colour observed (yellow to pink) on addition of ***rac*-3.7** (*rac*-Ind$^{\#}_2$ZrBz$_2$) to MAO in hexane during the preparation of a polymerisation run. This colour change is more dramatic than that observed for other complexes. Figure 5.5 illustrates clearly the improved activity on replacing the chloride ligands for benzyl groups across the entire temperature range. Like ***meso*-3.5**, ***rac*-3.7** displays an optimum temperature in the middle of the range (1059 kg$_{PE}$/mol$_{Zr}$/h/bar at 60 °C) but outperforms both dichloride

congeners almost two fold under all conditions tested. The benzyl compound, ***rac*-3.7**, almost matches the activity of $^{2\text{-Me,4-Ph}}$SBIZrCl$_2$ (1185 kg$_{PE}$/mol$_{Zr}$/h/bar), used as a solution phase ethylene polymerisation catalyst by Napoli and co-workers in 2011.[33] Nevertheless, the benzyl complex falls significantly short of the values reported for ***rac*-3.1** at all temperatures.

Previous reports of the use of benzyl complexes as ethylene polymerisation catalysts, such as those by Bochmann *et al*. use perfluoroborate initiators to generate the cationic species *in situ*.[34] The activities reported for Cp$_2$ZrBz$_2$ (as the pre-catalyst – 1,100 kg$_{PE}$/mol$_{Zr}$/h/bar at 60 °C) match well with the values reported here (1059 kg$_{PE}$/mol$_{Zr}$/h/bar). The runs reported in the paper were only 60 seconds in length, however, in a 50 ml reactor in toluene;[34] typically, short runs emphasise high activities (*vide infra*).

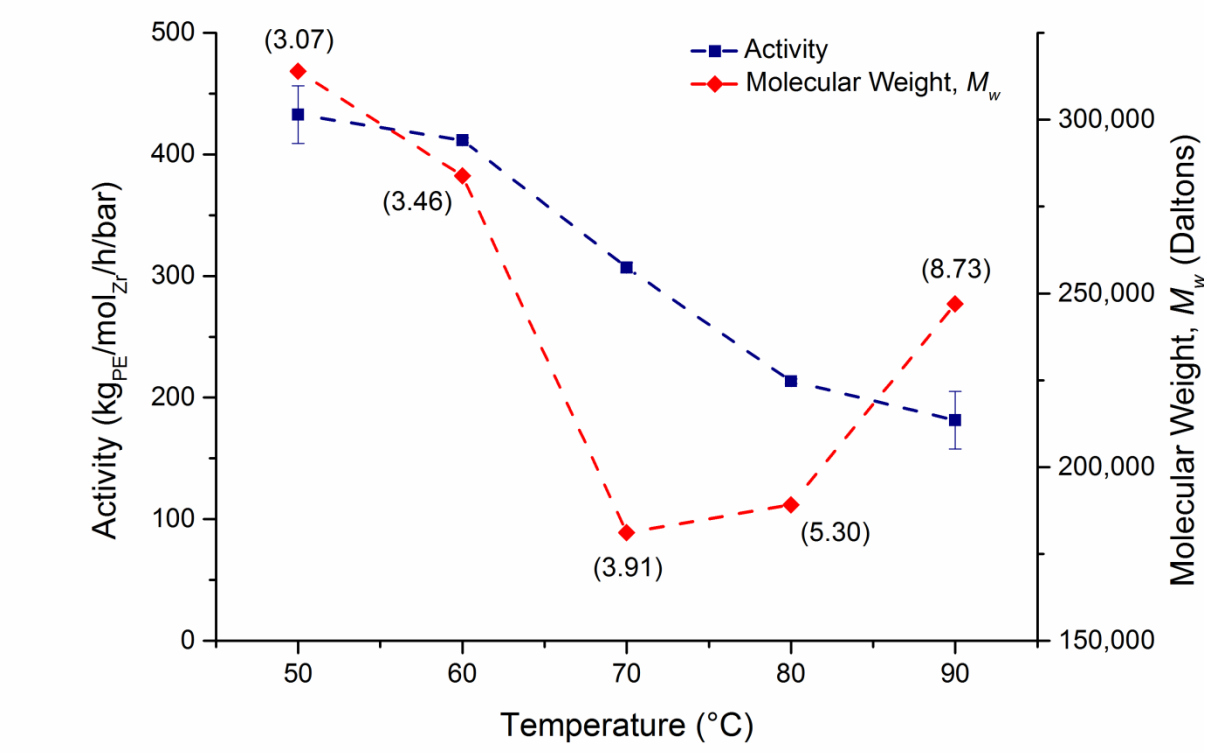


Figure 5.6: a graph showing the dependence of activity and M_w for ***rac*-3.5** on temperature. PDIs are given in parentheses. MAO (2000:1); 2 bar ethylene; 0.2 mg catalyst loading; 50 ml hexane; 30 minutes.

Figure 5.6 highlights the temperature dependence of both activity and molecular weight, M_w, for ***rac*-3.5**. The trend in activity decreases with increasing temperature (*vide supra*) but the trend in M_w is not as simple. It displays a trough, dropping from over 300,000 daltons at 50 °C to just over half that at 70 °C, before rising back to approximately 250,000 daltons by 90 °C. This contrasts with the polydispersity index which rises continuously from 50 to 90 °C with a particularly sharp increase from 5.30 at 80 °C to 8.73 at 90 °C.

The values for M_w and PDI at 70 °C for the four catalysts tested in solution are compared in Figure 5.7. The data show that the trends in molecular weight and MWD are opposing, with the former rising as the latter falls. No clear trend is identified with regards to the effect of an *ansa*-bridge on the molecular weight of polyethylene produced (PE) – the situation is more clear cut for polypropylene (PP).[26] Despite the suggestion from Kaminsky's paper that unbridged analogues consistently show high molecular weights, the variations observed here nowhere near match the 40-fold differential seen in previous PE studies.[26]

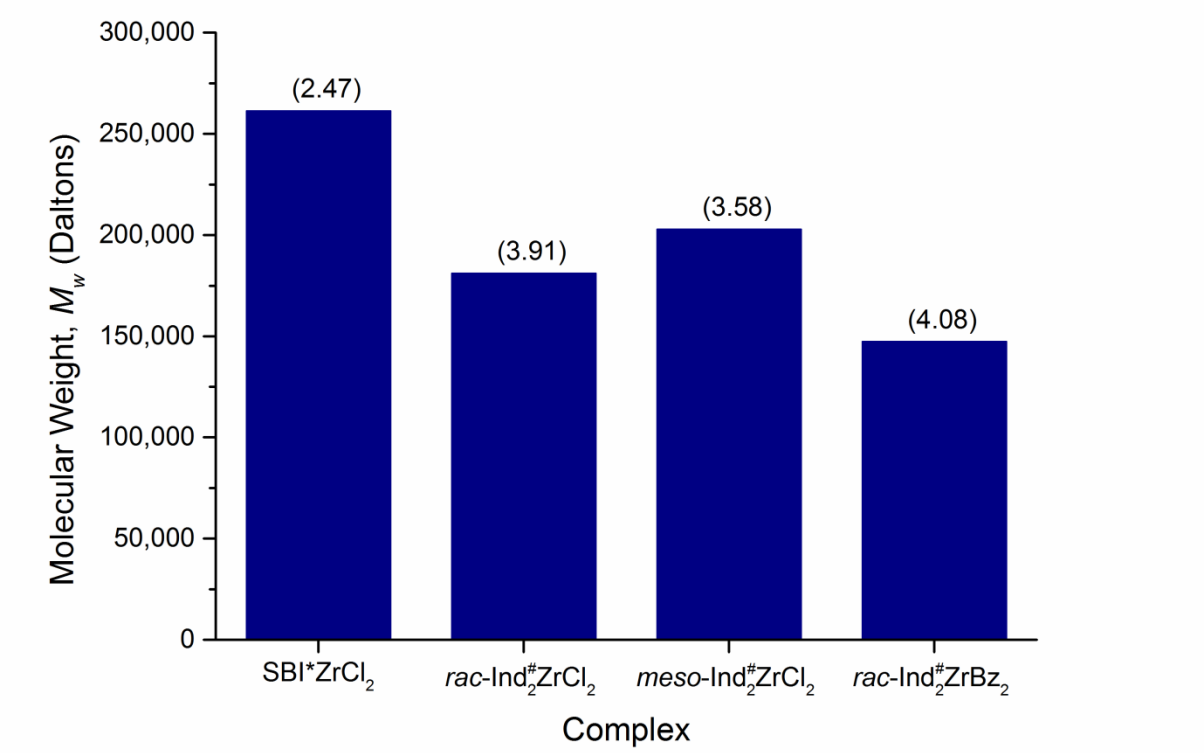


Figure 5.7: a graph showing the variation in molecular weight, M_w, of the polyethylene produced by four complexes in solution. PDIs are given in parentheses. 70 °C; 2 bar ethylene; 0.2 mg catalyst loading; 50 ml hexane; timed until cessation of stirring or 30 minutes, where possible.

While the solution-phase ethylene polymerisation experiments have shown mixed success in terms of the activities reported, a few interesting trends have been seen. Typically (but not always), optimum polymerisation temperatures are reached when the barriers to activation are easily overcome but the complex is not degraded. The benzyl complex, ***rac*-3.7**, seems to outperform the dichloride, **3.5**, which is, as discussed, not always the case in the literature. Perhaps most significantly of all, the peak activity for ***rac*-1**, 22,622 $kg_{PE}/mol_{Zr}/h/bar$ at 60 °C, is exceptional given the small scale of experimental set-up – a match for some of the highest reported values anywhere in the literature.

5.3 Slurry-phase polymerisation

5.3.1 EBI* complexes

Figure 5.8 depicts the ethylene polymerisation activity and the molecular weight data for the previously reported EBI*$ZrCl_2$ on silica supported MAO (SSMAO). This combination of a complex, silica and MAO, is ubiquitous and has even been referred to as the "Holy Trinity" of supported single-site catalysis.[22] In addition to the aforementioned ingredients, triisobutylaluminium (TIBA; Al^iBu_3) is also employed as a scavenger. The activities displayed in Figure 5.8 have an optimum (2151 $kg_{PE}/mol_{Zr}/h/bar$ at 60 °C) and are comparatively stable (i.e. above 1500 $kg_{PE}/mol_{Zr}/h/bar$) from 50-80 °C. A sharper drop off is noted at 90 °C (777 $kg_{PE}/mol_{Zr}/h/bar$). These values compare poorly with those reported for the solution phase polymerisation of EBI*$ZrCl_2$ (61,800 $kg_{PE}/mol_{Zr}/h/bar$ at 70 °C) but outperform the solution results for any of the Ind[#] complexes above (**3.5** or ***rac*-3.7**).

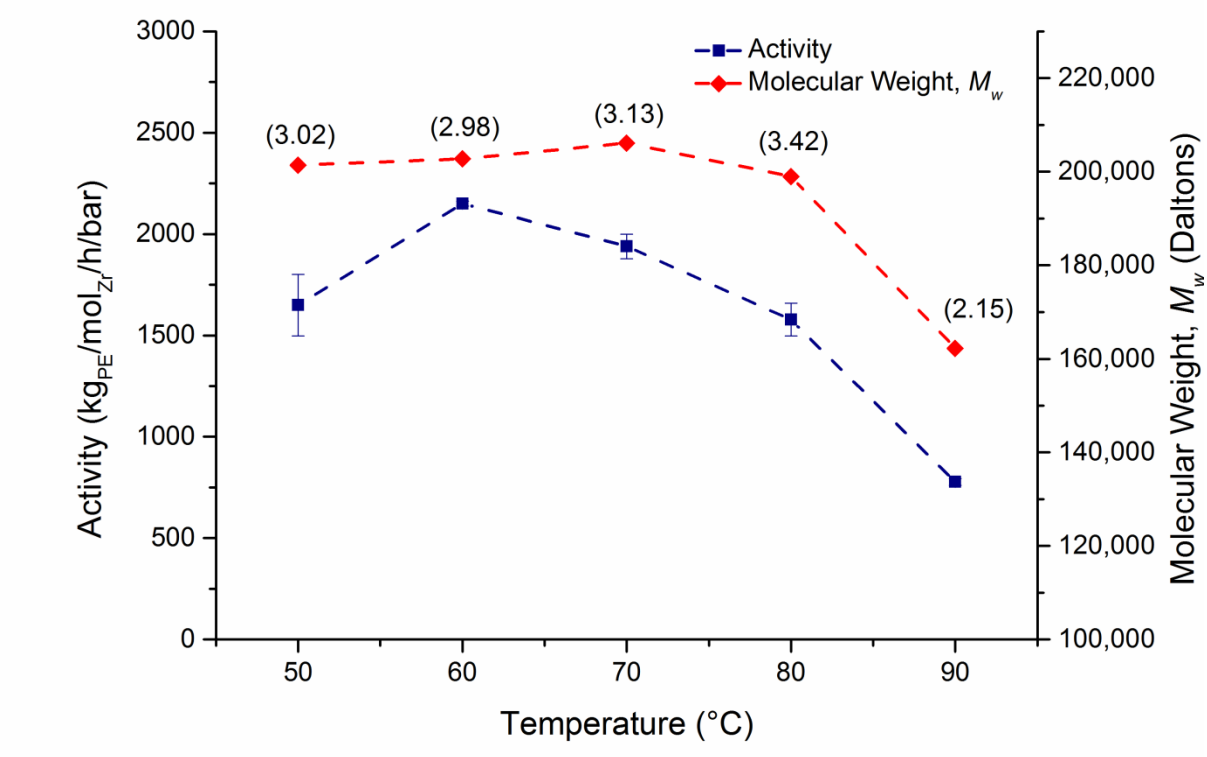


Figure 5.8: a graph showing the dependence of activity and M_w for *rac*-EBI*$ZrCl_2$ on temperature. PDIs are given in parentheses. Supported on SSMAO (200:1 loading); TIBA co-catalyst; 2 bar ethylene; 10 mg catalyst; 50 ml hexane; 1 hour.

A major change to consider when comparing the results in Figure 5.7 to the solution results from section 5.2 is the change from using MAO as the scavenger to TIBA. This is typically preferred to MAO by industry due to the greatly reduced cost; £195.15 mol^{-1} as

opposed to £635.90 mol^{-1} on a small scale from Sigma Aldrich. MAO is only used to affix the complex to the solid support.

The values reported for EBI*$ZrCl_2$ on SSMAO represent a big improvement over the reported results for Ind_2ZrCl_2 supported on silica with trimethylalumnium (400 $kg_{PE}/mol_{Zr}/h/bar$).[35]

The molecular weight observed in the temperature range 50-80 °C is remarkably constant at just over 200,000 daltons before dropping off to approximately 160,000 daltons at 90 °C. Similarly, the molecular weight distribution is roughly constant at approximately 3 until 80 °C where it rises to 3.42 before falling again at 90 °C to 2.15. This final drop in PDI is associated with a lowering in the molecular weight.

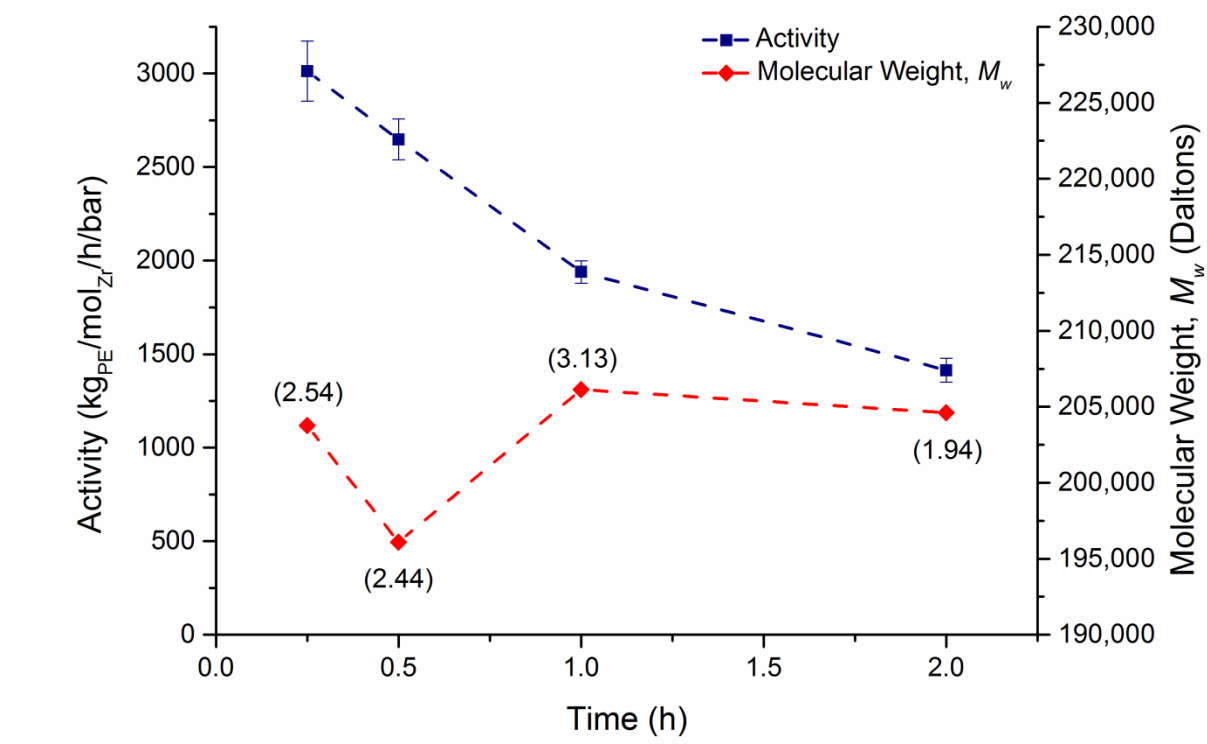


Figure 5.9: a graph showing the dependence of activity and molecular weight, M_w, for *rac*-EBI*$ZrCl_2$ on length of run. PDIs are given in parentheses. Supported on SSMAO (200:1 loading); TIBA co-catalyst; 70 °C; 2 bar ethylene; 10 mg catalyst; 50 ml hexane.

A study was undertaken to ascertain the effect that the length of the polymerisation run has on the activities obtained (Figure 5.9). The activity for the whole run was seen to decrease from 3,012 to 1,414 $kg_{PE}/mol_{Zr}/h/bar$ as the time increased from 15 minutes to two hours – a drop of over 50%. One factor in the explanation is that the catalytic species decomposes throughout the run, reducing the number of active sites effecting the polymerisation and hence reducing the rate.[29] It is also postulated that the slower stirring,

caused by the presence of more than one gram of polymer in the vessel may inhibit the introduction of ethylene into solution, meaning that the reaction is not limited by the turnover rate of the catalyst. Additionally, the build-up of PE around the active site could limit the diffusion of the monomer to the metal centre, inhibiting the observed activity.

The molecular weight holds approximately constant (approximately 200,000 daltons) across all the different run lengths. This behaviour is consistent with literature reports where the molecular weight is often observed to remain at a set value, despite the decrease in activity observed for longer polymerisations.[29]

As described extensively in Chapter Four, supports other than silica are commonly used to immobilise single-site metallocene catalysts. This work only analyses the performance of three of these: SSMAO, Solid MAO, and LDHMAO. Figure 5.10 presents a comparison of two of these, SSMAO and Solid MAO, for *rac*-EBI*$ZrCl_2$. While the loadings of the two catalysts are not the same (SSMAO 200:1, Solid MAO 300:1), it is crucial to bear in mind that these are mole ratios in relation to the support, and that the supports differ significantly in molecular mass. Therefore there is more supported precatalyst in the reaction vessel for Solid MAO than SSMAO (0.48 and 0.28 μmol respectively). More details are given in Chapters Four and Six.

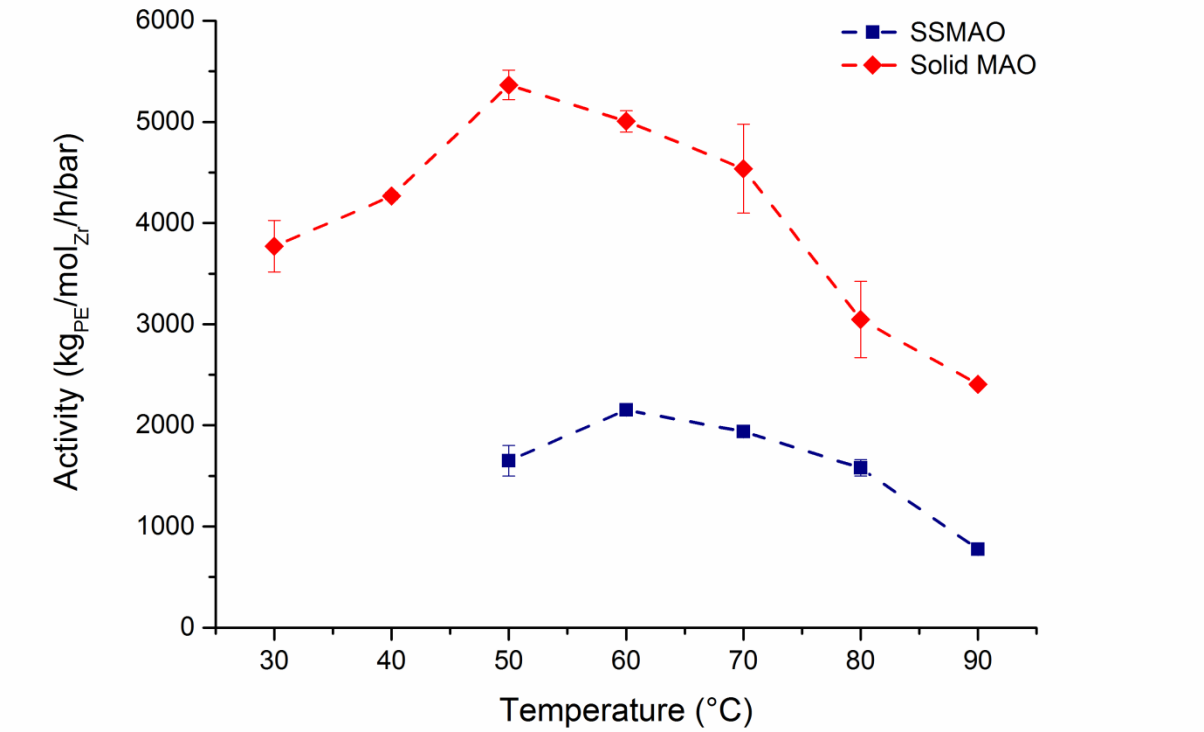


Figure 5.10: a graph showing the ethylene polymerisation activity dependence of *rac*-EBI*$ZrCl_2$ on temperature, supported on SSMAO (200:1) and Solid MAO (300:1). TIBA co-catalyst; 2 bar ethylene; 10 mg catalyst; 50 ml hexane; 1 hour (SSMAO), 30 minutes (Solid MAO).

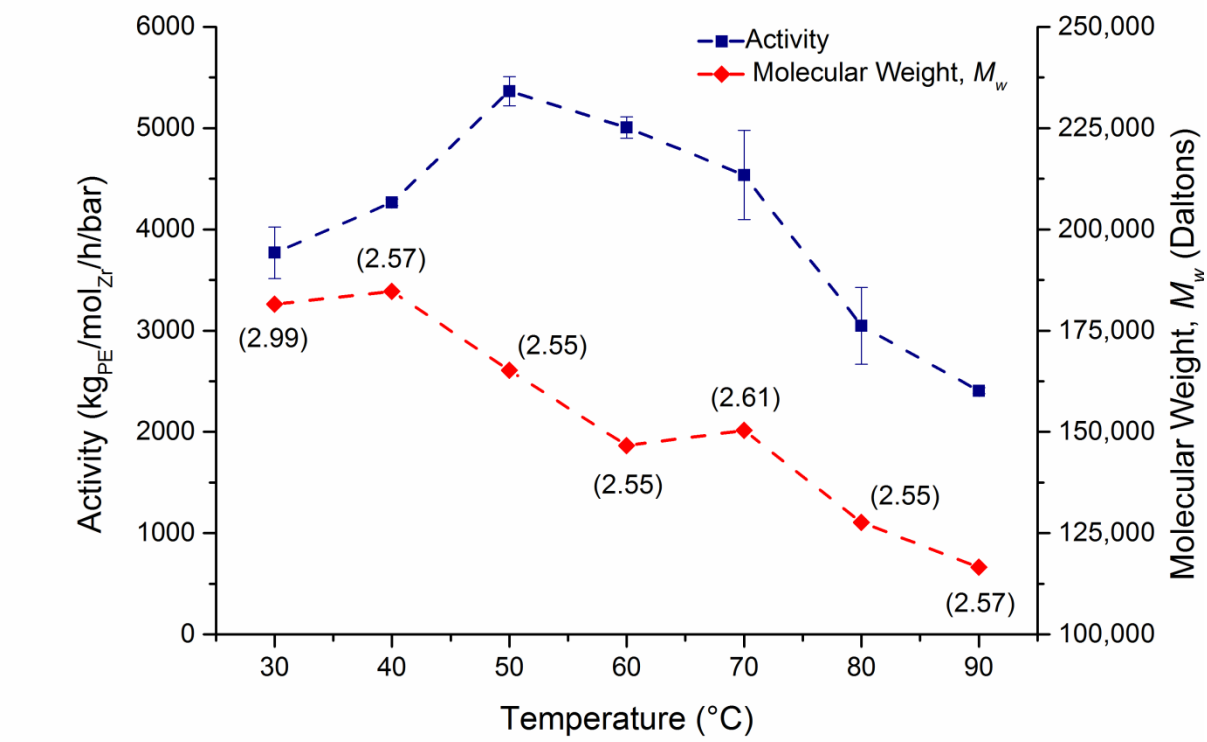


Figure 5.11: a graph showing the dependence of activity and M_W, for *rac*-EBI*$ZrCl_2$ on temperature. PDIs are given in parentheses. Supported on Solid MAO (200:1 loading); TIBA co-catalyst; 2 bar ethylene; 10 mg catalyst; 50 ml hexane; 30 minutes.

Figure 5.10 compares the activity data for *rac*-EBI*$ZrCl_2$ on SSMAO (also shown in Figure 5.8) and Solid MAO. At first glance, it is obvious that the performance of Solid MAO supported catalyst is vastly superior to that for the complex supported on SSMAO; the activity at all temperatures is double or greater. For this reason the polymerisation runs using Solid MAO as a support are carried out for 30 minutes and not a full hour to reduce diffusion limitation effects. The activity for *rac*-EBI*$ZrCl_2$ peaks at 50 °C (5,365 $kg_{PE}/mol_{Zr}/h/bar$) – more than three times that of the silica analogue at the same temperature (1,649 $kg_{PE}/mol_{Zr}/h/bar$). Activities from 50-70 °C remain in excess of 4500 $kg_{PE}/mol_{Zr}/h/bar$, while the nadir (2,406 $kg_{PE}/mol_{Zr}/h/bar$ at 90 °C) outperforms the zenith seen for the silica supported equivalent. No reports in the open literature are, to the author's knowledge, available on the use of Solid MAO as a catalyst support although the activities seen for *rac*-EBI*$ZrCl_2$ supported on Solid MAO match some of the best results reported in the literature. Dos Santos and co-workers studied SSMAO supported zirconocenes and noted that $EBIZrCl_2$ showed polymerisation activities of 490 $kg_{PE}/mol_{Zr}/h/bar$ at 60 °C.[36] However, this system was significantly outperformed by Cp_2ZrCl_2 and Cp'_2ZrCl_2 (Cp′ = C_5H_4Me) and $EBTHIZrCl_2$ [EBTHI = ethylenebis(tetrahydroindenyl)], which show activities of 5,400, 9180 and

4,320 $kg_{PE}/mol_{Zr}/h/bar$ (all at 60 °C) respectively. These values compare excellently with those shown in Figures 5.10 and 5.11 although they require an MAO scavenger. The MWD for *rac*-EBI*$ZrCl_2$ on Solid MAO is described in Figure 5.11 and the molecular weight shows a general decrease with increasing temperature from 180,000 to 115,000 daltons (40 to 90 °C). These values are consistently lower than the equivalent results on SSMAO. With the exception of 2.99 at 30 °C, the PDI remains almost constant across the temperature range (approximately 2.5).

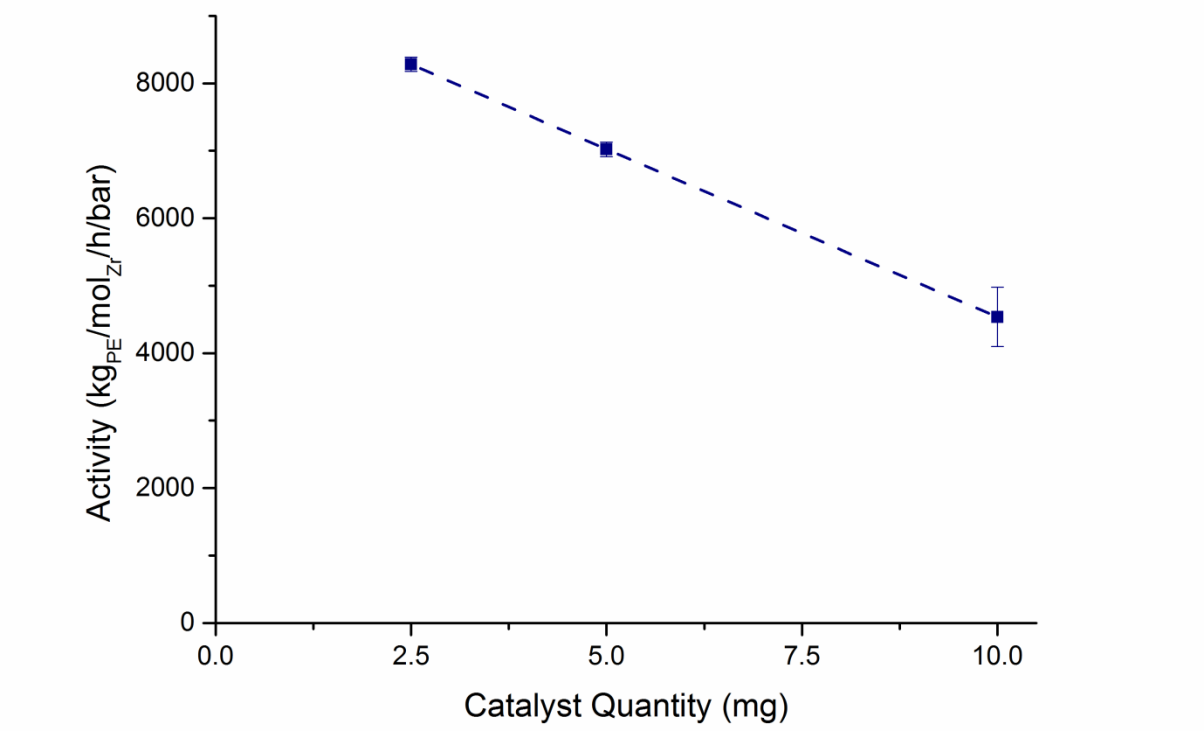


Figure 5.12: a graph showing the ethylene polymerisation activity dependence of *rac*-EBI*$ZrCl_2$ on amount of catalyst. Supported on Solid MAO (200:1 loading); TIBA co-catalyst; 70 °C; 2 bar ethylene; 10 mg catalyst; 50 ml hexane; 30 minutes.

Figure 5.12 highlights a striking trend of increasing activity with decreasing quantities of catalyst added to the reaction. The change from 10 mg to 2.5 mg represents a change in the moles of zirconium in the polymerisation run from 0.7 to 0.18 μmol and reduces the corresponding value of [Zr] to as low as 3.5 μM. The trend seems to be essentially linear, the activity increasing from 4,537 $kg_{PE}/mol_{Zr}/h/bar$ at 10 mg to 8,281 $kg_{PE}/mol_{Zr}/h/bar$ at 2.5 mg – an increase of almost 100%. This is consistent with reports in the literature where the results can be as great as halving the concentration doubling the activity.[30] This suggests that concentration of monomer or reactor capacity may well be the limiting factor. Although no data are provided here, this increase in activity is typically accompanied by an increase in M_w.

A comparison was also made between different catalyst loadings on the surface of the support. Catalysts bearing a 200:1 and 300:1 loadings were successfully synthesised but it was not possible, even heating to 80 °C to immobilise enough complex to generate 100:1 and the prolonged heating significantly affected the activity. The lower loading increased the catalytic activity at 70 °C by approximately 50%: 4537 (200:1) and 6680 $kg_{PE}/mol_{Zr}/h/bar$ (300:1).

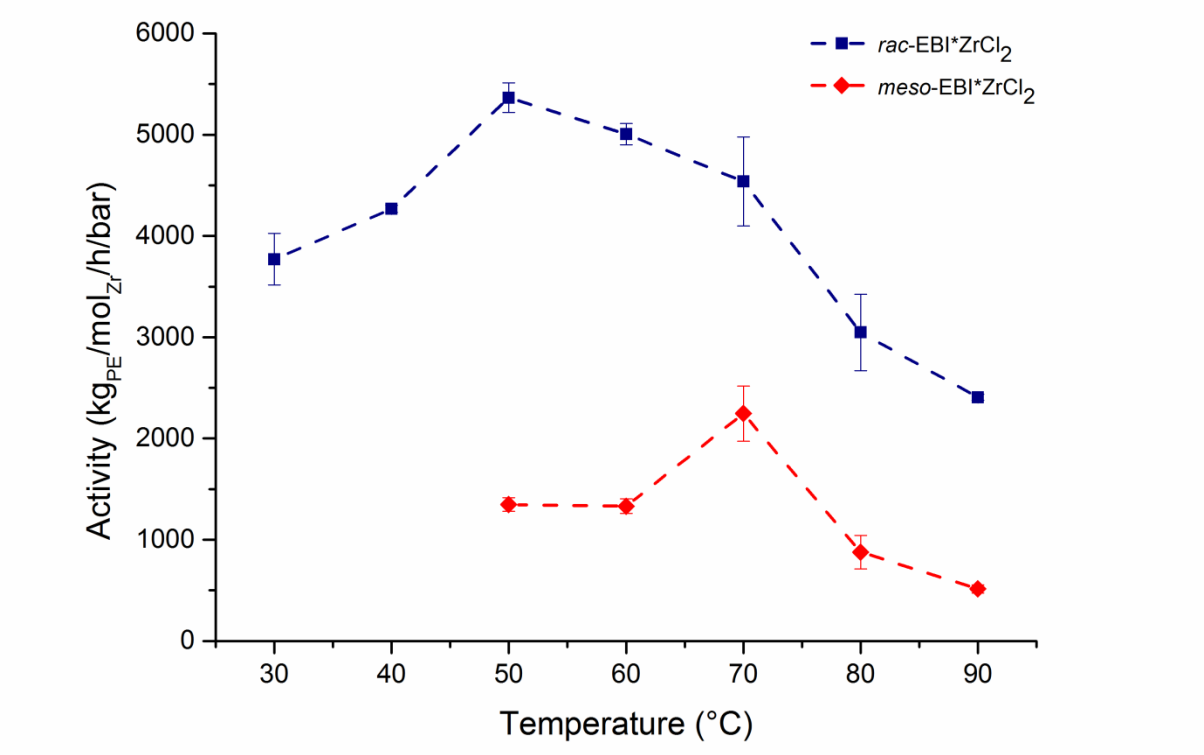


Figure 5.13: a graph showing the ethylene polymerisation activity dependence of *rac*-EBI*$ZrCl_2$ and *meso*-EBI*$ZrCl_2$ on temperature. Supported on Solid MAO (200:1 *rac*-EBI*$ZrCl_2$, 300:1 *meso*-EBI*$ZrCl_2$); TIBA co-catalyst; 2 bar ethylene; 10 mg catalyst; 50 ml hexane; 1 hour (*rac*-EBI*$ZrCl_2$), 30 minutes (*meso*-EBI*$ZrCl_2$).

Figure 5.13 re-emphasises the reported data from Ransom *et al*. that *rac*-EBI*$ZrCl_2$ outperforms *meso*-EBI*$ZrCl_2$.[24] In solution ethylene polymerisation runs, the *meso*-form trailed the *rac*-isomer in activity by a factor of 1.6 (38,300 to 61,800 $kg_{PE}/mol_{Zr}/h/bar$ at 80 °C). This discrepancy is exaggerated in the catalysts supported on Solid MAO where the differential is 3.5 at 80 °C and 4 at 50 °C. The desirability of *rac*-stereoisomers over their *meso*- counterparts is well documented in the literature;[37,38] this derives not only from the predisposition of the C_2 symmetric catalyst to form isotactic polypropylene (PP) but also from the increased rates of olefin polymerisation observed.[39] It is perhaps interesting to note that while *meso*-EBI*$ZrCl_2$ shows an optimum activity at 70 °C (2,246 $kg_{PE}/mol_{Zr}/h/bar$), *rac*-EBI*$ZrCl_2$ peaks at only 50 °C (5,365 $kg_{PE}/mol_{Zr}/h/bar$).

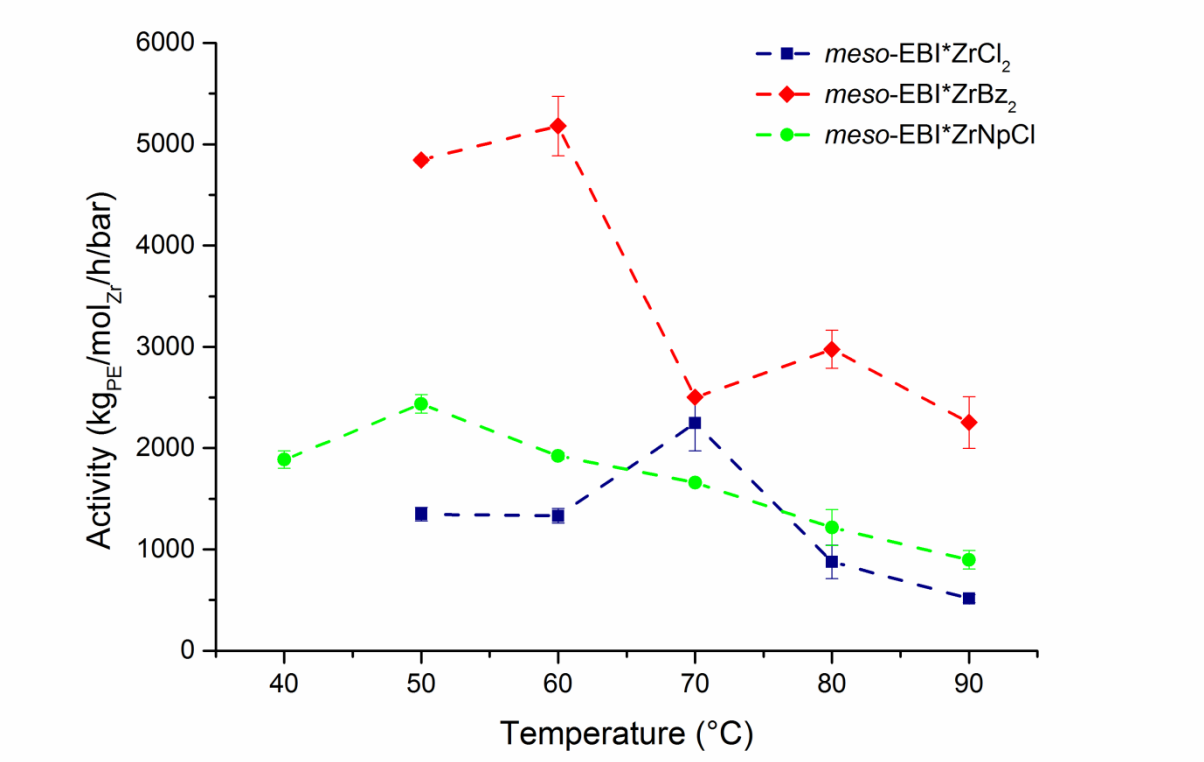


Figure 5.14: a graph showing the ethylene polymerisation activity dependence of *meso*-EBI*$ZrCl_2$, ***meso*-3.3** and ***meso*-3.4** on temperature, supported on Solid MAO (300:1). TIBA co-catalyst; 2 bar ethylene; 10 mg catalyst; 50 ml hexane; 30 minutes.

Given the large disparity in ethylene polymerisation activities between the *rac*- and *meso*-forms, illustrated by Figure 5.13, it was hoped that changing the chloride ligands for alkyl groups may dramatically increase the activities reported. A significant increase was reported for ***rac*-3.7** over ***rac*-3.5** in solution (section 5.2). Both ***meso*-3.3** and ***meso*-3.4** show optimum activities higher than the 2,246 $kg_{PE}/mol_{Zr}/h/bar$ for *meso*-EBI*$ZrCl_2$ (5,179 and 2,436 $kg_{PE}/mol_{Zr}/h/bar$ respectively). While the neopentyl chloride only marginally outperforms the dichloride congener, and at a lower, less commercially suitable temperature, the peak performance of the benzyl is more than twice that of the others. At 60 °C, the activity values for both *rac*-EBI*$ZrCl_2$ (Figure 5.13) and ***meso*-3.3** are in agreement, within error, and both represent some of the highest values for supported ethylene polymerisation catalysts in the literature. Figure 5.15 illustrates the molecular weight data for ***meso*-3.3** and ***meso*-3.4**. In both cases unusual trends are observed.

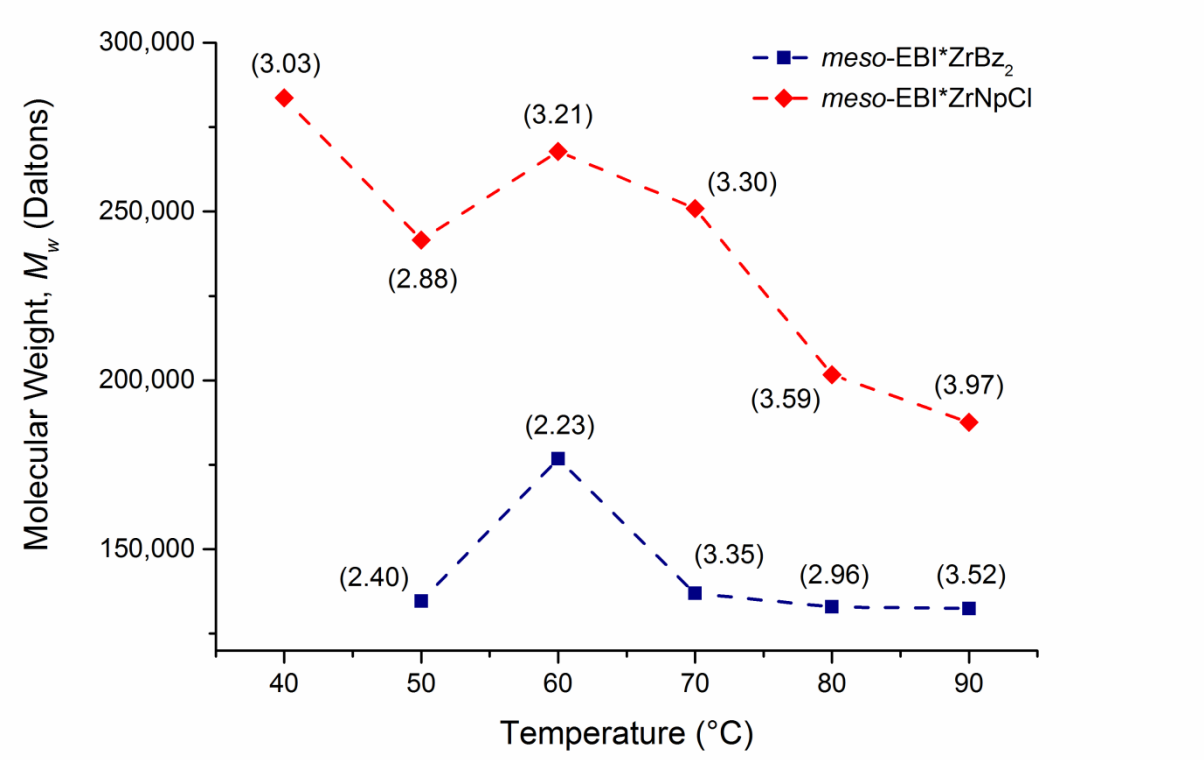


Figure 5.15: a graph showing the dependence of M_W, for ***meso*-3.3** and ***meso*-3.4** on temperature. PDIs are given in parentheses. Supported on Solid MAO (300:1 loading); TIBA co-catalyst; 2 bar ethylene; 10 mg catalyst; 50 ml hexane; 30 minutes.

A comparison of the molecular weight data for the two complexes highlights two significant points. Firstly that the molecular weight of the PE produced by ***meso*-3.4** is higher at all temperatures (minimum 187,530 daltons; 90 °C) than the PE of ***meso*-3.3** (maximum 176,708 daltons; 60 °C). Secondly, it is clear that both plots show an uncharacteristic value: 50 °C for ***meso*-3.4**, 60 °C for ***meso*-3.3**. This disrupts the, otherwise smooth, negative trend in M_w with increasing temperature for ***meso*-3.4**, interpreted as being caused by increasing chain transfer processes occurring.[28] On the other hand, the M_w of the PE synthesised by ***meso*-3.3** remains almost constant at just above 130,000 daltons.

As with the solution-phase ethylene polymerisation runs reported in section 5.2, the use of EBI* complexes as immobilised single-site catalysts has generated activities comparable with the most active in the literature. Judicious substitution of the chloride ligands for alkyls such as benzyl and neopentyl, alters the properties of the resulting PE and brings about a significant improvement in the activity of the, otherwise underperforming, *meso*-isomer.

5.3.2 SBI* complexes

In addition to the EBI* complexes immobilised on solid supports in the preceding section, ***rac*-3.1** was also selected as a precatalyst to support, not least due to its excellent activity in

solution. Numerous reports in the literature indicated that a dimethylsilyl bridge can provide catalysts as effective as those containing an ethylene bridge under standardised conditions.[26]

Figure 5.16 compares the ethylene polymerisation activities of ***rac*-3.1** immobilised on two different solid supports, both activated with MAO: silica and layered double hydroxide (LDH). LDHs are inorganic layered clays and have been the subject of fewer publications than silica as catalyst supports. As described in Chapter Four, the LDH used as a support for ***rac*-3.1** is MgAl-SO_4. When the activities are compared to those reported for any of the EBI* complexes (*vide supra*), the activities reported in Figure 5.16 are notably lower. The LDH supported catalyst displays a higher activity (953 $kg_{PE}/mol_{Zr}/h/bar$ at 70 °C) than that achieved by its silica counterpart (759 $kg_{PE}/mol_{Zr}/h/bar$ at 80 °C). The trends identified are similar with an optimum seen in both cases and the activity diminishing on either heating or cooling.

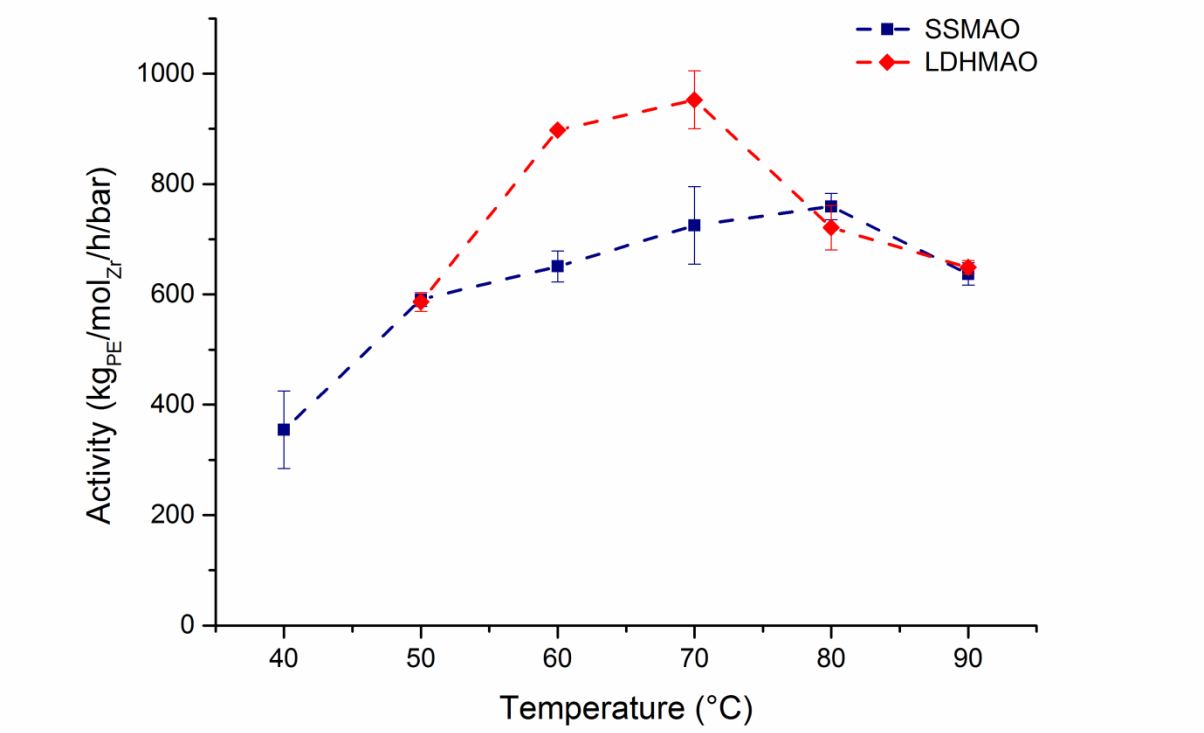


Figure 5.16: a graph showing the ethylene polymerisation activity dependence of ***rac*-3.1** on temperature, supported on SSMAO (200:1 loading) and LDHMAO (300:1 loading). TIBA co-catalyst; 2 bar ethylene; 10 mg catalyst; 50 ml hexane; 30 minutes.

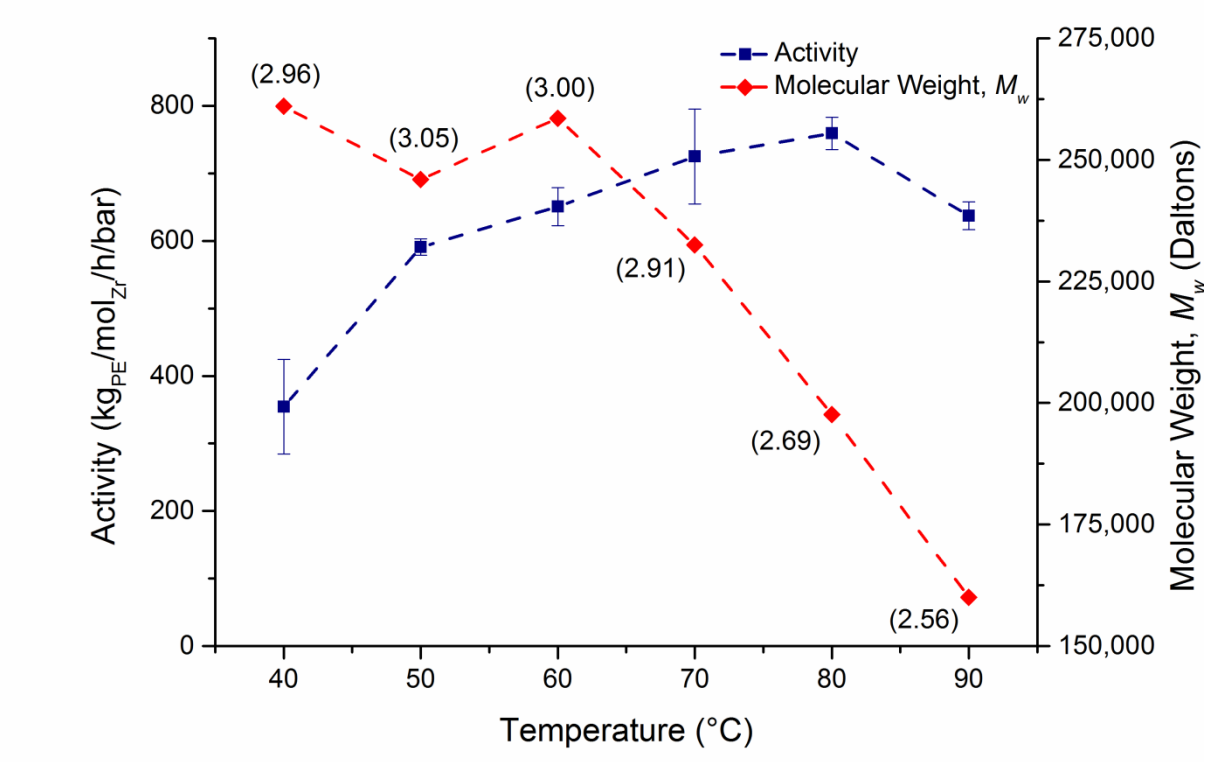


Figure 5.17: a graph showing the dependence of activity and M_w for ***rac*-3.1** on temperature. PDIs are given in parentheses. Supported on SSMAO (200:1 loading); TIBA co-catalyst; 2 bar ethylene; 10 mg catalyst; 50 ml hexane; 30 minutes.

However, as highlighted by Figure 5.16, while the activities shown by ***rac*-3.1** on SSMAO and LDHMAO are lower than for *rac*-EBI*$ZrCl_2$, the molecular weights on SSMAO are higher (258,536 and 202,746 daltons; 60 °C). The molecular weight trend for ***rac*-3.1** on SSMAO sees a decline in molecular weight with increasing temperature (Figure 5.17). This is coupled with a decrease in PDI, which has previously been attributed to the better solubilisation of the PE chains at higher temperatures leading to greater homogeneity in sites and, hence, a smaller MWD.[28]

As with *rac*-EBI*$ZrCl_2$, ***rac*-3.1** on SSMAO was tested to see the effect of increasing the residence time on the activity and M_w (Figure 5.18). The activity trends in both cases are very similar, with the rate decreasing on increased length of run. However, the relative decrease in activity is not as severe for ***rac*-3.1**: a reduction of 1.4× as opposed to 2.1×. The value of M_w drops off at two hours which is not seen for *rac*-EBI*$ZrCl_2$ on SSMAO.

A comparison of two different loadings of ***rac*-3.1** on SSMAO led to the observation of the opposite trend seen for *rac*-EBI*$ZrCl_2$. The activities obtained were lower on decreased loading at 70 °C: 725 and 611 $kg_{PE}/mol_{Zr}/h/bar$ (200:1 and 300:1 respectively).

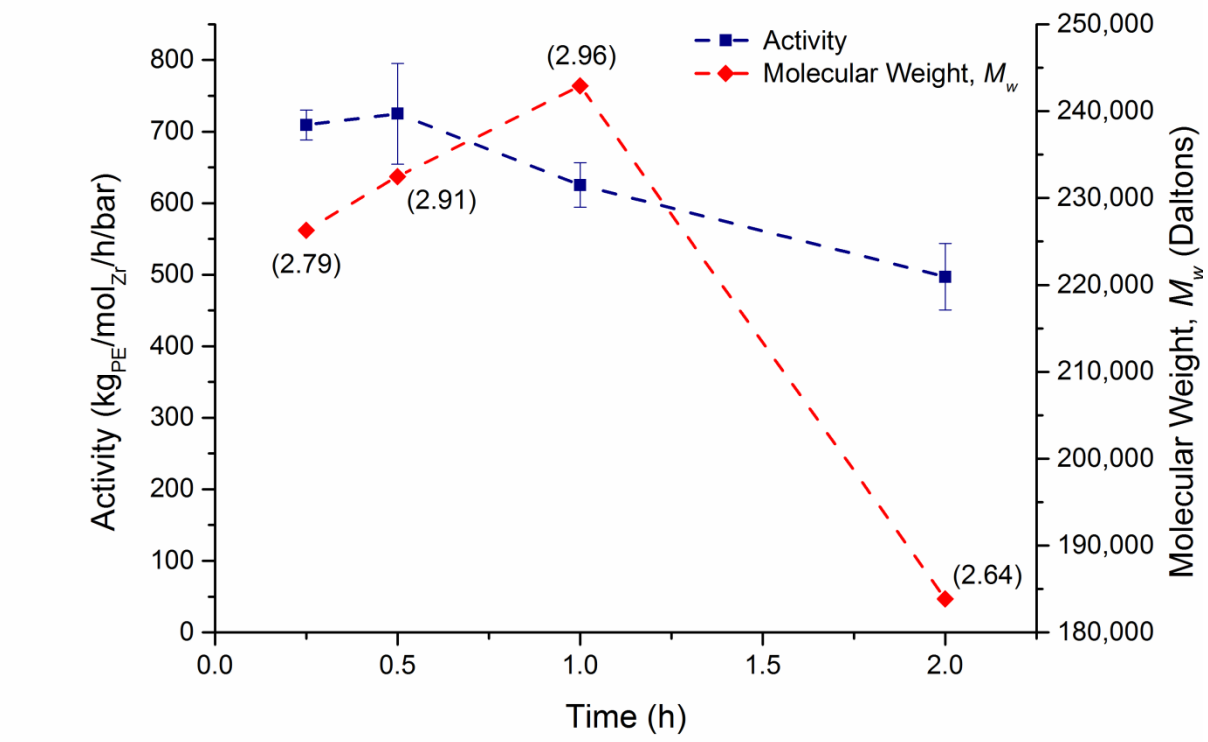


Figure 5.18: a graph showing the dependence of activity and M_w for ***rac*-3.1** on length of run. PDIs are given in parentheses. Supported on SSMAO (200:1 loading); TIBA co-catalyst; 70 °C; 2 bar ethylene; 10 mg catalyst; 50 ml hexane.

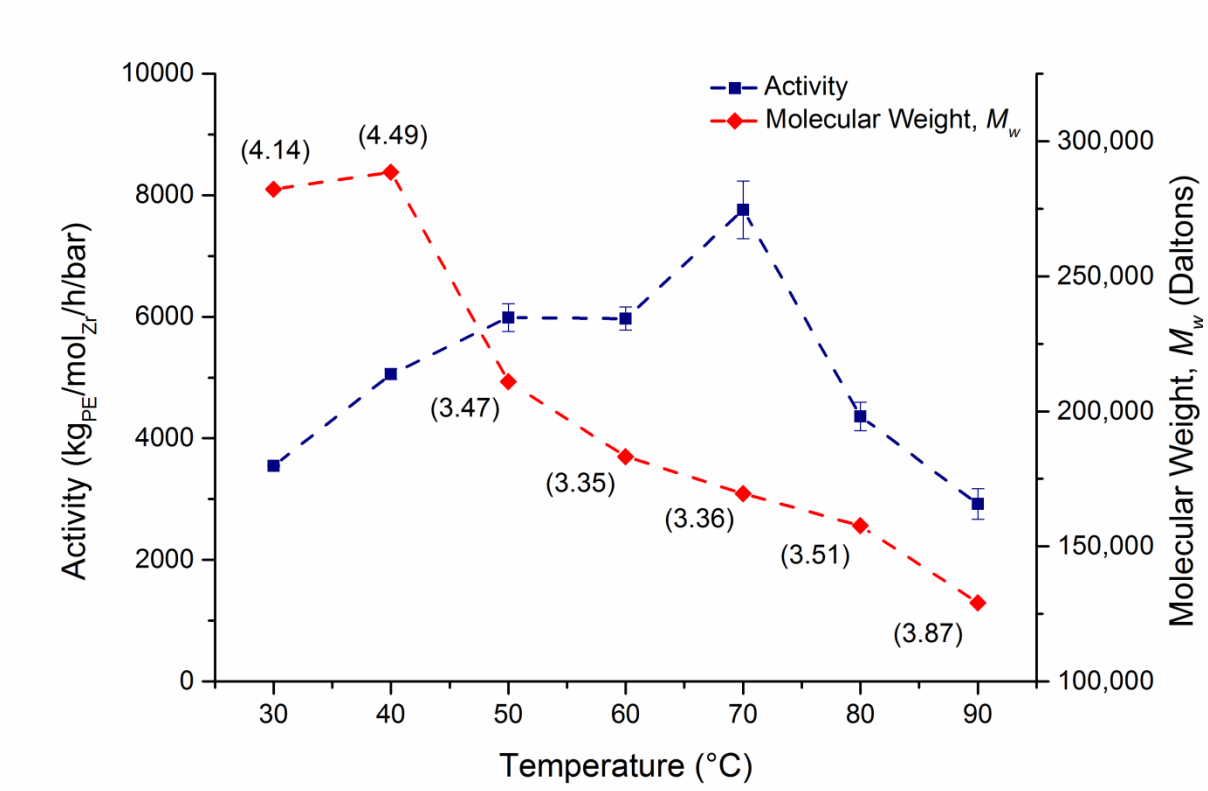


Figure 5.19: a graph showing the dependence of activity and M_w, for ***rac*-3.1** on temperature. PDIs are given in parentheses. Supported on Solid MAO (300:1 loading); TIBA co-catalyst; 2 bar ethylene; 10 mg catalyst; 50 ml hexane; 30 minutes.

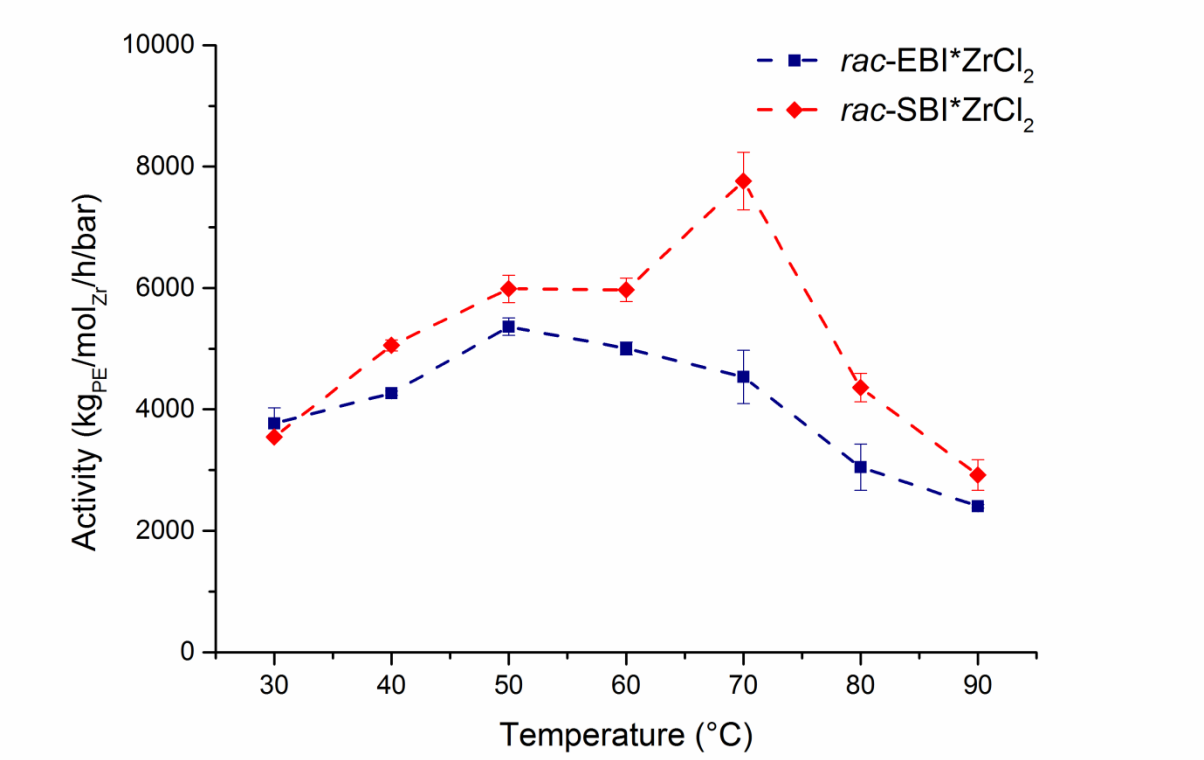


Figure 5.20: a graph showing the ethylene polymerisation activity dependence of *rac*-EBI*$ZrCl_2$ and ***rac*-3.1** on temperature. Supported on Solid MAO (200:1 *rac*-EBI*$ZrCl_2$, 300:1 *meso*-EBI*$ZrCl_2$); TIBA co-catalyst; 2 bar ethylene; 10 mg catalyst; 50 ml hexane; 30 minutes.

Figures 5.19 and 5.20 focus on ***rac*-3.1** immobilised on Solid MAO – Figure 5.19 displaying both activity and molecular weight data with Figure 5.20 offering a comparison of the activity with *rac*-EBI*$ZrCl_2$. Clearly the activity of ***rac*-3.1** on Solid MAO is very high, bordering on exceptional in comparison with literature, and peaking at 70 °C (7,760 $kg_{PE}/mol_{Zr}/h/bar$). As outlined above, the best values reported hitherto are Cp_2ZrCl_2, EBTHIZrCl_2, and Cp'_2ZrCl_2 which show activities of 5,400, 4,320, and 9,180 $kg_{PE}/mol_{Zr}/h/bar$ (all at 60 °C) respectively;[36] all of these bar the dimethylzirconocene dichloride are improved upon by ***rac*-3.1**. In addition, the high activities reported are remarkably temperature stable, maintaining ethylene polymerisation activities in excess of 6,000 $kg_{PE}/mol_{Zr}/h/bar$, and outperforming *rac*-EBI*$ZrCl_2$ on Solid MAO, from 50 to 70 °C. At either end of the temperature spectrum measured, the activity is seen to dip but still remains as one of the highest activity supported catalysts known in the academic literature.

M_w is also high and a value of 288,557 daltons is recorded at 40 °C. This decreases rapidly on heating, falling below 150,000 daltons by 90 °C. The PDIs narrow in the middle of the temperature range as previously described.[28]

The synergy of complex and support is clearly demonstrated here as the activities reported for ***rac*-3.1** on SSMAO and LDHMAO clearly trail those for *rac*-EBI*$ZrCl_2$.[40] However, on changing the immobilisation surface to Solid MAO, ***rac*-3.1** experiences a much more marked improvement than *rac*-EBI*$ZrCl_2$. There is a ten-fold increase in performance from SSMAO to Solid MAO for ***rac*-3.1** compared to just 2.5 times for *rac*-EBI*$ZrCl_2$. While this increase is remarkable, the drop from the reported value of 22,622 $kg_{PE}/mol_{Zr}/h/bar$ in solution is also very significant. In contrast to the large variation observed across different media for ***rac*-3.1**, the molecular weight and PDI are comparatively constant (Figure 5.21). The excellent activity of Solid MAO is not matched by its molecular weight data, reporting the broadest distribution and lowest M_w at 70 °C (3.36 and 169,554 daltons respectively). The well-ordered layered structure of LDHMAO gives rise to high molecular weight polymer and a narrow PDI (297,583 daltons and 2.74) at the cost of activity. The values for the solution polymerisation and the SSMAO immobilised run are intermediate.

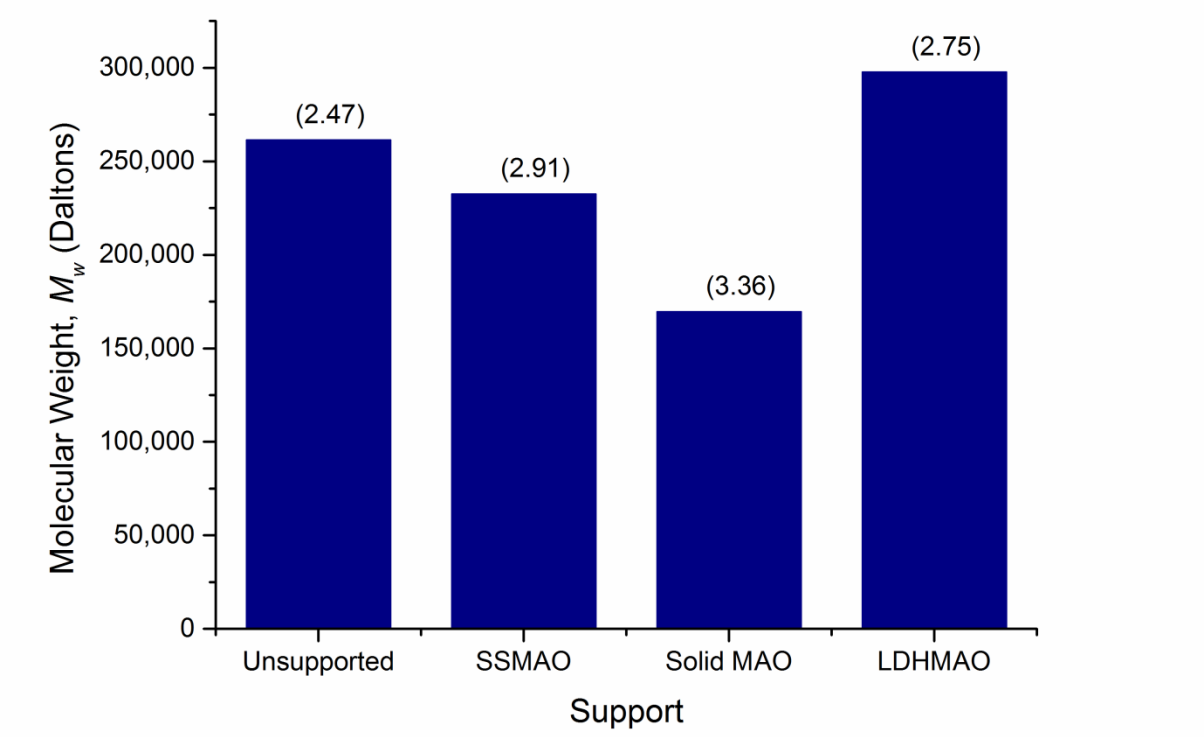


Figure 5.21: a graph showing the variation in molecular weight, M_w, of the polyethylene produced by ***rac*-3.1** in solution and on three different supports. PDIs are given in parentheses. 70 °C; 2 bar ethylene; 0.2 mg catalyst (solution), 10 mg catalyst (slurry); 50 ml hexane; timed until cessation of stirring or 30 minutes, where possible.

In terms of peak activity, and sustained activity across a range of temperatures, ***rac*-3.1** outperforms its ethylene-bridged analogue. While not exceptional in terms of PE properties, the PDI displayed compares well with others in the literature.[36]

5.3.3 Ind$^{\#}$ complexes

In solution polymerisations, the unbridged complexes based on the "Ind$_2^{\#}$" motif, yielded disappointing activities relative to those based on SBI*. It was decided only to test the unbridged complexes on Solid MAO, since their activities were so much lower and it had been shown to give consistently more active catalysts than SSMAO or LDHMAO.

Figure 5.22 compares the activities of the dichloride compounds as pure *rac*-, pure *meso*- and a 50:50 mix of the two. Most surprisingly of all the isomeric mixture of Ind$_2^{\#}$ZrCl$_2$ gave rise to higher activities than either of the single isomers on their own (1,152 kg$_{PE}$/mol$_{Zr}$/h/bar at 70 °C). It is difficult to be sure of what causes this phenomenon, but it is suspected that some cooperative effect between the two catalytic sites must be at work with a chain-shuttling process in operation. The peak activity for ***rac*-3.5**, 870 kg$_{PE}$/mol$_{Zr}$/h/bar at 60 °C, is double the 433 kg$_{PE}$/mol$_{Zr}$/h/bar (50 °C) reported in solution as well as being faster than the *meso*-isomer. This is a rare, if not unprecendented, instance of supported metallocene polymerisation improving upon its homogeneous counterpart.[41] The same is true for ***meso*-3.5** which registers 442 kg$_{PE}$/mol$_{Zr}$/h/bar ahead of the 335 kg$_{PE}$/mol$_{Zr}$/h/bar (both 70 °C) in solution. In the case of both isomers, the temperature dependence remains the same on immobilisation.

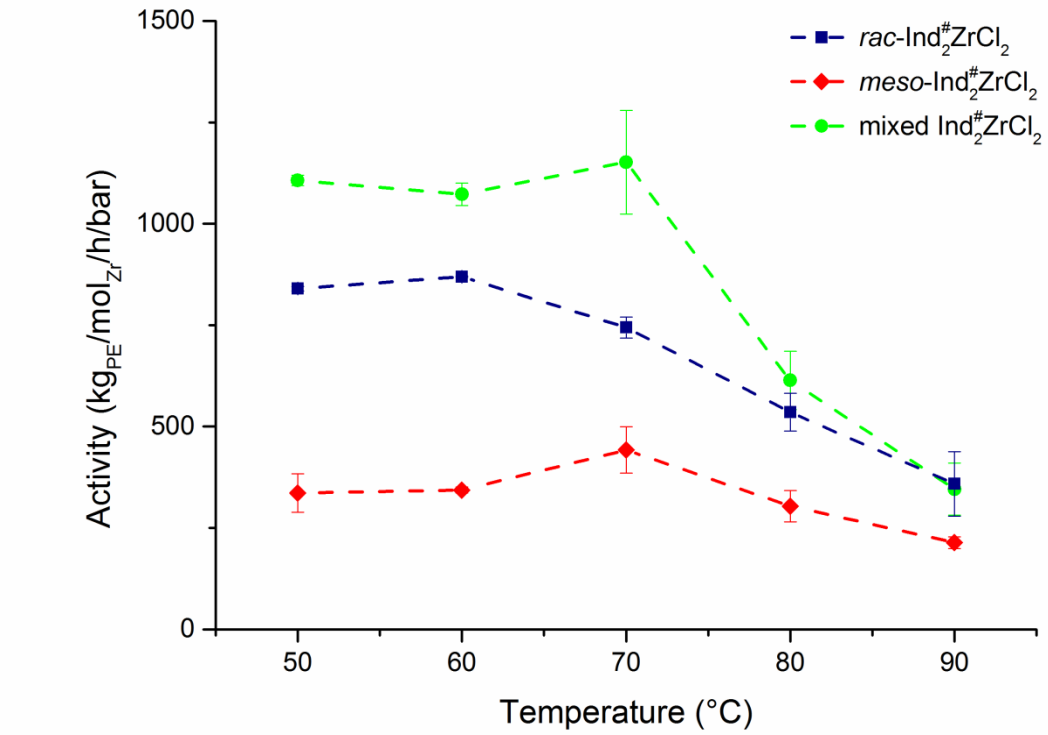


Figure 5.22: a graph showing the ethylene polymerisation activity dependence of *rac*-, *meso*- and mixed-Ind$_2^{\#}$ZrCl$_2$ on temperature. Supported on Solid MAO (300:1); TIBA co-catalyst; 2 bar ethylene; 10 mg catalyst; 50 ml hexane; 30 minutes.

The GPC trace for the mixed isomers of **3.5** (Figure 5.23) shows that the PE molecular weight distribution is bimodal with an M_w of 322,680 daltons and a PDI of 19.57. These figures are totally different from that of either single isomer – *rac*: 164,667 daltons, 4.17; *meso*: 157,161 daltons, 4.29. These are much narrower MWDs with a lower M_w in each case. To the author's knowledge, no precedence exists in the literature for an M_w for a dual-catalyst system which is higher than that of either component. Typical chain-shuttling processes narrow the MWD at an intermediate value between the two individual systems.[42,43] As only TIBA is present in the reaction to act as a chain transfer agent (CTA), a system as efficient as the $ZnEt_2$ catalysed chain growth reactions is not anticipated. TIBA is reported to be a poorer chain transfer agent than linear aluminium alkyls.[44] Similarly, no tendency is noted in the MWD towards a Poisson distribution.[45]

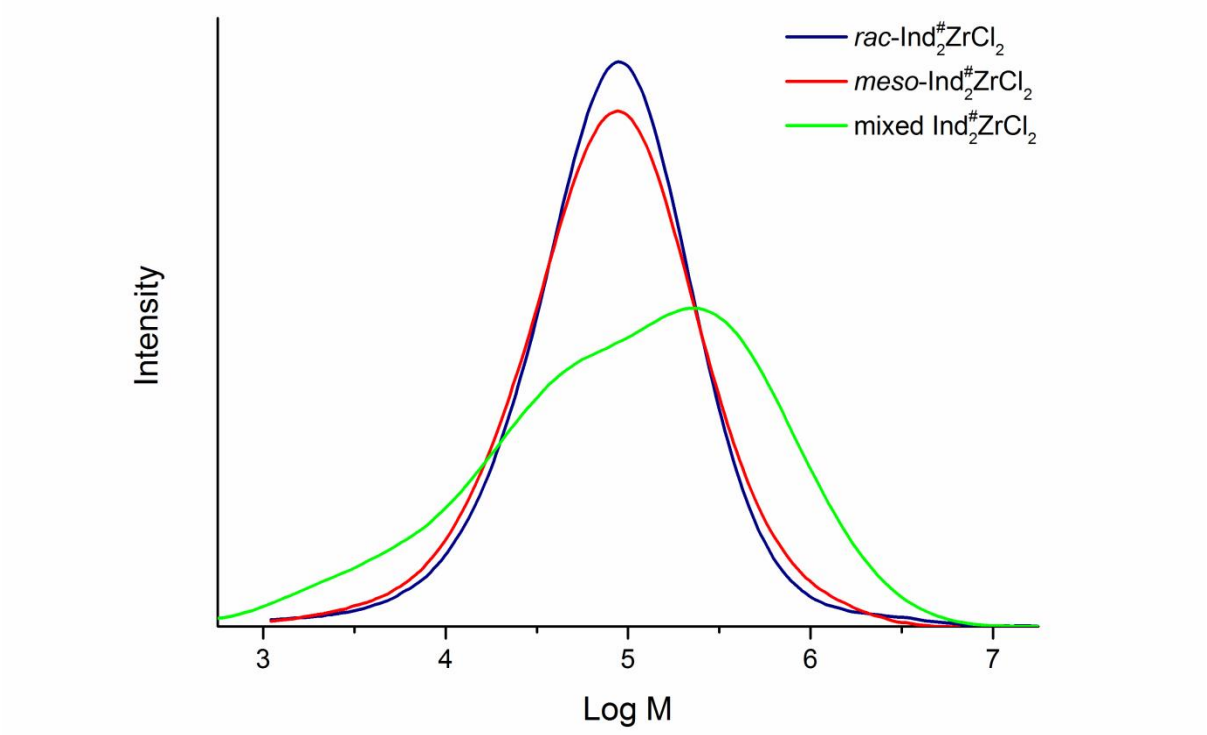


Figure 5.23: GPC traces for ***rac*-3.5**, ***meso*-3.5** and a 50:50 mixture of isomers of **3.5**. Supported on Solid MAO (300:1); 70 °C; TIBA co-catalyst; 2 bar ethylene; 10 mg catalyst; 50 ml hexane; 30 minutes.

As with the isomers of $Ind^{\#}_2ZrCl_2$ above, ***rac*-3.7** is shown to be more active on Solid MAO than in solution (Figure 5.24), and it too retains the trend in temperature dependence, showing an activity peak at 50 °C (1,538 $kg_{PE}/mol_{Zr}/h/bar$). This outperforms both dichloride isomers and the 50:50 mixture. The activity of ***rac*-3.7** tails off strongly above 50 °C and from 70 to 90 °C agrees with that reported for ***rac*-3.5** within error. The molecular weight reported for ***rac*-3.7**, 300,877 daltons at 70 °C, is almost double that reported for the

dichloride congener of either single isomer. It also shows PDI of 3.95, indicative of a single site catalyst.

A comparison of the Solid MAO supported complexes bearing the Ind$^{\#}$ ligand, show remarkable similarities with the results obtained from solution-phase polymerisation runs. the activities remain poor compared to their bridged counterparts and the temperature dependences observed are the same. Nonetheless, the activity reported for ***rac*-3.7** falls into the definition of a very active catalyst according to Britovsek *et al*.[2]

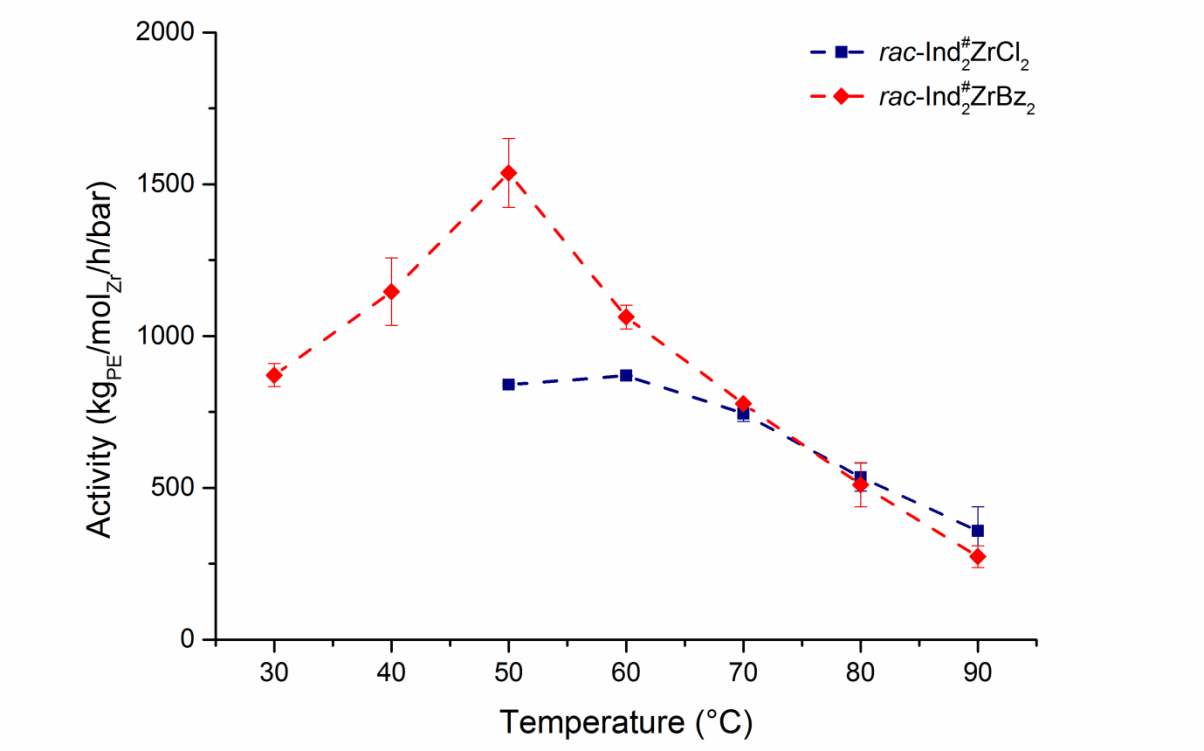


Figure 5.24: a graph showing the ethylene polymerisation activity dependence of ***rac*-3.5** and ***rac*-3.7** on temperature. Supported on Solid MAO (300:1); TIBA co-catalyst; 2 bar ethylene; 10 mg catalyst; 50 ml hexane; 30 minutes.

5.3.4 Ind$^{\#}$SiMe$_2$^{n}BuZrCl$_3$

An excellent precedent has been set in the literature for the use of complexes with an *n*-butyl chain attached as supported ethylene polymerisation catalysts.[36,41] Cp$_2^{n\text{Bu}}$ZrCl$_2$ is the complex most usually employed, but following the fortuitous synthesis of **3.8**, it was anticipated that it might be active. However, zirconium half-sandwich complexes are not typically renowned for their use as ethylene polymerisation catalysts (although CpZrCl$_3$ was reported as being active).[46]

3.8 on Solid MAO was found to be an ethylene polymerisation catalyst and the activity data are given in Figure 5.25. The optimum activity (811 kg$_{PE}$/mol$_{Zr}$/h/bar) is found at 70 °C

and is seen to decrease quite rapidly with a change of temperature in either direction. This activity compares well with that reported for ***rac*-3.5** (870 $kg_{PE}/mol_{Zr}/h/bar$ at 60 °C). The molecular weight is significantly higher than any of the complexes so far reported in this chapter (568,389 daltons at 70 °C) but at the cost of a high PDI value (32.03). As with the mixed isomers of $Ind^{\#}_2ZrCl_2$, the MWD was clearly bimodal (Figure 5.26), explaining the high value PDI.

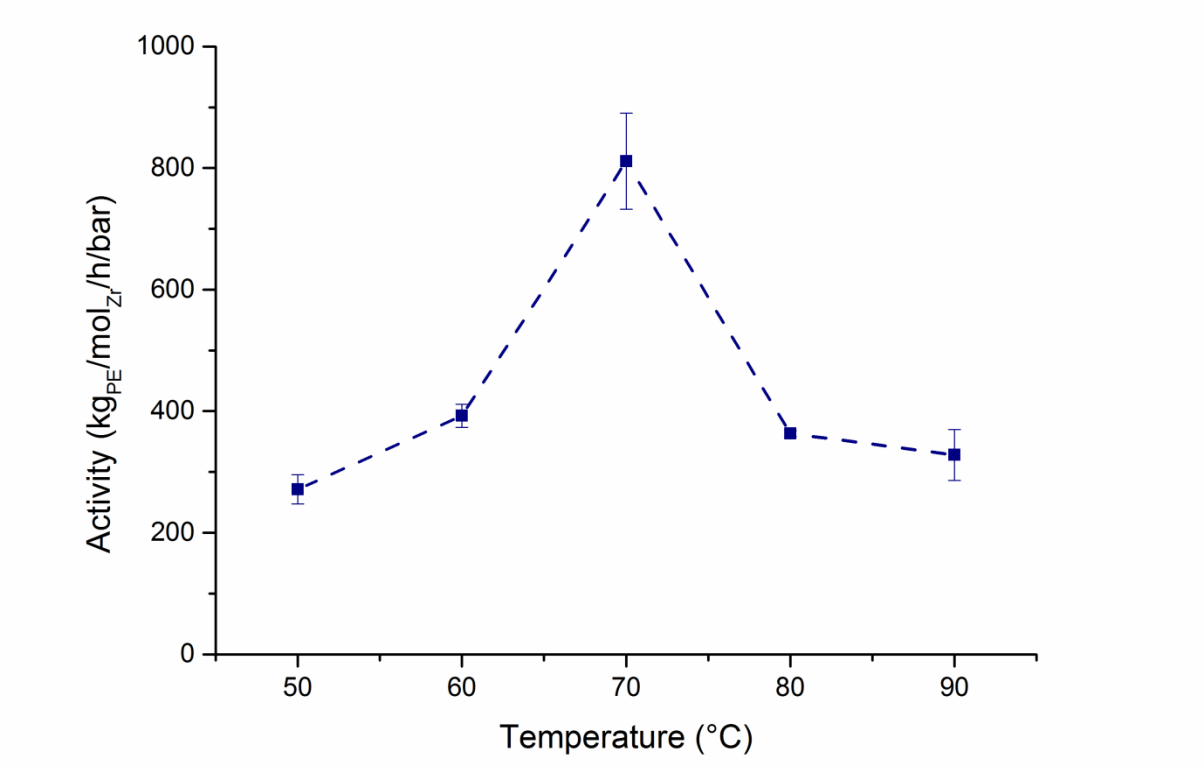


Figure 5.25: a graph showing the ethylene polymerisation activity dependence of **3.8** on temperature. Supported on Solid MAO (300:1); TIBA co-catalyst; 2 bar ethylene; 10 mg catalyst; 50 ml hexane; 30 minutes.

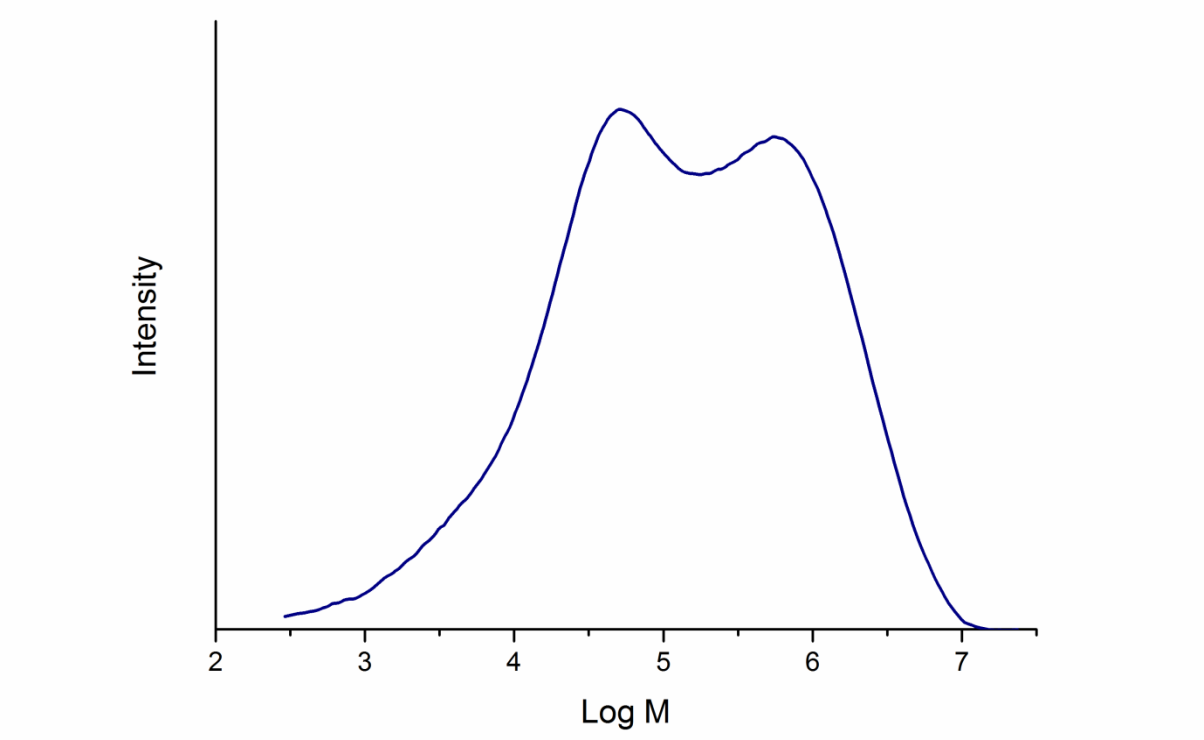
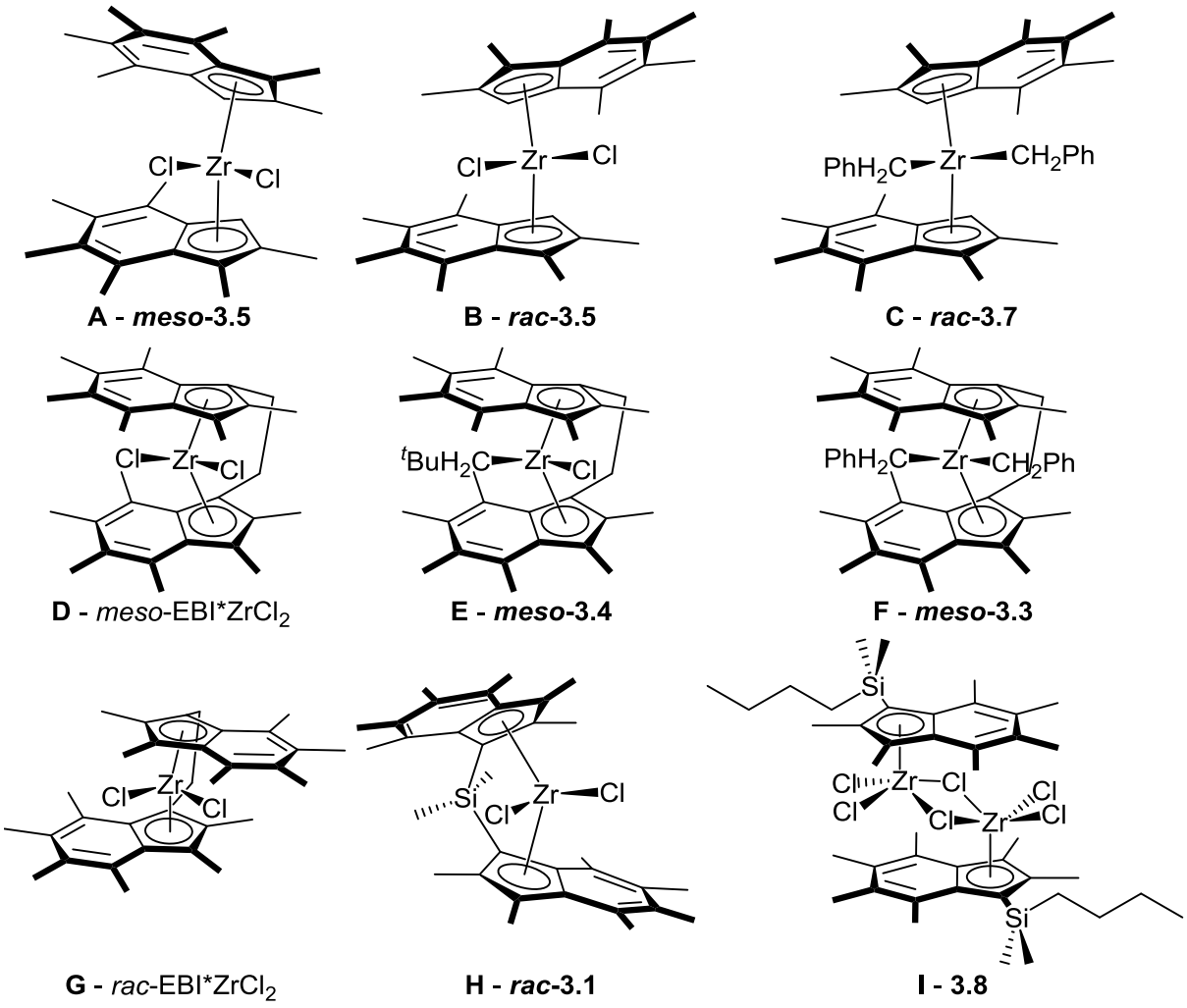


Figure 5.26: GPC trace for **3.8**. Supported on Solid MAO (300:1); 70 °C; TIBA co-catalyst; 2 bar ethylene; 10 mg catalyst; 50 ml hexane; 30 minutes.

5.3.5 Summary

Figures 5.27 and 5.28 give a broad overview of the complexes used in this chapter and their comparative activities and MWDs when supported on Solid MAO at two different temperatures: 50 and 70 °C. Perhaps the most striking point is the large difference in activities despite the structural similarities between the complexes (**3.8** excepted). The most active (***rac*-3.1**, 70 °C) is 23 times faster than the least active (***meso*-3.5**, 50 °C).



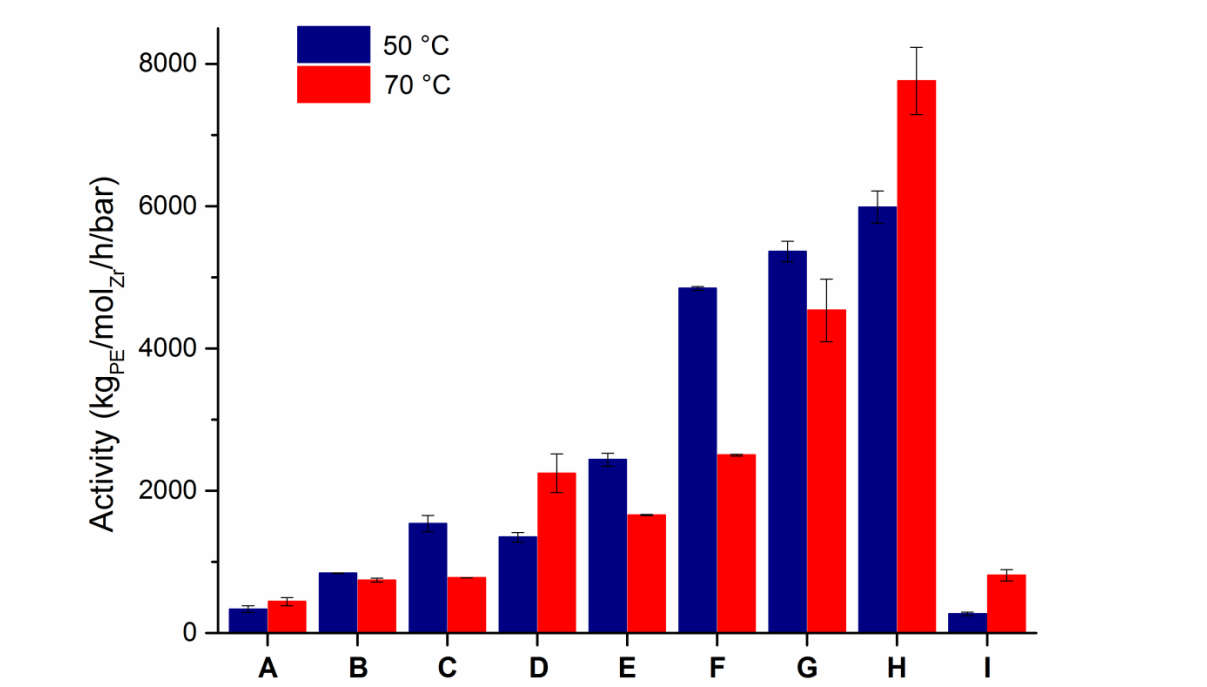


Figure 5.27: ethylene polymerisation activity for complexes **A** to **I** (complexes used for polymerisation in this chapter) at 50 and 70 °C. Supported on Solid MAO (300:1 except **G**, 200:1), TIBA co-catalyst; 2 bar ethylene; 10 mg catalyst; 50 ml hexane; 30 minutes (except **G**, 1 hour).

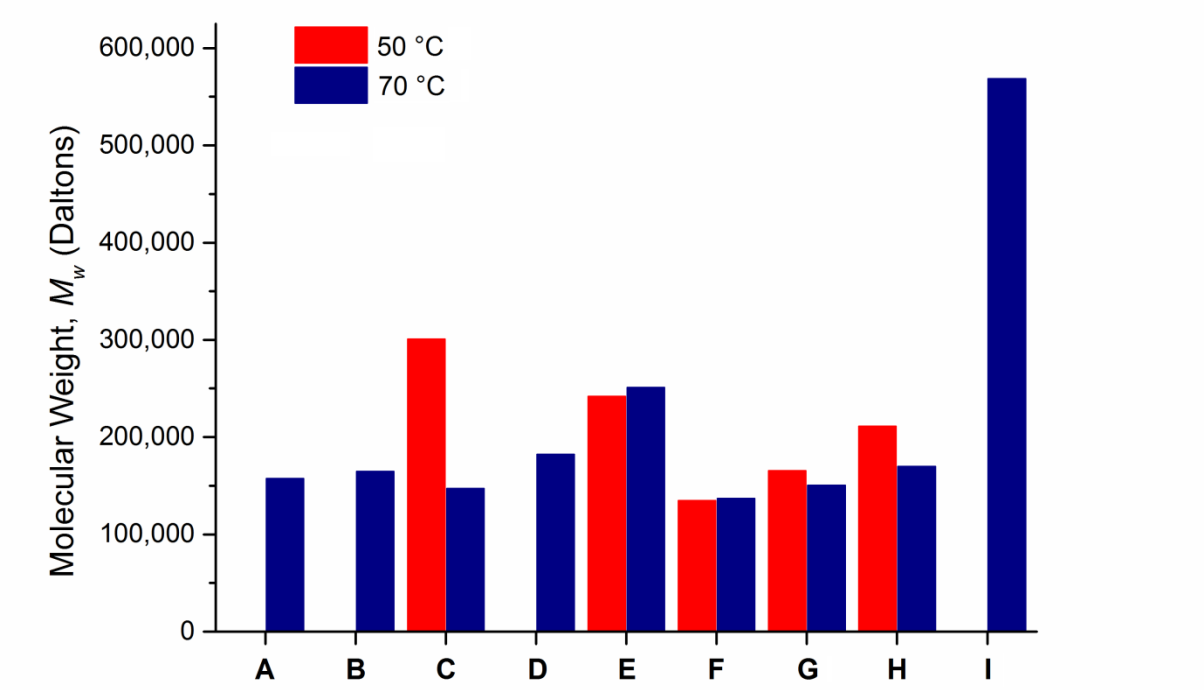


Figure 5.28: molecular weight data for complexes **A** to **I** at 50 and 70 °C (not all samples were analysed by GPC). Supported on Solid MAO (300:1 except **G**, 200:1), TIBA co-catalyst; 2 bar ethylene; 10 mg catalyst; 50 ml hexane; 30 minutes (except **G**, 1 hour).

Another point of interest is that four (of the nine) complexes are faster at 70 °C, while the other five are more active at 50 °C, showing no obvious trend. Similarly, in five of the examples shown, the activity differential between the two temperatures is less than 30% while in the other four it is significantly greater than this, reaching almost double for ***meso*-3.3** and more than that for the half-sandwich, **3.8**.

The molecular weight data are incomplete due to the long lead time on GPC analysis but appear more similar than the activities (Figure 5.27). The majority of the molecular weights shown on the graph fall in the range 150,000 to 200,000 daltons. ***meso*-3.4** improves on this, with values for M_w of approximately 250,000 daltons at both temperatures. **3.8**, presumably due to its anomalous structure, shows an outlier value of over 500,000 daltons.

5.4 High-throughput screening

Following on from the numerous polymerisation runs carried out in the laboratory in Oxford, three catalysts supported on Solid MAO were selected for a high-throughput screening process to analyse a variety of conditions. The complexes selected were *rac*- and *meso*-EBI*$ZrCl_2$ and ***rac*-3.1**. The catalysts were supported in the Chemistry Research Laboratory, Oxford, and the screening was run in the laboratory of Prof. Vicenzo Busico at the Universita degli Studi di Napoli Federico II.

Before any catalytic measurements were taken in the presence of ethylene, the catalysts were tested for their zirconium abundance. A value of 0.43 wt% was expected in each case and the values recorded were in approximate agreement: 0.38(2), 0.35(3) and 0.41(2)% for *rac*- and *meso*-EBI*$ZrCl_2$, and ***rac*-3.1** respectively.

Table 5.1: selected parameters for the homo-polymerisation of ethylene using Solid MAO supported catalysts during the high-throughput screening

Catalyst	70 °C			80 °C		
	Activity	M_w	PDI	Activity	M_w	PDI
rac-EBI*$ZrCl_2$	13,000	199,000	2.3	15,000	194,000	2.7
meso-EBI*$ZrCl_2$	1,100	242,000	2.7	1,500	210,000	2.7
***rac*-3.1**	22,000	273,000	3.1	19,000	367,000	3.3

Activity measured in $kg_{PE}/mol_{Zr}/h/bar$ (2 s.f.). M_w given in daltons. Polymerisation conditions: supported on Solid MAO (300:1); 800 seconds; 5 ml heptane; 10 μmol $AlEt_3$; 8.274 bar ethylene; 0.1-0.5 mg catalyst.

Table 5.1 summarises the data for the homo-polymerisation of ethylene; the activity data is limited to two significant figures. It is pertinent to note that the effect of changing the scavenger from TEA to TIBA had little impact on the polymerisation runs. It was also noted that all the catalysts tested here showed a significant decay in activity with time, and hence all activities were measured at 800 seconds, to give an idea of the initial rate. The activities reported for *rac*-EBI*$ZrCl_2$ and ***rac*-3.1** are considered high enough for hot-spot formation on catalyst particles to be an issue for consideration.

A comparison of the activities with those obtained in the laboratory shows that the values have increased significantly for the two *rac*- compounds but that *meso*-EBI*$ZrCl_2$ shows a slight decrease. In addition to the increase in activity of ***rac*-3.1** from the lab to the high-throughput trial (7,760 to 22,000 $kg_{PE}/mol_{Zr}/h/bar$; 70 °C), the molecular weight of the polymer increases significantly (169,554 to 273,000 daltons) as well. The *rac*-EBI*$ZrCl_2$ also experiences an activity surge from 4,357 to 13,000 $kg_{PE}/mol_{Zr}/h/bar$ at 70 °C. This increase in activity is attributed in part to the increase in pressure, which empiricism suggests does not have a linear impact on catalyst performance.

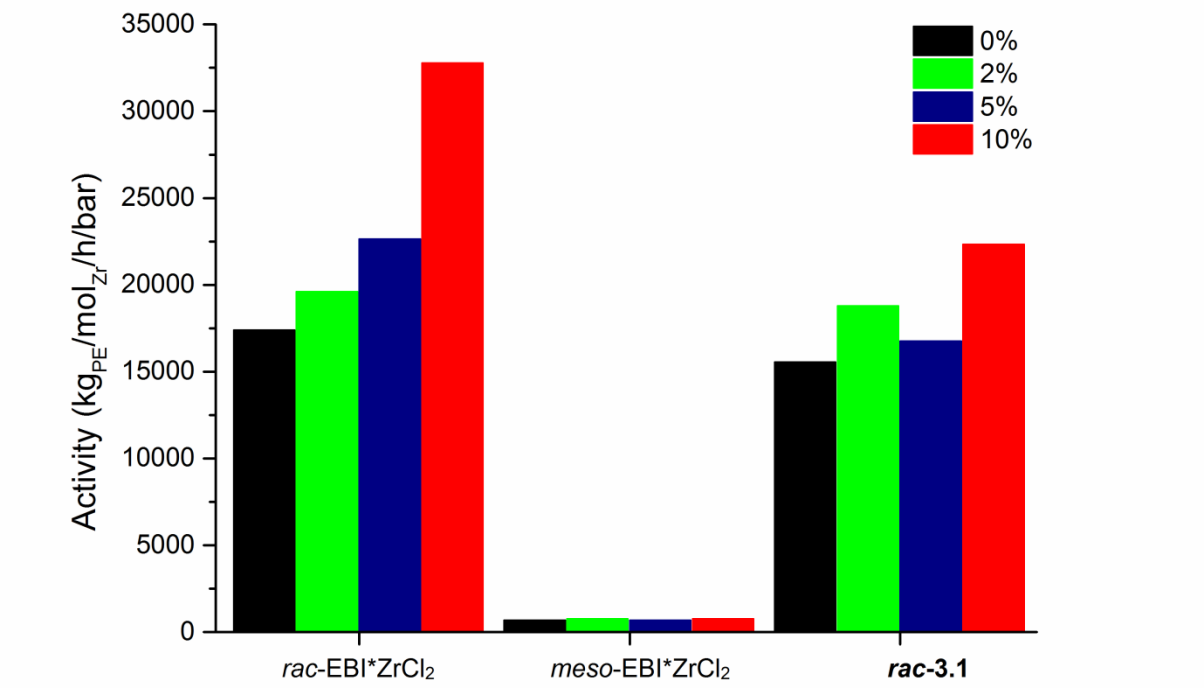


Figure 5.29: activity data for *rac*- and *meso*-EBI*$ZrCl_2$ and ***rac*-3.1** at different concentrations of 1-hexene (v/v). Supported on Solid MAO (300:1); 70 °C; 5 ml heptane; 15 µmol $AlEt_3$; 8.274 bar ethylene; 0.1-0.5 mg catalyst.

In addition to the homo-polymerisation of ethylene, co-polymerisation with 1-hexene was carried out to test the co-monomer incorporation with each catalyst (Figure 5.29). All three catalysts showed a clear "co-monomer effect", enhanced activity with respect to the homo-polymerisation up to 5% (v/v) loading of 1-hexene. While the activity of *meso*-EBI*$ZrCl_2$ remained poor in comparison, *rac*-EBI*$ZrCl_2$ showed an increase of 90% (to a peak of almost 33,000 $kg_{PE}/mol_{Zr}/h/bar$) on the addition of 10% 1-hexene by volume. ***rac*-3.1** did not demonstrate the same improvement in activity (40%) but on analysis of the ^{13}C NMR spectroscopy data for the resulting polymer the rate of 1-hexene incorporation was impressive (Table 5.2).

Table 5.2: 1-hexene incorporation (mol%) into the final polymer as determined by ^{13}C NMR spectroscopy at different concentrations of co-monomer.

Catalyst	5% (v/v) 1-hexene	10% (v/v) 1-hexene
	1-hexene incorporation (mol%)	1-hexene incorporation (mol%)
rac-EBI*$ZrCl_2$	0.2	0.4
meso-EBI*$ZrCl_2$	0.2	0.5
***rac*-3.1**	0.4	0.8

Polymerisation conditions: supported on Solid MAO (300:1); 70 °C; 5 ml heptane; 15 µmol $AlEt_3$; 8.274 bar ethylene; 0.1-0.5 mg catalyst.

While the two isomers of EBI*$ZrCl_2$ were only able to incorporate up to 0.5% of 1-hexene into the co-polymer, ***rac*-3.1** was able to incorporate effectively double the proportion of co-monomer: 0.4 and 0.8 mol% at 5 and 10% concentrations of 1-hexene respectively.

Table 5.3: M_w (daltons) and PDI data for the final polymer as determined by GPC at different concentrations of 1-hexene.

Catalyst	2% (v/v) 1-hexene		5% (v/v) 1-hexene		10% (v/v) 1-hexene	
	M_w	PDI	M_w	PDI	M_w	PDI
rac-EBI*$ZrCl_2$	231,000	2.9	227,000	2.5	228,000	2.6
meso-EBI*$ZrCl_2$	231,000	2.8	271,000	3.3	224,000	2.8
***rac*-3.1**	384,000	4.4	302,000	3.3	244,000	2.8

Polymerisation conditions: supported on Solid MAO (300:1); 70 °C; 5 ml heptane; 15 μmol $AlEt_3$; 8.274 bar ethylene; 0.1-0.5 mg catalyst.

As well as improved levels of 1-hexene incorporation, ***rac*-3.1** maintains the highest molecular weights on addition of co-monomer at all concentrations, although a steep decline is noted as the 1-hexene concentrations increases (Table 5.3). In contrast the value for M_w for *rac*-EBI*$ZrCl_2$ remains constant as more co-monomer is incorporated, and higher than the value recorded for the homopolymer at the same temperature (199,000 daltons). The polydispersities in all cases are low and indicative of single-site activity.

Further to the characterisation by ^{13}C NMR spectroscopy, the co-polymer was analysed by crystallisation elution fractionation (CEF). This corroborated the 1-hexene incorporation data as well as analysing the amorphous fractions (AF) and temperatures of melting (Table 5.4).

Table 5.4: temperature at maximum elution (°C) and amorphous fraction (%) data for the final polymer as determined by CEF at different concentrations of 1-hexene.

Catalyst	2% (v/v) 1-hexene		5% (v/v) 1-hexene		10% (v/v) 1-hexene	
	$T_{el.\ max.}$ (°C)	AF (%)	$T_{el.\ max.}$ (°C)	AF (%)	$T_{el.\ max.}$ (°C)	AF (%)
rac-EBI*$ZrCl_2$	111.5	-	111.0	-	110.1	0.1
meso-EBI*$ZrCl_2$	111.5	0.1	111.0	0.3	110.3	0.3
***rac*-3.1**	111.3	-	110.4	-	109.2	-

Polymerisation conditions: supported on Solid MAO (300:1); 70 °C; 5 ml heptane; 15 μmol $AlEt_3$; 8.274 bar ethylene; 0.1-0.5 mg catalyst.

The data for the temperature at maximum elution ($T_{el.\ max.}$) fits very well with the 1-hexene incorporation data: $T_{el.\ max.}$ decreases as the proportion of 1-hexene in the co-polymer rises. Poly(1-hexene) has a much lower glass transition temperature (T_g) and melting

temperature than PE, and this is reflected in the reduction of $T_{el.\ max.}$ with increasing 1-hexene concentration. At 0.8% incorporation, the temperature of elution has decreased to 109.2 °C (***rac*-3.1** at 10% 1-hexene). Viscosity measurements were also recorded and these were found to be in good agreement with the molecular weight data obtained by GPC.

5.5 Large-scale polymerisation runs

In addition to the high throughput screening data shown above, both *rac*-EBI*$ZrCl_2$ and ***rac*-3.1** were selected for scale-up polymerisation runs. These runs were carried out by an operator under the instruction Dr. Khamnaen at SCG Chemicals' research centre in Rayong, Thailand.

Table 5.6: polymerisation data for the scale-up runs in Rayong, Thailand.

Catalyst	PE produced (g)	Activity ($kg_{PE}/mol_{Zr}/h/bar$)	M_w (daltons)	PDI
rac-EBI*$ZrCl_2$	99.8	10,664	178,242	2.96
***rac*-3.1**	48.4	5,082	373,834	5.46

Polymerisation conditions: supported on Solid MAO (300:1); 80 °C; 1000 ml hexane; 2.5 ml $AlEt_3$; 8 bar ethylene; 25 mg catalyst.

The Solid MAO supported catalysts were run in 1 l hexane for one hour at 80 °C. 2.5 ml $AlEt_3$ was used as a scavenger and the ethylene pressure was 8 bar. *rac*-EBI*$ZrCl_2$ outperformed the ***rac*-3.1** on scale-up, producing almost 100 g PE in one hour. This represents a threefold increase in activity from the laboratory scale (3,047 $kg_{PE}/mol_{Zr}/h/bar$) to 10,664 $kg_{PE}/mol_{Zr}/h/bar$ in the two litre reactor at 80 °C. The values recorded for ***rac*-3.1** are the same (within error) both in Oxford and on scale-up. This was an unexpectedly poor result and is due to be repeated. ***rac*-3.1** generates higher molecular weight polymer than *rac*-EBI*$ZrCl_2$, although there is a significant jump in PDI.

5.6 Polymer characterisation

Selected polymer samples from runs in Oxford were analysed by SEM, high temperature ^1H and ^{13}C NMR spectroscopy and powder X-ray diffraction. The data obtained were consistent with HDPE and are given below.

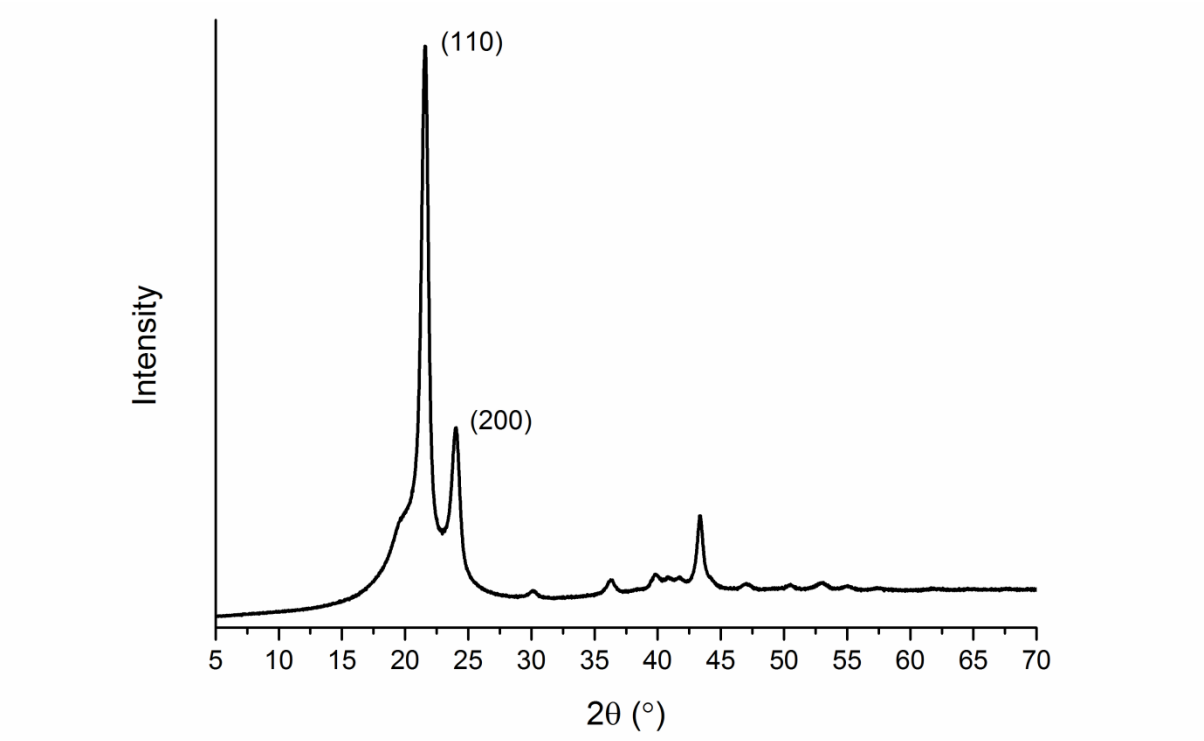


Figure 5.30: powder X-ray diffraction pattern for polyethylene (synthesised by ***rac*-3.1** on Solid MAO, 60 °C) showing two reflections, 110 and 200, and that of the aluminium sample holder (*c*. 43°).

The X-ray diffraction pattern presented in Figure 5.30 shows the two characteristic reflections, identified from the literature, for HDPE.[47] These occur at 21.5° and 24.0° and correspond to the 110 and 200 planes respectively. The sharp nature of the reflections gives an indication of the high crystallinity of the sample.[48]

Figures 5.31 to 5.33 highlight the differing particle sizes and morphologies shown by varying the supports. For all supports, the PE shown is synthesised by catalysts with ***rac*-3.1** immobilised, as well as two other complexes in the case of Solid MAO (Figure 5.30). In each case the polymer appears to emulate the morphology of the inorganic support: Solid MAO is spherical, SSMAO block-like and LDHMAO aggregated smaller particles. Similarly, the size of the resulting polymer particle appears to be reasonably well controlled by the support; an increase of approximately ten times in each direction is observed. Finally, comparing the different surface complexes on Solid MAO suggests that polymer particle size might also be determined, in part, by activity with ***rac*-3.1** and *rac*-EBI*$ZrCl_2$ (Figure 5.31 (b) and (c) respectively) generating larger particles than the slower ***rac*-3.5** (d).

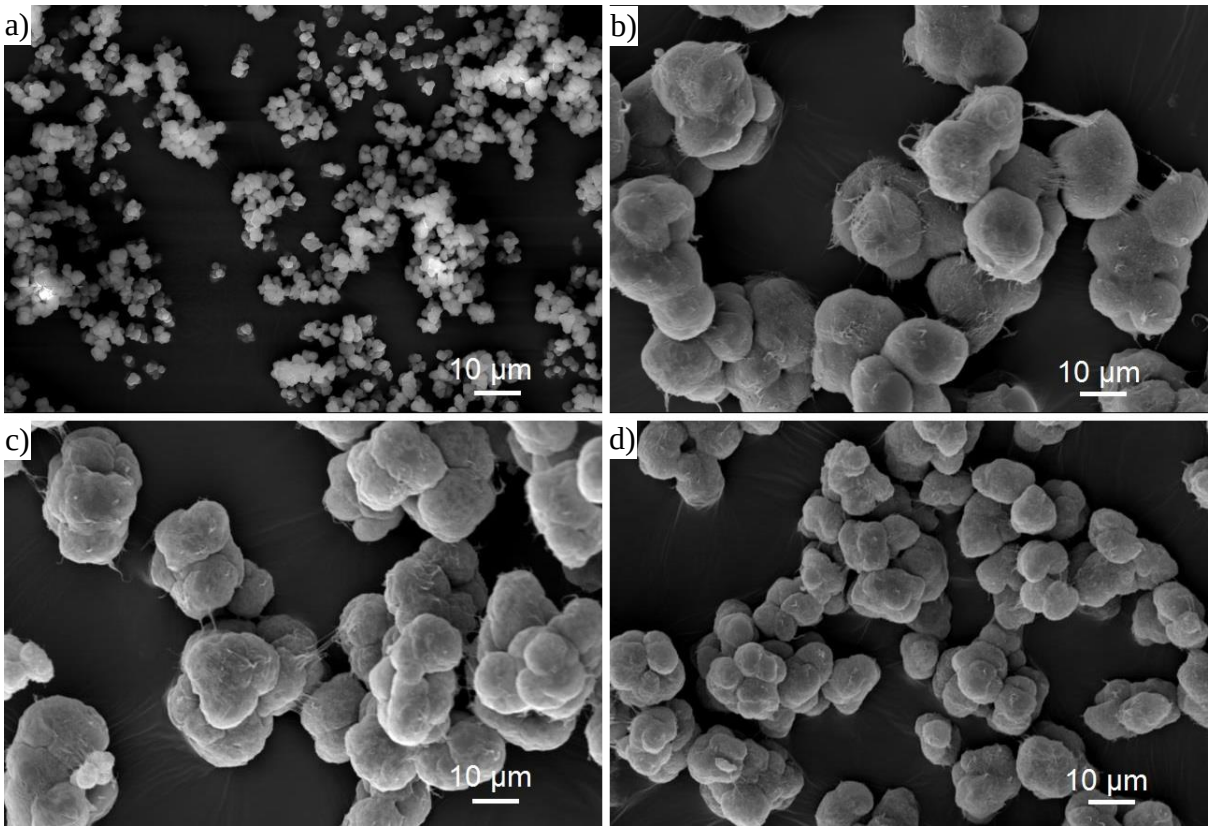


Figure 5.31: scanning electron microscopy (1000×) images of catalyst and polymer: a) Solid MAO-SBI*$ZrCl_2$; b) PE (Solid MAO-SBI*$ZrCl_2$); c) PE (Solid MAO-EBI*$ZrCl_2$); d) PE (Solid MAO-$Ind^{\#}_2ZrCl_2$).

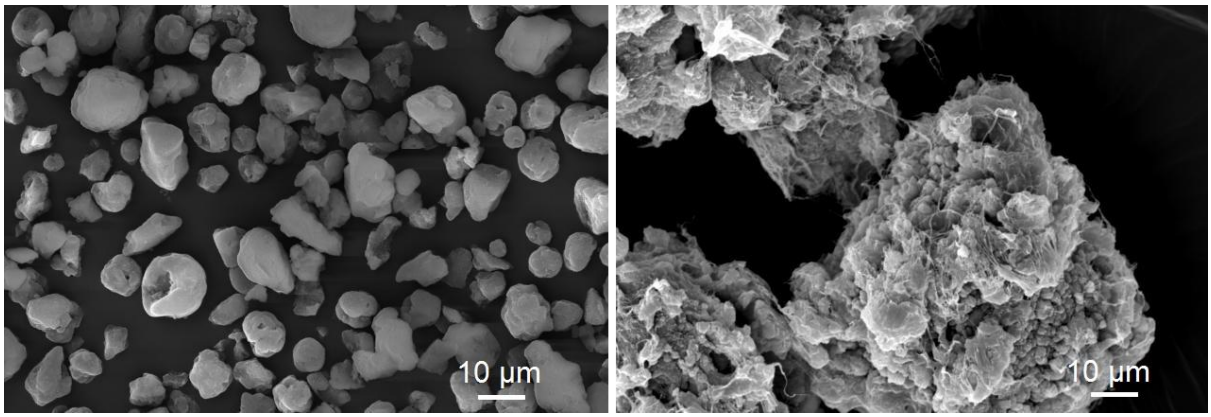


Figure 5.32: scanning electron microscopy (1000×) images of catalyst and polymer: a) SSMAO-SBI*$ZrCl_2$; b) PE (SSMAO-SBI*$ZrCl_2$).

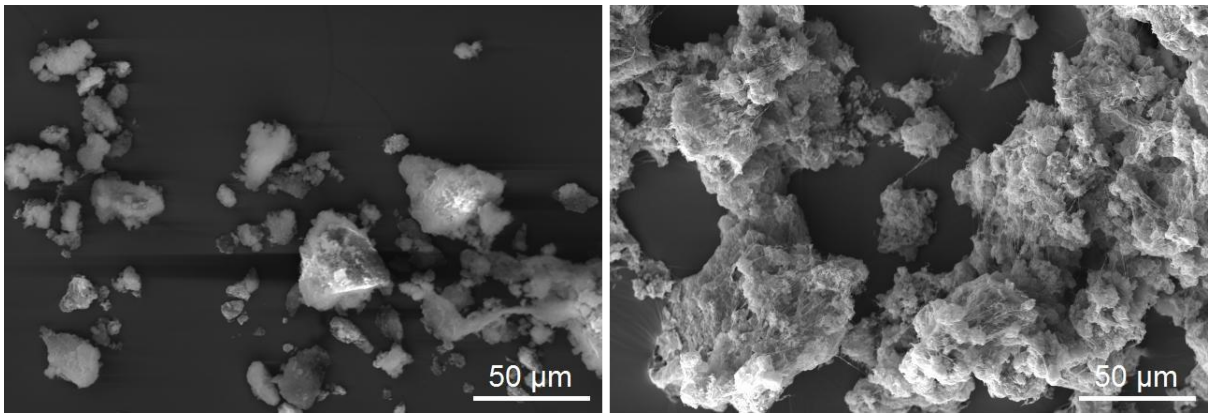


Figure 5.33: scanning electron microscopy (500×) images of catalyst and polymer: a) LDHMAO-SBI*$ZrCl_2$; b) PE (LDHMAO-SBI*$ZrCl_2$).

The PE generated by the solution-phase polymerisation with ***rac*-3.1** (Figure 5.34) contrasts sharply with the supported morphologies seen above. The polymer does not form discrete particles and has a less uniform shape. Some aggregation is also observed. It is thought that HDPE synthesised in this way will be more challenging to process on an industrial scale.

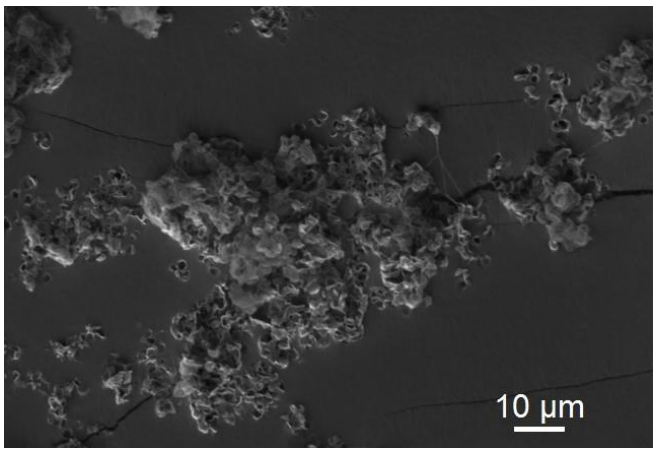


Figure 5.34: scanning electron microscopy (1000×) images of PE (synthesised by ***rac*-3.1** in solution).

Four strong absorptions are observed in the IR spectrum of the HDPE (Figure 5.35), synthesised by ***rac*-3.1** on Solid MAO at 60 °C. These agree well with the literature values where two bands at 1462 and 1472 cm^{-1} are identified as CH_2 bending modes.[49] The very intense signals at 2849 and 2917 cm^{-1} correspond to the asymmetric and symmetric CH_2 stretches respectively. The absence of any other major features within the range 3000-1000 cm^{-1} indicates that only crystalline HDPE is present.

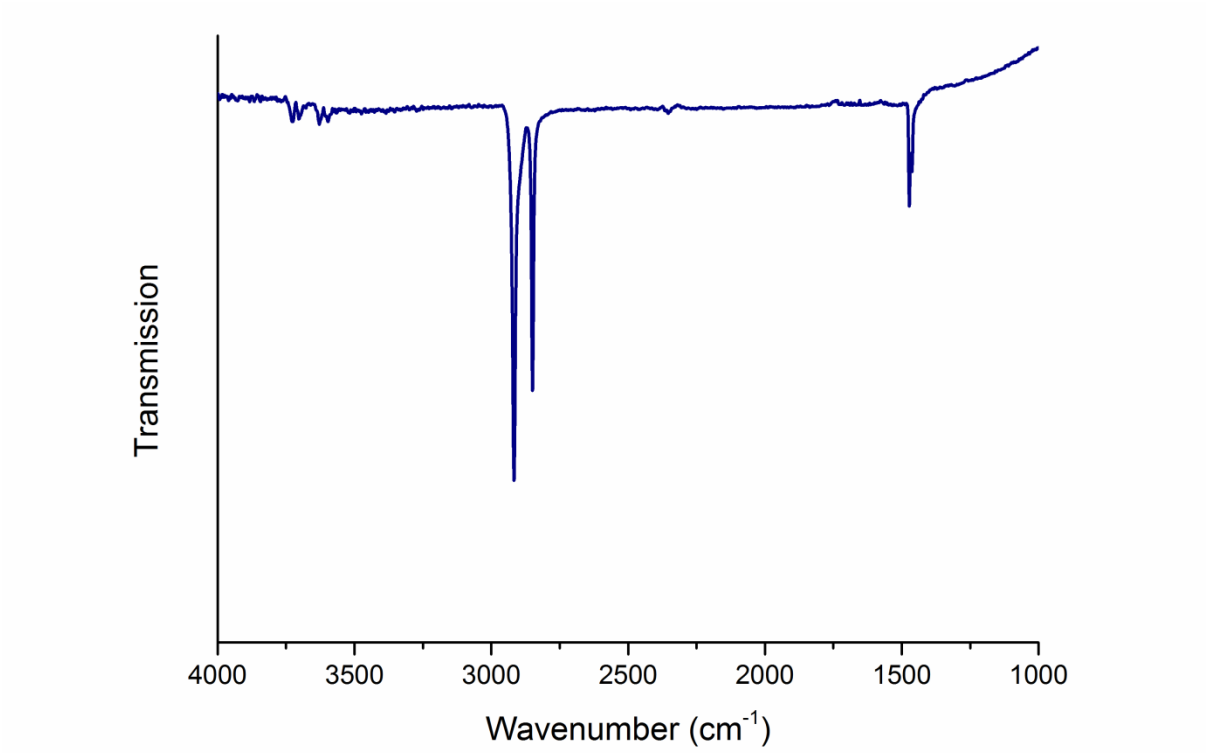


Figure 5.35: infrared spectrum of PE (synthesised by ***rac*-3.1** on Solid MAO, 60 °C).

Similarly, the ^{1}H and ^{13}C NMR spectra (Figures 5.36 and 5.37 respectively) are very simple indicating the presence of only one species. The proton resonance occurs at 1.27 ppm while the carbon resonance comes at 29.98 ppm – both are in good agreement with the literature.[50,51] A very small signal appears at 29.80 ppm, although no such resonance has previously been assigned in the literature.[52–55]

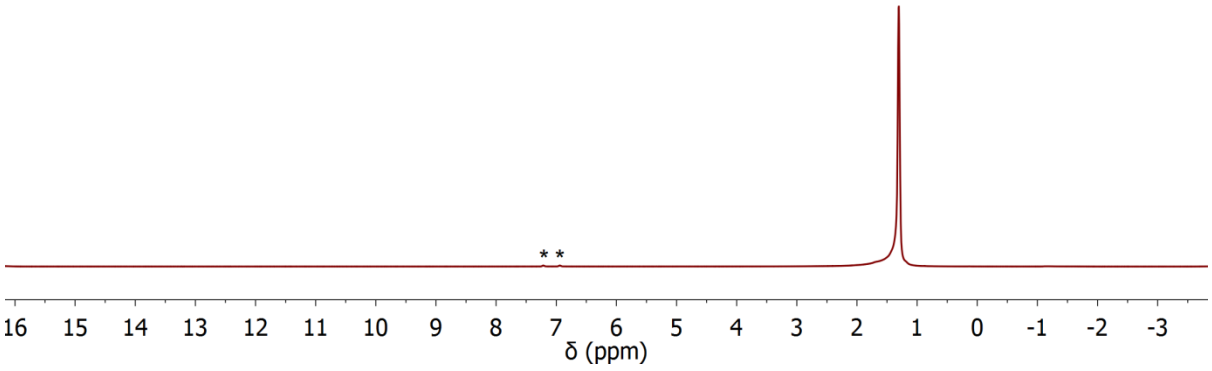


Figure 5.36: ^{1}H NMR (400 MHz) spectrum of PE at 120 °C (synthesised by ***rac*-3.1** on Solid MAO, 60 °C) in 1,2-dichlorobenzene-d_4.

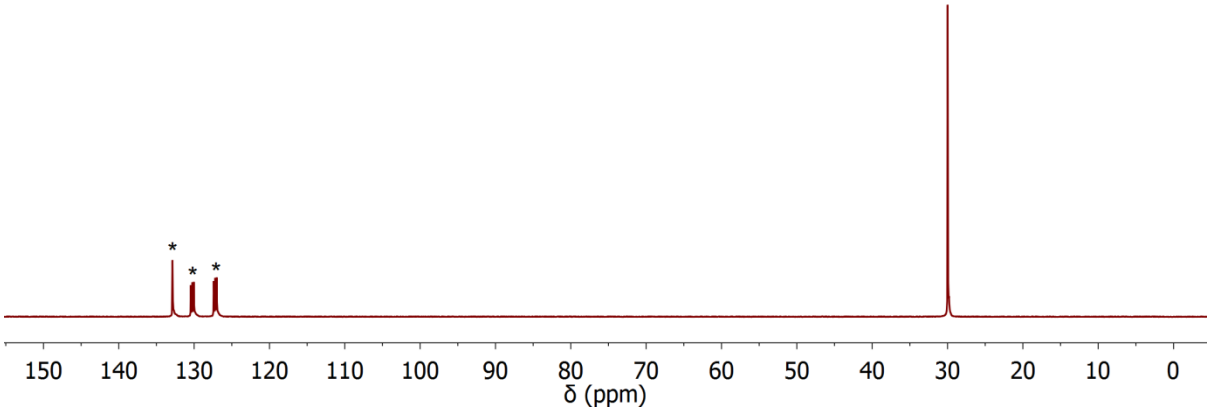


Figure 5.37: ^{13}C NMR (400 MHz) spectrum of PE at 120 °C (synthesised by ***rac*-3.1** on Solid MAO, 60 °C) in 1,2-dichlorobenzene-d_4.

5.7 Conclusion

The aims of this chapter were to test the polymerisation of a variety of indenyl zirconocenes and develop a highly active immobilised system for the polymerisation of ethylene. Nine complexes have been tested in total, with polymerisation runs carried out in solution and as slurries, affixed to three different supports. Almost all of the values recorded fall within the "very high activity" class of catalyst and some exceed this by a factor of ten or more. Of particular note were the peaks in activity for ***rac*-3.1** in solution (22,622 $kg_{PE}/mol_{Zr}/h/bar$) and on Solid MAO in the laboratory scale runs (7,760 $kg_{PE}/mol_{Zr}/h/bar$). These values have been further augmented in high-throughput screening (22,000 $kg_{PE}/mol_{Zr}/h/bar$) and both ***rac*-3.1** and *rac*-EBI*$ZrCl_2$ demonstrated excellent incorporation of 1-hexene and a strong co-monomer effect, the latter peaking at almost 33,000 $kg_{PE}/mol_{Zr}/h/bar$.

In addition to the measurement of activity, the polymer has been characterised by GPC and in some cases CEF and high temperature ^{13}C NMR spectroscopy. This has given us insight into the molecular weight of the polymers produced, and confirmed that all the single isomer metallocene catalysts tested yield HDPE with single-site MWDs. Further characterisation by standard laboratory techniques confirms that the physical characteristics of the HDPE synthesised agrees well with literature reports.

5.8 References

(1) Piringer, O. G.; Baner, A. L. *Plastic Packaging: Interactions with Food and Pharmaceuticals*; 2nd Ed.; Wiley, **2008**.
(2) Britovsek, G. J. P.; Gibson, V. C.; Wass, D. F. *Angew. Chem. Int. Ed.* **1999**, *38*, 428.
(3) Chen, E. Y.; Marks, T. J. *Chem. Rev.* **2000**, *100*, 1391.
(4) Delferro, M.; Marks, T. J. *Chem. Rev.* **2011**, *111*, 2450.

(5) Severn, J. R.; Chadwick, J. C.; Duchateau, R.; Friederichs, N. *Chem. Rev.* **2005**, *105*, 4073.
(6) Ziegler, K.; Gellert, H. G.; Zosel, K.; Lehmkuhl, W.; Pfohl, W. *Angew. Chemie* **1955**, *67*, 424.
(7) Breslow, D. S.; Newburg, N. R. *J. Am. Chem. Soc.* **1957**, *79*, 5072.
(8) Natta, G.; Pino, P.; Mazzanti, G.; Giannini, U. *J. Am. Chem. Soc.* **1957**, *79*, 2975.
(9) Kaminsky, W.; Sinn, H. *Liebigs Ann. Chem.* **1975**, *1975*, 424.
(10) Andresen, A.; Cordes, H.-G.; Herwig, J.; Kaminsky, W.; Merck, A.; Mottweiler, R.; Pein, J.; Sinn, H.; Vollmer, H.-J. *Angew. Chemie* **1976**, *88*, 689.
(11) Shapiro, P. J.; Bunel, E.; Schaefer, W. P.; Bercaw, J. E. *Organometallics* **1990**, *9*, 867.
(12) Okuda, J. *Chem. Ber.* **1990**, *123*, 1649.
(13) McKnight, A. L.; Waymouth, R. M. *Chem. Rev.* **1998**, *98*, 2587.
(14) Britovsek, G. J. P.; Gibson, V. C.; McTavish, S. J.; Solan, G. A.; White, A. J. P.; Williams, D. J.; Kimberley, B. S.; Maddox, P. J. *Chem. Commun.* **1998**, 849.
(15) Small, B. L.; Brookhart, M.; Bennett, A. M. A. *J. Am. Chem. Soc.* **1998**, *120*, 4049.
(16) Gibson, V. C.; Spitzmesser, S. K. *Chem. Rev.* **2003**, *103*, 283.
(17) Ittel, S. D.; Johnson, L. K.; Brookhart, M. *Chem. Rev.* **2000**, *100*, 1169.
(18) Böhm, L. L. *Angew. Chem. Int. Ed.* **2003**, *42*, 5010.
(19) Wang, B. *Coord. Chem. Rev.* **2006**, *250*, 242.
(20) Bochmann, M. *J. Organomet. Chem.* **2004**, *689*, 3982.
(21) Hlatky, G. G. *Chem. Rev.* **2000**, *100*, 1347.
(22) Severn, J. R.; Chadwick, J. C. *Taylor-Made Polymers. Via Immobilisation of Alpha-Olefin Polymerization Catalysts*; Wiley-VCH, **2008**.
(23) Kaminsky, W. *J. Chem. Soc. Dalton Trans.* **1998**, 1413.
(24) Ransom, P.; Ashley, A. E.; Brown, N. D.; Thompson, A. L.; O'Hare, D. *Organometallics* **2011**, *30*, 800.
(25) Alt, H. G.; Köppl, A. *Chem. Rev.* **2000**, *100*, 1205.
(26) Kaminsky, W.; Engehausen, R.; Zoumis, K.; Spaleck, W.; Rohrmann, J. *Makromol. Chem.* **1992**, *193*, 1643.
(27) Casely, I. J. Unpublished results, **2012**.
(28) Eskelinen, M.; Seppälä, J. V. *Eur. Polym. J.* **1996**, *32*, 331.
(29) D'Agnillo, L.; Soares, J. B. P.; Penlidis, A. *Macromol. Chem. Phys.* **1998**, *199*, 955.
(30) Rieger, B.; Janiak, C. *Angew. Makromol. Chemie* **1994**, *215*, 35.
(31) Piccolrovazzi, N.; Pino, P.; Consiglio, G.; Sironi, A.; Moret, M. *Organometallics* **1990**, *9*, 3098.
(32) Lee, I. M.; Gauthier, W. J.; Ball, J. M.; Iyengar, B.; Collins, S. *Organometallics* **1992**, *11*, 2115.
(33) Napoli, M.; De Vita, R.; Immediata, I.; Longo, P.; Guerra, G. *Polym. Adv. Technol.* **2011**, *22*, 458.
(34) Bochmann, M.; Lancaster, S. J. *Organometallics* **1993**, *12*, 633.
(35) Lee, D.-H.; Shin, S.-Y.; Lee, D.-H. *Macromol. Symp.* **1995**, *97*, 195.
(36) Guimarães, R.; Stedile, F. C.; dos Santos, J. H. . *J. Mol. Catal. A Chem.* **2003**, *206*, 353.
(37) Diamond, G. M.; Petersen, R. F. J. L.; Jordan, R. F.; Petersen, J. L. *Organometallics* **1996**.
(38) Diamond, G. M.; Jordan, R. F.; Petersen, J. L. *J. Am. Chem. Soc.* **1996**, *118*, 8024.
(39) Kaminsky, W.; Külper, K.; Brintzinger, H. H.; Wild, F. R. W. P. *Angew. Chem. Int. Ed.* **1985**, *24*, 507.
(40) Buffet, J.-C. Unpublished results.

(41) Buffet, J.-C.; Turner, Z. R.; Cooper, R. T.; O'Hare, D. *Polym. Chem.* **2015**, 10.1039/c4py01742k.
(42) Arriola, D. J.; Carnahan, E. M.; Hustad, P. D.; Kuhlman, R. L.; Wenzel, T. T. *Science* **2006**, *312*, 714.
(43) Li, H.; Marks, T. J. *Proc. Natl. Acad. Sci. U. S. A.* **2006**, *103*, 15295.
(44) Britovsek, G. J. P.; Cohen, S. A.; Gibson, V. C.; Maddox, P. J.; van Meurs, M. *Angew. Chem. Int. Ed.* **2002**, *41*, 489.
(45) Van Meurs, M.; Britovsek, G. J. P.; Gibson, V. C.; Cohen, S. A. *J. Am. Chem. Soc.* **2005**.
(46) Chien, J. C. W.; Wang, B. P. *J. Polym. Sci. Part A Polym. Chem.* **1990**, *28*, 15.
(47) Li, K. T.; Dai, C. L.; Kuo, C. W. *Catal. Commun.* **2007**, *8*, 1209.
(48) Mirabella, F. M.; Ford, E. a. *J. Polym. Sci. Part B Polym. Phys.* **1987**, *25*, 777.
(49) Krimm, S.; Liang, C. Y.; Sutherland, G. B. B. M. *J. Chem. Phys.* **1956**, *25*, 549.
(50) Hansen, E. W.; Blom, R.; Bade, O. M. *Polymer* **1997**, *38*, 4295.
(51) Hsieh, E. T.; Randall, J. C. *Macromolecules* **1982**, *15*, 1402.
(52) Liu, W.; Ray, D. G.; Rinaldi, P. L. *Macromolecules* **1999**, *32*, 3817.
(53) Liu, W.; Rinaldi, P. L.; McIntosh, L. H.; Quirk, R. P. *Macromolecules* **2001**, *34*, 4757.
(54) Sahoo, S. K.; Zhang, T.; Reddy, D. V.; Rinaldi, P. L.; McIntosh, L. H.; Quirk, R. P. *Macromolecules* **2003**, *36*, 4017.
(55) Seger, M. R.; Maciel, G. E. *Anal. Chem.* **2004**, *76*, 5734.

Chapter Six
Experimental Details

6.1 General Procedures

All reactions, unless specified otherwise, were performed under an atmosphere of nitrogen, using standard Schlenk techniques on a dual vacuum/inert gas manifold or within an MBraun UNIlab glovebox. All glassware was placed in an oven at 160 °C for at least two hours prior to use.

Pentane, hexane, toluene, benzene and dichloromethane were dried on an MBraun SPS-800 solvent purification system and degassed prior to use. The non-chlorinated solvents were stored in ampoules over a potassium mirror while dichloromethane was stored over molecular sieves. Tetrahydrofuran was distilled from purple sodium/benzophenone ketyl radical and stored on molecular sieves. Diethyl ether was collected off a Na/K still which had been refluxing for at least five days and was stored in a potassium mirrored ampoule. Pyridine was dried over calcium hydride, filtered and stored over molecular sieves. 1,4-dioxane was dried on molecular sieves and stored on a potassium mirror. Ligand preparation procedures were carried out in a ChemGlass ChemRxnHub reactor – a mechanically stirred 2 l reaction vessel with temperature control jacket, linked to an automated Huber cooling/heating system (range: −35 to 200 °C). The "reactor" can be kept under an atmosphere of N_2 although this is not entirely rigourous.

Benzene-d_6 (99.6%, Sigma Aldrich) and toluene-d_8 (99.5%, Goss Scientific) were dried over Na/K. Chloroform-d_1 (99.8%, Sigma Aldrich), pyridine-d_5 (99.5%, Goss Scientific) and tetrahydrofuran-d_8 (99.6%, Goss Scientific) were dried over calcium hydride. All deuterated solvents were vacuum transferred and freeze-pump-thaw degassed three times prior to use.

Molecular sieves (3 Å, 8-12 mesh) were supplied from Acros Organics and were baked at 140 °C under vacuum (< 10^{-1} mbar) for at least six hours before use.

6.2 Physical measurements

6.2.1 Single crystal X-ray diffraction

Crystals were mounted on MiTeGen Micromounts with a perfluoropolyether oil (Fomblin YR1800, Alfa Aesar) and cooled rapidly to either 100(1) or 150(1) K using an Oxford Cryosystems Cryostream unit.[1] Three different diffractometer setups were used as follows:

i. An Enraf-Nonius Kappa CCD diffractometer using graphite monochromated Mo Kα radiation (λ = 0.71073 Å). Raw frame data were reduced using the DENZO-SMN package,[2] and corrected for absorption using SORTAV.[3] Intensity data were collected using a multi-scan method with SCALEPACK (within DENZO-SMN).

ii. An Oxford Diffraction Supernova using multilayer, orthogonal, micro-focus Cu Kα radiation (λ = 1.5405 Å). Raw frame data were collected, reduced and processed using CrysAlis.

iii. A Crystal Logic Goniometer with a Rigaku Saturn 734+ detector on Beamline I19, Diamond Light Source operating at λ = 0.68890 Å.[4] Raw frame data were collected, reduced and processed using CrysAlis.

The structures were solved using either direct methods with SIR92,[5] or using charge-flipping with SuperFlip,[6] and refined using a full-matrix least squares refinement on all F^2 data using the CRYSTALS program suite.[7,8] In general, distances were calculated using the full variance/co-variance matrix. Dihedral angles were calculated with CCDC's Mercury[9] or using PLATON.[10]

Illustrations of the solid-state molecular structures were created using ORTEP.[11] Thermal ellipsoids were shown at 50% probability and octant shading (seven lines, except for carbon: four) was used for all non-hydrogen atoms. Hydrogens were depicted using black spheres. Colours were chosen as follows: carbon, grey-50%; oxygen, red; zirconium, spicy pink; chlorine, green; silicon, plum; and hafnium, old gold.

6.2.2 Density functional theory calculations

All DFT calculations were performed with the ORCA program package.[12] The geometry optimisations of the complexes and single-point calculations on the optimised geometries were carried out at the B3LYP[13–15] and BP86[16,17] levels of DFT. These hybrid functionals often give better analyses for transition metal complexes than pure gradient-corrected functionals with respect to metal-ligand covalency.[18] For the geometry optimisations, the all-electron Gaussian basis sets were those developed by the Ahlrichs group.[19,20] Triple-ζ quality scalar relativistic basis sets def2-TZVP with one set of polarization functions on the metals and on the atoms directly coordinated to the metal center were used.[21,22] For the carbon and hydrogen atoms, slightly smaller polarized split-valence def2-SV(P) basis sets were used, that were of double-ζ quality in the valence region and contained a polarizing set of d-functions

on the non-hydrogen atoms. Auxiliary basis sets were chosen to match the orbital basis.[23–25] The RIJCOSX15 approximation was used to accelerate the calculations.[26–28]

Illustrations depicting the frontier molecular orbitals were generated using USCF Chimera 1.10,[29] with the isosurface limits at ± 0.05. Bonds were set to wires (width two) and halfbond mode was activated.

6.2.3 Solution phase NMR spectroscopy

All air- and moisture-sensitive compounds were prepared in a glovebox under a nitrogen atmosphere and sealed in 5mm Young's type concentric stopcocks. Spectra were recorded on a Bruker AVIII 400 MHz NMR spectrometer, an Agilent Mercury 300 MHz NMR spectrometer or a Bruker AVIII 500 MHz NMR spectrometer. ^{1}H and ^{13}C NMR spectra were referenced internally to the residual *protio*-solvent resonance. ^{7}Li NMR spectra were referenced externally with LiCl.

6.2.4 Solid-state NMR spectroscopy

All samples were prepared in a glovebox under a nitrogen atmostphere and sealed in 4 mm ZrO_2 rotors. Solid-state NMR spectra were recorded by Dr. Nick Rees, University of Oxford, on a Bruker AVIII HD NanoBay 400 MHz Solid-State NMR spectrometer. Samples were spun at the magic angle (54.71°) at spin rates of 10 kHz for ^{13}C, ^{27}Al and ^{29}Si CPMAS, and ^{29}Si DPMAS NMR. ^{13}C NMR spectra were referenced to adamantane, ^{27}Al to $Al(NO_3)_3$ and ^{29}Si to kaolinite.

6.2.5 Infrared spectroscopy

Air-sensitive samples were prepared in the glovebox and ground with anhydrous KBr and then formed into discs using a specially designed press and airtight holder. IR spectra were recorded on a Nicolet iS5 ThermoScientific spectrometer (range 4000-400 cm^{-1}, resolution 1 cm^{-1}) as KBr discs in transmission mode. Air-stable samples were collected on the same instrument, using an iS3 diamond surface.

6.2.6 Ultraviolet/visible spectroscopy

UV/visible spectroscopy measurements were performed in the solid-state using an Agilent Cary 4000 UV Vis Spectrometer. Data were recorded with a grating of 70 × 45 mm from 200-800 nm. Samples were packed into the ceramic crucible in the glovebox and seled in an airtight temperature-controlled cell, custom-designed for diffuse reflectance by Prof.

Andrew Weller, University of Oxford. The cell was mounted on a PIKE Veemac Diffuse IR accessory and samples were run at room temperature.

6.2.7 Mass spectrometry

Samples were run as electron impact (EI) mass spectra and the data were collected by Mr. Colin Sparrow of the Chemistry Research Laboratory, University of Oxford.

6.2.8 Scanning electron microscopy

Scanning electron microscopy (SEM) images were collected by Phakpoom Angpanitcharoen, University of Oxford, on a JEOL JSM 6610 scanning electron microscope. Particles were cast onto a silica wafer. Before imaging, the samples were coated with platinum to prevent charging, improving the image quality. Energy dispersive X-ray (EDX) spectroscopy was also performed on this instrument to determine the relative percentages of elements on the surface.

6.2.9 Powder X-ray diffraction

Powder X-ray diffraction data were collected by Dr. Chunping Chen on a PANAnalytical X'Pret Pro diffractometer in reflection mode and a PANAnalytical Empyrean Series 2 at 40 kV and 40 mA using Cu K_α radiation ($K_{\alpha1}$ = 1.54057 Å, $K_{\alpha2}$ = 1.54433 Å). Scans were recorded in the range $3° \leq 2\theta \leq 70°$ with varying scan speed. Samples were mounted onto aluminium sample holders, accounting for the reflections in the region of 44°.

6.2.10 Gel permeation chromatography

Gel permeation chromatography (GPC) samples were collected under the supervision of Dr. Thipphaya Pathaweeisariyakul at SCG Chemicals, Thailand.

6.2.11 Elemental analysis

Samples were prepared in the glovebox and sealed in glass tubes (i.d. 2.5 mm, o.d. 5 mm) under vacuum. CHN analyses were carried out by Dr. Stephen Boyer, London Metropolitan University in duplicate.

6.2.12 EXAFS measurements

The Zr K-edge EXAFS studies were carried out on the B18 beamline at the Diamond Light Source, Didcot, UK with the help of Dr. Peter Wells and Dr. Emma Gibson. Measurements were performed using a QEXAFS set-up with a fast-scanning Si (111) double

crystal monochromator. The time resolution of the spectra reported herein was 30 s/spectrum (k_{max} = 14.5, step size 0.49 eV), on average 12 scans were acquired to improve the signal to noise level of the data for transmission measurements. Samples were handled in a glove box where they were pressed into pellets, placed on Kapton tape and sealed in a Swagelok gas cell under N_2 before being measured in transmission mode using ion chamber detectors. All XAFS spectra were acquired concurrently with a Zr foil placed between I_t and I_{ref}. XAFS data processing was performed using IFEFFIT[30] with the Horae package[31] (Athena and Artemis). The amplitude reduction factor, S_0^2, was derived from EXAFS data analysis of a known reference compound, ZrO_2, (with known coordination numbers which were fixed during analysis) to be 0.8, which was used as a fixed input parameter.

6.3 Starting Materials

6.3.1 Commercially supplied reagents

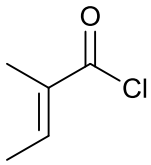
All reagents were used as received unless specified otherwise. Solvents were supplied by Sigma Aldrich, Fisher Scientific or Rathburn and dried as outlined in section 6.1. MeLi (1.6 M in Et_2O), ^{n}BuLi (2.5 M in hexane), MeMgBr (3.0 M in Et_2O), BrCN, tiglic acid, lithium aluminium hydride, sodium borohydride, calcium hydride, N,N-dimethylformamide, Al^iBu_3, $AlMe_3$, $AlCl_3$ (anhydrous), $LiAlH_4$ (2.0 M in THF), Li (wire), Na and K were all supplied from Sigma Aldrich. $PhSiH_3$ was supplied from Sigma Aldrich, dried over molecular sieves, and freeze-pump that degassed three times before use. 1,2,3,4-tetramethylbenzene, **2.3**, was supplied either from Alfa Aesar or from China (c/o SCG Chemicals). Oxalyl chloride was supplied from Alfa Aesar. Methylaluminoxane (MAO; 1.0 M in toluene) was supplied by Sigma Aldrich and was dried under vacuum before use. NEt_3 was supplied by Sigma Aldrich and was dried over CaH_2 and distilled under vacuum before use. $ZrCl_4$ and $HfCl_4$ were supplied by Sigma Aldrich and were dried at 140 °C overnight prior to use. Naphthalene was sourced from Sigma Aldrich and sublimed before use.

6.3.2 Literature preparations

The following species were prepared according to the literature procedures: $TiCl_4$·2THF,[32] $NaCH_2SiMe_3$,[33] KBz,[34] LiNp,[35] [H][B(3,5-$(CF_3)_2$-$C_6H_3)_4$],[36] AMO-LDH (MgAl-SO_4),[37,38] [Na][B(3,5-$(CF_3)_2$-$C_6H_3)_4$].[39]

6.4 Experimental details for Chapter Two

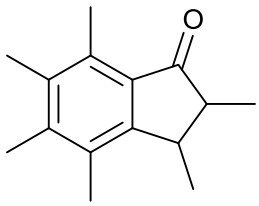
6.4.1 Synthesis of tigloyl chloride (2.2)



60.65 g oxalyl chloride (477 mmol, 0.9 eq.) was quickly added at room temperature to a stirred solution of 53.00 g tiglic acid [trans-2-methylbutenoic acid, **2.1**] (531 mmol, 1 eq.) in 200 ml DCM in a 500 ml two-necked, round-bottomed flask and was placed under an N_2 bubbler. The solution began to bubble slowly, and, on addition of one drop of catalytic, dry, degassed DMF, the effervescence increased dramatically. When no more gas was evolved (*c.* 3 h), the solution was reduced *in vacuo* (40 °C, 550 mbar) in order to remove the volatile DCM. The product was obtained by short-path distillation (25 °C, 0.1 mbar) of the remaining solution as a clear, colourless liquid in 81% yield (43.15 g, 386 mmol).

^{1}H NMR ($CDCl_3$): δ 1.90 (s, 3H, α-**Me**), 1.93 (d, 3H, $^3J_{HH}$ = 7.1 Hz, β-**Me**), 7.30 (q, 1H, $^3J_{HH}$ = 7.0 Hz, $^4J_{HH}$ = 1.0 Hz, vinylic-**H**).

6.4.2 Synthesis of hexamethylindanone (2.4)

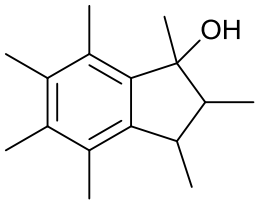


26.70 g anhydrous aluminium trichloride (200 mmol, 1.07 eq.) was stirred in 250 ml DCM in a 500 ml two-necked, round-bottomed flask under a flow of N_2 for 15 minutes before cooling to 0 °C. 22.25 g **2.2** (187 mmol, 1 eq.) was combined with 25.00 g 1,2,3,4-tetramethylbenzene (**2.3**;187 mmol, 1 eq.) and was slowly added dropwise by syringe to the pale yellow $AlCl_3$ suspension effecting a rapid change in colour to dark orange. The reaction mixture was allowed to warm to room temperature under a positive pressure of N_2, and was stirred for a further 12 h, turning dark red-brown, before quenching with a 500 ml mixture of conc. hydrochloric acid and ice 1:1 (v/v), causing the solution to decolourise to pale pink. The product was extracted in DCM (3 × 250 ml), dried over anhydrous magnesium sulphate, and the solvent removed under vacuum (40 °C, 10 mbar) affording a light brown oil which crystallised on cooling to room temperature. The product was washed with pentane (3 × 30 ml) at −35 °C to give a white crystalline solid in 93% yield (37.39 g, 174 mmol).

^{1}H NMR ($CDCl_3$): δ 1.06 (s, 3H, $^3J_{HH}$ = 7.0 Hz, α-**Me**), 1.23 (d, 3H, $^3J_{HH}$ = 7.2 Hz, β-**Me**), 2.23 (s, 3H, Ar-**Me**), 2.28 (s, 3H, Ar-**Me**), 2.31 (s, 3H, Ar-**Me**), 2.62 (s, 3H, Ar-**Me**), 2.76 (dq, 1H, $^3J_{HH}$ = 7.3 Hz, 7.3 Hz, β-**H**), 3.47 (dq, 1H, $^3J_{HH}$ = 7.1 Hz, 7.1 Hz, α-**H**).

Unit cell data: Orthorhombic, *Pca2$_1$*, a = 13.6257(3), b = 8.6250(2), c = 10.5161(2), α = β = γ = 90°.

6.4.3 Synthesis of Ind*OH (2.5)

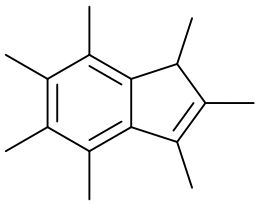


20.00 g anhydrous cerium trichloride (81.1 mmol, 1.5 eq.) was activated by stirring in 300 ml dry, degassed THF in a 500 ml Schlenk tube under a nitrogen atmosphere for 24 h, before cooling to −78 °C. 47.3 ml methyllithium (1.6 M in Et_2O; 75.7 mmol, 1.4 eq.) was added fast dropwise to the white suspension turning it bright yellow. The solution was allowed to stir for a further hour warming to −35 °C before dropwise addition of 11.69 g **2.4** (54.1 mmol, 1 eq.) in 100 ml THF, warming to room temperature and stirring for a further 12 h. The reaction mixture was quenched with 400 ml saturated aqueous ammonium chloride solution and was extracted in DCM (3 × 150 ml), dried over anhydrous magnesium sulphate and reduced *in vacuo* (40 °C, 10 mbar) affording a light brown oil. This oil was triturated with 2 ml hexane (4 °C), which was decanted after one hour affording an off-white crystalline solid in 96% yield (12.05 g, 51.9 mmol).

^{1}H NMR ($CDCl_3$): δ 0.5 (bs, 1H, $\Delta\nu_{½}$ = 105 Hz, -O**H**), 1.68 (s, 3H, Ar-**Me**), 2.20 (dq, 1H, $^3J_{HH}$ = 7.4 Hz, 7.4 Hz, β-**H**), 2.24 (s, 6H, Ar-**Me**), 2.26 (s, 3H, Ar-**Me**), 2.46 (s, 3H, 1-**Me**), 3.17 (dq, 1H, $^3J_{HH}$ = 7.3 Hz, 7.3 Hz, α-**H**).

Unit cell data: Tetragonal, $I4_1/a$, a = b =24.7261(4), c = 9.1915(2), α = β = γ = 90°.

6.4.4 Synthesis of Ind*H (2.6)

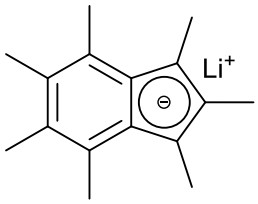


9.21 g **2.5** (39.7 mmol, 1 eq.) was dissolved in 150 ml dry DMSO and was added to a 250 ml round-bottomed flask and allowed to stir under N_2. 2.53 g hygroscopic, anhydrous lithium chloride (59.5 mmol, 1.5 eq) was quickly added to the pale brown solution, a Liebig condenser was set up and the flask was heated to 110 °C and allowed to stir for 48 h, darkening in colour. Upon cessation of stirring, a dark brown immiscible layer can be seen to form which congeals to a pale-yellow wax on cooling of the reaction mixture to room temperature. The product is extracted in pentane (3 × 150 ml), washed vigourously with distilled water (150 ml) to remove residual DMSO and dried over anhydrous magnesium sulphate, and the solvent removed under reduced pressure (40 °C, 10 mbar) affording a pale brown crystalline solid in 92% yield (7.85 g, 36.6 mmol).

^{1}H NMR ($CDCl_3$): δ 1.24 (d, 3H, $^3J_{HH}$ = 7.2 Hz, 1-**Me**), 1.96 (s, 3H, α-**Me**), 2.24 (s, 3H, Ar-**Me**), 2.25 (s, 6H, Ar-**Me**), 2.33 (s, 3H, Ar-**Me**), 2.51 (s, 3H, β-**Me**), 3.19 (q, 1H, $^3J_{HH}$ = 7.2 Hz, 1-**H**).[40]

Unit cell data: monoclinic, $P2_1/a$, a = 9.0940(8), b =10.9228(11), c = 13.0429(12), α = γ = 90°, β = 91.932(4).

6.4.5 Synthesis of Ind*Li (2.7)

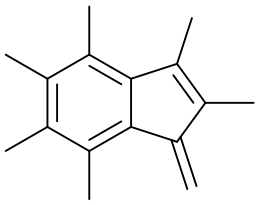


10.21 g **2.6** (47.7 mmol, 1 eq.) was dissolved in 150 ml dry, degassed THF and was cooled, in a 300 ml Schlenk tube under N_2, to −78 °C before fast dropwise addition of 24.7 ml *n*-butyllithium (2.5 M in hexanes; 61.9 mmol, 1 eq.), affording a clear pale red-pink solution which was allowed to warm to room temperature over one hour. The solution was dried *in vacuo* (25 °C, 0.1 mbar) and scraped out in a glovebox, giving a beige powder. The powder was returned to the Schlenk tube and washed, first with toluene (3 × 150 ml), and then with pentane (150 ml), until the solvent carried no colour, before finally drying residue under vacuum (25 °C, 0.1 mbar) yielding a white solid in 96% yield (10.06 g, 45.7 mmol).

^{1}H NMR (C_5D_5N): δ 2.90 (s, 6H, Ar-**Me**), 2.88 (s, 6H, Ar-**Me**), 2.49 (s, 6H, Cp-**Me**), 2.43 (s, 3H, Cp-**Me**).

^{13}C{^{1}H} NMR (C_5D_5N): δ 12.68 (Cp-**Me**), 15.86 (Cp-**Me**), 17.43(Ar-**Me**), 18.64 (Ar-**Me**), 97.10 (**Cp**), 119.52 (**Ar**), 123.95 (**Ar**). Two quaternary resonances are not observed in the spectrum.

6.4.6 Synthesis of hexamethylindenyl fulvene (2.8)

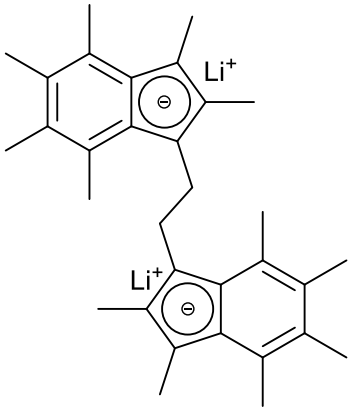


9.1 g **2.7** (41.3 mmol, 1 eq.) was slurried in 200 ml dry, degassed Et_2O in a 300 ml Schlenk tube under a nitrogen atmosphere and cooled to −78 °C. 5.23 g cyanogen bromide (BrCN; 49.3 mmol, 1.2 eq.) was quickly added under a flush of N_2 causing the white slurry to turn pale yellow. The reaction mixture was allowed to warm to room temperature and was stirred for a further 12 h, turning dark red-brown. 10 ml dry triethylamine (7.26 g, 71.8 mmol, 1.75 eq.) was gently added by syringe to the Schlenk tube causing the suspension to lighten in colour. The solution was stirred for a further six hours before an additional 10 ml NEt_3 was added, and the reaction mixture was reduced to dryness *in vacuo* (60 °C, 0.1 mbar). The air-stable product was extracted in hexane (3 × 200 ml) at 60 °C which was removed under vacuum (25 °C, 0.1 mbar) affording a yellow solid in 89% yield (7.80 g, 36.8 mmol).

^{1}H NMR ($CDCl_3$): δ 2.09 (s, 3H, α-**Me**), 2.31 (s, 3H, Ar-**Me**), 2.35 (s, 3H, Ar-**Me**), 2.36 (s, 3H, Ar-**Me**), 2.53 (s, 3H, Ar-**Me**), 2.54 (s, 3H, β-**Me**), 5.70 (s, 1H, C=C**H**$_2$), 5.96 (s, 1H, C=C**H**$_2$).[41]

$^{13}C\{^{1}H\}$ NMR ($CDCl_3$): δ 9.93 (**Me**), 15.87 (**Me**), 16.25 (**Me**), 16.46 (**Me**), 16.84 (**Me**), 16.92 (**Me**), 21.70 (**C**H_2), 126.68 (**Ar**), 129.75 (**Ar**), 131.21 (**Ar**), 132.01(**Ar**), 132.70 (**Ar**), 13.54 (**Ar**), 136.98 (**Ar**), 140.22 (**Ar**), 149.97(**Ar**).

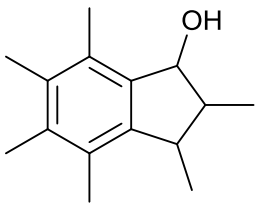
6.4.7 Synthesis of EBI*Li_2 (2.9)



158 mg freshly cut lithium (22.6 mmol, 1.2 eq.) was quickly added under a flush of argon to a 300 ml Schlenk tube containing 3.38 g sublimed naphthalene (26.4 mmol, 1.4 eq.) and was dissolved in 100 ml dry, degassed THF, turning the solution dark green after approximately five minutes. The solution was stirred for 18 h under an argon atmosphere before cooling to −78 °C. Fast dropwise addition of a solution containing 4.00 g **2.8** (18.8 mmol, 1 eq.) in 100 ml dry, degassed THF, and further stirring at room temperature for 18 h afforded a chocolate-brown reaction mixture which was concentrated to dryness (25 °C, 0.1 mbar). The Schlenk tube was scraped out in a nitrogen glovebox, yielding a beige powder. The product was washed with Et_2O (3 × 200 ml) until no more colour was taken up and the solid was collected, as the THF adduct (EBI*)Li_2·0.29THF, in 82% yield (3.38 g, 15.4 mmol).

^{1}H NMR (C_5D_5N) δ 2.42 (s, 6H, Cp-**Me**), 2.45 (s, 6H, Cp-**Me**), 2.62 (s, 6H, Ar-**Me**), 2.88 (s, 6H, Ar-**Me**), 2.91 (s, 6H, Ar-**Me**), 3.07 (s, 6H, Ar-**Me**), 3.79 (s, 4H, C**H**$_2$).[42]

6.4.8 Synthesis of Ind$^{\#}$OH (2.10)

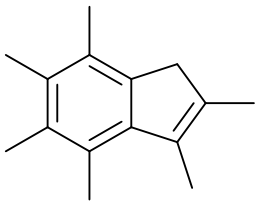


15.5 g $LiAlH_4$ (387 mmol, 1.1 eq.) was weighed into a 400 ml Schlenk flask in the glovebox and 300 ml dry, degassed THF was causing a significant rise in temperature. The resulting light grey slurry was added to the reactor with an additional 500 ml THF and the mixture was cooled to 8 °C. 76 g **2.4** (352 mmol, 1 eq.) was dissolved in 400 ml dry, degassed THF and this was added to the reactor in a fast dropwise manner over the course of 10 minutes causing a rise in the temperature of the reactor. The reaction was allowed to stir for 16 hours at room temperature before re-cooling to 8 °C and addition of 500 ml chloroform. The reaction was further quenched with distilled water until no further effervescence was observed and the mixture had turned white, eventually totaling 500 ml. 300 ml HCl (diluted 1:2 with H_2O) was added to ease separation of the layers. The organic layer was decanted off and the aqueous layer was extracted with two additional 500 ml portions of chloroform. After

removing the aqueous layer from the reaction vessel, the combined organic layer was washed with 500 ml brine before decanting, drying with *c.* 100 g magnesium sulfate, filtering and removing the solvent *in vacuo* (50 °C, 250 mbar). The product was obtained as a pale yellow oil in 88 % yield (70.58 g, 310 mmol).

^{1}H NMR ($CDCl_3$): δ 1.00 (s, 3H, $^{3}J_{HH}$ = 7.2 Hz, α-**Me**), 1.27 (d, 3H, $^{3}J_{HH}$ = 7.0 Hz, β-**Me**), 2.18 (q, 1H, $^{3}J_{HH}$ = 7.2 Hz, α-**H**), 2.22 (s, 6H, Ar-**Me**), 2.24 (s, 3H, Ar-**Me**), 2.39 (s, 3H, Ar-**Me**), 3.24 (q, 1H, $^{3}J_{HH}$ = 7.0 Hz, β-**H**), 4.92 (d, 1H, $^{3}J_{HH}$ = 8.2 Hz, *i*-**H**), 5.19 (d, 1H, $^{3}J_{HH}$ = 8.2 Hz, -O**H**).

6.4.9 Synthesis of Ind$^{\#}$H (2.11)



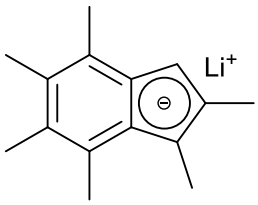
15.1 g **2.10** (69.1 mmol, 1 eq.) was dissolved in 500 ml DCM and transferred to the reactor and stirred vigourously at room temperature. 10 ml conc. H_2SO_4 was added to the solution in a fast dropwise manner causing the pale colour to change first to orange within the first five minutes and subsequently dark red. After 30 minutes, the reaction was quenched by the addition of 500 ml deionised water which caused the solution to turn a pale green and the reaction was stirred vigourously for an extra ten minutes. On cessation of stirring, the biphasic mixture separated very easily, being complete after only 20 seconds, and the organic layer was decanted off. The aqueous layer was extracted with DCM (2 × 250 ml) and the combined organic phase was washed with a further 500 ml H_2O. The organic layer was dried over magnesium sulphate, filtered and the volatiles removed *in vacuo* affording the product as an off white solid in 94 % yield (13.0 g, 64.9 mmol).

^{1}H NMR ($CDCl_3$): δ 2.03 (s, 3H, Cp-**Me**), 2.24 (s, 12H, Ar-**Me**), 2.50 (s, 3H, Cp-**Me**), 3.13 (bs, 2H, C**H$_2$**).

^{13}C{^{1}H} NMR ($CDCl_3$): δ 14.25 (Cp-**Me**), 15.33 (Ar-**Me**), 15.87 (Cp-**Me**), 16.26 (Ar-**Me**), 16.40 (Ar-**Me**), 16.43 (Ar-**Me**), 42.11 (**C**H$_2$), 126.44 (**Ar**), 128.36 (**Ar**), 130.43 (**Ar**), 133.72 (**Ar**), 134.09 (**Ar**), 137.33 (**Ar**), 139.25 (**Ar**), 142.01 (**Ar**).

Unit cell data: monoclinic, *P2$_1$/c*, a = 7.7961(3), b =18.3690(7), c = 8.0144(3), α = γ = 90°, β =90.3299(19).

6.4.10 Synthesis of Ind$^{\#}$Li (2.12)

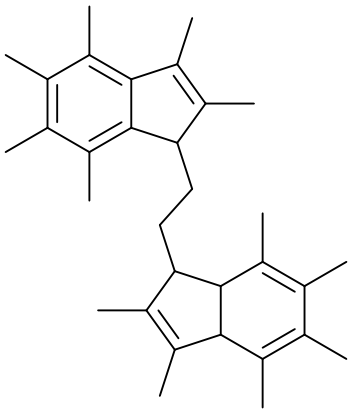


250 ml dry, degassed pentane was added to a Schlenk tube containing 24.4 g **2.11** (122 mmol, 1 eq.) and on stirring, the starting material was only partially dissolved. 63.5 ml *n*-butyllithium (2.5 M in hexanes; 159 mmol, 1.3 eq.) was transferred to the solution at room temperature in a fast dropwise manner, causing a slight rise in temperature. The slurry was allowed to stir for 18 hours before air-sensitive filtration and washing of the residue with a further 150 ml pentane. Care was taken not to use an excessive volume of pentane as the product is known to be partially soluble in aliphatic solvents and it was noted that the product immediately decolourised and smoked on contact with air. After drying *in vacuo* (20 °C, 0.1 mbar), the product was scraped collected as a light, white solid in 97 % yield (98.8 mmol, 20.3 g).

^{1}H NMR (C_5D_5N): δ 2.42 (s, 3H, Cp-**Me**), 2.46 (s, 3H, Cp-**Me**), 2.59 (s, 6H, Ar-**Me**), 2.90 (s, 3H, Ar-**Me**), 2.91 (s, 3H, Ar-**Me**), 6.30 (s, 1H, Cp-**H**).

^{13}C{^{1}H} NMR (C_5D_5N): δ 15.86 (**Me**), 15.97 (**Me**), 17.23 (**Me**), 17.40 (**Me**), 17.46 (**Me**), 18.18 (**Me**), 90.33 (**Cp**-H), 100.39 (**Ar**), 118.89 (**Ar**), 119.38 (**Ar**), 121.99 (**Ar**), 123.86 (**Ar**), 124.63 (**Ar**), 126.08 (**Ar**), 128.11 (**Ar**).

6.4.11 Synthesis of EBI*H$_2$ (2.13)

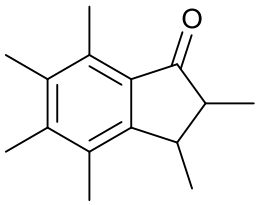


2.39 g of dry 1,2-dichloroethane (24 mmol, 1 eq.) was mixed with 200 ml THF. This solution was added dropwise to an orange solution containing 10 g **2.12** (10 g, 0.048 mol) in 800 ml THF. The reaction mixture was stirred for 15 h at room temperature, the colour changed from orange to yellow. The solution was dried under vacuum, the product was extracted with toluene, filtered, and finally dried under vacuum to afford an off-white solid as a 1:1 mixture of *rac*- and *meso*- isomers in 40% yield (9.6 mmol, 4.09 g).

^{1}H NMR ($CDCl_3$): δ 1.02 (m, 1H, bridge), 1.20 (d, 2H, bridge), 1.44 (m, 1H, bridge), 1.63 (s, 3H, **Me**), 1.81 (s, 3H, **Me**), 1.83 (s, 3H, **Me**), 2.14 (s, 3H, **Me**), 2.17 (s, 3H, **Me**), 2.21 (s, 15H, **Me**), 2.48 (s, 6H, **Me**), 3.03 (s, 2H, C**H**).

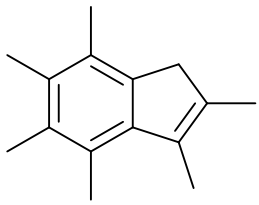
^{13}C{^{1}H} NMR ($CDCl_3$): δ 12.20 (**Me**), 12.49 (**Me**), 15.40 (**Me**), 16.12 (**Me**), 16.28 (**Me**), 16.48 (**Me**), 16.52 (**Me**), 16.65 (**Me**), 20.90 (**Me**), 21.10 (**Me**), 50.48 (**Cp**). Quaternary carbon resonances were not observed and numerous resonances were coincident.

6.4.12 Synthesis of hexamethylindanone (2.4) *via* a one-pot method



38.75 g **2.1** (387 mmol, 1 eq.) was dissolved in 1 l DCM and was transferred to the reactor under a flow of N_2. To this mixture 48.74 g oxalyl chloride (384 mmol, 1 eq.) was added which was washed in with a 100 ml portion of DCM. Five drops of N,N-dimethylformamide (DMF) were pipetted into the vigorously stirred solution causing a large amount of effervescence. The reaction was left stirring under nitrogen and an aliquot was taken after two hours showing that the reaction was 50 % complete. Another aliquot was taken after five hours showing that the reaction had reached 90 % completion and the reactor was cooled to 8 °C and allowed to equilibrate. 52.62 g aluminium trichloride (394 mmol, 1.02 eq.) was quickly added to the reactor under a flow of nitrogen, causing a small temperature rise and the resulting DCM slurry to become light orange. 49.18 g **2.3** (367 mmol, 0.95 eq.) was mixed with 100 ml DCM and transferred to a pressure-equalising dropping-funnel which was attached to the reactor under N_2. The solution of **2.3** was added to the stirred reaction mixture in a fast dropwise manner effecting a colour change through dark-orange to red. After stirring for a further seven hours at room temperature, a solution of 500 ml conc. HCl and 500 g ice was made-up and was transferred to the reaction mixture to quench it, dropwise at first and then more quickly over 10 minutes. This caused the dark-red slurry to decolourise to a light pink solution. The stirring was stopped and the organic layer was decanted before extracting the aqueous layer with more DCM (2 × 500 ml). After removing the aqueous layer from the reaction vessel, the combined organics were washed with 500 ml deionised water in the reactor before decanting, drying with *c.* 100 g magnesium sulfate, filtering and removing the solvent *in vacuo* (40 °C, 550 mbar). The product was obtained as a light brown oil in 96% yield (76 g, 352 mmol). Spectral details are given in section 6.4.2.

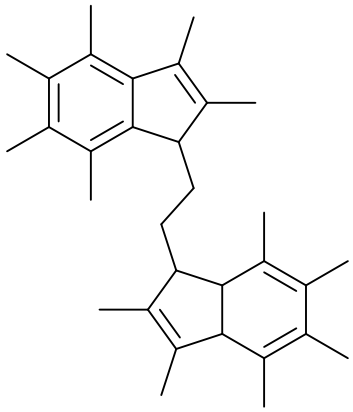
6.4.13 Synthesis of Ind$^{\#}$H (2.11) *via* a one-pot method



100 ml $LiAlH_4$ (2.0 M in THF; 200 mmol, 0.5 eq.) was combined with 100 ml dry, degassed THF and the mixture was cooled to 8 °C under N_2. 86.53 g **2.4** (400 mmol, 1 eq.) was dissolved in 150 ml dry, degassed THF and this was added to the stirred reaction mixture in a fast dropwise manner over the course of 10 minutes causing a small rise in temperature. The reaction was stirred for four hours before careful, portionwise quenching with 14.4 ml H_2O (800 mmol, 2 eq.) over approximately 30 minutes. 113 ml conc. H_2SO_4 (>95 %; 2 mol, 5 eq.)

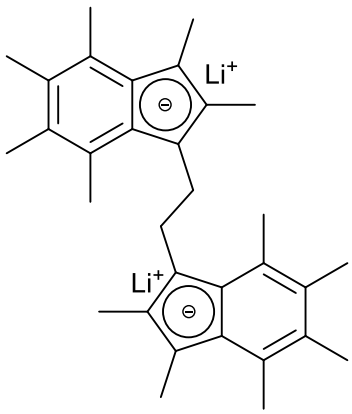
was added, slowly at first, causing the colour to change to a medium-dark grey over 30 minutes. The reaction was quenched with an additional 500 ml H_2O and extracted with DCM (3 × 500 ml). The combined organic layer was washed with a further 500 ml H_2O, dried over magnesium sulphate and the volatiles removed *in vacuo* (40 °C, 250 mbar), affording the product as a dark brown oil in 98% yield (78.51 g, 392 mmol). Spectral details are given in section 6.4.9.[43]

6.4.14 Synthesis of EBI*H_2 *via* a one-pot method



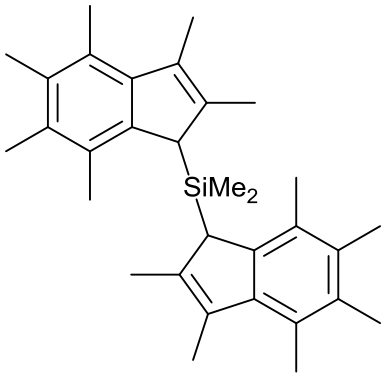
5 ml of *n*-butyllithium (2.4 M in hexanes; 12 mmol, 1.2 eq.) was added to a green solution of 2 g **2.11** (10 mmol, 1 eq.) in 50 ml THF at room temperature. The solution turned yellow instantly, and was left to stir for six hours at room temperature Then 0.93 g 1,2-dichloroethane (5 mmol, 0.5 eq.) in 10 ml THF was added to the solution and stirred for a further four hours at room temperature. The solution was dried under vacuum and the product was extracted with toluene to afford a yellow solution and a white solid (comprising lithium chloride); the solution was filtered, and finally dried under reduced pressure to afford an off-white solid in 45% yield (0.96 g, 2.25 mmol). Spectral details are given in section 6.4.11.

6.4.15 Synthesis of EBI*Li_2 (2.9) from EBI*H_2



300 ml THF was added to a Schlenk tube containing 12.45 g EBI*H_2 (29.2 mmol, 1 eq.) and on stirring, the starting material was only partially dissolved. 25.7 ml *n*-butyllithium (2.5 M in hexanes; 64.2 mmol, 2.2 eq.) was transferred to the solution at room temperature in a fast dropwise manner, causing a slight rise in temperature. The white slurry turned clear while adding the ^{n}BuLi. After 1 h stirring at room temperature, a pale green precipitate formed. The slurry was allowed to stir for four hours before air-sensitive filtration. The light green solid obtained was dried (20 °C, 0.1 mbar) and the product, **2.9**·THF, was collected as a light, white solid in 94% yield (13.66 g, 27.4 mmol). No colour was taken up on washing with pentane. Spectral details are given in section 6.4.7.

6.4.16 Synthesis of SBI*H_2 (2.14)



250 ml dry, degassed pentane was added to a Schlenk tube containing 10 g **2.11** (50 mmol, 1 eq.) and on stirring, the starting material was only partially dissolved. 22 ml *n*-butyllithium (2.5 M in hexanes; 55 mmol, 1.1 eq.) was transferred to the solution at room temperature by cannula in a fast dropwise manner, causing a slight rise in temperature. 3.52 g dimethyldichlorosilane (3.75 ml, 27.5mmol, 0.5 eq.), dried over molecular sieves and magnesium powder, was mixed with a further 10 ml THF and added in a slow dropwise fashion to the stirred reactor causing a slight lightening in colour. An aliquot was taken after two hours, and the ^{1}H NMR spectrum showed the reaction to be complete. The solution was reduced to dryness *in vacuo* (40 °C, 150 mbar), extracted in toluene, and dried once more affording the product as an off white solid in 75 % yield (9.39 g, 20.6 mmol).

***rac*-2.14**

^{1}H NMR ($CDCl_3$): δ −0.59 (s, 6H, Si**Me$_2$**), 2.16 (s, 6H, **Me**), 2.19 (s, 6H, **Me**), 2.23 (s, 6H, **Me**), 2.27 (s, 6H, **Me**), 2.30 (s, 6H, **Me**), 2.52 (s, 6H, **Me**), 3.71 (s, 2H, Cp-**H**).

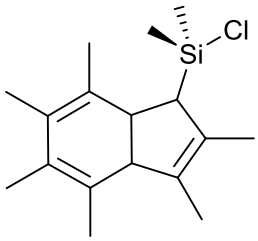
^{13}C{^{1}H} NMR ($CDCl_3$): δ −4.07 (Si**Me$_2$**), 15.17 (Ar-**Me**), 15.97 (Ar-**Me**), 16.27 (Ar-**Me**), 16.33 (Ar-**Me**), 16.40 (Ar-**Me**), 19.04 (Ar-**Me**), 47.22 (**Cp**-H), 126.22 (**Ar**), 127.16 (**Ar**), 129.79 (**Ar**), 132.29 (**Ar**), 132.87 (**Ar**), 139.70 (**Ar**), 141.59 (**Ar**), 142.24 (**Ar**).

Unit cell data: triclinic, $P\bar{1}$, a = 9.2291(7), b = 9.7804(7), c = 15.8873(12), α = 89.600(6), β = 81.392(6), γ = 73.234(6).

***meso*-2.14**

^{1}H NMR ($CDCl_3$): δ −0.54 (s, 3H, Si**Me$_2$**), −0.40 (s, 3H, Si**Me$_2$**), 1.98 (s, 6H, **Me**), 2.20 (s, 6H, **Me**), 2.21 (s, 6H, **Me**), 2.25 (s, 12H, **Me**), 2.52 (s, 6H, **Me**), 3.59 (s, 2H, Cp-**H**).[43]

6.4.17 Synthesis of HIndSiMe$_2$Cl (2.16)



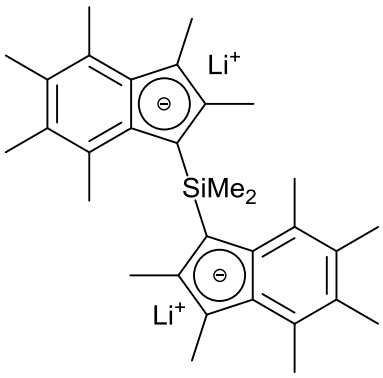
2 g **2.12** (9.7 mmol, 1 eq.) was dissolved in 50 ml THF and added to a stirred solution containing 6.14 g Me_2SiCl_2 (5.77 ml, 48 mmol, 5 eq.) in 30 ml THF. This addition caused a change in colour from pink to pale yellow. The reaction mixture was stirred for one further hour, before removing the volatiles under vacuum, affording the product as an off-white powder in 95% yield (2.69 g, 9.2 mmol). Care must be taken with the separation

of **2.16** from the LiCl byproduct as silyl chlorides are very sensitive to nucleophilic attack by H_2O and, hence, **2.16** should be treated as moisture-sensitive.

^{1}H NMR (C_6D_6): δ −0.08 (s, 3H, Si**Me**$_2$), 0.20 (s, 3H, Si**Me**$_2$), 2.09 (s, 3H, **Me**), 2.12 (s, 3H, **Me**), 2.13 (s, 3H, **Me**), 2.15 (s, 3H, **Me**), 2.16 (s, 3H, **Me**), 2.43 (s, 3H, **Me**), 3.49 (s, 1H, Cp-**H**).

^{13}C{^{1}H} NMR (C_6D_6): δ −0.41 (Si**Me**$_2$), 3.26 (Si**Me**$_2$), 15.22 (**Me**), 15.36 (**Me**), 16.27 (**Me**), 16.35 (**Me**), 16.41 (**Me**), 19.25 (**Me**), 49.75 (**Cp**-H), 126.57 (**Ar**), 127.62 (**Ar**), 130.48 (**Ar**), 133.13 (**Ar**), 134.50 (**Ar**), 137.83 (**Ar**), 139.76 (**Ar**), 142.14 (**Ar**).

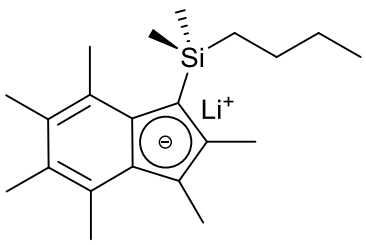
6.4.18 Synthesis of SBI*Li$_2$ (2.15)



2 g **2.14** (mixed isomers; 4.38 mmol, 1 eq.) were dissolved in 100 ml THF and 3.9 ml *n*-butyllithium (2.5 M in hexanes; 9.64 mmol, 2.2 eq.) was added slowly causing a slight colour change to pale pink and a moderate exotherm. The solution was allowed to stir for ten hours before removing the solvent *in vacuo*. The beige solid was scraped out in a glovebox and washed with pentane (3 × 50 ml). The product was obtained as an off-white powder in 68% yield (1.40 g, 2.98 mmol).

^{1}H NMR ($CDCl_3$): δ 1.18 (s, 6H, Si**Me**$_2$), 2.23 (s, 6H, **Me**), 2.38 (s, 6H, **Me**), 2.80 (s, 6H, **Me**), 2.89 (s, 6H, **Me**), 2.90 (s, 6H, **Me**), 2.96 (s, 6H, **Me**).

6.4.19 Synthesis of LiInd$^{\#}$SiMe$_2$^{n}Bu (2.17)



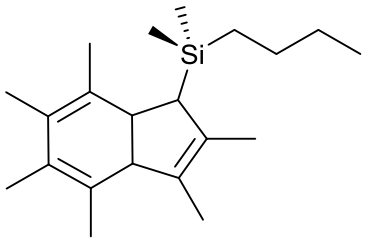
2 g **2.11** (10 mmol, 1 eq.) was dissolved in 50 ml THF and 4.4 ml *n*-butyllithium (2.5 M in hexanes; 11 mmol, 1.1 eq.) was added dropwise at room temperature, effecting a change in colour to pale pink. After two hours, 0.64 g Me_2SiCl_2 (0.60 ml, 5 mmol, 0.5 eq.) was added cauing a slight decolouration in the solution to pale yellow. After one hour, another 4.4 ml ^{n}BuLi (2.5 M in hexanes; 11 mmol, 1.1 eq.) was added to the reaction mixture and, following stirring at room temperature for three hours, the reaction was dried under vacuum and the product was obtained as an off white solid in an 83 % yield (1.33 g, 4.15 mmol). This is not a recommended synthesis of **2.17**, and a more efficient process would require the treatment of **2.16** (*vide infra*) with two equivalents of ^{n}BuLi.

^{1}H NMR (C_5D_5N): δ 0.73 (s, 6H, Si**Me$_2$**), 0.92 (t, 3H, $^{3}J_{HH}$ = 7.0 Hz, δ-Bu), 1.27 (m, 2H, α-Bu), 1.48 (m, 2H, γ-Bu), 1.72 (m, 2H, β-Bu), 2.47 (s, 3H, Ar-**Me**), 2.29 (s, 3H, Ar-**Me**), 2.82 (s, 3H, Cp-**Me**), 2.97 (s, 3H, Ar-**Me**), 3.03 (s, 3H, Cp-**Me**), 3.05 (s, 3H, Ar-**Me**).

^{13}C{^{1}H} NMR (C_5D_5N): δ 5.96 (Si**Me$_2$**), 14.84 (δ-Bu), 16.78 (**Me**), 17.33 (**Me**), 17.99 (**Me**), 18.33 (**Me**), 18.69 (**Me**), 23.11 (**Me**), 23.30 (α-Bu), 28.04 (γ-Bu), 28.77 (β-Bu), 90.71 (**C**-Si), 105.11 (**Cp**), 119.02 (**Ar**), 119.48 (**Ar**), 122.49 (**Ar**), 122.97 (**Ar**), 132.30 (**Ar**), 135.69 (**Cp**), 138.02 (**Ar**).

^{7}Li NMR (pyridine-d_5): δ 1.54.

6.4.20 Synthesis of HInd$^{\#}$SiMe$_2$^{n}Bu (2.18)

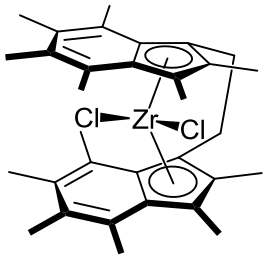


2.18 was synthesised by the careful protonation of **2.17** using a mixture of propan-2-ol and toluene (1:4 v:v). After thorough swirling the reaction is complete. The product is obtained by washing the organic layer with water, drying with magnesium sulphate and removal of the solvent *in vacuo*, leaving a white solid in quantitative yield.

^{1}H NMR (C_6D_6): δ −0.12 (s, 3H, Si**Me$_2$**), −0.04 (s, 3H, Si**Me$_2$**), 0.45 (m, 2H, α-**Bu**), 0.86 (t, 3H, $^{3}J_{HH}$ = 7.0 Hz, δ-**Bu**), 1.11 (m, 2H, γ-**Bu**), 1.24 (m, 2H, β-**Bu**), 1.98 (s, 3H, **Me**), 2.19 (s, 3H, **Me**), 2.21 (s, 3H, **Me**), 2.22 (s, 3H, **Me**), 2.26 (s, 3H, **Me**), 2.52 (s, 3H, **Me**), 3.32 (bs, 1H, Cp-**H**).

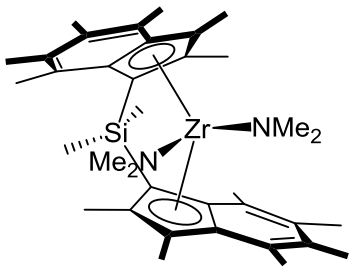
6.5 Experimental details for Chapter Three

6.5.1 Synthesis of EBI*ZrCl$_2$



The reported procedure for the synthesis of EBI*ZrCl$_2$ has been updated with a change of solvent.[42] 6 g **2.9**.THF (19.2 mmol, 1 eq.) was mixed with 4.41 g $ZrCl_4$ (19.2 mmol, 1 eq.) in a Schlenk tube in the glovebox and 200 ml benzene was added. The reaction was stirred for 17 hours before filtration at room temperature. The supernatant was allowed to stand for 72 hours affording a crop of bright orange solid, *rac*-EBI*ZrCl$_2$. Reduction of the benzene solution in vacuo and extraction into hexane at room temperature left more *rac*-EBI*ZrCl$_2$ as a residue and a solution containing exclusively *meso*-EBI*ZrCl$_2$. The solid of each isomer were combined affording a total yield of 25% (2.80 g, 4.8 mmol).

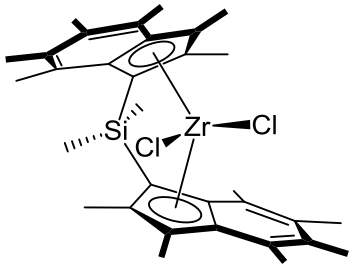
6.5.2 Synthesis of SBI*Zr(NMe_2)$_2$



20 mg **2.14** (mixed isomers; 43.8 μmol, 1 eq.) and 11.7 mg $Zr(NMe_2)_4$ (43.8 μmol, 1 eq.) were combined in a Young's tap NMR tube and 1 ml $CDCl_3$ was added forming an off-white slurry. After heating the NMR tube at 80 °C for 24 hours, the reaction appeared complete, and the tube contained a pale yellow solution. The resonance relating to $Zr(NMe_2)_4$ had disappeared and a resonance attributed to NMe_2H had grown in. Only one isomer of the product was seen to form. Attempts to scale up the reaction proved unsuccessful so no isolated yield is reported and the product was only characterised by ^{1}H NMR spectroscopy.

^{1}H NMR ($CDCl_3$): δ −0.13 (s, 3H, Si**Me**$_2$), −0.11 (s, 3H, Si**Me**$_2$), 2.03 (s, 3H, Ar-**Me**), 2.20 (s, 6H, Ar-**Me**), 2.23 (s, 12H, Ar-**Me**), 2.31 (s, 9H, Ar-**Me**), 2.51 (s, 6H, Ar-**Me**), 2.63 (s, 12H, N**Me**$_2$).

6.5.3 Synthesis of SBI*ZrCl_2 (3.1)



2 g **2.15** (4.27 mmol, 1 eq.) was combined with 0.98 g $ZrCl_4$ (4.27 mmol, 1 eq.) in a Schlenk tube in the glovebox and 60 ml benzene was added. The beige mixture was stirred, turning first pale- then dark orange. After two hours, the reaction was heated until boiling and filtered hot, giving a rich orange supernatant and an orange/brown residue. The benzene filtrate was allowed to stand at room temperature overnight affording a small crop of bright orange solid identified as ***rac*-3.1**. The decanted liquor was dried *in vacuo* and extracted in hexane, reduced to minimum volume and placed at −35 °C for four days. An orange crystalline solid was formed, with crystals suitable for X-ray analysis. The solids were combined giving a total isolated yield of 34% (891 mg, 1.45 mmol). No evidence was seen for a *meso*-isomer.

^{1}H NMR ($CDCl_3$): δ 1.34 (s, 6H, Si**Me**$_2$), 1.88 (s, 6H, Cp-**Me**), 2.18 (s, 6H, Ar-**Me**), 2.30 (s, 6H, Ar-**Me**), 2.39 (s, 6H, Cp-**Me**), 2.45 (s, 12H, Ar-**Me**).

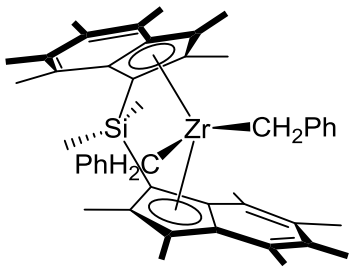
^{13}C{^{1}H} NMR ($CDCl_3$): δ 10.94 (Si**Me**$_2$), 15.93 (Ar-**Me**), 16.09 (Ar-**Me**), 16.50 (Ar-**Me**), 17.52 (Cp-**Me**), 17.71 (Ar-**Me**), 22.12 (Cp-**Me**), 78.02 (**Cp**-Si), 127.81 (**Me**), 129.90 (**Me**), 130.17 (**Me**), 130.35 (**Me**), 130.89 (**Me**), 133.17 (**Me**), 134.31 (**Me**), 135.40 (**Me**).

Unit cell data: monoclinic, $P2_1/n$, a = 14.10780(10), b =14.2840(2), c = 14.3753(2), α = γ = 90°, β = 96.8940(5).

IR (KBr) (cm^{-1}): 2961, 2923, 1543, 1454, 1384, 1260, 1097, 1020, 850, 813, 668.

MS (EI): found 615.7972; calculated 615.7908. Major fragmentation peaks noted for M−Me (600.78).

6.5.4 Synthesis of SBI*ZrBz$_2$ (3.2)



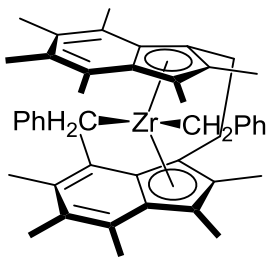
20 ml benzene was added to a small Schlenk tube containing 200 mg ***rac*-3.1** (326 μmol, 1 eq.) and 93 mg KBz (717 μmol, 2.2 eq.) and the reaction mixture was stirred vigourously for 17 hours. The reaction was deemed incomplete by ^{1}H NMR spectroscopy and the tube was sonicated for 30 minutes, before the red/brown mixture was dried under reduced pressure. Extraction of the resultant solid with hexane gave a yellow solution which, when dried, afforded a yellow solid, ***rac*-3.2**, in 61% yield (144 mg, 199 μmol). Attempts were made to crystallise ***rac*-3.2** from pentane, hexane, toluene and Et_2O but no crystals suitable for X-ray diffraction were obtained.

^{1}H NMR (400 MHz, C_6D_6): δ 1.10 (s, 6H, Si-**Me**), 1.69 (s, 6H, Ar-**Me**), 1.79 (s, 6H, Ar-**Me**), 2.11 (s, 12H, Ar-**Me**), 2.13 (s, 4H, Ph-C**H**$_2$), 2.37 (s, 6H, Ar-**Me**), 2.40 (s, 6H, Ar-**Me**), 6.75 (d, *J* = 7.1 Hz, 4H, *o*-**Ph**), 6.85 (t, *J* = 6.5 Hz, 2H, *p*-**Ph**), 7.13 (t, *J* = 7.0 Hz, 4H, *m*-**Ph**).

^{13}C{^{1}H} NMR (400 MHz, C_6D_6): δ 11.31 (Si-**Me**), 14.20 (Ar-**Me**), 15.25 (Ar-**Me**), 16.41 (Ar-**Me**), 17.43 (Ar-**Me**), 17.89 (Ar-**Me**), 22.00 (Ar-**Me**), 70.49 (Ph**C**H$_2$), 121.48 (*o*-**Ph**), 124.30 (**Ar**), 125.70 (**Ar**), 126.81 (*p*-**Ph**), 127.94 (**Ar**), 128.18 (**Ar**), 128.41 (**Ar**), 128.57 (*m*-**Ph**), 129.33 (**Ar**), 129.64 (**Ar**), 131.21 (**Ar**), 133.72 (**Ar**), 134.00 (**Ar**).

IR (KBr) (cm^{-1}): 2962, 1544, 1434, 1261, 1093, 1022, 802, 668.

6.5.5 Synthesis of EBI*ZrBz$_2$ (3.3)



50 ml benzene was added to a Schlenk tube containing 600 mg *meso*-EBI*ZrCl$_2$ (1.03 mmol, 1 eq.) and 295 mg KBz (2.27 mmol, 2.2 eq.) and the reaction mixture was stirred for 18 hours. The reaction was deemed incomplete by ^{1}H NMR spectroscopy and the tube stirred for a further 24 hours, before the dark red/brown mixture was dried *in vacuo*. Extraction of the resultant solid with hexane (2 × 80 ml) gave a yellow

solution which, when dried, afforded a yellow solid, ***rac*-3.3**, in 64% yield (459 mg, 659 μmol). Single crystals were grown from a concentrated solution of hexane at −35 °C.

^{1}H NMR (400 MHz, C_6D_6): δ −0.70 (s, 2H, PhC**H**$_2$), 1.83 (s, 2H, PhC**H**$_2$), 1.85 (s, 6H, Cp-**Me**), 2.01 (s, 6H, Ar-**Me**), 2.04 (s, 12H, Cp/Ar-**Me**), 2.41 (s, 6H, Ar-**Me**), 2.50 (s, 6H, Ar-**Me**), 3.07 (m, 3.02-3.13, 2H, C**H**$_2$), 3.67 (m, 3.62-3.73, 2H, C**H**$_2$), 6.39 (d, *J* = 7.5 Hz, 2H, *o*-**Ph**), 6.58 (d, *J* = 7.5 Hz, 2H, *o*-**Ph**), 6.80 (t, *J* = 7.2 Hz, 1H, *p*-**Ph**), 6.95 (t, *J* = 7.3 Hz, 1H, *p*-**Ph**), 7.04 (t, *J* = 7.6 Hz, 2H, *m*-**Ph**), 7.16 (t, *J* = 7.6 Hz, 2H, *m*-**Ph**).

^{1}H NMR (400 MHz, C_4D_8O): δ −1.01 (s, 2H, PhC**H**$_2$), 1.60 (s, 2H, PhC**H**$_2$), 2.04 (s, 6H, Cp-**Me**), 2.13 (s, 6H, Ar-**Me**), 2.15 (s, 6H, Ar-**Me**), 2.16 (s, 6H, Cp-**Me**), 2.39 (s, 6H, Ar-**Me**), 2.60 (s, 6H, Ar-**Me**), 3.44 (q, $^2J_{HH}$ = 6.8 Hz, $^3J_{HH}$ = 6.2 Hz, 2H, C**H**$_2$), 3.92 (q, $^2J_{HH}$ = 6.3 Hz, $^3J_{HH}$ = 6.2 Hz, 2H, C**H**$_2$), 6.07 (d, *J* = 7.6 Hz, 2H, *o*-**Ph**), 6.26 (d, *J* = 7.5 Hz, 2H, *o*-**Ph**), 6.50 (t, *J* = 7.3 Hz, 1H, *p*-**Ph**), 6.66 (t, *J* = 7.2 Hz, 1H, *p*-**Ph**), 6.77 (t, *J* = 7.5 Hz, 2H, *m*-**Ph**), 6.86 (t, *J* = 7.4 Hz, 2H, *m*-**Ph**).

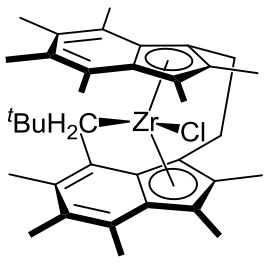
^{13}C{^{1}H} NMR (400 MHz, C_6D_6): δ 13.48 (Cp-**Me**), 15.36 (Cp-**Me**), 16.81 (Ar-**Me**), 16.95 (Ar-**Me**), 17.89 (Ar-**Me**), 18.66 (Ar-**Me**), 30.70 (**C**$_2$H$_4$), 64.71 (**C**H$_2$Ph), 69.41 (**C**H$_2$Ph), 110.57 (**Ar**), 115.81 (**Ar**), 120.95 (*p*-**Ph**), 121.85 (*p*-**Ph**), 125.55 (**Ar**), 126.36 (**Ar**), 127.18 (*o*-**Ph**), 127.20 (*m*-**Ph**), 127.68 (**Ar**), 127.94 (*m*-**Ph**), 128.65 (*o*-**Ph**), 129.03 (**Ar**), 129.56 (**Ar**), 132.32 (**Ar**), 133.32 (**Ar**), 151.39 (*i*-**Ph**), 151.63 (*i*-**Ph**).

Unit cell data: monoclinic, *P2$_1$/n*, a = 12.1915(3), b = 19.1827(4), c = 15.3626(3), α = γ = 90°, β = 93.2526(18).

MS (EI): found 726.2760; calculated 726.3198. Major fragmentation peaks noted at 635, 544 and 91 corresponding to [EBI*ZrBz]$^+$, [EBI*Zr]$^+$ and [Bz]$^+$ respectively.

IR (KBr) (cm^{-1}): 2962, 1738, 1543, 1434, 1374, 1261, 1205, 1094, 1022, 802, 668.

6.5.6 Synthesis of EBI*ZrNpCl (3.4)



53.5 mg lithium neopentyl (685 μmol, 2 eq.) was dissolved in 10 ml benzene and, at room temperature, added to a Schlenk tube containing 200 mg *meso*-EBI*ZrCl$_2$ (342 μmol, 1 eq.) in 40 ml benzene. The mixture was stirred for one hour before drying under reduced pressure. Care was taken to ensure the thorough removal of neopentane. The pale orange solid was extracted in hexane, giving a pale orange solution which was dried *in vacuo*. Careful washing with pentane (*c*. 5ml) at −78 °C removed any excess LiNp but was noted to take colour from the solid. The product was collected in 21%

yield (44.5 mg, 71.82 μmol). Very small, pale orange crystalline blocks were grown from hexane at −35 °C in the glovebox freezer.

^{1}H NMR (400 MHz, C_6D_6): δ −2.23 (s, 2H, C**H**$_2$^{t}Bu), 0.74 (s, 9H, C**Me**$_3$), 1.92 (s, 6H, Cp-**Me**), 2.07 (s, 6H, Ar-**Me**), 2.14 (s, 6H, Ar-**Me**), 2.44 (s, 6H, Ar-**Me**), 2.47 (s, 6H, Ar-**Me**), 2.53 (s, 6H, Ar-**Me**), 3.16 (m, 3.10-3.25, 2H, C**H**$_2$), 3.63 (m, 3.56-3.69, 2H, C**H**$_2$).

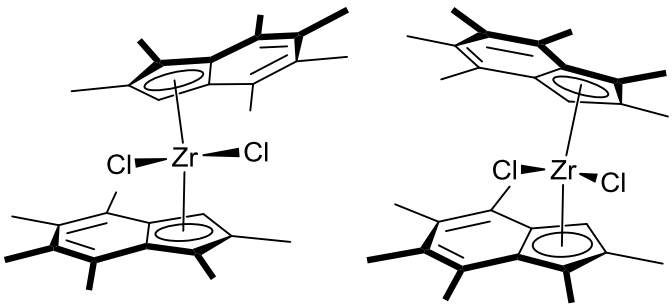
^{13}C{^{1}H} NMR (400 MHz, C_6D_6): δ 14.06 (Ar-**Me**), 16.30 (Ar-**Me**), 16.77 (Ar-**Me**), 16.86 (Ar-**Me**), 17.71 (Ar-**Me**), 18.81 (Ar-**Me**), 30.86 (**C**H$_2$), 34.95 (C**Me**$_3$), 77.24 (**C**H$_2$^{t}Bu) 111.79 (**Cp**), 116.90 (**Cp**), 125.22 (**Ar**), 127.53 (**Ar**), 127.95 (**Ar**), 129.50 (**Cp**), 130.27 (**Ar**), 132.47 (**Ar**), 133.72 (**Ar**).

Unit cell data: triclinic, $P\bar{1}$, a = 11.4222(5), b = 15.9204(6), c = 19.5395(7), α = 92.805(3), β = 90.490(3), γ = 108.372(4).

MS (EI): no molecular ion peak was found. Major fragmentation peaks at 592 and 551, corresponding to [EBI*ZrNp]$^+$ and [EBI*ZrCl]$^+$ respectively. Fragmentation patterns corresponding to the loss of Cl^- and Np^- were noted throughout the spectrum.

IR (KBr) (cm^{-1}): 3386 (b), 2962, 1640, 1459, 1261, 1095, 1020, 801.

6.5.7 Synthesis of $Ind^{\#}_2ZrCl_2$ (3.5)



4 g $Ind^{\#}Li$ (19.4 mmol, 2 eq.) were added to 2.26 g $ZrCl_4$ (9.71 mmol, 1 eq.) in a Schlenk tube inside a glovebox, and were stirred in 100 ml benzene under nitrogen for 72 h at room temperature during which time the beige solution turned dark orange. The mixture was allowed to settle, and the solution decanted. The solid was extracted with further benzene (2 × 50 ml) and the filtrates combined and reduced *in vacuo*. The mixture was recrystallised from hot hexane affording an orange crystalline solid in 45 % yield (2.43 g, 4.35 mmol). This solid comprised an equal mixture of both the *rac*- and *meso*-isomeric forms which proved inseparable by fractional crystallisation from hexane, pentane, toluene, Et_2O and THF. A further recrystallisation from acetone yielded large dark orange crystals of *meso*-$Ind^{\#}_2ZrCl_2$ which were isolated. On reduction in volume, the acetone solution precipitated *rac*-$Ind^{\#}_2ZrCl_2$ as a pale-orange microcrystalline solid. It is not recommended to the let the reaction mixture settle (due the slow rate at which this occurs) but preferably to augment

the volume of benzene used as the reaction solvent and to use an air-sensitive frit to remove the residue.

CHN Analysis (%). Expected: C 64.50, H 6.86. Found: C 64.35, H 6.74.

***rac*-3.5**

^{1}H NMR (400 MHz, $CDCl_3$): δ 1.60 (s, 6H, Cp-**Me**), 2.25 (s, 6H, Ar-**Me**), 2.26 (s, 6H, Ar-**Me**), 2.43 (s, 6H, Ar-**Me**), 2.54 (s, 6H, Cp-**Me**), 2.60 (s, 6H, Ar-**Me**), 6.26 (s, 2H, Cp-**H**).

^{1}H NMR (400 MHz, C_6D_6): δ 1.55 (s, 6H, Cp-**Me**), 2.08 (s, 6H, Ar-**Me**), 2.15 (s, 6H, Ar-**Me**), 2.39 (s, 6H, Ar-**Me**), 2.49 (s, 6H, Cp-**Me**), 2.57 (s, 6H, Ar-**Me**), 6.12 (s, 2H, Cp-**H**).

^{1}H NMR (400 MHz, pyridine-d_5): δ 1.67 (s, 6H, Cp-**Me**), 2.23 (s, 6H, Ar-**Me**), 2.25 (s, 6H, Ar-**Me**), 2.51 (s, 6H, Ar-**Me**), 2.59 (s, 6H, Cp-**Me**), 2.64 (s, 6H, Ar-**Me**), 6.42 (s, 2H, Cp-**H**).

^{13}C{^{1}H} NMR (400 MHz, $CDCl_3$): δ 14.06 (Cp-**Me**), 14.96 (Ar-**Me**), 16.47 (Ar-**Me**), 16.78 (Ar-**Me**), 17.42 (Cp-**Me**), 17.63 (Ar-**Me**), 93.49 (**Cp**-H), 119.15 (**Cp**), 124.08 (**Ar**), 124.96 (**Ar**), 129.44 (**Ar**), 130.64 (**Cp**), 131.58 (**Ar**), 132.99 (**Ar**), 133.35 (**Ar**).

Unit cell data: monoclinic, $P2_1/c$, a = 17.2538(13), b = 9.0136(5), c = 18.3402(16), $\alpha = \gamma = 90°$, $\beta = 114.553(10)$.

HRMS (EI): found 558.1390; calculated 558.1398. Major fragmentation peaks at 359 corresponding to $[Ind^{\#}ZrCl_2]^+$ were found.

IR (KBr) (cm^{-1}): 2962, 1543, 1441, 1261, 1022, 800.

***meso*-3.5**

^{1}H NMR (400 MHz, $CDCl_3$): δ 2.13 (s, 6H, Cp-**Me**), 2.18 (s, 6H, Ar-**Me**), 2.19 (s, 6H, Ar-**Me**), 2.23 (s, 6H, Ar-**Me**), 2.51 (s, 6H, Cp-**Me**), 2.52 (s, 6H, Ar-**Me**), 5.83 (s, 2H, Cp-**H**).

^{1}H NMR (400 MHz, C_6D_6): δ 2.00 (s, 6H, Cp-**Me**), 2.02 (s, 6H, Ar-**Me**), 2.05 (s, 6H, Ar-**Me**), 2.06 (s, 6H, Ar-**Me**), 2.54 (s, 6H, Cp-**Me**), 2.55 (s, 6H, Ar-**Me**), 5.60 (s, 2H, Cp-**H**).

^{1}H NMR (500 MHz, C_7D_8): δ 1.98 (s, 6H, Cp-**Me**), 2.02 (s, 6H, Ar-**Me**), 2.04 (s, 6H, Ar-**Me**), 2.05 (s, 6H, Ar-**Me**), 2.49 (s, 6H, Cp-**Me**), 2.50 (s, 6H, Ar-**Me**), 5.57 (s, 2H, Cp-**H**).

^{1}H NMR (400 MHz, pyridine-d_5): δ 2.14 (s, 6H, Cp-**Me**), 2.15 (s, 6H, Ar-**Me**), 2.20 (s, 6H, Ar-**Me**), 2.22 (s, 6H, Ar-**Me**), 2.56 (s, 6H, Cp-**Me**), 2.58 (s, 6H, Ar-**Me**), 5.98 (s, 2H, Cp-**H**).

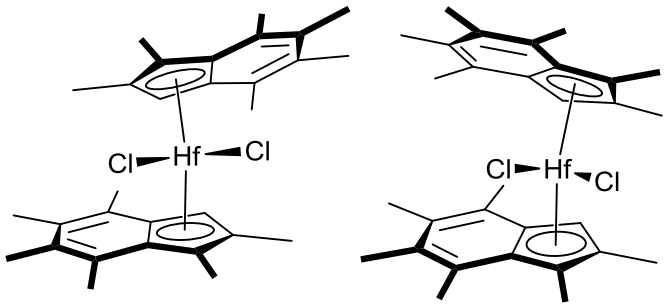
^{13}C{^{1}H} NMR (400 MHz, $CDCl_3$): δ 15.04 (Cp-**Me**), 15.95 (Ar-**Me**), 16.51 (Ar-**Me**), 16.53 (Ar-**Me**), 16.70 (Cp-**Me**), 17.10 (Ar-**Me**), 96.63 (**Cp**-H), 120.81 (**Cp**), 126.67 (**Ar**), 126.81 (**Ar**), 126.94 (**Ar**), 129.59 (**Cp**), 130.41 (**Ar**), 133.10 (**Ar**), 133.51 (**Ar**).

Unit cell data: monoclinic, $P2_1/n$, a = 12.55987(11), b = 14.56043(10), c = 14.41692(11), α = γ = 90°, β = 98.3967(8).

HRMS (EI): found 558.1390; calculated 558.1398. Major fragmentation peaks at 359 corresponding to $[Ind^{\#}ZrCl_2]^+$ were found.

IR (KBr) (cm^{-1}): 2920, 1542, 1441, 1382, 1261, 1064, 1024, 792.

6.5.7 Synthesis of $Ind^{\#}_2HfCl_2$ (3.6)



2 g $Ind^{\#}Li$ (9.71 mmol, 2 eq.) were added to 1.55 g $HfCl_4$ (4.86 mmol, 1 eq.) in a Schlenk tube inside a glove box, and were stirred in 70 ml benzene under nitrogen for 72 h at room temperature during which time the beige solution turned dark orange. The mixture was allowed to settle, and the solution decanted. The solid was extracted with further benzene (1 × 50 ml) and the filtrates combined and reduced *in vacuo*. The mixture was recrystallised from hot hexane affording an orange crystalline solid in 34 % yield (1.06 g, 1.64 mmol). This solid comprised an equal mixture of both the *rac*- and *meso*-isomeric forms which proved inseparable by fractional crystallisation from all common laboratory solvents. Crystals of each isomer suitable for X-ray diffraction were picked by eye under a microscope.

CHN Analysis (%). Expected: C 55.54, H 5.91. Found: C 55.63, H 6.01.

***rac*-3.6**

^{1}H NMR (400 MHz, C_6D_6): δ 1.63 (s, 6H, Cp-**Me**), 2.10 (s, 6H, Ar-**Me**), 2.17 (s, 6H, Ar-**Me**), 2.41 (s, 6H, Ar-**Me**), 2.51 (s, 6H, Cp-**Me**), 2.56 (s, 6H, Ar-**Me**), 5.99 (s, 2H, Cp-**H**).

^{13}C{^{1}H} NMR (400 MHz, C_6D_6): δ 14.06 (Cp-**Me**), 14.93 (Cp-**Me**), 16.39 (Ar-**Me**), 16.57 (Ar-**Me**), 17. 64 (Ar-**Me**), 17.64 (Ar-**Me**), 91.89 (**Cp**-H), 116.29 (**Cp**), 123.37 (**Ar**), 124.83 (**Ar**), 127.94 (**Ar**), 129.27 (**Cp**), 130.18 (**Ar**), 130.79 (**Ar**), 132.36 (**Ar**).

Unit cell data: monoclinic, $P2_1/c$, a = 17.3610(2), b = 9.08256(7), c = 18.4055(2), α = γ = 90°, β = 114.8387(16).

HRMS (EI): found 648.1780; calculated 648.1801. Major fragmentation peaks at 449 corresponding to $[Ind^{\#}HfCl_2]^+$ were found.

IR (KBr) (cm^{-1}): 2923, 1543, 1442, 1382, 1261, 1027, 792.

***meso*-3.6**

^{1}H NMR (400 MHz, C_6D_6): δ 2.00 (s, 6H, Cp-**Me**), 2.08 (s, 12H, Ar-**Me**), 2.11 (s, 6H, Ar-**Me**), 2.53 (s, 6H, Cp-**Me**), 2.59 (s, 6H, Ar-**Me**), 5.48 (s, 2H, Cp-**H**).

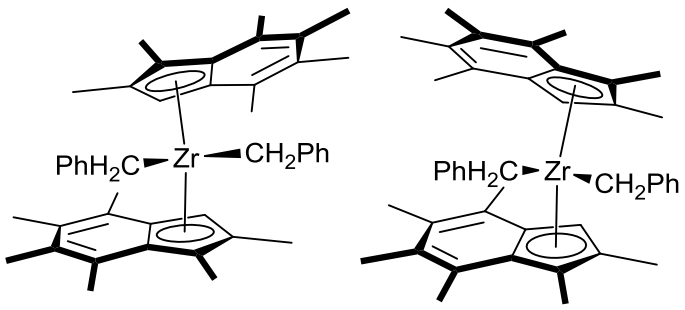
^{13}C{^{1}H} NMR (400 MHz, C_6D_6): δ 14.93 (Ar-**Me**), 15.86 (Ar-**Me**), 16.33 (Ar-**Me**), 16.57 (Ar-**Me**), 16.60 (Cp-**Me**), 17.29 (Cp-**Me**), 94.27 (**Cp**-H), 118.10 (**Cp**), 126.27 (**Ar**), 126.34 (**Ar**), 126.56 (**Ar**), 128.40 (**Cp**), 130.60 (**Ar**), 132.64 (**Ar**), 132.94 (**Ar**).

Unit cell data: monoclinic, *P2$_1$/n*, a = 12.56910(10), b = 14.62720(10), c = 14.3927(2), $\alpha = \gamma = 90°$, $\beta = 98.6310(9)$.

HRMS (EI): found 648.1780; calculated 648.1801. Major fragmentation peaks at 449 corresponding to $[Ind^{\#}HfCl_2]^+$ were found.

IR (KBr) (cm^{-1}): 2923, 1543, 1442, 1382, 1261, 1027, 792.

6.5.8 Synthesis of $Ind^{\#}_2ZrBz_2$ (3.7)



100 mg ***rac*-3.5** (179 μmol, 1 eq.) was stirred with 51 mg $K(CH_2Ph)$ (394 μmol, 1 eq.) in 20 ml benzene for 18 hours with periodic sonication. The reaction mixture was dried *in vacuo* and the residues extracted with hexane. The product, ***rac*-3.7**, was obtained as a yellow powder precipitated from hexane at −35 °C in 59% yield (70.8 mg, 106 μmol). Crystals suitable for X-ray analysis were grown from a saturated toluene solution cooled to −35 °C.

100 mg ***meso*-3.5** (179 μmol, 1 eq.) was stirred with 51 mg $K(CH_2Ph)$ (394 μmol, 1 eq.) in 20 ml benzene for 18 hours with periodic sonication. The reaction mixture was dried *in vacuo* and the residues extracted with hexane. ***meso*-3.7** was noted to be extremely soluble in hexane and all attempts at crystallisation were unsuccessful. The product, ***meso*-3.7**, was obtained as a yellow powder (with slight impurities) in a 68% yield (81.6 mg, 122 μmol).

***rac*-3.7**

^{1}H NMR (400 MHz, C_6D_6): δ 1.01 (d, J = 11.1 Hz, 2H, PhC**H**$_2$), 1.19 (d, J = 11.1 Hz, 2H, PhC**H**$_2$), 1.80 (s, 6H, Cp-**Me**), 2.02 (s, 6H, Ar-**Me**), 2.08 (s, 6H, Ar-**Me**), 2.10 (s, 6H, Ar-**Me**), 2.17 (s, 6H, Cp-**Me**), 2.39 (s, 6H, Ar-**Me**), 4.90 (s, 2H, Cp-**H**), 6.91 (d, J = 7.6 Hz, 4H, *o*-**Ph**), 6.94 (t, J = 7.4 Hz, 2H, *p*-**Ph**), 7.21 (d, J = 7.6 Hz, 4H, *m*-**Ph**).

^{1}H NMR (500 MHz, C_7D_8): δ 0.94 (d, J = 11.1 Hz, 2H, PhC**H**$_2$), 1.10 (d, J = 11.1 Hz, 2H, PhC**H**$_2$), 1.78 (s, 6H, Cp-**Me**), 1.98 (s, 6H, Ar-**Me**), 2.08 (s, 6H, Ar-**Me**), 2.09 (s, 6H, Ar-**Me**), 2.16 (s, 6H, Cp-**Me**), 2.38 (s, 6H, Ar-**Me**), 4.83 (s, 2H, Cp-**H**), 6.83 (d, J = 7.6 Hz, 4H, *o*-**Ph**), 6.86 (t, J = 7.6 Hz, 2H, *p*-**Ph**), 7.14 (d, J = 7.5 Hz, 4H, *m*-**Ph**).

^{13}C{^{1}H} NMR (400 MHz, C_6D_6): δ 13.58 (Ar-**Me**), 15.02 (Ar-**Me**), 16.37 (Ar-**Me**), 16.52 (Ar-**Me**), 16.61 (Ar-**Me**), 17.66 (Ar-**Me**), 66.75 (**C**H$_2$Ph), 100.77 (**Cp**-H), 114.04 (**Cp**), 121.59 (*p*-**Ph**), 125.12 (**Ar**), 126.71(**Ar**), 127.76 (*o*-**Ph**), 127.99 (*m*-**Ph**), 128.17 (**Ar**), 128.62 (**Ar**), 128.76 (**Cp**), 130.70 (**Ar**), 132.93 (**Ar**), 152.84(*i*-**Ph**).

Unit cell data: monoclinic, $P2_1/n$, a = 13.39700(10), b = 18.33180(10), c = 14.31300(10), $\alpha = \gamma = 90°$, $\beta = 93.7834(7)$.

HRMS (EI): no molecular ion peak was found. Major fragmentation peaks at 471 corresponding to $[Ind^{\#}ZrBz_2]^+$ were found.

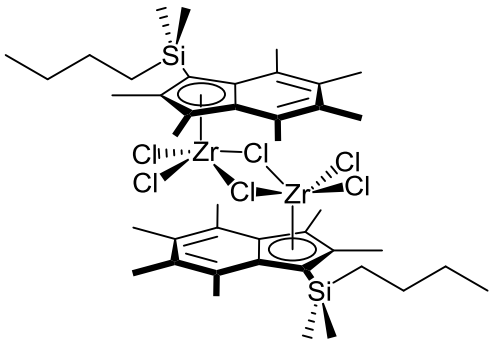
IR (KBr) (cm^{-1}): 2963, 1543, 1261, 1094 1022, 802.

***meso*-3.7**

^{1}H NMR (400 MHz, C_6D_6): δ 0.54 (s, 2H, PhC**H**$_2$), 1.39 (s, 2H, PhC**H**$_2$), 1.68 (s, 6H, Cp-**Me**), 2.04 (s, 6H, Ar-**Me**), 2.05 (s, 6H, Ar-**Me**), 2.09 (s, 12H, Ar-**Me**), 2.38 (s, 6H, Cp-**Me**), 5.45 (s, 2H, Cp-**H**), 6.75 (d, J = 7.6 Hz, 2H, *o*-**Ph**), 6.88 (m, 6H, **Ph**), 7.15 (t, J = 7.5 Hz, 2H, *m*-**Ph**).

HRMS (EI): no molecular ion peak was found. Major fragmentation peaks at 471 corresponding to $[Ind^{\#}ZrBz_2]^+$ were found.

6.5.9 Synthesis of $Ind^{\#}SiMe_2{}^nBuZrCl_3$ (3.8)



50 ml toluene was added to a Schlenk tube containing 1 g **2.17** (3.12 mmol, 1 eq.) and 0.72 g $ZrCl_4$ (3.12 mmol, 1 eq.). As immediate change in colour, from white to bright orange, was noted on addition of the solvent and the reaction mixture had turned vermillion on stirring for a further two hours. The slurry was allowed to settle and the supernatant was filtered off and left to stand at −35 °C for three days affording a red crystalline solid suitable for X-ray analysis in 73% yield (1.16 g, 2.28 mmol).

^{1}H NMR (400 MHz, C_6D_6): δ 0.55 (s, 3H, Si-**Me**$_2$), 0.65 (s, 3H, Si-**Me**$_2$), 0.86 (t, $^3J_{HH}$ = 7.0 Hz, 3H, δ-Bu), 1.01 (m, 2H, α-Bu), 1.25 (m, 2H, β-Bu), 1.29 (m, 2H, γ-Bu), 1.96

(s, 3H, Ar-**Me**), 2.03 (s, 3H, Ar-**Me**), 2.31 (s, 3H, Cp-**Me**), 2.42 (s, 3H, Ar-**Me**), 2.48 (s, 3H, Cp-**Me**), 2.57 (s, 3H, Ar-**Me**).

$^{13}C\{^{1}H\}$ NMR (400 MHz, C_6D_6): δ 3.37 (Si-**Me**$_2$), 3.75 (Si-**Me**$_2$), 13.98 (δ-Bu), 15.92 (Cp-**Me**), 16.78 (Ar-**Me**), 17.31 (Ar-**Me**), 17.31 (Ar-**Me**), 17.87 (Cp-**Me**), 19.79 (α-Bu), 21.71 (Ar-**Me**), 26.82 (γ-Bu), 26.89 (β-Bu), 116.31 (**Cp**), 126.23 (**Cp**), 130.46 (**Ar**), 132.48 (**Ar**), 133.23 (**Ar**), 134.05 (**Ar**), 136.57 (**Ar**), 137.24 (**Ar**), 143.54 (**Cp**).

Unit cell data: triclinic, $P\bar{1}$, a = 9.52710(10), b = 11.12740(10), c = 11.36160(10), α = 78.1654(5), β = 87.3403(5), γ = 77.9022(5).

HRMS (EI): found 508.0464; calculated 508.0460.

IR (KBr) (cm^{-1}): 3573, 2957, 1457, 1385, 1261, 1217, 1098, 814, 690, 480.

No satisfactory CHN analysis data were obtained for **3.1**, **3.3**, **3.7** and **3.8** due to the temperature sensitivity of the samples and the possible formation of carbide species. Insufficient material was prepared for **3.2** and **3.4** to allow for CHN analysis.

6.6 Experimental details for Chapter Four

6.6.1 Synthesis of supported catalysts

The quantity of catalyst immobilised on the surface of the support is given in terms of the Al:M (M = Zr, Hf) ratio of the methylaluminoxane component to the organometallic complex. In the case of SSMAO and LDHMAO, 0.5 eq. MAO is used to activate the surface of each support. The ratios used in this work are 300:1 and 200:1. The molecular weights used for SiO_2 and LDH ($Mg_{0.75}Al_{0.25}(OH)_2(SO_4)_{0.125}$) are 59.97 and 70.73 daltons respectively. This gives rise to molecular masses of SSMAO and LDHMAO of 177.94 and 199.46 daltons. Solid MAO is known to contain 39.7% Al by mass and so is calculated to have an effective molecular weight of 67.96 daltons. SSMAO and LDHMAO are prepared by weighing out both silica/LDH and the MAO into a Schlenk tube in the glovebox and adding toluene to the mixture which is then heated at 80 °C for two hours with regular swirling, until no further effervescence is observed. The white solid is allowed to settle, the solution decanted, and the product dried under vacuum at 50 °C to ensure complete solvent removal.

In the glovebox, the activated support (e.g. 293 mg Solid MAO, 4.31 mmol, 300 eq.) is weighed out into a Schlenk tube, while the complex (e.g. 8.8 mg ***rac*-3.1**, 14.3 μmol, 1 eq.) is weighed out into a second Schlenk tube. Toluene (e.g. 50 ml) is added *via* cannula to the tube containing the organometallic reagent and it is swirled until fully dissolved. The solution is

added to the support and the reaction mixture swirled at 60 °C for one hour. The coloured solid is allowed to settle from the clear, colourless solution which is decanted, and the solid is dried *in vacuo* (40 °C, 1×10^{-2} mbar). The product is scraped out in the glovebox in quantitative yield. It is imperative that the toluene solution is clear and colourless otherwise appreciable levels of unsupported catalyst contaminate the product and can lead to reactor fouling and the distortion of results. In some cases (e.g. *rac*-EBI*$ZrCl_2$), additional solvent may be required to completely dissolve the complex.

6.6.2 UV/visible spectroscopy data

***rac*-3.1**: λ_{max} = 460 nm.

***rac*-3.7**: λ_{max} = 430 nm.

Solid MAO: λ_{max} = 235 nm.

Solid MAO-SBI*$ZrCl_2$: λ_{max} = 395 nm.

Solid MAO-$Ind^{\#}_2ZrCl_2$: λ_{max} = 470 nm.

Solid MAO- $Ind^{\#}_2ZrBz_2$: λ_{max} = 505 nm.

LDHMAO: λ_{max} = 260 nm.

LDHMAO-SBI*$ZrCl_2$: λ_{max} = 395 nm.

SSMAO: λ_{max} = 265 nm.

SSMAO-EBI*$ZrCl_2$: λ_{max} = 390 nm.

6.6.3 Solid-state NMR spectroscopy data

LDHMAO-SBI*$ZrCl_2$

^{13}C CPMAS NMR: δ −9.32 (AlO**Me**), 12.87 (Si**Me_2**), 22.44 (Ar-**Me**), 24.57 (Ar-**Me**), 29.54 (Ar-**Me**), 31.10 (Ar-**Me**), 74.97 (**Cp**), 128.39 (**Ar**).

^{27}Al CPMAS NMR: δ −527, −28, 470.

SSMAO-EBI*$ZrCl_2$

^{13}C CPMAS NMR: δ −9.03 (AlO**Me**).

^{27}Al CPMAS NMR: δ −309, −113, 3, 182, 336.

^{29}Si CPMAS NMR: δ −106.

Solid MAO-SBI*$ZrCl_2$

^{13}C CPMAS NMR: δ −8.16 (AlO**Me**).

^{27}Al CPMAS NMR: δ −271, −102, 176, 322.

Solid MAO-$Ind^{\#}_2ZrBz_2$

^{13}C CPMAS NMR: δ −8.05 (AlO**Me**).

^{27}Al CPMAS NMR: δ −529, −30, 473.

6.6.4 EXAFS fit data

Sample	Abs-Sc	N	R (Å)	$2\sigma^2$ (Å^2)	E_0 (eV)	R_{factor}
#1 $MgAlSO_4$ -EBIZrMe_2	Zr-C (Cp ring)	10	2.53(5)	0.011(1)	0(2)	0.035
	Zr-C-C (m. s.)	20	3.23(3)	0.004		
	Zr-O	1	2.5(1)	0.004		
	Zr-Al	1	3.36(5)	0.004		
#2 $MgAlSO_4$ -EBIZrCl_2 + TIBA	Zr-C (Cp ring)	10	2.48(1)	0.005(1)	-8(2)	0.040
	Zr-C-C (m. s.)	20	3.22(4)	0.004		
	Zr-O	1	2.20	0.004		
	Zr-Al	1	3.32(3)	0.004		
#3 MgAlCl -EBIZrCl_2	Zr-C (Cp ring)	10	2.51(2)	0.006(1)	-2(2)	0.049
	Zr-C-C (m. s.)	20	3.21(4)	0.004		
	Zr-O	1	2.26(4)	0.004		
	Zr-Al	1	3.34(5)	0.004		
#4 $MgAlSO_4$ -EBIZrCl_2	Zr-C (Cp ring)	10	2.50(2)	0.007(1)	-4(2)	0.052
	Zr-C-C (m. s.)	20	3.20(3)	0.004		
	Zr-O	1	2.22(3)	0.004		
	Zr-Al	1	3.33(4)	0.004		
#5 MgAlBorate -EBIZrCl_2	Zr-C (Cp ring)	10	2.50(2)	0.006(1)	-3(2)	0.048
	Zr-C-C (m. s.)	20	3.26(3)	0.004		
	Zr-O	1	2.20(4)	0.004		
	Zr-Al	1	3.30(5)	0.004		

Fitting parameters: $S_0^2 = 0.8$ as deduced by ZrO_2 standard; Fit range 3<k<11.5, 1.1<R<4; number of independent points = 15

6.7 Experimental details for Chapter Five

6.7.1 Laboratory polymerisation runs

A typical slurry-phase laboratory polymerisation run was performed as follows. 150 mg TIBA was added to a 150 ml Rotaflo ampoule containing a stirrer bar and rinsed in with 10 ml hexane. 10 mg supported catalyst was added to the ampoule and washed in with a further 40 ml hexane. The vessel was sealed and was pumped on to a vacuum line and degassed under reduced pressure. It was cycled a further three times using an ethylene purge

while the reaction was brought to temperature in an oil bath with the stirring was set at 1000 rpm. The stopcock was opened to ethylene at a pressure of 2 bar and the timer was started. On completion of the run, the vessel was closed to ethylene and degassed, before filtration on a glass sintered frit (porosity 3) and washing with 50 ml pentane. The PE was dried in the vacuum oven at 50 °C overnight and weighed.

A typical laboratory solution-phase polymerisation run was performed as above after the following modification. A stock solution of the pre-catalyst (organometallic complex) was prepared at a concentration of 0.2 mg/ml. 2000 equivalents MAO were added to a 150 ml Rotaflo ampoule and washed in with 10 ml hexane. 1 ml stock solution was added to the ampoule along with a further 40 ml hexane. The run was continued as above.

All polymerisation runs were carried out, at least, in duplicate. The quantity of TIBA was kept constant, replicating the process used in industry. Given the changing loadings and mass of the catalysts, $[Al]_0$:$[Zr]_0$ varied significantly from *c.* 1000:1 (Solid MAO-*rac*-EBI*$ZrCl_2$ at 200:1) to 4500:1 (LDHMAO-*rac*-SBI*$ZrCl_2$ at 300:1). For the majority of runs (300:1 loading on Solid MAO), $[Al]_0$:$[Zr]_0$ = 1600:1.

6.7.2 Polymer characterisation

Powder XRD: 21.5°, 24.0°.

IR (diamond plate; cm^{-1}): 2917, 2849, 1472, 1462.

^1H NMR (*o*-$C_6D_4Cl_2$; 373 K): δ 1.27.

$^{13}C\{^1H\}$ NMR (*o*-$C_6D_4Cl_2$; 373 K): δ 29.98.

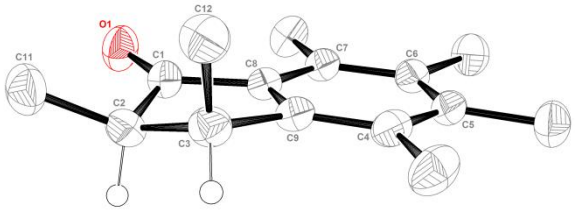
6.8 References

(1) Cosier, J.; Glazer, A. M. *J. Appl. Crystallogr.* **1986**, *19*, 105.
(2) Otwinowski, Z.; Minor, W. *Methods Enzymol.* **1997**, *276*, 307.
(3) Blessing, R. H. *Acta Crystallogr. Sect. A* **1995**, *51*, 33.
(4) Nowell, H.; Barnett, S. A.; Christensen, K. E.; Teat, S. J.; Allan, D. R. *J. Synchrotron Rad.* **2012**, *19*, 435.
(5) Altomare, A.; Cascarano, G.; Giacovazzo, C.; Guagliardi, A.; Burla, M. C.; Polidori, G.; Camalli, M. *J. Appl. Crystallogr.* **1994**, *27*, 435.
(6) Palatinus, L.; Chapuis, G. *J. Appl. Crystallogr.* **2007**, *40*, 786.
(7) Betteridge, P. W.; Carruthers, J. R.; Cooper, R. I.; Prout, K.; Watkin, D. J. *J. Appl. Crystallogr.* **2003**, *36*, 1487.
(8) Cooper, R. I.; Thompson, A. L.; Watkin, D. J. *J. Appl. Crystallogr.* **2010**, *43*, 1100.
(9) Macrae, C. F.; Bruno, I. J.; Chisholm, J. A.; Edgington, P. R.; McCabe, P.; Pidcock, E.; Rodriguez-Monge, L.; Taylor, R.; Van De Streek, J.; Wood, P. A. *J. Appl. Crystallogr.* **2008**, *41*, 466.
(10) Spek, A. L. *J. Appl. Crystallogr.* **2003**, *36*, 7.
(11) Farrugia, L. J. *J. Appl. Crystallogr.* **2012**, *45*, 849.

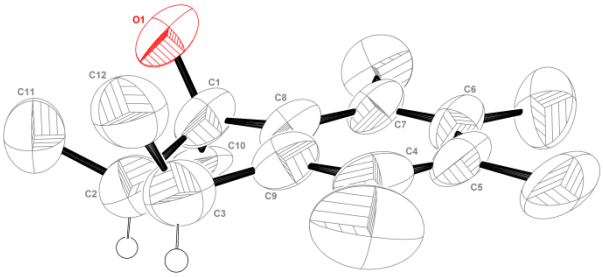
(12) Neese, F. Orca - an ab initio DFT and semi-empirical electronic structure package, 2011.
(13) Becke, A. D. *J. Chem. Phys.* **1986**, *84*, 4524.
(14) Becke, A. D. *J. Chem. Phys.* **1993**, *98*, 5648.
(15) Lee, C.; Yang, W.; Parr, R. G. *Phys. Rev. B* **1988**, *37*, 785.
(16) Becke, A. D. *Phys. Rev. A* **1988**, *38*, 3098.
(17) Perdew, J. *Phys. Rev. B* **1986**, *33*, 8822.
(18) Neese, F.; Solomon, E. I. *Magnetism: From Molecules to Materials*; Wiley (New York), 2002; p. 345.
(19) Schäfer, A.; Huber, C.; Ahlrichs, R. *J. Chem. Phys.* **1994**, *100*, 5829.
(20) Weigend, F.; Ahlrichs, R. *Phys. Chem. Chem. Phys.* **2005**, *7*, 3297.
(21) Pantazis, D. A.; Chen, X.-Y.; Landis, C. R.; Neese, F. *J. Chem. Theory Comput.* **2008**, *4*, 908.
(22) Pantazis, D. A.; Neese, F. *J. Chem. Theory Comput.* **2009**, *5*, 2229.
(23) Eichkorn, K.; Treutler, O.; Öhm, H.; Häser, M.; Ahlrichs, R. *Chem. Phys. Lett.* **1995**, *242*, 652.
(24) Eichkorn, K.; Weigend, F.; Treutler, O.; Ahlrichs, R. *Theor. Chem. Accounts Theory, Comput. Model. (Theoretica Chim. Acta)* **1997**, *97*, 119.
(25) Eichkorn, K.; Treutler, O.; Öhm, H.; Häser, M.; Ahlrichs, R. *Chem. Phys. Lett.* **1995**, *240*, 283.
(26) Neese, F.; Wennmohs, F.; Hansen, A.; Becker, U. *Chem. Phys.* **2009**, *356*, 98.
(27) Kossmann, S.; Neese, F. *Chem. Phys. Lett.* **2009**, *481*, 240.
(28) Neese, F. *J. Comput. Chem.* **2003**, *24*, 1740.
(29) Pettersen, E. F.; Goddard, T. D.; Huang, C. C.; Couch, G. S.; Greenblatt, D. M.; Meng, E. C.; Ferrin, T. E. *J. Comput. Chem.* **2004**, *25*, 1605.
(30) Newville, M. *J. Synchrotron Rad.* **2001**, *8*, 322.
(31) Ravel, B.; Newville, M. *J. Synchrotron Rad.* **2005**, *12*, 537.
(32) *Inorg. Syn.* **1982**, *21*, 135.
(33) Matson, E. M.; Forrest, W. P.; Fanwick, P. E.; Bart, S. C. *Organometallics* **2012**, *31*, 4467.
(34) Bailey, P. J.; Coxall, R. A.; Dick, C. M.; Fabre, S.; Henderson, L. C.; Herber, C.; Liddle, S. T.; Loroño-González, D.; Parkin, A.; Parsons, S. *Chem. Eur. J.* **2003**, *9*, 4820.
(35) Schrock, R. R.; Fellmann, J. D. *J. Am. Chem. Soc.* **1978**, *100*, 3359.
(36) Taylor, R. G.; Habimana J. d. l. C.; Leadley, S. Process for the condensation of compounds having silicon bonded hydroxy or alkoxy groups. WO0179330 (A1), **2001**.
(37) Wang, Q.; O'Hare, D. *Chem. Commun.* **2013**, *49*, 6301.
(38) Chen, C.; Yang, M.; Wang, Q.; Buffet, J.-C.; O'Hare, D. *J. Mater. Chem. A* **2014**, *2*, 15102.
(39) Buschmann, W. E.; Miller, J. S. *Inorg. Synth.* **2002**, *33*, 83.
(40) O'Hare, D.; Green, J. C.; Marder, T.; Collins, S.; Stringer, G.; Kakkar, A. K.; Kaltsoyannis, N.; Kuhn, A.; Lewis, R. *Organometallics* **1992**, *11*, 48.
(41) Ransom, P. *D.Phil. Thesis*, University of Oxford, **2009**.
(42) Ransom, P.; Ashley, A. E.; Brown, N. D.; Thompson, A. L.; O'Hare, D. *Organometallics* **2011**, *30*, 800.
(43) Alias, F. M.; Barlow, S.; Tudor, J. S.; O'Hare, D.; Perry, R. T.; Nelson, J. M.; Manners, I. *J. Organomet. Chem.* **1997**, *528*, 47.

Appendix

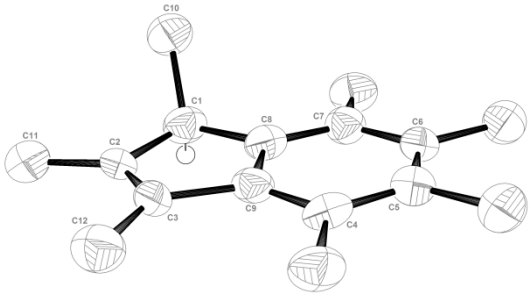
Crystallographic Data



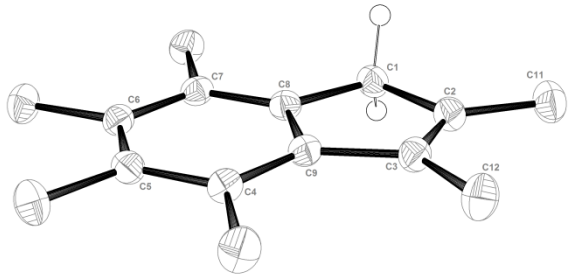
001TAQA11 (**2.4**)	
Chemical formula	$C_{15}H_{20}O$
M_r	216.32
Crystal system, space group	Orthorhombic, $Pca2_1$
Temperature (K)	150
a, b, c (Å)	13.6257 (3), 8.6250 (2), 10.5161 (2)
V (Å^3)	1235.87 (5)
Z	4
Radiation type	Mo Ka
μ (mm^{-1})	0.07
Crystal size (mm)	0.40 × 0.32 × 0.14
Data collection	
Diffractometer	Nonius KappaCCD diffractometer
Absorption correction	Multi-scan *DENZO*/*SCALEPACK*
T_{min}, T_{max}	0.88, 0.99
No. of measured, independent and observed [$I > 2.0\sigma(I)$] reflections	22158, 1463, 1288
R_{int}	0.013
$(\sin \theta/\lambda)_{max}$ (Å^{-1})	0.649
Refinement	
$R[F^2 > 2\sigma(F^2)]$, $wR(F^2)$, S	0.039, 0.111, 0.83
No. of reflections	1463
No. of parameters	145
No. of restraints	1
H-atom treatment	H-atom parameters constrained
$\Delta\rho_{max}$, $\Delta\rho_{min}$ (e Å^{-3})	0.18, −0.19



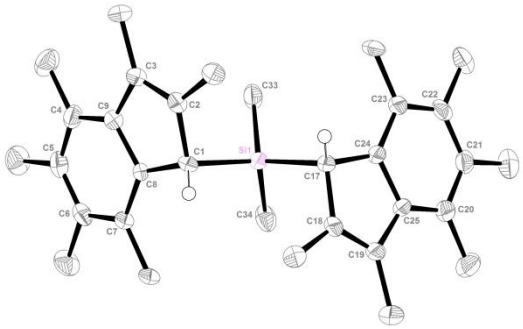
005TAQA11 (**2.5**)	
Chemical formula	$C_{16}H_{24}O$
M_r	232.37
Crystal system, space group	Tetragonal, I41/a
Temperature (K)	150
a, *b*, *c* (Å)	24.7261 (4), 9.1915 (2)
V (Å^3)	5619.50 (18)
Z	16
Radiation type	Mo *K*α
μ (mm^{-1})	0.07
Crystal size (mm)	0.16 × 0.14 × 0.13
Data collection	
Diffractometer	Nonius KappaCCD diffractometer
Absorption correction	Multi-scan *DENZO*/*SCALEPACK*
T_{min}, T_{max}	0.92, 0.92
No. of measured, independent and observed [$I > 2.0\sigma(I)$] reflections	3193, 3193, 1604
R_{int}	0.027
$(\sin\theta/\lambda)_{max}$ (Å^{-1})	0.649
Refinement	
$R[F^2 > 2\sigma(F^2)]$, $wR(F^2)$, *S*	0.165, 0.403, 0.91
No. of reflections	2006
No. of parameters	208
No. of restraints	194
H-atom treatment	H-atom parameters constrained
$\Delta\rho_{max}$, $\Delta\rho_{min}$ (e Å^{-3})	0.86, −0.81



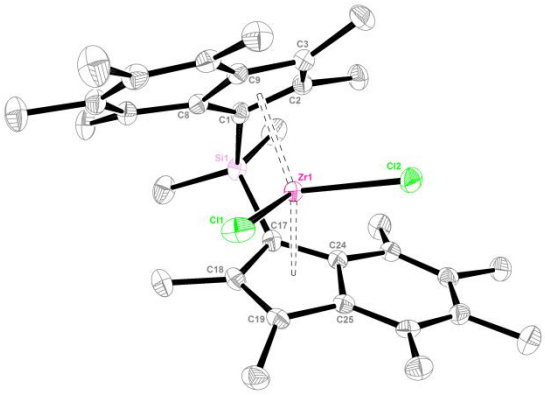
002TAQA11 (**2.6**)	
Chemical formula	$C_{16}H_{22}$
M_r	214.35
Crystal system, space group	Monoclinic, P21/a
Temperature (K)	150
a, *b*, *c* (Å)	9.0940 (8), 10.9228 (11), 13.0429 (12)
β (°)	91.932 (4)
V (Å^3)	1294.8 (2)
Z	4
Radiation type	Mo Kα
μ (mm^{-1})	0.06
Crystal size (mm)	0.30 × 0.16 × 0.12
Data collection	
Diffractometer	Nonius KappaCCD diffractometer
Absorption correction	Multi-scan *DENZO*/*SCALEPACK*
T_{min}, T_{max}	0.88, 0.99
No. of measured, independent and observed [$I > 2.0\sigma(I)$] reflections	2516, 2516, 1156
R_{int}	0.070
$(\sin\theta/\lambda)_{max}$ (Å^{-1})	0.622
Refinement	
$R[F^2 > 2\sigma(F^2)]$, $wR(F^2)$, S	0.095, 0.095, 1.09
No. of reflections	1156
No. of parameters	146
H-atom treatment	H-atom parameters constrained
$\Delta\rho_{max}$, $\Delta\rho_{min}$ (e Å^{-3})	0.22, −0.26



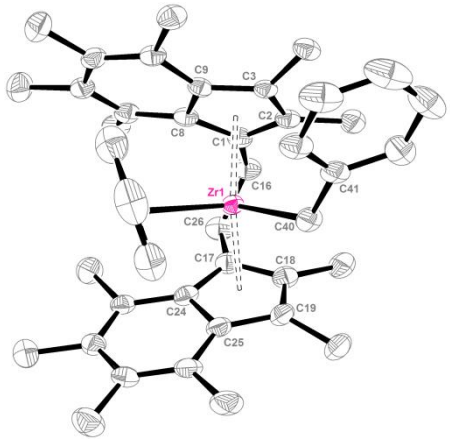
003SCB12 (**2.11)**	
Chemical formula	$C_{15}H_{20}$
M_r	200.32
Crystal system, space group	Monoclinic, $P2_1/c$
Temperature (K)	150
a, *b*, *c* (Å)	7.7961 (3), 18.3690 (7), 8.0144 (3)
β (°)	90.3299 (19)
V (Å^3)	1147.70 (8)
Z	4
Radiation type	Mo *K*a
μ (mm^{-1})	0.06
Crystal size (mm)	0.40 × 0.30 × 0.20
Data collection	
Diffractometer	Nonius KappaCCD diffractometer
Absorption correction	Multi-scan *DENZO*/*SCALEPACK*
T_{min}, T_{max}	0.88, 0.99
No. of measured, independent and observed [$I > 2.0\sigma(I)$] reflections	9353, 2597, 1852
R_{int}	0.026
$(\sin\theta/\lambda)_{max}$ (Å^{-1})	0.649
Refinement	
$R[F^2 > 2\sigma(F^2)]$, $wR(F^2)$, S	0.048, 0.134, 0.95
No. of reflections	2596
No. of parameters	216
H-atom treatment	H atoms treated by a mixture of independent and constrained refinement
$\Delta\rho_{max}$, $\Delta\rho_{min}$ (e Å^{-3})	0.34, −0.31



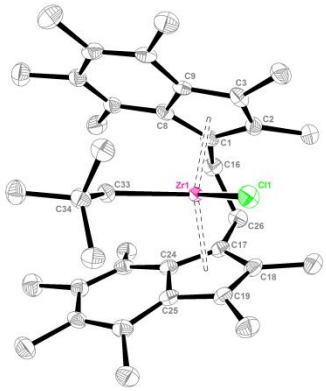
028TAQA12 (***rac*-2.14)**	
Chemical formula	$C_{32}H_{44}Si$
M_r	456.79
Crystal system, space group	Triclinic, $P\bar{1}$
Temperature (K)	150
a, *b*, *c* (Å)	9.2291 (7), 9.7804 (7), 15.8873 (12)
β (°)	89.600 (6), 81.392 (6), 73.234 (6)
V (Å^3)	1356.64 (18)
Z	2
Radiation type	Cu Kα
μ (mm^{-1})	0.87
Crystal size (mm)	0.15 × 0.05 × 0.03
Data collection	
Diffractometer	Oxford Diffraction SuperNova diffractometer
Absorption correction	Multi-scan CrysAlis
T_{min}, T_{max}	0.52, 0.97
No. of measured, independent and observed [$I > 2.0\sigma(I)$] reflections	5617, 5617, 4511
R_{int}	0.081
$(\sin \theta/\lambda)_{max}$ (Å^{-1})	0.631
Refinement	
$R[F^2 > 2\sigma(F^2)]$, $wR(F^2)$, S	0.097, 0.279, 0.97
No. of reflections	5595
No. of parameters	301
H-atom treatment	H-atom parameters constrained
$\Delta\rho_{max}$, $\Delta\rho_{min}$ (e Å^{-3})	0.57, −0.39



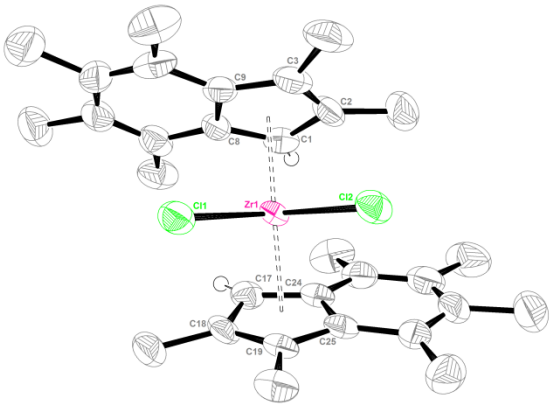
201TAQA13 (***rac*-3.1**)	
Chemical formula	$C_{32}H_{42}Cl_2SiZr$
M_r	616.90
Crystal system, space group	Monoclinic, $P2_1/n$
Temperature (K)	150
a, *b*, *c* (Å)	14.1078 (1), 14.2840 (2), 14.3753 (2)
β (°)	96.8940 (5)
V (Å^3)	2875.91 (6)
Z	4
Radiation type	Mo Kα
μ (mm^{-1})	0.63
Crystal size (mm)	0.35 × 0.30 × 0.25
Data collection	
Diffractometer	Nonius KappaCCD diffractometer
Absorption correction	Multi-scan *DENZO*/*SCALEPACK*
T_{min}, T_{max}	0.77, 0.85
No. of measured, independent and observed [$I > 2.0\sigma(I)$] reflections	46194, 6558, 5879
R_{int}	0.013
$(\sin\theta/\lambda)_{max}$ (Å^{-1})	0.649
Refinement	
$R[F^2 > 2\sigma(F^2)]$, $wR(F^2)$, S	0.030, 0.073, 0.91
No. of reflections	6556
No. of parameters	325
H-atom treatment	H-atom parameters constrained
$\Delta\rho_{max}$, $\Delta\rho_{min}$ (e Å^{-3})	0.49, −0.58



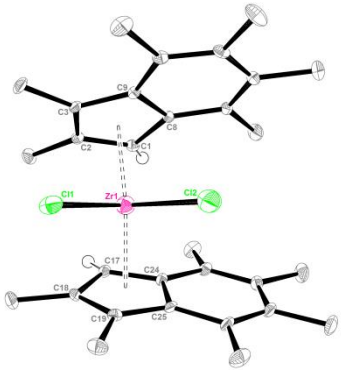
011TAQA14 (***meso*-3.3)**	
Chemical formula	$C_{46}H_{54}Zr$
M_r	698.15
Crystal system, space group	Monoclinic, $P2_1/n$
Temperature (K)	150
a, b, c (Å)	12.1915 (3), 19.1827 (4), 15.3626 (3)
β (°)	93.2526 (18)
V (Å^3)	3587.00 (13)
Z	4
Radiation type	Cu Ka
μ (mm^{-1})	2.73
Crystal size (mm)	0.20 × 0.07 × 0.05
Data collection	
Diffractometer	Oxford Diffraction SuperNova diffractometer
Absorption correction	–
No. of measured, independent and observed [$I > 2.0\sigma(I)$] reflections	21352, 7430, 5705
R_{int}	0.054
$(\sin \theta/\lambda)_{max}$ (Å^{-1})	0.630
Refinement	
$R[F^2 > 2\sigma(F^2)]$, $wR(F^2)$, S	0.046, 0.109, 1.00
No. of reflections	7403
No. of parameters	424
H-atom treatment	H-atom parameters constrained
$\Delta\rho_{max}$, $\Delta\rho_{min}$ (e Å^{-3})	1.48, −0.75



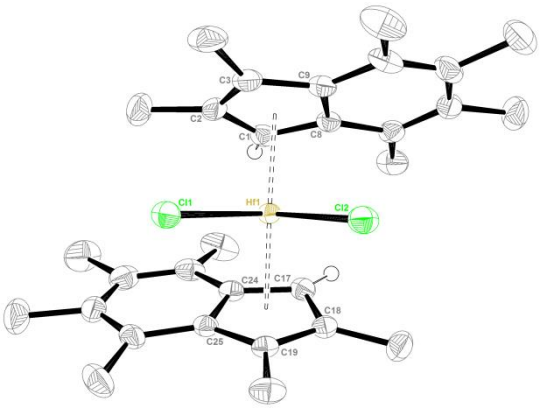
023TAQA14 (***meso*-3.4**)	
Chemical formula	$C_{40}H_{58}ClZr$
M_r	665.57
Crystal system, space group	Triclinic, $P\bar{1}$
Temperature (K)	100
a, b, c (Å)	11.4222 (5), 15.9204 (6), 19.5395 (7)
β (°)	92.805 (3), 90.490 (3), 108.372 (4)
V (Å^3)	3367.0 (2)
Z	4
Radiation type	Synchrotron, λ = 0.68890 Å
μ (mm^{-1})	0.43
Crystal size (mm)	0.04 × 0.01 × 0.01
Data collection	
Diffractometer	Rigaku Saturn724+ (2x2 bin mode) diffractometer
Absorption correction	Multi-scan CrysAlis
T_{min}, T_{max}	0.82, 1.00
No. of measured, independent and observed [$I > 2.0\sigma(I)$] reflections	48267, 14738, 8979
R_{int}	0.062
$(\sin\theta/\lambda)_{max}$ (Å^{-1})	0.673
Refinement	
$R[F^2 > 2\sigma(F^2)]$, $wR(F^2)$, S	0.042, 0.102, 0.93
No. of reflections	11809
No. of parameters	757
H-atom treatment	H-atom parameters constrained
$\Delta\rho_{max}$, $\Delta\rho_{min}$ (e Å^{-3})	0.63, −0.54



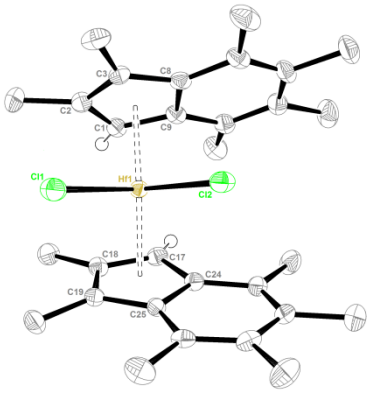
009TAQA14 (***rac*-3.5**)	
Chemical formula	$C_{30}H_{38}Cl_2Zr$
M_r	560.76
Crystal system, space group	Monoclinic, $P2_1/c$
Temperature (K)	100
a, b, c (Å)	17.2538 (13), 9.0136 (5), 18.3402 (16)
β (°)	114.553 (10)
V (Å^3)	2594.3 (4)
Z	4
Radiation type	Synchrotron, λ = 0.68890 Å
μ (mm^{-1})	0.65
Crystal size (mm)	0.01 × 0.01 × 0.01
Data collection	
Diffractometer	Rigaku Saturn724+ (2x2 bin mode) diffractometer
Absorption correction	Multi-scan CrysAlis
T_{min}, T_{max}	0.40, 1.00
No. of measured, independent and observed [$I > 2.0\sigma(I)$] reflections	22027, 5499, 2546
R_{int}	0.126
$(\sin \theta/\lambda)_{max}$ (Å^{-1})	0.657
Refinement	
$R[F^2 > 2\sigma(F^2)]$, $wR(F^2)$, S	0.046, 0.116, 0.93
No. of reflections	3466
No. of parameters	298
H-atom treatment	H-atom parameters constrained
$\Delta\rho_{max}$, $\Delta\rho_{min}$ (e Å^{-3})	0.54, −0.54



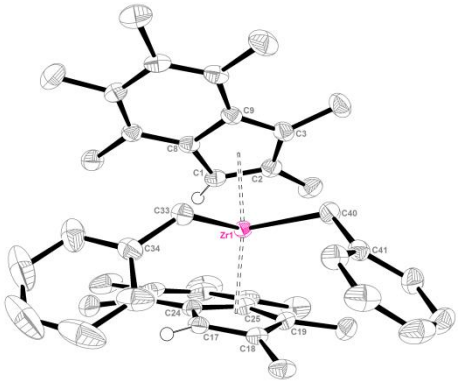
018TAQA14 (***meso*-3.5**)	
Chemical formula	$C_{30}H_{38}Cl_2Zr$
M_r	560.76
Crystal system, space group	Monoclinic, $P2_1/n$
Temperature (K)	100
a, b, c (Å)	12.55987 (11), 14.56043 (10), 14.41692 (11)
β (°)	98.3967 (8)
V (Å^3)	2608.26 (3)
Z	4
Radiation type	Mo Ka
μ (mm^{-1})	0.64
Crystal size (mm)	0.08 × 0.05 × 0.04
Data collection	
Diffractometer	Rigaku Saturn724+ (2x2 bin mode) diffractometer
Absorption correction	Multi-scan CrysAlis
T_{min}, T_{max}	0.89, 0.97
No. of measured, independent and observed [$I > 2.0\sigma(I)$] reflections	58287, 9280, 7913
R_{int}	0.053
$(\sin \theta/\lambda)_{max}$ (Å^{-1})	0.773
Refinement	
$R[F^2 > 2\sigma(F^2)]$, $wR(F^2)$, S	0.061, 0.196, 0.93
No. of reflections	9259
No. of parameters	298
H-atom treatment	Modified Sheldrick $w = 1/[s^2(F^2) + (0.1P)^2 + 14.53P]$ where $P = (\max(F_o^2,0) + 2F_c^2)/3$
$\Delta\rho_{max}$, $\Delta\rho_{min}$ (e Å^{-3})	1.06, −2.48



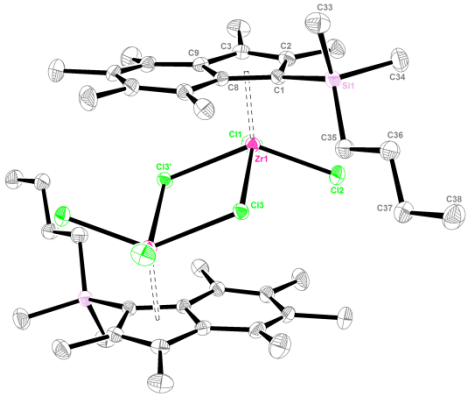
056TAQA14 (***rac*-3.6**)	
Chemical formula	$C_{30}H_{38}Cl_2Hf$
M_r	648.03
Crystal system, space group	Monoclinic, $P2_1/c$
Temperature (K)	150
a, b, c (Å)	17.3610 (2), 9.08256 (7), 18.4055 (2)
β (°)	114.8387 (16)
V (Å^3)	2633.74 (6)
Z	4
Radiation type	Cu $K\alpha$
μ (mm^{-1})	9.30
Crystal size (mm)	0.18 × 0.08 × 0.07
Data collection	
Diffractometer	Oxford Diffraction SuperNova diffractometer
Absorption correction	Multi-scan CrysAlis
T_{min}, T_{max}	0.28, 0.52
No. of measured, independent and observed [$I > 2.0\sigma(I)$] reflections	28455, 5492, 5278
R_{int}	0.021
$(\sin \theta/\lambda)_{max}$ (Å^{-1})	0.629
Refinement	
$R[F^2 > 2\sigma(F^2)]$, $wR(F^2)$, S	0.017, 0.042, 1.00
No. of reflections	5473
No. of parameters	298
H-atom treatment	H-atom parameters constrained
$\Delta\rho_{max}$, $\Delta\rho_{min}$ (e Å^{-3})	0.67, −0.54



055TAQA14 (***meso*-3.6**)	
Chemical formula	$C_{30}H_{38}Cl_2Hf$
M_r	648.03
Crystal system, space group	Monoclinic, $P2_1/n$
Temperature (K)	150
a, b, c (Å)	12.5691 (1), 14.6272 (1), 14.3927 (2)
β (°)	98.6310 (9)
V (Å^3)	2616.14 (5)
Z	4
Radiation type	Cu Ka
μ (mm^{-1})	9.36
Crystal size (mm)	0.30 × 0.12 × 0.08
Data collection	
Diffractometer	Oxford Diffraction SuperNova diffractometer
Absorption correction	Multi-scan CrysAlis
T_{min}, T_{max}	0.06, 0.47
No. of measured, independent and observed [$I > 2.0\sigma(I)$] reflections	26328, 5435, 5261
R_{int}	0.036
$(\sin \theta/\lambda)_{max}$ (Å^{-1})	0.629
Refinement	
$R[F^2 > 2\sigma(F^2)]$, $wR(F^2)$, S	0.027, 0.076, 1.02
No. of reflections	5415
No. of parameters	298
H-atom treatment	H-atom parameters constrained
$\Delta\rho_{max}$, $\Delta\rho_{min}$ (e Å^{-3})	1.68, −1.28



050TAQA14 (***rac*-3.7**)	
Chemical formula	$C_{44}H_{52}Zr$
M_r	672.12
Crystal system, space group	Monoclinic, $P2_1/n$
Temperature (K)	150
a, b, c (Å)	13.3970 (1), 18.3318 (1), 14.3130 (1)
β (°)	93.7834 (7)
V (Å^3)	3507.48 (4)
Z	4
Radiation type	Cu Ka
μ (mm^{-1})	2.77
Crystal size (mm)	0.18 × 0.14 × 0.12
Data collection	
Diffractometer	Oxford Diffraction SuperNova diffractometer
Absorption correction	Multi-scan CrysAlis
T_{min}, T_{max}	0.52, 0.72
No. of measured, independent and observed [$I > 2.0\sigma(I)$] reflections	19921, 7269, 6809
R_{int}	0.016
$(\sin \theta/\lambda)_{max}$ (Å^{-1})	0.630
Refinement	
$R[F^2 > 2\sigma(F^2)]$, $wR(F^2)$, S	0.025, 0.066, 1.00
No. of reflections	7240
No. of parameters	406
H-atom treatment	H-atom parameters constrained
$\Delta\rho_{max}$, $\Delta\rho_{min}$ (e Å^{-3})	0.37, −0.41



002TAQA13 (**3.8**)	
Chemical formula	$C_{21}H_{33}Cl_3SiZr$
M_r	511.16
Crystal system, space group	Triclinic, $P\bar{1}$
Temperature (K)	150
a, *b*, *c* (Å)	9.5271 (1), 11.1274 (1), 11.3616 (1)
β (°)	78.1654 (5), 87.3403 (5), 77.9022 (5)
V (Å^3)	1152.67 (2)
Z	2
Radiation type	Mo *K*a
μ (mm^{-1})	0.88
Crystal size (mm)	0.36 × 0.32 × 0.22
Data collection	
Diffractometer	Nonius KappaCCD diffractometer
Absorption correction	Multi-scan *DENZO*/*SCALEPACK*
T_{min}, T_{max}	0.72, 0.82
No. of measured, independent and observed [$I > 2.0\sigma(I)$] reflections	34494, 5248, 4881
R_{int}	0.013
$(\sin\theta/\lambda)_{max}$ (Å^{-1})	0.649
Refinement	
$R[F^2 > 2\sigma(F^2)]$, $wR(F^2)$, S	0.027, 0.070, 0.93
No. of reflections	5248
No. of parameters	235
H-atom treatment	H-atom parameters constrained
$\Delta\rho_{max}$, $\Delta\rho_{min}$ (e Å^{-3})	0.50, −0.62